

Knowledge wins



Take the
360° view

Immuno-oncology



Understanding how the immune system fights cancer and how cancer cells evade these attacks is the key to developing effective immunotherapies. A multi-omics approach provides a 360° view of tumor heterogeneity and the tumor microenvironment and yields an in-depth perspective contributing to rapid clinical advances.

Researchers in the field are advancing immunotherapy with products and services from Affymetrix for gene-, protein-, and cell-level analysis.



Scan the QR code or visit our website to download
the *Immuno-oncology Application Guide*.

www.affymetrix.com/view360

© 2016 Affymetrix, Inc. All rights reserved. For Research Use Only. Not for use in diagnostic procedures.

Immunity

Best of 2015



Including a New SnapShot from *Immunity*

immunoSEQ®

The most quantitative way to sequence
millions of T- and B-cell receptors



immunoSEQ Technology combines:

- Bias-controlled multiplex PCR
- High-throughput sequencing
- Sophisticated bioinformatics

VISIT US AT BOOTH #446

We'll show you how easy it is to analyze and visualize your
data with the immunoSEQ Analyzer.

Explore immunology-focused applications

www.immunoSEQ.com/AAI-2016



PROTEINTECH GROUP: THE BENCHMARK IN ANTIBODY VALIDATION

Antibodies detected with siRNA treated samples to demonstrate specificity.

Look out for the **Tested with siRNA** icon when searching for your antibody to ensure it is specific.

The Benchmark
In Antibodies

www.ptglab.com

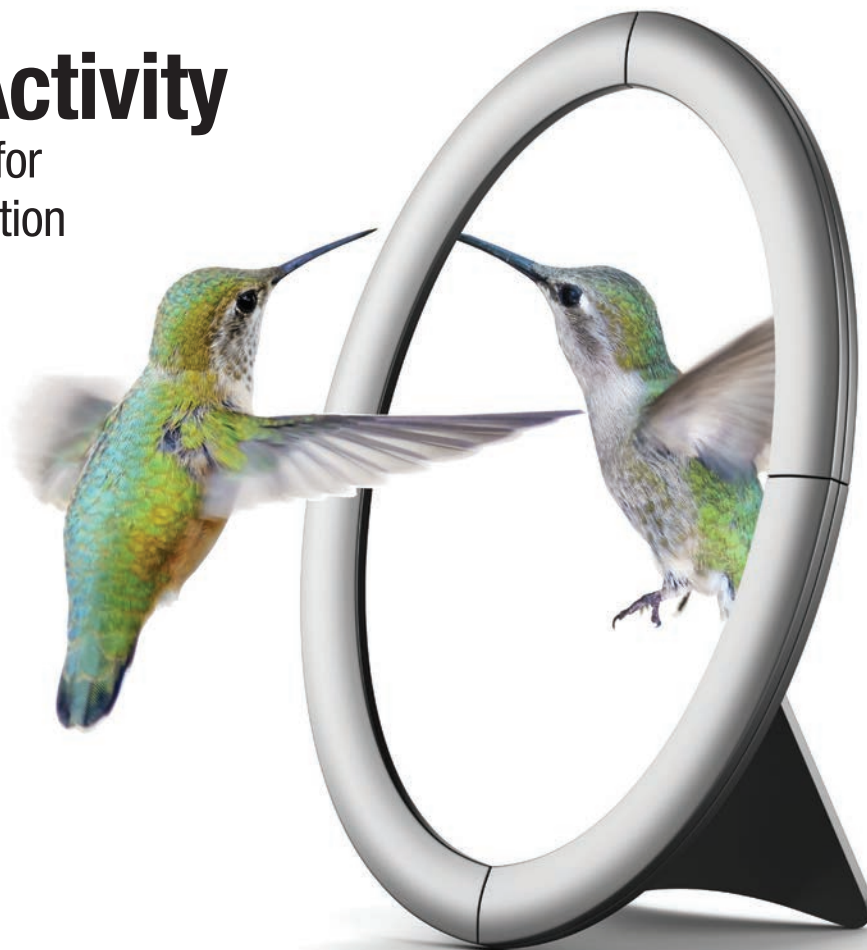
PROTEINTECH GROUP: THE BENCHMARK IN ANTIBODY VALIDATION

Winner of the Citeab 2016 award for
“Most Exciting Validation Initiative.”



Mimic True Activity

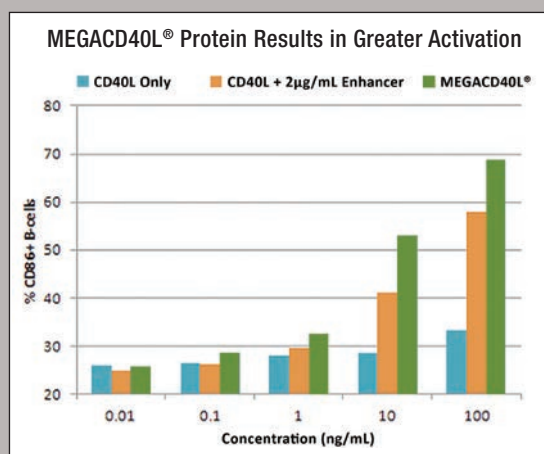
MEGACD40L[®] Construct for
Immune Response Activation



High-activity, high-purity construct for co-stimulating activation of an immune response

MEGACD40L[®] protein is an optimized, oligomeric construct which mimics *in vivo* membrane-assisted CD40L aggregation and stimulation without the need for enhancers. Enzo's expertise in the production of challenging protein complexes, such as MEGACD40L[®] protein, results in a product you can rely on for the duration of your study.

- Engages with immune cell receptors and acts as a potent and sustained immunostimulator
- Improved stability and enhanced activity, when compared to CD40L, alone or with enhancers
- Superior purity eliminates experimental artifacts—100-fold lower endotoxin levels than comparable products
- Guarantees reliable results through consistent lot-to-lot performance



Autoimmunity | Cancer Immunotherapy | Endocrinology | Vaccine Development

SEEING IS BELIEVING

Fluorescent *in vivo* imaging probes allow you to see cellular processes and get a more complete understanding of the activity of a potential therapeutic.

Image: apoptotic cells labeled with CAS-MAP™ red. Countestained with DNA dye (blue).

Non-invasive imaging enables you to see how, where and when cellular processes are affected by potential therapies.

Vergent Bioscience carries a line of *in vivo* imaging probes that are easy to use. Simply inject the probe IV and image at the desired time points using standard optical animal imaging systems.

- Optimized for live cell imaging, fluorescent microscopy and live animal imaging.
- Near infrared (NIR) probes for deeper tissue penetration and reduced tissue autofluorescence.
- Activatable probes for high signal-to-noise target biology.

SEE MORE:

vergentbio.com/imaging
844.803.0346

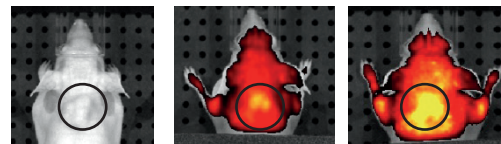


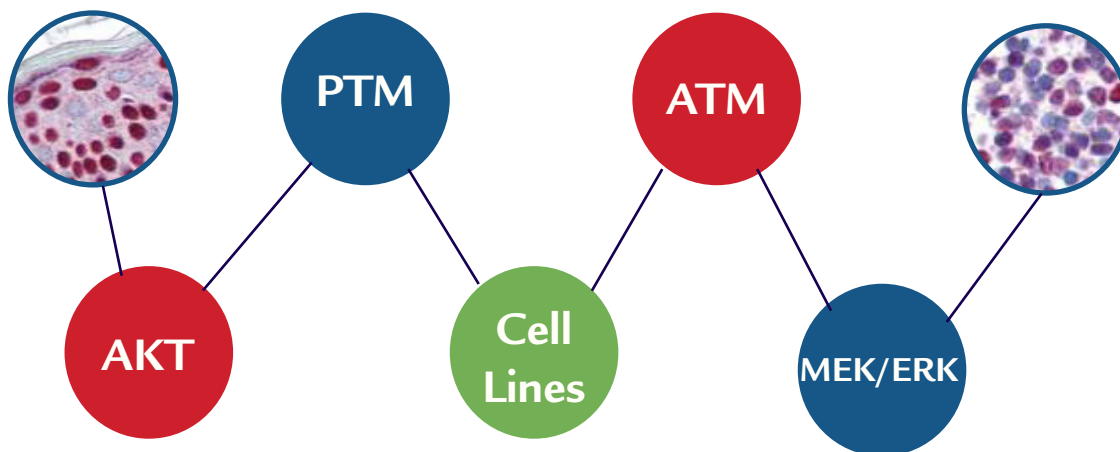
Figure 1: Apoptotic cells are labeled green using CAS-MAP™ probes in an *in vivo* study of postnatal development. Figure 2: Apoptotic COLO205 tumor cells are labeled in response to treatment.



All Your Cancer Research Needs

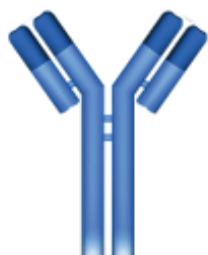
Available from Rockland

www.rockland-inc.com/cancertools



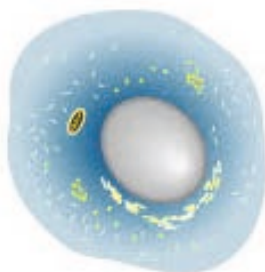
Rockland offers a comprehensive portfolio of antibodies and antibody-based tools for the numerous methods needed in cancer research.

Cancer Antibodies



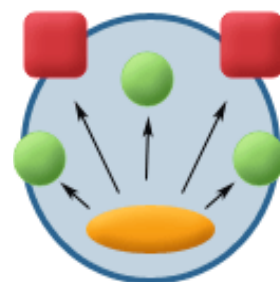
We provide over 1000 cancer antibodies in our extensive portfolio. We offer NCI validated antibodies for a wide range of applications such as ELISA, western blot, IHC and more.

Cell Lines



Our highly characterized melanoma cell line models are able to predict clinical activity as they are biologically stable in terms of gene expression pattern, tumor architecture and mutation status. Key applications include genetic studies, xenograft production, drug testing and drug target discovery.

Cell Signaling



Rockland produces antibodies that assist in cancer research in numerous cell signaling pathways, including AKT, MEK/ERK, NF-kB, Notch signaling, and more.

UBIQUITIN is everywhere:

GET IT ALL



ACTIVITY

Enzymes, substrates, and activity assays

ISOLATION + ID

Pull-downs from lysates, Western blots, and imaging applications

EXPRESSION

Patented SUMO system: increase purity and solubility, decrease cost and time

SERVICES

Protein microarrays, substrate production, and biologically active protein expression

LifeSensors: We build UbiRelations for life

TALK WITH US

**AAI Meeting
Booth #2114**

May 2016

Deepen your understanding of the Ubiquitome:

- Quantify substrate ubiquitylation
- Identify enzymes and substrates
- Discover modulators

DIY, or let our team give your project a lift with our **Ubiquitin Research Toolbox**

Conjugating Enzymes & Assays

Deubiquitinating enzymes (DUBs) & Isopeptidase Substrates

Ubiquitin-Proteasome Pathway Inhibitors

Proteasome Research tools

Call +1 610 644 8845
info@lifesensors.com

www.lifesensors.com

Use promo code LS201605CELL for 10% off*

*Single use per customer and cannot be combined with other offers.

Foreword



Four years ago, Cell Press launched the “Best of” reprint collections across a number of our journals, including *Immunity*. We proudly welcome you to the 2015 edition of *Best of Immunity*. In looking back at the papers published during 2015, we wanted to provide our readers with a sense of the various topics and findings in which they and their colleagues have shown significant interest. *Immunity* is published monthly in two volumes each year, with each volume covering 6 months. In order to account for the amount of time since publication, we have selected 10 of the most-accessed articles from volumes 42 and 43, which cover the first and second halves of 2015, respectively. We use the number of requests for PDF and full-text HTML versions of a given article up until the end of March 2016 to determine the “most-accessed” articles. We acknowledge that no single measurement can truly be indicative of “the best” research papers over a given period of time. This is especially true when sufficient time has not necessarily passed to allow one to fully appreciate the relative importance of a discovery. That said, we think it is still informative to look back at our readers’ interest in the immunology that *Immunity* published over the course of 2015.

In this reprint collection, we present for your consideration one perspective, one review, and eight research articles from throughout 2015. You will see a range of the exciting topics that have widely captured the attention and enthusiasm of our readers, including an examination of how regulatory T cells in tumor-associated tertiary lymphoid structures suppress anti-tumor T cell responses, a review of mitochondrial regulation of innate and adaptive immunity, and an investigation into the origin, phenotype, and function of regulatory B cells.

Additionally, we present a SnapShot on integrated type 2 immune responses. To access the complete collection of SnapShots, visit snapshots.cell.com.

We hope that you will enjoy reading this special collection and that you will visit www.cell.com/immunity to check out the latest findings that we have had the privilege to publish. Also be sure to visit www.cell.com to find other high-quality papers published in the full collection of Cell Press journals.

Finally, we are grateful for the generosity of our sponsors, who helped to make this reprint collection possible.

Immunity



For information for the Best of Series, please contact:

Jonathan Christison
Program Director, Best of Cell Press
e: jchristison@cell.com
p: 617-397-2893
t: @CellPressBiz

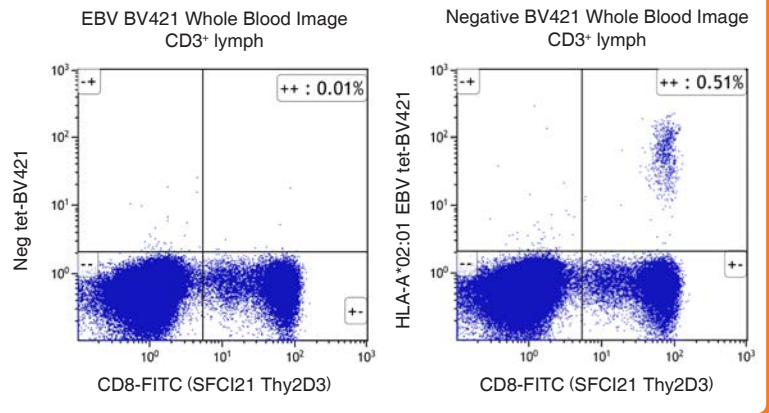
Data You Can Trust

- MHC Class I & II Tetramers
- MHC Monomers
- CD1d Tetramers
- Qa-1b tetramers

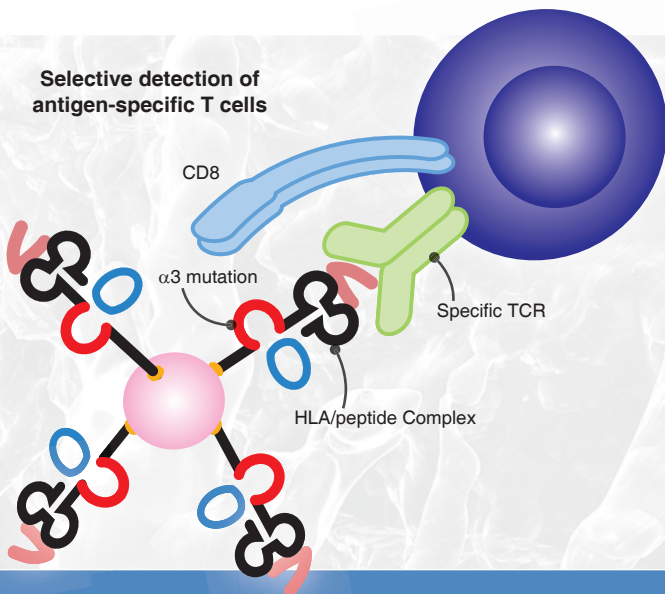
MBL has been providing tetramer reagents for over a decade and is your source for quality reagents for detection of antigen-specific T cells and NKT cells.

- Class I and class II tetramers for detection of antigen-specific CD8⁺ and CD4⁺ T cells
- Patented $\alpha 3$ domain mutation to reduce non-specific binding
- Non-classical MHC HLA-E and Qa-1b
- Human, Mouse, Rhesus Macaque, Mauritian Cyno, Chicken, and Chimeric alleles
- MHC Monomers

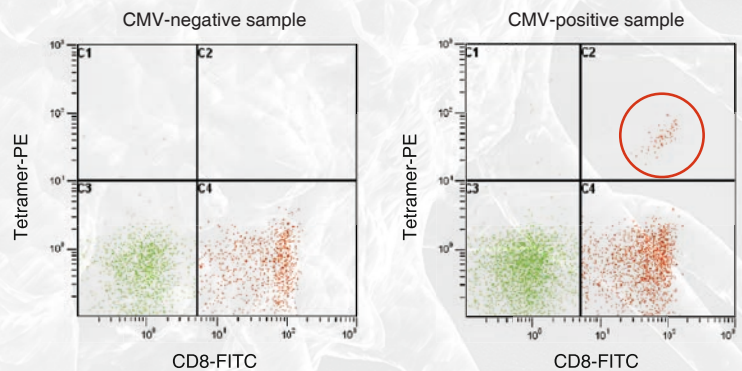
NEW! Brilliant Violet™ 421



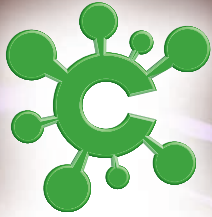
Selective detection of antigen-specific T cells



HLA-A*02:01 CMV pp65 Tetramer



Contact MBL International today to learn more about our products and how we can help you discover ways to make your science more efficient and effective.

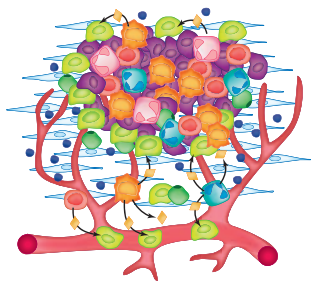


CELLECTA

Obtain a Molecular Snapshot of the Tumor Microenvironment

Driver-Map™ ImmuneNet™

NEW Driver-Map™, a novel, quantitative, multiplexed **GPS** (comprehensive **G**ene expression **P**rofilng **S**ervice) from Cellecta allows you to characterize cellular composition of tumor samples. This quantitative, targeted RNA-Seq approach leverages the power of multiplex PCR technologies and NGS and allows you to simultaneously profile thousands of genes in one reaction. ImmuneNet™ is a panel specifically designed to obtain cellular composition of tumor stroma.



- Detect cellular composition of immune/stromal/cancer cells in the tumor microenvironment
- Identify immunity status and immunoediting mechanisms
- Discover novel biomarkers for immunotherapy
- Profile immunotherapy targets & all FDA-approved drug targets
- Understand role of cancer driver genes

Interested? Email us at driver-map@cellecta.com to participate in the early access program. Visit www.driver-map.com for more details, or call us at (877) 938-3910.

And check out Booth #2426 at the 2016 AAI Annual Meeting!

(877) 938-3910

Discovery is yours.

www.cellecta.com

Knowledge wins



Take the
360° view

Immuno-oncology



Understanding how the immune system fights cancer and how cancer cells evade these attacks is the key to developing effective immunotherapies. A multi-omics approach provides a 360° view of tumor heterogeneity and the tumor microenvironment and yields an in-depth perspective contributing to rapid clinical advances.

Researchers in the field are advancing immunotherapy with products and services from Affymetrix for gene-, protein-, and cell-level analysis.



Scan the QR code or visit our website to download
the *Immuno-oncology Application Guide*.

www.affymetrix.com/view360

© 2016 Affymetrix, Inc. All rights reserved. For Research Use Only. Not for use in diagnostic procedures.

Immunity

Best of 2015

Perspective

Regulatory B Cells: Origin, Phenotype, and Function

Elizabeth C. Rosser and Claudia Mauri

Review

Mitochondria in the Regulation of Innate and Adaptive Immunity

Samuel E. Weinberg, Laura A. Sena, and Navdeep S. Chandel

Articles

Human Monocytes Undergo Functional Re-programming during Sepsis Mediated by Hypoxia-Inducible Factor-1 α

Irina N. Shalova, Jyue Yuan Lim, Manesh Chittezhath, Annelies S. Zinkernagel, Federico Beasley, Enrique Hernández-Jiménez, Victor Toledano, Carolina Cubillos-Zapata, Annamaria Rapisarda, Jinmiao Chen, Kaibo Duan, Henry Yang, Michael Poidinger, Giovanni Melillo, Victor Nizet, Francisco Arnalich, Eduardo López-Collazo, and Subhra K. Biswas

Network Integration of Parallel Metabolic and Transcriptional Data Reveals Metabolic Modules that Regulate Macrophage Polarization

Abhishek K. Jha, Stanley Ching-Cheng Huang, Alexey Sergushichev, Vicky Lampropoulou, Yulia Ivanova, Ekaterina Loginicheva, Karina Chmielewski, Kelly M. Stewart, Juliet Ashall, Bart Everts, Edward J. Pearce, Edward M. Driggers, and Maxim N. Artyomov

C-Myb⁺ Erythro-Myeloid Progenitor-Derived Fetal Monocytes Give Rise to Adult Tissue-Resident Macrophages

Guillaume Hoeffel, Jinmiao Chen, Yonit Lavin, Donovan Low, Francisca F. Almeida, Peter See, Anna E. Beaudin, Josephine Lum, Ivy Low, E. Camilla Forsberg, Michael Poidinger, Francesca Zolezzi, Anis Larbi, Lai Guan Ng, Jerry K.Y. Chan, Melanie Greter, Burkhard Becher, Igor M. Samokhvalov, Miriam Merad, and Florent Ginhoux

Interleukin-33 and Interferon- γ Counter-Regulate Group 2 Innate Lymphoid Cell Activation during Immune Perturbation

Ari B. Molofsky, Frédéric Van Gool, Hong-Erh Liang, Steven J. Van Dyken, Jesse C. Nussbaum, Jinwoo Lee, Jeffrey A. Bluestone, and Richard M. Locksley

Regulatory T Cells in Tumor-Associated Tertiary Lymphoid Structures Suppress Anti-tumor T Cell Responses

Nikhil S. Joshi, Elliot H. Akama-Garren, Yisi Lu, Da-Yae Lee, Gregory P. Chang, Amy Li, Michel DuPage, Tuomas Tammela, Natanya R. Kerper, Anna F. Farago, Rebecca Robbins, Denise M. Crowley, Roderick T. Bronson, and Tyler Jacks

Distinct Commensals Induce Interleukin-1 β via NLRP3 In ammasome in In ammatory Monocytes to Promote Intestinal In amamation in Response to Injury

Sang-Uk Seo, Nobuhiko Kamada, Raúl Muñoz-Planillo, Yun-Gi Kim, Donghyun Kim, Yukiko Koizumi, Mizuho Hasegawa, Stephanie D. Himpfl, Hilary P. Browne, Trevor D. Lawley, Harry L.T. Mobley, Naohiro Inohara, and Gabriel Núñez

(continued)

Spatiotemporally Distinct Interactions with Dendritic Cell Subsets Facilitates CD4⁺ and CD8⁺ T Cell Activation to Localized Viral Infection

Jyh Liang Hor, Paul G. Whitney, Ali Zaid, Andrew G. Brooks, William R. Heath, and Scott N. Mueller

The Cytokine GM-CSF Drives the Inflammatory Signature of CCR2⁺ Monocytes and Licenses Autoimmunity

Andrew L. Croxford, Margit Lanzinger, Felix J. Hartmann, Bettina Schreiner, Florian Mair, Pawel Pelczar, Björn E. Clausen, Steffen Jung, Melanie Greter, and Burkhard Becher

SnapShot

Integrated Type 2 Immune Responses

Bart N. Lambrecht and Stephen J. Galli

A MAJOR LEAP FORWARD IN METABOLIC PHENOTYPING

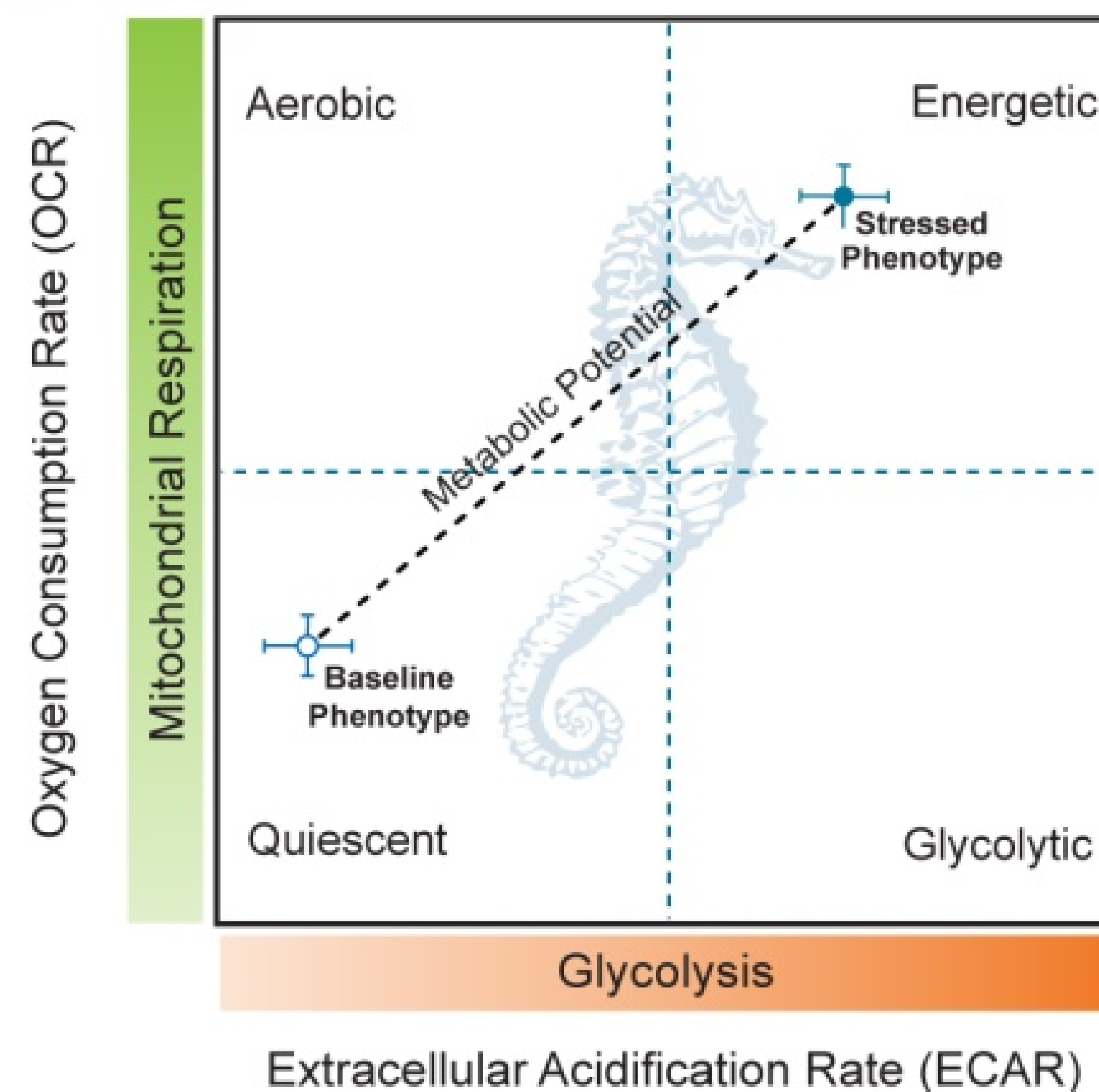
Determine the functional impact of genes, proteins, or drugs on metabolism in an hour



The XF^e Extracellular Flux Analyzer

With the Seahorse XF^e Analyzer and XF Cell Energy Phenotype Test Kit you can quickly and easily identify your cells' metabolic phenotype, as well as metabolic potential - the utilization of mitochondrial respiration and glycolysis.

Get a **FREE** energy phenotype analysis of your cells at www.seahorsebio.com/pheno



NEW FROM THE JACKSON LABORATORY

THE HUMANIZED NSG™-SGM3 MOUSE

A SUPERIOR MOUSE MODEL FOR IMMUNO-ONCOLOGY AND INFECTIOUS DISEASE RESEARCH.

BENEFITS

- FASTER IMMUNE CELL REPOPULATION*
- HIGHER MYELOID CELL ENGRAFTMENT*
- FASTER LYMPHOID CELL ENGRAFTMENT*
- HIGHER T CELL AND DENDRITIC CELL POPULATIONS*
- ENHANCED AML ENGRAFTMENT*

**When compared to humanized NSG™*

LIFESPAN

- LONG-TERM
- GREATER THAN 12 MONTHS

**READILY AVAILABLE FOR
WORLDWIDE SHIPMENT.**

PLACE YOUR ORDER TODAY!

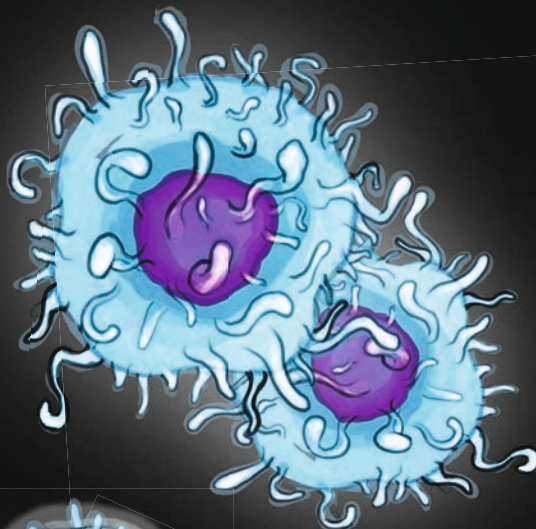
jax.org/regional-reps

1-800-422-6423 (US, Canada & Puerto Rico)

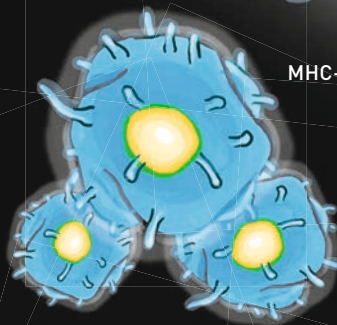
1-207-288-5845 (from any location)



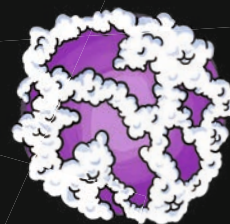
IMMUNE DEVELOPMENT



MHC-restricted CD4 and CD8 T cells



Monocytes



Macrophages



Dendritic cells

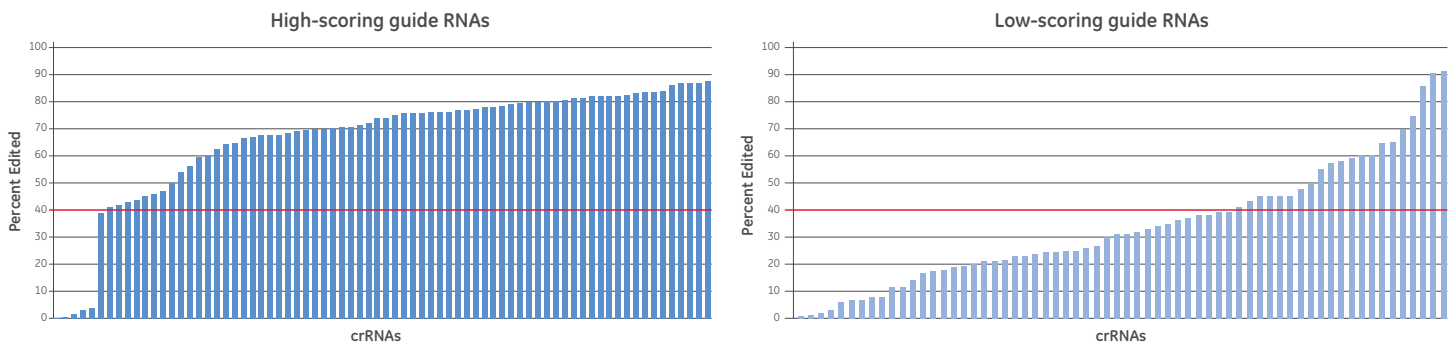
CRISPR

Dharmacon reagents help you move forward. Faster.

Simplify your gene editing workflow with the Dharmacon™ Edit-R™ CRISPR-Cas9 platform. Custom or predesigned ready-to-use DNA and synthetic RNA leverage a validated algorithm to select highly functional, specific targets for gene knockout – enabling you to quickly assess multiple target sites per gene across one or hundreds of genes.

CRISPR Guide RNAs | CRISPR Screening Libraries | Cas9 Nucleases

crRNAs that have high functionality scores show high editing efficiency



HEK293T-CAG-Cas9 cells were transfected with either high-scoring or low-scoring crRNAs (50 nM crRNA:tracrRNA) using DharmaFECT 1 transfection reagent (0.25 μ L/well) in 96-well format. Gene editing efficiencies were determined using next-generation sequencing. 93% of the top 10 high-scoring crRNAs targeting ten different genes have > 40% indel formation and only 33% of the 10 lowest scoring designs have > 40% indel formation.



What's in Your Sample?



Choose the right immunoassay
to get your answers!

[rndsystems.com/
Immunoassays](https://rndsystems.com/Immunoassays)

Regulatory B Cells: Origin, Phenotype, and Function

Elizabeth C. Rosser¹ and Claudia Mauri^{1,*}

¹Centre for Rheumatology Research, Division of Medicine, University College London, 5 University Street, London WC1E 6JF, UK

*Correspondence: c.mauri@ucl.ac.uk

<http://dx.doi.org/10.1016/j.immuni.2015.04.005>

Regulatory B (Breg) cells are immunosuppressive cells that support immunological tolerance. Through the production of interleukin-10 (IL-10), IL-35, and transforming growth factor β (TGF- β), Breg cells suppress immunopathology by prohibiting the expansion of pathogenic T cells and other pro-inflammatory lymphocytes. Recent work has shown that different inflammatory environments induce distinct Breg cell populations. Although these findings highlight the relevance of inflammatory signals in the differentiation of Breg cells, they also raise other questions about Breg cell biology and phenotype. For example, what are the functional properties and phenotype of Breg cells? Can a Breg cell arise at every stage in B cell development? Is inflammation the primary requisite for Breg cell differentiation? Here, we use these questions to discuss the advances in understanding Breg cell biology, with a particular emphasis on their ontogeny; we propose that multiple Breg cell subsets can be induced in response to inflammation at different stages in development.

Introduction

The hallmark of an effective immune response is inflammation. After infection, the inflammatory response is critical for clearing pathogens and initiating protein cascades that control wound healing (Medzhitov, 2008). If unresolved, this inflammatory response causes injury to host tissues, which can lead to the development of a wide variety of immune-mediated pathologies (Medzhitov, 2008). In the healthy individual, inflammation is self-limiting, and resolution is controlled by the release of anti-inflammatory mediators and cytokines, such as interleukin-10 (IL-10), produced by cells that have been termed “suppressive” or “regulatory” (Nathan and Ding, 2010). Conversely, in individuals with chronic inflammation, the immune system is persistently activated, often characterized by a deficiency in the number and function of these suppressor cells in circulation and at the site of inflammation (Nathan and Ding, 2010). Over the past decade, a population of suppressor B cells, collectively known as regulatory B (Breg) cells, have been associated with the inhibition of excessive inflammation (Mauri and Bosma, 2012). The use of genetically altered mice that lack B cells (Wolf et al., 1996), and more specifically IL-10-producing B cells (Fillatreau et al., 2002), has shown that defective Breg cell development and function result in chronic inflammation. This suggests that these cells could be targeted therapeutically for alleviating a wide variety of immune-mediated inflammatory conditions. For Breg cells to be useful therapeutically, greater clarity regarding the phenotype, induction, and stability of these cells *in vivo* is needed. Here, we will discuss the principal advances made in our understanding of the function, phenotype, and developmental origin of Breg cells. In particular, we will focus on newly emerging evidence demonstrating the importance of inflammation in the differentiation of Breg cells.

What Are the Functional Properties of Breg Cells?

A suppressive function for B cells was first postulated in the 1970s after the observation that B-cell-depleted splenocytes were unable to suppress delayed-type hypersensitivity in guinea pigs on adoptive transfer (Katz et al., 1974; Neta and Salvin,

1974). However, the molecular or biochemical mechanism responsible for these initial observations was never characterized, and the field of “suppressor” B cells was abandoned. The present revival of the study of B cell suppression can be traced back to the observation that B-cell-deficient mice were unable to recover from experimental autoimmune encephalitis (EAE) (Wolf et al., 1996). After this, three studies showing that B cells could suppress inflammation by the provision of IL-10 in models of colitis (Mizoguchi et al., 2002), EAE (Fillatreau et al., 2002), and arthritis (Mauri et al., 2003) were published. Over the last decade, much progress has been made to characterize immunosuppressive B cells, or “Breg cells,” leading to more rigorous study of the multiple mechanisms they employ to suppress pro-inflammatory responses *in vivo*. Primarily, Breg cells function by skewing T cell differentiation in favor of a regulatory phenotype in both mice (Carter et al., 2011) and humans (Flores-Borja et al., 2013). The importance of B cells in the maintenance of the regulatory T (Treg) cell compartment can be derived from early studies showing that Treg cells are reduced in B-cell-deficient μ MT mice (Sun et al., 2008; Tadmor et al., 2011). Later studies have shown that mice harboring a B-cell-specific deletion of IL-10 also display a Treg cell deficiency, which is associated with an outgrowth of pro-inflammatory T cells after the induction of autoimmunity (Carter et al., 2012; Carter et al., 2011). Directly, cognate interactions between Breg cells and T cells are thought to control Treg cell induction, given that B cells deficient in major histocompatibility complex class II (Yoshizaki et al., 2012) and B7 (Mann et al., 2007) do not exhibit regulatory function (Rosser et al., 2014a). Indirectly, Breg cells suppress the differentiation of T helper 1 (Th1) and Th17 cells by suppressing pro-inflammatory cytokine production by dendritic cells (Matsumoto et al., 2014; Sun et al., 2005). In addition to expressing IL-10, Breg cells express other immune-regulatory cytokines, including transforming growth factor β (TGF- β) and IL-35. Through the production of TGF- β , lipopolysaccharide (LPS)-activated B cells can induce both apoptosis of CD4⁺ (Tian et al., 2001) and anergy in CD8⁺ (Parekh et al., 2003) effector T cells. The identification of IL-35 as a key



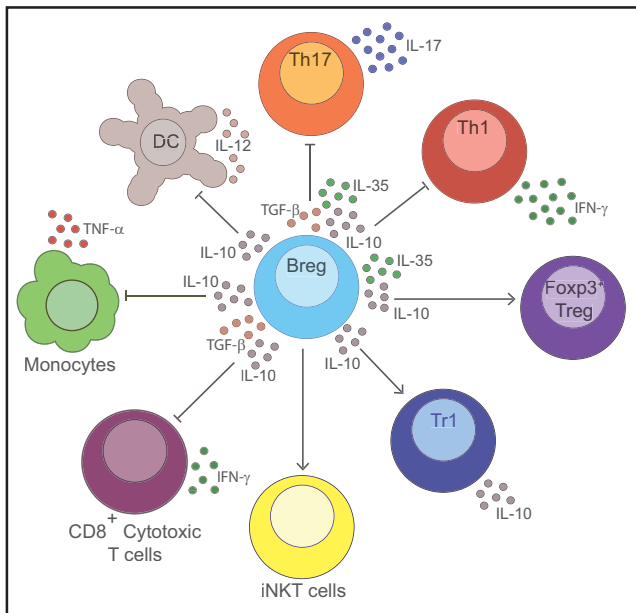


Figure 1. Functional Properties of Breg Cells

Through the production of IL-10, TGF- β , and IL-35, Breg cells can suppress the differentiation of pro-inflammatory lymphocytes, such as tumor necrosis factor α (TNF- α)-producing monocytes, IL-12-producing dendritic cells, Th17 cells, Th1 cells, and cytotoxic CD8⁺ T cells. Breg cells can also induce the differentiation of immunosuppressive T cells, Foxp3⁺ T cells, and T regulatory 1 (Tr1) cells. Breg cells also support the maintenance of iNKT cells.

immunoregulatory cytokine produced by Breg cells is a relatively recent breakthrough in the field. Chimeric mice lacking expression of IL-35 subunits, either p35 or EB13, in B cells alone develop exacerbated EAE and are provided with greater protection against *Salmonella*-induced sepsis. In the *Salmonella* model, lack of IL-35 expression by B cells resulted in enhanced Th1 cell responses and an increase in the number of macrophages in the spleen (Shen et al., 2014). Another independent study has shown that IL-35-stimulated B cells produce IL-35 and are able to inhibit experimental uveitis on adoptive transfer (Wang et al., 2014). It has also been proposed that Breg cells are critical in maintaining invariant natural killer (iNKT) cell homeostasis in humans (Bosma et al., 2012). These examples also show the advancement in the understanding of the pleiotropic role of Breg cells in the suppression of immune responses, given that Breg cells have the capacity to target many immune-system cells to exert suppression (Figure 1).

What Is the Phenotype of Breg Cells? Is There a Breg-Cell-Specific Transcription Factor?

Although a partial consensus regarding the effector function of Breg cells has been reached, the field has yet to produce a unified view concerning their phenotype. To date, multiple Breg cell subsets with many similarities in phenotype and effector functions have been described. Whether the differences observed are due to the existence of distinct Breg cell lineages or to changes dependent upon the immunological environment has yet to be elucidated. In mice, multiple subsets of IL-10-producing Breg cells have been described; these include transitional 2

marginal-zone precursor (T2-MZP) cells (Evans et al., 2007; Rosser et al., 2014b), CD5⁺CD1d^{hi} B (B10) cells (Yanaba et al., 2008; Yoshizaki et al., 2012), marginal-zone (MZ) B cells (Gray et al., 2007), Tim-1⁺ B cells (Ding et al., 2011), CD138⁺ plasma cells (Neves et al., 2010; Shen et al., 2014), and plasmablasts (Matsumoto et al., 2014). In humans, both CD19⁺CD24^{hi}CD38^{hi}CD1d^{hi} (Blair et al., 2010; Flores-Borja et al., 2013) and CD19⁺CD24^{hi}CD27⁺ (Iwata et al., 2011) Breg cells have been identified. The phenotypes of published Breg cell subsets and a summary of their associated effector functions can be found in Table 1. At present, it is unknown whether and how subsets of Breg cells are developmentally linked.

Although the expression of IL-10 has been useful in defining populations of suppressive B cells in mice and humans, many surface markers that have been used for identifying Breg cells are up- or downregulated during immune activation, leading to inherent problems in the definition of different Breg cell subsets among different experimental settings, which possibly accounts for some of the discrepancies in described Breg cell subsets. Thus, as a result of the heterogeneity of Breg cell subsets, a principal challenge of Breg cell research has been the identification of a Breg-cell-specific transcription factor, similar to Foxp3 in Treg cells (Rudensky, 2011). The identification of such a molecule would allow some resolution regarding the phenotype of Breg cells and would help answer the question of whether these cells represent a distinct lineage. To date, two models of Breg cell development can be suggested. The first is that Breg cells, similar to thymus-derived Treg cells, are a dedicated lineage of B cells where a specific factor controls the expression of genes responsible for their suppressive nature. The second is that in response to certain stimuli, B cells take on a regulatory phenotype to suppress local inflammation. Despite considerable effort, no study that has performed gene arrays on Breg cells in both mice (Shen et al., 2014) and humans (van de Veen et al., 2013) has conclusively identified a lineage-specific marker equivalent to Foxp3. The inability to identify a unique transcription factor, together with the heterogeneity of the phenotype of Breg cells, supports the idea that suppressor B cells are not lineage specific but rather are “reactive.” Thus, unlike natural Treg cells, any B cell might potentially differentiate into a “Breg” cell in response to the right environmental stimuli.

Can Breg Cells Arise at Every Stage of B cell Development?

A recent publication demonstrating that, in addition to previously described Breg cell subsets, plasmablasts can also suppress inflammatory responses supports the proposal that any B cell has the potential to differentiate into a Breg cell; mice whose B cells are deficient in *Irf4* and *Prdm1*, genes necessary for plasma cell differentiation, develop exacerbated EAE (Matsumoto et al., 2014). This is not the first time that antibody-producing B cells have been attributed with regulatory function: CD138⁺ plasma cells that produce IL-10 and IL-35 suppress pro-inflammatory responses during EAE and *Salmonella* infection (Shen et al., 2014). Furthermore, an earlier report suggested that splenic B10 cells have the propensity to differentiate into antibody-producing plasmablasts after stimulation in vivo and in vitro (Maseda et al., 2012). Matsumoto et al. also suggest a developmental link between CD19⁺CD24^{hi}CD38^{hi} B cells, previously

Table 1. Different Breg Cell Subsets

Type of Breg Cell	Mouse	Human	Key Features	Reference
T2-MZP cells	CD19 ⁺ CD21 ^{hi} CD23 ^{hi} CD24 ^{hi}	–	found in spleen, produce IL-10, induce Treg cells, and suppress effector CD4 ⁺ and CD8 ⁺ T cells	Blair et al., 2009; Carter et al., 2011; Evans et al., 2007; Schioppa et al., 2011
MZ cells	CD19 ⁺ CD21 ^{hi} CD23 [–]	–	found in spleen, produce IL-10, induce Treg cells, and suppress effector CD4 ⁺ and CD8 ⁺ T cells	Bankoti et al., 2012; Gray et al., 2007; Miles et al., 2012
B10 cells	CD5 ⁺ CD1d ^{hi}	CD24 ^{hi} CD27 ⁺	found in spleen (mice) and blood (humans), produce IL-10, and suppress effector CD4 ⁺ T cells, monocytes, and DCs	Horikawa et al., 2013; Iwata et al., 2011; Matsushita et al., 2010; Yanaba et al., 2008
Plasma cells	CD138 ⁺ MHC-11 ^{lo} B220 ⁺	–	found in spleen, produce IL-10 and IL-35, and suppress NK cells, neutrophils, and effector CD4 ⁺ T cells	Neves et al., 2010; Shen et al., 2014
Tim-1 ⁺ B cells	Tim-1 ⁺ CD19 ⁺	–	found in spleen (mice), produce IL-10, and suppress effector CD4 ⁺ T cells	Ding et al., 2011; Xiao et al., 2012
Plasmablasts	CD138 ⁺ CD44 ^{hi}	CD19 ⁺ CD24 ^{hi} CD27 ^{int}	found in dLNs (mice) and blood (humans), produce IL-10, and suppress DCs and effector CD4 ⁺ T cells	Matsumoto et al., 2014
Immature cells	–	CD19 ⁺ CD24 ^{hi} CD38 ^{hi}	found in blood and at site of inflammation, produce IL-10, induce Treg cells, suppress Th1 and Th17 cells, suppress virus-specific CD8 ⁺ T cell responses, are defective in patients with SLE and RA, and support iNKT cell homeostasis	Blair et al., 2010; Bosma et al., 2012; Das et al., 2012; Flores-Borja et al., 2013
Br1 cells	–	CD19 ⁺ CD25 ^{hi} CD71 ^{hi}	found in blood and produce IL-10 and IgG4	van de Veen et al., 2013

This table shows currently described subsets of Breg cells in mice and humans. Abbreviations are as follows: Br1, B regulatory 1; DC, dendritic cell; dLN, draining lymph node; IgG4, immunoglobulin G4; MHC, major histocompatibility complex; MZ, marginal zone; NK, natural killer; RA, rheumatoid arthritis; SLE, systemic lupus erythematosus; T2-MZP, transitional 2 marginal-zone precursor.

ascribed with a regulatory phenotype (Blair et al., 2010), and IL-10-producing plasmablasts in humans. This suggests that a similar fate—the development into plasma cells—exists for Breg cells in both mice and humans (Matsumoto et al., 2014). The idea that antibody-producing B cells are also regulators of immune responses is hard to reconcile with current knowledge that plasma cells drive inflammatory responses through the production of antibody, which is often pathogenic in the context of autoimmunity or allergy. Thus, it might be possible that a subset of plasmablasts maintain the ability to regulate inflammatory responses while producing antibody. This is supported by data showing that the lack of *Bcl6* has no effect on regulatory plasmablast generation (Matsumoto et al., 2014), which is known to be important for the expansion of class-switched cells through B cell proliferation in germinal centers (Dent et al., 1997), suggesting that regulatory plasmablasts are contained within an immunoglobulin-M-positive subset (Matsumoto et al., 2014).

Taking into account these latest studies, it has now been demonstrated that immature B cells, mature B cells, and plasmablasts all have the capacity to differentiate into IL-10-producing Breg cells in both mice and humans. This supports the concept that the primary requisite for Breg cell differentiation is not the expression of a Breg-cell-specific lineage factor but rather the environment in which a B cell finds itself. With this in mind, the identification of stimuli necessary to induce B cells to become regulatory is an important consideration in the assessment of the origin of Breg cells. Toll-like receptor (TLR)

and/or CD40 activation is the most well-characterized signal known to induce their differentiation (reviewed in Mauri and Bosma, 2012). However, a spate of recent publications has revealed that pro-inflammatory cytokines can also drive the induction of IL-10-producing Breg cells.

Is Inflammation the Primary Requisite for the Differentiation of Breg Cells?

There is strong evidence that the number and suppressive ability of Breg cells increase in response to inflammation. For example, although they are present in naive mice, Breg cells increase in number during the inflammatory phase of several autoimmune disorders (Evans et al., 2007; Mizoguchi et al., 2002). Moreover, it is known that Breg cells are functionally suppressive in the inflammatory phase of autoimmunity, given that in their absence, mice develop exacerbated arthritis or unremitting EAE (Carter et al., 2012; Carter et al., 2011; Fillatreau et al., 2002). This suggests that Breg cells are activated in response to the same inflammatory signals that drive autoimmune disease and thus limit damaging inflammation that would otherwise develop. Recently, it was demonstrated that Breg cells arise in response to IL-1 β and IL-6, pro-inflammatory cytokines that are produced after the induction of antigen-induced arthritis (Rosser et al., 2014b). The production of these cytokines in arthritic mice is controlled by the community of bacteria in the gut, collectively known as the microbiota, a pathway that has been previously shown to induce the differentiation of pro-arthritisogenic Th17

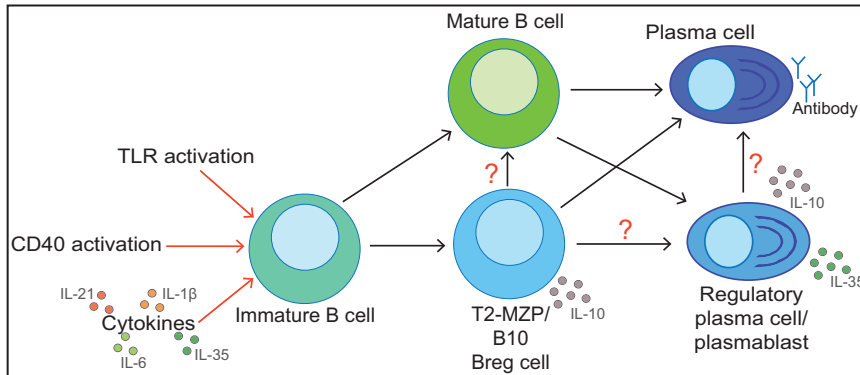


Figure 2. Proposed Developmental Pathways for Breg Cell Differentiation

After CD40 activation, TLR activation, or activation with cytokines, immature B cells can differentiate into B10 cells, IL-10-producing T2-MZP cells, and mature B cells. It is possible that while B10 and T2-MZP cells are differentiating into plasmablasts and/or plasma cells, they retain their ability to produce IL-10 and/or IL-35. B10 and T2-MZP cells can also differentiate into mature B cells. IL-10- and/or IL-35-producing plasmablasts and/or plasma cells can also develop directly from mature B cells. All Breg cell types can terminally differentiate into antibody-producing plasma cells.

cells (Wu et al., 2010). In the absence of IL-1R1 or IL-6R expression on B cells, mice housed in non-sterile conditions develop exacerbated arthritis (Rosser et al., 2014b). Thus, perhaps Breg cells are expanded in response to IL-1 β and IL-6 in order to keep the immune system in check, preventing the uncontrolled expansion of pro-inflammatory lymphocytes such as Th17 cells. Other inflammatory cytokines that are known to be critical for Th17 cell differentiation, such as IL-21 (Yoshizaki et al., 2012) and granulocyte macrophage colony-stimulating factor (GM-CSF, in combination with IL-15) (Rafei et al., 2009), have also been shown to be important in Breg cell differentiation. Importantly, different cellular sources of the cytokines that can induce IL-10 production by B cells have been identified. Myeloid-derived cells producing IL-6 (in the mesenteric lymph nodes) and both IL-6 and IL-1 β (in the spleen) are responsible for Breg cell induction in arthritis (Rosser et al., 2014b), whereas IL-21-producing CD4⁺ T cells located in the spleen are responsible for Breg cell induction in EAE (Yoshizaki et al., 2012). Conversely, it has been reported that treatment of mice with the anti-inflammatory cytokine IL-35 induces a population of IL-10- and IL-35-expressing B cells and thus suppresses the development of uveitis (Wang et al., 2014). This suggests that anti-inflammatory cytokines might also have a role in Breg cell differentiation. However, there is evidence suggesting that IL-35 is not constitutively expressed but is induced in response to inflammation (Li et al., 2012).

Although non-cognate inflammatory stimuli, e.g., IL-1 β , IL-6, and IL-21, are clearly important in the generation of Breg cells, it should not be forgotten that evidence suggests that B cell receptor (BCR) recognition is important in Breg cell induction. In MD4 mice, where the BCR is fixed for an irrelevant antigen, Breg cell activation is impaired; bone marrow chimeras that have MD4 B cells are unable to resolve EAE (Fillatreau et al., 2002), and MD4 mice produce less B-cell-derived IL-10 in response to TLR-9 activation (Miles et al., 2012) and have fewer B10 cells than do wild-type mice (Yanaba et al., 2009). Further evidence of the importance of BCR recognition in Breg cell function has been provided by experiments utilizing mice with a B-cell-specific deletion of stromal interaction molecule 1 (STIM-1) and STIM-2. STIM-1 and STIM-2 are important for mediating the influx of calcium into the B cell cytosol from outside the cell after antigen recognition of the BCR. Mice lacking STIM-1 and STIM-2 exclusively on B cells produce less IL-10 after stimulation with the auto-antigen MOG and anti-CD40 (Matsumoto et al.,

2011). Taken together, these data show that antigen-specific recognition by the BCR is important for Breg cell function and development, but it is still not clear whether Breg cells are reactive to the auto-antigens or putative endogenous ligands. Thus, in response to BCR recognition and inflammation, B cells might differentiate into both regulatory and antibody-producing cells.

The importance of inflammation in the differentiation of Breg cells calls into question the location of their maturation. To date, most studies have characterized splenic populations of B cells. However, other publications have reported that Breg cells are found in the lymph node draining the site of inflammation after the development of colitis (Mizoguchi et al., 2002) and EAE (Matsumoto et al., 2014). Importantly, the study in EAE by Matsumoto et al. (2014) demonstrates that Breg cells can develop and acquire their suppressive capabilities outside the spleen, in the draining lymph node, given that splenectomy has no effect on their generation. This supports the idea that the induction of Breg cells is dictated by inflammatory environment but is at odds with previously published data characterizing the spleen as the primary location for Breg cell development.

Breg Cells: What Next?

Although it cannot be ruled out that a transcriptional regulator that defines Breg cell function might be discovered in the future, at present there is no evidence to support this model. Thus, on the basis of the idea that Breg cells are not lineage specific but rather are expanded in response to inflammation, different models can be suggested for their development. These include the proposal that Breg cells are short-lived effector cells that are expanded in response to inflammation or, alternatively, that Breg cells are an inflammation-inducible subset that enters a further differentiation pathway after the resolution of an inflammatory response, such as the maturation of immature B cells into plasmablasts. There is evidence for both hypotheses, yet without the development of a fate reporter mouse that allows the identification of the historical expression of IL-10, it is currently not possible to be certain exactly what happens to a Breg cell after the cessation of an inflammatory response. Thus, at the moment, more questions have been raised than answered. For example, is the acquisition of regulatory function tissue dependent? Do certain stimuli direct B cells to traffic to the site of inflammation? Can we separate the stimuli necessary to induce the differentiation of antibody-producing and regulatory B cells? We believe that it is these questions that need to be

addressed before we can understand how to harness these cells therapeutically.

Concluding Remarks

Experimental evidence concerning the role of Breg cells in the suppression of inflammatory responses has been confused by the description of multiple Breg cell subsets. We propose that immunosuppression is not the purview of a devoted Breg cell lineage with a specific phenotype but rather is the outcome of the dynamic balance between multiple B cell subsets and other cells of the immune system. This hypothesis is supported by recent data underlining the importance of inflammatory cytokines in the induction of Breg cells, suggesting that Breg cells arise in response to inflammation, when immunosuppression is most needed. More recent publications suggest a developmental link between B cell subsets previously ascribed a regulatory phenotype and antibody-producing B cells, suggesting that although Breg cells might be inducible from multiple developmental stages, they might all share the capacity to become terminally differentiated plasma cells (Figure 2). In conclusion, although the Breg cell field has in the last year made many advances regarding the biological processes that control Breg cell differentiation, more resolution is needed before we can fully understand what happens during the life cycle of a Breg cell in vivo.

ACKNOWLEDGMENTS

This work was funded by a program grant (MP/17707 to C.M.) and PhD studentship (MP/19314 to C.M.) from Arthritis Research UK. We would like to thank Dr. Kiran Nistala and Dr. Paul Blair for their constructive criticism of the manuscript.

REFERENCES

- Bankoti, R., Gupta, K., Levchenko, A., and Stäger, S. (2012). Marginal zone B cells regulate antigen-specific T cell responses during infection. *J. Immunol.* *188*, 3961–3971.
- Blair, P.A., Chavez-Rueda, K.A., Evans, J.G., Shlomchik, M.J., Eddaoudi, A., Isenberg, D.A., Ehrenstein, M.R., and Mauri, C. (2009). Selective targeting of B cells with agonistic anti-CD40 is an efficacious strategy for the generation of induced regulatory T2-like B cells and for the suppression of lupus in MRL/lpr mice. *J. Immunol.* *182*, 3492–3502.
- Blair, P.A., Noreña, L.Y., Flores-Borja, F., Rawlings, D.J., Isenberg, D.A., Ehrenstein, M.R., and Mauri, C. (2010). CD19(+)CD24(hi)CD38(hi) B cells exhibit regulatory capacity in healthy individuals but are functionally impaired in systemic Lupus Erythematosus patients. *Immunity* *32*, 129–140.
- Bosma, A., Abdel-Gadir, A., Isenberg, D.A., Jury, E.C., and Mauri, C. (2012). Lipid-antigen presentation by CD1d(+) B cells is essential for the maintenance of invariant natural killer T cells. *Immunity* *36*, 477–490.
- Carter, N.A., Vasconcellos, R., Rosser, E.C., Tulone, C., Muñoz-Suano, A., Kamanaka, M., Ehrenstein, M.R., Flavell, R.A., and Mauri, C. (2011). Mice lacking endogenous IL-10-producing regulatory B cells develop exacerbated disease and present with an increased frequency of Th1/Th17 but a decrease in regulatory T cells. *J. Immunol.* *186*, 5569–5579.
- Carter, N.A., Rosser, E.C., and Mauri, C. (2012). Interleukin-10 produced by B cells is crucial for the suppression of Th17/Th1 responses, induction of T regulatory type 1 cells and reduction of collagen-induced arthritis. *Arthritis Res. Ther.* *14*, R32.
- Das, A., Ellis, G., Pallant, C., Lopes, A.R., Khanna, P., Peppas, D., Chen, A., Blair, P., Dusheiko, G., Gill, U., et al. (2012). IL-10-producing regulatory B cells in the pathogenesis of chronic hepatitis B virus infection. *J. Immunol.* *189*, 3925–3935.
- Dent, A.L., Shaffer, A.L., Yu, X., Allman, D., and Staudt, L.M. (1997). Control of inflammation, cytokine expression, and germinal center formation by BCL-6. *Science* *276*, 589–592.
- Ding, Q., Yeung, M., Camirand, G., Zeng, Q., Akiba, H., Yagita, H., Chalasani, G., Sayegh, M.H., Najafian, N., and Rothstein, D.M. (2011). Regulatory B cells are identified by expression of TIM-1 and can be induced through TIM-1 ligation to promote tolerance in mice. *J. Clin. Invest.* *121*, 3645–3656.
- Evans, J.G., Chavez-Rueda, K.A., Eddaoudi, A., Meyer-Bahlburg, A., Rawlings, D.J., Ehrenstein, M.R., and Mauri, C. (2007). Novel suppressive function of transitional 2 B cells in experimental arthritis. *J. Immunol.* *178*, 7868–7878.
- Fillatreau, S., Sweeney, C.H., McGeachy, M.J., Gray, D., and Anderton, S.M. (2002). B cells regulate autoimmunity by provision of IL-10. *Nat. Immunol.* *3*, 944–950.
- Flores-Borja, F., Bosma, A., Ng, D., Reddy, V., Ehrenstein, M.R., Isenberg, D.A., and Mauri, C. (2013). CD19+CD24hiCD38hi B cells maintain regulatory T cells while limiting TH1 and TH17 differentiation. *Sci. Transl. Med.* *5*, 73ra23.
- Gray, M., Miles, K., Salter, D., Gray, D., and Savill, J. (2007). Apoptotic cells protect mice from autoimmune inflammation by the induction of regulatory B cells. *Proc. Natl. Acad. Sci. USA* *104*, 14080–14085.
- Horikawa, M., Weimer, E.T., DiLillo, D.J., Venturi, G.M., Spolski, R., Leonard, W.J., Heise, M.T., and Tedder, T.F. (2013). Regulatory B cell (B10 Cell) expansion during *Listeria* infection governs innate and cellular immune responses in mice. *J. Immunol.* *190*, 1158–1168.
- Iwata, Y., Matsushita, T., Horikawa, M., DiLillo, D.J., Yanaba, K., Venturi, G.M., Szabolcs, P.M., Bernstein, S.H., Magro, C.M., Williams, A.D., et al. (2011). Characterization of a rare IL-10-competent B-cell subset in humans that parallels mouse regulatory B10 cells. *Blood* *117*, 530–541.
- Katz, S.I., Parker, D., and Turk, J.L. (1974). B-cell suppression of delayed hypersensitivity reactions. *Nature* *251*, 550–551.
- Li, X., Mai, J., Virtue, A., Yin, Y., Gong, R., Sha, X., Gutchigian, S., Frisch, A., Hodge, I., Jiang, X., et al. (2012). IL-35 is a novel responsive anti-inflammatory cytokine—a new system of categorizing anti-inflammatory cytokines. *PLoS ONE* *7*, e33628.
- Mann, M.K., Maresz, K., Shriver, L.P., Tan, Y., and Dittel, B.N. (2007). B cell regulation of CD4+CD25+ T regulatory cells and IL-10 via B7 is essential for recovery from experimental autoimmune encephalomyelitis. *J. Immunol.* *178*, 3447–3456.
- Maseda, D., Smith, S.H., DiLillo, D.J., Bryant, J.M., Candando, K.M., Weaver, C.T., and Tedder, T.F. (2012). Regulatory B10 cells differentiate into antibody-secreting cells after transient IL-10 production in vivo. *J. Immunol.* *188*, 1036–1048.
- Matsumoto, M., Fujii, Y., Baba, A., Hikida, M., Kurosaki, T., and Baba, Y. (2011). The calcium sensors STIM1 and STIM2 control B cell regulatory function through interleukin-10 production. *Immunity* *34*, 703–714.
- Matsumoto, M., Baba, A., Yokota, T., Nishikawa, H., Ohkawa, Y., Kayama, H., Kallies, A., Nutt, S.L., Sakaguchi, S., Takeda, K., et al. (2014). Interleukin-10-producing plasmablasts exert regulatory function in autoimmune inflammation. *Immunity* *41*, 1040–1051.
- Matsushita, T., Horikawa, M., Iwata, Y., and Tedder, T.F. (2010). Regulatory B cells (B10 cells) and regulatory T cells have independent roles in controlling experimental autoimmune encephalomyelitis initiation and late-phase immunopathogenesis. *J. Immunol.* *185*, 2240–2252.
- Mauri, C., and Bosma, A. (2012). Immune regulatory function of B cells. *Annu. Rev. Immunol.* *30*, 221–241.
- Mauri, C., Gray, D., Mushtaq, N., and Londei, M. (2003). Prevention of arthritis by interleukin 10-producing B cells. *J. Exp. Med.* *197*, 489–501.
- Medzhitov, R. (2008). Origin and physiological roles of inflammation. *Nature* *454*, 428–435.
- Miles, K., Heaney, J., Sibinska, Z., Salter, D., Savill, J., Gray, D., and Gray, M. (2012). A tolerogenic role for Toll-like receptor 9 is revealed by B-cell interaction with DNA complexes expressed on apoptotic cells. *Proc. Natl. Acad. Sci. USA* *109*, 887–892.
- Mizoguchi, A., Mizoguchi, E., Takedatsu, H., Blumberg, R.S., and Bhan, A.K. (2002). Chronic intestinal inflammatory condition generates IL-10-producing

- regulatory B cell subset characterized by CD1d upregulation. *Immunity* 16, 219–230.
- Nathan, C., and Ding, A. (2010). Nonresolving inflammation. *Cell* 140, 871–882.
- Neta, R., and Salvin, S.B. (1974). Specific suppression of delayed hypersensitivity: the possible presence of a suppressor B cell in the regulation of delayed hypersensitivity. *J. Immunol.* 113, 1716–1725.
- Neves, P., Lampropoulou, V., Calderon-Gomez, E., Roch, T., Stervbo, U., Shen, P., Kühl, A.A., Loddenkemper, C., Haury, M., Nedospasov, S.A., et al. (2010). Signaling via the MyD88 adaptor protein in B cells suppresses protective immunity during *Salmonella typhimurium* infection. *Immunity* 33, 777–790.
- Parekh, V.V., Prasad, D.V., Banerjee, P.P., Joshi, B.N., Kumar, A., and Mishra, G.C. (2003). B cells activated by lipopolysaccharide, but not by anti-Ig and anti-CD40 antibody, induce anergy in CD8+ T cells: role of TGF- β 1. *J. Immunol.* 170, 5897–5911.
- Rafei, M., Hsieh, J., Zehntner, S., Li, M., Forner, K., Birman, E., Boivin, M.N., Young, Y.K., Perreault, C., and Galipeau, J. (2009). A granulocyte-macrophage colony-stimulating factor and interleukin-15 fusokine induces a regulatory B cell population with immune suppressive properties. *Nat. Med.* 15, 1038–1045.
- Rosser, E.C., Blair, P.A., and Mauri, C. (2014a). Cellular targets of regulatory B cell-mediated suppression. *Mol. Immunol.* 62, 296–304.
- Rosser, E.C., Oleinika, K., Tonon, S., Doyle, R., Bosma, A., Carter, N.A., Harris, K.A., Jones, S.A., Klein, N., and Mauri, C. (2014b). Regulatory B cells are induced by gut microbiota-driven interleukin-1 β and interleukin-6 production. *Nat. Med.* 20, 1334–1339.
- Rudensky, A.Y. (2011). Regulatory T cells and Foxp3. *Immunol. Rev.* 241, 260–268.
- Schioppa, T., Moore, R., Thompson, R.G., Rosser, E.C., Kulbe, H., Nedospasov, S., Mauri, C., Coussens, L.M., and Balkwill, F.R. (2011). B regulatory cells and the tumor-promoting actions of TNF- α during squamous carcinogenesis. *Proc. Natl. Acad. Sci. USA* 108, 10662–10667.
- Shen, P., Roch, T., Lampropoulou, V., O'Connor, R.A., Stervbo, U., Hilgenberg, E., Ries, S., Dang, V.D., Jaimes, Y., Daridon, C., et al. (2014). IL-35-producing B cells are critical regulators of immunity during autoimmune and infectious diseases. *Nature* 507, 366–370.
- Sun, C.M., Deriaud, E., Leclerc, C., and Lo-Man, R. (2005). Upon TLR9 signaling, CD5+ B cells control the IL-12-dependent Th1-priming capacity of neonatal DCs. *Immunity* 22, 467–477.
- Sun, J.B., Flach, C.F., Czerkinsky, C., and Holmgren, J. (2008). B lymphocytes promote expansion of regulatory T cells in oral tolerance: powerful induction by antigen coupled to cholera toxin B subunit. *J. Immunol.* 181, 8278–8287.
- Tadmor, T., Zhang, Y., Cho, H.M., Podack, E.R., and Rosenblatt, J.D. (2011). The absence of B lymphocytes reduces the number and function of T-regulatory cells and enhances the anti-tumor response in a murine tumor model. *Cancer Immunol. Immunother.* 60, 609–619.
- Tian, J., Zekzer, D., Hanssen, L., Lu, Y., Olcott, A., and Kaufman, D.L. (2001). Lipopolysaccharide-activated B cells down-regulate Th1 immunity and prevent autoimmune diabetes in nonobese diabetic mice. *J. Immunol.* 167, 1081–1089.
- van de Veen, W., Stanic, B., Yaman, G., Wawrzyniak, M., Söllner, S., Akdis, D.G., Rückert, B., Akdis, C.A., and Akdis, M. (2013). IgG4 production is confined to human IL-10-producing regulatory B cells that suppress antigen-specific immune responses. *J. Allergy Clin. Immunol.* 131, 1204–1212.
- Wang, R.X., Yu, C.R., Dambuzza, I.M., Mahdi, R.M., Dolinska, M.B., Sergeev, Y.V., Wingfield, P.T., Kim, S.H., and Egwuagu, C.E. (2014). Interleukin-35 induces regulatory B cells that suppress autoimmune disease. *Nat. Med.* 20, 633–641.
- Wolf, S.D., Dittel, B.N., Hardardottir, F., and Janeway, C.A., Jr. (1996). Experimental autoimmune encephalomyelitis induction in genetically B cell-deficient mice. *J. Exp. Med.* 184, 2271–2278.
- Wu, H.J., Ivanov, I.I., Darce, J., Hattori, K., Shima, T., Umesaki, Y., Littman, D.R., Benoist, C., and Mathis, D. (2010). Gut-residing segmented filamentous bacteria drive autoimmune arthritis via T helper 17 cells. *Immunity* 32, 815–827.
- Xiao, S., Brooks, C.R., Zhu, C., Wu, C., Sweere, J.M., Petecka, S., Yeste, A., Quintana, F.J., Ichimura, T., Sobel, R.A., et al. (2012). Defect in regulatory B-cell function and development of systemic autoimmunity in T-cell Ig mucin 1 (Tim-1) mucin domain-mutant mice. *Proc. Natl. Acad. Sci. USA* 109, 12105–12110.
- Yanaba, K., Bouaziz, J.D., Haas, K.M., Poe, J.C., Fujimoto, M., and Tedder, T.F. (2008). A regulatory B cell subset with a unique CD1dhiCD5+ phenotype controls T cell-dependent inflammatory responses. *Immunity* 28, 639–650.
- Yanaba, K., Bouaziz, J.D., Matsushita, T., Tsubata, T., and Tedder, T.F. (2009). The development and function of regulatory B cells expressing IL-10 (B10 cells) requires antigen receptor diversity and TLR signals. *J. Immunol.* 182, 7459–7472.
- Yoshizaki, A., Miyagaki, T., DiLillo, D.J., Matsushita, T., Horikawa, M., Kountikov, E.I., Spolski, R., Poe, J.C., Leonard, W.J., and Tedder, T.F. (2012). Regulatory B cells control T-cell autoimmunity through IL-21-dependent cognate interactions. *Nature* 491, 264–268.



We don't compromise on quality.



We understand that respect is not a given, it's earned. Our standards are high, but you wouldn't have it any other way. That's why you choose to publish with us.

When you choose Cell Press you get the attention you deserve.

For more information visit: www.cell.com/values

Your **work** is our **life**



Mitochondria in the Regulation of Innate and Adaptive Immunity

Samuel E. Weinberg,¹ Laura A. Sena,¹ and Navdeep S. Chandel^{1,*}

¹Department of Medicine, Feinberg School of Medicine Northwestern University, Chicago, IL 60615, USA

*Correspondence: nav@northwestern.edu

<http://dx.doi.org/10.1016/j.immuni.2015.02.002>

Mitochondria are well appreciated for their role as biosynthetic and bioenergetic organelles. In the past two decades, mitochondria have emerged as signaling organelles that contribute critical decisions about cell proliferation, death, and differentiation. Mitochondria not only sustain immune cell phenotypes but also are necessary for establishing immune cell phenotype and their function. Mitochondria can rapidly switch from primarily being catabolic organelles generating ATP to anabolic organelles that generate both ATP and building blocks for macromolecule synthesis. This enables them to fulfill appropriate metabolic demands of different immune cells. Mitochondria have multiple mechanisms that allow them to activate signaling pathways in the cytosol including altering in AMP/ATP ratio, the release of ROS and TCA cycle metabolites, as well as the localization of immune regulatory proteins on the outer mitochondrial membrane. In this Review, we discuss the evidence and mechanisms that mitochondrial dependent signaling controls innate and adaptive immune responses.

Introduction

Over the last 30 years, the molecular events that drive immune responses have been characterized in great detail in numerous cell types. A successful immune response requires a delicate balance of activation and inhibition of distinct signaling pathways in diverse cell types. Classically, these signaling pathways are conceptualized as linear phosphorylation-based cascades initiated at the cell surface and transmitted to the nucleus. However, increasing data suggest that many of these signaling pathways are highly integrated with cellular metabolism, which not only fuels active cells but also provides guidance for cell-fate decisions. These studies have led to the creation of the new field of investigation termed immunometabolism.

For decades, we have observed that immune cells transform from a state of relative metabolic quiescence to a highly active metabolic state during the activation phase of an immune response. Predictably, this conversion requires a shift in cellular metabolism from a catabolic to an anabolic metabolic program (Pearce and Pearce, 2013). In a catabolic state, macromolecules are completely degraded and shuttled through energy-generating pathways to produce ATP to maintain cellular homeostasis and allow long-term survival during quiescence. Alternatively, in an anabolic state, cellular metabolism is reorganized to balance a need for ATP with the need for metabolic intermediates that are required for de novo synthesis of macromolecules. Yet our lab and others have observed that during both catabolism and anabolism, metabolic pathways provide more than just ATP and biosynthetic intermediates and importantly provide signaling intermediates that are essential for cellular function. An emerging concept is that metabolism not only sustains diverse immune cell phenotypes as a consequence of alterations in cellular signaling, but metabolism also feeds back and alters signaling to drive immune-cell phenotypes. Mitochondria are central hubs of metabolism that thus have emerged to be necessary for both the maintenance and establishment of immune cell

phenotypes. In this review, we will create a conceptual framework to establish mitochondria as signaling organelles that are critical for innate and adaptive immune responses.

Mitochondria are Bioenergetic, Biosynthetic, and Signaling Organelles

Historically, the major role of mitochondria is thought to be to the efficient coupling of metabolite oxidation through the tricarboxylic acid (TCA) cycle to ATP production by the electron transport chain (ETC). Fatty acids or pyruvate are oxidized into acetyl-CoA by fatty-acid oxidation or pyruvate dehydrogenase (PDH), respectively. Subsequently, the TCA cycle is initiated by the enzyme citrate synthase that catalyzes the condensation reaction of acetyl-CoA with oxaloacetate to generate citrate. The TCA cycle generates reducing equivalents NADH and FADH₂ that provide electrons to the electron transport chain. The ETC complexes ultimately transfer electrons to molecular oxygen and concomitantly pump protons across the inner mitochondrial membrane resulting in a generation of a proton-motive force that is utilized to produce ATP by the FoF₁ ATP synthase. Mitochondria that fail to generate a mitochondrial membrane potential are targeted for destruction through mitophagy. Mitochondrial oxidation of pyruvate and fatty acids such as palmitate generates 31.5 and 113 ATP, respectively, compared to 2 ATP generated by glycolysis (Mookerjee et al., 2015). Thus, mitochondria are the most efficient source of cellular ATP (Figure 1).

An equally important primordial function of mitochondria is the utilization of TCA cycle metabolites for the building of macromolecules (Figure 1). For example, citrate can be transported into the cytosol where ATP-citrate lyase (ACLY) converts citrate into acetyl-CoA and oxaloacetate. Cytosolic acetyl-CoA is utilized for protein acetylation, as well as de novo fatty-acid synthesis (Wellen and Thompson, 2012). Citrate depletion from the TCA cycle for de novo lipid synthesis necessitates replenishment of the TCA cycle (termed anaplerosis) to allow it to continue

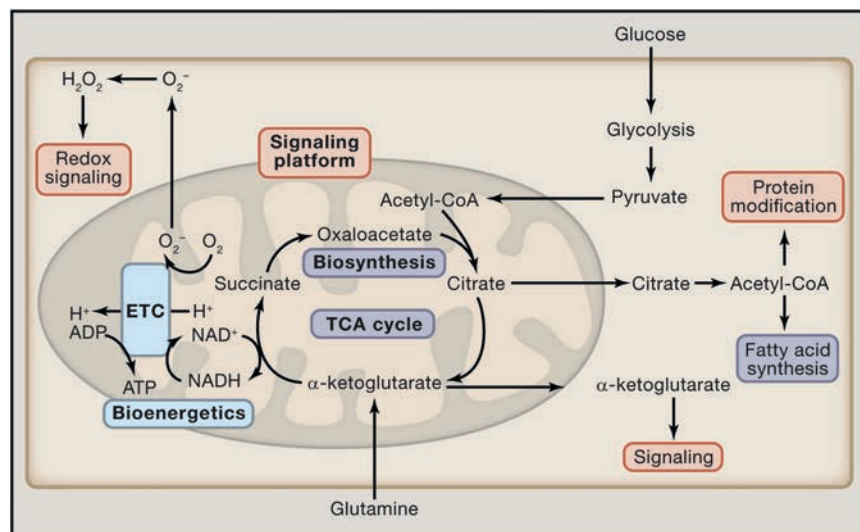


Figure 1. Mitochondria Are Essential Metabolic and Signaling Organelles

Cytosolic metabolic pathways funnel into the mitochondria where they constantly replenish the TCA cycle. Depending on the cellular metabolic state, TCA cycle intermediates can be further oxidized to generate ATP (blue) or they can be shuttled out of the mitochondria into subsidiary pathways to generate cellular building blocks such as fatty acids (purple). Finally, TCA cycle metabolites (orange) in addition to other byproducts of mitochondrial metabolism, such as ROS, function as important signaling molecules that control cellular functions.

availability of TCA cycle intermediates acetyl-CoA, succinate, fumarate, and α -ketoglutarate, which can alter protein function (Metallo and Vander Heiden, 2010). Acetyl-CoA is utilized for protein acetylation, α -ketoglutarate is required

for functioning. Glutamine replenishes the TCA cycle through glutaminolysis, which results in the generation of α -ketoglutarate (Hensley et al., 2013).

These two functions of mitochondria to generate ATP and to support biosynthesis must be carefully balanced to support specific cellular demands. Thus, mitochondria are metabolic hubs within the cell that alter their function to meet cellular needs. Clearly this necessitates that mitochondria receive signals to change their function. But importantly, more and more data suggest that mitochondrial pathways are not just reactive but also actively provide signals back to the nucleus. This crosstalk might coordinate cell-fate decisions with metabolic capacity dependent on the cellular environment. Thus we propose that mitochondria are crucial cellular signaling organelles that are an integral part of the decision-making process when cells receives internal and external cues to trigger diverse biological outcomes ranging from metabolic adaptation, proliferation, differentiation, and cell death (Chandel, 2014).

There are several known types of signal transduction mechanisms between mitochondria and the rest of the cell (Figure 1). First, anterograde signaling is signal transduction from cytosol to mitochondria. The best example of this is the rapid sequestration of calcium into the mitochondrial matrix in response to elevations in cytosolic calcium (Rizzuto et al., 2012). The influx of calcium into the mitochondria results in activation of multiple enzymes of the TCA cycle and the ETC. Second, retrograde signaling is signal transduction from mitochondria to the cytosol. One of the earliest examples of retrograde signaling was the production of mitochondrial reactive oxygen species (ROS) regulating the activation of the transcription factor hypoxia inducible factor 1 (HIF-1) (Chandel et al., 1998). Recent studies indicate that mitochondrial ROS regulate metabolic adaptation, differentiation, and proliferation (Sena and Chandel, 2012). The ETC can produce superoxide, notably from complexes I and III, that can be converted into hydrogen peroxide and released into the cytosol where it can cause thiol oxidation of proteins (Murphy, 2009). There are a total of ten potential sites of ROS generation within mitochondria (Quinlan et al., 2013). Mitochondria can also impact signaling by altering the

for function of α -ketoglutarate-dependent dioxygenases family of proteins, which include the prolyl hydroxylases (PHDs) and Jumonji domain-containing histone demethylase (JHDM), and fumarate and succinate are inhibitors of these proteins (Kaelin and McKnight, 2013). PHDs and JHDM are negative regulators of the HIFs and are also sensitive to hydrogen peroxide. As such, the accumulation of fumarate, succinate, and hydrogen peroxide can result in inactivation of PHDs and JHDMS resulting in activation of HIFs and hypermethylation of histones. Mitochondrial bioenergetic status can also influence signaling pathways. Notably, the decrease in mitochondrial ATP production typically increases AMP concentrations that cause a shift from an anabolic state to a catabolic state to sustain high ATP/ADP ratio necessary to thermodynamically favor ATP coupled reactions. The increase in AMP/ATP ratio triggers activation of AMP-activated protein kinase (AMPK) that decreases mammalian target of rapamycin (mTOR) activity to diminish anabolic reactions thus reducing ATP demand and activate autophagy to increase metabolic supply by providing nutrients to mitochondria for generation of ATP (Pearce et al., 2013). AMPK activation also promotes fatty-acid oxidation while suppressing fatty-acid synthesis. Lastly, the outer mitochondrial membrane is known to serve as a signaling platform to align multiple proteins to allow for coordinated interaction and subsequent signaling (West et al., 2011a).

Mitochondrial Signaling Dictates Macrophage Polarization and Function

Macrophages are commonly distinguished into two lineages, classically activated (M1) and alternatively activated (M2). M1 macrophages display marked production of inflammatory mediators following exposure to pro-inflammatory mediators such as LPS while M2 polarized macrophages display a pro-fibrotic and anti-inflammatory signature in response to the cytokine interleukin-4 (IL-4). Although this classification scheme is imperfect and there almost certainly exists many more macrophage subtypes, it is a useful model for studying how metabolism differs in macrophages with differing functions (Mosser and Edwards, 2008). M1 polarized macrophages exhibit robust glycolysis

even in the presence of ample oxygen and decreased oxygen consumption compared to unpolarized macrophages, suggesting minimal reliance on mitochondrial metabolism and a dependence on glycolytic ATP production compared with the M0 unpolarized macrophages (Haschemi et al., 2012; Huang et al., 2014). In contrast, M2 polarized macrophages demonstrate an increase in oxygen consumption. The importance of these difference in mitochondrial metabolism between M1 and M2 *in vivo* is supported by the finding that mice deficient in NDUFS4, a subunit of complex I of the ETC, exhibit an enhanced M1 polarization and diminished M2 polarization (Jin et al., 2014).

The induction of M2 polarization is driven by IL-4 stimulation of signal transducer and activator of transcription 6 (STAT6) resulting in PPAR γ -coactivator-1 β (PGC-1 β) induction of mitochondrial biogenesis and fatty-acid oxidation (Vats et al., 2006). The carnitine palmitoyltransferase-1 (CPT1) inhibitor etomoxir, which inhibits fatty-acid translocation into the mitochondria, is sufficient to inhibit expression of classic M2 genes indicating that the increase in mitochondrial metabolism is not simply an effect of STAT6 activation needed for sustaining the M2 phenotype, but is in fact a driver of M2 macrophage activation and function. Furthermore, the loss of the transcription factors of the peroxisome proliferator-activated receptor (PPAR) family, transcription factors known to activate oxidative metabolism in numerous tissues, leads to a deficit in M2 polarization (Kang et al., 2008; Odegaard et al., 2007, 2008). In contrast, overexpression of PGC-1 β promotes M2 polarization that could be reversed following pharmacologic blockade of fatty-acid oxidation or mitochondrial ATP production (Vats et al., 2006). These data are consistent with the observation that M2 macrophages require AMPK, a stimulator of fatty-acid oxidation, for proper activation *in vivo* (Mounier et al., 2013) (Carroll et al., 2013). Interestingly, the potential source of fatty acids required for M2 polarization is internal lysosomal stores. Thus, M2 macrophages require cell autonomous lysosomal-based lipolysis to increased internal fatty acids to fuel the enhanced mitochondrial metabolism (Huang et al., 2014). Going forward it will be important to specifically ablate fatty-acid oxidation or lysosomal-dependent lipolysis in macrophages to confirm *in vivo* significance lysosomal-dependent lipolysis and fatty-acid oxidation in establishing and maintaining the M2 phenotype.

A critical question that remains unanswered is what are the advantages of conducting enhanced glycolysis and mitochondrial metabolism in establishing the M1 and M2 phenotype, respectively? A clue might come from the observation that M1 macrophages require glucose-dependent metabolism for anabolic functions, whereas the role of mitochondria is restricted to signaling organelles in response to microorganism-derived pathogen-associated molecular patterns (PAMPs) and endogenous tissue injury-derived damage-associated molecular patterns (DAMPs).

Mitochondrial Signaling Is Necessary for Responses to Activators of Innate Immune Signaling

Pathogen-associated molecular patterns (PAMPs) and damage-associated molecular patterns (DAMPs) bind to specific receptors, including RIG-I-like receptors (RLRs), NOD-like receptors (NLRs), and Toll-like receptors (TLRs), to generate cytokines that are essential for eliminating pathogens or repairing tissue

damage. Interestingly, mitochondrial DNA and N-formyl peptides represent two sources of mitochondrial DAMPs that activate pattern-recognition receptors (PRRs). N-formyl-methionine is the initiating residue for both mitochondria and bacterial protein synthesis. Bacterial N-formyl peptides serve as PAMPs by activating G-protein-coupled formyl peptide receptors (FPRs) (Rabiet et al., 2007), and mitochondrial N-formyl peptides act as DAMPs through activation of the receptor FPR-1 to stimulate cytokine secretion (Carp, 1982; Zhang et al., 2010). Mitochondrial DNA is similar to bacterial DNA in that both share hypomethylated CpG motifs, which activate TLR9 (West et al., 2011a). Direct injection of mitochondrial (but not nuclear) DNA into mouse joints induces a pro-inflammatory response (Collins et al., 2004), and systemic injection of mitochondrial DNA induces lung and liver inflammation (Zhang et al., 2010). Mitochondrial DNA is also released systemically during trauma injury to induce inflammation (Zhang et al., 2010). Thus, mitochondrial DAMPs drive hyperactivation of innate immunity in an absence of an infection by a microorganisms *i.e.*, sterile inflammation. In the next section we review the evidence for mitochondria-dependent signaling in regulating responses to both DAMPs and PAMPs.

Initial studies implicating mitochondria as signaling organelles in innate immunity came from the observations that LPS through TLR4 and tumor necrosis factor- α (TNF- α) through TNF receptor associated factors (TRAFs) activate inflammatory cytokines through the generation of mitochondrial generated ROS (Chandel et al., 2000, 2001). More recent studies have shown that decreasing mitochondrial ROS diminishes multiple TLR-initiated pathways and bactericidal activity of macrophages (West et al., 2011b). TLR1, 2, and 4 activation results in mitochondrial translocation of TRAF6 that interacts with ECSIT, a protein that has been implicated in mitochondrial respiratory complex I assembly, leading to increased mitochondrial ROS that aid in the destruction of phagocytosed bacteria. It is not clear how ECSIT regulates mitochondrial ROS production upon TLR stimulation. Furthermore, patients with tumor necrosis factor receptor-associated periodic syndrome (TRAPS) have heightened responsiveness to LPS due to increased mitochondrial ROS production that promotes inflammation (Bulua et al., 2011).

Aside from ROS, the TCA cycle intermediate succinate has also been implicated in LPS-induced inflammatory cytokine signaling (Figure 2). In the TCA cycle, succinate is produced from succinyl-CoA and subsequently converted to fumarate by succinate dehydrogenase. Succinate dehydrogenase is the only TCA enzyme that also functions as an electron carrier in the electron transport chain, which might position it to also modulate ROS signaling (Mills and O'Neill, 2014). In LPS-activated macrophages, increases in succinate concentrations stabilize HIF-1 α through inhibition of PHDs (Tannahill et al., 2013), an effect that has previously been reported to occur in tumors (Selak et al., 2005). This stabilization of HIF-1 α induces the expression of the pro-inflammatory cytokine IL-1 β . In addition to directly activating HIF-1 through PHD inactivation, succinate might also increase mROS production, which is known to activate HIF-1 α in macrophages (Wang et al., 2010). Interestingly, a recent study demonstrated that succinate buildup results in increased reverse electron transport and ROS production from complex I of the ETC (Chouchani et al., 2014). Going forward,

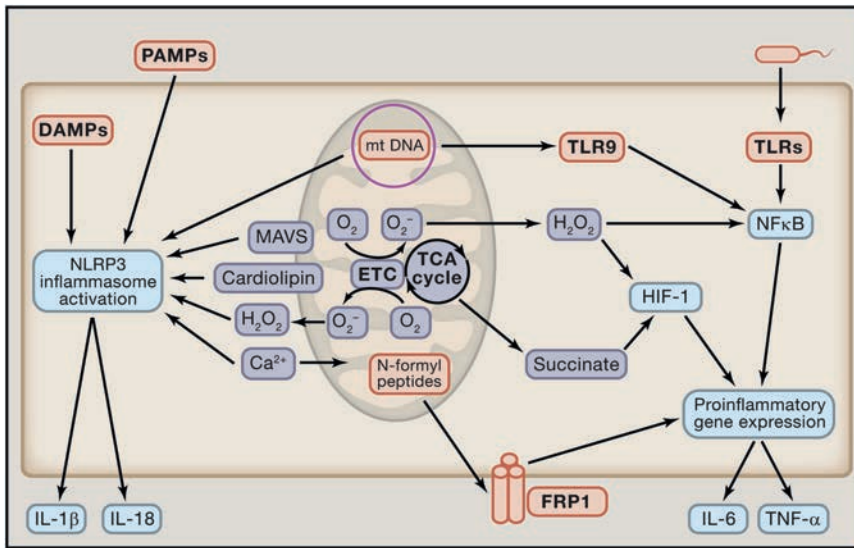


Figure 2. Mitochondria Are Critical to Activation of the Immune Response

Mitochondrial components such as mitochondrial DNA (mtDNA) and N-formyl peptides can act as damage-associated molecular patterns (DAMPs). Specifically, mtDNA can activate the NLRP3 inflammasome and TLR9 to induce an inflammatory response, while N-formyl peptides activate proinflammatory gene expression through the N-formyl peptide receptor-1 (FRP1). In addition to production and presentation of DAMPs, mitochondrial metabolism and signaling further promote the induction of inflammation to pathogens. Mitochondrial-derived metabolites such as mROS and succinate enhance pro-inflammatory gene expression, and mROS also can function directly as an anti-microbial effector molecule and NLRP3 activator. Additionally, mitochondrial localized proteins and lipids, MAVS, and cardiolipin respectively, are required for proper activation of the NLRP3 inflammasome. Finally, cellular calcium flux is linked to NLRP3 activation and mitochondrial function and signaling.

it will be important to decipher the mechanism by which LPS results in accumulation of succinate and whether succinate activation of IL-1 β expression requires mitochondrial ROS. Citrate is another TCA cycle intermediate implicated in LPS activation of pro-inflammatory gene expression. It is known that it is exported from the mitochondria to the cytosol and converted to acetyl-CoA; however, the precise mechanism by which it thereby alters cytokine production is unclear (Infantino et al., 2011).

In addition to TLRs, other PRRs are known to depend on mitochondrial ROS signaling including nuclear oligomerization domain (NOD)-like receptors (NLRs) (Figure 2). Upon activation, NLRs form multi-subunit protein complexes termed inflammasomes that activate caspase-1, resulting in proteolytic cleavage and maturation of the pro-inflammatory cytokine IL-1 β (Schroder and Tschopp, 2010). Diverse PAMPs and DAMPs such as lipopolysaccharide (LPS), asbestos, ATP, and uric acid lead to NLRP3 activation through increase in ROS (Cruz et al., 2007; Dostert et al., 2008). Specifically, pharmacological manipulations resulting in diminished mitochondrial ROS decrease NLRP3 inflammasome activation, but not other inflammasome subsets (Zhou et al., 2011). Furthermore, pharmacologic or genetic blockade of autophagy, which increases mitochondrial ROS concentrations, enhances inflammasome activation (Saitoh et al., 2008; Zhou et al., 2011). The release of mitochondrial ROS leads to lysosomal membrane permeabilization necessary for proper NLRP3 activation (Heid et al., 2013). A consequence of NLRP3 activation is the induction of mitochondrial damage with concomitant block in mitophagy to remove damaged mitochondria (Yu et al., 2014). Apart from mitochondrial ROS, release of mitochondrial DNA (mtDNA) into the cytosol was found to enhance NLRP3 activation (Nakahira et al., 2011). Later it was shown that oxidized mtDNA is actually required to activate NLRP3 (Shimada et al., 2012). This finding is provocative because it suggests that mtDNA is released from mitochondria without release of cytochrome c and induction of cell death. Further study of this observation is likely to reveal new mitochondrial transport mechanisms. Another recent finding linking mito-

chondria to NLRP3 is the observation that cardiolipin on the mitochondrial outer membrane directly binds to NLRP3 resulting in its activation (Iyer et al., 2013). Importantly, although many studies suggest an important role of mitochondrial ROS, cardiolipin, and DNA for in regulating NLRP3 activation, direct genetic evidence is still lacking in vivo.

It is important to note that mitochondrial ROS are necessary for optimal activation of NLRP3 inflammasome as other key activators such as influx of calcium and potassium efflux are also major regulators of NLRP3 inflammasome (Gurung et al., 2014). Calcium influx also contributes to mitochondrial damage which might increase mitochondrial ROS and release of mitochondrial DNA to amplify NLRP3 inflammasome activation (Murakami et al., 2012). The specific mechanisms by which diverse PAMPs and DAMPs increase mitochondrial ROS and by which mitochondrial ROS and ions such as calcium cooperate to optimally activate NLRP3 have yet to be delineated.

An emerging theme in the past decade is that the mitochondrial outer membrane serves as a signaling platform for innate immune responses. The most studied example of this is a class of PRRs that respond to viral infection known as the retinoic-acid-inducible protein I (RIG-I)-like receptor family (RLRs). The three members of RLRs are RIG-I, MDA5 and DHX58 that function in antiviral immunity by sensing viral 5'-triphosphorylated and uncapped single- or double-stranded RNA resulting in the production of type I interferons and pro-inflammatory cytokines (Reikine et al., 2014). A breakthrough in establishing the role for mitochondria in RLR-activated antiviral immunity was the identification of the RLR mitochondrial adaptor protein MAVS (mitochondrial antiviral-signaling protein) (Kawai et al., 2005; Meylan et al., 2005; Seth et al., 2005; Xu et al., 2005) localization to the outer mitochondrial membrane is indispensable for its function. MAVS contains a C-terminal transmembrane domain, which targets the protein to the outer membrane of mitochondria (Figure 3). Subsequent studies demonstrated that MAVS does not bind to free mitochondria but to mitochondrial associated membrane (MAM), which physically connects endoplasmic

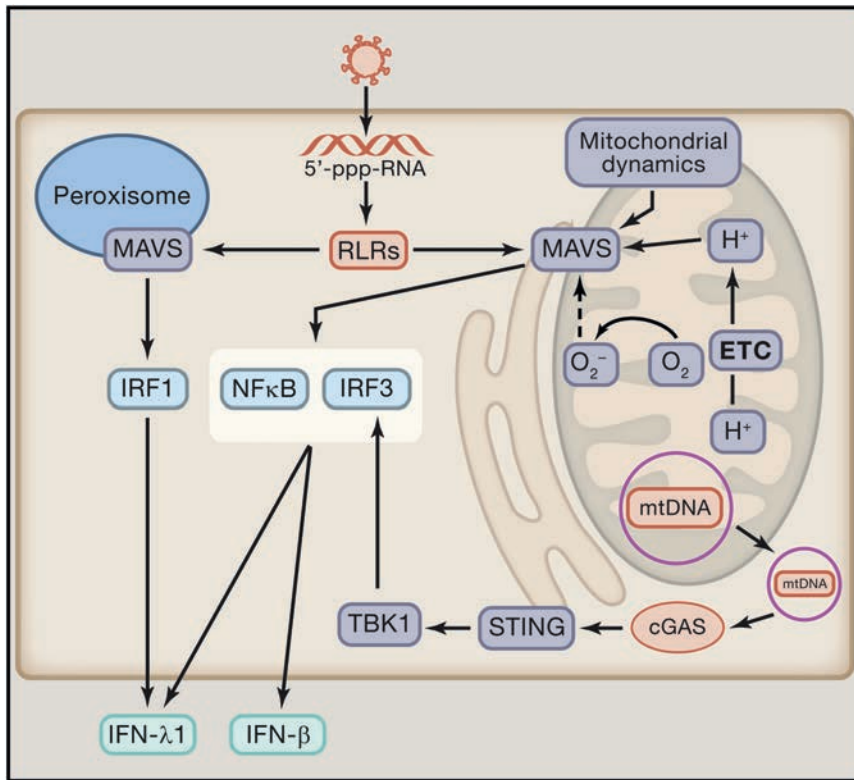


Figure 3. The Mitochondria Are Essential for the Proper Induction of Antiviral Signaling

The mitochondrial antiviral signaling protein (MAVS) is required for proper induction of RLR mediated activation of antiviral immunity. Importantly, mitochondrial dynamics, membrane potential, and ROS production are critical regulators of MAVS signaling. MAVS also localizes to the peroxisome, an organelle with a well described role in fatty-acid oxidation and H_2O_2 generation. Stimulation of peroxisomal MAVS signaling induces IFN- λ 1 production through IRF1 activation, while mitochondrial-localized MAVS drives IFN- β and IFN- λ 1 production. Along with MAVS, the mitochondrial also function as an activator of the stimulator of interferon genes protein (STING). Specifically, mtDNA translocated to the cytoplasm activates cyclic GMP-AMP synthase (cGAS), which triggers STING signaling, which further enhances antiviral immunity.

isomal enzyme required for ether lipid synthesis, results in neutropenia (Lodhi et al., 2015).

MAVS activation is also regulated by mitochondrial dynamics. Healthy mitochondria displaying robust mitochondrial membrane potential are in a fused network, whereas fission is indicative of damaged depolarized mitochondria. Multiple studies have demonstrated that

reticulum (ER) specialized domain to outer mitochondrial membrane (Horner et al., 2011). MAM provides a mitochondrial/ER inter-organelle communication that regulates stress and metabolic signaling (Hayashi et al., 2009). Mice deficient in MAVS are impaired in their ability to produce type I IFNs and thus are highly susceptible to RNA virus infection (Sun et al., 2006). RIG-I and MDA5 interact with MAVS through mutual caspase activation and recruitment domains (CARDs) upon recognition of viral RNA. Subsequently, RIG-I interaction with MAVS induces prion-like aggregates of MAVS on the outer mitochondrial membrane leads to activation of downstream pathways such as interferon regulatory factor 3 (IRF3), MAP kinases, and nuclear factor- κ B (NF- κ B) (Hou et al., 2011).

It is important to note that MAVS is also localized to the membranes of peroxisomes, which is necessary for the rapid early but transient expression of antiviral genes called interferon-stimulated genes (ISGs) (Dixit et al., 2010). Furthermore, mitochondrial MAVS induces both IFN- β and IFN- λ while peroxisomal MAVS induces IFN- λ in a interferon regulatory factor 1 (IRF1)-dependent manner (Odendall et al., 2014). Thus, maximal antiviral response requires the coordination of both mitochondrial and peroxisomal MAVS (Figure 3). Peroxisomes like mitochondria carry out oxidation of fatty acids and generate ROS (Lodhi and Semenkovich, 2014). Peroxisomes also exchange proteins with mitochondria (Camões et al., 2009). Given the shared roles in ROS and lipid metabolism between the two organelles, we speculate that MAVS recruitment to mitochondrial and peroxisomal membranes could be related to lipid and/or ROS metabolism. Indeed peroxisomal lipid synthesis can regulate immune cells as highlighted by the recent finding that loss of PexRAP, a perox-

mitochondrial fusion promotes, whereas mitochondrial fission inhibits RLR signaling (Castanier et al., 2010; Yasukawa et al., 2009; Zhao et al., 2012). Further strengthening this link, mitochondrial membrane potential alone is required for proper induction of antiviral signaling (Koshiba et al., 2011). It is unclear why mitochondrial dynamics dramatically influences antiviral signaling. Moreover, the central question as to why mitochondrial localization is necessary for MAVS to propagate RIG-I signaling remains unanswered. A speculative idea is that initiation of MAVS aggregation requires a lipid or protein component in the outer mitochondrial membrane. Alternatively, mitochondria might release protein, lipids, metabolites, or ROS necessary for optimal MAVS dependent antiviral signaling. Indeed, mitochondrial ROS have been shown to enhance MAVS mediated antiviral signaling (Tal et al., 2009; Zhao et al., 2012). Interestingly, MAVS is also necessary for NLRP3 activation (Subramanian et al., 2014). Future experiments will have to delineate the mechanisms by which outer mitochondrial membrane as a signaling platform controls innate immune responses.

The induction of type I IFNs can also be invoked by release of mitochondrial DNA. Two recent studies demonstrate that Bak- and Bax-mediated mitochondrial damage in the absence of activating the downstream apoptotic caspases triggers the release of mitochondrial DNA (mtDNA), which cyclic GMP-AMP synthase (cGAS)/STING-mediated cytosolic DNA sensing pathway (Rongvaux et al., 2014; White et al., 2014). DNA binding to cGAS catalyzes the production of cyclic GMP-AMP dinucleotide (cGAMP), which binds to and activates STING resulting in induction of type I IFN transcription via the Tbk1-Irf3 signaling axis (Barber, 2014). STING localizes to endoplasmic reticulum

(ER)-mitochondrial contact sites (Ishikawa and Barber, 2008; Zhong et al., 2008). It remains to be tested whether there are physiological and pathological conditions where mitochondrial DNA is released without mitochondrial damage to increase IFN- β expression. There is precedent that mitochondria can transport proteins and lipids through small vesicular carriers (Sugiura et al., 2014).

Aside from macrophages, other important antigen-presenting cells are dendritic cells (DCs). Upon exposure to antigen, DCs rapidly increased their phagocytic capacity while simultaneously elevating expression of major histocompatibility complex I (MHC I) and MHC II. This process, termed DC maturation, also promotes migration of DCs to the T cell zones of the secondary immune organs and is required for proper activation and control of an adaptive immune response (Joffre et al., 2009). The activation of this program using TLR stimulation results in a robust increase in glycolytic flux in dendritic cells (Everts et al., 2012; Krawczyk et al., 2010). This alteration in metabolism is required to meet the increased bioenergetic and biosynthetic demands of an activated DC, specifically by funneling metabolites into pathways for lipid and protein synthesis (Everts et al., 2014). Other studies have correlated increased intracellular lipid concentrations in DCs with enhanced antigen presentation and polarization of T cells toward inflammatory lineages, suggesting that the rate of de novo fatty-acid synthesis might regulate the immunogenicity of dendritic cells (Ibrahim et al., 2012). Emerging data has recently demonstrated that dendritic cells can be grouped into distinct subsets that display unique characteristics, similar to macrophages and T cells. As with macrophages, DCs likely exist in numerous different subsets however for simplicity that are classically designated as either an immunogenic or tolerant subset. Immunogenic DCs display high phagocytic activity and MHC expression after activation and are thought to drive inflammatory T cell responses (Everts et al., 2014). In contrast, tolerogenic DCs are characterized by a resistance to maturation along with the expression of immune-modulatory factors, which corresponds to an increased T regulatory cell (Treg) response (Pulendran et al., 2010). New data suggest that tolerogenic DCs display a high levels of fatty-acid oxidation and low levels of glycolysis reminiscent of the anti-inflammatory M2 macrophage (Cook et al., 2012; Ferreira et al., 2012; Szanto et al., 2010) DCs lacking PPAR- γ show increased immunogenicity while simultaneously failing to induce tolerogenic T cell responses (Klotz et al., 2007), further promoting a link between fatty-acid oxidation and a suppressive immune phenotype. Future studies need to further explore how metabolism differs in different subsets of DCs, and whether alterations in metabolism specifically in these cells is necessary to activate the transcriptional networks that establish these subsets.

Mitochondrial Signaling Controls Adaptive Immunity

T cells respond to antigens and therefore are central orchestrators of adaptive immune responses. During infection, naive T cells (T_n) challenged with an antigen rapidly proliferate into effector T cells (T_e). The majority of T_e cells undergo cell death with a few long-lived memory T cells (T_m) after the infection diminishes. T_m cells can be reactivated into rapidly expanding into T_e cells if a similar infection occurs to quickly curtail the infection. There also exist active immunosuppressive cells

termed regulatory T cells (Tregs) that suppress proliferation and function of effector T cells. These T cells subtypes have different metabolic demands and functions therefore exhibit diverse metabolic profiles. Aberrant T cell function results in a myriad of pathologies including auto-immune diseases.

Mitochondrial ROS Regulate T Cell Activation

Antigen stimulation of the T cell receptor (TCR) along with engagement of co-stimulatory molecules on naive T cells shifts them from a quiescent catabolic state in which nutrients are utilized to generate ATP required for cellular survival to a robust anabolic state where nutrients feed into metabolic pathways that generate macromolecules necessary for cell proliferation. Classical studies demonstrate that the anabolism of activated T cells is supported by large increases in glucose consumption that feed into multiple pathways. More recent studies indicate that glutamine is also an important fuel source, which supports mitochondrial metabolism through glutaminolysis (Carr et al., 2010; Sinclair et al., 2013). The transcription factor myc is necessary for this increased mitochondrial flux (Wang et al., 2011). Pharmacologic inhibition of mitochondrial oxidative phosphorylation or glycolysis in vitro diminishes T cell proliferation indicating that mitochondrial metabolism and glycolysis support T cell proliferation (Chang et al., 2013; Sena et al., 2013). However, glycolysis but not mitochondrial metabolism is dispensable for T cell activation and production of the cytokine IL-2 prior to proliferation (Sena et al., 2013) (Figure 4). In fact, mitochondrial metabolism was found to be required for T cell activation through generation of mitochondrial ROS necessary for optimal activity of NFAT, NF- κ B, and proximal TCR signaling (Gill and Levine, 2013; Kaminski et al., 2010; Kamiński et al., 2012; Sena et al., 2013). It is known that mitochondrial localization to the immune synapse is required for T cell activation (Contento et al., 2010; Martín-Cófreces et al., 2014; Quintana et al., 2007), likely for efficiency of both calcium and ROS signals. Future studies will more clearly define the mitochondrial ROS molecular target in T cell activation. The notion that mitochondrial metabolism is necessary for T cell activation is further supported by the observations that chronically activated T cells isolated from mouse model of lupus are dependent on mitochondrial metabolism and peripheral blood lymphocytes from patients with lupus have increased mitochondrial metabolism and ROS production (Gergely et al., 2002; Wahl et al., 2010).

Differential Metabolic Pathways Regulate CD4⁺ T Cell Differentiation

Once activated, T cells differentiate into different T_e subsets ranging from pro-inflammatory T helper 1 (Th1), Th17, and Th22 cells to suppressive regulatory T (Tregs) cells to curtail infection. Traditionally, these subsets have been classified by specific transcription factor activation. Emerging data indicate that these different T cell subsets have distinctive metabolic phenotypes that can promote T cell subset differentiation. Perhaps the best-studied subsets are Treg and Th17 cells, which have different metabolic profiles that are essential to establish their phenotype. Tregs have elevated levels of oxidative phosphorylation and decreased glycolytic flux compared to Th17 cells (Michalek et al., 2011).

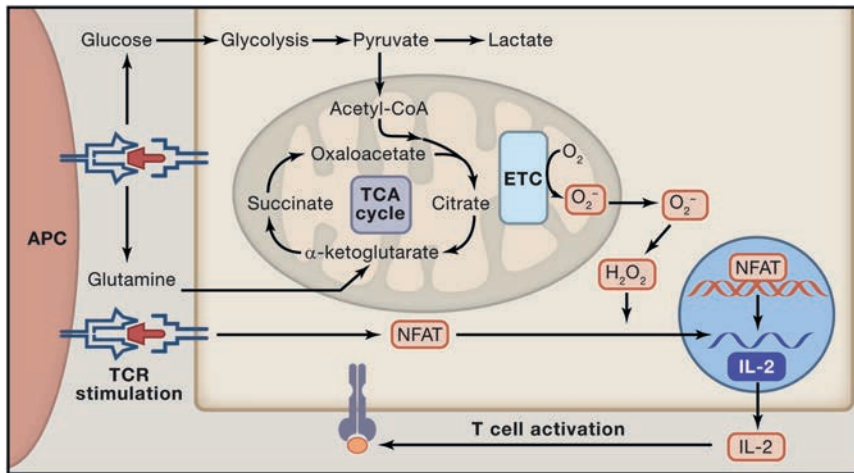


Figure 4. Mitochondrial Signaling Is Required for T Cell Activation

Upon binding of the TCR with MHC, numerous signaling cascades are activated. One of the activated pathways MYC activates an anabolic metabolic program that increases uptake of glucose and glutamine and allows for the cells to meet the increased metabolic demands of proliferation and induction of an adaptive immune response (blue). Importantly, in this model, metabolism works to sustain cellular activity required for a proper immune response. However, the mitochondria also alter cellular signaling upon ligation of the TCR. Specifically, mitochondrial ROS production following TCR stimulation is required for proper activation of NFAT and IL-2 production (orange). In this way, the mitochondrial signaling and metabolism are required for proper T cell activation.

This increased mitochondrial metabolism in Tregs was found to be due to increased AMPK-dependent fatty-acid oxidation (MacIver et al., 2011; Michalek et al., 2011). Pharmacologically attenuating fatty-acid oxidation by etomoxir impaired Treg differentiation, but did not affect other CD4 helper subsets *in vitro*. By contrast, Th17 cells engage in *de novo* fatty-acid synthesis that is necessary for the Th17 phenotype. Pharmacologic and genetic inhibition of the enzyme acetyl-CoA carboxylase 1 (ACC1), the enzyme that catalyzes the first step of *de novo* fatty-acid synthesis, impaired Th17 cell differentiation, and promoted Tregs *in vitro* and *in vivo*, as well as attenuated EAE in mice (Berod et al., 2014). It is presently not clear why fatty-acid oxidation versus synthesis appears to be a checkpoint in the T cell-fate decision between Treg and Th17 cells.

Increased glycolytic metabolism in Th17 cells also appears to be important to maintaining their Th17 lineage state. Pharmacological inhibition of glucose metabolism by administering 2-deoxyglucose attenuated Th17 cell development and interestingly promoted Treg cell development and diminished pathology in a Th17-dependent experimental autoimmune encephalomyelitis (EAE) (Shi et al., 2011). The increase in glycolysis observed in Th17 cells is due to an increase in HIF-1, and mice with T cells deficient in HIF-1 α display diminished Th17 cells, increased Treg cells, and resistance to EAE (Dang et al., 2011; Shi et al., 2011). Further evidence comes from the observation that the HIF-1 target PDHK1 is expressed in Th17 cells, but not in Treg cells, and diminishing PDHK1, the negative regulator of pyruvate dehydrogenase (PDH), suppressed Th17 formation and increased Treg formation *in vitro* (Gerriets et al., 2014). PDH is necessary for converting pyruvate to acetyl-CoA in mitochondrial matrix and increasing PDHK1 reduces PDH activity thus limiting mitochondrial acetyl-CoA availability. These data are supported *in vivo* by the observation that pharmacologic inhibition of PDHK by dichloroacetate (DCA) in mice diminishes Th17 and promotes Tregs resulting in inhibition of Th17 dependent colitis and EAE pathologies.

The mechanisms by which diminishing mitochondrial metabolism and/or enhancing glycolysis resulting in increased cells with concomitant decreased Treg cells is not fully understood. It is possible that the decrease in mitochondrial metabolism

concomitantly with an increase in glycolysis diminishes ROS through unknown mechanisms to promote Th17 differentiation. It is important to note that the ROS regulation of Th17/Treg axis has yet to be confirmed genetically. This is imperative because pharmacological inhibition of these pathways can affect multiple cell types, and conclusions drawn from these studies can be difficult to interpret. For example, unexpectedly fatty-acid oxidation inhibition by etomoxir reduces disease severity of EAE (Shriver and Manchester, 2011). On the basis of *in vitro* findings, fatty-acid oxidation inhibition is predicted to decrease Tregs cells, thus exacerbating EAE. Nevertheless, collectively these emerging metabolic studies suggest that mitochondrial metabolism function dictates the different inflammatory and suppressive CD4⁺ T helper lineages.

Mitochondrial Metabolism Regulates CD8⁺ Memory T Cell Formation

During the resolution phase of an infection, the majority of CD8⁺ T_e cells undergo cell death with the survival of a few long-lived CD8⁺ memory T cells (T_m). Re-infection with a pathogen containing similar antigens allows these T_m cells to be reactivated and rapidly expand into T cells to quickly control the infection. T_m cells are not rapidly proliferating and thus do not have high anabolic requirements. They efficiently catabolize nutrients to generate ATP to maintain long-term cell survival. Thus, T_m cells have a contrasting metabolic profile compared to T_e cells (Figure 5). T_m cells display increased mitochondrial number and spare respiratory capacity, which is fueled by fatty-acid oxidation to generate copious amount of ATP (Pearce et al., 2009; van der Windt et al., 2012). Fatty-acid oxidation generates almost three times more ATP than glucose oxidation by mitochondria. The source of fatty acids in T_m cells is not extracellular but rather internal lysosomal stores. T_m cells display reduced surface expression of CD36, necessary for fatty-acid uptake, compared with T_e cells and engage in *de novo* lipogenesis and store lipids in lysosomes (O'Sullivan et al., 2014). T_m cells utilize lysosomal acid lipase (LAL) in T_m cells to liberate free fatty acids from storage for the robust fatty-acid oxidation in the mitochondria. Thus, T_m cells appear to utilize a “futile cycle” whereby fatty-acid synthesis occurs concurrently with fatty-acid

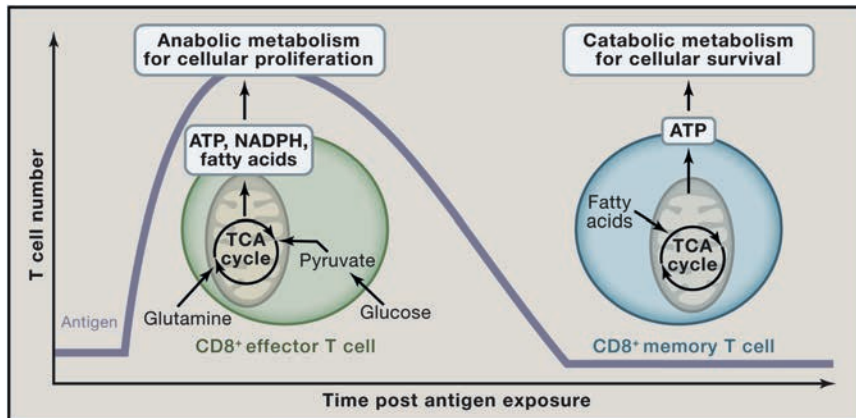


Figure 5. CD8⁺ Effector T Cells Display a Distinct Mitochondrial Metabolic Profile Compared to CD8⁺ Memory T Cells

Upon T cell activation, effector T cells rapidly increase uptake of glucose and glutamine, which is utilized to produce the ATP and cellular building blocks (NADPH and fatty acids) required for production of clonal T cells. The mitochondria in effector T cells functions as an anabolic hub where TCA cycle intermediates are shuttled into the cytoplasm to promote production of increase cellular biomass. In contrast, memory T cells utilize fatty-acid catabolism to efficiently generate ATP to fuel cellular survival.

oxidation, which is required for proper maintenance of memory T cells. The biochemical basis as to how and why T_m cells conduct concurrent fatty-acid synthesis and fatty-acid oxidation is not fully understood, because most cells utilize regulatory mechanisms that prevent this inefficiency. One possibility is that the availability of fatty acids from the extracellular environment *in vivo* might differ depending on the tissues where they reside; therefore, T_m cells continuously store lipids that can be utilized for fatty-acid oxidation. The importance of fatty-acid oxidation for T_m cells is bolstered by the observations that diminishing or enhancing AMPK, a positive regulator of fatty-acid oxidation, decreases or increases formation of memory T cells (MacIver et al., 2011; Pearce et al., 2009; Rolf et al., 2013; Tamás et al., 2010). Further evidence supporting the importance of mitochondrial metabolism comes from the observation that increasing or decreasing glycolytic flux, which reciprocally modulates mitochondrial metabolism, results in enhanced or diminished generation of memory T cells, respectively (Sukumar et al., 2013). Although there is mounting evidence that mitochondrial metabolism maintains the memory T cell phenotype, it remains unknown why this is and whether mitochondria participate in cell signaling necessary to establish the memory T cell phenotype.

Similar to T cells, B cells also undergo major transitions in their metabolic profiles as they transition from naive quiescent cells to anabolic proliferative cells. Upon activation, B cells greatly enhance glucose and glutamine metabolism during clonal expansion comparable to T cells (Doughty et al., 2006; Garcia-Manteiga et al., 2011; Le et al., 2012). Along with these changes in metabolism, B cell receptor (BCR) activation is regulated by ROS (Capasso et al., 2010; Singh et al., 2005). Specifically, BCR ligation stimulates calcium release into the cytoplasm that promotes ROS production and inactivation of receptor-coupled phosphates, allowing for activation of downstream signaling pathways. Depending on the magnitude of the ROS pulse, there is increased duration of BCR signaling and enhanced activation of downstream signaling pathways (Singh et al., 2005). Initially, the cytosolic NADPH oxidases were surmised to be source of ROS for B cell function. However, new data from primary B cells suggests that early ROS production by NADPH oxidases is dispensable for BCR signaling (Richards and Clark, 2009; Wheeler and DeFranco, 2012). Instead, long-

term elevations in ROS levels, potentially driven by increased production of mitochondrial ROS, are required for down-

stream BCR signaling and cellular proliferation in response to BCR cross-linking (Wheeler and DeFranco, 2012). Along with ROS signaling, new studies also suggest that other mitochondrial-derived molecules have important roles in B cell activation and effector function. Recent studies have suggested that plasma cells produce increased levels of phospholipids when compared to naive B cells, and plasma cell differentiation is dependent on mitochondrial citrate conversion to acetyl-CoA and oxaloacetate in the cytoplasm (Dufort et al., 2014; Fagone et al., 2007). Although the evidence is incomplete, these new studies indicate that mitochondrial metabolism is altered during B cell activation and plasma cell development. Future studies will delineate whether mitochondria metabolism is essential in driving differential B cell function in a manner similar to T cells.

Concluding Remarks

The mammalian immune response is extremely complex, requiring the coordination of multiple organ systems and a large variety of cells within those organs. These immune cells are so effective because they are able to rapidly respond to the stress of infection through activation and often proliferation, differentiation, and finally cell death. Furthermore, during an immune response, immune cells must decide to participate as an effector cell promoting inflammation or a suppressor cell ensuring adequate control of the inflammation. Within the capacity of an effector cell, various cells acquire more specific abilities necessary to fighting specific types of infections be it viral, bacterial, or parasitic. Thus, a rapid change in cell fate is absolutely essential to immunity. Although decades of study have shown that direct signaling from the cell surface to the nucleus is critical to these cell-fate decisions, more recent work has shown that these signaling pathways often include detours that transmit through metabolic machinery to ensure cooperation of metabolism in the cell-fate decision (Pearce et al., 2013) It is becoming clear that cellular metabolism plays a highly active role in determining cellular destiny in the immune system—in other words, we are learning that the immune cell is what it eats.

In this review, we highlight the mitochondrion as a central hub of immune-cell regulation. We outline that in immune cells, mitochondria participate in signaling through ROS production, metabolite availability, and by physically acting as scaffolding for protein interaction. Mitochondrial signals appear to be

necessary for the immune cell to fulfill its specific role in the immune response in both innate and adaptive settings to a variety of intruders. Ironically, this organelle of bacterial origin has established itself as a major conductor of the defense of the organism from invaders such as bacteria.

The studies we have discussed open several avenues for future investigation. First, we are lacking important mechanistic detail regarding the role of mitochondria in immune cells. Some questions include: what are the critical mitochondrial ROS targets in immune cell activation? How do the peroxisomes, ER, and mitochondria communicate to optimally regulate immune responses? Does availability of TCA cycle intermediates like acetyl-CoA, alpha-ketoglutarate, and citrate alter immune cell activation similar to succinate? If so, how? Second, several of the mechanisms discussed in this review are lacking in vivo evidence. Future study should use genetics and targeted small molecules to show that mitochondria are indeed important in the setting of a complex organismal immune response.

Lastly, the essential question remains whether targeting mitochondrial metabolism in humans will allow for modulation of the immune response in disease. We are very interested in determining the specific metabolic fuels and enzymes that sustain mitochondrial function in the immune response, as identification of these major crutches of mitochondrial function within immune cells might allow for development of small molecules for immune therapy. For example, the anti-diabetic drug metformin is being utilized an immunomodulator for tuberculosis (Singhal et al., 2014). It is not clear what the target of metformin in immune cells is but the anti-tumor effects of metformin are through inhibiting mitochondrial complex I (Wheaton et al., 2014). Moreover, Bz-423, a small-molecule inhibitor of the mitochondrial ATP-synthase, arrested established graft versus host disease (GVHD) in several bone marrow transplant models without affecting hematopoietic engraftment or lymphocyte reconstitution (Gatza et al., 2011). Beyond pharmaceuticals, modulation of total calorie availability, as well as type of calorie availability and subsequent support of specific cellular metabolic pathways, may also prove to be a useful method of immune modulation.

ACKNOWLEDGMENTS

This work is supported by R01CA123067, RO1HL12206201, and 5P01HL071643 to N.S.C. and T32HL076139 to S.E.W.

REFERENCES

- Barber, G.N. (2014). STING-dependent cytosolic DNA sensing pathways. *Trends Immunol.* *35*, 88–93.
- Berod, L., Friedrich, C., Nandan, A., Freitag, J., Hagemann, S., Harmrolfs, K., Sandouk, A., Hesse, C., Castro, C.N., Bähre, H., et al. (2014). De novo fatty acid synthesis controls the fate between regulatory T and T helper 17 cells. *Nat. Med.* *20*, 1327–1333.
- Bulua, A.C., Simon, A., Maddipati, R., Pelletier, M., Park, H., Kim, K.-Y., Sack, M.N., Kastner, D.L., and Siegel, R.M. (2011). Mitochondrial reactive oxygen species promote production of proinflammatory cytokines and are elevated in TNFR1-associated periodic syndrome (TRAPS). *J. Exp. Med.* *208*, 519–533.
- Camões, F., Bonekamp, N.A., Delille, H.K., and Schrader, M. (2009). Organelle dynamics and dysfunction: A closer link between peroxisomes and mitochondria. *J. Inher. Metab. Dis.* *32*, 163–180.
- Capasso, M., Bhamrah, M.K., Henley, T., Boyd, R.S., Langlais, C., Cain, K., Dinsdale, D., Pulford, K., Khan, M., Musset, B., et al. (2010). HVCN1 modulates BCR signal strength via regulation of BCR-dependent generation of reactive oxygen species. *Nat. Immunol.* *11*, 265–272.
- Carp, H. (1982). Mitochondrial N-formylmethionyl proteins as chemoattractants for neutrophils. *J. Exp. Med.* *155*, 264–275.
- Carr, E.L., Kelman, A., Wu, G.S., Gopaul, R., Senkevitch, E., Aghvanyan, A., Turay, A.M., and Frauwirth, K.A. (2010). Glutamine uptake and metabolism are coordinately regulated by ERK/MAPK during T lymphocyte activation. *J. Immunol.* *185*, 1037–1044.
- Carroll, K.C., Violette, B., and Suttles, J. (2013). AMPK α 1 deficiency amplifies proinflammatory myeloid APC activity and CD40 signaling. *J. Leukoc. Biol.* *94*, 1113–1121.
- Castanier, C., Garcin, D., Vazquez, A., and Arnoult, D. (2010). Mitochondrial dynamics regulate the RIG-I-like receptor antiviral pathway. *EMBO Rep.* *11*, 133–138.
- Chandel, N.S. (2014). Mitochondria as signaling organelles. *BMC Biol.* *12*, 34.
- Chandel, N.S., Maltepe, E., Goldwasser, E., Mathieu, C.E., Simon, M.C., and Schumacker, P.T. (1998). Mitochondrial reactive oxygen species trigger hypoxia-induced transcription. *Proc. Natl. Acad. Sci. USA* *95*, 11715–11720.
- Chandel, N.S., Trzyna, W.C., McClintock, D.S., and Schumacker, P.T. (2000). Role of oxidants in NF- κ B activation and TNF- α gene transcription induced by hypoxia and endotoxin. *J. Immunol.* *165*, 1013–1021.
- Chandel, N.S., Schumacker, P.T., and Arch, R.H. (2001). Reactive oxygen species are downstream products of TRAF-mediated signal transduction. *J. Biol. Chem.* *276*, 42728–42736.
- Chang, C.-H., Curtis, J.D., Maggi, L.B., Jr., Faubert, B., Villarino, A.V., O'Sullivan, D., Huang, S.C.-C., van der Windt, G.J.W., Blagih, J., Qiu, J., et al. (2013). Posttranscriptional control of T cell effector function by aerobic glycolysis. *Cell* *153*, 1239–1251.
- Chouchani, E.T., Pell, V.R., Gaude, E., Aksentijević, D., Sundier, S.Y., Robb, E.L., Logan, A., Nadtochiy, S.M., Ord, E.N.J., Smith, A.C., et al. (2014). Ischaemic accumulation of succinate controls reperfusion injury through mitochondrial ROS. *Nature* *515*, 431–435.
- Collins, L.V., Hajizadeh, S., Holme, E., Jonsson, I.-M., and Tarkowski, A. (2004). Endogenously oxidized mitochondrial DNA induces in vivo and in vitro inflammatory responses. *J. Leukoc. Biol.* *75*, 995–1000.
- Contento, R.L., Campello, S., Trovato, A.E., Magrini, E., Anselmi, F., and Viola, A. (2010). Adhesion shapes T cells for prompt and sustained T-cell receptor signalling. *EMBO J.* *29*, 4035–4047.
- Cook, P.C., Jones, L.H., Jenkins, S.J., Wynn, T.A., Allen, J.E., and MacDonald, A.S. (2012). Alternatively activated dendritic cells regulate CD4⁺ T-cell polarization in vitro and in vivo. *Proc. Natl. Acad. Sci. USA* *109*, 9977–9982.
- Cruz, C.M., Rinna, A., Forman, H.J., Ventura, A.L.M., Persechini, P.M., and Ojcius, D.M. (2007). ATP activates a reactive oxygen species-dependent oxidative stress response and secretion of proinflammatory cytokines in macrophages. *J. Biol. Chem.* *282*, 2871–2879.
- Dang, E.V., Barbi, J., Yang, H.Y., Jinasena, D., Yu, H., Zheng, Y., Bordman, Z., Fu, J., Kim, Y., Yen, H.R., et al. (2011). Control of T(H)17/T(reg) balance by hypoxia-inducible factor 1. *Cell* *146*, 772–784.
- Dixit, E., Boulant, S., Zhang, Y., Lee, A.S.Y., Odendall, C., Shum, B., Hacohen, N., Chen, Z.J., Whelan, S.P., Fransen, M., et al. (2010). Peroxisomes are signaling platforms for antiviral innate immunity. *Cell* *141*, 668–681.
- Dostert, C., Pétrilli, V., Van Bruggen, R., Steele, C., Mossman, B.T., and Tschopp, J. (2008). Innate immune activation through Nalp3 inflammasome sensing of asbestos and silica. *Science* *320*, 674–677.
- Doughty, C.A., Bleiman, B.F., Wagner, D.J., Dufort, F.J., Mataraza, J.M., Roberts, M.F., and Chiles, T.C. (2006). Antigen receptor-mediated changes in glucose metabolism in B lymphocytes: role of phosphatidylinositol 3-kinase signaling in the glycolytic control of growth. *Blood* *107*, 4458–4465.
- Dufort, F.J., Gumina, M.R., Ta, N.L., Tao, Y., Heyse, S.A., Scott, D.A., Richardson, A.D., Seyfried, T.N., and Chiles, T.C. (2014). Glucose-dependent de novo lipogenesis in B lymphocytes: a requirement for atp-citrate lyase in lipopolysaccharide-induced differentiation. *J. Biol. Chem.* *289*, 7011–7024.

- Everts, B., Amiel, E., van der Windt, G.J.W., Freitas, T.C., Chott, R., Yarasheski, K.E., Pearce, E.L., and Pearce, E.J. (2012). Commitment to glycolysis sustains survival of NO-producing inflammatory dendritic cells. *Blood* **120**, 1422–1431.
- Everts, B., Amiel, E., Huang, S.C.-C., Smith, A.M., Chang, C.-H., Lam, W.Y., Redmann, V., Freitas, T.C., Blagih, J., van der Windt, G.J.W., et al. (2014). TLR-driven early glycolytic reprogramming via the kinases TBK1-IKK ϵ supports the anabolic demands of dendritic cell activation. *Nat. Immunol.* **15**, 323–332.
- Fagone, P., Sriburi, R., Ward-Chapman, C., Frank, M., Wang, J., Gunter, C., Brewer, J.W., and Jackowski, S. (2007). Phospholipid biosynthesis program underlying membrane expansion during B-lymphocyte differentiation. *J. Biol. Chem.* **282**, 7591–7605.
- Ferreira, G.B., Kleijwegt, F.S., Waelkens, E., Lage, K., Nikolic, T., Hansen, D.A., Workman, C.T., Roep, B.O., Overbergh, L., and Mathieu, C. (2012). Differential protein pathways in 1,25-dihydroxyvitamin d(3) and dexamethasone modulated tolerogenic human dendritic cells. *J. Proteome Res.* **11**, 941–971.
- Garcia-Manteiga, J.M., Mari, S., Godejohann, M., Spraul, M., Napoli, C., Cenci, S., Musco, G., and Sitia, R. (2011). Metabolomics of B to plasma cell differentiation. *J. Proteome Res.* **10**, 4165–4176.
- Gatza, E., Wahl, D.R., Opipari, A.W., Sundberg, T.B., Reddy, P., Liu, C., Glick, G.D., and Ferrara, J.L.M. (2011). Manipulating the bioenergetics of alloreactive T cells causes their selective apoptosis and arrests graft-versus-host disease. *Sci. Transl. Med.* **3**, 67ra8.
- Gergely, P., Jr., Niland, B., Gonchoroff, N., Pullmann, R., Jr., Phillips, P.E., and Perl, A. (2002). Persistent mitochondrial hyperpolarization, increased reactive oxygen intermediate production, and cytoplasmic alkalization characterize altered IL-10 signaling in patients with systemic lupus erythematosus. *J. Immunol.* **169**, 1092–1101.
- Gerriets, V.A., Kishton, R.J., Nichols, A.G., Macintyre, A.N., Inoue, M., Ilkayeva, O., Winter, P.S., Liu, X., Priyadharshini, B., Slawinska, M.E., et al. (2014). Metabolic programming and PDHK1 control CD4+ T cell subsets and inflammation. *J. Clin. Invest.* **125**, 194–207.
- Gill, T., and Levine, A.D. (2013). Mitochondria-derived hydrogen peroxide selectively enhances T cell receptor-initiated signal transduction. *J. Biol. Chem.* **288**, 26246–26255.
- Gurung, P., Lukens, J.R., and Kanneganti, T.-D. (2014). Mitochondria: diversity in the regulation of the NLRP3 inflammasome. *Trends Mol. Med.* Published online November 27, 2014. <http://dx.doi.org/10.1016/j.molmed.2014.11.008>.
- Haschemi, A., Kosma, P., Gille, L., Evans, C.R., Burant, C.F., Starkl, P., Knapp, B., Haas, R., Schmid, J.A., Janil, C., et al. (2012). The sedoheptulose kinase CARKL directs macrophage polarization through control of glucose metabolism. *Cell Metab.* **15**, 813–826.
- Hayashi, T., Rizzuto, R., Hajnoczky, G., and Su, T.-P. (2009). MAM: more than just a housekeeper. *Trends Cell Biol.* **19**, 81–88.
- Heid, M.E., Keyel, P.A., Kamga, C., Shiva, S., Watkins, S.C., and Salter, R.D. (2013). Mitochondrial reactive oxygen species induces NLRP3-dependent lysosomal damage and inflammasome activation. *J. Immunol.* **191**, 5230–5238.
- Hensley, C.T., Wasti, A.T., and DeBerardinis, R.J. (2013). Glutamine and cancer: cell biology, physiology, and clinical opportunities. *J. Clin. Invest.* **123**, 3678–3684.
- Horner, S.M., Liu, H.M., Park, H.S., Briley, J., and Gale, M., Jr. (2011). Mitochondrial-associated endoplasmic reticulum membranes (MAM) form innate immune synapses and are targeted by hepatitis C virus. *Proc. Natl. Acad. Sci. USA* **108**, 14590–14595.
- Hou, F., Sun, L., Zheng, H., Skaug, B., Jiang, Q.X., and Chen, Z.J. (2011). MAVS forms functional prion-like aggregates to activate and propagate antiviral innate immune response. *Cell* **146**, 448–461.
- Huang, S.C.-C., Everts, B., Ivanova, Y., O'Sullivan, D., Nascimento, M., Smith, A.M., Beatty, W., Love-Gregory, L., Lam, W.Y., O'Neill, C.M., et al. (2014). Cell-intrinsic lysosomal lipolysis is essential for alternative activation of macrophages. *Nat. Immunol.* Published online August 3, 2014. <http://dx.doi.org/10.1038/ni.2956>.
- Ibrahim, J., Nguyen, A.H., Rehman, A., Ochi, A., Jamal, M., Graffeo, C.S., Henning, J.R., Zambirinis, C.P., Fallon, N.C., Barilla, R., et al. (2012). Dendritic cell populations with different concentrations of lipid regulate tolerance and immunity in mouse and human liver. *Gastroenterology* **143**, 1061–1072.
- Infantino, V., Convertini, P., Cucci, L., Panaro, M.A., Di Noia, M.A., Calvello, R., Palmieri, F., and Iacobazzi, V. (2011). The mitochondrial citrate carrier: a new player in inflammation. *Biochem. J.* **438**, 433–436.
- Ishikawa, H., and Barber, G.N. (2008). STING is an endoplasmic reticulum adaptor that facilitates innate immune signalling. *Nature* **455**, 674–678.
- Iyer, S.S., He, Q., Janczy, J.R., Elliott, E.I., Zhong, Z., Olivier, A.K., Sadler, J.J., Knepper-Adrian, V., Han, R., Qiao, L., et al. (2013). Mitochondrial cardiolipin is required for Nlrp3 inflammasome activation. *Immunity* **39**, 311–323.
- Jin, Z., Wei, W., Yang, M., Du, Y., and Wan, Y. (2014). Mitochondrial complex I activity suppresses inflammation and enhances bone resorption by shifting macrophage-osteoclast polarization. *Cell Metab.* **20**, 483–498.
- Joffre, O., Nolte, M.A., Spörri, R., and Reis e Sousa, C. (2009). Inflammatory signals in dendritic cell activation and the induction of adaptive immunity. *Immunol. Rev.* **227**, 234–247.
- Kaelin, W.G., Jr., and McKnight, S.L. (2013). Influence of metabolism on epigenetics and disease. *Cell* **153**, 56–69.
- Kaminski, M.M., Sauer, S.W., Klemke, C.-D., Süß, D., Okun, J.G., Krammer, P.H., and Gülow, K. (2010). Mitochondrial reactive oxygen species control T cell activation by regulating IL-2 and IL-4 expression: mechanism of ciprofloxacin-mediated immunosuppression. *J. Immunol.* **184**, 4827–4841.
- Kamiński, M.M., Sauer, S.W., Kamiński, M., Opp, S., Ruppert, T., Grigaričius, P., Grudnik, P., Gröne, H.-J., Krammer, P.H., and Gülow, K. (2012). T cell activation is driven by an ADP-dependent glucokinase linking enhanced glycolysis with mitochondrial reactive oxygen species generation. *Cell Rep.* **2**, 1300–1315.
- Kang, K., Reilly, S.M., Karabacak, V., Gangl, M.R., Fitzgerald, K., Hatano, B., and Lee, C.-H. (2008). Adipocyte-derived Th2 cytokines and myeloid PPAR- δ regulate macrophage polarization and insulin sensitivity. *Cell Metab.* **7**, 485–495.
- Kawai, T., Takahashi, K., Sato, S., Coban, C., Kumar, H., Kato, H., Ishii, K.J., Takeuchi, O., and Akira, S. (2005). IPS-1, an adaptor triggering RIG-I- and Mda5-mediated type I interferon induction. *Nat. Immunol.* **6**, 981–988.
- Klotz, L., Dani, I., Edenhofer, F., Nolden, L., Evert, B., Paul, B., Kolanus, W., Klockgether, T., Knolle, P., and Diehl, L. (2007). Peroxisome proliferator-activated receptor gamma control of dendritic cell function contributes to development of CD4+ T cell anergy. *J. Immunol.* **178**, 2122–2131.
- Koshiba, T., Yasukawa, K., Yanagi, Y., and Kawabata, S. (2011). Mitochondrial membrane potential is required for MAVS-mediated antiviral signaling. *Sci. Signal.* **4**, ra7.
- Krawczyk, C.M., Holowka, T., Sun, J., Blagih, J., Amiel, E., DeBerardinis, R.J., Cross, J.R., Jung, E., Thompson, C.B., Jones, R.G., and Pearce, E.J. (2010). Toll-like receptor-induced changes in glycolytic metabolism regulate dendritic cell activation. *Blood* **115**, 4742–4749.
- Le, A., Lane, A.N., Hamaker, M., Bose, S., Gouw, A., Barbi, J., Tsukamoto, T., Rojas, C.J., Slusher, B.S., Zhang, H., et al. (2012). Glucose-independent glutamine metabolism via TCA cycling for proliferation and survival in B cells. *Cell Metab.* **15**, 110–121.
- Lodhi, I.J., and Semenkovich, C.F. (2014). Peroxisomes: a nexus for lipid metabolism and cellular signaling. *Cell Metab.* **19**, 380–392.
- Lodhi, I.J., Wei, X., Yin, L., Feng, C., Adak, S., Abou-Ezzi, G., Hsu, F.-F., Link, D.C., and Semenkovich, C.F. (2015). Peroxisomal lipid synthesis regulates inflammation by sustaining neutrophil membrane phospholipid composition and viability. *Cell Metab.* **21**, 51–64.
- Maclver, N.J., Blagih, J., Saucillo, D.C., Tonelli, L., Griss, T., Rathmell, J.C., and Jones, R.G. (2011). The liver kinase B1 is a central regulator of T cell development, activation, and metabolism. *J. Immunol.* **187**, 4187–4198.
- Martín-Cófreces, N.B., Baixauli, F., and Sánchez-Madrid, F. (2014). Immune synapse: conductor of orchestrated organelle movement. *Trends Cell Biol.* **24**, 61–72.
- Metallo, C.M., and Vander Heiden, M.G. (2010). Metabolism strikes back: metabolic flux regulates cell signaling. *Genes Dev.* **24**, 2717–2722.

- Meylan, E., Curran, J., Hofmann, K., Moradpour, D., Binder, M., Bartenschlager, R., and Tschopp, J. (2005). Cardif is an adaptor protein in the RIG-I antiviral pathway and is targeted by hepatitis C virus. *Nature* *437*, 1167–1172.
- Michalek, R.D., Gerriets, V.A., Jacobs, S.R., Macintyre, A.N., MacIver, N.J., Mason, E.F., Sullivan, S.A., Nichols, A.G., and Rathmell, J.C. (2011). Cutting edge: distinct glycolytic and lipid oxidative metabolic programs are essential for effector and regulatory CD4+ T cell subsets. *J. Immunol.* *186*, 3299–3303.
- Mills, E., and O'Neill, L.A.J. (2014). Succinate: a metabolic signal in inflammation. *Trends Cell Biol.* *24*, 313–320.
- Mookerjee, S.A., Goncalves, R.L.S., Gerencser, A.A., Nicholls, D.G., and Brand, M.D. (2015). The contributions of respiration and glycolysis to extracellular acid production. *Biochim. Biophys. Acta - Bioenerg.* *1847*, 171–181.
- Mosser, D.M., and Edwards, J.P. (2008). Exploring the full spectrum of macrophage activation. *Nat. Rev. Immunol.* *8*, 958–969.
- Mounier, R., Théret, M., Arnold, L., Cuvellier, S., Bultot, L., Göransson, O., Sanz, N., Ferry, A., Sakamoto, K., Foretz, M., et al. (2013). AMPK α 1 regulates macrophage skewing at the time of resolution of inflammation during skeletal muscle regeneration. *Cell Metab.* *18*, 251–264.
- Murakami, T., Ockinger, J., Yu, J., Byles, V., McColl, A., Hofer, A.M., and Horng, T. (2012). Critical role for calcium mobilization in activation of the NLRP3 inflammasome. *Proc. Natl. Acad. Sci. USA* *109*, 11282–11287.
- Murphy, M.P. (2009). How mitochondria produce reactive oxygen species. *Biochem. J.* *417*, 1–13.
- Nakahira, K., Haspel, J.A., Rathinam, V.A., Lee, S.J., Dolinay, T., Lam, H.C., Englert, J.A., Rabinovitch, M., Cernadas, M., Kim, H.P., et al. (2011). Autophagy proteins regulate innate immune responses by inhibiting the release of mitochondrial DNA mediated by the NALP3 inflammasome. *Nat. Immunol.* *12*, 222–230.
- O'Sullivan, D., van der Windt, G.J.W., Huang, S.C.-C., Curtis, J.D., Chang, C.-H., Buck, M.D., Qiu, J., Smith, A.M., Lam, W.Y., DiPlato, L.M., et al. (2014). Memory CD8(+) T cells use cell-intrinsic lipolysis to support the metabolic programming necessary for development. *Immunity* *41*, 75–88.
- Odegaard, J.I., Ricardo-Gonzalez, R.R., Goforth, M.H., Morel, C.R., Subramanian, V., Mukundan, L., Red Eagle, A., Vats, D., Brombacher, F., Ferrante, A.W., and Chawla, A. (2007). Macrophage-specific PPAR γ controls alternative activation and improves insulin resistance. *Nature* *447*, 1116–1120.
- Odegaard, J.I., Ricardo-Gonzalez, R.R., Red Eagle, A., Vats, D., Morel, C.R., Goforth, M.H., Subramanian, V., Mukundan, L., Ferrante, A.W., and Chawla, A. (2008). Alternative M2 activation of Kupffer cells by PPAR δ ameliorates obesity-induced insulin resistance. *Cell Metab.* *7*, 496–507.
- Odendall, C., Dixit, E., Stavru, F., Bierne, H., Franz, K.M., Durbin, A.F., Boulant, S., Gehrke, L., Cossart, P., and Kagan, J.C. (2014). Diverse intracellular pathogens activate type III interferon expression from peroxisomes. *Nat. Immunol.* *15*, 717–726.
- Pearce, E.L., and Pearce, E.J. (2013). Metabolic pathways in immune cell activation and quiescence. *Immunity* *38*, 633–643.
- Pearce, E.L., Walsh, M.C., Cejas, P.J., Harms, G.M., Shen, H., Wang, L.-S., Jones, R.G., and Choi, Y. (2009). Enhancing CD8 T-cell memory by modulating fatty acid metabolism. *Nature* *460*, 103–107.
- Pearce, E.L., Poffenberger, M.C., Chang, C.-H., and Jones, R.G. (2013). Fueling immunity: insights into metabolism and lymphocyte function. *Science* *342*, 1242454.
- Pulendran, B., Tang, H., and Manicassamy, S. (2010). Programming dendritic cells to induce T(H)2 and tolerogenic responses. *Nat. Immunol.* *11*, 647–655.
- Quinlan, C.L., Perevoshchikova, I.V., Hey-Mogensen, M., Orr, A.L., and Brand, M.D. (2013). Sites of reactive oxygen species generation by mitochondria oxidizing different substrates. *Redox Biol.* *1*, 304–312.
- Quintana, A., Schwindling, C., Wenning, A.S., Becherer, U., Rettig, J., Schwarz, E.C., and Hoth, M. (2007). T cell activation requires mitochondrial translocation to the immunological synapse. *Proc. Natl. Acad. Sci. USA* *104*, 14418–14423.
- Rabiet, M.-J., Huet, E., and Boulay, F. (2007). The N-formyl peptide receptors and the anaphylatoxin C5a receptors: an overview. *Biochimie* *89*, 1089–1106.
- Reikine, S., Nguyen, J.B., and Modis, Y. (2014). Pattern Recognition and Signaling Mechanisms of RIG-I and MDA5. *Front. Immunol.* *5*, 342.
- Richards, S.M., and Clark, E.A. (2009). BCR-induced superoxide negatively regulates B-cell proliferation and T-cell-independent type 2 Ab responses. *Eur. J. Immunol.* *39*, 3395–3403.
- Rizzuto, R., De Stefani, D., Raffaello, A., and Mammucari, C. (2012). Mitochondria as sensors and regulators of calcium signalling. *Nat. Rev. Mol. Cell Biol.* *13*, 566–578.
- Rolf, J., Zarrouk, M., Finlay, D.K., Foretz, M., Viollet, B., and Cantrell, D.A. (2013). AMPK α 1: a glucose sensor that controls CD8 T-cell memory. *Eur. J. Immunol.* *43*, 889–896.
- Rongvaux, A., Jackson, R., Harman, C.C.D., Li, T., West, A.P., de Zoete, M.R., Wu, Y., Yordy, B., Lakhani, S.A., Kuan, C.-Y., et al. (2014). Apoptotic caspases prevent the induction of type I interferons by mitochondrial DNA. *Cell* *159*, 1563–1577.
- Saitoh, T., Fujita, N., Jang, M.H., Uematsu, S., Yang, B.-G., Satoh, T., Omori, H., Noda, T., Yamamoto, N., Komatsu, M., et al. (2008). Loss of the autophagy protein Atg16L1 enhances endotoxin-induced IL-1 β production. *Nature* *456*, 264–268.
- Schroder, K., and Tschopp, J. (2010). The inflammasomes. *Cell* *140*, 821–832.
- Selak, M.A., Armour, S.M., MacKenzie, E.D., Boulahbel, H., Watson, D.G., Mansfield, K.D., Pan, Y., Simon, M.C., Thompson, C.B., and Gottlieb, E. (2005). Succinate links TCA cycle dysfunction to oncogenesis by inhibiting HIF- α prolyl hydroxylase. *Cancer Cell* *7*, 77–85.
- Sena, L.A., and Chandel, N.S. (2012). Physiological roles of mitochondrial reactive oxygen species. *Mol. Cell* *48*, 158–167.
- Sena, L.A., Li, S., Jairaman, A., Prakriya, M., Ezponda, T., Hildeman, D.A., Wang, C.-R., Schumacker, P.T., Licht, J.D., Perlman, H., et al. (2013). Mitochondria are required for antigen-specific T cell activation through reactive oxygen species signaling. *Immunity* *38*, 225–236.
- Seth, R.B., Sun, L., Ea, C.-K., and Chen, Z.J. (2005). Identification and characterization of MAVS, a mitochondrial antiviral signaling protein that activates NF- κ B and IRF 3. *Cell* *122*, 669–682.
- Shi, L.Z., Wang, R., Huang, G., Vogel, P., Neale, G., Green, D.R., and Chi, H. (2011). HIF1 α -dependent glycolytic pathway orchestrates a metabolic checkpoint for the differentiation of TH17 and Treg cells. *J. Exp. Med.* *208*, 1367–1376.
- Shimada, K., Crother, T.R., Karlin, J., Dagvadorj, J., Chiba, N., Chen, S., Ramanujan, V.K., Wolf, A.J., Vergnes, L., Ojcius, D.M., et al. (2012). Oxidized mitochondrial DNA activates the NLRP3 inflammasome during apoptosis. *Immunity* *36*, 401–414.
- Shriver, L.P., and Manchester, M. (2011). Inhibition of fatty acid metabolism ameliorates disease activity in an animal model of multiple sclerosis. *Sci Rep* *1*, 79.
- Sinclair, L.V., Rolf, J., Emslie, E., Shi, Y.-B., Taylor, P.M., and Cantrell, D.A. (2013). Control of amino-acid transport by antigen receptors coordinates the metabolic reprogramming essential for T cell differentiation. *Nat. Immunol.* *14*, 500–508.
- Singh, D.K., Kumar, D., Siddiqui, Z., Basu, S.K., Kumar, V., and Rao, K.V.S. (2005). The strength of receptor signaling is centrally controlled through a cooperative loop between Ca²⁺ and an oxidant signal. *Cell* *121*, 281–293.
- Singhal, A., Jie, L., Kumar, P., Hong, G.S., Leow, M.K.-S., Paleja, B., Tsenova, L., Kurepina, N., Chen, J., Zolezzi, F., et al. (2014). Metformin as adjunct anti-tuberculosis therapy. *Sci. Transl. Med.* *6*, 263ra159–ra263ra159.
- Subramanian, N., Natarajan, K., Clatworthy, M., Wang, Z., and Germain, R. (2014). Mitochondria play a central role in NLRP3 inflammasome activation (349.1). *FASEB J* *28*, 349.
- Sugiura, A., McLelland, G.-L., Fon, E.A., and McBride, H.M. (2014). A new pathway for mitochondrial quality control: mitochondrial-derived vesicles. *EMBO J.* *33*, 2142–2156.
- Sukumar, M., Liu, J., Ji, Y., Subramanian, M., Crompton, J.G., Yu, Z., Roychoudhuri, R., Palmer, D.C., Muranski, P., Karoly, E.D., et al. (2013). Inhibiting glycolytic metabolism enhances CD8+ T cell memory and antitumor function. *J. Clin. Invest.* *123*, 4479–4488.

- Sun, Q., Sun, L., Liu, H.-H., Chen, X., Seth, R.B., Forman, J., and Chen, Z.J. (2006). The specific and essential role of MAVS in antiviral innate immune responses. *Immunity* *24*, 633–642.
- Szanto, A., Balint, B.L., Nagy, Z.S., Barta, E., Dezso, B., Pap, A., Szeles, L., Poliska, S., Oros, M., Evans, R.M., et al. (2010). STAT6 transcription factor is a facilitator of the nuclear receptor PPAR γ -regulated gene expression in macrophages and dendritic cells. *Immunity* *33*, 699–712.
- Tal, M.C., Sasai, M., Lee, H.K., Yordy, B., Shadel, G.S., and Iwasaki, A. (2009). Absence of autophagy results in reactive oxygen species-dependent amplification of RLR signaling. *Proc. Natl. Acad. Sci. USA* *106*, 2770–2775.
- Tamás, P., Macintyre, A., Finlay, D., Clarke, R., Feijoo-Carnero, C., Ashworth, A., and Cantrell, D. (2010). LKB1 is essential for the proliferation of T-cell progenitors and mature peripheral T cells. *Eur. J. Immunol.* *40*, 242–253.
- Tannahill, G.M., Curtis, A.M., Adamik, J., Palsson-McDermott, E.M., McGettrick, A.F., Goel, G., Frezza, C., Bernard, N.J., Kelly, B., Foley, N.H., et al. (2013). Succinate is an inflammatory signal that induces IL-1 β through HIF-1 α . *Nature* *496*, 238–242.
- van der Windt, G.J.W., Everts, B., Chang, C.-H., Curtis, J.D., Freitas, T.C., Amiel, E., Pearce, E.J., and Pearce, E.L. (2012). Mitochondrial respiratory capacity is a critical regulator of CD8+ T cell memory development. *Immunity* *36*, 68–78.
- Vats, D., Mukundan, L., Odegaard, J.I., Zhang, L., Smith, K.L., Morel, C.R., Wagner, R.A., Greaves, D.R., Murray, P.J., and Chawla, A. (2006). Oxidative metabolism and PGC-1 β attenuate macrophage-mediated inflammation. *Cell Metab.* *4*, 13–24.
- Wahl, D.R., Petersen, B., Warner, R., Richardson, B.C., Glick, G.D., and Opari, A.W. (2010). Characterization of the metabolic phenotype of chronically activated lymphocytes. *Lupus* *19*, 1492–1501.
- Wang, D., Malo, D., and Hekimi, S. (2010). Elevated mitochondrial reactive oxygen species generation affects the immune response via hypoxia-inducible factor-1 α in long-lived Mcl $k1^{+/-}$ mouse mutants. *J. Immunol.* *184*, 582–590.
- Wang, R., Dillon, C.P., Shi, L.Z., Milasta, S., Carter, R., Finkelstein, D., McCormick, L.L., Fitzgerald, P., Chi, H., Munger, J., and Green, D.R. (2011). The transcription factor Myc controls metabolic reprogramming upon T lymphocyte activation. *Immunity* *35*, 871–882.
- Wellen, K.E., and Thompson, C.B. (2012). A two-way street: reciprocal regulation of metabolism and signalling. *Nat. Rev. Mol. Cell Biol.* *13*, 270–276.
- West, A.P., Shadel, G.S., and Ghosh, S. (2011a). Mitochondria in innate immune responses. *Nat. Rev. Immunol.* *11*, 389–402.
- West, A.P., Brodsky, I.E., Rahner, C., Woo, D.K., Erdjument-Bromage, H., Tempst, P., Walsh, M.C., Choi, Y., Shadel, G.S., and Ghosh, S. (2011b). TLR signalling augments macrophage bactericidal activity through mitochondrial ROS. *Nature* *472*, 476–480.
- Wheaton, W.W., Weinberg, S.E., Hamanaka, R.B., Soberanes, S., Sullivan, L.B., Anso, E., Glasauer, A., Dufour, E., Mutlu, G.M., Budigner, G.S., and Chandel, N.S. (2014). Metformin inhibits mitochondrial complex I of cancer cells to reduce tumorigenesis. *eLife* *3*, e02242.
- Wheeler, M.L., and Defranco, A.L. (2012). Prolonged production of reactive oxygen species in response to B cell receptor stimulation promotes B cell activation and proliferation. *J. Immunol.* *189*, 4405–4416.
- White, M.J., McArthur, K., Metcalf, D., Lane, R.M., Cambier, J.C., Herold, M.J., van Delft, M.F., Bedoui, S., Lessene, G., Ritchie, M.E., et al. (2014). Apoptotic caspases suppress mtDNA-induced STING-mediated type I IFN production. *Cell* *159*, 1549–1562.
- Xu, L.-G., Wang, Y.-Y., Han, K.-J., Li, L.-Y., Zhai, Z., and Shu, H.-B. (2005). VISA is an adapter protein required for virus-triggered IFN- β signaling. *Mol. Cell* *19*, 727–740.
- Yasukawa, K., Oshiumi, H., Takeda, M., Ishihara, N., Yanagi, Y., Seya, T., Kawabata, S., and Kishimoto, T. (2009). Mitofusin 2 inhibits mitochondrial antiviral signaling. *Sci. Signal.* *2*, ra47.
- Yu, J., Nagasu, H., Murakami, T., Hoang, H., Broderick, L., Hoffman, H.M., and Horng, T. (2014). Inflammasome activation leads to Caspase-1-dependent mitochondrial damage and block of mitophagy. *Proc. Natl. Acad. Sci. USA* *111*, 15514–15519.
- Zhang, Q., Raoof, M., Chen, Y., Sumi, Y., Sursal, T., Junger, W., Brohi, K., Itagaki, K., and Hauser, C.J. (2010). Circulating mitochondrial DAMPs cause inflammatory responses to injury. *Nature* *464*, 104–107.
- Zhao, Y., Sun, X., Nie, X., Sun, L., Tang, T.-S., Chen, D., and Sun, Q. (2012). COX5B regulates MAVS-mediated antiviral signaling through interaction with ATG5 and repressing ROS production. *PLoS Pathog.* *8*, e1003086.
- Zhong, B., Yang, Y., Li, S., Wang, Y.-Y., Li, Y., Diaó, F., Lei, C., He, X., Zhang, L., Tien, P., and Shu, H.B. (2008). The adaptor protein MITA links virus-sensing receptors to IRF3 transcription factor activation. *Immunity* *29*, 538–550.
- Zhou, R., Yazdi, A.S., Menu, P., and Tschopp, J. (2011). A role for mitochondria in NLRP3 inflammasome activation. *Nature* *469*, 221–225.

Human Monocytes Undergo Functional Re-programming during Sepsis Mediated by Hypoxia-Inducible Factor-1 α

Irina N. Shalova,¹ Jyue Yuan Lim,¹ Manesh Chittezhath,¹ Annelies S. Zinkernagel,^{2,6} Federico Beasley,² Enrique Hernández-Jiménez,³ Víctor Toledano,³ Carolina Cubillos-Zapata,³ Annamaria Rapisarda,⁴ Jinmiao Chen,¹ Kaibo Duan,¹ Henry Yang,¹ Michael Poidinger,¹ Giovanni Melillo,⁴ Victor Nizet,² Francisco Arnalich,⁵ Eduardo López-Collazo,³ and Subhra K. Biswas^{1,*}

¹Singapore Immunology Network (SIgN), Agency for Science, Technology and Research (A*STAR), Biopolis, #04-06 Immunos building, 8A Biomedical Grove, Singapore 138648, Singapore

²Department of Pediatrics and Skaggs School of Pharmacy and Pharmaceutical Sciences, University of California, San Diego, 9500 Gilman Drive, La Jolla, CA 92093, USA

³Tumor Immunology Lab and Innate Immunity Group, IdiPAZ, “La Paz” Hospital, Pseo de La Castellana 261, Madrid 28046, Spain

⁴Development Therapeutic Program, Tumor Hypoxia Laboratory, Science Applications International Corporation-Frederick, Inc., National Cancer Institute, Frederick, MD 21701, USA

⁵Department of Internal Medicine, “La Paz” Hospital, Pseo de La Castellana 261, Madrid 28046, Spain

⁶Present address: Division of Infectious Diseases and Hospital Epidemiology, University Hospital Zurich, University of Zurich, Rämistr 100, Zurich 8091, Switzerland

*Correspondence: subhra_biswas@immunol.a-star.edu.sg

<http://dx.doi.org/10.1016/j.immuni.2015.02.001>

SUMMARY

Sepsis is characterized by a dysregulated inflammatory response to infection. Despite studies in mice, the cellular and molecular basis of human sepsis remains unclear and effective therapies are lacking. Blood monocytes serve as the first line of host defense and are equipped to recognize and respond to infection by triggering an immune-inflammatory response. However, the response of these cells in human sepsis and their contribution to sepsis pathogenesis is poorly understood. To investigate this, we performed a transcriptomic, functional, and mechanistic analysis of blood monocytes from patients during sepsis and after recovery. Our results revealed the functional plasticity of monocytes during human sepsis, wherein they transited from a pro-inflammatory to an immunosuppressive phenotype, while enhancing protective functions like phagocytosis, anti-microbial activity, and tissue remodeling. Mechanistically, hypoxia inducible factor-1 α (HIF1 α) mediated this functional re-programming of monocytes, revealing a potential mechanism for their therapeutic targeting to regulate human sepsis.

INTRODUCTION

Sepsis is a complex pathology that arises from dysregulated host inflammatory responses to systemic bacterial infection (Hotchkiss et al., 2009). Human sepsis is a leading cause of death in intensive care units (ICUs) worldwide. Yet, the immunological and molecular basis of this syndrome is poorly understood. In the last 20 years, numerous therapeutic strategies to ameliorate human sepsis have failed in clinical trials and reliable

biomarkers for sepsis are still lacking (Focus on sepsis, 2012). The reason for such a dismal scenario can be partially attributed to the complex and dynamic nature of the condition, as well as important species-specific differences in innate responses between mouse model systems and human patients (Schroder et al., 2012; Seok et al., 2013).

In line with the dynamic nature of sepsis, two phases have been recognized in this disease: an early inflammatory phase and a late immunosuppressive phase (Biswas and Lopez-Collazo, 2009; Hotchkiss et al., 2009). The early phase is characterized by leukocyte activation, cytokine storm, and a systemic inflammatory response, while the later phase is characterized by immunosuppression, leukocyte deactivation, increased risks of secondary infection, and high mortality (Boomer et al., 2011; Hotchkiss et al., 2009). The scenario might be even more complicated with the overlapping co-existence of inflammatory and immunosuppressive processes, as suggested by some (Adib-Conquy and Cavaillon, 2009; Xiao et al., 2011). Further, contrasting the common view that overt inflammation drives mortality in sepsis, this response is often effectively controlled by standard ICU practices, whereas recent evidence has emphasized how immunosuppression might contribute to increasing mortality risk in most sepsis patients (Boomer et al., 2011; Hotchkiss et al., 2009; Pachot et al., 2006; Tang et al., 2010). However, the lack of infection foci in sepsis patient organs and the emerging role of immunometabolism and neurophysiological mechanisms in organ dysfunction in sepsis reveal further complexity (Deutschman and Tracey, 2014). Nonetheless, the cellular and molecular mechanisms that regulate different aspects of human sepsis pathogenesis still remain poorly understood. Moreover, the failure of numerous human clinical trials as opposed to mice preclinical studies in sepsis also emphasize the divergence in the immune mechanisms between these species as reported recently. These facts further reinforce the immediate necessity for investigating sepsis and its effects in humans.

Monocytes and macrophages are believed to play an important role in orchestrating the host immune response during

sepsis (Biswas and Lopez-Collazo, 2009). They can potentially participate in both phases of sepsis by releasing inflammatory cytokines that contribute to “cytokine storm” and ultimately adopting an immunosuppressive phenotype whereupon they are unable to respond to secondary infections. However, whether monocytes and macrophages can actually perform such diverse functions to contribute to the pathogenesis of sepsis in humans needs investigation. A better definition of how the gene expression and functional activities of monocyte and macrophage are regulated in human sepsis patients can provide valuable insight into fundamental disease mechanisms and their possible therapeutic targeting.

In the current study, we have applied a combination of transcriptomic and functional approaches to immune profile blood monocytes during Gram-negative sepsis in adults, including follow-on analyses of the same individuals after sepsis resolution, to clarify how these cells contribute to progression of the disorder. We demonstrate that blood monocytes from patients displayed a functional plasticity, transiting from a pro-inflammatory to an immunosuppressive state during sepsis, and identify hypoxia inducible factor-1 α (HIF1 α) as a key mediator of monocyte re-programming under these conditions. Our data sheds light on the molecular and cellular basis of human sepsis progression that might inform the development of targeted therapeutic interventions.

RESULTS

Monocytes from Sepsis Patients Exhibit a Distinct Genetic Signature

Blood monocytes are believed to be major players in the dysregulated inflammatory response during sepsis and characterizing their response during this pathology provides insight into the disease mechanism (Biswas and Lopez-Collazo, 2009). We performed a transcriptomic characterization of human blood monocytes isolated from patients during Gram-negative sepsis (Sepsis-Monocytes) and following their resolution or recovery (Recovery-Monocytes); monocytes from healthy donors (Monocytes) were used as an additional baseline control population. Hierarchical clustering of the monocyte transcriptomes showed a clear segregation of the two populations, Sepsis-Monocytes versus Recovery-Monocytes, indicative of their distinct gene expression profiles (Figure 1A). However, Recovery-Monocytes clustered closely with the control Monocytes suggesting that their gene-expression profile represented a return toward the baseline condition.

The transcriptome analysis of Sepsis-Monocytes identified 1,170 (561, upregulated; 609, downregulated) differentially expressed genes in Sepsis-Monocytes compared to Recovery-Monocytes. Gene Ontology (GO) analysis was performed to assess the biological processes related to these differentially expressed genes as shown in Figure S1. The top ten statistically significant GO categories showed a prominence of essentially immune response-related processes as shown in Figures S1A and S1B and Figure 1B. In particular, immune response processes mostly related to the upregulated differentially expressed genes, whereas metabolic processes related to the downregulated differentially expressed genes (Figures S1B and S1C).

Because we were interested in characterizing the immune response of monocytes in sepsis, we focused on the im-

mune-related differentially expressed genes in Sepsis-Monocytes. The heatmap in Figure 1C shows that Sepsis-Monocytes upregulate a large number of immune-related genes encoding cytokines, chemokines, surface molecules, and transcription factors. Many of these cytokine and chemokine genes were also validated by qPCR array (Figure 1D). Analysis of Sepsis-Monocytes culture supernatants confirmed the significant upregulation of pro-inflammatory cytokines and chemokines including interleukin-1 β (IL-1 β), IL-6, and the chemokines CCL3 and CCL5, as compared to Recovery-Monocytes (Figure 1E). The anti-inflammatory cytokine, IL-10 was also found to be upregulated alongside pro-inflammatory cytokines and chemokines in the Sepsis-Monocytes. Consistent with these observations, NF- κ B, a central transcriptional regulator of inflammatory response, was found to be activated in the Sepsis-Monocytes, as indicated by the heightened expression of phospho-I κ B α (Figure 1F). Figure 1G presents a diagrammatic overview of some key immune-related genes modulated in Sepsis-Monocytes, indicating a gene-expression profile that is consistent with monocyte activation and inflammation during ongoing sepsis.

Blood Monocytes Display Altered Responses to Endotoxin in Sepsis Patients

The high risk of fatal secondary infections in sepsis is thought to be due to the immunosuppressive state of blood leukocytes in these patients (Boomer et al., 2011; Hotchkiss et al., 2009). We therefore sought to determine whether human blood monocytes displayed an altered response to endotoxin challenge in ongoing sepsis. To have a global view of this phenomenon, the response of Sepsis- and Recovery-Monocytes to ex vivo lipopolysaccharide (LPS) challenge was compared using microarray. Hierarchical clustering in Figure 2A showed a clear segregation of LPS-treated Recovery-Monocytes from their untreated counterparts (i.e., Recovery-Monocytes+LPS versus Recovery-Monocytes) suggesting a distinct transcriptomic response to LPS in these cells. In contrast, LPS-treated Sepsis-Monocytes did not segregate from their untreated counterpart (i.e., Sepsis-Monocytes+LPS versus Sepsis-Monocytes), indicating the failure to display a distinct transcriptomic response to LPS. The defective LPS response of Sepsis-Monocytes was also evident quantitatively by the markedly lesser number of differentially expressed genes (76) compared to Recovery-Monocytes (2,221 genes), in response to LPS (Figure 2B).

We further analyzed the LPS response of Sepsis- versus Recovery-Monocytes. Upregulation of inflammatory cytokine and chemokine genes is a key feature of LPS response in myelomonocytic cells (Schroder et al., 2012). Accordingly, we found many cytokines (e.g., tumor necrosis factor [TNF], IL1A, IL1B, IL6, IL12A, IL23A) and chemokines (e.g., CCL3, CCL4, CCL5, CCL20, CCL23, CXCL2, CXCL11) to be upregulated in the LPS transcriptome of Recovery-Monocytes, but not in that of Sepsis-Monocytes, indicating a defect in the LPS-induced inflammatory response of Sepsis-Monocytes (Figure 2C). A similar defect was also noted for the expression of genes encoding several surface molecules (e.g., CD80, CD44) and transcription factors (e.g., ATF5, NFKB1, NFKB2, REL, RELA) related to immune activation (Figure 2C, compare Sepsis- with Recovery-Monocytes). Figure 2D shows a diagrammatic overview of

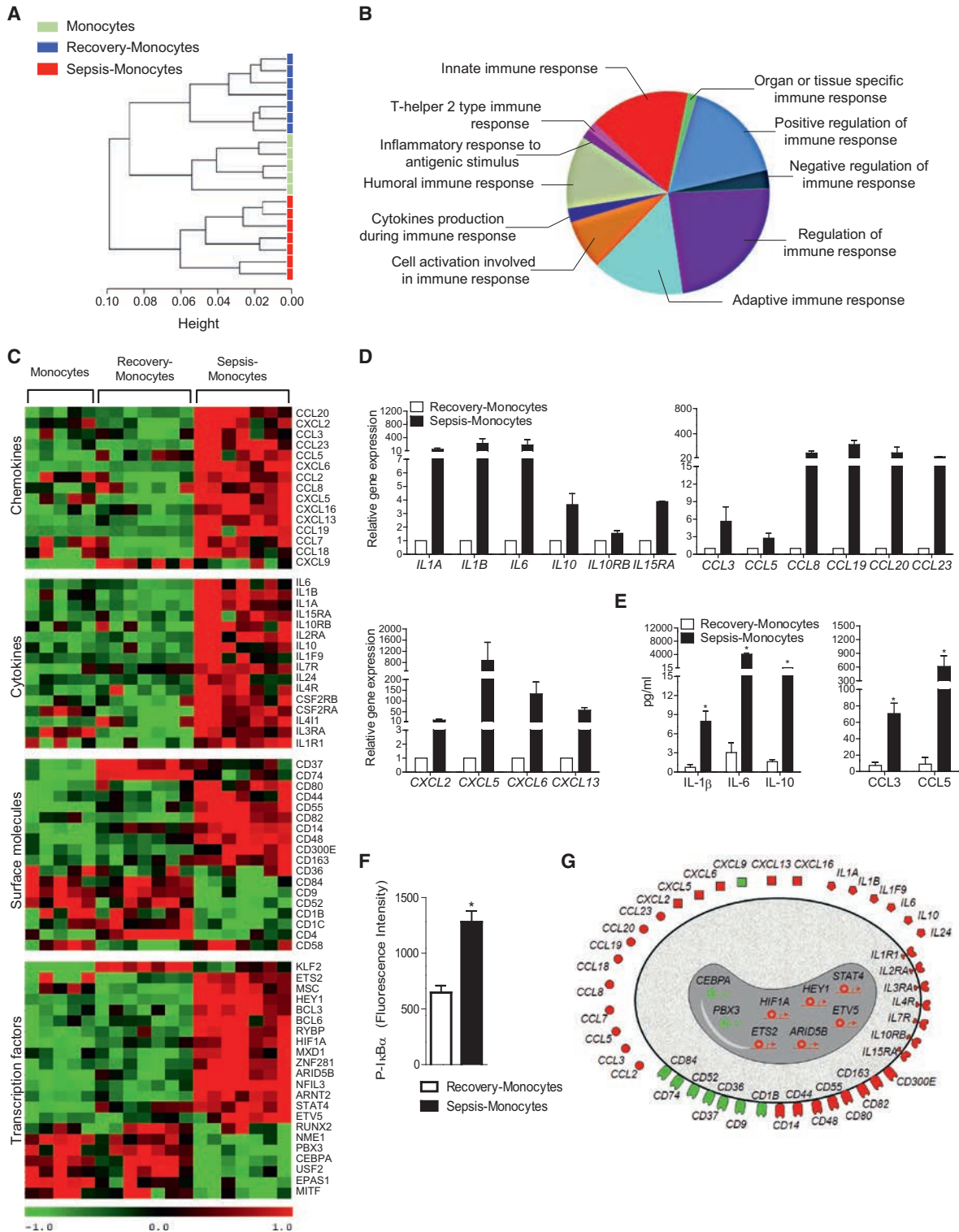


Figure 1. Transcriptome Profiling of Monocytes from Sepsis Patients

(A) Hierarchical clustering with Pearson's correlation and complete linkage of Sepsis-Monocytes (n = 7), Recovery-Monocytes (n = 7) and healthy donor Monocytes (n = 5).

(B) Gene Ontology (GO) classification of differentially expressed genes showing immune-related biological functions.

(C) Heatmap showing differential expression of genes belonging to cytokines, chemokines, selected surface molecules, and transcription factors in Sepsis-versus Recovery-Monocytes. Monocytes are shown as an additional baseline control population. Differentially expressed genes determined by Limma and row-based Z score were normalized.

(legend continued on next page)

the gene-expression data indicating impaired inflammatory response of Sepsis-Monocytes in response to LPS.

Distinct from the large number of immune-related genes (422) that showed downregulation in the LPS-treated Sepsis-Monocytes, an equal number of genes (504) were found to be still inducible or less repressed in the Sepsis-Monocytes than Recovery-Monocytes, in response to LPS treatment. GO analysis of these genes mapped them to miscellaneous functions including metabolism and phagocytosis-related processes (Figure S2). The anti-microbial gene *HAMP* also fell in the latter category and is investigated later in this study. Overall, these data indicate a profound gene “re-programming” in Sepsis-Monocytes associated with their altered response to LPS.

Monocytes Exhibit Hallmarks of Endotoxin Tolerance In Vivo in Human Sepsis

Given the altered transcriptomic response of monocytes to LPS in sepsis, we next investigated whether key monocyte functions were also disrupted under these conditions. Compared to Recovery-Monocytes, Sepsis-Monocytes exhibited a marked reduction in LPS-induced pro-inflammatory genes including *CCL3*, *4*, *5*; *CXCL2*, *11*; *IL1A*, *IL1B*, *IL6*, and *TNF*, by qPCR (Figure 3A), that mirrored our transcriptome data (Figure 2C). Reduced expression of some of these cytokines and chemokines was also confirmed in the culture supernatants of LPS-treated Sepsis-Monocytes (Figure 3B). Thus, Sepsis-Monocytes exhibit an attenuated inflammatory response to LPS. Consistent with this, LPS-treated Sepsis-Monocytes also showed reduced phospho- $\text{I}\kappa\text{B}\alpha$ expression, indicating an impaired activation of NF- κB , the key transcriptional regulator of inflammatory response (Figure 3C).

We next assessed the antigen-presenting function of Sepsis-Monocytes, because it is essential for immune activation and a sustained host immune response. Sepsis-Monocytes showed decreased expression of several key co-stimulatory and major histocompatibility complex class II (MHCII) molecule genes (*CD80*, *CD40*, and *HLA-DOB*) upon LPS treatment (Figure 3D), suggesting that the antigen-presenting ability of these cells might be impaired. Indeed, a mixed lymphocyte reaction (MLR) revealed LPS-treated Sepsis-Monocytes to induce a significantly lower T cell proliferation than Recovery-Monocytes counterpart (Figure 3E).

Monocytes and macrophages also mediated direct killing of pathogens via phagocytosis. Figure 3F shows Sepsis-Monocytes displayed a higher phagocytotic ability than control monocytes (Monocytes). Supernatants of Sepsis-Monocytes also demonstrated heightened ability to restrict growth of bacteria (*E. coli*) (Figure 3G). In line with this observation, Sepsis-Monocytes displayed enhanced expression of the anti-microbial gene *HAMP* upon LPS stimulation (Figure 3H).

Defective cytokine release in response to LPS, impaired antigen presenting function, and increased expression of anti-micro-

bial genes are features reported for in vitro endotoxin tolerance (Biswas and Lopez-Collazo, 2009; del Fresno et al., 2009; Foster et al., 2007). Therefore, the present observations on Sepsis-Monocytes strongly suggest them to be conditioned to a refractory or endotoxin tolerant phenotype in vivo during sepsis.

Sepsis-Monocytes Upregulate Tissue Re-modeling Functions

Acute inflammation during sepsis often involves tissue damage, which must be repaired to protect the host. Monocytes and macrophages release matrix metalloproteases (MMPs) and angiogenic factors such as vascular endothelial growth factors (e.g., VEGFA) and are known to contribute to tissue re-modeling and wound healing (Murray and Wynn, 2011). The heatmap in Figure 4A shows increased expression of several MMP genes in Sepsis-Monocytes compared to Recovery-Monocytes. qPCR confirmed increased *MMP9* and *MMP19* expression in the Sepsis-Monocytes (Figure 4B). MMP activity was confirmed using zymography, which showed increased gelatinase activity in the supernatants of Sepsis-Monocytes (Figure 4C). Functional consequence of this heightened MMP activity was demonstrated by the increased ability of Sepsis-Monocyte supernatants to stimulate re-epithelialization of wounded human fibroblasts (wound healing), as compared to Recovery-Monocyte (Figure 4D). Marked inhibition of this phenomenon using a pan-MMP inhibitor confirmed MMPs to mediate this event (Figure 4D).

Sepsis-Monocytes also exhibited marked upregulation of vascular endothelial growth factor-A (VEGFA) gene expression and release, compared to Recovery-Monocytes (Figures 4E and 4F). Increased VEGFA expression correlated with a significantly heightened human umbilical vein endothelial cell (HUVEC) tube formation by Sepsis-Monocyte supernatants, indicating their enhanced angiogenic activity (Figure 4G). This was mediated through VEGF as demonstrated by the ability of VEGFR2 blocking antibody to markedly inhibit this process (Figure 4G). Collectively, our above data indicate enhanced tissue re-modeling functions of Sepsis-Monocytes as compared to Recovery-Monocytes.

HIF1 α Expression and Activation Influence the Gene-Expression Profile of Sepsis-Monocytes

We investigated the potential mechanism(s) that might control the transcriptional and functional re-programming of monocytes during sepsis. The transcription factor, hypoxia inducible factor-1 α (HIF1 α) regulates mammalian cell response to hypoxia (low oxygen concentration) and is induced by Gram-negative endotoxin challenge in mice (Rius et al., 2008). Our microarray data indicated that *HIF1A* was differentially upregulated in Sepsis-Monocytes compared to Recovery-Monocytes (Figure 1C), also confirmed by increased *HIF1A* (not *HIF2A*) expression by qPCR and HIF1 α binding assay (Figures

(D) qPCR of indicated genes in Sepsis- versus Recovery-Monocytes.

(E) Cytokine expression in culture supernatants of Sepsis- versus Recovery-Monocytes.

(F) Phospho- $\text{I}\kappa\text{B}\alpha$ expression in Sepsis- versus Recovery-Monocytes. Values are mean \pm SEM (D and F: n = 3; E: n = 4), *p < 0.05 versus Recovery-Monocytes.

(G) Diagrammatic overview of Sepsis-Monocytes showing selected immune-related differentially expressed genes as compared to Recovery-Monocytes. Red represents upregulated; green represents downregulated; Panels showing transcriptome analysis represent data from the number of subjects as indicated in (A). See also Figure S1.

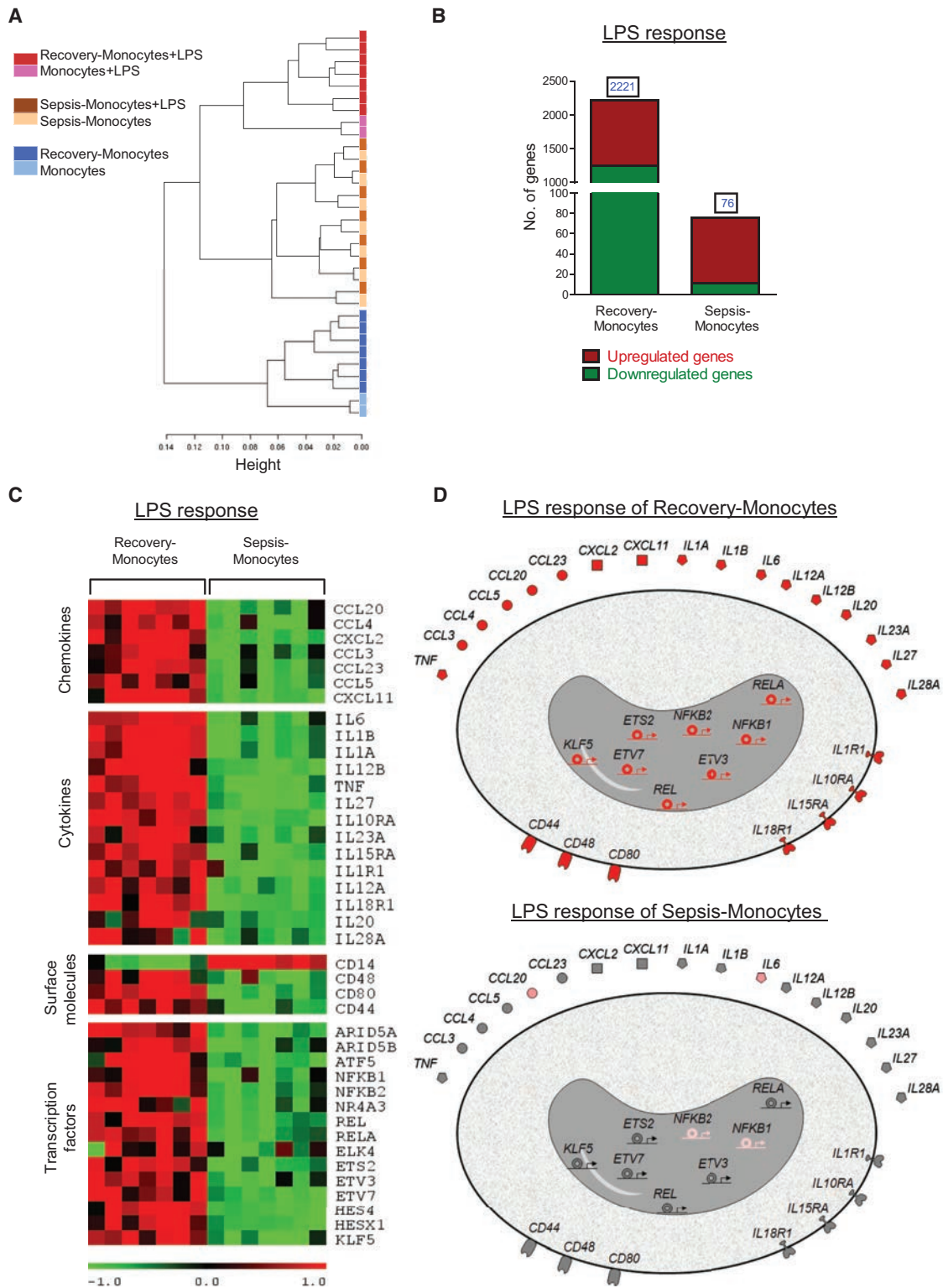


Figure 2. Blood Monocytes Display Altered Responses to Endotoxin in Sepsis Patients

(A) Hierarchical clustering with Pearson's correlation and complete linkage of Sepsis-Monocytes (n = 7), Recovery-Monocytes (n = 7), and healthy donor Monocytes (n = 2) in response to ex vivo LPS treatment (3 hr).

(B) Total number of LPS-induced differentially expressed genes in Sepsis- and Recovery-Monocytes. Box indicates the total number of differentially expressed genes.

(C) Heatmaps showing the differential modulation of indicated genes in Recovery- versus Sepsis-Monocytes, in response to LPS.

(legend continued on next page)

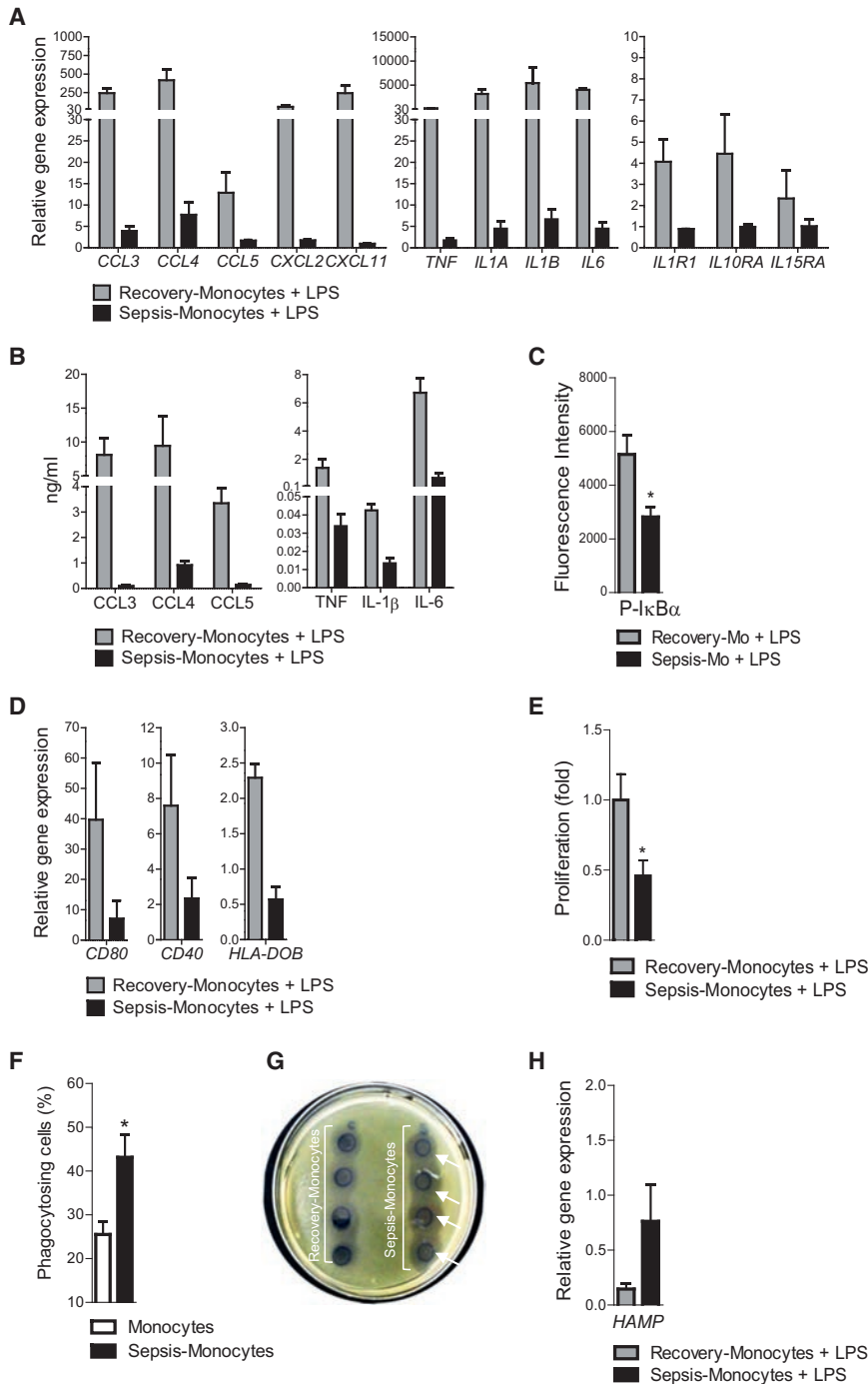


Figure 3. Monocytes Exhibit Hallmarks of Endotoxin Tolerance In Vivo in Human Sepsis

(A) qPCR of indicated genes in Sepsis- versus Recovery-Monocytes, upon LPS stimulation (3 hr). (B) Indicated cytokine and chemokine expression in culture supernatants of Sepsis- and Recovery-Monocytes, upon LPS treatment (12 hr). (C) Phospho-IκBα expression in response to LPS in Sepsis- versus Recovery-Monocytes, *p < 0.05 versus Recovery-Monocytes+LPS. (D) qPCR of indicated genes in Sepsis- and Recovery-Monocytes upon LPS challenge. (E) MLR assay showing proliferation of T cells from healthy donors upon incubation with LPS-treated Sepsis- or Recovery-Monocytes, *p < 0.05 versus Recovery-Monocytes+LPS. (F) Ability of Sepsis- versus Control-Monocytes (Monocytes) to phagocytose GFP-labeled *E. coli*, *p < 0.05 versus control Monocytes. (G) Anti-microbial activity of supernatants from Sepsis- or Recovery-Mo showing inhibition of *E. coli* growth (dark area, see arrow), on agar plates. Each spot represents the supernatant from a particular subject. (H) qPCR of anti-microbial gene *HAMP* in Sepsis- or Recovery-Mo following LPS stimulation. Values in all panels are mean ± SEM (A, C, D, H: n = 3; B, F, G: n = 4; E: n = 5).

lactor of Toll-like receptor (TLR) signaling (Bosco et al., 2006; Fang et al., 2009; Kobayashi et al., 2002; López-Collazo et al., 2006). We therefore checked the expression of this gene in Sepsis-Monocytes and confirmed its upregulation by qPCR (Figure 5D).

Taken together, the upregulation of HIF1α and enrichment of hypoxia inducible genes in Sepsis-Monocytes suggested the involvement of this transcription factor in the regulation of monocyte response in sepsis, which was further investigated.

HIF1α Is a Regulator of IRAKM Expression in Monocytes

IRAKM is one of the few conserved negative regulators of TLR pathway in mice and humans (van 't Veer et al., 2007), and is implicated in endotoxin tolerance

(Kobayashi et al., 2002). Hence, the upregulation of *IRAKM* in Sepsis-Monocytes (Figure 5D) is consistent with their impaired LPS response and endotoxin tolerant phenotype, as shown earlier (Figure 3). However, the mechanism by which *IRAKM* is

(Kobayashi et al., 2002). Hence, the upregulation of *IRAKM* in Sepsis-Monocytes (Figure 5D) is consistent with their impaired LPS response and endotoxin tolerant phenotype, as shown earlier (Figure 3). However, the mechanism by which *IRAKM* is

(D) Diagrammatic overview of the impaired LPS response of Sepsis-Monocytes. Expression of selected immune-related genes in Sepsis- and Recovery-Monocytes in response to LPS is indicated. Gene expression in response to LPS is presented relative to the respective non-LPS treated counterpart. Red-pink color coding indicates varying expression of genes that are differentially induced by LPS. Grey indicates genes not differentially induced by LPS. Transcriptome data in (B)–(D) are from n = 7 patients during Sepsis and Recovery, respectively. See also Figure S2.

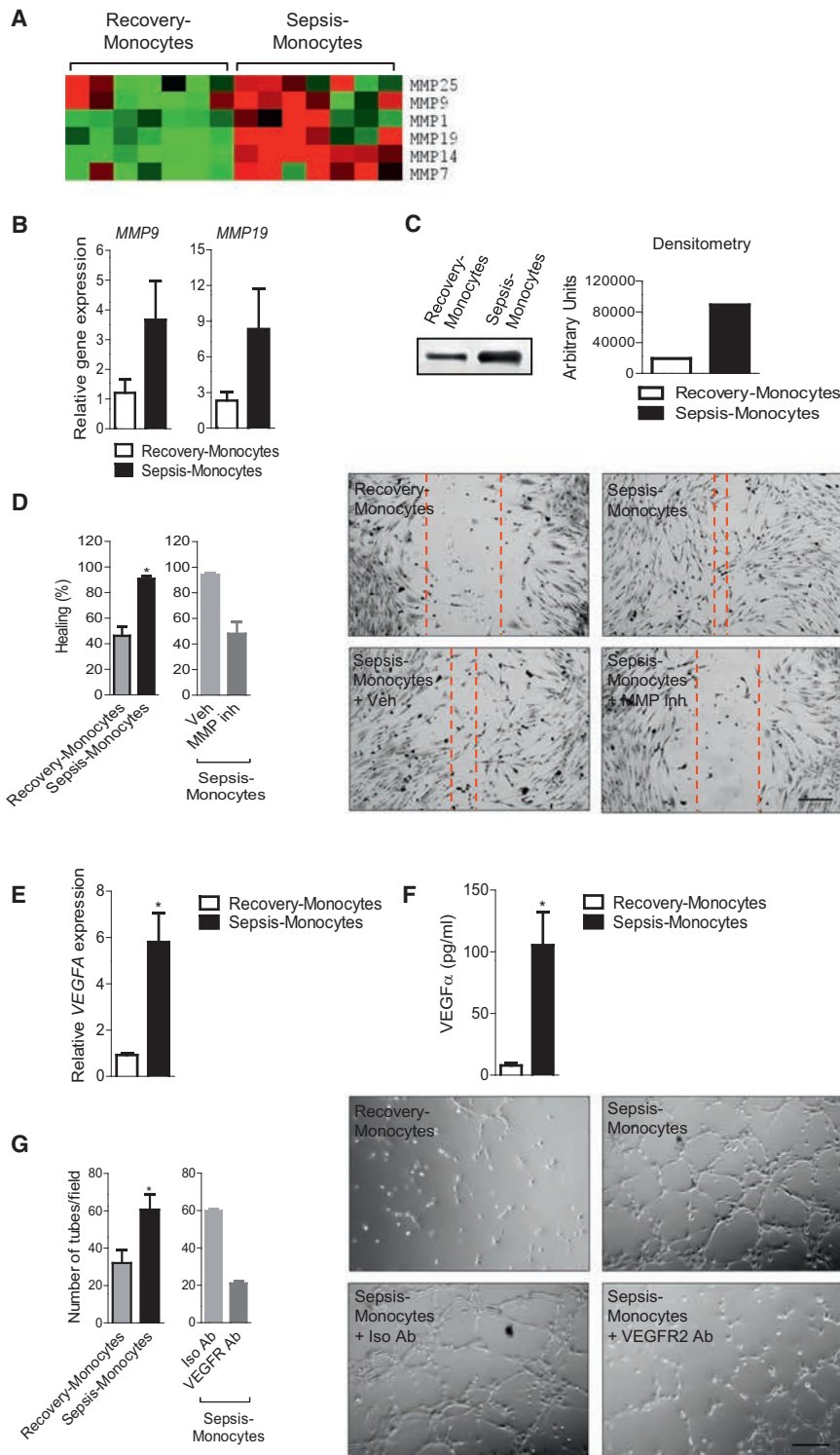


Figure 4. Sepsis-Monocytes Show Elevated Tissue Remodeling Functions

(A) Heatmap showing MMP gene modulation in Recovery- versus Sepsis-Monocytes (n = 7).

(B) qPCR for *MMP9* and *MMP19* in Sepsis- and Recovery-Mo.

(C) Zymography assay showing MMP(gelatinase) activity in culture supernatants of Sepsis- and Recovery-Monocytes.

(D) Wound-healing assay showing percent healing of wounded fibroblasts incubated with supernatant of Sepsis- or Recovery-Monocytes. Quantification and picture of wound healing (closure) is shown. Dotted line represents wound margin. Scale bar represents 0.5 mm. Wound healing in presence of a vehicle control (Veh) or MMP inhibitor is also shown. Data are representative of two independent experiments.

(E) VEGFA gene expression and (F) release by Sepsis- and Recovery-Monocytes.

(G) Enhanced angiogenesis (HUVEC tube formation) induced by supernatants of Sepsis-Monocytes. Quantification and pictures are shown. Scale bar represents 0.1 mm. The effect of VEGFR2 antibody or its isotype control (Iso Ab) on tube formation is also shown. Data are representative of two independent experiments; Values in all panels are mean \pm SEM (B, E: n = 3; D, F, G: n = 4), *p < 0.05 versus Recovery-Monocytes.

regulatory role of HIF1 (Figures 6A and 6B); concurrent upregulation of *VEGFA* and *HIF1A* served as positive controls. Similar results were also obtained in hypoxia-stimulated cells (Figure S3A). Because the sepsis condition is linked to persistent exposure to endotoxins, we next checked whether HIF1 activation combined with endotoxin exposure could augment monocyte expression of *IRAKM*. For this purpose, monocytes were treated with or without CoCl_2 for 12 hr and thereafter challenged with Lipid A (LPA, a key component of gram-negative endotoxins and a specific TLR4 ligand) for 4 hr and assessed for *IRAKM* expression. CoCl_2 +LPA treatment significantly increased expression of *IRAKM*, *VEGFA*, and *HIF1A*, as compared to monocytes treated with LPA alone (Figure 6C).

To directly demonstrate that HIF1 α was responsible for inducing *IRAKM* expression in LPA-treated monocytes, we over-expressed HIF1 α in monocytes and studied their response to LPA. Monocytes transfected with a HIF1 α plasmid markedly upregulated *IRAKM* (and *HIF1A*) compared to control plasmid transfected cells, upon LPA challenge (Figure 6D). We also performed HIF1 α small interfering RNA (siRNA)-silencing experiments in monocytes. LPA alone could induce *HIF1A* expression in monocytes (Figure S3B). However, LPA stimulation

induced and regulated in these cells is not known. Based on Figure 5, we decided to investigate whether HIF1 α regulates the expression of *IRAKM* in response to endotoxin. *IRAKM* expression was assessed in human monocytes treated with CoCl_2 , an activator of HIF1 (Huang et al., 2003). CoCl_2 -treated monocytes upregulated *IRAKM* gene expression and protein, indicating the

induced and regulated in these cells is not known. Based on Figure 5, we decided to investigate whether HIF1 α regulates the expression of *IRAKM* in response to endotoxin. *IRAKM* expression was assessed in human monocytes treated with CoCl_2 , an activator of HIF1 (Huang et al., 2003). CoCl_2 -treated monocytes upregulated *IRAKM* gene expression and protein, indicating the

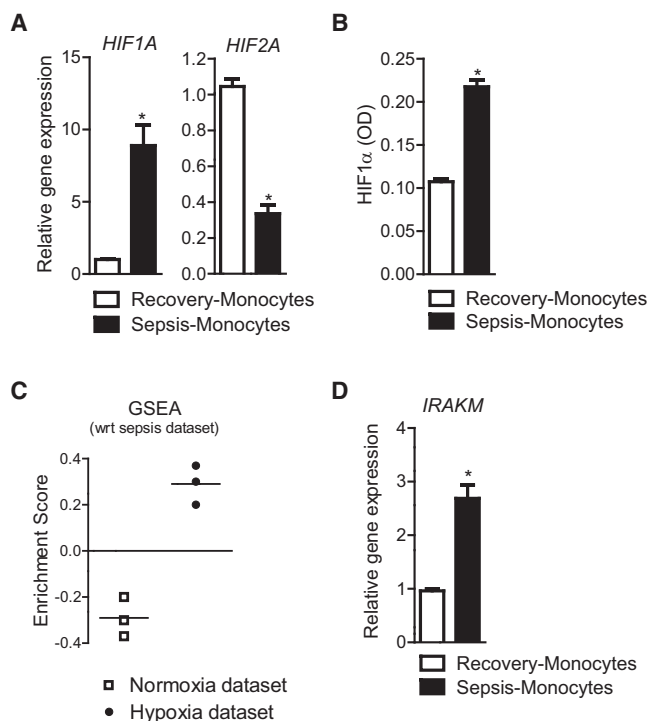


Figure 5. Sepsis-Monocytes Express Hypoxia-Inducible Genes
 (A and B) HIF1 α gene expression and binding assay in Sepsis- and Recovery-Monocytes.
 (C) GSEA was performed between normoxia versus hypoxia datasets (from GEO and ArrayExpress) and our Sepsis- versus Recovery-Monocytes dataset. A positive score indicates positive gene enrichment between the hypoxia-inducible genes and Sepsis differentially expressed genes.
 (D) Upregulated IRAKM gene expression in Sepsis-Monocytes. Values in (A), (B), and (D) are mean \pm SEM (n = 3), *p < 0.05 versus Recovery-Mo.

of siHIF1 α -silenced monocytes showed a significant decrease in the expression of *IRAKM* (as well as *VEGFA* and *HIF1A*) as compared to their control siRNA-treated counterparts, implicating HIF1 α in mediating LPA-induced *IRAKM* expression (Figure 6E).

Taken together, the results from the above approaches, i.e., pharmacological activation (via CoCl₂), overexpression, and silencing of HIF1 α , clearly establish HIF1 α as an important regulator of *IRAKM* expression in human monocytes.

Additional support to the above findings also came from meta-analysis of GEO-deposited datasets of sepsis patients wherein a statistically significant upregulation and correlation between *HIF1A* and *IRAKM* was observed in three independent patient cohorts as compared to their respective control population (Figures S3C–S3D).

HIF1 α -Induced Upregulation of *IRAKM* Skews Monocyte Pro-inflammatory Function

Although our results demonstrated HIF1 α to regulate *IRAKM* expression in monocytes in response to LPA, we wondered about the functional consequence of this phenomenon. Because *IRAKM* is a negative regulator of TLR pathway, it is conceivable that its upregulation (via HIF1 α) should concomitantly inhibit LPA-induced pro-inflammatory response. To demonstrate this, we assessed the expression of pro-inflammatory cytokines and chemokines

in all the experiments described above. Concomitant with the upregulation of *IRAKM* in CoCl₂+LPA-treated monocytes (Figure 6C), their expression of pro-inflammatory cytokine and chemokine genes like *TNF*, *IL6*, and *CCL5* was attenuated as compared to monocytes treated with LPA alone (Figure 6F). However, this attenuation was only visible in monocytes pre-treated with CoCl₂ for 12 hr but not 4 hr, possibly suggesting that HIF1 α activation at late time points mediated this effect (Figure S3E). Decrease in the corresponding cytokines was also detected by ELISA (Figure S3F). Further, we silenced *IRAKM* in these monocytes. Figure S3G, shows monocytes treated with *IRAKM* siRNA failed to repress the pro-inflammatory genes upon treatment with CoCl₂+LPA, directly implicating *IRAKM* in mediating the suppression of pro-inflammatory gene expression.

Mirroring the results of Figure 6F, HIF1 α overexpression also showed a marked downregulation of LPA-induced pro-inflammatory cytokines (Figure 6G, Figure S3H). Taken together, the results from Figures 6C–6G clearly demonstrate that HIF1 α , by inducing *IRAKM* expression in human monocytes, attenuates their pro-inflammatory response to endotoxin challenge.

To further demonstrate the functional impact of this attenuated pro-inflammatory response of monocytes, we also looked at the ability of these cells to polarize T cells. CoCl₂+LPA-treated monocytes showed downregulation of co-stimulatory molecule genes like *CD80* and *CD40* (Figure 6H). Testing their ability to polarize T cells revealed CoCl₂+LPA-treated monocytes to increase polarization to T regulatory (Tregs) cells (Figure 6I). This is in line with the decreased IL-6 (Figure 6F, Figure S3F) and increased TGF- β gene expression (Figure 6J) by these cells, the two key determinants for Treg cell polarization (Kimura and Kishimoto, 2010).

Collectively, the results presented in Figure 6 demonstrate that HIF1 α (via *IRAKM* upregulation) functionally re-programs monocytes to an immunosuppressive phenotype characterized by a defective pro-inflammatory response to endotoxin and skewing of T cells to Treg cells. This immunosuppressive phenotype is reminiscent of the phenotype we observed in the Sepsis-Monocytes and in in vitro endotoxin tolerance.

HIF1 α Upregulates Tissue Re-Modeling and Anti-microbial Functions of Monocytes

Since our earlier results showed sepsis monocytes to upregulate tissue re-modeling and anti-microbial functions (Figure 3 and 4), we next checked whether HIF1 α regulated these functions and their genes (e.g., *MMP9*, *MMP19*, *VEGFA*, *HAMP*) in response to endotoxin. As shown in Figure 7A, CoCl₂+LPA-treated monocytes showed a significant upregulation of *MMP9* and *MMP19* compare to LPA-treated monocytes, suggesting an involvement of HIF1 in the regulation of these genes. Confirming this, HIF1 α overexpression also upregulated *MMP9* and *MMP19* in response to LPA (Figure 7B). Conversely, HIF1 α siRNA significantly downregulated LPA-induced *MMP9* and *MMP19* in monocytes (Figure 7C).

Consistent with Figure 7A, at functional level, supernatants from CoCl₂+LPA-treated monocytes showed significantly heightened wounded healing (Figure 7D). Inhibition of this event by a pan-MMP inhibitor proved mediation through MMPs (Figure 7D).

Angiogenesis is an important aspect of tissue remodeling that is upregulated by Sepsis-Monocytes. Pharmacological

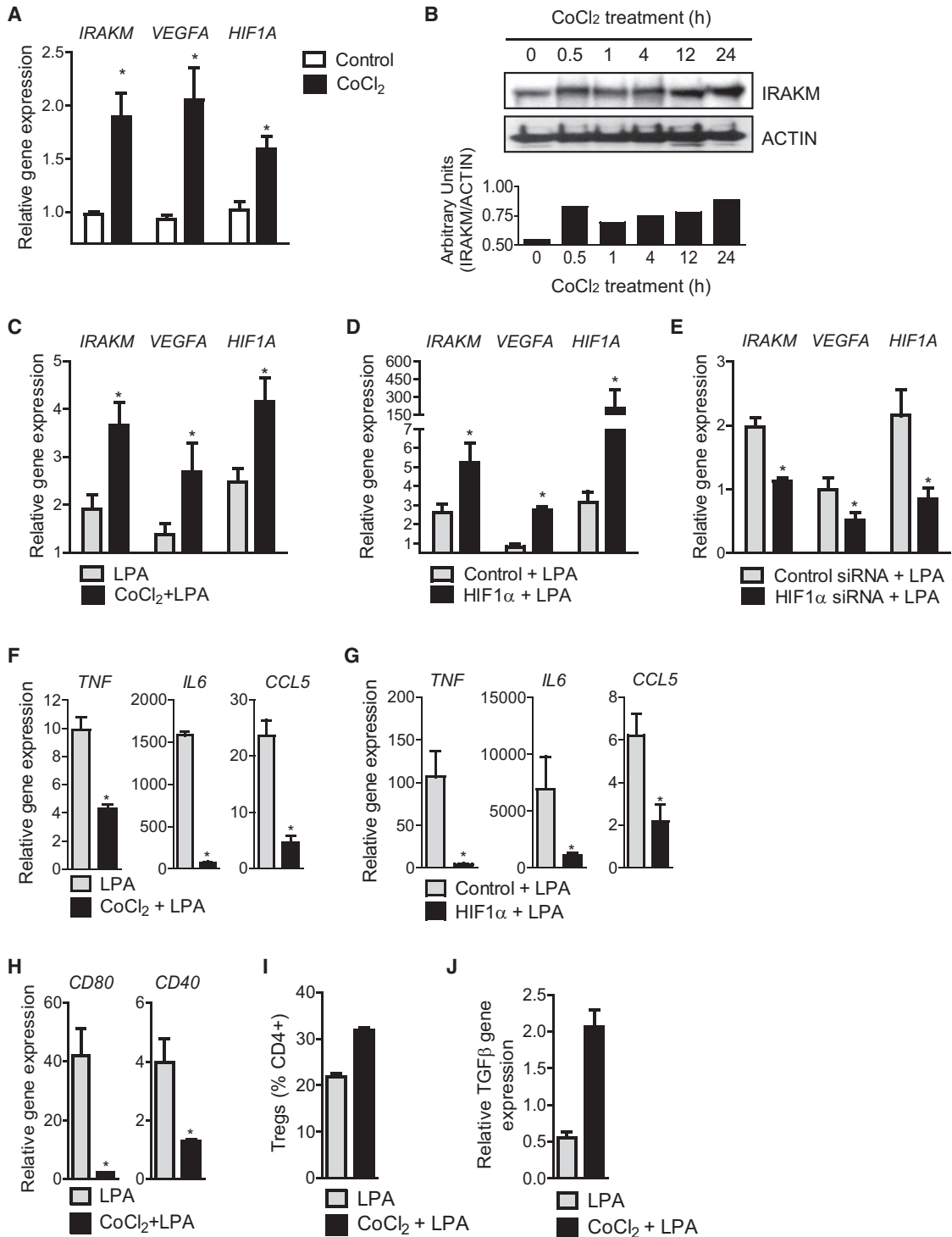


Figure 6. HIF1 α Induces the Expression of IRAKM that Skews Monocyte Pro-inflammatory Function

(A) qPCR of indicated genes in monocytes from healthy donors treated or not with CoCl_2 (0.25mM) for 12 hr, *p < 0.05 versus Control. (B) Immunoblot showing IRAKM expression in CoCl_2 -treated monocytes. Actin expression indicates loading control. Inset shows densitometry analysis; qPCR analysis of indicated genes in monocytes (C) treated or not with CoCl_2 (12 hr) and then exposed to LPA (100ng/ml) for 4 hr, *p < 0.05 versus LPA. (D) transfected with a control or $\text{HIF1}\alpha$ expressing plasmid following by LPA challenge (4 hr), *p < 0.05 versus Control+LPA. (E) Treated with control or $\text{HIF1}\alpha$ siRNA and stimulated with LPA (4 hr), *p < 0.05 versus Control siRNA+LPA; qPCR analysis of indicated genes in monocytes (F) treated with LPA or CoCl_2 +LPA, *p < 0.05 versus LPA and (G) transfected and treated as described in (D), *p < 0.05 versus Control+LPA. (H) qPCR analysis of indicated genes in LPA or CoCl_2 +LPA treated monocytes, *p < 0.05 versus LPA.

(legend continued on next page)

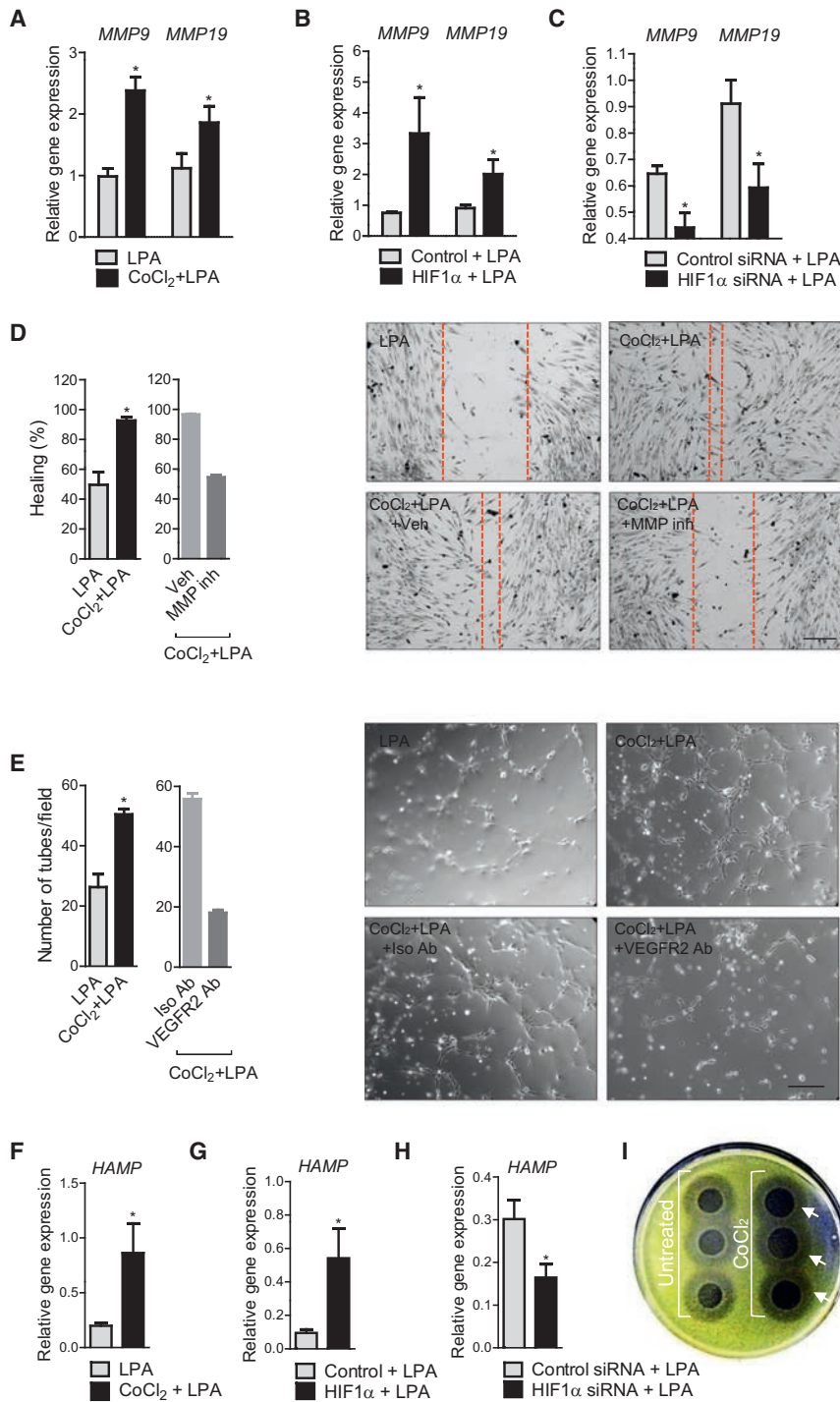


Figure 7. HIF1 α Upregulates Tissue Remodeling and Anti-microbial Functions of Monocytes

(A) qPCR of indicated genes in monocytes treated with LPA or CoCl₂+LPA, **p* < 0.05 versus LPA. (B) qPCR of indicated genes in monocytes transfected with control or HIF1 α plasmid and stimulated with LPA, **p* < 0.05 versus Control+LPA. (C) qPCR of indicated genes in monocytes treated with control or HIF1 α siRNA and stimulated with LPA, **p* < 0.05 versus Control siRNA+LPA. (D) Wound-healing assay showing percent healing of wounded fibroblasts incubated with supernatant of LPA or CoCl₂+LPA treated monocytes (n = 3), **p* < 0.05 versus LPA. Wound healing in presence of a vehicle control (Veh) or MMP inhibitor is also shown. Data are representative of two independent experiments. Dotted lines represent wound margin. Scale bar represents 0.5 mm. (E) Angiogenesis assay enumerating HUVEC tube formation induced by supernatants from LPA or CoCl₂+LPA treated monocytes (n = 3). The effect of VEGFR2 antibody or its isotype control (Iso Ab) on tube formation is also shown. Data are representative of two independent experiments. Scale bar represents 0.1 mm; qPCR of *HAMP* expression in monocytes (F) treated with LPA or CoCl₂+LPA, **p* < 0.05 versus LPA. (G) Transfected with control or HIF1 α plasmid following LPA stimulation, **p* < 0.05 versus Control+LPA. (H) Treated with control or HIF1 α siRNA following LPA treatment, **p* < 0.05 versus Control siRNA+LPA. (I) Anti-microbial activity of the supernatants from monocytes treated or not with CoCl₂ showing inhibition of bacterial (*E. coli*) growth on agar plates, as described in the legend for Figure 3G (n = 3). Values in all panels are mean \pm SEM (A, F, G: n = 4; B, C, H: n = 3). See also Figure S4.

tional level, supernatants from CoCl₂+LPA-treated monocytes markedly increase angiogenic tube formation compared to LPA-treated monocytes (Figure 7E). Inhibition of this process by a VEGFR2 blocking antibody demonstrates mediation through VEGFA (Figure 7E).

Anti-microbial activity is another vital function that is upregulated in Sepsis-Mo. These cells also upregulated the anti-microbial gene, *HAMP*. We show here that activation of HIF1 α by CoCl₂ or its overexpression significantly upregulated *HAMP* in response to LPA (Figures 7F and 7G). Conversely, HIF1 α siRNA treatment significantly downregulated *HAMP* (Figure 7H). At a functional level, CoCl₂-treated monocyte supernatants markedly restricted

activation (CoCl₂) and genetic overexpression of HIF1 α in monocytes was mirrored by increased *VEGFA*, a key angiogenic and well-known HIF1 α target gene (Forsythe et al., 1996), whereas HIF1 α siRNA abrogated this effect (Figures 6C–6E). At a func-

its overexpression significantly upregulated *HAMP* in response to LPA (Figures 7F and 7G). Conversely, HIF1 α siRNA treatment significantly downregulated *HAMP* (Figure 7H). At a functional level, CoCl₂-treated monocyte supernatants markedly restricted

(I) Bar graph showing % of CD4⁺ T cells polarized toward Tregs (CD25⁺FOXP3⁺) in an MLR assay performed in the presence of monocytes treated with LPA or CoCl₂+LPA.

(J) qPCR showing TGF- β gene expression in LPA or CoCl₂+LPA treated monocytes. Values in (A), (C)–(J) are mean \pm SEM (A and C: n = 4; D–H: n = 3; I and J: n = 2). See also Figure S3.

growth of *E. coli* bacteria, suggesting that HIF1 upregulates anti-microbial activity (Figure 7I). Bacterial killing also involves the generation of superoxides and phagocytosis. We showed that CoCl₂-treated monocytes increased their superoxide production in response to LPA (Figure S4A). Similarly, overexpression of HIF1 α in monocytes upregulated their phagocytic ability toward *E. coli* (Figure S4B).

In our biochemical studies on the regulation of tissue remodeling and anti-microbial genes by HIF1 α , we noted these genes to be upregulated only upon 12 hr, but not 4 hr, of CoCl₂ pretreatment, suggesting that HIF1 α activation at late rather than early time point was responsible for this effect (Figure S4C). Further, we also noted in the CoCl₂+LPA-treated monocyte experiments that silencing IRAKM in these cells did not affect the expression these genes, suggesting these genes to be regulated by HIF1 α , independent of IRAKM (Figure S4D).

Taken together, our above results present multiple evidence that establishes HIF1 α as an important regulator of tissue remodeling and anti-microbial function in human monocytes. However, these functions are regulated by HIF1 α directly, independent of IRAKM.

DISCUSSION

In the current report, we adopted a systems biology approach to reveal that blood monocytes undergo phenotypic and functional plasticity during the clinical course of Gram-negative sepsis in humans. Circulating human monocytes displayed a pro-inflammatory gene-expression profile in ongoing sepsis. These same cells also exhibited features of endotoxin tolerance such as blunted inflammatory cytokine and chemokine production and impaired antigen-presenting function when challenged with LPS *ex vivo*. Mechanistically, upregulated expression of HIF1 α in blood monocytes mediated the expression of IRAKM, a negative regulator of TLR signaling, leading to the conversion of these cells from a pro-inflammatory to an endotoxin-tolerant phenotype in sepsis. However, the capacity to phagocytose bacteria, express anti-microbial activity, and perform tissue re-modeling or repair functions were increased in blood monocytes from sepsis, indicating that monocyte function is re-configured rather than globally suppressed under these conditions.

Transcriptome profiling of blood monocytes sampled from patients both during and after resolution of Gram-negative sepsis revealed that a large number of pro-inflammatory cytokines, chemokines, and transcription factors were upregulated in monocytes from sepsis patients (Sepsis-Monocytes) compared with monocytes from the same subjects following resolution (Recovery-Monocytes). These data are consistent with the concept that blood monocytes (and likely tissue macrophages) directly support the induction of a “cytokine storm” in response to systemic bacterial infection in human sepsis. Supporting our transcriptome data, identification of soluble factors secreted by cultured Sepsis-Monocytes confirmed that blood monocytes secrete increased pro-inflammatory cytokines and chemokines including IL-1 β , IL-6, CCL3, and CCL5 in ongoing sepsis. Previous microarray analyses of blood mononuclear cells from pediatric, as well as adult sepsis patients, have indicated the differential regulation of several cytokine and chemokine genes such as *IL1*, *IL8*, *CCL3*, and *CCL4* (Pachot et al., 2006; Standage and Wong, 2011;

Tang et al., 2010). The objective of many of these studies was to identify a predictive gene signature or biomarker(s) for sepsis and its prognosis by comparing patients with healthy controls or between cohorts with different clinical symptoms or outcomes. However, identifying such biomarkers has been challenging due to the wide range of etiologies associated with sepsis. In contrast, our present study examined a well-defined population of sepsis patients, i.e., Gram-negative sepsis patients. In these patients, we examined the cellular and molecular basis of the aberrant immune response in sepsis, pinpointing monocytes as a key mediator of this response in humans. The importance of this cell population is heightened because apoptosis of a large number of immune subsets like lymphocytes and dendritic cells, but not blood monocytes or interstitial macrophages, has been reported in sepsis (Hotchkiss et al., 2013). Thus, characterizing Sepsis-Monocytes provides a snapshot of the immune-inflammatory response linked to sepsis. In addition, Sepsis-Monocytes also modulated anti-microbial activity, tissue re-modeling, and metabolism, suggesting other functions in sepsis.

Death in sepsis for most cases is not due to overt inflammation, which can be controlled by standard treatments such as antibiotics and steroids, but instead reflects host immunosuppression that confers high risk of fatal nosocomial infection (Hotchkiss et al., 2013). Indeed, post-mortem studies have shown unresolved opportunistic infections in a large number of patients dying of sepsis (Otto et al., 2011; Torgersen et al., 2009). In contrast, other studies report the absence of active infection in patients dying of sepsis and suggest the emerging role of immunometabolism and neurophysiology in organ dysfunction and death in sepsis (Deutschman and Tracey, 2014). It is likely that multiple events as mentioned above co-exist and contribute to this phenomenon. Among these, sepsis-related host immunosuppression has gained considerable attention recently (Hotchkiss et al., 2009; Hotchkiss et al., 2013; Pachot et al., 2006). The mechanism(s) underlying such immunosuppression (although not presently understood) might be varied such as relative changes in the abundance of different immune cell types (e.g., apoptosis of lymphocytes) (Hotchkiss et al., 2013) or change in an individual immune cell type (e.g., altered response or function). In line with the latter, a potential mechanism of immunosuppression in sepsis patients is the induction of endotoxin tolerance, a process by which host immune cells exposed to low doses of endotoxin over an extended period become refractory to further endotoxin challenge (Adib-Conquy and Cavillon, 2009; Biswas and Lopez-Collazo, 2009). Studies in murine macrophages and human monocytes have demonstrated that endotoxin tolerance can be induced *in vitro* by prolonged exposure of these cells to low doses of LPS, leading to downregulation of inflammatory cytokines TNF, IL-6, and IL-8, and upregulation of the regulatory cytokine IL-10 (Biswas and Lopez-Collazo, 2009; Foster et al., 2007; Medvedev et al., 2000). Similar impairment in the production of TNF, IL-6, and IL-1 was also reported for monocytes from gram-negative sepsis patients, upon *ex vivo* LPS challenge (Munoz et al., 1991). However, whether such an effect is restricted to a few genes or a more wide-scale event is not well-understood. To clarify this, we compared the LPS-stimulated transcriptome of Sepsis-Monocytes with that of Recovery-Monocytes to identify an impaired monocyte response to LPS during sepsis. These

findings together with qPCR results showed markedly reduced gene expression of several pro-inflammatory cytokines or chemokines, inflammation-related transcription factors, and antigen presentation-related molecules, corroborating with a downregulation of monocyte activation. Our data provide transcriptomic evidence confirming the *in vivo* endotoxin tolerance of human blood monocytes in ongoing sepsis.

While the above observations conform to the general characteristics of an endotoxin-tolerant phenotype in Sepsis-Monocytes, several genes and functions related to anti-microbial activity and tissue remodeling remain upregulated in these cells. This suggests that monocytes undergo a transcriptomic and functional “re-programming” in sepsis rather than a general suppression of genes and functions. Supporting this, *in vitro* endotoxin tolerance studies in human monocytes and murine bone-marrow-derived macrophages reported the downregulation of inflammatory genes concomitant with increased expression of anti-microbial genes in these cells (Biswas and Lopez-Collazo, 2009; del Fresno et al., 2009; Foster et al., 2007). In addition, *in vitro* endotoxin tolerant human peripheral blood mononuclear cells (PBMCs) and macrophages were recently shown to upregulate genes related to wound healing (*VEGFA*, *MMP9*) and phagocytosis (*MARCO*, *CD23*) (Pena et al., 2011), an observation supported *in vivo* by the upregulation of *VEGFA*, *MMPs*, and heightened phagocytosis in Sepsis-Monocytes. Some studies also link *in vitro* endotoxin tolerance to M2 macrophage polarization, upregulating *ARG1*, *YM1*, and *FIZZ1* genes in mice, and *CCL22*, *CCL24*, *CD163*, and *CD206* in humans (Pena et al., 2011; Porta et al., 2009). Although our array data show *CD163* upregulation in Sepsis-Monocytes, the fact that these cells co-express pro-inflammatory signature together with immunosuppressive (e.g., impaired response to LPS *ex vivo*), tissue remodeling, and anti-microbial characteristics suggests a more complex profile than a simple M1 or M2 polarization state. This is conceivable considering the multitude of stimuli encountered *in vivo* and the dynamic nature of the disease. In line with this fact, a recent study reported that the immune response in severely ill human patients exhibits both pro-inflammatory and anti-inflammatory components that function in parallel (Xiao et al., 2011). Similarly, another study profiling PBMCs from sepsis patients also failed to demonstrate a distinctive pro- or anti-inflammatory phase at the transcriptional level (Tang et al., 2010), suggesting their co-existence, as proposed by others (Adib-Conquy and Cavaillon, 2009). The phenotype of Sepsis-Monocytes emerging from our study suggests a general adaptation response to overt inflammation, which involves an impaired capacity to support further inflammation and immune activation, while promoting a protective response through an intact phagocytotic, anti-microbial, and tissue re-modeling functions.

Our transcriptomal and functional analyses of blood monocytes demonstrates their *in vivo* functional re-programming in course of human sepsis. Defining the mechanisms that support monocyte functional plasticity or re-programming in human sepsis is crucial in understanding the dysregulated host immune response in sepsis progression. Several lines of evidence in the current report suggest a mechanistic role for HIF1 α in guiding this functional re-programming of monocytes in human sepsis. Using gene-enrichment analysis, we found that a large proportion of the genes modulated in Sepsis-Monocytes were hypoxia

inducible. Consistent with this fact, the expression and activity of HIF-1 α was found to be upregulated in Sepsis-Monocytes as compared to Recovery-Monocytes. Further studies involving the modulation of HIF1 α using pharmacological, genetic overexpression and siRNA silencing approach established HIF1 α to regulate the expression of *IRAKM*, a well-known negative regulator of the TLR signaling pathway and inducer of endotoxin tolerance (Kobayashi et al., 2002; López-Collazo et al., 2006). Moreover, meta-analysis of sepsis leukocyte datasets showed a significant correlation between increased *HIF1A* and *IRAKM* expression in independent cohorts of sepsis patients. On the basis of our results, we propose that during sepsis, exposure to endotoxin triggers HIF1 α activation in the monocytes, which in turn induces *IRAKM* expression, thereby driving these cells into an endotoxin-tolerant state. This correlates well with our observations on HIF1 α activation, upregulation of *IRAKM* and the endotoxin tolerant phenotype of Sepsis-Monocytes. In fact, we could demonstrate that HIF1 α not only upregulated *IRAKM* in monocytes, but concomitantly downregulated the expression of pro-inflammatory cytokines like *TNF* and *IL-6* in response to LPA, consistent with the negative regulatory role of *IRAKM*. Indeed, using si*IRAKM* silencing in monocytes, we demonstrated that *IRAKM*, downstream of HIF1 α , was responsible for mediating this downregulation of pro-inflammatory cytokines in response to LPA. In contrast to these observations, earlier studies in conditional genetically ablated mice have shown HIF1 α to support myeloid cell-mediated inflammation and pro-inflammatory gene expression (Cramer et al., 2003; Nizet and Johnson, 2009). Recently, HIF1 α was also shown to mediate *IL-1 β* expression in LPS-treated macrophages (Tannahill et al., 2013). The apparent paradox could perhaps be explained by the fact that an initial HIF1 α activation will induce a pro-inflammatory program in human monocytes, whereas chronic activation of this pathway (as occurs in sepsis) would lead to the dampening of those same inflammatory responses via induction of negative regulators such as *IRAKM*. Supporting such a view, we showed that HIF1 α activation (by *CoCl₂* treatment) at late, but not early time points in monocytes suppressed their pro-inflammatory cytokine expression in response to LPA. Consistent with a role for HIF1 α in ameliorating ongoing inflammation, HIF1 α was reported to increase the frequency and suppressive properties of naturally occurring *CD4⁺CD25⁺* regulatory T cells (Ben-Shoshan et al., 2008). Tregs are increased in sepsis (Hotchkiss et al., 2013). Supporting these observations, we showed that HIF1 α activation by *CoCl₂*+LPA treatment in monocytes increased their ability to induce Treg cell polarization. This was possibly driven by the skewed *IL-6* versus *TGF- β* expression by monocytes, a hallmark for Treg cell polarization (Kimura and Kishimoto, 2010). An immunosuppressive role for HIF1 α is also supported by studies in tumors, where HIF1 α was instrumental in polarizing tumor associated macrophages to an M2-like phenotype and driving myeloid-derived suppressor cells to their immunosuppressive phenotype (Colegio et al., 2014; Corzo et al., 2010). In line with these, our finding that HIF1 α regulates *IRAKM* expression in monocytes identifies a potential mechanism for targeting the immunosuppressive response of monocytes in human sepsis.

In addition to the above data, we have presented biochemical and genetic evidence demonstrating HIF1 α to regulate tissue

remodeling and anti-microbial functions and their related genes (e.g., *VEGFA*, *MMP9*, *19*, and *HAMP*). However, HIF1 α directly regulated these independent of IRAKM. This is conceivable because many of these molecules like VEGFA and MMPs are target genes for HIF1 α and hypoxia (Forsythe et al., 1996). In line with our functional studies, mice studies have shown HIF1 α to mediate the anti-microbial activity in myeloid cells (Nizet and Johnson, 2009). Taken together, our mechanistic studies suggest HIF1 α as a crucial regulator of the functional plasticity of monocytes during sepsis: regulating inflammatory response on one hand and orchestrating protective responses on the other hand. However, further studies on these different aspects of HIF1 α in humans would shed more light on the situation.

Although HIF1 α regulates the expression of a diverse range of genes (e.g., inflammatory, negative regulator, tissue remodeling, and anti-microbial genes), it is pertinent to understand what controls the target specificity and temporal regulation of such HIF-induced genes. Recent studies indicate HIF to exert direct or indirect transcriptional regulation involving other interacting proteins, enhanceosomes, and epigenetic modifications (Schödel et al., 2011). While the relative contribution of these different modes of HIF transcriptional regulation remains unclear, future ChIP-Seq and epigenetic studies would clarify the extent of such direct versus indirect regulatory effects of HIF1 α on our genes of interest (e.g., *IRAKM*, *VEGFA*, *MMP* gene), as well as gene re-programming.

Another aspect of sepsis is its long-term effect on survivors. Sepsis survivors have been reported to show significant morbidity and mortality, with 5-year mortality rates of higher than 70% (Deutschman and Tracey, 2014; Iwashyna et al., 2010; Valdés-Ferrer et al., 2013). Although the events underlying such long-term effects remain unclear, elevated serum factors like IL-6, HMGB1, and inflammatory monocytes have been suggested in human and mice studies (Valdés-Ferrer et al., 2013; Yende et al., 2008). It is possible that persistence of such sub-clinical inflammation might induce long-term and specific changes in these immune cells that might contribute to the altered status of these survivors. Although our study involved sepsis survivors, its main focus was to characterize the immune response of monocytes during sepsis (hence comparing Sepsis-with Recovery-Monocytes), rather than post-sepsis susceptibility in these subjects. The latter is a different issue requiring future investigation of the immune response in survivors at different time points following recovery, in relation to healthy subjects.

In conclusion, using a systems biology approach, the present study demonstrates that blood monocytes undergo a phenotypic and functional re-programming during human sepsis that allows these cells to transit from an inflammatory to an immunosuppressive state, thereby contributing to both features of sepsis progression. Mechanistically, HIF1 α was identified as a key mediator of monocyte functional re-programming in sepsis, raising the possibility of pharmacologically targeting this molecule to modulate monocyte responses and human sepsis progression.

EXPERIMENTAL PROCEDURES

Human Blood Samples

All access to blood samples from patients or healthy subjects were in compliance with the guidelines approved by the local ethics committee. Further

information on healthy and patient blood samples, as well as patient clinicopathological features, are provided in the Supplemental Experimental Procedures.

qPCR Analysis

Cells were lysed in Trizol (Life Technologies, Invitrogen), and total RNA prepared using the RNeasy kit (QIAGEN) as per manufacturer's instructions. For PCR Array analysis, total RNA was reverse transcribed using the RT² First Strand Kit (SABiosciences, QIAGEN). cDNA was utilized for qPCR using PCR array plates for human inflammatory cytokines and their receptors (SABiosciences, QIAGEN) and run on an iCycler iQ5 Real-Time PCR detection system (Bio-Rad). Gene expression was analyzed using the manufacturer's analysis software (www.sabiosciences.com/pcrarraydataanalysis.php). For normal qPCRs, total RNA was reverse transcribed using the Taqman reverse transcription kit (Applied Biosystems) and cDNA ran for qPCR on iCycler iQ5 machine. Target gene expression was normalized to the expression of a housekeeping gene, β -actin gene. Relative gene expression was calculated using the standard 2- $\Delta\Delta$ Ct method.

siRNA Silencing and Overexpression Studies

RNA interference was performed using siRNAs targeted against human HIF1 α or IRAKM and compared with a control/scrambled siRNA (Invitrogen). Similarly, HIF1 α overexpression was performed by transfecting monocytes with a human HIF1 α expression plasmid or a control plasmid. Monocytes were nucleofected using Human Monocyte Nucleofector Kit (Amaxa Biosystems, Lonza) in the presence of the respective siRNAs (20 nM) or plasmids (0.5 μ g) as per the manufacturer's instructions. Overexpression or silencing was assessed by qPCR analysis.

Bio-Plex Assays

Cell-free culture supernatants of human monocytes (50 μ l) were assayed for the presence of the indicated cytokines, chemokines, and growth factors using the Bio-Plex Pro assay kit (Bio-Rad). For phospho-I κ B α protein, monocyte protein extracts were prepared and analyzed using the Bio-Plex phospho-protein detection kit (Bio-Rad) as per the manufacturer's instructions. All data were collected using the Bio-Plex 200 array system with Luminex xMap Technology and analyzed using Bio-Plex Manager 6.0 (Bio-Rad).

ELISA

Cell-free culture supernatants of human monocytes were tested for TNF, IL-6, and CCL5 using ELISA Kits (DuoSet Kits, R&D Systems) according to the manufacturer's instructions.

HIF1 α Binding Assay

Monocytes from septic and recovered patients were processed and assayed using the TransAM HIF1 kit (Active Motif) according to the manufacturer's protocol. The optical density of the samples was quantified using an Infinite M200 plate reader (Tecan).

Statistical Analysis

Statistical significance was calculated by Student's t test for comparisons between two groups, or by one-way ANOVA for comparisons of three or more groups. p values < 0.05 were considered significant.

Additional methods including microarray and bioinformatics analysis, patient details, cell isolation and culture, and biochemical and functional assays are provided in the Supplemental Experimental Procedures.

ACCESSION NUMBERS

The Gene Expression Omnibus (GEO) accession number for the microarray data reported in this paper is GSE46955.

SUPPLEMENTAL INFORMATION

Supplemental Information includes four figures and Supplemental Experimental Procedures and can be found with this article online at <http://dx.doi.org/10.1016/j.immuni.2015.02.001>.

ACKNOWLEDGMENTS

S.K.B. thanks core funding of SigN, A*STAR, and E.L.-C. thanks Fondos de Investigación Sanitaria (PI11/00350) for the funding this research. We thank the Health Sciences Authority, Singapore, for their kind support with the blood supply. We are grateful to Ms. Josephine Lum and Dr. Francesca Zolezzi for their kind help with the transcriptomics. We also thank the Flow Cytometry and Immunomonitoring Platforms (SigN). We thank Dr. John Common and Professor Birgitte Lane (Institute of Medical Biology, A*STAR) for their help in providing human fibroblasts for wound healing assay. Dr. Neil McCarthy of Insight Editing London edited the manuscript. G.M. is presently an employee of AstraZeneca and has no conflict of interest related to this work.

Received: July 30, 2013

Revised: October 27, 2014

Accepted: December 30, 2014

Published: March 3, 2015

REFERENCES

- Adib-Conquy, M., and Cavaillon, J.M. (2009). Compensatory anti-inflammatory response syndrome. *Thromb. Haemost.* *101*, 36–47.
- Ben-Shoshan, J., Maysel-Auslender, S., Mor, A., Keren, G., and George, J. (2008). Hypoxia controls CD4+CD25+ regulatory T-cell homeostasis via hypoxia-inducible factor-1alpha. *Eur. J. Immunol.* *38*, 2412–2418.
- Biswas, S.K., and Lopez-Collazo, E. (2009). Endotoxin tolerance: new mechanisms, molecules and clinical significance. *Trends Immunol.* *30*, 475–487.
- Boomer, J.S., To, K., Chang, K.C., Takasu, O., Osborne, D.F., Walton, A.H., Bricker, T.L., Jarman, S.D., 2nd, Kreisel, D., Krupnick, A.S., et al. (2011). Immunosuppression in patients who die of sepsis and multiple organ failure. *JAMA* *306*, 2594–2605.
- Bosco, M.C., Puppo, M., Santangelo, C., Anfosso, L., Pfeffer, U., Fardin, P., Battaglia, F., and Varesio, L. (2006). Hypoxia modifies the transcriptome of primary human monocytes: modulation of novel immune-related genes and identification of CC-chemokine ligand 20 as a new hypoxia-inducible gene. *J. Immunol.* *177*, 1941–1955.
- Colegio, O.R., Chu, N.Q., Szabo, A.L., Chu, T., Rhebergen, A.M., Jairam, V., Cyrus, N., Brokowski, C.E., Eisenbarth, S.C., Phillips, G.M., et al. (2014). Functional polarization of tumour-associated macrophages by tumour-derived lactic acid. *Nature* *513*, 559–563.
- Corzo, C.A., Condamine, T., Lu, L., Cotter, M.J., Youn, J.I., Cheng, P., Cho, H.I., Celis, E., Quiceno, D.G., Padya, T., et al. (2010). HIF-1 α regulates function and differentiation of myeloid-derived suppressor cells in the tumor microenvironment. *J. Exp. Med.* *207*, 2439–2453.
- Cramer, T., Yamanishi, Y., Clausen, B.E., Förster, I., Pawlinski, R., Mackman, N., Haase, V.H., Jaenisch, R., Corr, M., Nizet, V., et al. (2003). HIF-1alpha is essential for myeloid cell-mediated inflammation. *Cell* *112*, 645–657.
- del Fresno, C., García-Río, F., Gómez-Piña, V., Soares-Schanoski, A., Fernández-Ruiz, I., Jurado, T., Kajiji, T., Shu, C., Marin, E., Gutierrez del Arroyo, A., et al. (2009). Potent phagocytic activity with impaired antigen presentation identifying lipopolysaccharide-tolerant human monocytes: demonstration in isolated monocytes from cystic fibrosis patients. *J. Immunol.* *182*, 6494–6507.
- Deutschman, C.S., and Tracey, K.J. (2014). Sepsis: current dogma and new perspectives. *Immunity* *40*, 463–475.
- Fang, H.Y., Hughes, R., Murdoch, C., Coffelt, S.B., Biswas, S.K., Harris, A.L., Johnson, R.S., Imityaz, H.Z., Simon, M.C., Fredlund, E., et al. (2009). Hypoxia-inducible factors 1 and 2 are important transcriptional effectors in primary macrophages experiencing hypoxia. *Blood* *114*, 844–859.
- Focus on sepsis (2012). *Nature Medicine* *18*, 997.
- Forsythe, J.A., Jiang, B.H., Iyer, N.V., Agani, F., Leung, S.W., Koos, R.D., and Semenza, G.L. (1996). Activation of vascular endothelial growth factor gene transcription by hypoxia-inducible factor 1. *Mol. Cell. Biol.* *16*, 4604–4613.
- Foster, S.L., Hargreaves, D.C., and Medzhitov, R. (2007). Gene-specific control of inflammation by TLR-induced chromatin modifications. *Nature* *447*, 972–978.
- Hotchkiss, R.S., Coopersmith, C.M., McDunn, J.E., and Ferguson, T.A. (2009). The sepsis seesaw: tilting toward immunosuppression. *Nat. Med.* *15*, 496–497.
- Hotchkiss, R.S., Monneret, G., and Payen, D. (2013). Sepsis-induced immunosuppression: from cellular dysfunctions to immunotherapy. *Nat. Rev. Immunol.* *13*, 862–874.
- Huang, Y., Du, K.M., Xue, Z.H., Yan, H., Li, D., Liu, W., Chen, Z., Zhao, Q., Tong, J.H., Zhu, Y.S., and Chen, G.Q. (2003). Cobalt chloride and low oxygen tension trigger differentiation of acute myeloid leukemic cells: possible mediation of hypoxia-inducible factor-1alpha. *Leukemia* *17*, 2065–2073.
- Iwashyna, T.J., Ely, E.W., Smith, D.M., and Langa, K.M. (2010). Long-term cognitive impairment and functional disability among survivors of severe sepsis. *JAMA* *304*, 1787–1794.
- Kimura, A., and Kishimoto, T. (2010). IL-6: regulator of Treg/Th17 balance. *Eur. J. Immunol.* *40*, 1830–1835.
- Kobayashi, K., Hernandez, L.D., Galán, J.E., Janeway, C.A., Jr., Medzhitov, R., and Flavell, R.A. (2002). IRAK-M is a negative regulator of Toll-like receptor signaling. *Cell* *110*, 191–202.
- López-Collazo, E., Fuentes-Prior, P., Arnalich, F., and del Fresno, C. (2006). Pathophysiology of interleukin-1 receptor-associated kinase-M: implications in refractory state. *Curr. Opin. Infect. Dis.* *19*, 237–244.
- Medvedev, A.E., Kopydlowski, K.M., and Vogel, S.N. (2000). Inhibition of lipopolysaccharide-induced signal transduction in endotoxin-tolerized mouse macrophages: dysregulation of cytokine, chemokine, and toll-like receptor 2 and 4 gene expression. *J. Immunol.* *164*, 5564–5574.
- Munoz, C., Carlet, J., Fitting, C., Misset, B., Blériot, J.P., and Cavaillon, J.M. (1991). Dysregulation of in vitro cytokine production by monocytes during sepsis. *J. Clin. Invest.* *88*, 1747–1754.
- Murray, P.J., and Wynn, T.A. (2011). Protective and pathogenic functions of macrophage subsets. *Nat. Rev. Immunol.* *11*, 723–737.
- Nizet, V., and Johnson, R.S. (2009). Interdependence of hypoxic and innate immune responses. *Nat. Rev. Immunol.* *9*, 609–617.
- Otto, G.P., Sossdorf, M., Claus, R.A., Rödel, J., Menge, K., Reinhart, K., Bauer, M., and Riedemann, N.C. (2011). The late phase of sepsis is characterized by an increased microbiological burden and death rate. *Crit. Care* *15*, R183.
- Pachot, A., Lepape, A., Vey, S., Bienvenu, J., Mouglin, B., and Monneret, G. (2006). Systemic transcriptional analysis in survivor and non-survivor septic shock patients: a preliminary study. *Immunol. Lett.* *106*, 63–71.
- Pena, O.M., Pistolic, J., Raj, D., Fjell, C.D., and Hancock, R.E. (2011). Endotoxin tolerance represents a distinctive state of alternative polarization (M2) in human mononuclear cells. *J. Immunol.* *186*, 7243–7254.
- Porta, C., Rimoldi, M., Raes, G., Brys, L., Ghezzi, P., Di Liberto, D., Dieli, F., Ghisletti, S., Natoli, G., De Baetselier, P., et al. (2009). Tolerance and M2 (alternative) macrophage polarization are related processes orchestrated by p50 nuclear factor kappaB. *Proc. Natl. Acad. Sci. USA* *106*, 14978–14983.
- Rius, J., Guma, M., Schachtrup, C., Akassoglou, K., Zinkernagel, A.S., Nizet, V., Johnson, R.S., Haddad, G.G., and Karin, M. (2008). NF-kappaB links innate immunity to the hypoxic response through transcriptional regulation of HIF-1alpha. *Nature* *453*, 807–811.
- Schödel, J., Oikonomopoulos, S., Ragoussis, J., Pugh, C.W., Ratcliffe, P.J., and Mole, D.R. (2011). High-resolution genome-wide mapping of HIF-binding sites by ChIP-seq. *Blood* *117*, e207–e217.
- Schroder, K., Irvine, K.M., Taylor, M.S., Bokil, N.J., Le Cao, K.A., Masterman, K.A., Labzin, L.I., Semple, C.A., Kapetanovic, R., Fairbairn, L., et al. (2012). Conservation and divergence in Toll-like receptor 4-regulated gene expression in primary human versus mouse macrophages. *Proc. Natl. Acad. Sci. USA* *109*, E944–E953.
- Seok, J., Warren, H.S., Cuenca, A.G., Mindrinos, M.N., Baker, H.V., Xu, W., Richards, D.R., McDonald-Smith, G.P., Gao, H., Hennessy, L., et al.; Inflammation and Host Response to Injury, Large Scale Collaborative

- Research Program (2013). Genomic responses in mouse models poorly mimic human inflammatory diseases. *Proc. Natl. Acad. Sci. USA* *110*, 3507–3512.
- Standage, S.W., and Wong, H.R. (2011). Biomarkers for pediatric sepsis and septic shock. *Expert Rev. Anti Infect. Ther.* *9*, 71–79.
- Tang, B.M., Huang, S.J., and McLean, A.S. (2010). Genome-wide transcription profiling of human sepsis: a systematic review. *Crit. Care* *14*, R237.
- Tannahill, G.M., Curtis, A.M., Adamik, J., Palsson-McDermott, E.M., McGettrick, A.F., Goel, G., Frezza, C., Bernard, N.J., Kelly, B., Foley, N.H., et al. (2013). Succinate is an inflammatory signal that induces IL-1 β through HIF-1 α . *Nature* *496*, 238–242.
- Torgersen, C., Moser, P., Luckner, G., Mayr, V., Jochberger, S., Hasibeder, W.R., and Dünser, M.W. (2009). Macroscopic postmortem findings in 235 surgical intensive care patients with sepsis. *Anesth. Analg.* *108*, 1841–1847.
- Valdés-Ferrer, S.I., Rosas-Ballina, M., Olofsson, P.S., Lu, B., Dancho, M.E., Ochani, M., Li, J.H., Scheinerman, J.A., Katz, D.A., Levine, Y.A., et al. (2013). HMGB1 mediates splenomegaly and expansion of splenic CD11b+ Ly-6C(high) inflammatory monocytes in murine sepsis survivors. *J. Intern. Med.* *274*, 381–390.
- van 't Veer, C., van den Pangaart, P.S., van Zoelen, M.A., de Kruijff, M., Birjmohun, R.S., Stroes, E.S., de Vos, A.F., and van der Poll, T. (2007). Induction of IRAK-M is associated with lipopolysaccharide tolerance in a human endotoxemia model. *J. Immunol.* *179*, 7110–7120.
- Xiao, W., Mindrinos, M.N., Seok, J., Cuschieri, J., Cuenca, A.G., Gao, H., Hayden, D.L., Hennessy, L., Moore, E.E., Minei, J.P., et al.; Inflammation and Host Response to Injury Large-Scale Collaborative Research Program (2011). A genomic storm in critically injured humans. *J. Exp. Med.* *208*, 2581–2590.
- Yende, S., D'Angelo, G., Kellum, J.A., Weissfeld, L., Fine, J., Welch, R.D., Kong, L., Carter, M., and Angus, D.C.; GenIMS Investigators (2008). Inflammatory markers at hospital discharge predict subsequent mortality after pneumonia and sepsis. *Am. J. Respir. Crit. Care Med.* *177*, 1242–1247.

Network Integration of Parallel Metabolic and Transcriptional Data Reveals Metabolic Modules that Regulate Macrophage Polarization

Abhishek K. Jha,¹ Stanley Ching-Cheng Huang,² Alexey Sergushichev,^{2,3} Vicky Lampropoulou,² Yulia Ivanova,² Ekaterina Loginicheva,² Karina Chmielewski,¹ Kelly M. Stewart,¹ Juliet Ashall,² Bart Everts,^{2,5} Edward J. Pearce,^{2,4} Edward M. Driggers,^{1,4,6,*} and Maxim N. Artyomov^{2,4,*}

¹Agios Pharmaceuticals, 38 Sidney Street, Cambridge, MA 02139, USA

²Department of Pathology & Immunology, Washington University in St. Louis, 660 S. Euclid Avenue, St. Louis, MO 63110, USA

³ITMO University, 49 Kronverksky Prospekt, Saint Petersburg 197101, Russia

⁴Co-senior author

⁵Present address: Department of Parasitology, Leiden University Medical Center, Albinusdreef 2, Leiden 2333 ZA, the Netherlands

⁶Present address: General Metabolics, 30 Arlington Street, Winchester, MA 01890, USA

*Correspondence: edward.driggers@generalmetabolics.com (E.M.D.), martyomov@pathology.wustl.edu (M.N.A.)

<http://dx.doi.org/10.1016/j.immuni.2015.02.005>

SUMMARY

Macrophage polarization involves a coordinated metabolic and transcriptional rewiring that is only partially understood. By using an integrated high-throughput transcriptional-metabolic profiling and analysis pipeline, we characterized systemic changes during murine macrophage M1 and M2 polarization. M2 polarization was found to activate glutamine catabolism and UDP-GlcNAc-associated modules. Correspondingly, glutamine deprivation or inhibition of N-glycosylation decreased M2 polarization and production of chemokine CCL22. In M1 macrophages, we identified a metabolic break at *ldh*, the enzyme that converts isocitrate to alpha-ketoglutarate, providing mechanistic explanation for TCA cycle fragmentation. ¹³C-tracer studies suggested the presence of an active variant of the aspartate-arginosuccinate shunt that compensated for this break. Consistently, inhibition of aspartate-aminotransferase, a key enzyme of the shunt, inhibited nitric oxide and interleukin-6 production in M1 macrophages, while promoting mitochondrial respiration. This systems approach provides a highly integrated picture of the physiological modules supporting macrophage polarization, identifying potential pharmacologic control points for both macrophage phenotypes.

INTRODUCTION

The ability to assume different activation states in response to environmental factors is critical to the role played by murine macrophages in a broad range of responses. Resting macrophages (M0) develop pro-inflammatory microbicidal and tumoricidal properties after stimulation with interferon- γ (IFN- γ) and

toll-like receptor (TLR) agonists (M1 or classical activation), but they will promote adipose tissue homeostasis and wound healing and mediate anti-helminth immune responses when stimulated with interleukin-4 (IL-4) and IL-13 (M2 or alternative activation). This phenotypic polarization of murine macrophages in response to their microenvironment is highly regulated at both transcriptional and metabolic levels (McGettrick and O'Neill, 2013; O'Neill and Hardie, 2013).

The metabolism of M1 macrophages is characterized by increased glycolytic flux and reduced mitochondrial oxidative phosphorylation compared to M0 cells (Rodríguez-Prados et al., 2010). This metabolic shift occurs in the context of an altered TCA cycle, which is needed to support the production of key M1 cellular products such as acetyl CoA (AcCoA), succinate, and nitric oxide (NO) (Tannahill et al., 2013). However, the precise metabolic flows that alter the mitochondrial activity and the corresponding compensatory mechanisms that maintain basic cellular metabolic functions in the absence of an active TCA cycling in M1 macrophages are unclear. Likewise, although it is understood that M2 activation is coupled to changes in polyamine synthesis, iron metabolism, and fatty acid oxidation (Biswas and Mantovani, 2012; Vats et al., 2006), we currently lack a systems-level understanding of central metabolic rewiring during alternative activation.

In principle, integration of top-down transcriptional and metabolic “omics” approaches provide a strategy for non-targeted characterization of systems-level changes, but two obstacles impede realization of such a strategy. First is the lack of parallel experimental approaches to enable synchronized metabolomic and transcriptional profiling on simultaneously prepared biomass; the throughput of current experimental approaches for metabolic profiling are typically quite low and require a considerable amount of input material, making it difficult to perform parallel sample preparation for transcriptional profiling. A second challenge is the uncertainty associated with integrating the two data types in a physiologically meaningful way that can be further validated through functional testing. Here, we introduce a combined experimental and computational pipeline, concordant metabolomics integration with transcription (CoMBI-T),

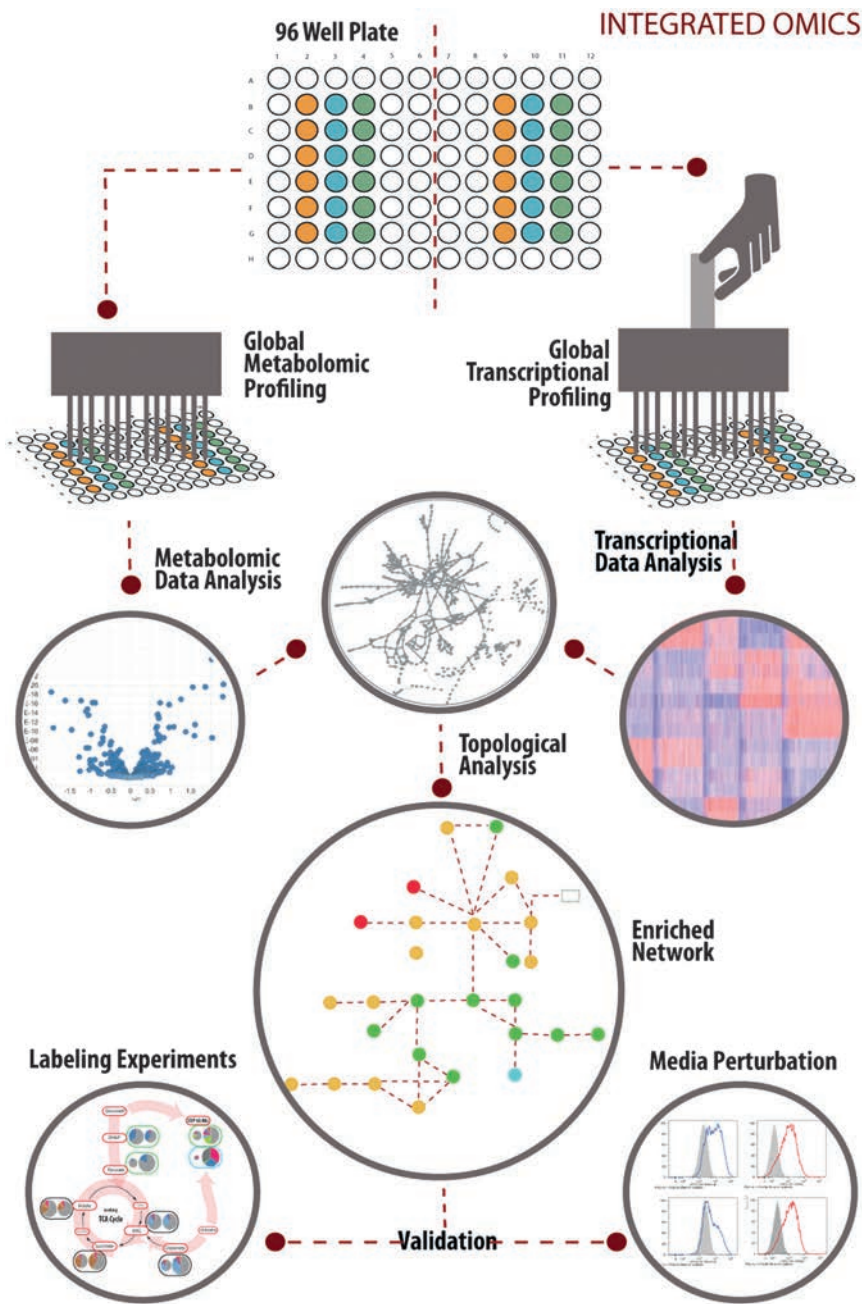


Figure 1. Integrated Metabolic-Transcriptional Profiling and Analysis Pipeline

Cells derived from the same culture batch are grown in 96-well plates, stimulated, then lysed and processed in 96-well format to collect global metabolic and RNA-seq-based transcriptional profiles. Individual datasets are then processed and differential regulation data are mapped onto a global metabolic network that includes both enzymes and metabolites. Integrated network analysis then identifies the most coordinately responsive subnetwork and uncovers novel points of metabolic rewiring during macrophage polarization. Predictions of CoMBI-T profiling analysis are then validated mechanistically through labeling experiments and through the effects of targeted media perturbation and pharmacologic agents on cell phenotype.

glutamine deprivation is shown to be associated with profound functional consequences in M2 macrophages, such as decreased chemokine *Ccl22* production. On the other hand, in M1 macrophages, CoMBI-T identified a metabolic interruption in the tricarboxylic acid (TCA) cycle carbon flow during M1 polarization, which was validated by isotope labeling. Based on that labeling data, we propose that a variant of the aspartate-arginosuccinate shunt connects the fragmented (ana-pleurotic) TCA cycle metabolites with NO production during the inflammatory response. Consistent with this model, inhibition of a key enzyme in the shunt, aspartate aminotransferase (AAT), led to decreased NO production and increased oxygen consumption rates (OCR) due to mitochondrial respiration in M1 macrophages. Overall, our data and analysis provide a comprehensive view of the integrated transcriptional and central metabolic changes during murine macrophage polarization, yielding a deeper contextual understanding of established polarization markers, while simultaneously uncovering

that overcomes these challenges and provides a non-targeted systems-level characterization of coordinated transcriptional and metabolic rewiring during the macrophage polarization process. This approach identified statistically significant modules within the metabo-transcriptional network that contribute to and define M1 versus M2 polarization, which were functionally validated via a combination of targeted media perturbations, pharmacological inhibition, and ^{13}C -glucose and ^{13}C - and ^{15}N -glutamine labeling experiments. In M2-polarized macrophages, CoMBI-T reveals involvement of two new previously uncharacterized modules: a glutamine-associated module and a UDP-GlcNAc-associated module. Perturbation of either of these pathways led to impairment of M2 polarization. Furthermore,

targets for pharmacological intervention and control of the polarization process.

RESULTS

CoMBI-T Data Acquisition: Parallel High-Throughput Metabolic and Transcriptional Profiling

The CoMBI-T pipeline to generate and integrate mass spectrometry-based metabolic profiling with RNA-seq-based transcriptional profiling data sets is shown schematically in Figure 1. To provide the raw biological material for the data acquisition, bone marrow cells were isolated from a single mouse and seeded into 96-well plates as described previously (Everts

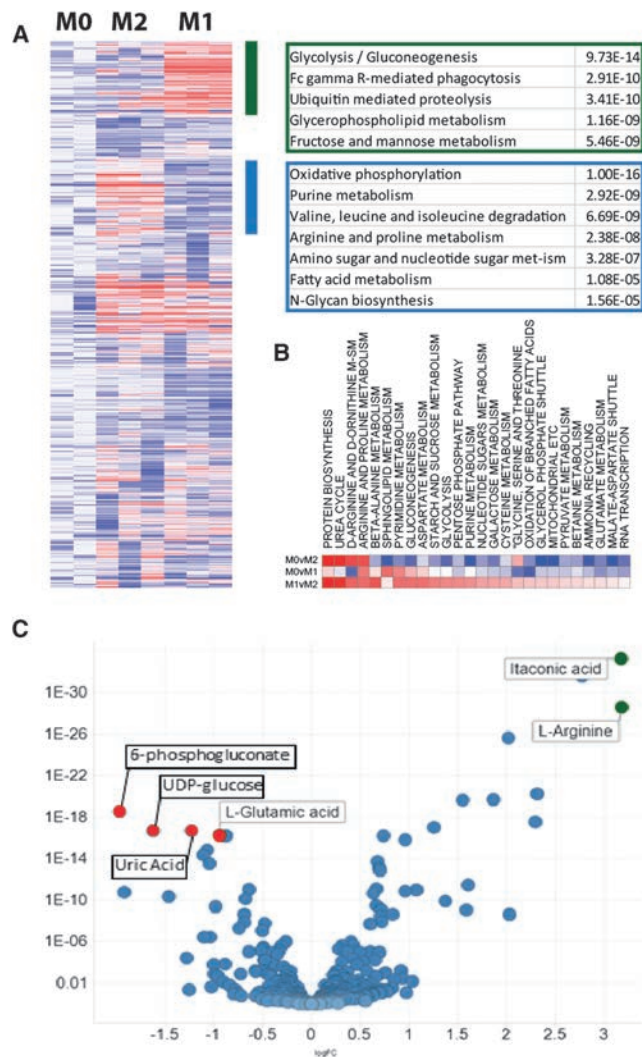


Figure 2. Knowledge-Based Pathway Analysis of Metabolic and Transcriptional Data

(A) Pathway analysis of enzymes that are transcriptionally upregulated in M1 or M2 states. Green bar points to the enzymes upregulated in M1 conditions (blue for M2) and corresponding enriched pathways are listed in the green box on the right (blue for M2).

(B) Pathway enrichment analysis across metabolome profiling data shows KEGG pathways that are differentially regulated between all possible pairs of conditions (M1 versus M0, M2 versus M0, M1 versus M2).

(C) Volcano plot shows metabolites differentially expressed between M1 and M2 conditions. x axis shows log-fold change between M1 and M2 conditions with positive values corresponding to metabolites upregulated in M1 macrophages. y axis shows p value for corresponding metabolite. Top M1-specific metabolites (itaconate and arginine) are highlighted in green, and top M2-specific metabolites are marked as red circles.

et al., 2014). At day 7, the bone-marrow-derived macrophages (BMDMs) were stimulated with either lipopolysaccharide (LPS) and IFN- γ or IL-4 treatment for 24 hr to obtain M1- and M2-polarized cells (respectively, as confirmed by expression of major markers such as *Ii12b*, *Nos2*, *Arg1*, etc.). Cultures destined for either of the two analyses were treated identically until cells were lysed for metabolite and RNA extractions, providing mini-

mal divergence in cell handling and maximum degree of consistency between metabolic and transcriptional profiles. To obtain metabolic profiles, we used a non-targeted, flow-injection-analysis (FIA) mass spectrometry (MS) method (Fuhrer et al., 2011), enabling broad metabolite coverage between 50 and 1,000 daltons and yielding quantitative information on approximately 10,000 MS spectral features (Fuhrer et al., 2011), of which approximately 2,200 were annotated as high-confidence metabolites in these studies. For transcriptional profiling, we used 3' end focused RNA sequencing with a barcode-first strategy that allows sample pooling at the cDNA stage, improving sensitivity and consistency between samples and allowing construction of a high-throughput library from material extracted from cell lysates in a single well of a 96-well plate (Sojka et al., 2014) (Experimental Procedures). Overall, we analyzed five and three bio-replicates per condition for metabolic and transcriptional profiles, respectively.

CoMBI-T Analysis: Network-Based Integration of High-Throughput Metabolic and Transcriptional Profiles

To date, predictive powers of integrated analysis have been tested only to a very limited degree, largely due to a lack of large-scale, parallel metabo-transcriptional datasets. Overall, analytical strategies used for integration of metabolic and transcriptional data can be broadly divided into two major classes: modifications of constraint-based models (such as flux balance analysis) (Bordbar et al., 2012; Patil and Nielsen, 2005) and network-based approaches (Beisser et al., 2012; Zhu et al., 2012). In order to leverage the large metabolite coverage achieved in our profiling experiments, we adopted a network-based strategy that integrates the power of both transcriptional and metabolic profiles while minimizing the drawbacks inherent to each dataset with respect to computational analysis. For instance, metabolic profiling often has a high false negative rate, being neither exhaustive nor adequately sensitive for low-abundance metabolites. Nevertheless, metabolism is described by a relatively well-defined network, capturing the interconversion of various metabolites in a framework particularly suitable for systems-scale analysis. The opposite is true for transcriptional data: RNA-seq profiling provides an exhaustive list of mature transcripts, but their corresponding regulatory networks are defined very loosely, limiting the ability to follow causal relationships. Our integration strategy seeks to identify functional modules characteristic to the M1 and M2 states based on proximity of differentially regulated metabolites and enzymes in the global metabolic network. Such core subnetworks typically consist of combinations of metabolites and enzymes from multiple canonical metabolic pathways (see examples below) and provide relatively unbiased characterization of metabolic changes in the system of interest.

As such, this approach differs from the typical knowledge-based pathway enrichment analysis (PEA) because it allows the capture of major routes of metabolic rewiring that occur on a global level but that do not necessarily follow known definitions of pathways. For instance, pathway analysis of obtained metabolic and transcriptional profiles (Figure 2A) revealed a combination of known pathways regulating macrophage polarization without specific understanding of functional interconnections between them. Genes involved in glycolysis and phospholipid

metabolism, differentially expressed between M1 (LPS + IFN- γ stimulation) and M2 (IL-4 stimulation) macrophages, are major distinguishing features of inflammatory (M1) macrophages, whereas oxidative phosphorylation, purine synthesis, arginine, and nucleotide sugar metabolism are enhanced in M2 macrophages. Global metabolic changes showed differential regulation of glycolysis/gluconeogenesis, urea cycle, arginine, mitochondrial, and fatty acid metabolism (Figure 2B). However, the interpretative utility of these findings is severely limited because the interconnections between these pathways are not revealed even though macrophage polarization requires them to be globally coordinated. Furthermore, pathway-based analysis fails to account for many of the most differentially expressed metabolites: in M1 macrophages itaconic acid (Figure 2C, green circle) is currently not annotated to be the part of any individual pathway, and a number of the most altered M2 metabolites such as UDP-glucose and 6-phosphogluconate (Figure 2C, red circles) are not associated with any of the enriched pathways. Finally, pathway analyses that are carried out on the individual levels of regulation (whether transcriptional or metabolic) inherently fail to leverage the notion of coherent changes between these regulatory events, diminishing their power to identify important regulators of metabolic rewiring.

In order to address these issues, we constructed a global murine cellular reaction network (CRN) that connects \sim 3,000 metabolites and corresponding enzymes based on the latest edition of the KEGG database (Kanehisa et al., 2012) (see Experimental Procedures). We then sought the most differentially regulated subnetwork (typically of the size \sim 100 nodes) within the CRN, accounting for both the nodal connectivity and the degree of differential expression of metabolites and enzymes in the network. We first assign weights to nodes in the global cellular reaction network: differential expression p values for M1 versus M2 comparison were transformed to enzymatic node weights, and differential intensity p values of metabolites corresponded to metabolic node weights. By structuring the CRN in this manner, we were able to apply the BioNet algorithm (Beisser et al., 2010), developed for integration of protein-protein interaction databases with microarray datasets, to identify the most differentially regulated network as a maximum-weight connected subgraph (MWCS) problem (Figure 3; Experimental Procedures). Overall, CoMBI-T analysis indicated that divergent macrophage polarization is characterized by significant differences in three metabo-transcriptional modules (the UDP-GlcNAc biosynthesis module, a glutamine/glutamate-associated module in M2 macrophages, and an *ldh*-centered TCA pathway break-point coupled with dramatic itaconate production in M1-polarized macrophages) that together with known regulatory pathways make up a densely connected core that governs macrophage metabolic response to polarization stimuli (Figure 3). Next, we sought to investigate the function of these modules in greater detail.

CoMBI-T Reveals Increased UDP-GlcNAc Synthesis as a Critical Feature of M2 Polarization

CoMBI-T identified two previously unreported M2-specific metabolic modules. First, increased amino sugar and nucleotide sugar metabolism, characterized by high levels of UDP-GlcNAc, UDP-glucose, and UDP-glucuronate, and corresponding tran-

scriptional upregulation of enzymes involved in the production of these intermediates (e.g., *Enpp1*, *Pgm1*), were observed in M2 macrophages (Figure 3). To validate that this module is indeed metabolically active in M2-polarized macrophages, we traced the fate of ^{13}C -glucose and ^{13}C -glutamine in M2 cells to the intermediates of these pathways. Labeling distribution analyses revealed partially labeled forms of TCA metabolites (malate, citrate, AKG, succinate) in M0 and M2 macrophages (Figure 4A), reflecting reported active oxygen consumption rates and complete TCA cycling in M2 macrophages (Haschemi et al., 2012). Consistent with the known hexosamine biosynthetic route, we found glucose and glutamine as the major sources of carbon and nitrogen, respectively, in UDP-GlcNAc, an important intermediate that links signaling to metabolism (Figure 4A; Wellen and Thompson, 2012; Yi et al., 2012). Together with transcriptional upregulation of steps in the N-glycan pathway revealed through pathway enrichment analysis (see Figure 2A), this observation suggests the importance of N-glycosylation in M2 macrophages. It is well established that highly glycosylated lectin/mannose receptors are among the most typical M2 polarization markers (Sica and Mantovani, 2012). We investigated the functional importance of the UDP-GlcNAc pathway by asking directly whether N-glycosylation plays a role in M2 activation. Accordingly, we stimulated macrophages with IL-4 in the presence or absence of the N-glycosylation inhibitor tunicamycin (Varki, 2009). We found that tunicamycin significantly inhibited expression of the canonical M2 activation markers *Relm α* (Figure 4B), *CD206*, and *CD301* (Figure 4C), only mildly affecting M1 polarization as measured by inducible nitric oxide synthase (*iNOS*) protein expression (Figure S1A) or regulation of major M1-specific cytokines (Figure S1B). Similarly, M2-specific defects were observed when we inhibited the hexosamine pathway via glucosamine (Figure S1C; Koch et al., 1979). Thus, the UDP-GlcNAc synthesis pathway identified by CoMBI-T as being upregulated in M2 macrophages plays a direct, specific, and critical role in the M2 polarization process.

CoMBI-T Reveals Glutamine Metabolism as a Characteristic Feature of M2 Polarization

The second M2-specific module revealed by CoMBI-T was centered on glutamate management and included glutamate, AKG, ornithine, and corresponding transcripts of *Gatm*, *Arg1*, *Oat*, *Got2*, and *Gpt2* as well as several other closely related transcripts and metabolites (Figure 3). This result together with the participation of glutamine in supporting an active TCA cycle and providing structural features for UDP-GlcNAc synthesis led us to hypothesize that this amino acid plays a crucial, specific role in M2 polarization. The extent of glutamine dependence in M2 macrophages was suggested by the fact that a third of all carbons in TCA metabolites in M2 cells originated from glutamine (versus \sim 20% for M1) and that within 4 hr of addition of ^{15}N -labeled glutamine, more than half of the nitrogen in UDP-GlcNAc derived from glutamine (Figure 4A). To functionally validate these findings from CoMBI-T, we transiently (for 4 hr prior to stimulation) deprived macrophages of glutamine and assessed M2 commitment, using expression of *CD206*, *CD301*, and *Relm α* as markers of M2 activation. We found that glutamine deprivation had a substantial effect on M2 polarization, reducing the committed population by

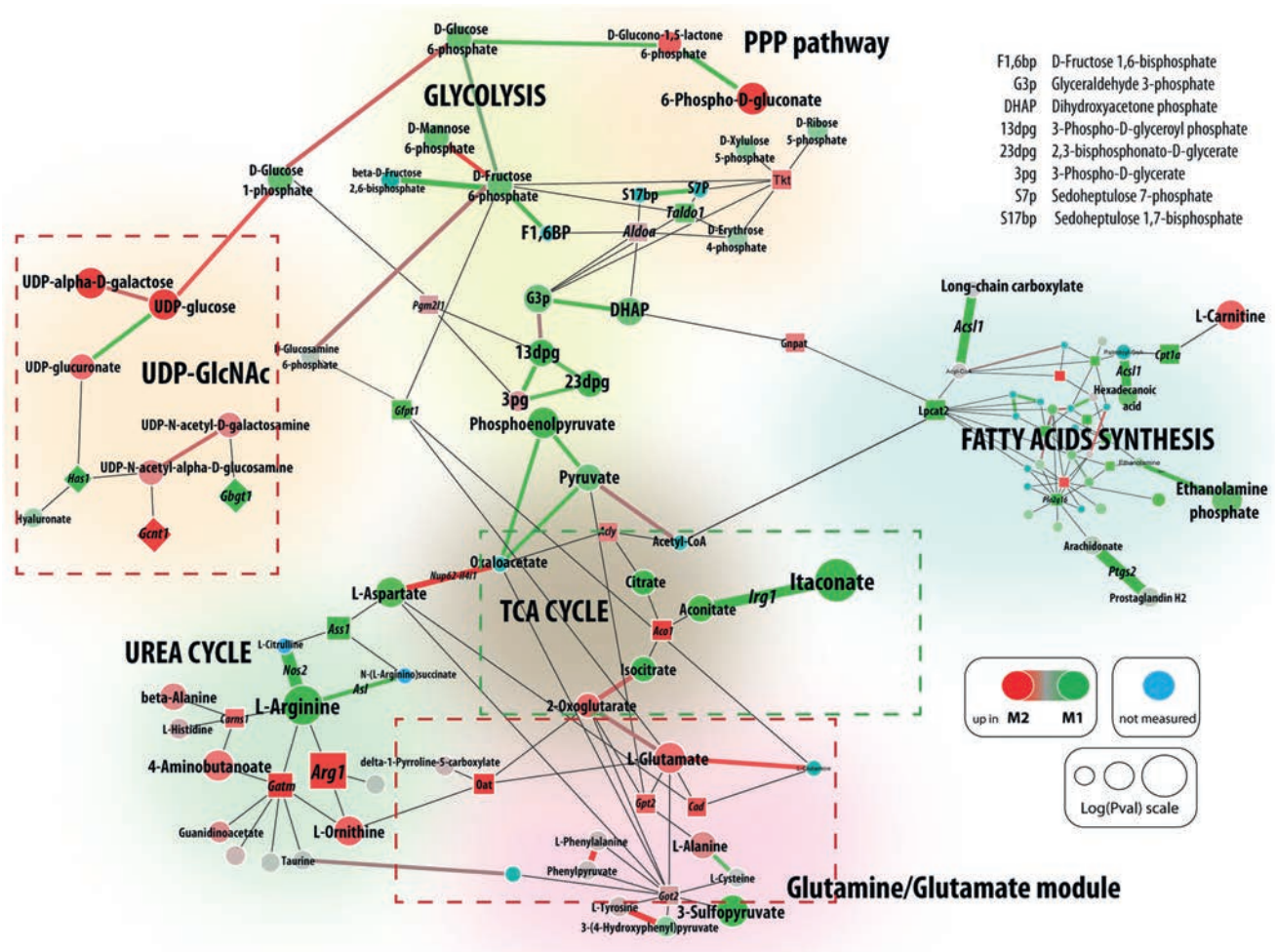


Figure 3. Major Metabolic Modules Are Rewired during Macrophage Polarization

CoMBI-T reveals the most regulated subnetwork within global murine metabolic network that consists of more than 2,000 enzymes and metabolites measured through the CoMBI-T profiling pipeline. For comparison between M1- and M2-polarized macrophages, the most regulated metabolic subnetwork encompasses seven distinct modules highlighted by distinct background shading. Three major novel features of macrophage polarization identified by CoMBI-T are highlighted with dotted line squares—green for M1-specific module and red for M2. Round nodes represent metabolites within core regulatory network. Enzymes are represented by square nodes. Differential expression of corresponding enzyme/metabolite is indicated by the size of the node, and fold-change by red (M2) to green (M1) color scale. Enzymes in reactions with single product-substrate pair are represented by thick edges for visual convenience with thickness and color of the edge reflecting $-\log(p)$ and fold-change of differential expression correspondingly. For visual convenience, nodes of fatty acid synthesis module are not labeled. The complete metabolomic data used for CoMBI-T are available in Table S1.

about 50% (Figure 5A), whereas removal of glutamine had no effect on capacity for M1 polarization as measured by *Nos2* up-regulation (Figure 5B).

We next sought to determine specific functional defects in M2-polarized macrophages due to glutamine deprivation. We obtained transcriptional profiles for macrophages polarized in either complete media or in glutamine-deprived media and found that most of the differentially expressed transcripts that are downregulated upon glutamine withdrawal are M2-specific marker genes, including *Irf4*, *Klf4*, *Ccl22*, and *Ii4i1*. Notably, glutamine-deprived M2 macrophages exhibited a distinctly downregulated transcriptional signature of TCA cycle activity (Figure 5C) when compared to M2 macrophages polarized in full media, thus providing support for a causal link between glutamine usage, regulation of oxidative phosphorylation, and

M2 polarization, as opposed to other possibilities such as an effect via the mTOR pathway (Byles et al., 2013), which was not regulated upon glutamine deprivation (Figures S2A–S2C). This is consistent with literature reporting that transient glutamine deprivation in a human cell line led to perturbation of TCA cycle and autophagy as opposed to the activation of mTOR signaling typically seen in more severe starvation conditions (Shanware et al., 2014). Strikingly, the chemokine pathway (Figure S2B) was found to be among those most downregulated upon glutamine deprivation, and therefore we tested the effect of glutamine depletion on production of CCL22, because expression of the encoding gene *Ccl22* is markedly upregulated in M2 macrophages and it is the second most-downregulated transcript upon glutamine deprivation ($p = 10^{-57}$; Figure 5D, in red are shown transcripts that are

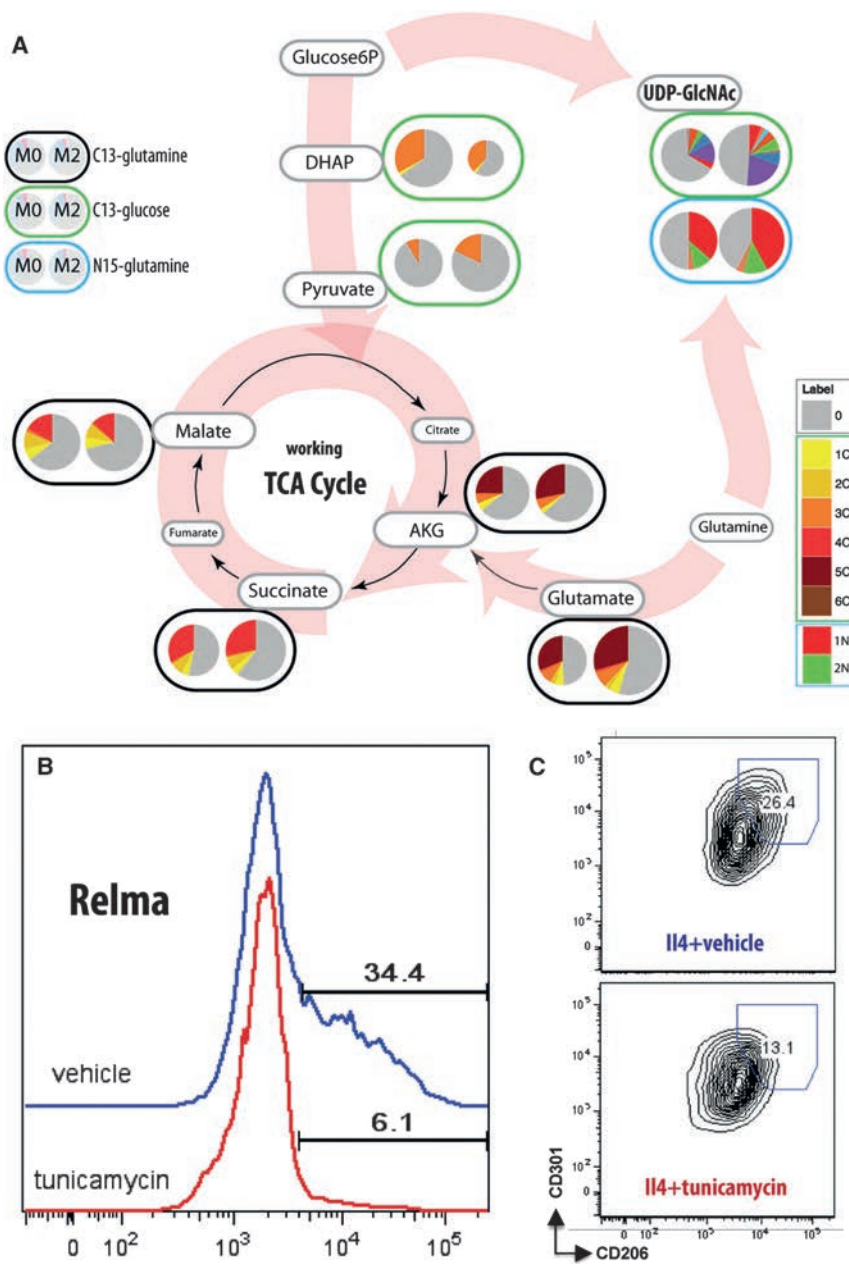


Figure 4. Labeling and Pharmacological Inhibition Experiments Validate the Critical Role of UDP-GlcNAc Pathway in M2 Polarization

(A) U-¹³C glucose (green outline) and U-¹³C (black outline), ¹⁵N₂ (blue outline) glutamine were used as media for unstimulated/II4-stimulated macrophages. Circle sizes are scaled with respect to pool sizes for individual metabolites in each condition. Exact labeling distributions and patterns are detailed in Table S2 for each metabolite. Thin black arrows represent known metabolic pathway connections; background arrows indicate deduced major metabolic flows in M2 macrophages.

(B and C) Results of inhibition of N-glycosylation by tunicamycin: in the presence of the inhibitor, M2 commitment is significantly blocked by both Relm α (B) and CD206-CD301 staining (C).

(Biswas and Mantovani, 2012) and associated defects in the TCA cycle. However, the specific mechanism leading to such mitochondrial dysfunction is not understood. CoMBI-T analysis revealed a potential breakpoint in the metabolic flow of the TCA cycle at the isocitrate-to-oxoglutarate (AKG) conversion, which was specific to M1 versus M2 macrophages (Figure 3, green square). This effect was characterized by a significantly increased pool of (iso)citrate and decreased pool of AKG (the ratio of (iso)citrate:AKG is ~3 times higher in M1 compared to M0; Table S2) and was accompanied by significant transcriptional downregulation of *Idh1*, the enzyme that interconverts these two metabolites (7-fold decrease in M1). To further validate that this alteration of citrate and AKG steady-state levels results from reduced flow through IDH, we performed stable isotopic labeling experiments, tracing the fate of ¹³C-labels from U-¹³C-glucose and U-¹³C-glutamine in M1 macrophages with a single time point

M2-specific up- or downregulated markers). Accordingly, secreted protein levels of CCL22 was lower in supernatants of M2 macrophages activated in the absence of glutamine compared to in complete medium, reflecting a marked and M2-specific downstream functional defect due to media perturbation (Figure 5E). The CCR2 transcript was expressed in only low amounts basally, and hence differential transcript expression did not translate to differences in surface protein expression (Figure S2D).

TCA Breakpoint at IDH Coupled with Itaconate Synthesis Is a Major Feature of M1 Polarization

One of the major metabolic signatures of macrophage activation upon LPS stimulation is a defect in overall mitochondrial function

analysis to estimate relative rates of accumulation (4 hr labeling time). Consistent with CoMBI-T results, we observed that ~20% of citrate was synthesized from glucose, whereas the AKG pool accumulated 0% glucose-derived carbon labeling at the 4 hr time point (Figure 6). Carbon flow from glutamine to AKG was detectable in M1 macrophages (Figure 6: 10%–12% U-¹³C-AKG from U-¹³C-glutamine after 4 hr labeling), yet still significantly smaller than in the M0 state, where ~25% of the AKG pool acquired uniform labeling. Of note, partially labeled forms in the AKG pool present in M0 state reflective of active TCA cycling disappeared from the AKG pool in M1 macrophages (Figure 6, pie charts in black and green ovals next to AKG). Such a lack of partial labeling indicates interrupted TCA cycle activity and provides a mechanistic explanation for the

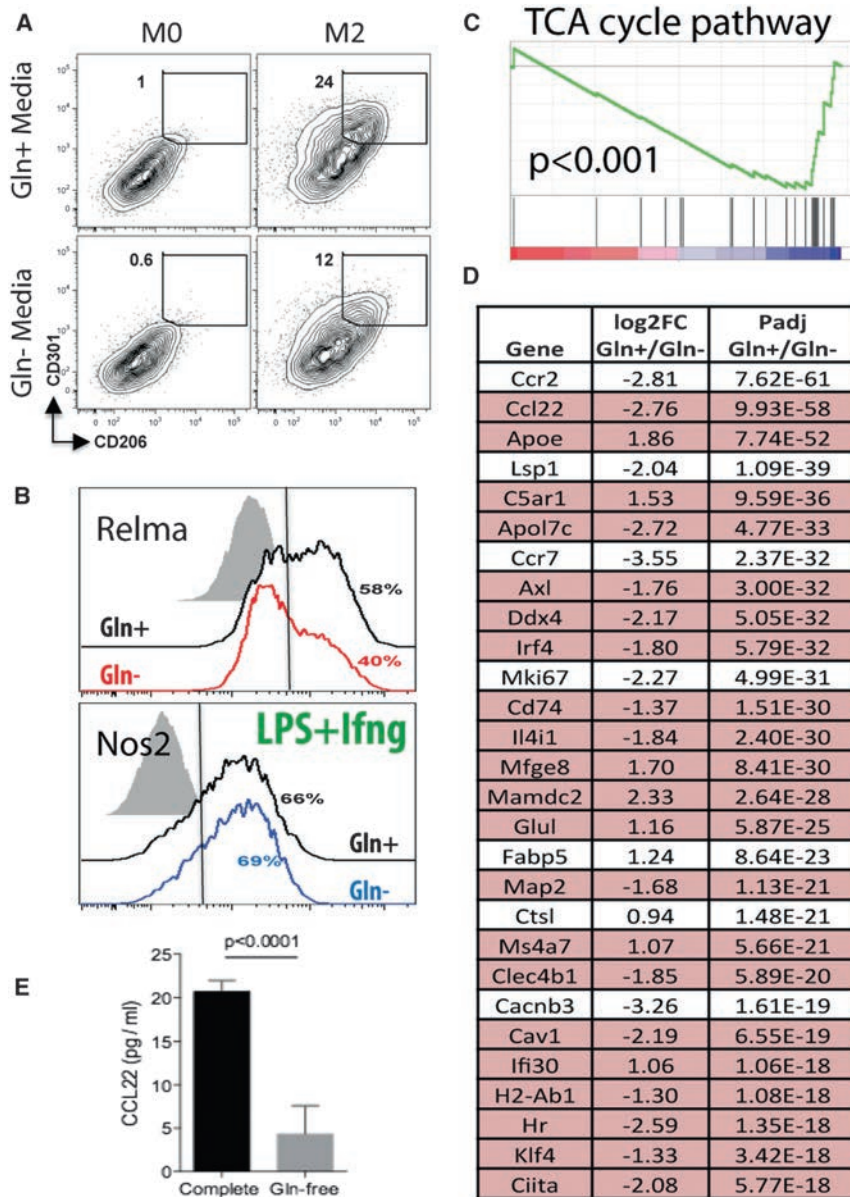


Figure 5. Labeling and Media Perturbation Experiments Validate the Critical Role of Glutamine in M2 Polarization

(A) Glutamine deprivation shows significant (~50%) defect in M2 commitment in glutamine-deprived media based on CD301-CD206.

(B) Relm α staining and Nos2 upregulation indicate a comparative lack of effect for glutamine deprivation on M1 versus M2 commitment.

(C) Gene set enrichment analysis identifies significant transcriptional downregulation of TCA cycle.

(D) Top 30 differentially expressed genes between M2 macrophages polarized in full media versus glutamine-deprived media. Corresponding p values are shown for glutamine-no glutamine M2 macrophages, genes that are statistically different between M0 and M2 macrophages are indicated in red.

(E) Serum protein production of M2-specific chemokine CCL22 are downregulated when macrophages are polarized in glutamine-deprived conditions (error bars computed based on at least three independent experiments).

Inflammatory Aspartate-Argininosuccinate Shunt Connects Anapleurosis of the TCA Cycle and NO Synthesis

The U-¹³C-glutamine tracing experiments suggested an additional breakpoint in the TCA for M1 macrophages (Figure 7A). After 4 hr of labeling, initiated after 20 hr of exposure to LPS, approximately 35% of the succinate pool but only 22% of malate can be attributed to glutamine in M1s, as opposed to comparable labeling of these metabolites in M0 conditions (~39% and ~35%, respectively, Figure 7A). Additionally, the total pool of malate increased significantly in M1 conditions contrary to the only moderate increase in the steady-state concentration of succinate (see relative M0/M1 sizes of pie charts in Figure 7A).

These data together suggest that the succinate-to-fumarate transition in M1 cells is not as efficient as it is in M0 macrophages, and there might be an alternative route for malate accumulation. Further examination revealed that the glutamine carbon-labeling pattern and M0/M1 pool ratio for malate were strikingly consistent to those observed for argininosuccinate, aspartate, and citrate (Figure 7A; Table S2). Such conserved labeling distribution patterns are characteristic of metabolites partaking in common metabolic cycles, in which pool sizes and labels are equilibrated among all members of the cycle, as illustrated by TCA cycle metabolites in M0 and M2 macrophages (Figure 4A). Notably, aspartate, argininosuccinate, malate, and fumarate are common components of the aspartate-argininosuccinate shunt (Lehninger et al., 2008), a set of transformations connecting the TCA cycle with the urea cycle (Allen et al., 2011), with active ornithine-to-citrulline conversion. An inflammation-associated version of this shunt would account for the observed

reports of mitochondrial dysfunction in M1 state. Notably, reverse flow at *Idh* is also undetectably low based on the absence of 5 carbon label from glutamine feed in citrate (from 5-labeled AKG).

It is important to point out that in the context of greatly reduced *Idh* activity and associated reduction of carbon flow to AKG, citric acid is redirected to serve as a precursor for itaconic acid synthesis, an important anti-microbial metabolite identified recently (Michelucci et al., 2013). Our U-¹³C-glucose and U-¹³C-glutamine labeling studies here are consistent with citrate serving as the direct chemical source for itaconic acid (Figure 6). Further supporting this possibility, we found *Irg1*, which encodes the enzyme catalyzing the aconitate-to-itaconate reaction (Michelucci et al., 2013), to be one of the most up-regulated transcripts in M1 relative to M0 macrophages (Figure 3).

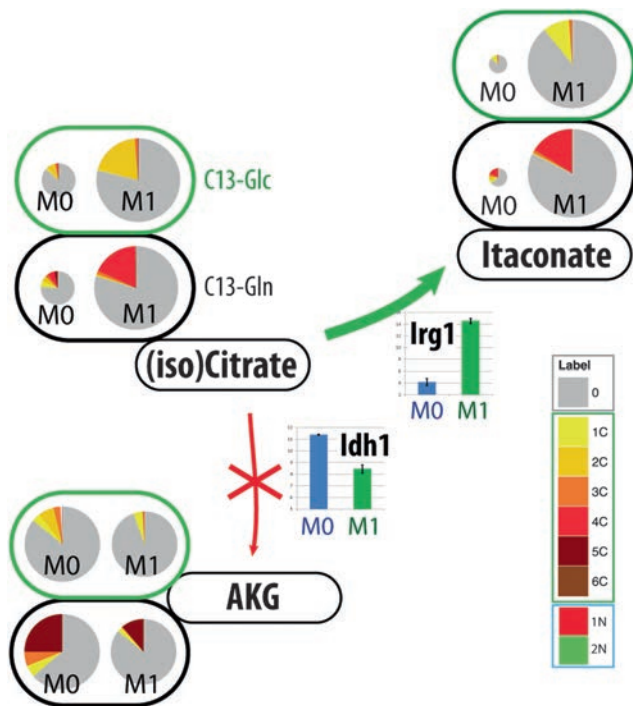


Figure 6. A Breakpoint in TCA Cycle Is a Major Metabolic Marker of Macrophage M1 Polarization

Labeling data show that (iso)citrate labeled by glucose does not transfer carbon to AKG in M1 macrophages, consistently with transcriptional downregulation of *Idh1*, resulting in isocitrate-to-2-oxoglutarate (AKG) transition blocked in M1-activated macrophages.

labeling patterns in these TCA intermediates and amino acids in M1 macrophages, connecting the TCA cycle metabolites with the NO cycle.

To functionally validate the importance of this apparent aspartate-arginosuccinate shunt, we pharmacologically inhibited the aspartate aminotransferase *Got1* (marked with lightning in Figure 7A) by using aminooxyacetic acid (AOAA) (Kauppinen et al., 1987). As expected from the U-¹³C-glutamine labeling results, pretreatment with AOAA at concentrations ranging from 1 to 10 μM inhibited M1 polarization as measured by NO production (Figure 7B) and by iNOS expression (Figure S3A, left) in a dose-dependent manner, although it did not affect macrophage viability (Figure S3B). Because NO production plays a role in the suppression of mitochondrial respiration in TLR-agonist-activated dendritic cells (Everts et al., 2012), we asked whether oxygen consumption rates (OCRs) increased in AOAA-treated M1 macrophages in which NO production was inhibited. As expected, untreated M1 macrophages exhibited very little mitochondrion-dependent (rotenone- and antimycin-inhibitable) oxygen consumption, and rather had very high, compensatory extracellular acidification rates (ECARs), a mark of exaggerated aerobic glycolysis (Everts et al., 2012). In contrast, M1 macrophages in which *Got1/2* was inhibited retained mitochondrial respiratory function and exhibited ECARs similar to M0 macrophages (Figure 7C). This observation could reflect an inability of macrophages to execute anapleurosis of the TCA cycle in the presence of NO-based inhibition of succinate dehydroge-

nase if there is no proper balancing mechanism provided by the aspartate-aminotransferase as a part of aspartate-arginosuccinate shunt. Furthermore, we observe that perturbation of the shunt leads to profound functional consequences, such as a defect in inflammatory cytokine production, e.g., IL6 (Figure 7B, right).

CoMBI-T Provides Insight into Redox Balance Regulation in M1-Polarized Macrophages

A related aspect of de novo fatty acid synthesis and the production of NO is the significant stoichiometric demand for nicotinamide adenine dinucleotide phosphate (NADPH) in these processes (Knowles and Moncada, 1994). Another NADPH-demanding process is the regulation of reactive oxygen species (ROS) levels, mediated in M1 macrophages by *Cybb*-encoded NADPH oxidase (*Nox2*), which we found to be transcriptionally upregulated in M1 macrophages and downregulated in M2 cells (Figure S4). Downregulation of *Idh* in M1-polarized cells compromises one of the sources for NADPH (Geisbrecht and Gould, 1999). In the context of macrophage polarization, two major sources of NADPH production are typically discussed: conversion of malate to pyruvate by malic enzyme and the oxidative branch of the pentose phosphate pathway (PPP), which was previously shown to play a role in macrophage polarization (Haschemi et al., 2012) and is also one of the seven M1 versus M2 defining modules identified by CoMBI-T (Figure 3). In our data, we did not detect signatures of malic enzyme activity in M1 macrophages, corresponding to labeled pyruvate or lactate from U-¹³C-glutamine (Figures S5A and S5B). We did, however, confirm significant carbon flow through the oxidative arm of PPP (Haschemi et al., 2012) in M1 macrophages by using ¹³C-glucose carbon tracing experiments, finding that both the total pool of pentose-5-phosphates and their labeled fraction increased significantly in M1 relative to M0 cells (Figure S5C). In addition to the previously described role of *Cark1* (Haschemi et al., 2012), metabolic and transcriptional regulation of the PPP pathway was indicated by the relation of levels of early PPP metabolites (D-Glucono-1,5-lactone 6-phosphate and 6-Phospho-D-gluconate, Figure 3) and transcriptional regulation of the downstream enzyme *Pgd* that converts 6-Phospho-D-gluconate to ribulose-5P. *Pgd*'s upregulation under M1 conditions (Figure S6A) is consistent with increased flux through the PPP, leading to a decrease in steady-state levels of early PPP metabolites relative to levels in M0 and M2 cells (hence, these metabolites are marked in red in Figure 3). These effects of oxidative stress are typically counterbalanced by reducing agents such as glutathione, and indeed, we observed coordinated transcriptional regulation of glutathione reductase (*Gsr*, upregulated in M1 cells) and glutathione peroxidase (*Gpx1*, downregulated in M1 cells) (Figure S6B), which was consistent with labeling data showing increased labeling of oxidized glutathione by glutamine-derived carbon in M1, but not M2, macrophages (Figure S6C).

DISCUSSION

In this work, we developed a pipeline for high-throughput parallel metabolic and transcriptional data profiling with integration of these datasets that allows non-targeted identification of

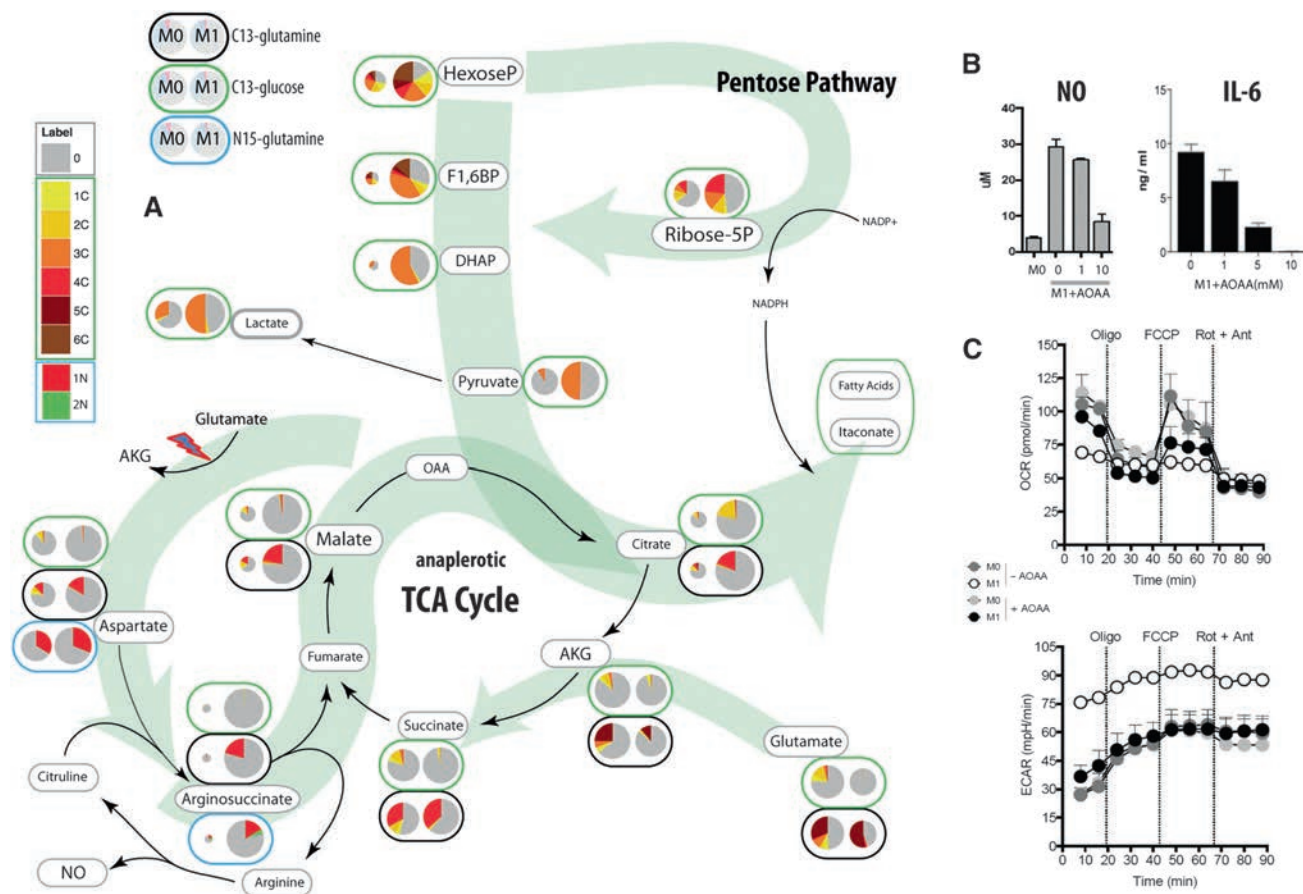


Figure 7. Labeling Data Reveal an Inflammatory Version of the Aspartate-Arginosuccinate Shunt in M1-Polarized Macrophages

(A) U-¹³C glucose (green outline), U-¹⁵N₂-glutamine (blue outline), and U-¹³C glucose (black outline) were used as media for unstimulated and M1-stimulated macrophages. Circle sizes are scaled with respect to pool sizes for individual metabolites in each condition. Exact labeling distributions and patterns are detailed in Table S2 for each metabolite.

(B) Inhibition of Got1/2 (aspartate-aminotransferase, marked with lightning sign in A) with AOAA decreases nitric oxide and IL-6 production in a dose-dependent manner without affecting macrophage viability (Figure S3B) (error bars computed based on at least three independent experiments).

(C) SeaHorse data on oxygen consumption rate (OCR) and extracellular acidification rates (ECAR), both rotenone and antimycin inhibited, and very high, compensatory M1 macrophages in which Got1/2 was inhibited, retain mitochondrial respiratory function (top), and exhibited ECARs similar to M0 macrophages (bottom).

regulated metabolic modules. We applied this approach to uncover an integrated global picture of the metabolic rewiring that characterizes macrophage polarization and revealed a set of known and novel modules that define the M1- and M2-polarized states, including the UDP-GlcNAc biosynthesis pathway, glutamine-related pathway flows, an M1-specific TCA cycle breakpoint at *ldh*, and the engagement of aspartate-arginosuccinate shunt to balance carbon flow in the presence of NO production. We additionally confirmed previously recognized metabolic features, such as elevated glycolytic activity and reduction in oxidative phosphorylation activity upon polarization to M1, which are metabolically consistent with, and gain mechanistic context from, our findings of flux discontinuity within the canonical TCA cycle (at *ldh* and succinate dehydrogenase). The discontinuity at *ldh* is evident at both the transcriptional and the steady-state metabolic level and was confirmed by the pathway flow studies. The metabolic role of this pathway flow constriction downstream of isocitrate, in parallel with high carbon flow into the TCA up-

stream of citrate, appears to be the metabolic mechanism to enable significant production of large pools of fatty acids and itaconate, which exhibits a labeling pattern identical with its upstream precursors citrate/isocitrate (the LCMS methods used here do not distinguish the two citrate isomers). Itaconate itself was recently described as an important anti-microbial agent, disrupting the glyoxylate shunt, a pathway used in some pathogens (e.g., *Mycobacterium tuberculosis*) but not mammalian cells (Michelucci et al., 2013). The significance of flux re-direction in M1 macrophages at the level of citrate/aconitate is also evident from recent studies, where knock-down of the mitochondrial citrate carrier was shown to lead to defects in macrophage activation in response to LPS (Infantino et al., 2011; O'Neill, 2011) due to blocking production of cytosolic AcCoA. Overall, our data show that the module embodying citrate/isocitrate, *Irg1*, and itaconate constitutes a systems-level marker of M1 polarization that is at least as robust as the well-established *Cox2*-PGE2 and *iNOS*-NO transcriptional-metabolic duos (see Figure 3).

Analysis of labeling patterns in M1 macrophages supports a role for the aspartate-arginosuccinate shunt in coordinating the NO cycle with anapleurosis of the TCA cycle. Such a route of anapleurosis would likely be necessary in the context of a TCA break-point at succinate dehydrogenase. Note that the flow from aspartate to oxaloacetate via aspartate transaminase replenishes the cycle immediately downstream of this break and provides substrate for citrate synthase to handle an increased flux producing itaconic acid from the same carbon skeleton. Functionally, inhibition of aspartate transaminase led to a decrease in NO production and the maintenance of mitochondrial respiration, a finding that is consistent with the known inhibitory effects of NO on the electron transport chain (Everts et al., 2012). The ability of AOAA to inhibit NO production has been previously demonstrated for astrocytes (Schmidlin and Wiesinger, 1998), where the transamination inhibitor eliminates flow from the aspartate nitrogen to citrulline and the citrulline-arginine-NO cycle. These findings indicate that the aspartate-arginosuccinate shunt might be an adaptation to the fact that NO, a major effector molecule of M1 macrophages, competes with oxygen to inhibit complex II of the electron transport chain and, by doing so, attenuates succinate-to-fumarate conversion creating the aforementioned second break-point in the TCA cycle (Stadler et al., 1991). Furthermore, the presence of this break point would be consistent with the release of succinate from the local metabolic network, enabling it to participate in signaling pathways that are central to M1 polarization such as IL-1 β induction (Tannahill et al., 2013).

CoMBI-T analysis allowed us to identify two pathways critical for M2 polarization: glutamine-related metabolism and the UDP-GlcNAc pathway. These features of M2 polarization have, to the best of our knowledge, not been discussed previously. We found that transient glutamine deprivation had negative effects on the M2 activation program, which was associated with its effects on the TCA cycle. mTOR signaling has been shown to regulate macrophage polarization (Byles et al., 2013) and prolonged or harsher starvation conditions will probably lead to an interesting interplay between macrophage polarization, metabolism, and mTOR signaling, which is an exciting avenue for future exploration. Moreover, targeted inhibition of N-glycosylation, a pathway highlighted in M2 macrophages and one that requires UDP-GlcNAc as a sugar donor, also inhibited M2 activation (as measured by Relm α , CD206, and CD301 expression). This finding, which could reflect the requirement for N-glycosylation to correctly fold and traffic proteins such as Relm α , CD206, and CD301, which are destined for export to the cell surface, or for secretion, emphasizes the importance of glutamine-dependent pathways in these cells. Our findings do not exclude the possibility that UDP-GlcNAc is also serving as a sugar donor for O-glycosylation, a pathway that is recognized to serve as a major connecting hub between cellular metabolism and signaling (Wellen and Thompson, 2012). The dependence of M2 activation on glutamine is intriguing not least because of the recognized role of M2 macrophages in wound healing (Murray and Wynn, 2011) and the findings that glutamine supplementation might provide a viable means to support recovery after surgery (Wilmore, 2001).

We are optimistic that these findings summarized above will spur activity into the development of approaches to manipulate the newly identified metabolic modules to affect macrophage function in clinically relevant settings.

EXPERIMENTAL PROCEDURES

Animals and Mouse Bone-Marrow-Derived Macrophage Culture

C57BL/6J (The Jackson Laboratory) mice were bred and maintained under specific-pathogen-free conditions according to protocols approved by the institutional animal care at Washington University School of Medicine and were used at age of 8–12 weeks. BM cells were harvested from femurs and tibia of C57BL6/J mice and differentiated in the presence of recombinant mouse M-CSF (20 ng/ml; R&D Systems) in complete RPMI 1640 (Corning) containing 10 mM glucose, 2 mM L-glutamine, 100 U/ml of penicillin/streptomycin, and 10% FCS for 7 days. Day 7 BMDMs were washed and cultured in presence or absence (for 4 hr) of 2 mM glutamine medium containing 10 mM glucose and 10% dialyzed FCS prior to IL-4 (20 ng/ml; PeproTech) or lipopolysaccharide (LPS, 20 ng/ml; Sigma) + IFN- γ (50 ng/ml; R&D Systems) 24 hr stimulation. In Got1/2 inhibition experiments, day 7 BMDMs were treated for 1 hr with 10 mM, 5 mM, or 1 mM aminooxetic acid (AOAA; Sigma) prior to 24 hr stimulation with LPS + IFN- γ . For inhibition of N-glycosylation, tunicamycin (1 μ M or 2 μ M as indicated; Sigma) was added on day 7 BMDMs 1 hr prior to 24 hr stimulation with IL-4.

Quantification of CCL22, IL-6, and Nitric Oxide in Culture Supernatants

CCL22, IL-6, and nitric oxide concentrations were determined with, respectively, the CCL22/MDC DuoSet ELISA kit (R&D Systems), the IL-6 ELISA Ready-Set-Go! Kit, and the Griess Reagent System (Promega), according to manufacturers' instructions.

Flow Cytometry and Extracellular Flux Analysis

Cells were blocked with 5 μ g/ml of anti-CD16/32 (clone 93, eBiosciences) before the surface staining with antibodies to F4/80 (clone BM8, eBiosciences), CD206 (clone C068C2, Biolegend), CD301 (clone ER-MP23, AbD Serotec). For intracellular staining of RELM α and iNOS, cells were fixed with a fixation buffer (BD Biosciences) and stained with rabbit anti-RELM α (PeproTech) and mouse anti-NOS2 (clone C-11; Santa Cruz Biotechnology), followed by incubation with appropriate fluorochrome-conjugated anti-rabbit or anti-mouse IgG (both Jackson Immunoresearch). Cells were also stained with LIVE/DEAD (Invitrogen) or 7-amino-actinomycin D (eBiosciences). Data were acquired on a FACSCanto II flow cytometer (BD Biosciences) and analyzed with FlowJo v.9.5.2 (Tree Star). Measurements of oxygen consumption rates and extracellular acidification rates were made with a Seahorse extracellular flux analyzer as described previously (Everts et al., 2012, 2014).

LC-MS and Data Analysis for Metabolomics

Data generated from a Quadrupole Time-of-flight mass spectrometer was used as the MS input for our CoMBI-T analysis; all steps of MS data processing were performed with Matlab R2010b (The Mathworks) using functions native to the Bioinformatics, Statistics, Database, and Parallel Computing toolboxes (Fuhrer et al., 2011). For the subsequent isotopic labeling experiments to validate the CoMBI-T findings (amino acid and central metabolite analyses), either triple-quadrupole MS data were acquired using scheduled selective reaction monitoring (SRM) in negative mode, or high-resolution accurate mass (HRAM) LC-MS data were acquired with a QExactive Orbitrap mass spectrometer (Thermo Fisher Scientific), in either positive or negative mode as appropriate; acquisition was controlled by Xcalibur 2.2 software (Thermo Fisher Scientific). U-¹³C-L-glutamine and U-¹³C-D-glucose were purchased from Sigma. Cell extracts were prepared from live cultures on Hamilton StarPlus system running an automated metabolite extraction protocol using hot 70% aq. ethanol (70°C). Supernatant of extracted samples were dried under vacuum and resuspended in LC-MS grade water for analysis of the relative abundance of ¹³C and ¹⁵N metabolites (Munger et al., 2008).

RNA Sequencing

mRNA was extracted from cell lysates by means of oligo-dT beads (Invitrogen). For cDNA synthesis, we used custom oligo-dT primer with a barcode and adaptor-linker sequence (CCTACACGACGCTCTTCCGATCT-XXXX-XXXX-T15). After first-strand synthesis, samples were pooled together based on Actb qPCR values and RNA-DNA hybrid was degraded with consecutive acid-alkali treatment. Then, a second sequencing linker (AGATCGGAAGAG

CACACGTCTG) was ligated with T4 ligase (NEB) followed by SPRI clean-up. The mixture then was PCR enriched 12 cycles and SPRI purified to yield final strand-specific RNA-seq libraries. Data were sequenced on HiSeq 2500 by 50bpX25bp pair-end sequencing. Second mate was used for sample demultiplexing, at which point individual single-end fastqs were aligned to mm9 genome via TopHat and gene expression was obtained via ht-seq and DESeq2 for differential expression.

Integrated Network Analysis

To construct the network for integrated analysis of metabolomic and RNA-seq data, we downloaded KEGG REACTION, KEGG ENZYME, KEGG COMPOUND, and KEGG GLYCAN databases (August 2013 version) (Kanehisa et al., 2012). Additionally, the reaction converting *cis*-aconitate to itaconate controlled by *Irg1* (Michelucci et al., 2013) was added to the network manually. A global combined network that connects nodes representing reactions to the nodes representing metabolites was constructed, in which nodes representing each reaction are connected to its respective substrates and products. Then we mapped reactions to enzymes REACTION and ENZYME databases. COMPOUND and GLYCAN databases were used to algorithmically access names for compounds. Reactions lacking at least one enzyme with an associated mouse gene were excluded from the network; sub-reactions embedded in multi-step metabolic transformations were masked, keeping only net reaction in the network. Based on names, anomeric metabolites were collapsed into a single species. Then we masked some common highly connected metabolites in the network: non-organic metabolites (water, ammonia, etc.), (deoxy)nucleosides phosphates (ATP, ADP, dATP, etc.), common cofactors (NADH, FAD, etc.), some generic metabolites (acceptors, ROH, etc.), and ubiquitin. The resulting network represents topological description of murine metabolism, independent of specific data. After data acquisition and application to the integrated model network, p values for metabolites and genes were calculated with limma and DESeq R-packages for differential expressions (Anders and Huber, 2010). For analysis, reactions with transcripts not detected in any sample (number of matching reads <5, leading to 14,276 significantly expressed genes) were excluded from the network. Next, reactions were assigned a differential regulation p value, corresponding to a differential expression p value for the transcript specific to the reaction. In cases where more than one enzyme (transcript) was associated with the reaction, we selected the single enzyme (transcript) that had the minimal p value; these p values were assigned as reaction p values. Then groups of reactions having at least one common metabolite and a shared most-significant gene were collapsed into single nodes. The problem for finding most significant module in the network was thus reduced to a maximum-weight connected subgraph (MWCS) problem (Beisser et al., 2010). Scores were assigned to all metabolites and reactions based on their p values and FDR threshold fitting a FitBum-Model distribution separately to metabolites and genes: metabolite and reaction p values with low p value had positive scores; ones with high p values had negative scores. The score for metabolites absent from the data is a parameter and was chosen to be -10 . MWCS instances were solved by heinz solver (<http://www.mi.fu-berlin.de/w/LISA/Heinz>). Resulting networks were annotated and plotted in Cytoscape.

ACCESSION NUMBERS

Raw and processed sequencing data are deposited to PubMed GEO under GSE53053.

SUPPLEMENTAL INFORMATION

Supplemental Information includes six figures, two tables, and Supplemental Experimental Procedures and can be found with this article online at <http://dx.doi.org/10.1016/j.immuni.2015.02.005>.

ACKNOWLEDGMENTS

We would like to thank Eugene Oltz for useful comments and help with the manuscript. We would also like to thank Ananya Mukherjee for helping with the figures used in the manuscript. M.N.A. would like to thank J.A. for support

and stimulating discussions. E.M.D. declares competing financial interest as a founder and shareholder of General Metabolics. K.C., K.M.S., and A.K.J. were employees of Agios when this study was conducted.

Received: April 29, 2014

Revised: November 24, 2014

Accepted: January 15, 2015

Published: March 17, 2015

REFERENCES

- Allen, A.E., Dupont, C.L., Oborník, M., Horák, A., Nunes-Nesi, A., McCrow, J.P., Zheng, H., Johnson, D.A., Hu, H., Fernie, A.R., and Bowler, C. (2011). Evolution and metabolic significance of the urea cycle in photosynthetic diatoms. *Nature* 473, 203–207.
- Anders, S., and Huber, W. (2010). Differential expression analysis for sequence count data. *Genome Biol.* 11, R106.
- Beisser, D., Klau, G.W., Dandekar, T., Müller, T., and Dittrich, M.T. (2010). BioNet: an R-Package for the functional analysis of biological networks. *Bioinformatics* 26, 1129–1130.
- Beisser, D., Grohme, M.A., Kopka, J., Frohme, M., Schill, R.O., Hengherr, S., Dandekar, T., Klau, G.W., Dittrich, M., and Müller, T. (2012). Integrated pathway modules using time-course metabolic profiles and EST data from *Milnesium tardigradum*. *BMC Syst. Biol.* 6, 72.
- Biswas, S.K., and Mantovani, A. (2012). Orchestration of metabolism by macrophages. *Cell Metab.* 15, 432–437.
- Bordbar, A., Mo, M.L., Nakayasu, E.S., Schrimpe-Rutledge, A.C., Kim, Y.M., Metz, T.O., Jones, M.B., Frank, B.C., Smith, R.D., Peterson, S.N., et al. (2012). Model-driven multi-omic data analysis elucidates metabolic immunomodulators of macrophage activation. *Mol. Syst. Biol.* 8, 558.
- Byles, V., Covarrubias, A.J., Ben-Sahra, I., Lamming, D.W., Sabatini, D.M., Manning, B.D., and Horng, T. (2013). The TSC-mTOR pathway regulates macrophage polarization. *Nat. Commun.* 4, 2834.
- Everts, B., Amiel, E., van der Windt, G.J., Freitas, T.C., Chott, R., Yarasheski, K.E., Pearce, E.L., and Pearce, E.J. (2012). Commitment to glycolysis sustains survival of NO-producing inflammatory dendritic cells. *Blood* 120, 1422–1431.
- Everts, B., Amiel, E., Huang, S.C., Smith, A.M., Chang, C.H., Lam, W.Y., Redmann, V., Freitas, T.C., Blagih, J., van der Windt, G.J., et al. (2014). TLR-driven early glycolytic reprogramming via the kinases TBK1-IKKe supports the anabolic demands of dendritic cell activation. *Nat. Immunol.* 15, 323–332.
- Fuhrer, T., Heer, D., Begemann, B., and Zamboni, N. (2011). High-throughput, accurate mass metabolome profiling of cellular extracts by flow injection-time-of-flight mass spectrometry. *Anal. Chem.* 83, 7074–7080.
- Geisbrecht, B.V., and Gould, S.J. (1999). The human PICD gene encodes a cytoplasmic and peroxisomal NADP(+)-dependent isocitrate dehydrogenase. *J. Biol. Chem.* 274, 30527–30533.
- Haschemi, A., Kosma, P., Gille, L., Evans, C.R., Burant, C.F., Starkl, P., Knapp, B., Haas, R., Schmid, J.A., Jandl, C., et al. (2012). The sedoheptulose kinase CARL directs macrophage polarization through control of glucose metabolism. *Cell Metab.* 15, 813–826.
- Infantino, V., Convertini, P., Cucci, L., Panaro, M.A., Di Noia, M.A., Calvello, R., Palmieri, F., and Iacobazzi, V. (2011). The mitochondrial citrate carrier: a new player in inflammation. *Biochem. J.* 438, 433–436.
- Kanehisa, M., Goto, S., Sato, Y., Furumichi, M., and Tanabe, M. (2012). KEGG for integration and interpretation of large-scale molecular data sets. *Nucleic Acids Res.* 40, D109–D114.
- Kauppinen, R.A., Sihra, T.S., and Nicholls, D.G. (1987). Aminoxyacetic acid inhibits the malate-aspartate shuttle in isolated nerve terminals and prevents the mitochondria from utilizing glycolytic substrates. *Biochim. Biophys. Acta* 930, 173–178.
- Knowles, R.G., and Moncada, S. (1994). Nitric oxide synthases in mammals. *Biochem. J.* 298, 249–258.

- Koch, H.U., Schwarz, R.T., and Scholtissek, C. (1979). Glucosamine itself mediates reversible inhibition of protein glycosylation. A study of glucosamine metabolism at inhibitory concentrations in influenza-virus-infected cells. *Eur. J. Biochem.* *94*, 515–522.
- Lehninger, A., Nelson, D., and Cox, M. (2008). *Lehninger Principles of Biochemistry*. (W.H. Freeman), p. 684.
- McGettrick, A.F., and O'Neill, L.A. (2013). How metabolism generates signals during innate immunity and inflammation. *J. Biol. Chem.* *288*, 22893–22898.
- Michelucci, A., Cordes, T., Ghelfi, J., Pailot, A., Reiling, N., Goldmann, O., Binz, T., Wegner, A., Tallam, A., Rausell, A., et al. (2013). Immune-responsive gene 1 protein links metabolism to immunity by catalyzing itaconic acid production. *Proc. Natl. Acad. Sci. USA* *110*, 7820–7825.
- Munger, J., Bennett, B.D., Parikh, A., Feng, X.J., McArdle, J., Rabitz, H.A., Shenk, T., and Rabinowitz, J.D. (2008). Systems-level metabolic flux profiling identifies fatty acid synthesis as a target for antiviral therapy. *Nat. Biotechnol.* *26*, 1179–1186.
- Murray, P.J., and Wynn, T.A. (2011). Protective and pathogenic functions of macrophage subsets. *Nat. Rev. Immunol.* *11*, 723–737.
- O'Neill, L.A. (2011). A critical role for citrate metabolism in LPS signalling. *Biochem. J.* *438*, e5–e6.
- O'Neill, L.A., and Hardie, D.G. (2013). Metabolism of inflammation limited by AMPK and pseudo-starvation. *Nature* *493*, 346–355.
- Patil, K.R., and Nielsen, J. (2005). Uncovering transcriptional regulation of metabolism by using metabolic network topology. *Proc. Natl. Acad. Sci. USA* *102*, 2685–2689.
- Rodríguez-Prados, J.C., Través, P.G., Cuenca, J., Rico, D., Aragonés, J., Martín-Sanz, P., Cascante, M., and Boscá, L. (2010). Substrate fate in activated macrophages: a comparison between innate, classic, and alternative activation. *J. Immunol.* *185*, 605–614.
- Schmidlin, A., and Wiesinger, H. (1998). Argininosuccinate synthetase: localization in astrocytes and role in the production of glial nitric oxide. *Glia* *24*, 428–436.
- Shanware, N.P., Bray, K., Eng, C.H., Wang, F., Follettie, M., Myers, J., Fantin, V.R., and Abraham, R.T. (2014). Glutamine deprivation stimulates mTOR-JNK-dependent chemokine secretion. *Nat. Commun.* *5*, 4900.
- Sica, A., and Mantovani, A. (2012). Macrophage plasticity and polarization: in vivo veritas. *J. Clin. Invest.* *122*, 787–795.
- Sojka, D.K., Plougastel-Douglas, B., Yang, L., Pak-Wittel, M.A., Artyomov, M.N., Ivanova, Y., Zhong, C., Chase, J.M., Rothman, P.B., Yu, J., et al. (2014). Tissue-resident natural killer (NK) cells are cell lineages distinct from thymic and conventional splenic NK cells. *eLife* *3*, e01659.
- Stadler, J., Billiar, T.R., Curran, R.D., Stuehr, D.J., Ochoa, J.B., and Simmons, R.L. (1991). Effect of exogenous and endogenous nitric oxide on mitochondrial respiration of rat hepatocytes. *Am. J. Physiol.* *260*, C910–C916.
- Tannahill, G.M., Curtis, A.M., Adamik, J., Palsson-McDermott, E.M., McGettrick, A.F., Goel, G., Frezza, C., Bernard, N.J., Kelly, B., Foley, N.H., et al. (2013). Succinate is an inflammatory signal that induces IL-1 β through HIF-1 α . *Nature* *496*, 238–242.
- Varki, A. (2009). *Essentials of Glycobiology*, Second Edition. (Cold Spring Harbor Laboratory Press).
- Vats, D., Mukundan, L., Odegaard, J.I., Zhang, L., Smith, K.L., Morel, C.R., Wagner, R.A., Greaves, D.R., Murray, P.J., and Chawla, A. (2006). Oxidative metabolism and PGC-1 β attenuate macrophage-mediated inflammation. *Cell Metab.* *4*, 13–24.
- Wellen, K.E., and Thompson, C.B. (2012). A two-way street: reciprocal regulation of metabolism and signalling. *Nat. Rev. Mol. Cell Biol.* *13*, 270–276.
- Wilmore, D.W. (2001). The effect of glutamine supplementation in patients following elective surgery and accidental injury. *J. Nutr.* *131*, 2543S–2549S, discussion 2550S–2551S.
- Yi, W., Clark, P.M., Mason, D.E., Keenan, M.C., Hill, C., Goddard, W.A., 3rd, Peters, E.C., Driggers, E.M., and Hsieh-Wilson, L.C. (2012). Phosphofructokinase 1 glycosylation regulates cell growth and metabolism. *Science* *337*, 975–980.
- Zhu, J., Sova, P., Xu, Q., Dombek, K.M., Xu, E.Y., Vu, H., Tu, Z., Brem, R.B., Bumgarner, R.E., and Schadt, E.E. (2012). Stitching together multiple data dimensions reveals interacting metabolomic and transcriptomic networks that modulate cell regulation. *PLoS Biol.* *10*, e1001301.

C-Myb⁺ Erythro-Myeloid Progenitor-Derived Fetal Monocytes Give Rise to Adult Tissue-Resident Macrophages

Guillaume Hoeffel,¹ Jinmiao Chen,¹ Yonit Lavin,^{2,3} Donovan Low,¹ Francisca F. Almeida,¹ Peter See,¹ Anna E. Beaudin,⁴ Josephine Lum,¹ Ivy Low,¹ E. Camilla Forsberg,⁴ Michael Poidinger,¹ Francesca Zolezzi,¹ Anis Larbi,¹ Lai Guan Ng,¹ Jerry K.Y. Chan,^{1,5,6,7} Melanie Greter,⁸ Burkhard Becher,⁸ Igor M. Samokhvalov,⁹ Miriam Merad,^{2,3} and Florent Ginhoux^{1,*}

¹Singapore Immunology Network (SiGN), Agency for Science, Technology and Research (A*STAR), 8A Biomedical Grove, IMMUNOS Building #3-4, BIOPOLIS, 138648 Singapore

²Department of Oncological Sciences, The Tisch Cancer Institute, 1425 Madison Avenue, New York, NY 10029, USA

³The Immunology Institute, Icahn school of Medicine at Mount Sinai, 1425 Madison Avenue, New York, NY 10029, USA

⁴Institute for the Biology of Stem Cells, Department of Biomolecular Engineering, University of California-Santa Cruz, 1156 High Street, Santa Cruz, CA 95064, USA

⁵Experimental Fetal Medicine Group, NUHS Tower Block level 12, Yong Loo Lin School of Medicine, National University of Singapore, 1E Kent Ridge Road, 119228 Singapore

⁶Reproductive Medicine, KK Women's and Children's Hospital, 100 Bukit Timah Road, 229899 Singapore

⁷Singapore and Cancer and Stem Cell Biology Program, Duke-NUS Graduate Medical School, 8 College Road, 169857 Singapore

⁸Institute of Experimental Immunology, University of Zürich, Winterthurerstrasse 190, CH-8057 Zürich, Switzerland

⁹Guangzhou Institutes of Biomedicine and Health, Chinese Academy of Science, 190 Kai Yuan Avenue, Science Park, Guangzhou, 510530 China

*Correspondence: florent_ginhoux@immunol.a-star.edu.sg

<http://dx.doi.org/10.1016/j.immuni.2015.03.011>

SUMMARY

Although classified as hematopoietic cells, tissue-resident macrophages (MFs) arise from embryonic precursors that seed the tissues prior to birth to generate a self-renewing population, which is maintained independently of adult hematopoiesis. Here we reveal the identity of these embryonic precursors using an in utero MF-depletion strategy and fate-mapping of yolk sac (YS) and fetal liver (FL) hematopoiesis. We show that YS MFs are the main precursors of microglia, while most other MFs derive from fetal monocytes (MOs). Both YS MFs and fetal MOs arise from erythro-myeloid progenitors (EMPs) generated in the YS. In the YS, EMPs gave rise to MFs without monocytic intermediates, while EMP seeding the FL upon the establishment of blood circulation acquired c-Myb expression and gave rise to fetal MOs that then seeded embryonic tissues and differentiated into MFs. Thus, adult tissue-resident MFs established from hematopoietic stem cell-independent embryonic precursors arise from two distinct developmental programs.

INTRODUCTION

Macrophages (MFs) are mononuclear phagocytes with crucial roles in development, tissue homeostasis, and the induction of immunity. However, they can also contribute to the pathological processes of tumor growth and metastasis, as well as chronic

inflammatory diseases including atherosclerosis and diabetes (Lavin and Merad, 2013). There is growing interest in the clinical manipulation of MF populations, but realizing their therapeutic potential will require improved knowledge of their origins and the mechanisms underlying their homeostasis.

Since the definition of the mononuclear phagocyte system (MPS) (van Furth et al., 1972), the prevailing dogma has stated that tissue-resident MF populations are replenished by monocytes (MOs) from the blood. While this proves true for dermal and gut MFs (Bain et al., 2014; Tamoutounour et al., 2013), MOs do not substantially contribute to many adult tissue MF populations either in the steady state, or even during inflammation (Hashimoto et al., 2013; Jakubzick et al., 2013; Jenkins et al., 2011; Yona et al., 2013); rather, the majority of tissue-resident MF populations are established during development by embryonic precursors and maintain themselves in adults by self-renewal (Epelman et al., 2014; Ginhoux et al., 2010; Williams et al., 2013; Hoeffel et al., 2012; Schneider et al., 2014; Schulz et al., 2012). Despite these advances in knowledge, the nature and origin of the embryonic precursors of MFs remain unknown.

Several spatially and temporally regulated waves of hematopoietic cells are produced in mammalian embryos, culminating with the establishment of hematopoietic stem cells (HSCs) in the bone marrow (BM) (Orkin and Zon, 2008; Taviani and Péault, 2005). In mice, the first hematopoietic progenitors appear in the extra-embryonic yolk sac (YS), around embryonic age 7.0 (E7.0), where they initiate primitive hematopoiesis, producing mainly nucleated erythrocytes and MFs (Moore and Metcalf, 1970). From E8.25, multi-lineage erythro-myeloid progenitors (EMPs) and lympho-myeloid progenitors (LMPs) emerge in the YS as a “second wave,” termed the transient definitive stage (Frame et al., 2013; Lin et al., 2014; Palis et al., 1999). EMPs are also

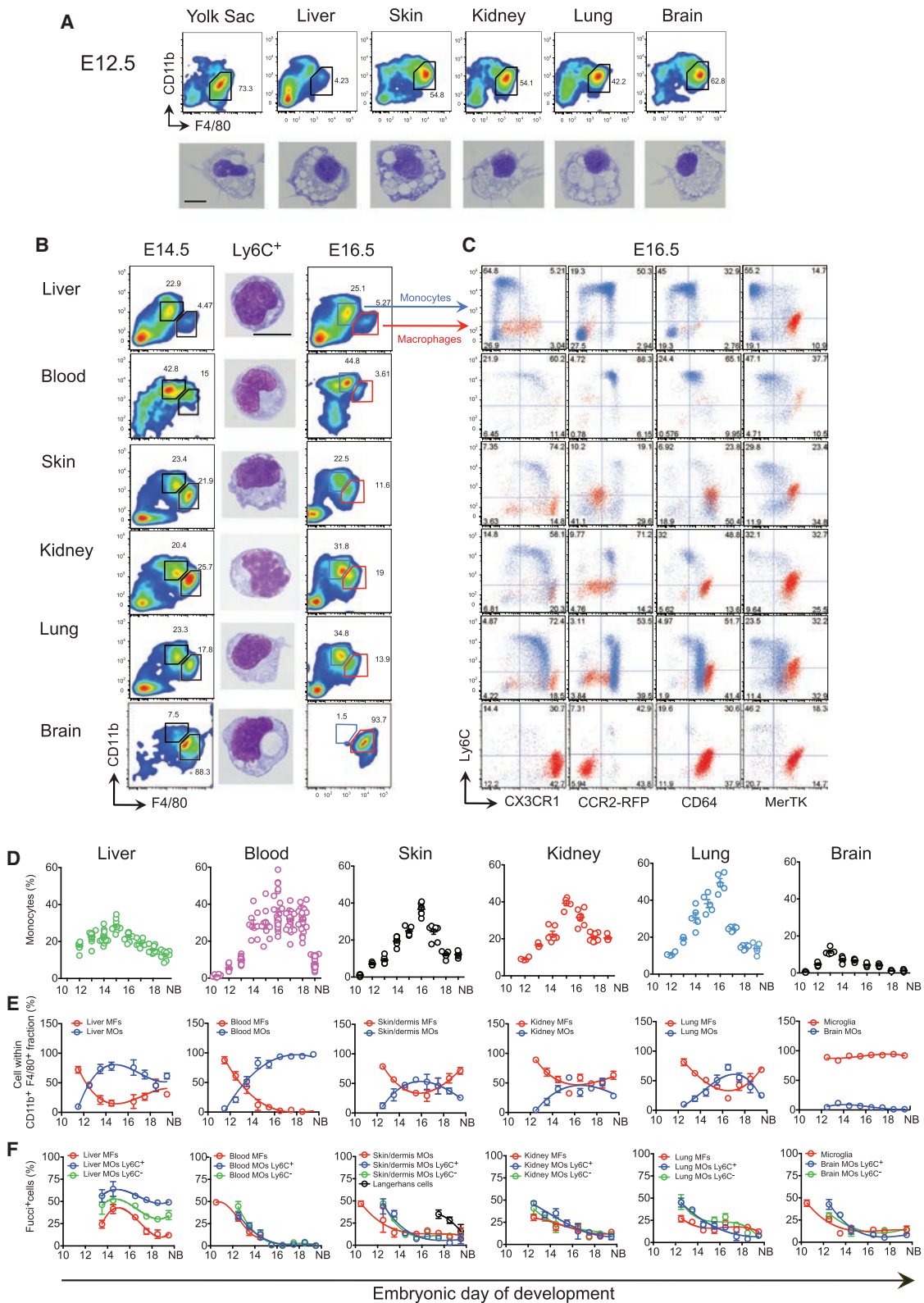


Figure 1. Fetal Macrophages Arise Sequentially from YS Macrophages and Fetal Monocytes

(A) Flow cytometry analysis of cells from E12.5 embryonic tissues and GIEMSA staining of purified doublet $\text{DAPI}^- \text{CD45}^+ \text{CD11b}^{\text{lo}} \text{F4/80}^{\text{hi}} \text{CD64}^+ \text{Ly6C}^-$ YS MFs from each tissue.

(legend continued on next page)

found in other hemogenic tissues such as the placenta and umbilical cord (Dzierzak and Speck, 2008) and enter the circulation to colonize the fetal liver (FL) from E9.5 (Lin et al., 2014). After E8.5, the intra-embryonic mesoderm commits to the hematopoietic lineage and new waves of hematopoietic progenitors emerge: first in the para-aortic splanchnopleura (P-Sp) region and then in the aorta, gonads, and mesonephros (AGM) region (Lin et al., 2014). The hematopoietic activities of the P-Sp and AGM regions generate the pre-HSC and mature HSC that colonize the FL around E10.5 (Kieusseian et al., 2012; Kumaravelu et al., 2002) to finally establish definitive hematopoiesis (Golub and Cumanò, 2013; Medvinsky et al., 2011; Orkin and Zon, 2008). The FL becomes the major hematopoietic organ after E11.5, generating all hematopoietic lineages and expanding the definitive HSC population before their migration to the spleen and the BM (Christensen et al., 2004).

YS MFs first appear within the YS blood islands at E9.0 in both mouse and rat, and develop without passing through a monocytic intermediate stage (Takahashi et al., 1989). They are the primary source of microglia, the resident MFs of the central nervous system (Ginhoux et al., 2010), and also give rise to a minor fraction of Langerhans cells (LCs), the specialized antigen-presenting cells of the skin (Hoeffel et al., 2012). The major fraction of adult LCs derives from fetal MOs generated in the FL from E12.5 and recruited into fetal skin around E14.5 (Hoeffel et al., 2012). Fetal MOs also contribute to populations of adult MFs in lung alveoli (Guilliams et al., 2013; Schneider et al., 2014) and in the heart (Epelman et al., 2014). Using fate-mapping to distinguish cells arising from primitive versus definitive hematopoiesis initially suggested that adult MF populations in lung, dermis, and spleen arise predominantly from definitive hematopoiesis with negligible contribution from YS MFs (Ginhoux et al., 2010). However, a new approach exploiting the differential dependence of MFs on the transcription factor *c-Myb* has since indicated that *c-Myb*-independent YS MFs may be the sole origin of MFs in the lung, liver, and pancreas, as well as of microglia and LCs (Schulz et al., 2012). Hence, the embryonic route of origin of tissue-resident MF populations in the adult remains controversial. Our understanding is further hampered by not knowing whether fetal MOs actually arise from definitive HSC or HSC-independent progenitors such as LMPs or EMPs.

We combined *in vivo* YS MF depletion with several fate-mapping models of YS MFs and/or FL MOs to conclusively show that YS MFs are the main precursors of microglia, whereas most other MF populations derive from fetal MOs that seed the tissues around E13.5. Fetal MOs in turn are revealed to derive sequentially from HSC-independent and -dependent routes, the former being the major pathway arising from *c-Myb*⁺ EMPs.

RESULTS

Tissue-Resident Macrophages Are Seeded Before Birth and Proliferate In Situ

MF embryonic precursors include YS MFs and fetal MOs generated in the FL (Epelman et al., 2014; Guilliams et al., 2013; Hoeffel et al., 2012; Schneider et al., 2014). At E10.5, YS MFs (CD45⁺CD11b^{lo}F4/80^{hi}Ly6C⁻), but not MOs, are present in the YS and throughout the body of the embryo proper (Hoeffel et al., 2012; Naito et al., 1990). At E12.5, YS MFs, but not MOs, were found in liver, skin, kidney, lung, and brain rudiments (Figure 1A). However, as in the developing skin (Hoeffel et al., 2012), an influx of fetal MOs (CD45⁺CD11b^{hi}F4/80^{lo}Ly6C⁺) was evident at E14.5 in all tissue rudiments tested (Figure 1B, blue population), except the brain (Figures 1B–1D). Fetal MOs appear in the FL around E12.5 (Naito et al., 1990) and exist as two populations differentially expressing Ly6C, similar to adult MOs in the BM (Geissmann et al., 2003). Both populations of fetal MOs also express the chemokine receptor CCR2 (Figure 1C), though it is not required for their emigration from the FL or recruitment into tissues (Figure S1), unlike in their adult counterparts (Serbina and Pamer, 2006). Ly6G⁺CCR2⁻ granulocyte progenitors were also detected at E14.5 (Figure S1). In contrast to adult BM MOs, fetal MOs only began to express the chemokine receptor CX3CR1 in the blood, following FL emigration (Figure 1C). Upon tissue infiltration, fetal MOs further upregulated expression of CX3CR1 and the MF markers CD64 and MerTK, and downregulated Ly6C (Figure 1C), suggesting their differentiation into tissue MFs. The early tissue MF populations (Figure 1B–1E, red population) decreased in numbers between E10.5 and E16.5, so that fetal MOs became the major myeloid cell population in the tissues at E16.5 (Figures 1D and 1E). The initial abundant proliferation of both fetal MO sub-populations and MFs within the tissues also gradually diminished with time (Figure 1F, Figure S2). By late embryogenesis, these populations coexisted in every tissue, without presenting any clear signs of apoptosis (Figure S2). Thus, both YS MFs and fetal MOs contribute to tissue MF populations present in the developing embryo.

YS Macrophages Are Not Required for Fetal Macrophage Development

To understand whether YS MFs were the sole progenitors of MFs in the adult, we asked what impact their *in utero* depletion would have on the subsequent generation of tissue MFs. The colony-stimulating factor 1 receptor (CSF-1R) is expressed on YS MFs and fetal MOs, but only the development of the former is dependent on CSF-1R (Ginhoux et al., 2010; Hoeffel et al., 2012). Thus, we attempted to deplete YS MFs by transiently inhibiting the CSF-1R signaling pathway with a blocking anti-CSF-1R antibody

(B) Flow cytometry analysis of cells from E14.5 and E16.5 embryos and GEMSA staining of purified doublet⁻ DAPI⁻ CD45⁺ CD11b^{hi} F4/80^{lo} CD64⁺ Ly6C⁺ MOs from each E14.5 tissue. (A and B) Scale bar represents 5 μ m.

(C) Flow cytometry analysis of cells from E16.5 *Cx3cr1*^{+/gfp}, *Ccr2*^{+/rfp}, and WT embryos. Overlay of MFs (red population) and fetal MOs (blue population) is depicted (see also Figure S1A for FL analysis). Representative data from five embryos from two litters of each strain are shown.

(D) Kinetics of fetal MO tissue infiltration. Percentage of fetal CD11b^{hi} F4/80^{lo} CD64⁺ Ly6C^{+/−} MOs within doublet⁻ DAPI⁻ CD45⁺ cells on alternate days of embryonic development (see also Figure S1B for CCR2^{-/-} data). Each dot represents one embryo (n = 5–12).

(E) MFs gated as in (A) and fetal MOs gated as in (B) within total CD11b⁺ F4/80⁺ cells (n = 5–12).

(F) Percentage of proliferative MFs gated as in (A), Ly6C⁺ and Ly6C⁻ MOs gated as in (B) determined in Fucci reporter mice (see Supplemental Information, n = 5–8) (see also Figure S2A for representative plots). Mean \pm SEM from three independent litters is presented in (D)–(F).

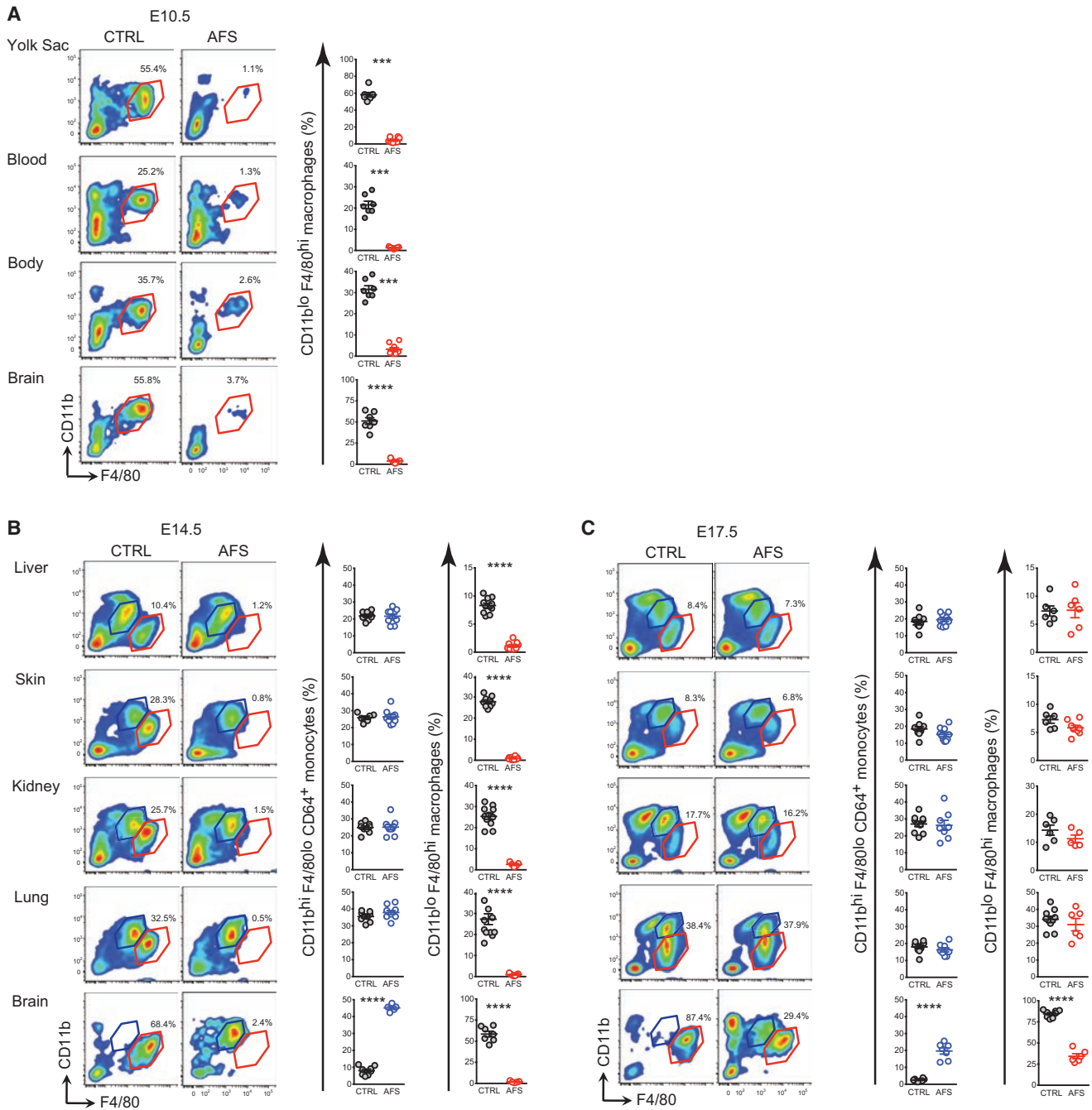


Figure 2. YS Macrophages Are Not Essential for Fetal Macrophage Development

(A–C) Pregnant females were untreated or injected with AFS98 at E6.5 and cells from embryos were analyzed by flow cytometry at E10.5 (A), E14.5 (B), and E17.5 (C). Percentages of MFs (red) and fetal MOs (blue) gated as in Figure 1 are shown. Each dot represents one embryo. Bars represent mean \pm SEM ($p < 0.05$; $**p < 0.01$; $***p < 0.001$; $****p < 0.0001$). Analysis of $n = 5$ –12 embryos per group from 2–3 independent litters (see also Figure S2B).

(clone AFS98), as recently described (Squarzoni et al., 2014). AFS98 injection at E6.5 efficiently depleted MFs in the E10.5 YS (Figure 2A), as well as most embryonic tissue MFs from E10.5 to E14.5 (Figure 2B, red population), but not circulating MOs (Figure 2B, blue population). The depletion of most MFs in AFS98-exposed embryos was transient and receded around

E17.5 (Figure 2C, red population). In contrast, embryonic microglia were fully depleted from E10.5 to E14.5, and only partially repopulated at E17.5 (Figures 2A–2C), but fully repopulated after birth (Squarzoni et al., 2014). These data suggest that YS MFs are dispensable for generating tissue-resident MFs in the embryo, and therefore another CSF-1R-independent

embryonic precursor can functionally replace YS MFs during development.

Except for Microglia, Only a Minor Fraction of Tissue Macrophages Derives from YS Macrophages

To define the relative contribution of YS MFs to the tissue MF compartment, we used a fate-mapping mouse model expressing the tamoxifen-inducible Cre recombinase gene (*MerCreMer*) under the control of the CSF-1R promoter (*Csf1r^{Cre/WT}*) (Qian et al., 2011). We crossed the *Csf1r^{Cre/WT}* mice with the Cre-reporter mouse strain *Rosa26^{R26-EYFP/R26-EYFP}* (*Rosa^{EYFP}*) and induced recombination in embryos by a single injection of Hydroxytamoxifen (4'OHT) into E8.5 pregnant females. Because CSF-1R is expressed on YS MFs, which appear in the YS from E9.0 (Ginhoux et al., 2010; Hoeffel et al., 2012), this strategy should specifically EYFP-label YS MFs and their progeny. We then measured the relative numbers of EYFP⁺ myeloid cells in E8.5 4'OHT-exposed embryos at E13.5 and E16.5, at birth, and in adulthood (Figure 3A). At E13.5, approximately 63.2% (± 5.6) of MFs in the YS and rudiments of brain, liver, skin, kidney, and lung were EYFP⁺, indicating their common YS MFs origin. From E13.5 onward, the extent of labeling of most MFs declined, reaching 2%–3% at birth, whereas microglia maintained a labeling frequency above 60% throughout adulthood.

To confirm the data from the *Csf1r^{Cre/WT}* mice, we used a fate-mapping model possessing a tamoxifen-inducible Cre recombinase gene (*MerCreMer*) under the control of one of the endogenous promoters of the runt-related transcription factor 1 (*Runx1*) locus (Samokhvalov et al., 2007). Because *Runx1* is expressed in hematopoietic progenitors, YS MF or fetal MO progeny could be traced by injecting 4'OHT at E7.5 or E8.5, respectively (Hoeffel et al., 2012). To assess the contribution of YS MFs to myeloid cell populations, we analyzed the frequency of EYFP⁺ myeloid cells in embryos and adult mice exposed to 4'OHT at E7.5 (Figure 3B). E13.5 embryos contained similar proportions of labeled MFs in the YS (22.2% \pm 0.9%) and brain rudiment (23.6% \pm 1.1%), suggesting their common origin. However, in liver, lung, skin, and kidney rudiments, significantly fewer fetal MFs were labeled (15.5% \pm 1.3; $p = 0.002$) (Figure 3B). After this time, EYFP labeling decreased to 2%–3% by birth and into adulthood; the same basal amounts as other leukocytes (Ginhoux et al., 2010). These data are consistent with the minor contribution of YS progenitors to the adult HSC pool shown previously (Samokhvalov et al., 2007). In contrast, the microglial population maintained abundant EYFP labeling from E13.5 into adulthood, confirming their YS MF origin (Ginhoux et al., 2010; Hoeffel et al., 2012). Therefore, while YS MFs seed embryonic tissues prior to the emergence of FL hematopoiesis, they do not contribute to adult tissue MF populations, apart from microglia. The absence of apoptosis within the YS MF population in tissues (Figure S2) suggests that the decreasing relative abundance of these cells from E13.5 likely results from dilution by unlabeled immigrant cells.

Adult Tissue-Resident Macrophages Derive Predominantly from Fetal Monocytes Generated during Definitive Hematopoiesis

On the basis of our observations in the skin (Hoeffel et al., 2012), we hypothesized that the fetal MOs infiltrating the tissue

rudiments (Figure 1) were the diluting cell population. As expected, fetal MOs were not labeled in *Csf1r^{Cre/WT}* \times *Rosa^{EYFP}* (*Csf1r^{Cre/EYFP}*) embryos activated at E8.5 or in *Runx1^{Cre/WT}* \times *Rosa^{EYFP}* (*Runx1^{Cre/EYFP}*) embryos activated at E7.5 (Figure 3C), while injecting 4'OHT into pregnant *Runx1^{Cre/WT}* mice at E8.5 is known to mark fetal MOs and their progeny (Hoeffel et al., 2012). Exposure to 4'OHT at E8.5 led to EYFP expression in most tissue MFs in both embryos and adult mice, and not in microglia (Figure 3D). The proportion of EYFP⁺ MFs and fetal MOs from E16.5 onward was comparable, suggesting that fetal MOs likely contribute to the EYFP signal observed in tissue MFs (Figure 3E).

To establish whether fetal MOs directly give rise to the tissue MFs that are maintained into adulthood, we devised a Cre-based fate-mapping model to specifically track fetal MOs and their progeny. Following comparative gene-expression analysis in fetal MOs and MFs (Figure 3F and complete list in Figure S3), and confirmation by quantitative RT-PCR (Figure 3G), we based our model on the specific expression of *S100A4* (*FSP1*) in fetal MOs, because this approach has previously been successful in fate-mapping of myeloid cells (Bhowmick et al., 2004; Hashimoto et al., 2013). We then crossed *S100a4^{Cre/WT}* mice with the Cre-reporter mouse strain *Rosa^{EYFP}* and analyzed the labeling of myeloid cells during development. Fetal MOs exhibited a high labeling frequency (64.5% \pm 6.7) (Figure 3H), whereas E10.5 YS MFs, YS progenitors such as EMPs, and most other leukocytes were labeled far less frequently (17.8% \pm 2.7) (Figure 3I and Figure S3). Therefore, we concluded that *S100a4^{Cre/WT}* mice represent a specific fetal MO fate-mapping model, and so proceeded to assess the labeling of tissue-resident MFs (Figure 3I). We hypothesized that MFs derived from fetal MOs should exhibit the same extent of EYFP labeling as fetal MOs. From E14.5 onward, the percentage of EYFP⁺ fetal MFs (28.4% \pm 3.6%) was markedly greater than the percentage of EYFP⁺ YS MFs and microglia (18.6% \pm 2.3%) and plateaued at the same extent as that of the fetal MO population (64.5% \pm 6.7%; Figures 3H and 3I). This implies that fetal MFs do not arise solely from YS MFs, and that fetal MOs are the dominant source of MFs throughout development. Because EYFP labeling reached a plateau between E17.5 and birth, and remained stable into adulthood (Figure S3), fetal MO-derived MFs must also be capable of maintenance by self-renewal. This is in agreement with newborn BM transplant experiments that showed minor post-natal contribution before 12 weeks after transplantation to adult tissue-resident MFs in the brain, epidermis, liver, kidney, and lung, while dermal, gut, and peritoneal MFs exhibited significant donor origin (Figure S3), likely arising from postnatal blood MO as previously published (Bain et al., 2014; Tamoutounour et al., 2013). Of note, the relative number of EYFP⁺ FL MFs was relatively greater than at other sites as early as E12.5, suggesting that fetal MOs differentiate locally into MFs in the FL before moving to other tissues (Figure 3I).

Fetal Monocytes Derive from HSC -Dependent and -Independent Progenitors

We next investigated the origin of MOs generated in the FL and observed a differentiation continuum of progenitors, as in adult BM (Figure 4A), where MOs derive sequentially from macrophage-dendritic cell precursors (MDPs) and common monocyte

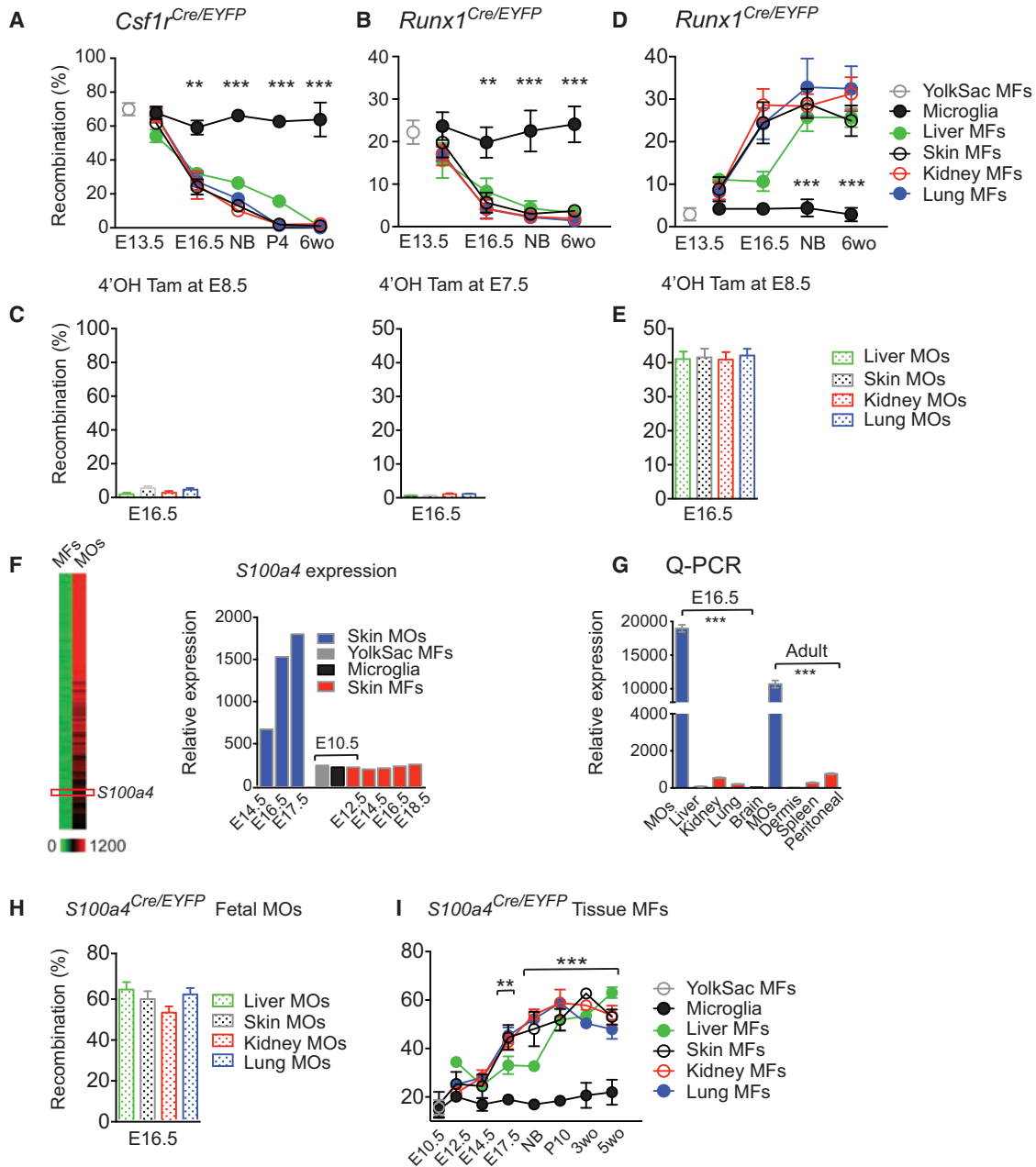


Figure 3. YS Macrophages in Embryonic Tissues Are Progressively Replaced by Fetal Monocyte-Derived Macrophages

(A–E) Fate-mapping of YS MFs and fetal MOs from early development into adulthood (6 weeks old). Percentage of recombination in MFs at various time points (A), (B), and (D) or MOs at E16.5 (C) and (E) after a single injection of 4'OHT at E8.5 in *Csf1r^{Cre/WT}* pregnant mice (A, C, left) (two pooled experiments, $n = 5–12$ for each time point), or at E7.5 (B, C, right) (three pooled experiments, $n = 8–16$, for each time point), or E8.5 (D) and (E) (two pooled experiments, $n = 5–16$ for each time point) in *Runx1^{Cre/WT}* pregnant mice.

(F) Heatmap depicting differentially expressed genes (DEG) in fetal MOs (See Supplemental Information and Figure S3A) and representative histograms of relative *S100a4* mRNA expression in MOs and MFs by gene array analysis. (G) *S100a4* mRNA expression determined by Q-PCR in MFs and fetal MOs ($n = 3$, each sample derives from at least eight embryos or five adult mice respectively).

(H and I) Percentage of recombination in MOs at E16.5 (two pooled experiments, $n = 5–10$) (H), and in MFs (two pooled experiments, $n = 5–10$ for each time point) (I) of *S100a4^{Cre/eyfp}* embryos and adult mice (see Figures S3B and S3C for controls). Bars represent mean \pm SEM (* $p < 0.05$; ** $p < 0.01$; *** $p < 0.001$).

progenitors (cMoPs) (Ginhoux and Jung, 2014; Hettinger et al., 2013). We found $\text{Lin}^{-}\text{cKit}^{+}\text{Fli3}^{+}\text{CSF-1R}^{+}\text{Ly6C}^{-}$ MDP-like progenitors in the FL (FL MDP) at E12.5–16.5 (Figure 4A and Figure S4)

alongside $\text{Lin}^{-}\text{cKit}^{+}\text{Fli3}^{-}\text{CSF-1R}^{+}\text{Ly6C}^{+/-}$ myeloid progenitors (MPs), all of which were highly proliferative (Figure 4B) and exhibited nucleolar structures typical of chromatin reorganization

(Figure 4C). The phenotype of the Ly6C⁺ MP fraction is equivalent to that of cMoP (Hettinger et al., 2013), whereas the Ly6C⁻ fraction of MP is absent in adult BM, and therefore might be a transient embryonic MP population specific to the FL (Figure 4A). We thus named them, FL cMoP and FL MP, respectively.

To clarify the relationships between these progenitors, we isolated them from E14.5 FL and adult BM and compared their gene-expression profiles (GEO GSE66970). Unsupervised clustering analysis revealed the close proximity of each of the FL progenitors to their BM counterparts (Figure 4D), but while fetal MOs selectively expressed genes related to cell cycle and differentiation, adult MOs exhibited an expression profile consistent with their roles in immune responses and pathogen recognition (Figure 4E). We also compared the gene-expression signatures of each progenitor population by Connectivity Map (CMAP) analysis (Figure 4F and Supplemental Methods). This showed that FL MPs and FL MDPs are most closely related; FL cMoP thus, seem to be an intermediate between these two populations and fetal MOs, consistent with their higher proliferative capacity (Figure 4B) and lower expression of CCR2, CX3CR1 and Lysozyme (Figure S4) compared to fetal MOs. Upon culture in vitro with CSF-1, both FL MDPs and FL MPs gave rise to MOs through a cMoP stage (Figure S4), as seen in adult BMs (Hettinger et al., 2013). However, the FL MP stage was not detected in FL MDP cultures, suggesting that these two progenitors are independent from each other. Thus, we hypothesized that two pathways of fetal MO generation coexist in the E14.5 FL, perhaps differing in their dependence on HSCs.

To assess the contribution of HSC to fetal MO generation, we examined progenitors and myeloid cells at different fetal stages in mice expressing the Cre-recombinase under the control of the Flt3 promoter, which labels HSC progeny in adult BM (Boyer et al., 2011). As HSC specification and maintenance are Flt3-independent (Boyer et al., 2011; Buza-Vidas et al., 2011), few HSC were labeled at E13.5 (2.17±0.99%) (Figure 4G), while the FL MDP population exhibited steadily increased labeling (from 20% at E13.5, to 67% at E17.5, and 82% at birth) (Figure 4G). Labeling of cMoP, MOs, and MFs at E17.5 was significantly lower than of MDP and remained low throughout (Figure 4G), suggesting a minor contribution from Flt3-dependent MDP to fetal MOs and MFs. These data suggest that fetal MOs arise via a Flt3⁻, and perhaps also HSC⁻, independent pathway.

To distinguish the roles of the two pathways in fetal MO generation, we investigated the lineage potential of FL progenitors. We identified differentially expressed genes in each population (Figure S4) and performed a Gene Set Enrichment Analysis (GSEA) using recently published lineage-associated genes (Böiers et al., 2013; Table S1). A significant enrichment in lymphoid genes expression including *Gata3*, *Rag1*, *Rag2*, and *Irf1* is shown in FL MDP (Figure S4, Table S2), similar to the E9.5 YS lymphomyeloid progenitors (LMPs) that colonize the FL at E11.5 (Böiers et al., 2013). This might indicate some heterogeneity within the fetal MDP population, consisting first of YS-derived LMP during late development and then of bona fide MDP after birth, which are related to those in adult BMs and derive from HSCs. In contrast, FL MPs expressed erythroid- and megakaryocyte-associated genes (Figure S4, Table S2) including as *Klf1*, *Gata1*, and *Itga2b* (CD41), similar to YS erythro-myeloid progenitors (EMPs), which colonize the FL around E10.0 (Frame

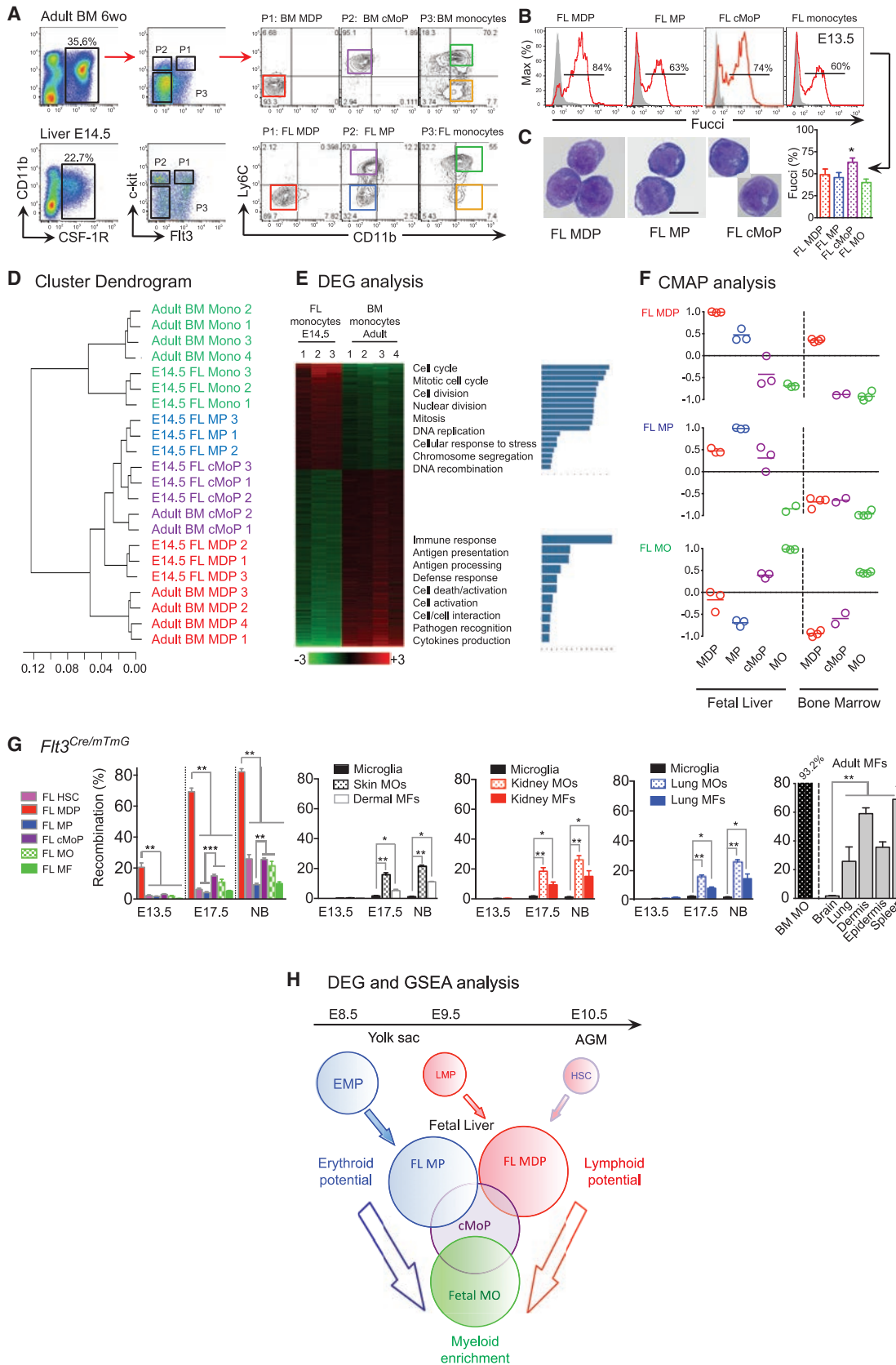
et al., 2013): thus FL MPs might derive from EMPs. Finally, FL cMoP and fetal MOs shared an enrichment in myeloid gene expression, whereas lymphocyte, erythrocyte, and megakaryocyte potentials were lost at the cMoP stage, consistent with their monocytic commitment (Figure 4H and Table S2). A heatmap of the genes that were differentially expressed in each progenitor population, based on recently published myeloid-associated genes and transcription factors (Friedman, 2002; Molawi and Sieweke, 2013), highlights the distinction between fetal MDPs and the other fetal myeloid populations (Figure S4), suggesting a closer proximity between FL MPs, FL cMoPs, and fetal MOs and implying that the transient FL MPs, likely the progeny of EMPs, are the main source of fetal MOs.

c-Myb⁺ EMPs Colonize the Fetal Liver and Generate Fetal Monocytes

To conclusively define the origin of fetal MOs, we returned to the *Runx1^{Cre/WT}* fate-mapping model and asked whether we could label the “transient definitive” wave that generates EMPs in the YS (Palis et al., 1999). We injected 4'OHT either at E7.5, E8.5, or E9.5 and compared the frequency of EYFP⁺ FL progenitors, Lin⁻CD48⁻c-Kit⁺Sca-1⁺CD150⁺ HSCs, MOs, and MFs at E13.5 (Figure 5A). Injection of 4'OHT at E7.5 exclusively labeled YS MFs in the FL, while injection at E9.5 predominantly led to labeling of HSCs and sequentially decreasing labeling frequencies in FL MDPs, FL MPs, FL cMoPs, fetal MOs, and MFs. Thus, E9.5 injection labels HSC-progeny, and reconfirms the limited involvement of HSCs in the generation of fetal MOs and MFs, as shown in Figure 4. 4'OHT injection at E8.5 led to a high frequency of EYFP⁺ FL MPs, FL cMoPs, fetal MOs, and MFs, but labeled only a minor fraction of HSCs, FL MDPs (Figure 5A), and did not label the pre-HSCs, which are generated in the P-Sp/AGM at E9.0 before seeding the FL at E11.0 (Figure S5). More precisely, 4'OHT injection at E8.5 labels YS CD41⁺ EMPs (Frame et al., 2013) en route to the FL at E10.0, and their progeny (Figure 5B). Thus, E8.5 injection labels EMPs and their progeny.

Because YS EMPs have been implicated in the generation of YS MFs (Kierdorf et al., 2013), while in our hands they also give rise to fetal MOs once they seed the FL, we decided to investigate their fate in these sites. As expected, EMPs arise before YS MFs, which appear from E9.5 (Figures 5C and 5D and Figure S5), in line with their developmental relationship (Cline and Moore, 1972; Kierdorf et al., 2013). Moreover, MFs were seen in the absence of any monocytic precursors before E12.5 (Figure 1), and as described (Cline and Moore, 1972; Hoeffel et al., 2012; Takahashi et al., 1989). In the *Runx1^{Cre/WT}* model, both E7.5 and E8.5 YS EMPs gave rise locally to YS MFs able to migrate to the FL (Figures 5E and 5F), however, E7.5-labeled EMPs remained in the YS and poorly entered the blood circulation, whereas E8.5-labeled EMPs efficiently reached the blood circulation and the FL (Figure 5E, left panel). This suggests that early EMPs differentiate locally, mainly generating YS MFs and erythrocytes before the onset of blood circulation, whereas later EMPs can reach the FL through the blood circulation, as reported (Palis and Yoder, 2001). Of note, E8.5 labeled EMPs that seed the FL still produced MFs locally, but did not substantially contribute to the microglial population at E13.5 (Figure 5E, right panel).

We then followed the fate of late EMPs from the YS to the FL using the *Runx1^{Cre/WT}* model, focusing on their E8.5



(legend on next page)

EYFP⁺ progeny (Figures 5F and 5G). EMPs lost the ability to generate MFs with time. From E11.5, intermediate CD11b^{hi} F4/80^{lo} CSF-1R^{+/-} populations emerge, suggesting that EMPs give rise to multiple myeloid progenitors, which in turn generate granulocytes and MOs. MF populations only enlarge again at E16.5 once the fetal MO population is established (Figure 5G). Hence, we hypothesized that the YS Runx1⁺ hemogenic endothelium initially gives rise to two types of EMPs: early EMPs (labeled at E7.5), which only generate local YS MFs, and late multipotent EMPs (labeled at E8.5) that reach the FL and differentiate into multiple lineages, including MOs that ultimately generate tissue MFs. This is supported by a previous study indicating two waves of phenotypically-similar MF-committed precursors possessing distinct clonal differentiation potentials and arising sequentially in the YS, the first at E8.0 and the second at E8.25 (Bertrand et al., 2005).

We confirmed this hypothesis using the *Csf1r*^{Cre/WT} fate-mapping model. 4'OHT injection at E8.5 in the *Csf1r*^{Cre/WT} model efficiently labeled EMPs and YS MFs at E10.5 in the YS and the FL (Figure 5H). However, increased decoupling between the tagging frequencies of EMPs and MFs occurred with time, suggesting that early EMPs are not maintained but are instead rapidly replaced by later EMPs. Accordingly, in CSF-1R reporter mice, EMPs did not express CSF-1R on their surface at E9.0 but did express it at the mRNA level (Figure S5), while from E10.0 in the inducible *Csf1r*^{Cre/WT} fate-mapping model EMPs were EYFP⁻, explaining why neither late EMPs nor fetal MOs were labeled. In summary, in agreement with our previous data suggesting the presence of two distinct types of EMPs, over time EMPs lose their ability to produce YS MFs but likely become able to give rise to other lineages in the FL, including MOs. As the c-Kit⁺ population that contains EMPs was absent in the FL of mice lacking c-Myb (Schulz et al., 2012), expansion and/or differentiation of later EMPs might be regulated by c-Myb expression, as previously suggested (Mucenski et al., 1991). Indeed, c-Myb was expressed in EMPs, LMPs, and cMoPs in the FL, as well as in the YS at E9.5, when EMPs ceased to give rise to YS MFs (Figure 5I). Thus, tissue-resident MFs rely on the generation of fetal MOs from c-Myb⁺ EMPs.

DISCUSSION

Here, we defined the origin and nature of the embryonic progenitors of major adult tissue-resident MF populations. Combining

in utero YS MF depletion and fate-mapping models revealed that YS MFs colonize every tissue at mid-gestation, but are dispensable for the generation of all adult tissue-resident MFs. The exception to this was the microglial population of the central nervous system: elsewhere YS MFs were replaced by MFs derived from fetal MOs. By using a fate-mapping model for fetal MOs, we showed that they colonized all embryonic tissues, apart from the brain, and differentiated into tissue MFs able to self-renew into adulthood. We also showed that these fetal MOs arose mostly from YS-derived late EMPs, while YS MFs arose from early EMPs. Thus, although arising from HSC-independent EMPs, fetal tissue MF populations are generated via two distinct developmental programs from two fundamentally different precursors: YS macrophages and FL monocytes.

Our results shed light on fetal monoipoiesis, identifying and characterizing the early embryonic progenitors of fetal MOs. Fetal MOs appeared to differentiate through a process related to adult BM monoipoiesis, starting from the FL MDP or FL MP that differentiated into FL cMOP intermediates and then Ly6C⁺ MOs. Two sources of fetal MOs existed: a first, HSC-independent, wave that arose mostly from YS-derived EMPs and accounted for the majority of fetal MOs present from E12.5–17.5; and a second, HSC-dependent, wave that generated a minor fraction of the fetal MO population after E17.5. In mice expressing the Cre-recombinase under the control of the *Flt3* promoter (Boyer et al., 2011), the fetal MDP population was abundantly labeled, indicating their derivation through an *Flt3*-dependent pathway. However, labeling frequency in fetal MFs did not increase to the same amount as FL MDPs, suggesting a minor contribution to fetal MOs and MFs from the *Flt3*-dependent pathway. Fetal MDPs exhibited a lymphoid gene-expression signature, consistent with a contribution from LMPs to fetal monoipoiesis, though this could not be assessed in the fate-mapping models used. Recent data from a *Rag1*^{Cre} fate-mapping model suggested that LMPs are unlikely to contribute to adult myeloid populations (Böiers et al., 2013). However, as only 50% of LMPs express *Rag1*, their contribution may have been underestimated. Whether the *Flt3* lineage-tracing model allows us to unambiguously follow fetal HSC or LMP progeny remains to be formally established.

Primitive hematopoiesis begins within the YS blood islands from E7.0 (Moore and Metcalf, 1970), and is characterized by the emergence of nucleated erythrocytes, hence the denomination “primitive” which relates to the red cells of inferior species

Figure 4. Fetal Monocytes Arise from HSC-Independent and -Dependent Pathways

(A) Gating strategy (from doublet⁻ DAPI⁻ cells) for myeloid progenitor identification in adult BM and E14.5 FL: MDP (P1, then red gate), MP (P2, then blue gate), cMoP (P2, then purple gate), fetal Ly6C⁺ MOs (P3, then green gate) and Ly6C⁻ MOs (P3, then yellow gate) (see other time point and phenotype in Figures S4A and S4B).

(B and C) Proliferative activity analyzed in Fucci-reporter mice (n = 3–6) (B) and morphology visualized by GIEMSA staining of corresponding sorted FL myeloid progenitors (scale bar represents 5 μM; two independent experiments).

(D) Unsupervised clustering analysis of E14.5 FL and adult BM myeloid progenitors.

(E) Heatmap of DEG between FL and BM MOs with specific gene functionalities annotated.

(F) CMAP analysis identifies FL MDP and FL MP as early progenitors, and cMoP as an intermediate, in generating fetal MOs (See also Figures S4C–S4E, Supplemental Information and Table S1).

(G) Percentage of recombination in *Flt3*^{Cre/mTmG} embryos/mice for FL MDP, FL MP, FL cMoP, FL MOs, or FL MFs (left), in MOs and MFs in skin, kidney and lung compared to microglia (middle) and in adult MOs and adult tissue MFs (right). Throughout the figure, bars represent mean ± SEM (n = 3–6, two pooled experiments, *p < 0.05; **p < 0.01; ***p < 0.001).

(H) Scheme representing fetal monoipoiesis based on GSEA of each FL progenitor DEG combined with CMAP analysis (see also heatmap of FL myeloid progenitors DEG in Figure S4E, Tables S2 and S3 for GSEA details and Figure S4D for myeloid gene heatmap).

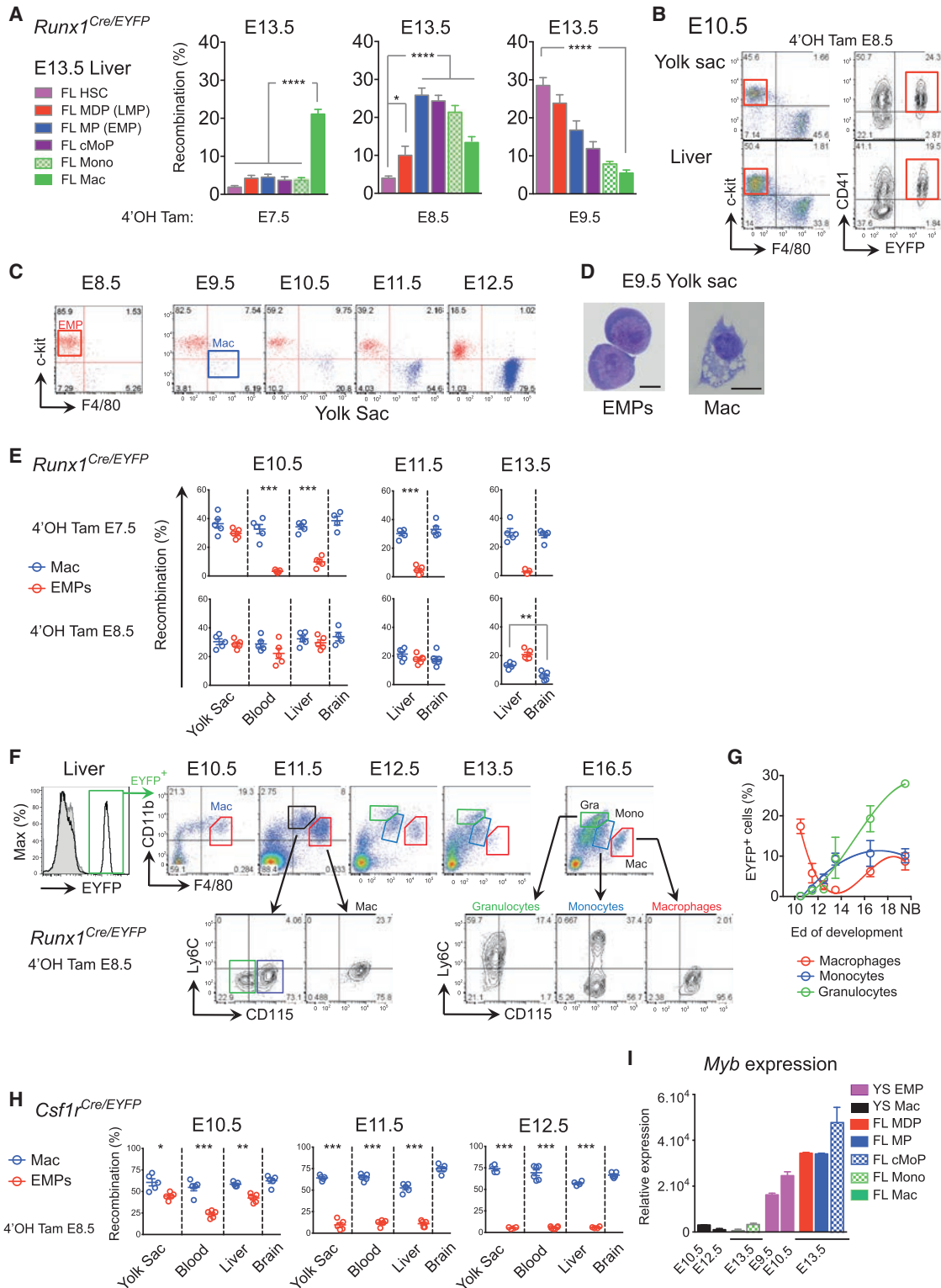


Figure 5. c-Myb⁺ EMPs Colonizes the Fetal Liver and Give Rise to Monocytes

Runx1^{Cre/Eyfp} embryos activated either at E7.5, E8.5 or E9.5. Percentage of recombination in FL HSC, MDP, MP, cMoP, MOs, and MFs (two pooled litters, n = 7–13) (A) and in YS CD41⁺ EMPs (B) (see also Figure S5 for gating strategy, pre-HSC, and EMP analysis).

(C) The YS from E8.5 to E12.5 embryos were analyzed by flow cytometry for presence of c-Kit⁺ progenitors and F4/80⁺ MF.

(D) E9.5 EMPs (doublet⁻ DAPI⁻ CD11b⁻ F4/80⁻ c-Kit⁺ CD41⁺) and YS MFs (doublet⁻ DAPI⁻ CD11b⁺ F4/80⁺) were sorted and visualized by GIEMSA staining.

(legend continued on next page)

such as fish, amphibians, and birds that remain nucleated throughout their lifespan (Palis, 2014). Such denomination was extended to MFs in the YS due to their concomitant development before the emergence of FL hematopoiesis. However, the notion of primitive versus definitive has been rather ambiguous for MFs but could now be clarified by our findings. Here, we have revealed a further layer of complexity to fetal MF generation: using our Runx1 fate-mapping system, we identified an early wave of E7.5 Runx1⁺ progenitors that give rise to the EMPs, which differentiate locally into YS MF, and a distinct second later wave of E8.5 Runx1⁺ progenitors that give rise to the EMPs, which retain the ability to differentiate locally into YS MFs, or migrate to seed the FL following the establishment of blood circulation from E9.0. The two waves of EMPs differed in their lineage potency and capacity to generate MO intermediates in the FL and YS. MFs deriving in the YS from either early or late EMPs did not seem to go through a monocytic intermediate stage, but rather followed a “fast-track” differentiation pathway, as previously described (Takahashi et al., 1989). Hence, the denomination “primitive macrophage” could now be used to refer to MFs generated in the YS without a monocytic intermediate, and might even be extended to early EMPs that differentiate locally in the YS, to distinguish them from definitive EMPs that give rise to MO intermediates in the FL. Whether early primitive EMPs and late definitive EMPs represent two heterogeneous progenitors arising from independent sources or rather a single population arising from a shared hematopoietic wave of progenitors and exists along a continuum of maturation stages in response to external stimuli, requires clarification. However, it is tempting to speculate that the contrasts in differentiation potential do not reside in the intrinsic potential given by their ontogeny, but rather in the extrinsic signals provided by the local environment. In fact, their multi-lineage potential is revealed upon establishment of blood circulation, which allows late YS EMPs to access the FLs where they encounter a microenvironment that permits their development along multiple lineages at the expense of uni-lineage MF progenitors.

Recent work by the Rodewald's group suggested that fetal MFs arise from HSC-independent YS EMPs (Perdiguer et al., 2014); while we agree that EMPs arise in the YS and contribute to most tissue-resident MFs, our data clearly demonstrate that two waves of EMPs exist and differentially contribute to tissue MF populations. The primitive wave gives rise mostly to local YS MFs without monocytic intermediates, and then to microglia, and the definitive wave gives rise to FL MOs (among other lineages) which subsequently differentiate into tissue MFs. Our work emphasizes the necessary contribution of FL MOs to most tissue-resident MFs with the exception of microglia. Of note, in this prior study and as shown in our work, injection of

4'OHT at E8.5 or E9.5 in the inducible *Csf1r*^{Cre/WT} model does not efficiently tag late EMPs and FL MOs, while efficiently labeling YS MFs. This is likely because early EMPs express CSF-1R mRNA, while late EMPs do not. Such differential expression of CSF-1R highlights the molecular heterogeneity of early versus late EMPs. Finally, absence of long-term follow up of the tagged cell progeny in the inducible *Csf1r*^{Cre/WT} model limits the capacity to differentiate between the contribution of primitive versus definitive EMPs in this later study (Perdiguer et al., 2014).

The differences in EMP lineage potential could be acquired through expression of c-Myb, a transcription factor required for expansion and differentiation along each of the hematopoietic cell lineages (Ramsay and Gonda, 2008). C-Myb ablation compromises definitive hematopoiesis and leads to embryonic death at E15.5 (Mucenski et al., 1991); while the earliest YS progenitors, which give rise to microglia, do not express c-Myb (Kierdorf et al., 2013), we show that EMPs arising from E8.5 do. This agrees with previous reports indicating that primitive hematopoiesis can occur independently of c-Myb (Clarke et al., 2000), whereas EMPs from definitive hematopoiesis both express and depend upon c-Myb (Palis et al., 1999; Sumner et al., 2000; Yoder et al., 1997). Because fetal MOs are absent in c-Myb-deficient embryos (Mucenski et al., 1991; Schulz et al., 2012) and c-Myb expression is upregulated during fetal monopoiesis, it is likely that the change in EMP fate between the YS and the FL is orchestrated by c-Myb. Consequently, most tissue-resident MFs deriving from either HSC-dependent or independent fetal MOs, rely on c-Myb activity for their generation. Earlier findings in a different model suggested that tissue MFs derive from a c-Myb-independent lineage via YS MFs (Schulz et al., 2012). While embryonic YS MF numbers were unaffected by the absence of c-Myb, far fewer c-Kit⁺ cells were present in the FL of *Myb*^{-/-} embryos than wild-type (Schulz et al., 2012). Because our data suggest that EMPs express c-Myb in the YS and in the FL, whereas E10.5 YS MFs do not, we support the notion that late multipotent EMPs are Myb-dependent. As a result, their contribution to tissue-resident MF populations could not be evaluated in the *Myb*^{-/-} embryos (Schulz et al., 2012). It may be that fetal MFs are unaffected in E16.5 *Myb*^{-/-} embryos (Schulz et al., 2012) because they derive from c-Myb-independent early EMPs giving rise to primitive MFs able to occupy the empty niche left by the absence of c-Myb-dependent myeloid cells, as a compensatory mechanism.

Microglia have a unique origin, arising from YS MFs that maintain themselves by proliferating in situ throughout adulthood, and not from fetal MOs (Ginhoux et al., 2010; Kierdorf et al., 2013). The lack of contribution from MOs to the microglial progenitor pool could result either from a lack of intrinsic potential or a lack of access to the developing brain. The dual

(E) *Runx1*^{Cre/eyfp} embryos were activated at E7.5 (upper panels) or E8.5 (lower panels). Recombination profile in YS, blood and FL and brain MFs (blue) or EMPs (red) at E10.5, E11.5, and E13.5 are shown (n = 5–6 from two experiments).

(F) EYFP⁺ EMPs from *Runx1*^{Cre/eyfp} activated at E8.5 and EMP progeny were followed in the FL during development. Primitive MFs (red), fetal MOs (blue), and granulocyte (green) generation is depicted.

(G) Quantification of MFs (red), fetal MOs (blue), and granulocytes (green) during development (n = 5–12 embryos from two independent experiments).

(H) *Csf1r*^{Cre/eyfp} embryos were activated at E8.5. EYFP recombination at E10.5, E11.5, and E12.5 in YS, blood, FL and brain MFs (blue), or EMPs (red) are shown (n = 5–6 from two experiments).

(I) YS EMP, YS MF, FL myeloid progenitors, MOs, and MFs were sorted and c-Myb mRNA expression was measured by Q-PCR. Data are represented as mean ± SEM from triplicate samples where each sample was comprised of at least eight embryos. Throughout the figure, each dot represents one embryo; bars represent mean ± SEM (*p < 0.05; **p < 0.01; ***p < 0.001).

origin of LCs suggests that the progenitor differentiation program is not intrinsic to either YS- or FL-derived progenitors, but rather depends on tissue-specific extrinsic factors (Hoeffel et al., 2012). Corroborating the latter hypothesis, the blood-brain barrier is starting to be established around E13.5 (Daneman et al., 2010), precisely when fetal MOs colonize the tissues, thereby explaining the minor influx of fetal MOs to the embryonic brain. In addition, upon depletion of YS MFs, we observed the disappearance of microglial progenitors from E10.5 to E14.5, followed by a partial repopulation at E17.5 that will be completed after birth (Squarzone et al., 2014), raising the question of the origin of the repopulating cells. The nature of the repopulating cell is under investigation, but we noted a major influx of MOs in the brain at E14.5, a population that is not found normally. In addition, preliminary data using our *S100a4^{Cre/WT}* fate-mapping model combined with in utero depletion of YS MFs suggest that fetal MOs give rise to all repopulating fetal MF populations including microglia (data not shown), excluding the possibility that tissue MFs might formally be derived from YS MFs that escaped antibody depletion. This suggests that fetal MOs might give rise to microglia if they are able to access the brain rudiment (provided after YS MF depletion). Finally, these findings highlight the crucial role that tissues play in shaping the MF compartment, from the stage of controlling recruitment of MF progenitors right through until the maturation of recruited cells into the adult MF population.

Altogether our data provide a framework for the future investigation of adult MF population heterogeneity in both regard to their ontogeny, as well as their homeostasis at the progenitor level. This forms a firm grounding for our understanding of their roles in tissues in the steady state, as well as their involvement in diverse pathological settings and their potential as therapeutic targets including metabolic diseases, fibrosis, and carcinogenesis, and opens the door to MF-targeted therapeutic interventions.

EXPERIMENTAL PROCEDURES

Cell Suspension Preparations

Mouse ears (split into dorsal and ventral parts) or whole skin (starting from E17.5) were first incubated for 2 hr in Hank's balanced salt solution (HBSS) containing Dispase (2.4 mg/ml, working activity of 1.7 U/mg; Invitrogen) to separate dermal and epidermal sheets before subsequent collagenase incubation. Whole tissues from adult mice, newborns or embryos were cut into small pieces, incubated in HBSS containing 10% fetal bovine serum and collagenase type IV (0.2 mg/ml, working activity of 770 U/mg; Sigma; 1 hr for adult tissues and newborns and 30 min for embryonic tissues) and then passaged through a 19G needle to obtain a homogeneous cell suspension. Embryonic blood cells were collected by decapitation in PBS 10 mM EDTA and red blood cells were lysed. When embryos were harvested prior to E13.5, the different tissues were isolated under a binocular microscope (Leica M320). For fetal liver cell suspensions, the whole liver was isolated and passed through a 19G needle without collagenase treatment. Analysis was carried out by flow cytometry, gating on singlets of DAPI⁺ (4,6-diamidino-2-phenylindole) CD45⁺ cells.

Induction of Cell Tagging with 4-Hydroxytamoxifen

For fate-mapping experiments, *Runx1^{MerCreMer/WT} × Rosa^{R26R-EYFP/R26R-EYFP}* mice were used as described (Samokhvalov et al., 2007). Briefly, 4-hydroxytamoxifen (4'OHT) (Sigma) was prepared as previously reported and administered by intraperitoneal injection (3–5 mg) to pregnant mice at 7.0–10.0 days post-conception (dpc). Day of embryonic development was estimated by

taking the day of vaginal plug observation as 0.5 dpc. As 4'OHT treatment during pregnancy interferes with normal delivery, to trace cells marked during embryogenesis into adulthood, caesarean sections were carried out at term and neonates were fostered by lactating females. Active recombination in these genetically targeted mice occurs in a narrow time frame that does not exceed 24 hr post-injection and leads to irreversible expression of the enhanced yellow fluorescent protein (EYFP) in *Runx1⁺* cells and their progeny (Samokhvalov et al., 2007). Similar procedures were followed for the use of *Csf1^{MerCreMer/WT}* mice.

Flow Cytometry

Flow cytometric studies were performed using a BD FACSCanto and a BD LSR II (BD Biosciences) with subsequent data analysis using FlowJo software (Tree Star). Fluorochrome- or biotin- conjugated monoclonal antibodies (mAbs) (see Supplemental Experimental Procedures), the corresponding isotype-matched controls, and secondary reagents were purchased either from BD Biosciences or eBioscience. Annexin-V staining was performed using the Annexin kit (BD PharMingen) according to the manufacturer's protocol.

Yolk Sac Macrophage Depletion

Pregnant C57BL/6 females were treated with anti-CSF-1R mAb (α CSF-1R, clone AFS98) or the rat IgG2a isotype control (clone R35-95; BD Biosciences) at E6.5 by intraperitoneal injection (3 mg, in sterile PBS). α CSF-1R mAb was purified from culture supernatant of AFS98 hybridoma (Sudo et al., 1995), grown in a CELLLine Flask (BD) in serum-free medium (PFHM-II; Invitrogen).

In Vivo Proliferation Assay

Proliferation of monocyte and macrophage populations was investigated using the fluorescent ubiquitination-based cell-cycle indicator (Fucci) transgenic mouse model in which the green-emitting fluorescent protein Azami Green is fused to Geminin, a ubiquitination oscillator whose expression is regulated by cell-cycle-dependent proteolysis, resulting in the expression of fluorescence in cells in S/G2/M phases (Sakaue-Sawano et al., 2008) and their identification by flow cytometry.

Statistical Analysis

Repeated-measures ANOVA, Mann-Whitney tests, and unpaired t tests (with a 95% confidence) were performed using Prism 6.0 (GraphPad Software). All p-values are two-tailed. *p < 0.05; **p < 0.01; and ***p < 0.001.

ACCESSION NUMBERS

The microarray data are available in the Gene Expression Omnibus (GEO) database (<http://www.ncbi.nlm.nih.gov/gds>) under the accession number GSE66970.

SUPPLEMENTAL INFORMATION

Supplemental Information includes five figures, three tables, and Supplemental Experimental Procedures and can be found with this article online at <http://dx.doi.org/10.1016/j.immuni.2015.03.011>.

AUTHOR CONTRIBUTIONS

F.G. and G.H. conceived the study; G.H., Y.L., D.L., F.F.A., P.S., A.E.B., J.L., I.L., and M.G. performed experiments; G.H., Y.L., A.E.B., E.C.F., and M.G. analyzed data; G.H., J.C., M.P., F.Z., and F.G. analyzed bioinformatics data; L.G.N., A.L., J.K.Y.C., and I.M.S. provided reagents; B.B., I.M.S., and M.M. provided intellectual guidance; and F.G., M.M., and G.H. wrote the paper.

ACKNOWLEDGMENTS

This work was supported by core grants of the Singapore Immunology Network to F.G., by NIH grants CA112100, HL086899, and AI080884 to M.M., by the NMRC Singapore (NMRC/CSA/012/2009) for J.K.Y.C. *Runx1-MerCreMer* mice have RIKEN CDB Acc. No. CDB0524K. We thank Dr. Lucy

Robinson of Insight Editing London for her assistance in preparing the manuscript.

Received: December 20, 2014

Revised: February 17, 2015

Accepted: March 27, 2015

Published: April 21, 2015

REFERENCES

- Bain, C.C., Bravo-Blas, A., Scott, C.L., Gomez Perdiguero, E., Geissmann, F., Henri, S., Malissen, B., Osborne, L.C., Artis, D., and Mowat, A.M. (2014). Constant replenishment from circulating monocytes maintains the macrophage pool in the intestine of adult mice. *Nat. Immunol.* **15**, 929–937.
- Bertrand, J.Y., Jalil, A., Klaine, M., Jung, S., Cumano, A., and Godin, I. (2005). Three pathways to mature macrophages in the early mouse yolk sac. *Blood* **106**, 3004–3011.
- Bhowmick, N.A., Chytil, A., Plieth, D., Gorska, A.E., Dumont, N., Shappell, S., Washington, M.K., Neilson, E.G., and Moses, H.L. (2004). TGF- β signaling in fibroblasts modulates the oncogenic potential of adjacent epithelia. *Science* **303**, 848–851.
- Böiers, C., Carrelha, J., Lutteropp, M., Luc, S., Green, J.C., Azzoni, E., Woll, P.S., Mead, A.J., Hultquist, A., Swiers, G., et al. (2013). Lymphomyeloid contribution of an immune-restricted progenitor emerging prior to definitive hematopoietic stem cells. *Cell Stem Cell* **13**, 535–548.
- Boyer, S.W., Schroeder, A.V., Smith-Berdan, S., and Forsberg, E.C. (2011). All hematopoietic cells develop from hematopoietic stem cells through Flk2/Flt3-positive progenitor cells. *Cell Stem Cell* **9**, 64–73.
- Buza-Vidas, N., Woll, P., Hultquist, A., Duarte, S., Lutteropp, M., Bouriez-Jones, T., Ferry, H., Luc, S., and Jacobsen, S.E. (2011). FLT3 expression initiates in fully multipotent mouse hematopoietic progenitor cells. *Blood* **118**, 1544–1548.
- Christensen, J.L., Wright, D.E., Wagers, A.J., and Weissman, I.L. (2004). Circulation and chemotaxis of fetal hematopoietic stem cells. *PLoS Biol.* **2**, E75.
- Clarke, D., Vegiopoulos, A., Crawford, A., Mucenski, M., Bonifer, C., and Frampton, J. (2000). In vitro differentiation of c-myb(-/-) ES cells reveals that the colony forming capacity of unilineage macrophage precursors and myeloid progenitor commitment are c-Myb independent. *Oncogene* **19**, 3343–3351.
- Cline, M.J., and Moore, M.A. (1972). Embryonic origin of the mouse macrophage. *Blood* **39**, 842–849.
- Daneman, R., Zhou, L., Kebede, A.A., and Barres, B.A. (2010). Pericytes are required for blood-brain barrier integrity during embryogenesis. *Nature* **468**, 562–566.
- Dzierzak, E., and Speck, N.A. (2008). Of lineage and legacy: the development of mammalian hematopoietic stem cells. *Nat. Immunol.* **9**, 129–136.
- Epelman, S., Lavine, K.J., Beaudin, A.E., Sojka, D.K., Carrero, J.A., Calderon, B., Brijja, T., Gautier, E.L., Ivanov, S., Satpathy, A.T., et al. (2014). Embryonic and adult-derived resident cardiac macrophages are maintained through distinct mechanisms at steady state and during inflammation. *Immunity* **40**, 91–104.
- Frame, J.M., McGrath, K.E., and Palis, J. (2013). Erythro-myeloid progenitors: “definitive” hematopoiesis in the conceptus prior to the emergence of hematopoietic stem cells. *Blood Cells Mol. Dis.* **51**, 220–225.
- Friedman, A.D. (2002). Transcriptional regulation of granulocyte and monocyte development. *Oncogene* **21**, 3377–3390.
- Geissmann, F., Jung, S., and Littman, D.R. (2003). Blood monocytes consist of two principal subsets with distinct migratory properties. *Immunity* **19**, 71–82.
- Ginhoux, F., and Jung, S. (2014). Monocytes and macrophages: developmental pathways and tissue homeostasis. *Nat. Rev. Immunol.* **14**, 392–404.
- Ginhoux, F., Greter, M., Leboeuf, M., Nandi, S., See, P., Gokhan, S., Mehler, M.F., Conway, S.J., Ng, L.G., Stanley, E.R., et al. (2010). Fate mapping analysis reveals that adult microglia derive from primitive macrophages. *Science* **330**, 841–845.
- Golub, R., and Cumano, A. (2013). Embryonic hematopoiesis. *Blood Cells Mol. Dis.* **51**, 226–231.
- Guilliams, M., De Kleer, I., Henri, S., Post, S., Vanhoutte, L., De Prijck, S., Deswarte, K., Malissen, B., Hammad, H., and Lambrecht, B.N. (2013). Alveolar macrophages develop from fetal monocytes that differentiate into long-lived cells in the first week of life via GM-CSF. *J. Exp. Med.* **210**, 1977–1992.
- Hashimoto, D., Chow, A., Noizat, C., Teo, P., Beasley, M.B., Leboeuf, M., Becker, C.D., See, P., Price, J., Lucas, D., et al. (2013). Tissue-resident macrophages self-maintain locally throughout adult life with minimal contribution from circulating monocytes. *Immunity* **38**, 792–804.
- Hettinger, J., Richards, D.M., Hansson, J., Barra, M.M., Joschko, A.C., Krijgsveld, J., and Feuerer, M. (2013). Origin of monocytes and macrophages in a committed progenitor. *Nat. Immunol.* **14**, 821–830.
- Hoeffel, G., Wang, Y., Greter, M., See, P., Teo, P., Malleret, B., Leboeuf, M., Low, D., Oller, G., Almeida, F., et al. (2012). Adult Langerhans cells derive predominantly from embryonic fetal liver monocytes with a minor contribution of yolk sac-derived macrophages. *J. Exp. Med.* **209**, 1167–1181.
- Jakubzick, C., Gautier, E.L., Gibbings, S.L., Sojka, D.K., Schlitzer, A., Johnson, T.E., Ivanov, S., Duan, Q., Bala, S., Condon, T., et al. (2013). Minimal differentiation of classical monocytes as they survey steady-state tissues and transport antigen to lymph nodes. *Immunity* **39**, 599–610.
- Jenkins, S.J., Ruckerl, D., Cook, P.C., Jones, L.H., Finkelman, F.D., van Rooijen, N., MacDonald, A.S., and Allen, J.E. (2011). Local macrophage proliferation, rather than recruitment from the blood, is a signature of TH2 inflammation. *Science* **332**, 1284–1288.
- Kierdorf, K., Erny, D., Goldmann, T., Sander, V., Schulz, C., Perdiguero, E.G., Wieghofer, P., Heinrich, A., Riemke, P., Hölscher, C., et al. (2013). Microglia emerge from erythromyeloid precursors via Pu.1- and Irf8-dependent pathways. *Nat. Neurosci.* **16**, 273–280.
- Kiuseseian, A., Brunet de la Grange, P., Burlen-Defranoux, O., Godin, I., and Cumano, A. (2012). Immature hematopoietic stem cells undergo maturation in the fetal liver. *Development* **139**, 3521–3530.
- Kumaravelu, P., Hook, L., Morrison, A.M., Ure, J., Zhao, S., Zuyev, S., Ansell, J., and Medvinsky, A. (2002). Quantitative developmental anatomy of definitive haematopoietic stem cells/long-term repopulating units (HSC/RUs): role of the aorta-gonad-mesonephros (AGM) region and the yolk sac in colonisation of the mouse embryonic liver. *Development* **129**, 4891–4899.
- Lavin, Y., and Merad, M. (2013). Macrophages: gatekeepers of tissue integrity. *Cancer immunology research* **1**, 201–209.
- Lin, Y., Yoder, M.C., and Yoshimoto, M. (2014). Lymphoid progenitor emergence in the murine embryo and yolk sac precedes stem cell detection. *Stem Cells Dev.* **23**, 1168–1177.
- Medvinsky, A., Rybtsov, S., and Taoudi, S. (2011). Embryonic origin of the adult hematopoietic system: advances and questions. *Development* **138**, 1017–1031.
- Molawi, K., and Sieweke, M.H. (2013). Transcriptional control of macrophage identity, self-renewal, and function. *Adv. Immunol.* **120**, 269–300.
- Moore, M.A., and Metcalf, D. (1970). Ontogeny of the haemopoietic system: yolk sac origin of in vivo and in vitro colony forming cells in the developing mouse embryo. *Br. J. Haematol.* **18**, 279–296.
- Mucenski, M.L., McLain, K., Kier, A.B., Swerdlow, S.H., Schreiner, C.M., Miller, T.A., Pietryga, D.W., Scott, W.J., Jr., and Potter, S.S. (1991). A functional c-myb gene is required for normal murine fetal hepatic hematopoiesis. *Cell* **65**, 677–689.
- Naito, M., Takahashi, K., and Nishikawa, S. (1990). Development, differentiation, and maturation of macrophages in the fetal mouse liver. *J. Leukoc. Biol.* **48**, 27–37.
- Orkin, S.H., and Zon, L.I. (2008). Hematopoiesis: an evolving paradigm for stem cell biology. *Cell* **132**, 631–644.
- Palis, J. (2014). Primitive and definitive erythropoiesis in mammals. *Frontiers in physiology* **5**, 3.
- Palis, J., and Yoder, M.C. (2001). Yolk-sac hematopoiesis: the first blood cells of mouse and man. *Exp. Hematol.* **29**, 927–936.

- Palis, J., Robertson, S., Kennedy, M., Wall, C., and Keller, G. (1999). Development of erythroid and myeloid progenitors in the yolk sac and embryo proper of the mouse. *Development* *126*, 5073–5084.
- Perdiguerro, E.G., Klapproth, K., Schulz, C., Busch, K., Azzoni, E., Crozet, L., Garner, H., Trouillet, C., de Bruijn, M.F., Geissmann, F., and Rodewald, H.R. (2014). Tissue-resident macrophages originate from yolk-sac-derived erythro-myeloid progenitors. *Nature* *518*, 547–551.
- Qian, B.Z., Li, J., Zhang, H., Kitamura, T., Zhang, J., Campion, L.R., Kaiser, E.A., Snyder, L.A., and Pollard, J.W. (2011). CCL2 recruits inflammatory monocytes to facilitate breast-tumour metastasis. *Nature* *475*, 222–225.
- Ramsay, R.G., and Gonda, T.J. (2008). MYB function in normal and cancer cells. *Nat. Rev. Cancer* *8*, 523–534.
- Sakaue-Sawano, A., Kurokawa, H., Morimura, T., Hanyu, A., Hama, H., Osawa, H., Kashiwagi, S., Fukami, K., Miyata, T., Miyoshi, H., et al. (2008). Visualizing spatiotemporal dynamics of multicellular cell-cycle progression. *Cell* *132*, 487–498.
- Samokhvalov, I.M., Samokhvalova, N.I., and Nishikawa, S. (2007). Cell tracing shows the contribution of the yolk sac to adult haematopoiesis. *Nature* *446*, 1056–1061.
- Schneider, C., Nobs, S.P., Kurrer, M., Rehrauer, H., Thiele, C., and Kopf, M. (2014). Induction of the nuclear receptor PPAR- γ by the cytokine GM-CSF is critical for the differentiation of fetal monocytes into alveolar macrophages. *Nat. Immunol.* *15*, 1026–1037.
- Schulz, C., Gomez Perdiguerro, E., Chorro, L., Szabo-Rogers, H., Cagnard, N., Kierdorf, K., Prinz, M., Wu, B., Jacobsen, S.E., Pollard, J.W., et al. (2012). A lineage of myeloid cells independent of Myb and hematopoietic stem cells. *Science* *336*, 86–90.
- Serbina, N.V., and Pamer, E.G. (2006). Monocyte emigration from bone marrow during bacterial infection requires signals mediated by chemokine receptor CCR2. *Nat. Immunol.* *7*, 311–317.
- Squarzoni, P., Oller, G., Hoeffel, G., Pont-Lezica, L., Rostaing, P., Low, D., Bessis, A., Ginhoux, F., and Garel, S. (2014). Microglia modulate wiring of the embryonic forebrain. *Cell Rep.* *8*, 1271–1279.
- Sudo, T., Nishikawa, S., Ogawa, M., Kataoka, H., Ohno, N., Izawa, A., Hayashi, S., and Nishikawa, S. (1995). Functional hierarchy of c-kit and c-fms in intramarrow production of CFU-M. *Oncogene* *11*, 2469–2476.
- Sumner, R., Crawford, A., Mucenski, M., and Frampton, J. (2000). Initiation of adult myelopoiesis can occur in the absence of c-Myb whereas subsequent development is strictly dependent on the transcription factor. *Oncogene* *19*, 3335–3342.
- Takahashi, K., Yamamura, F., and Naito, M. (1989). Differentiation, maturation, and proliferation of macrophages in the mouse yolk sac: a light-microscopic, enzyme-cytochemical, immunohistochemical, and ultrastructural study. *J. Leukoc. Biol.* *45*, 87–96.
- Tamoutounour, S., Guilliams, M., Montanana Sanchis, F., Liu, H., Terhorst, D., Malosse, C., Pollet, E., Ardouin, L., Luche, H., Sanchez, C., et al. (2013). Origins and functional specialization of macrophages and of conventional and monocyte-derived dendritic cells in mouse skin. *Immunity* *39*, 925–938.
- Tavian, M., and Péault, B. (2005). Embryonic development of the human hematopoietic system. *Int. J. Dev. Biol.* *49*, 243–250.
- van Furth, R., Cohn, Z.A., Hirsch, J.G., Humphrey, J.H., Spector, W.G., and Langevoort, H.L. (1972). The mononuclear phagocyte system: a new classification of macrophages, monocytes, and their precursor cells. *Bull. World Health Organ.* *46*, 845–852.
- Yoder, M.C., Hiatt, K., Dutt, P., Mukherjee, P., Bodine, D.M., and Orlic, D. (1997). Characterization of definitive lymphohematopoietic stem cells in the day 9 murine yolk sac. *Immunity* *7*, 335–344.
- Yona, S., Kim, K.W., Wolf, Y., Mildner, A., Varol, D., Breker, M., Strauss-Ayali, D., Viukov, S., Guilliams, M., Misharin, A., et al. (2013). Fate mapping reveals origins and dynamics of monocytes and tissue macrophages under homeostasis. *Immunity* *38*, 79–91.

Interleukin-33 and Interferon- γ Counter-Regulate Group 2 Innate Lymphoid Cell Activation during Immune Perturbation

Ari B. Molofsky,^{4,5} Frédéric Van Gool,² Hong-Erh Liang,¹ Steven J. Van Dyken,^{1,4} Jesse C. Nussbaum,^{3,4} Jinwoo Lee,⁴ Jeffrey A. Bluestone,^{2,4} and Richard M. Locksley^{1,3,4,*}

¹Howard Hughes Medical Institute

²Diabetes Center

³Department of Medicine

⁴Department of Microbiology & Immunology

⁵Department of Laboratory Medicine

University of California, San Francisco, San Francisco, CA 94143-0795, USA

*Correspondence: locksley@medicine.ucsf.edu

<http://dx.doi.org/10.1016/j.immuni.2015.05.019>

SUMMARY

Group 2 innate lymphoid cells (ILC2s) and regulatory T (Treg) cells are systemically induced by helminth infection but also sustain metabolic homeostasis in adipose tissue and contribute to tissue repair during injury. Here we show that interleukin-33 (IL-33) mediates activation of ILC2s and Treg cells in resting adipose tissue, but also after helminth infection or treatment with IL-2. Unexpectedly, ILC2-intrinsic IL-33 activation was required for Treg cell accumulation *in vivo* and was independent of ILC2 type 2 cytokines but partially dependent on direct co-stimulatory interactions via ICOSL-ICOS. IFN- γ inhibited ILC2 activation and Treg cell accumulation by IL-33 in infected tissue, as well as adipose tissue, where repression increased with aging and high-fat diet-induced obesity. IL-33 and ILC2s are central mediators of type 2 immune responses that promote tissue and metabolic homeostasis, and IFN- γ suppresses this pathway, likely to promote inflammatory responses and divert metabolic resources necessary to protect the host.

INTRODUCTION

Allergic, or type 2, immunity occurs in response to parasitic helminths, restricting sites permissive for parasite reproduction and limiting tissue damage. Such responses involve activation of group 2 innate lymphoid cells (ILC2s) and adaptive CD4⁺ Th2 cells, which together secrete the cytokines interleukin-4 (IL-4), IL-5, and IL-13 necessary for the accumulation of eosinophils and alternatively activated macrophages (AAMs) in involved tissues (Walker and McKenzie, 2013). In turn, chronic parasitism induces regulatory T (Treg) cells, which dampen immune pathology not only in helminth infection, but also in a variety of mouse and human conditions characterized by excess immune

activation, such as autoimmunity, graft-versus-host disease, and metabolic syndrome (Johnston et al., 2014; McSorley and Maizels, 2012; Wiria et al., 2014). Indeed, one of the key issues during allergic pathology provoked by common environmental allergens might be the failure to induce or maintain Treg cells (Allen and Maizels, 2011). Although transcriptional networks are establishing connections between Treg cells and the subsets of effector T cells they restrain (Chaudhry and Rudensky, 2013), cellular networks that link these effector and regulatory modules are incompletely understood. Further insights will be important in considering therapeutic strategies to control chronic pathologic states characterized by loss (allergy, atopy) or gain (cancer, chronic infectious diseases) in this regulatory-to-effector cell balance.

Recent reports have called attention to the confluence of innate cells associated with type 2 immunity, including ILC2s, eosinophils, and AAMs, with Treg cells in visceral adipose tissue (VAT) of resting mice (Cipolletta et al., 2012; Feuerer et al., 2009; Molofsky et al., 2013; Odegaard et al., 2007; Qiu et al., 2014; Vasanthakumar et al., 2015; Wu et al., 2011). Maintaining this cellular architecture is necessary for metabolic homeostasis, and its loss during obesity is associated with increased inflammatory T cells, macrophages, and the development of insulin resistance and type 2 diabetes. Adipose ILC2s and Treg cells constitutively express interleukin-1 receptor-like 1, (IL1RL1, ST2), the regulated subunit of the receptor for the IL-1 family member IL-33, a cytokine maintained in the nucleus of some epithelial, endothelial, and mesenchymal cells (Pichery et al., 2012) (Cayrol and Girard, 2014). IL-33 is released during necrosis or possibly via other regulated mechanisms, and stimulates ILC2s to produce cytokines like IL-13 and IL-5, important for the response to helminths and allergens (Neill et al., 2010). Exogenous IL-33 induces expansion of adipose tissue ILC2 and Treg cells (Molofsky et al., 2013; Vasanthakumar et al., 2015) and beneficial metabolic effects (Miller et al., 2010), acting in part via ILC2-mediated induction of “beige” adipose tissue associated with increased heat production (Brestoff et al., 2014; Lee et al., 2015). IL-33 administration also expands systemic Treg cells that suppress the rejection of allogeneic cardiac transplants (Brunner et al., 2011; Turnquist et al., 2011), and IL-33 promotes

resolution of tissue damage in models of colitis (Duan et al., 2012; Schiering et al., 2014), hepatitis (Liang et al., 2013), cutaneous wounding (Yin et al., 2013), central nervous system injury (Gadani et al., 2015), and atherosclerosis (Miller et al., 2008). On the basis of these prior findings, here we determine the role of ILC2s in regulating Treg cells under conditions of elevated IL-33, including resting adipose tissue and during helminth infection. We found that ILC2-intrinsic IL-33 signaling and ICOSL expression promoted Treg cell accumulation, whereas the inflammatory cytokine IFN- γ counter-regulated the effects of IL-33, in part through direct effects on ILC2s.

RESULTS

Visceral Adipose Tissue IL-33 Promotes ILC2 Function and Treg Cell Maintenance

We documented high concentrations of IL-33 in adipose tissue as compared to lung or spleen (Figure 1A), corroborating prior studies (Miller et al., 2010; Vasanthakumar et al., 2015; Zeyda et al., 2012). IL-33 was expressed selectively in the nuclei of many adipose tissue endothelial cells (Figure 1B, Figure S1A and S1B, data not shown). Although we confirmed IL-33-positive cells in mouse lung and spleen, where expression has been reported for alveolar type 2 pneumocytes and fibroblastic reticular cells (FRC), respectively, endothelium from these tissues did not express IL-33 (Figure S1A, and Pichery et al., 2012). In contrast, human endothelial expression of IL-33 is more widespread (Pichery et al., 2012). VAT ILC2s express IL1RL1 (ST2) and localize near the adipose tissue vasculature (Figure S1B and Molofsky et al., 2013) suggesting they might be sensitized by endothelial IL-33. We used previously described “Red5” IL-5^{tdtomato-cre} reporter mice (Nussbaum et al., 2013) to assess the expression of IL-5 in ILC2 without the need for ex vivo stimulation. ILC2 IL-5 production was diminished in adipose ILC2s from IL1RL1-deficient mice (Figure 1C, Figure S1C). Although less numerous than ILC2s, IL-5⁺ CD4⁺ Th2 cells that accumulate in adipose tissue also showed diminished IL-5 expression in the absence of IL-33 signals (Figures S1D and S1E). Despite their lower IL-5 production, the numbers of ILC2s and primed, IL-4-competent CD4⁺ Th2 cells in VAT were not decreased by the loss of IL-33 signaling (Figure S1C, data not shown). The attenuated IL-5 expression in VAT of IL1RL1-deficient mice resulted in a diminution in numbers of VAT eosinophils, consistent with a biologically relevant effect that was not evident in blood or lung (Figure 1D).

Treg cells accumulate in VAT of 4- to 6-month-old mice and express high amounts of GATA3, IL1RL1, KLRG1, and CD25 (Figure 1E, Figure S1F, data not shown), consistent with an activated or “effector” tissue-resident phenotype (Burzyn et al., 2013b; Cipolletta et al., 2012; Feuerer et al., 2009; Vasanthakumar et al., 2015). Accumulation of Treg cells was attenuated by loss of IL-33 signals in VAT, but not in lung or spleen (Figures 1F and 1G, Figure S1G). Even on normal chow diet, IL1RL1-deficient animals develop significant increases in VAT CD8⁺ T cells after 12–16 weeks (wild-type 6,801+/-1221 cells, IL1RL1-deficient 10,670+/-1176 cells, $p = 0.03$, $n = 16$ –18). Thus, IL-33 promotes VAT ILC2 cytokine expression associated with the accumulation of VAT eosinophils and activated Treg cells, and suppresses the accumulation of CD8⁺ T cells, thus potentially limiting adipose inflammation and obesity (Miller et al., 2010).

Next we tested the ability of isolated Treg cells and ILC2s to respond directly to IL-33. Although splenic Treg cells, which are largely IL1RL1⁻ at the time of isolation, were not affected by addition of IL-33 to short-term in vitro suppression assays, VAT IL1RL1⁺ Treg cells demonstrated enhanced suppression in the presence of IL-33, particularly at low Treg-to-Teffector ratios (Figure 2A). Given once in vivo, IL-33 rapidly enhances CD25 expression on VAT IL1RL1⁺ Treg cells and drives their entry into the cell cycle (Figures S2A and S2B). VAT IL1RL1⁺ ILC2 and Th2 also respond to IL-33 by increasing CD25, proliferating, and increasing IL-5 production, as assessed by MFI of the IL-5 reporter (Figures S2C–S2E). Non-IL-5⁺ CD4⁺ T cells and NK cells in VAT do not respond to IL-33 or IL-2 over this time period (data not shown). Thus, IL-33 can directly promote the proliferation, activation and function of IL1RL1⁺ lymphocytes, including VAT Treg cells, ILC2s, and rare IL-5⁺ Th2 cells. IL-33 also increases CD25 expression on Treg cells and ILC2s, potentially increasing their sensitivity to IL-2.

IL-2-Mediated Expansion of Treg Cells and ILC2 Is Augmented by Endogenous IL-33

Low-dose IL-2 has been used to expand Treg cells and treat patients with autoimmune disease and graft-versus-host disease (Liao et al., 2011). ILC2 and Treg cells constitutively express the high-affinity IL-2 receptor, including CD25 (IL-2R α), and both expand in vivo to IL-2 (Van Gool et al., 2014). Because IL-33 maintains VAT Treg cells and promotes their expression of CD25 (Figure S2B), we assessed whether systemic responses to IL-2 are reinforced by endogenous IL-33 in vivo. IL-2 promotes systemic expansion of Treg cells that express IL1RL1 and high levels of CD25 (Figure 2B). IL-2 modestly increased Treg cell cycling (Figure S2F), and the greatest proliferation occurred in IL1RL1⁺ Treg cells (Figure 2C). The IL-2-mediated expansion of VAT and lung Treg cells, and their upregulation of CD25, was attenuated in IL1RL1-deficient mice (Figure 2D–E, Figure S2G). Co-administration of IL-33 with IL-2 further enhanced Treg cell accumulation (Figure S2H). ILC2 also expanded to IL-2 in VAT and lungs, and expansion was blunted in both tissues in the absence of IL1RL1 (Figure 2F). These data show that endogenous tissue IL-33 cooperates with IL-2 to promote the expansion of both Treg cells and ILC2.

ILC2s Mediate IL-33-Dependent Treg Cell Homeostasis In Vivo

Despite direct effects of IL-33 in promoting IL1RL1⁺ Treg cells (Figure 2, Figure S2) (Schiering et al., 2014; Vasanthakumar et al., 2015), our data did not exclude indirect effects of IL-33 in vivo through its ability to activate ILC2s. Unexpectedly, loss of ILC2s via IL-5^{cre}-mediated cell deletion (Molofsky et al., 2013) significantly impaired the age-related Treg cell accumulation in VAT (Figure 3A, Figure S3A); this was particularly apparent in the IL1RL1⁺ Treg cell population (Figure 3B). ILC2-deficient mice displayed no overt signs of autoimmunity and young mice had normal numbers of VAT, lung, and spleen Treg cells (data not shown). To assess whether ILC2 were required for IL-33-mediated induction of Treg cells, we administered IL-33 to mice rendered ILC2-deficient using IL-5^{cre} or IL-13^{cre} strains crossed to deleter alleles (Molofsky et al., 2013; Nussbaum et al., 2013).

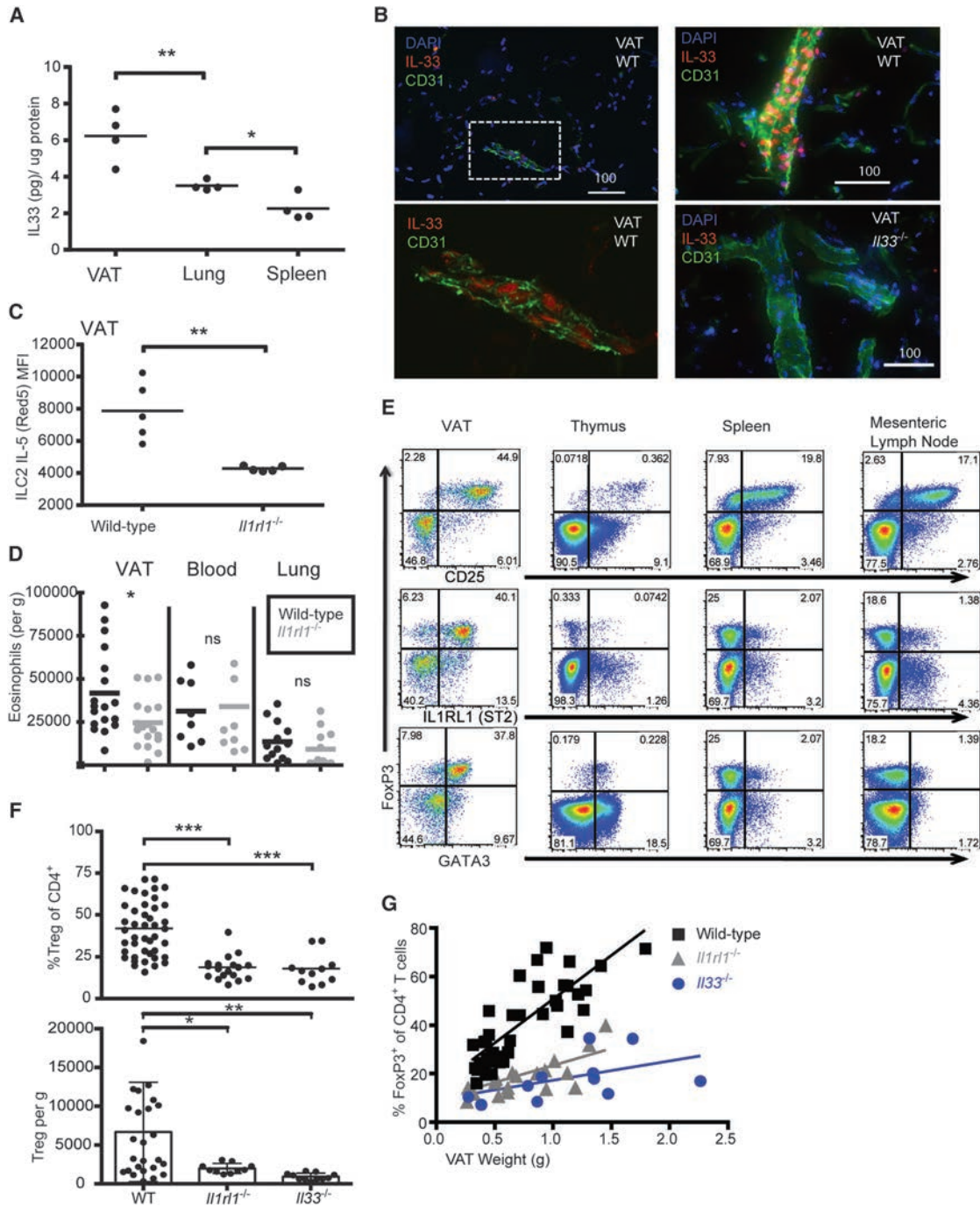


Figure 1. IL-33 Is an Endothelial Cytokine that Promotes ILC2 IL-5 Production, Eosinophilia, and Treg Cells in Visceral Adipose Tissue

(A) Total tissue IL-33 concentrations measured by ELISA.

(B) VAT immunofluorescence microscopy demonstrating IL-33 and CD31 endothelial cell co-localization in wild-type (WT) but not IL-33-deficient mice.

(C) Quantification of IL-5 reporter (Red5 tdTomato) mean fluorescence intensity, MFI) from wild-type or IL1RL1-deficient (*Il1rl1^{-/-}*) *Il5^{tdTomato-cre/+}* animals.

(D) Enumeration of total eosinophils in the indicated tissues and strains.

(E) Representative flow cytometric plots pre-gated on CD4⁺ T cells of 4- to 6-month-old male animals with (F) quantification of percent (top) and total per gram

(bottom) FoxP3⁺ CD4⁺ Treg cells from the tissues and strains indicated or (G) percent Treg cell expressed as a function of VAT weight. * = p < 0.05, ** = p < 0.01,

*** = p < 0.001, ns = not significant. Data are representative of three or more experiments (A–C, E) or pooled from three or more experiments (D, F, and G). Error bars represent SEM.

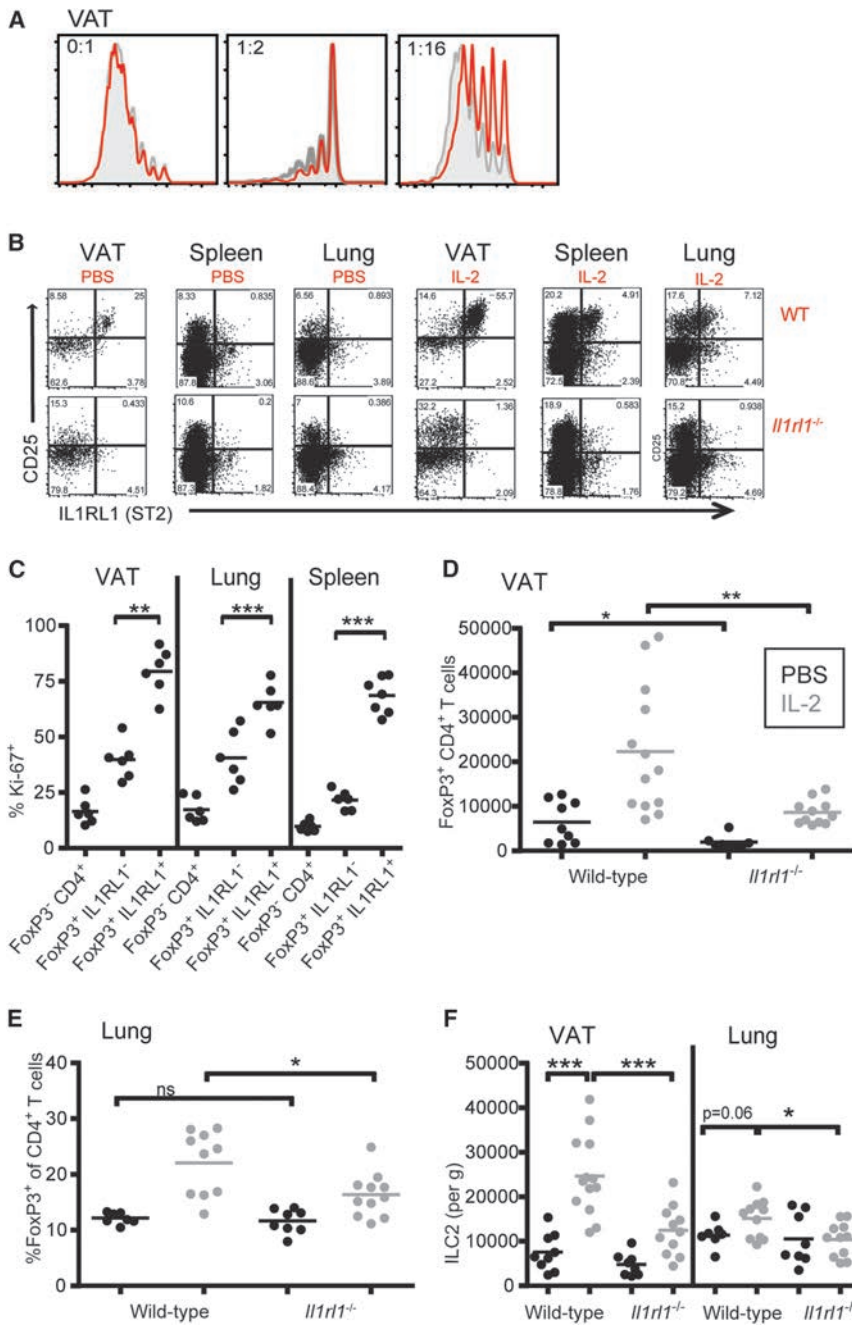


Figure 2. IL-2 Coordinates with IL-33 to Promote IL1RL1 (ST2)⁺ Treg Cells and ILC2 Expansion and Function

(A) VAT FoxP3GFP⁺ Treg cells from multiple mice were sort-purified and used in an in vitro suppression assay at the indicated Treg/Teff ratios by assessing CTV dilution in naive CD4⁺ T cells in the presence (red lines) or absence (gray lines) of IL-33.

(B) Flow cytometric plots pre-gated on CD4⁺ T cells from the indicated tissues of wild-type (top) or IL1RL1-deficient (*Il1rl1*^{-/-}) mice (bottom) treated with PBS (left) or IL-2 complexes (right), as indicated.

(C) Quantitation of Ki-67⁺ proliferative cells from the indicated CD4⁺ T cell subsets of IL-2-treated mice.

(D–F) FoxP3⁺ CD4⁺ Treg cells (D and E) or ILC2 (F) were quantitated from the indicated tissues after PBS or IL-2 complexes in wild-type or IL1RL1-deficient mice, as indicated. Black dots (PBS), gray dots (IL-2 complex). Data are representative of two to three experiments (A and B) or pooled from three experiments (C–F). Error bars represent SEM.

and Treg cell accumulation was blunted (Figures 3F–3H, Figure S3G, data not shown). In contrast, mice lacking MyD88 in FoxP3⁺ Treg cells (*Foxp3*^{YFP-cre} × *Myd88* flox) showed normal proliferation and accumulation of ILC2 and Treg cells in response to IL-33, although a modest reduction in the KLRG1⁺ IL1RL1⁺ Treg cell subset was noted (Figures 3G–3I). These ILC2-mediated effects of IL-33 on Treg cell accumulation were not mediated by IL-5, IL-4, IL-13, or IL-9; Treg cell expansion to IL-33 was normal in mice lacking these cytokines (Figure 3C, Figures S3D and S3E, data not shown). FoxP3⁺ Treg cells, in contrast to CD4⁺ Th2 cells, did not express reporters for either IL-5 or IL-13 (data not shown). Thus, ILC2-intrinsic responses to IL-33, but not ILC2 canonical cytokines, are required for optimal IL-33-mediated expansion of Treg cells in vivo.

IL-33 robustly increased ILC2 in VAT, lung, and spleen of wild-type mice; IL-33 also promoted Treg cells comparably to IL-2 (Figures S3B and S3C, data not shown). In contrast, in ILC2-deficient mice, IL-33-induced Treg cell expansion was impaired (Figures 3C–3E, Figure S3D–S3F), and this was particularly marked in the subset of “activated” GATA3⁺ IL1RL1⁺ KLRG1⁺ Treg cells (data not shown). MyD88 is a shared adaptor for TLR and IL-1 family signaling and is required for IL-33 signaling. To assess the cell-intrinsic role of IL-33 signaling in ILC2-directed Treg cell accumulation, we gave IL-33 to mice lacking the adaptor protein MyD88 in IL-5⁺ ILC2s (*IL-5*^{tdTomato-cre} × *Myd88* flox). In multiple tissues, ILC2 expansion and proliferation were impaired

We next determined whether ILC2s mediate the normal expansion of Treg cells during helminth infection, a challenge associated with elevated IL-33. During primary infection with the nematode *Nippostrongylus brasiliensis*, which transiently passes through the lung before reaching the small intestine, lung KLRG1⁺ Treg cell accumulation was significantly diminished in ILC2-deficient (IL-5 deleter) mice (Figure 3J); similar trends were observed in mice lacking the adaptor MyD88 in IL-5⁺ cells (Figure S3H, data not shown). Although smaller numbers of IL-5-expressing Th2 cells were also depleted in these mice, and might contribute to these ILC2-dependent effects, we noted that after secondary helminth infection, accumulation of lung ILC2,

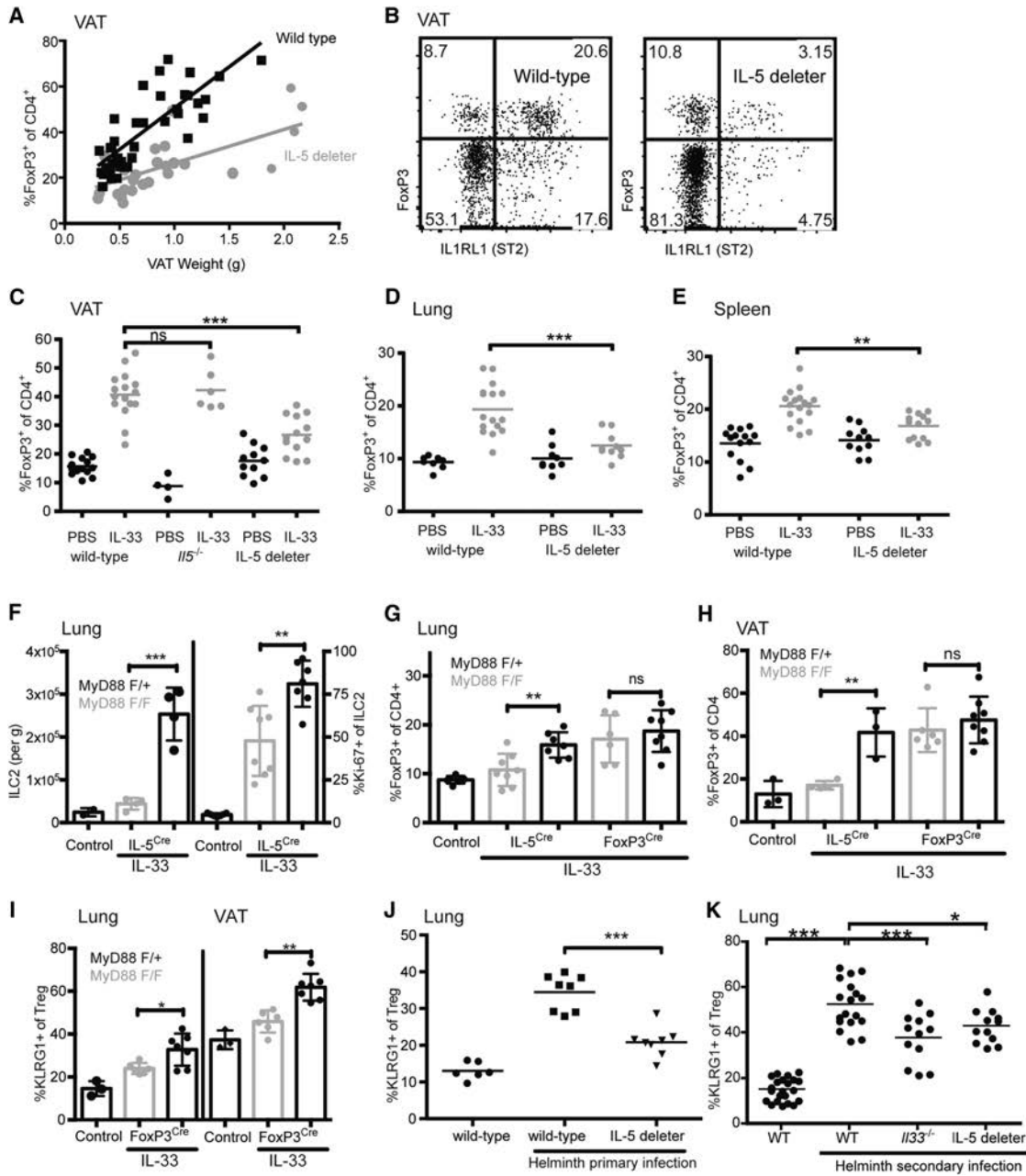


Figure 3. ILC2 Are Required for IL-33- and Helminth-Dependent Treg Cell Accumulation In Vivo

(A) FoxP3⁺ CD4⁺ Treg cells from VAT of 2- to 6-month-old male wild-type or IL-5 deleter (*Il5*^{tdtomato-cre/tdtomato-cre} × *Rosa26*^{DTA/DTA}) animals expressed as a correlation with VAT weight. (B) Representative flow cytometric plots of resting VAT CD4⁺ T cells from wild-type or IL-5 deleter mice. (C–E) Percent FoxP3⁺ Treg cells of CD4⁺ T cells measured in wild-type, IL-5-deficient (*Il5*^{tdtomato-cre/tdtomato-cre}), or IL-5 deleter animals after control PBS (black dots) or IL-33 treatment (gray dots) from the indicated tissues. (F–I) Cells were enumerated from the indicated tissues (VAT, Lung) and strains (*Il5*^{tdtomato-cre/tdtomato-cre} or FoxP3^{YFP-cre/y} × MyD88 flox/flox or flox/+) after three doses of IL-33 or from untreated controls. (J and K) Percent KLRG1⁺ of FoxP3⁺ Treg cells in lung was enumerated on (J) day 7–8 of primary infection or (K) 2 weeks after secondary infection with *N. brasiliensis* from the indicated strains. Data represent three or more experiments (B) or pooled from two (J and K) or three or more experiments (A, C–I). Note the double y axis in (F). Error bars represent SEM.

but not total CD4⁺ Th2 cells, remained impaired in IL-33-deficient and IL-5 deleter mice (Figures S3I and S3J). KLRG1⁺ Treg cells proportionately increased in lung, mesenteric lymph

node (MLN) and VAT, and optimal accumulation depended on both IL-33 signaling and IL-5⁺ ILC2s (Figure 3K, Figures S3K and S3L). Thus, IL-33, whether induced endogenously in

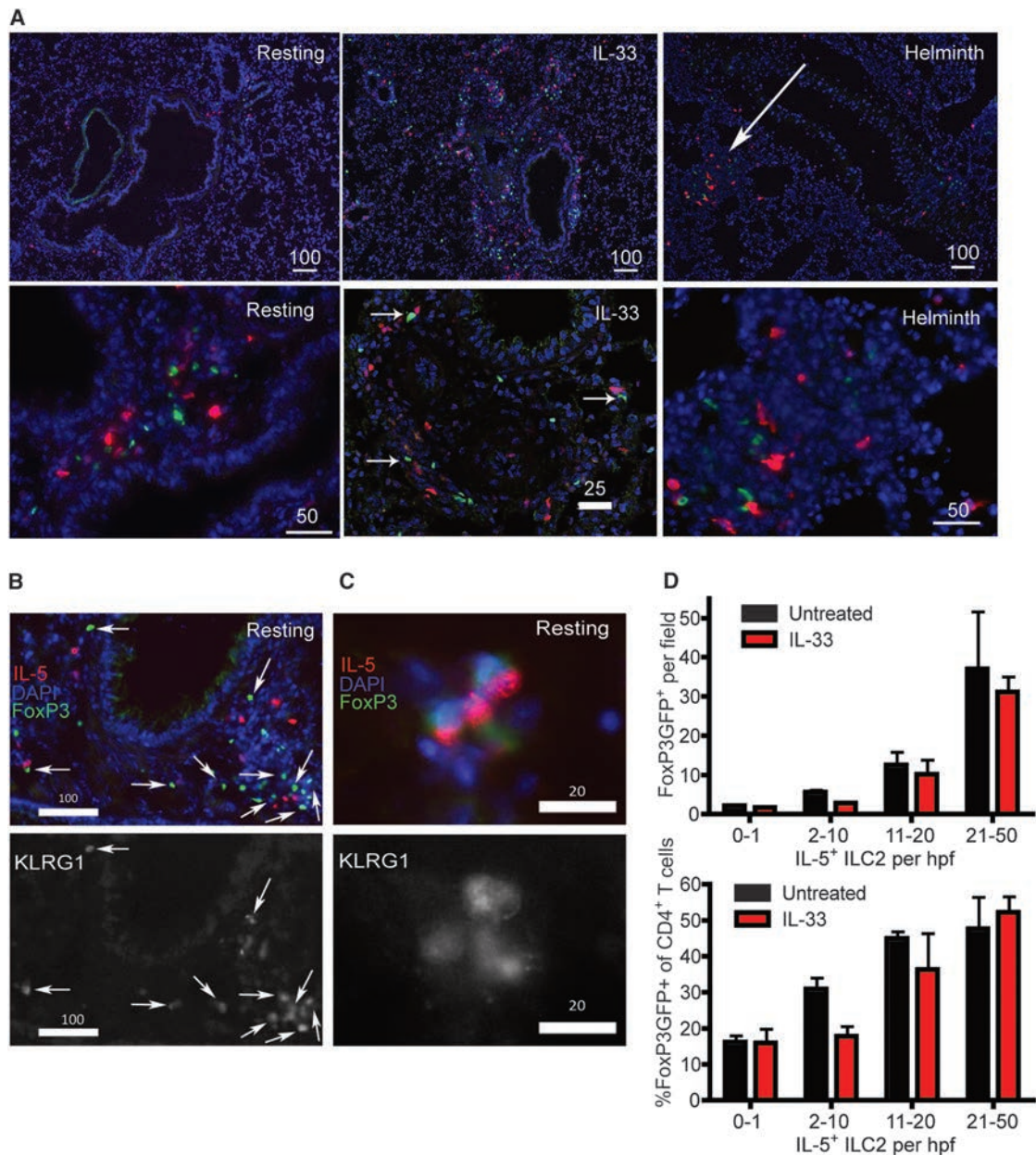


Figure 4. ILC2 and Treg Cells Co-Localize In Vivo

(A–C) Representative immunofluorescence microscopy images of lung under resting conditions (Resting), after IL-33 administration $\times 3$ doses (IL-33), or 2 weeks after *N. brasiliensis* infection (Helminth) identifying IL-5⁺ (tdtomato⁺) cells, FoxP3⁺ (GFP⁺) cells, and (B and C) KLRG1⁺ cells from Red5 (*Il5*^{tdtomato-cre/+}) Foxp3GFP double reporter animals.

(D) Quantification of total FoxP3GFP⁺ cells and IL-5⁺ ILC2 (top) or percent FoxP3GFP⁺ of CD4⁺ T cells and total IL-5⁺ ILC2 (bottom) per high-powered field (400 \times total magnification). Data are expressed as total or percent FoxP3⁺ Treg cells per IL-5⁺ ILC2 and grouped as bins. (A–D) Representative data from two experiments with two or mice per group. Error bars represent SEM.

response to migratory helminths or provided exogenously, promoted ILC2-dependent increases in “activated” Treg cells in multiple tissues.

ILC2 and Treg Cells Interact In Vitro and In Vivo

IL-5⁺ ILC2 and KLRG1⁺ FoxP3⁺ Treg cells localize to similar areas of the lung and VAT under resting conditions and in multiple

tissues after induction by IL-33 or helminth infection (Figures 4A–4D, Figure S4A–S4E), suggesting these cells may interact in vivo. The co-stimulatory protein ICOS was reported to function in sustaining tissue Treg cells, as opposed to the role for IL-2 in promoting Treg cell survival in lymphoid organs (Smigielski et al., 2014). When assessed directly ex vivo, ILC2s express ICOS ligand (ICOSL) at amounts comparable to B cells

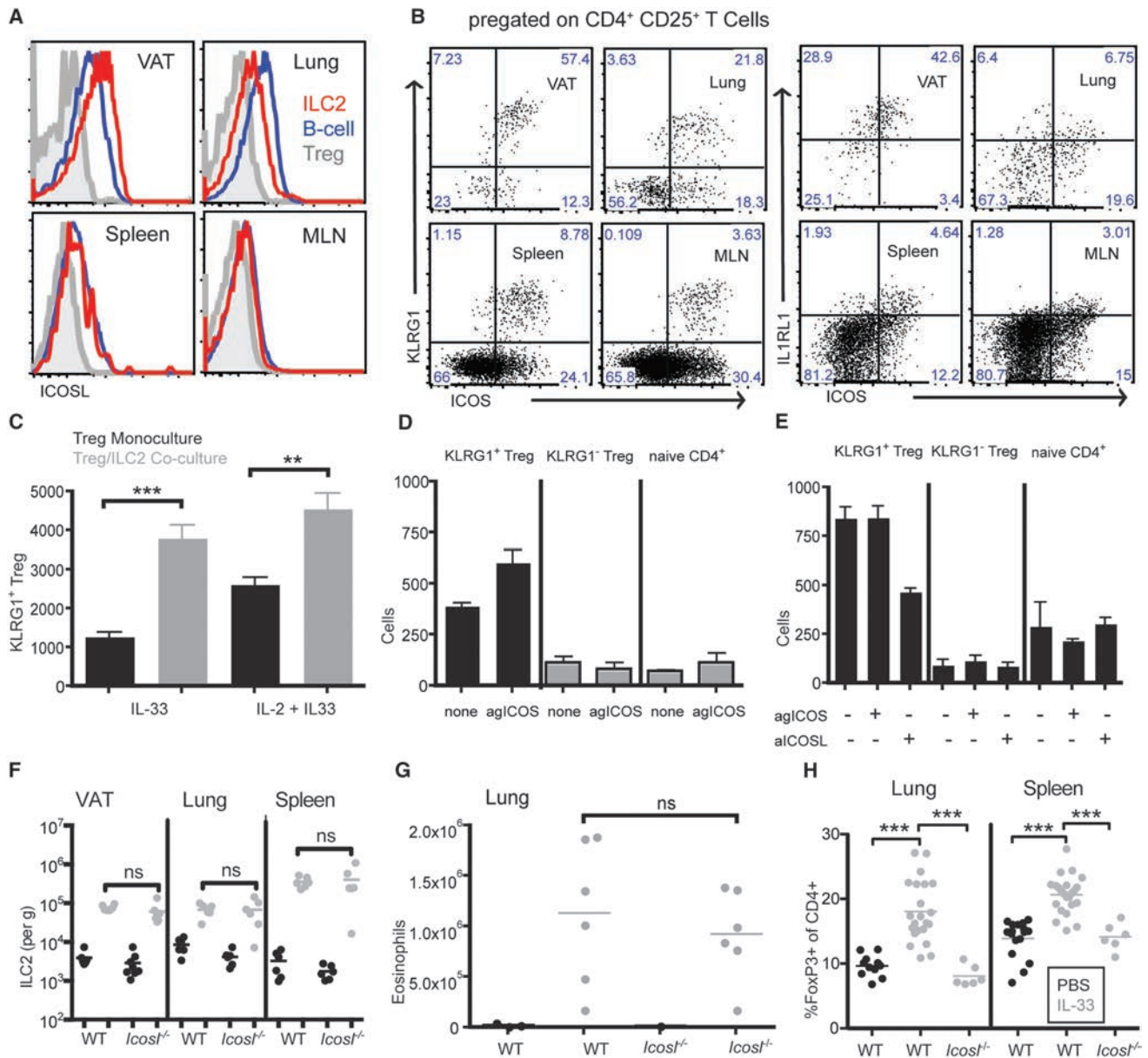


Figure 5. ILC2 ICOSL Engages Treg Cell ICOS to Promote Treg Cell Tissue Accumulation

(A and B) Flow cytometric analysis of (A) ICOSL or (B) ICOS, KLRG1, and IL1RL1 expression from the indicated tissues and populations. (C–E) In vitro 3 day culture of (C) KLRG1⁺ Treg cells \pm ILC2, (D) KLRG1⁺ Treg, KLRG1⁻ Treg, or naive CD4⁺ T cells alone \pm agonist ICOS antibody, or (E) CD4⁺ populations indicated co-cultured with ILC2 \pm blocking ICOSL antibody, enumerating Treg cell survival. (F and G) Treatment with three doses of IL-33 (gray dots) or control PBS (black dots) and (F) total ILC2 or ILC2 per g (VAT), (G) eosinophils, or (H) percent FoxP3⁺ Treg cells of CD4⁺ T cells were enumerated from wild-type and ICOSL deficient (*Icosl*^{-/-}) animals. Data are representative of two to three experiments (A–E) or pooled from two or more experiments (F–H). Error bars represent SEM.

(Figure 5A); expression is particularly high in VAT (Figure S5A). ICOSL was also expressed on the small numbers of IL-5⁺ KLRG1⁺ GATA3^{hi} Th2 cells in VAT, but not on CD8⁺ T cells, FoxP3⁺ CD4⁺ Treg, other CD4⁺ T cells, or NK cells (Figures S5B and S5C; and data not shown). In peripheral tissues, Treg cells comprised the major ICOS^{hi} lymphocytes, and, among these, KLRG1⁺ IL1RL1⁺ Treg cells were uniformly ICOS^{hi} (Figure 5B). ICOS^{hi} Treg cells have been associated with IL-2 therapy, helminth infection, and neoplasms, and are activated and highly

suppressive Treg cells (Busse et al., 2012; Redpath et al., 2013; Sim et al., 2014).

After administration of IL-33 or infection with *N. brasiliensis*, ICOSL⁺ ILC2 and ICOS^{hi} Treg cells accumulate in tissues and persist for prolonged periods (Figures S5D–S5F, data not shown). Although ILC2 and Th2 both express ICOS, the expression was much lower than on Treg cells, was inversely correlated with ICOSL expression, and was induced in response to IL-2 but not IL-33 (data not shown). Genetic deficiency or

antibody blockade of ICOSL led to increased lymphocyte expression of ICOS (data not shown), suggesting the possibility of ICOSL/ICOS shedding after binding. Whereas ICOS activation (agICOS) supported KLRG1⁺ Treg cell survival in vitro, co-culture of ILC2 and KLRG1⁺ IL1RL1⁺ Treg cells, but not other CD4⁺ lymphocytes, promoted Treg cell survival that was blocked by ICOSL antibody (aICOSL) (Figures 5C–5E). Following administration of systemic IL-33, ILC2 and eosinophil expansion was normal in ICOSL-deficient mice, but Treg cell expansion was impaired (Figures 5F–5H). In VAT there was a trend toward impaired total Treg cell accumulation ($p = 0.1$, data not shown). We conclude that ILC2s can interact with ICOS^{hi}, KLRG1⁺ Treg cells and promote Treg cell accumulation via ICOSL-ICOS interactions, although additional mechanism(s) also contribute, particularly in VAT. After secondary helminth infection, a subset of IL-5⁺ Th2 cells that express ICOSL also increase (Figures S5D–S5F) and may contribute additionally to enhance Treg cell accumulation.

Interferon- γ Inhibits ILC2 Activation by IL-33

Although VAT IL-33 is increased in obesity (data not shown and Zeyda et al., 2012), ILC2s, Treg cells, eosinophils, and AAMs decline (Feuerer et al., 2009; Molofsky et al., 2013), suggesting that loss of IL-33 does not account for this effect. However, interferon- γ -producing T cells and NK cells increase in obese VAT and IFN- γ can promote inflammation and systemic insulin resistance (Nishimura et al., 2009; Stolarczyk et al., 2013; Wensveen et al., 2015; Winer et al., 2009). ILC2s express both components of the IFN- γ receptor (Robinette et al., 2015; data not shown), and we found IFN- γ directly represses ILC2 activation, cytokine production, and proliferation in vitro (Figure 6A, Figures S6A–S6C). Although ILC2s express receptors for IL-10, IL-18, and IL-27 (data not shown), these cytokines did not impair ILC2 activation by IL-33 (Figure S6D). In vivo, lung tissue ILC2 proliferation and accumulation in response to IL-33 were blocked by co-administration of IFN- γ (Figure 6B), and this was accompanied by decreases in ILC2 and Th2 IL-5 production (Figure 6C) and in Treg cell accumulation (Figure 6D). Similar effects were noted in VAT (Figures S6E–S6G), although the ability of a short course of IFN- γ to repress IL-33-driven ILC2 and Treg cell activation was less marked, possibly due to the constitutively high expression of IL1RL1 by VAT ILC2s and Treg cells. We could not detect IL1RL1 on NK cells or CD8⁺ T cells either at rest or following challenge with IL-33 or IL-33 and IFN- γ ; although IFN- γ promoted CD8⁺ T cell and NK cell proliferation, IL-33 alone had minimal effects (data not shown).

To assess effects of endogenous IFN- γ on ILC2 function, we used Yeti mice (Stetson et al., 2003), in which the 3' untranslated region (UTR) of IFN- γ is stabilized by a YFP-bovine growth hormone poly-A construct, leading to constitutive increases in IFN- γ ; heterozygous mice were used here, thus avoiding overt IFN- γ -induced auto-inflammation (Reinhardt et al., 2015). Similar to wild-type mice on high-fat diet (Molofsky et al., 2013), young heterozygous Yeti mice on normal diet have fewer total adipose tissue ILC2s, eosinophils, and Treg cells, show attenuated IL-5 and ICOSL expression by ILC2s and rare Th2 cells, and accumulate NK cells, Th1 CD4⁺ T cells, and CD8⁺ T cells (Figures 6E–6I, Figure S6H, and data not shown). VAT

Treg cells in Yeti mice express diminished levels of GATA3, IL1RL1, KLRG1, and CD25 (Figure 6H). In the lung, where endogenous IL-33-driven type 2 immunity is constitutively less active as compared to VAT, ILC2 numbers, and IL-5 production, eosinophils and Treg cell were minimally affected in Yeti mice (Figures S6I and S6J).

Next, we used knockin IFN- γ reporter mice to identify NK cells, CD4⁺ T cells, and CD8⁺ T cells as IFN- γ -producing adipose tissue cells under conditions of excess (Yeti mice; Figure S6K) and normal IFN- γ (Great mice; Figure S6L) (Price et al., 2012); accumulation of IFN- γ -expressing CD4⁺ Th1 and CD8⁺ T cells was particularly dynamic in resting VAT as compared to lung. Indeed, wild-type IL-5 reporter mice older than 15 months showed decreases in VAT, but not lung, ILC2 numbers, IL-5 production, and eosinophil accumulation, which correlated with increased inflammatory CD4⁺ and CD8⁺ T cells (Figure 7A, Figures S7A–S7C). VAT Tregs, which accumulate in animals 4–9 months of age, decline with further aging (Figure S7D). Similarly, young animals fed high-fat diet (HFD) develop increased VAT IFN- γ -producing T cells (Nishimura et al., 2009; Stolarczyk et al., 2013; Winer et al., 2009) and VAT-specific loss of IL-5⁺ ILC2 and Th2, eosinophils, and Treg cells (Figure 7B, Figures S7E and S7F, data not shown). Together, we conclude that VAT IL-33 promotes ILC2 activation previously associated with metabolic homeostasis, including the accumulation of Treg cells, and that IFN- γ -producing lymphocytes infiltrate VAT in response to aging and high-fat diet and repress ILC2-mediated function.

To assess the role of IFN- γ in repressing ILC2 activation during infection, we challenged heterozygous Yeti mice with *N. brasiliensis*. Although helminth infection induces IL-33 (Moro et al., 2010), ILC2 proliferation, ILC2 and Th2 ICOSL expression and IL-5 production, and accumulation of KLRG1⁺ Treg cells, each of these responses was attenuated in the lungs of Yeti mice (Figures 7C–7E, Figures S7G–S7I). Helminth clearance from the gastrointestinal tract was also delayed (Figure 7F). To assess the effects of biologically induced IFN- γ , we infected mice with *Listeria monocytogenes*, intracellular gram-positive bacteria that elicit potent IFN- γ -mediated responses necessary to clear infection. *Listeria* co-infection with *N. brasiliensis* repressed lung ILC2s and KLRG1⁺ Treg cell expansion, ILC2 and rare Th2 IL-5 production, and eosinophilia (Figures 7G–7K), and promoted the accumulation of CD8⁺ T cells (Figure 7G). These effects were dependent on IFN- γ , as IFN γ R1 deficient co-infected mice did not display impaired ILC2 activation or Treg cell expansion (data not shown). Helminth infection is protective in mouse models of type 2 diabetes (Hussaarts et al., 2015; Wu et al., 2011; Yang et al., 2013), promoting short-term VAT ILC2 activation and eosinophilia (Molofsky et al., 2013). We found that VAT ILC2s, Th2, and eosinophils remain elevated 1 month after helminth infection, and VAT eosinophils are elevated up to 10 months post-infection (Figures S7J and S7K). In contrast, self-limited *Listeria* infection promotes persistent elevations in VAT IFN- γ -producing CD8⁺ T cells and decreased VAT ILC2 IL-5 production (Figure S7L). Together, we conclude that IFN- γ inhibits ILC2 activation and limits both the constitutive IL-33-dependent maintenance of activated ILC2 and Treg cells in VAT and the helminth- and IL-33-induced activation of ILC2s

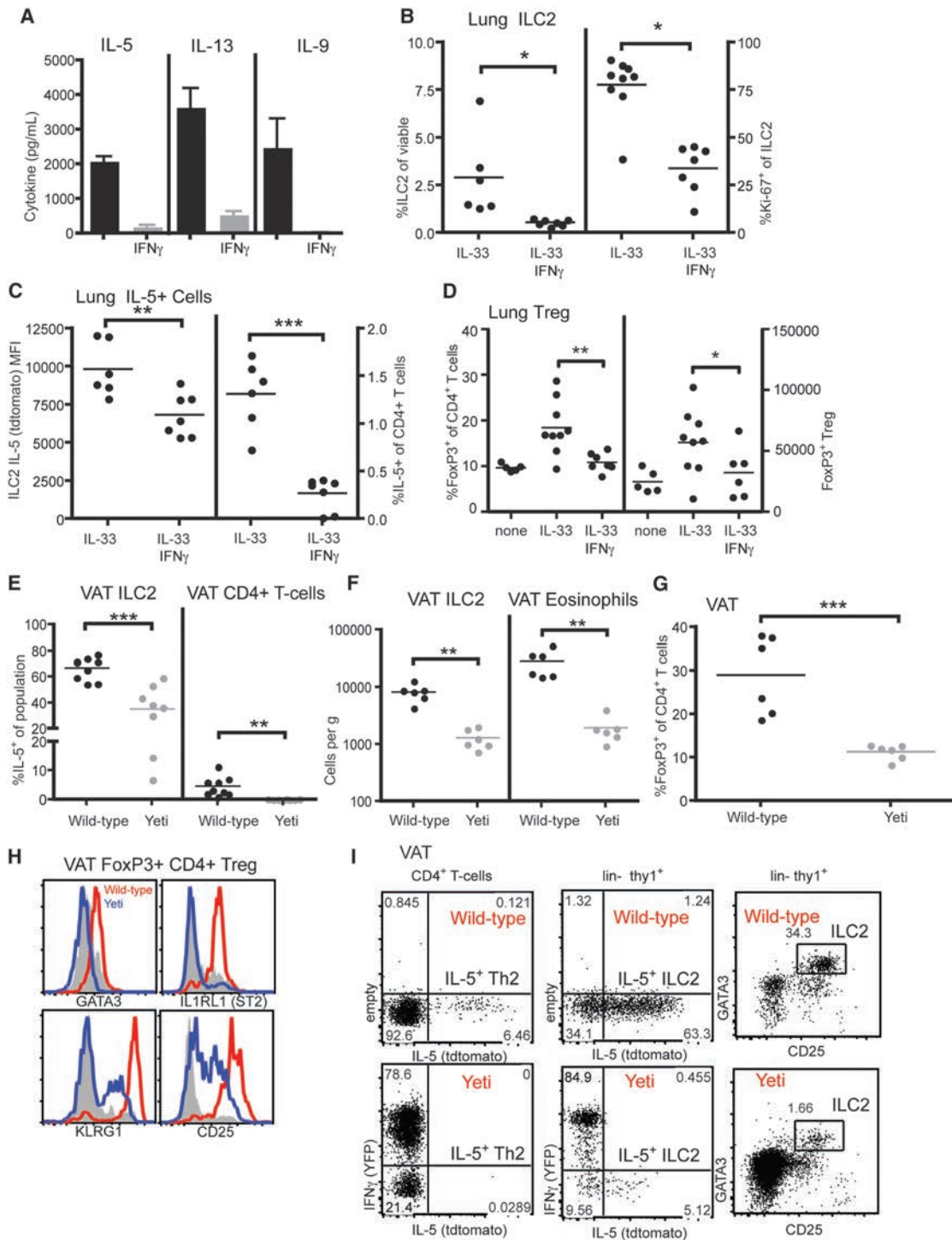


Figure 6. IFN- γ Represses ILC2 Activation and Limits IL-33-Driven ILC2s and Treg Cells

(A) Naive lung ILC2s (lin- thy1 $^{+}$ KLRG1 $^{+}$ CD25 $^{+}$) were sort purified and cultured in vitro with IL-2 and IL-33 with or without IFN- γ for 3 days, and supernatants were assayed for the indicated cytokines.

(B–D) Mice were treated with IL-33 \pm IFN- γ for three doses and lungs were assayed using flow cytometry for (B) ILC2 and Ki-67 $^{+}$ proliferating ILC2, (C) IL-5 production from ILC2 and CD4 $^{+}$ Th2, and (D) percent FoxP3 $^{+}$ Treg cells and total Treg cells (note secondary y axis on each).

(E–G) VAT from animals with constitutive excess IFN- γ (Yeti \times Red5, gray dots) or wild-type (Red5) controls (black dots) were assayed by flow cytometry for (E) IL-5 $^{+}$ ILC2 and IL-5 $^{+}$ Th2, (F) total ILC2 and eosinophils, or (G) percent FoxP3 $^{+}$ Treg cells of CD4 $^{+}$ T cells.

(H) VAT Treg cell expression of markers indicated from Yeti and wild-type animals.

(I) Representative FACS plots of VAT from wild-type IL-5 reporter and Yeti \times IL-5 reporter mice. Data are representative of two to three experiments (H and I) or pooled from two to three experiments (A–G). Error bars represent SEM.

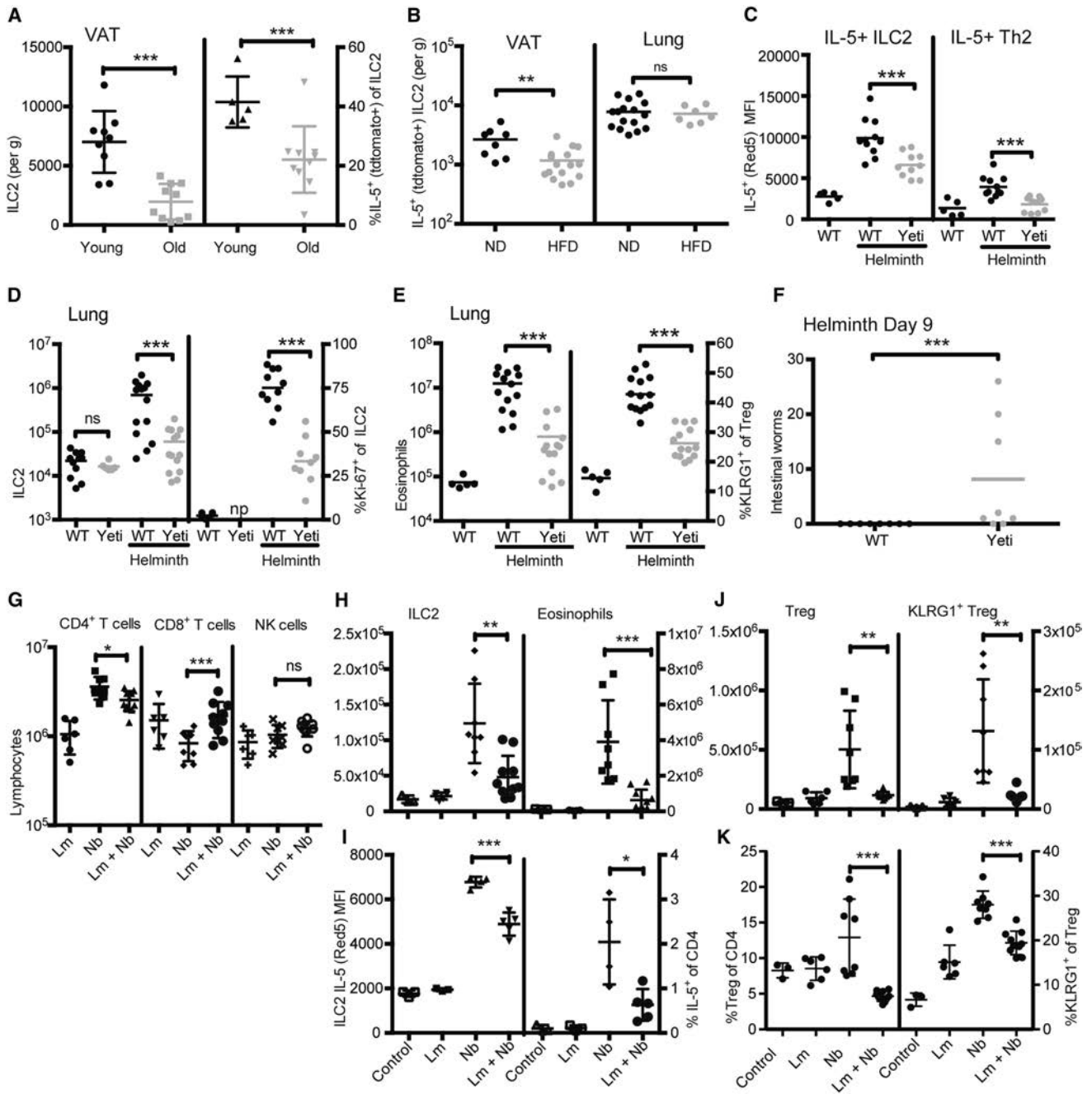


Figure 7. IFN- γ Associated with Age, Obesity, and *Listeria* Infection Limit ILC2-Mediated Immunity in Adipose Tissue and Helminth-Infected Lung
 (A) VAT ILC2 and IL-5 expression (tdtomato MFI) were assessed in 15-month-“old” and 8- to 12-week-“young” IL-5 reporter (*Il5^{tdtomato-cre/+}*) male mice.
 (B) Mice were placed on normal diet or high fat diet (60% kcal fat) for 16 weeks and IL-5⁺ ILC2 were enumerated in VAT versus lung.
 (C-E) Wild-type or Yeti IL-5 reporter mice were infected with *N. brasiliensis* and lung tissue harvested on days 7–9 post-infection, with the populations quantitated by flow cytometry as indicated (note secondary y axis on each).
 (F) *N. brasiliensis* were enumerated on day 9 post infection from small intestine of wild-type and Yeti mice.
 (G-K) Wild-type IL-5 reporter mice were infected with *N. brasiliensis*, *L. monocytogenes*, or co-infected, and lung tissue harvested on day 7 post-infection, with the populations quantitated by flow cytometry as indicated (note secondary y axis on each). Data are pooled from two to three experiments (A–J). Error bars represent SEM.

and Treg cells in lung. Further, our findings suggest adipose tissue is a dynamic immunologic organ that retains a prolonged “metabolic memory” of diverse infections and may lead to lasting metabolic alterations for the organism.

DISCUSSION

ILC2 cytokines, particularly IL-5 and IL-13, are critical in sustaining the accumulation of eosinophils and AAMs necessary to

maintain adipose tissue homeostasis and local tissue responses to perturbations mediated by allergens and helminths (Molofsky et al., 2013; Odegaard et al., 2007; Walker and McKenzie, 2013; Wu et al., 2011). Adipose tissue homeostasis and immunity to helminths also involve tissue accumulation of Treg cells (Cipolletta et al., 2012; Feuerer et al., 2009; McSorley and Maizels, 2012), but mechanisms that link ILC2 activation and Treg cells remain incompletely understood. Here, we identify IL-33 in coordinating ILC2s and Treg cell residence in resting VAT, but also during tissue perturbations induced by systemic IL-2 treatment or during migratory helminth infection. Although Treg cell activation by IL-33 was in part direct, as suggested by recent studies (Schiering et al., 2014; Vasanthakumar et al., 2015), optimal activation *in vivo* was ILC2-dependent by a process requiring intrinsic ILC2 MyD88 and interactions between ICOSL on ILC2s and ICOS on Treg. Although this IL-33-dependent pathway may serve to protect adipose tissue or injured tissues during allergen- or helminth-mediated injury, IFN- γ produced during acute inflammatory responses associated with infection inhibited these processes, potentially providing an overriding safeguard following invasion by rapidly replicating organisms, such as bacteria or viruses. Chronic inflammation linked to IFN- γ in the setting of obesity and aging also attenuated the normal organization of ILC2s and Treg cells in adipose tissue. These data position IL-33, IFN- γ , and ILC2s as critical regulators in the balance between tissue injury, metabolic homeostasis, and host defense.

Normal VAT contains high levels of IL-33 (Miller et al., 2010; Zeyda et al., 2012), which we demonstrate in endothelial cell nuclei in close proximity to resident ILC2s. Although others have reported IL-33 in both endothelium (Zeyda et al., 2012) and human adipocytes (Wood et al., 2009), our studies identify endothelium as a predominant source in resting mice. IL-33 was necessary to sustain normal ILC2 function and Treg cell numbers and function in VAT, as assessed in both IL1RL1- and IL-33-deficient mice. Although necrotic cell death can release IL-33, where it can be further activated by inflammatory proteases (Cayrol and Girard, 2014), the mechanisms by which VAT IL-33 titrates ILC2 and Treg cell function remain unknown. It is intriguing that VAT, a dynamic storage for high-energy fuels, would be a site constitutively impacted by IL-33, but perhaps such localization serves to protect the host from the detrimental metabolic effects of VAT inflammation. Recent reports have called attention to the role of IL-33 in promoting adipose tissue “beiging” via activation of ILC2s, leading to increased heat production and a loss of adipose tissue mass (Brestoff et al., 2014; Lee et al., 2015). The relative metabolic contribution of IL-33-induced beiging during normal physiology or cold-exposure is unknown.

We previously reported that IL-2, which is used therapeutically to expand Treg cells, activates ILC2 to proliferate, increase IL-5 production and promote eosinophilia (Van Gool et al., 2014). Here, we also demonstrate that IL-2 synergizes with endogenous IL-33 to promote expansion of IL1RL1⁺ KLRG1⁺ Treg cells, a subpopulation with high suppressive capacity (Burzyn et al., 2013b; Cheng et al., 2012; Feuerer et al., 2010; Wohlfert et al., 2011). Such a mechanism may work to expand the local Treg cell population and limit damage at immunologically active sites where IL-2 and IL-33 co-localize following tissue injury and

recruitment or activation of IL-2 producing cells. IL-7, TSLP, and IL-9 are cytokines that also signal through STAT5 and, similar to IL-2, could cooperate with local IL-33 to enhance Treg cell and ILC2 function.

Unexpectedly, expansion of Treg cells by IL-33 was optimally dependent on ILC2s, as revealed using both IL-5- and IL-13-driven cell deletion. Although we cannot rule out contributions by small numbers of Th2 cells, which are partially deleted in these mice, ILC2s comprise the vast majority of cells secreting high levels of these cytokines under the conditions examined. ILC2 cell-intrinsic IL-33 signaling was required for this effect, as assessed using IL-5-mediated deletion of the MyD88 adaptor protein. Treg-intrinsic IL-33 signaling was not necessary for Treg cell expansion but was important in optimally sustaining KLRG1⁺ “effector” Treg cells. Intriguingly, IL-4, IL-5, IL-9, and IL-13 were not required to mediate effects of ILC2s on Treg cells, suggesting that the downstream cellular targets of these cytokines, eosinophils and AAMs, are also not necessary. Nonetheless, it is possible that these cellular targets of ILC2s indirectly contribute to Treg cell accumulation in certain models. We were unable to implicate other ILC2-produced soluble mediators affecting Treg cell activation, including IL-2, IL-10, and amphiregulin (data not shown). Instead, we demonstrate that ILC2s and Treg cells co-localize in tissues, raising the possibility that direct interactions occur between these cells. Prior studies have called attention to a role for ICOSL:ICOS in maintaining the survival of tissue Treg cells (Redpath et al., 2013; Smigiel et al., 2014), and we demonstrate that activated ILC2s express high levels of ICOSL and are maintained in tissues for prolonged periods after administration of IL-33 or migratory helminth infection. A recent study also observed high levels of ICOSL on ILC2s, finding ICOSL/ICOS autocrine signals can promote ILC2 STAT5 signaling to promote ILC2 numbers and function in an asthma model (Maazi et al., 2015). We do not observe impaired ILC2 or eosinophil numbers at rest or after systemic IL-33 administration in ICOSL-deficient C57BL/6 mice, although autocrine signaling in ILC2s may be important in other contexts or strains. We found that treatment with ICOSL-Fc and IL-33 failed to promote Treg cell accumulation in ILC2-deficient mice (data not shown), and Treg cell expansion was compromised, but not abolished, in the absence of ICOSL. Together, these findings suggest ILC2s contribute to Treg cell expansion or maintenance through additional pathways. Recent studies have reported that innate lymphoid cells can express MHCII and perhaps present antigen to CD4⁺ T cells (Hepworth et al., 2013; Oliphant et al., 2014); such interactions, in combination with ICOSL co-stimulation, could also contribute to Treg cell maintenance. Other VAT immune cells, such as NKT cells, can produce IL-2 and may also cooperate with ILC2 to maintain Treg cells (Lynch et al., 2015). Of note, IL-33 alone can induce significant Treg cell proliferation independently of ILC2s, suggesting that ILC2s act primarily to promote the survival of Treg cells.

Although few inhibitory signals for ILC2s have been described, IFN- γ proved to be a potent inhibitor of ILC2 activation. We demonstrate that resting ILC2s respond directly to IFN- γ *in vitro*, restricting both cytokine production and cellular proliferation. Although the mechanisms by which IFN- γ restricts ILC2s activation are unknown, IFN- γ signals through STAT1 and STAT2 and could repress the expression and/or phosphorylation

of GATA3 (Schiering et al., 2014). SOCS1 is highly elevated in cells treated with IFN- γ , and could also repress IL-33 signaling. Although IL1RL1⁺ Treg cells in the colon were repressed directly by IL-23 (Schiering et al., 2014), naive ILC2s are not inhibited by IL-23 or IL-12 in vitro (data not shown). Lack of IFN- γ signaling has been associated with enhanced IL-5 and eosinophilia in allergic models (Coyle et al., 1996) and patients with defects in the IFN- γ receptor have elevated immunoglobulin E and increased atopic disease (Wood et al., 2005). Conversely, IFN- γ is effective in the treatment of atopic dermatitis (Reinhold et al., 1993). Together, these results suggest that IFN- γ is potent at limiting both resting and pathologic type 2 immune responses, although further work will be required to determine the specific role of ILC2s and other leukocytes in these processes. IFN- γ -mediated immunity is beneficial in the context of life-threatening infection, when pathogens must be contained and metabolic energy diverted to glycolytic support of host defense. Indeed, our data with bacterial/helminth co-infections suggest bacterial infections limit helminth-induced ILC2 expansion and function. In chronic obesity and aging, however, invasion of adipose tissues by IFN- γ -expressing lymphocytes, such as CD8⁺ T cells and Th1 cells, correlates with loss of adipose tissue ILC2s, Treg cells, eosinophils, and AAMs (Molofsky et al., 2013) and the development of systemic insulin resistance. Our data suggest these IFN- γ -expressing lymphocytes can directly repress ILC2s, leading to disruption of VAT metabolic homeostasis. As such, therapeutic interruption of IFN- γ signaling, possibly coupled with activation of ILC2s, may provide a strategy for re-establishing adipose immune homeostasis after obesity-driven dysregulation.

Our findings reveal novel interactions between ILC2s and Treg cells, and raise questions regarding the underlying role and function of “allergic immunity.” Increasingly, studies of these pathways have uncovered interactions with basal metabolism, mucosal homeostasis, and tissue repair (Burzyn et al., 2013b; 2013a; Cipolletta et al., 2012; Heredia et al., 2013; Molofsky et al., 2013; Qiu et al., 2014; Schiering et al., 2014; Wu et al., 2011). Not surprisingly, these pathways proceed independently from activation of adaptive effector cells, which focus on pathogen-derived peptides presented during microbial invasion. Prior studies have called attention to the destructive forms of type 2 immunity that occur in the absence of Treg cells (Brunkow et al., 2001; Fontenot et al., 2003) or following deletion of GATA3 or IRF4 in FoxP3⁺ lineage cells (Wang et al., 2011; Wohlfert et al., 2011; Zheng et al., 2009). Although we have been unable to document overt autoimmunity in IL-33- or IL1RL1-deficient mice (data not shown), we speculate that the IL-33-ILC2-Treg cell interactions we define may exist in part to protect local tissues during injury or microbial invasion and may be particularly important at sites where excess or chronic inflammation is detrimental. In the right setting, however, IFN- γ can suppress this pathway to enable development of host defense against rapidly proliferating microbes and perhaps contributes to the metabolic shifts in fuel utilization that accompany inflammation. The thresholds that define activation of these fundamental pathways in distinct tissues may be underpinned by the endogenous levels and regulation of IL-33, thus positioning this cytokine as a key regulator linking ILC2 and Treg cells in protecting the host during pathogen invasion or other challenges that disrupt tissue integrity.

EXPERIMENTAL PROCEDURES

Flow Cytometry

ILC2 are identified as lineage negative (CD11b⁻, F4/80⁻, CD3e⁻, CD4⁻, CD8 α ⁻, CD19⁻, Siglec F⁻, Fc ϵ R1⁻, NK1.1⁻), FSC/SSC-low-to-moderate, CD45⁺, CD127 (IL7R α)⁺ or Thy1.2 (CD90.2)⁺, and IL1RL1 (ST2)⁺, CD25 (IL-2R α)⁺, or KLRG1⁺, as indicated. CD4⁺ T cells are identified as FSC/SSC-lo, CD45⁺, CD3e⁺, CD4⁺. CD8⁺ T cells are identified as FSC/SSC-lo, CD45⁺, CD3e⁺, CD8⁺. Eosinophils are identified as CD45⁺, side-scatter high, DAPI-lo, CD11b⁺, and Siglec F⁺. NK cells are identified as CD45⁺ CD3e⁻ CD4⁻ CD8⁻ NK1.1⁺ CD11b variable. Treg cell are identified as CD45⁺ CD3e⁺ CD4⁺ FoxP3⁺. In some cases, FoxP3GFP mice were used to identify Treg cell as GFP⁺ CD4 cells. Populations were back-gated to verify purity and gating. Samples were analyzed on an LSR II or, for cell sorting, a FACSARIA II (both BD Biosciences). Live lymphocytes were gated by DAPI exclusion, size, and granularity based on forward- and side-scatter. Data were analyzed using FlowJo software (TreeStar) and compiled using Prism (Graphpad Software). Visceral adipose tissue (VAT) was normalized per gram adipose or as a percent of total viable cells or percent of CD45⁺ hematopoietic cells, as indicated.

Immunofluorescence Microscopy

Animals were anesthetized and injected in vivo with 4% paraformaldehyde (PFA). Tissues were harvested (VAT, lung, spleen, small intestine), fixed for 3 hr in 2% PFA, washed overnight with PBS, cryoprotected with 30% sucrose for 12–36 hr, and embedded in OCT (Sakura Finetek) prior to freezing in blocks. For whole mounts, tissues were fixed as above and imaged after permeabilization with 0.4% triton X and DAPI nuclear counterstaining. Frozen sections were processed on a Leica CM 3050S cryomicrotome (45 μ m in VAT, 8 μ m all others), dried on slides for 30 min, and kept at -80° until staining. Tissues were blocked with 5% goat or horse serum, and maintained in PBS + 5% serum + 0.4% triton X throughout antibody treatments. Primary and secondary antibodies were incubated for 1 hr at room temperature. Primary antibodies used include goat-anti IL-33 (R&D Systems, 1:100), hamster-anti-KLRG1 (eBioscience, 1:50), anti-CD4-APC (BD Biosciences, 1:50), rat-anti-Siglec F (BD Biosciences, 1:100), rat anti-CD31 (BD Biosciences, 1:100), chicken anti-GFP (Aves labs, 1:500), or rabbit anti-dsRed (Clontech, 1:500). When necessary, secondary antibodies were used at 1:1000 dilution. Slides were mounted with Vectashield hardset mounting media. Where indicated, 5 min before sacrifice, animals were injected with 20 μ g anti-CD31-APC (Clone 390, eBioScience) to label the vasculature. Whole-mount tissue or slides were examined with a Zeiss AxioVision M2 fluorescent microscope or a laser-scanning confocal microscope (Nikon C1si), as indicated. Confocal images were resolved to 1.2 μ m per pixel in the xy plane and 1.0 μ m in the z plane.

Infections

500 third-stage larvae of *N. brasiliensis* were injected subcutaneously as described (Voehringer et al., 2006). Mice were killed at the indicated time points and tissues were harvested and analyzed. Wild-type *Listeria monocytogenes* strain 10403s was infected intravenously (i.v.) at 3,000–4,000 CFU per mouse.

Experimental Design and Statistical Analysis

All data were analyzed by comparison of means using unpaired two-tailed Student's t tests using Prism (GraphPad Software), with * = $p < 0.05$, ** = $p < 0.01$, *** = $p < 0.001$. Figures display means \pm SE of the mean unless otherwise noted. When possible, results from independent experiments were pooled. All data points reflect individual biological replicates.

SUPPLEMENTAL INFORMATION

Supplemental Information includes seven figures and Supplemental Experimental Procedures and can be found with this article online at <http://dx.doi.org/10.1016/j.immuni.2015.05.019>.

AUTHOR CONTRIBUTIONS

A.B.M. designed experiments, performed research, analyzed data, and wrote the manuscript. F.V.G. designed experiments, performed research, and

analyzed data. J.C.N., H.-E.L., S.J.V.D., and J.L. provided reagents, performed research, and analyzed data. J.A.B. and R.M.L. designed experiments, analyzed data, and wrote the manuscript.

ACKNOWLEDGMENTS

We thank Drs. S. Akira, J.-P. Girard, A. DeFranco, and A. Rudensky for mice; Drs. A. DeFranco, A. Abbas, and C. Lowell for comments on the manuscript; Z.-E. Wang for technical assistance; and G. Rizzuto and J.D. Sauer for assistance with *Listeria* infections. This work was supported by AI026918, AI030663, AI078869, HL107202, and K08DK101604 (A.B.M.) from the NIH, the UCSF Diabetes Family Fund (A.B.M.), the UCSF REAC Pilot Grant (A.B.M.), the Sandler Asthma Basic Research Center at UCSF, and the Howard Hughes Medical Institute.

Received: November 7, 2014

Revised: March 25, 2015

Accepted: May 14, 2015

Published: June 16, 2015

REFERENCES

- Allen, J.E., and Maizels, R.M. (2011). Diversity and dialogue in immunity to helminths. *Nat. Rev. Immunol.* *11*, 375–388.
- Brestoff, J.R., Kim, B.S., Saenz, S.A., Stine, R.R., Monticelli, L.A., Sonnenberg, G.F., Thome, J.J., Farber, D.L., Lutfy, K., Seale, P., et al. (2014). Group 2 innate lymphoid cells promote beiging of white adipose tissue and limit obesity. *Nature* *519*, 1–17.
- Brunkow, M.E., Jeffery, E.W., Hjerrild, K.A., Paepfer, B., Clark, L.B., Yasayko, S.A., Wilkinson, J.E., Galas, D., Ziegler, S.F., and Ramsdell, F. (2001). Disruption of a new forkhead/winged-helix protein, scurfy, results in the fatal lymphoproliferative disorder of the scurfy mouse. *Nat. Genet.* *27*, 68–73.
- Brunner, S.M., Schiechl, G., Falk, W., Schlitt, H.J., Geissler, E.K., and Fichtner-Feigl, S. (2011). Interleukin-33 prolongs allograft survival during chronic cardiac rejection. *Transpl. Int.* *24*, 1027–1039.
- Burzyn, D., Benoist, C., and Mathis, D. (2013a). Regulatory T cells in nonlymphoid tissues. *Nat. Immunol.* *14*, 1007–1013.
- Burzyn, D., Kuswanto, W., Kolodin, D., Shadrach, J.L., Cerletti, M., Jang, Y., Sefik, E., Tan, T.G., Wagers, A.J., Benoist, C., and Mathis, D. (2013b). A special population of regulatory T cells potentiates muscle repair. *Cell* *155*, 1282–1295.
- Busse, M., Krech, M., Meyer-Bahlburg, A., Hennig, C., and Hansen, G. (2012). ICOS mediates the generation and function of CD4+CD25+Foxp3+ regulatory T cells conveying respiratory tolerance. *J. Immunol.* *189*, 1975–1982.
- Cayrol, C., and Girard, J.-P. (2014). IL-33: an alarmin cytokine with crucial roles in innate immunity, inflammation and allergy. *Curr. Opin. Immunol.* *31*, 31–37.
- Chaudhry, A., and Rudensky, A.Y. (2013). Control of inflammation by integration of environmental cues by regulatory T cells. *J. Clin. Invest.* *123*, 939–944.
- Cheng, G., Yuan, X., Tsai, M.S., Podack, E.R., Yu, A., and Malek, T.R. (2012). IL-2 receptor signaling is essential for the development of KlrG1+ terminally differentiated T regulatory cells. *J. Immunol.* *189*, 1780–1791.
- Cipolletta, D., Feuerer, M., Li, A., Kamei, N., Lee, J., Shoelson, S.E., Benoist, C., and Mathis, D. (2012). PPAR- γ is a major driver of the accumulation and phenotype of adipose tissue Treg cells. *Nature* *486*, 549–553.
- Coyle, A.J., Tsuyuki, S., Bertrand, C., Huang, S., Aguet, M., Alkan, S.S., and Anderson, G.P. (1996). Mice lacking the IFN- γ receptor have impaired ability to resolve a lung eosinophilic inflammatory response associated with a prolonged capacity of T cells to exhibit a Th2 cytokine profile. *J. Exp. Med.* *184*, 2680–2685.
- Duan, L., Chen, J., Zhang, H., Yang, H., Zhu, P., Xiong, A., Xia, Q., Zheng, F., Tan, Z., Gong, F., and Fang, M. (2012). Interleukin-33 ameliorates experimental colitis through promoting Th2/Foxp3+ regulatory T-cell responses in mice. *Mol. Med.* *18*, 753–761.
- Feuerer, M., Herrero, L., Cipolletta, D., Naaz, A., Wong, J., Nayer, A., Lee, J., Goldfine, A.B., Benoist, C., Shoelson, S., and Mathis, D. (2009). Lean, but not obese, fat is enriched for a unique population of regulatory T cells that affect metabolic parameters. *Nat. Med.* *15*, 930–939.
- Feuerer, M., Hill, J.A., Kretschmer, K., von Boehmer, H., Mathis, D., and Benoist, C. (2010). Genomic definition of multiple ex vivo regulatory T cell subphenotypes. *Proc. Natl. Acad. Sci. USA* *107*, 5919–5924.
- Fontenot, J.D., Gavin, M.A., and Rudensky, A.Y. (2003). Foxp3 programs the development and function of CD4+CD25+ regulatory T cells. *Nat. Immunol.* *4*, 330–336.
- Gadani, S.P., Walsh, J.T., Smirnov, I., Zheng, J., and Kipnis, J. (2015). The gliaderived alarmin IL-33 orchestrates the immune response and promotes recovery following CNS injury. *Neuron* *85*, 703–709.
- Hepworth, M.R., Monticelli, L.A., Fung, T.C., Ziegler, C.G.K., Grunberg, S., Sinha, R., Mantegazza, A.R., Ma, H.-L., Crawford, A., Angelosanto, J.M., et al. (2013). Innate lymphoid cells regulate CD4+ T-cell responses to intestinal commensal bacteria. *Nature* *498*, 113–117.
- Heredia, J.E., Mukundan, L., Chen, F.M., Mueller, A.A., Deo, R.C., Locksley, R.M., Rando, T.A., and Chawla, A. (2013). Type 2 innate signals stimulate fibro/adipogenic progenitors to facilitate muscle regeneration. *Cell* *153*, 376–388.
- Husaaarts, L., Garcia-Tardon, N., van Beek, L., Heemskerck, M.M., Haeberlein, S., van der Zon, G.C., Ozir-Fazalalikhani, A., Berbee, J.F.P., Willems van Dijk, K., van Harmelen, V., et al. (2015). Chronic helminth infection and helminth-derived egg antigens promote adipose tissue M2 macrophages and improve insulin sensitivity in obese mice. *Faseb J.* *29*, 2662–2673.
- Johnston, C.J.C., McSorley, H.J., Anderton, S.M., Wigmore, S.J., and Maizels, R.M. (2014). Helminths and immunological tolerance. *Transplantation* *97*, 127–132.
- Lee, M.-W., Odegaard, J.I., Mukundan, L., Qiu, Y., Molofsky, A.B., Nussbaum, J.C., Yun, K., Locksley, R.M., and Chawla, A. (2015). Activated type 2 innate lymphoid cells regulate beige fat biogenesis. *Cell* *160*, 74–87.
- Liang, Y., Jie, Z., Hou, L., Aguilar-Valenzuela, R., Vu, D., Soong, L., and Sun, J. (2013). IL-33 induces neutrophils and modulates liver injury in viral hepatitis. *J. Immunol.* *190*, 5666–5675.
- Liao, W., Lin, J.-X., and Leonard, W.J. (2011). IL-2 family cytokines: new insights into the complex roles of IL-2 as a broad regulator of T helper cell differentiation. *Curr. Opin. Immunol.* *23*, 598–604.
- Lynch, L., Michelet, X., Zhang, S., Brennan, P.J., Moseman, A., Lester, C., Besra, G., Vomhof-Dekrey, E.E., Tighe, M., Koay, H.-F., et al. (2015). Regulatory iNKT cells lack expression of the transcription factor PLZF and control the homeostasis of T(reg) cells and macrophages in adipose tissue. *Nat. Immunol.* *16*, 85–95.
- Maazi, H., Patel, N., Sankaranarayanan, I., Suzuki, Y., Rigas, D., Soroosh, P., Freeman, G.J., Sharpe, A.H., and Akbari, O. (2015). ICOS:ICOS-ligand interaction is required for type 2 innate lymphoid cell function, homeostasis, and induction of airway hyperreactivity. *Immunity* *42*, 538–551.
- McSorley, H.J., and Maizels, R.M. (2012). Helminth infections and host immune regulation. *Clin. Microbiol. Rev.* *25*, 585–608.
- Miller, A.M., Xu, D., Asquith, D.L., Denby, L., Li, Y., Sattar, N., Baker, A.H., McInnes, I.B., and Liew, F.Y. (2008). IL-33 reduces the development of atherosclerosis. *J. Exp. Med.* *205*, 339–346.
- Miller, A.M., Asquith, D.L., Hueber, A.J., Anderson, L.A., Holmes, W.M., McKenzie, A.N., Xu, D., Sattar, N., McInnes, I.B., and Liew, F.Y. (2010). Interleukin-33 induces protective effects in adipose tissue inflammation during obesity in mice. *Circ. Res.* *107*, 650–658.
- Molofsky, A.B., Nussbaum, J.C., Liang, H.-E., Van Dyken, S.J., Cheng, L.E., Mohapatra, A., Chawla, A., and Locksley, R.M. (2013). Innate lymphoid type 2 cells sustain visceral adipose tissue eosinophils and alternatively activated macrophages. *J. Exp. Med.* *210*, 535–549.
- Moro, K., Yamada, T., Tanabe, M., Takeuchi, T., Ikawa, T., Kawamoto, H., Furusawa, J., Ohtani, M., Fujii, H., and Koyasu, S. (2010). Innate production of T(H)2 cytokines by adipose tissue-associated c-Kit(+)Sca-1(+) lymphoid cells. *Nature* *463*, 540–544.
- Neill, D.R., Wong, S.H., Bellosi, A., Flynn, R.J., Daly, M., Langford, T.K.A., Bucks, C., Kane, C.M., Fallon, P.G., Pannell, R., et al. (2010). Neutrophils represent a new innate effector leukocyte that mediates type-2 immunity. *Nature* *464*, 1367–1370.

- Nishimura, S., Manabe, I., Nagasaki, M., Eto, K., Yamashita, H., Ohsugi, M., Otsu, M., Hara, K., Ueki, K., Sugiura, S., et al. (2009). CD8+ effector T cells contribute to macrophage recruitment and adipose tissue inflammation in obesity. *Nat. Med.* *15*, 914–920.
- Nussbaum, J.C., Van Dyken, S.J., von Moltke, J., Cheng, L.E., Mohapatra, A., Molofsky, A.B., Thornton, E.E., Krummel, M.F., Chawla, A., Liang, H.-E., and Locksley, R.M. (2013). Type 2 innate lymphoid cells control eosinophil homeostasis. *Nature* *502*, 245–248.
- Odegaard, J.I., Ricardo-Gonzalez, R.R., Goforth, M.H., Morel, C.R., Subramanian, V., Mukundan, L., Red Eagle, A., Vats, D., Brombacher, F., Ferrante, A.W., and Chawla, A. (2007). Macrophage-specific PPAR γ controls alternative activation and improves insulin resistance. *Nature* *447*, 1116–1120.
- Oliphant, C.J., Hwang, Y.Y., Walker, J.A., Salimi, M., Wong, S.H., Brewer, J.M., Englezakis, A., Barlow, J.L., Hams, E., Scanlon, S.T., et al. (2014). MHCII-mediated dialog between group 2 innate lymphoid cells and CD4(+) T cells potentiates type 2 immunity and promotes parasitic helminth expulsion. *Immunity* *41*, 283–295.
- Pichery, M., Mirey, E., Mercier, P., Lefrancais, E., Dujardin, A., Ortega, N., and Girard, J.-P. (2012). Endogenous IL-33 is highly expressed in mouse epithelial barrier tissues, lymphoid organs, brain, embryos, and inflamed tissues: in situ analysis using a novel IL-33-LacZ gene trap reporter strain. *J. Immunol.* *188*, 3488–3495.
- Price, A.E., Reinhardt, R.L., Liang, H.-E., and Locksley, R.M. (2012). Marking and quantifying IL-17A-producing cells in vivo. *PLoS ONE* *7*, e39750.
- Qiu, Y., Nguyen, K.D., Odegaard, J.I., Cui, X., Tian, X., Locksley, R.M., Palmiter, R.D., and Chawla, A. (2014). Eosinophils and type 2 cytokine signaling in macrophages orchestrate development of functional beige fat. *Cell* *157*, 1292–1308.
- Redpath, S.A., van der Werf, N., Cervera, A.M., MacDonald, A.S., Gray, D., Maizels, R.M., and Taylor, M.D. (2013). ICOS controls Foxp3(+) regulatory T-cell expansion, maintenance and IL-10 production during helminth infection. *Eur. J. Immunol.* *43*, 705–715.
- Reinhardt, R.L., Liang, H.-E., Bao, K., Price, A.E., Mohrs, M., Ben L Kelly, and Locksley, R.M. (2015). A Novel Model for IFN- γ -Mediated Autoinflammatory Syndromes. *1401992*.
- Reinhold, U., Kukul, S., Brzoska, J., and Kreysel, H.W. (1993). Systemic interferon gamma treatment in severe atopic dermatitis. *J. Am. Acad. Dermatol.* *29*, 58–63.
- Robinette, M.L., Fuchs, A., Cortez, V.S., Lee, J.S., Wang, Y., Durum, S.K., Gillfillan, S., Colonna, M., Shaw, L., Yu, B., et al.; Immunological Genome Consortium (2015). Transcriptional programs define molecular characteristics of innate lymphoid cell classes and subsets. *Nat. Immunol.* *16*, 306–317.
- Schiering, C., Krausgruber, T., Chomka, A., Fröhlich, A., Adelmann, K., Wohlfert, E.A., Pott, J., Griseri, T., Bollrath, J., Hegazy, A.N., et al. (2014). The alarmin IL-33 promotes regulatory T-cell function in the intestine. *Nature* *513*, 564–568.
- Sim, G.C., Martin-Orozco, N., Jin, L., Yang, Y., Wu, S., Washington, E., Sanders, D., Lacey, C., Wang, Y., Vence, L., et al. (2014). IL-2 therapy promotes suppressive ICOS+ Treg expansion in melanoma patients. *J. Clin. Invest.* *124*, 99–110.
- Smigielski, K.S., Richards, E., Srivastava, S., Thomas, K.R., Dudda, J.C., Klonowski, K.D., and Campbell, D.J. (2014). CCR7 provides localized access to IL-2 and defines homeostatically distinct regulatory T cell subsets. *J. Exp. Med.* *211*, 121–136.
- Stetson, D.B., Mohrs, M., Reinhardt, R.L., Baron, J.L., Wang, Z.-E., Gapin, L., Kronenberg, M., and Locksley, R.M. (2003). Constitutive cytokine mRNAs mark natural killer (NK) and NK T cells poised for rapid effector function. *J. Exp. Med.* *198*, 1069–1076.
- Stolarczyk, E., Vong, C.T., Perucha, E., Jackson, I., Cawthorne, M.A., Wargent, E.T., Powell, N., Canavan, J.B., Lord, G.M., and Howard, J.K. (2013). Improved insulin sensitivity despite increased visceral adiposity in mice deficient for the immune cell transcription factor T-bet. *Cell Metab.* *17*, 520–533.
- Turnquist, H.R., Zhao, Z., Rosborough, B.R., Liu, Q., Castellana, A., Isse, K., Wang, Z., Lang, M., Stolz, D.B., Zheng, X.X., et al. (2011). IL-33 expands suppressive CD11b+ Gr-1(int) and regulatory T cells, including ST2L+ Foxp3+ cells, and mediates regulatory T cell-dependent promotion of cardiac allograft survival. *J. Immunol.* *187*, 4598–4610.
- Van Gool, F., Molofsky, A.B., Morar, M.M., Rosenzweig, M., Liang, H.-E., Klatzmann, D., Locksley, R.M., and Bluestone, J.A. (2014). Interleukin-5-producing group 2 innate lymphoid cells control eosinophilia induced by interleukin-2 therapy. *Blood* *124*, 3572–3576.
- Vasanthakumar, A., Moro, K., Xin, A., Liao, Y., Gloury, R., Kawamoto, S., Fagarasan, S., Mielke, L.A., Afshar-Sterle, S., Masters, S.L., et al. (2015). The transcriptional regulators IRF4, BATF and IL-33 orchestrate development and maintenance of adipose tissue-resident regulatory T cells. *Nat. Immunol.* Published January 19, 2015. <http://dx.doi.org/10.1038/ni.3085>.
- Voehringer, D., Reese, T.A., Huang, X., Shinkai, K., and Locksley, R.M. (2006). Type 2 immunity is controlled by IL-4/IL-13 expression in hematopoietic non-eosinophil cells of the innate immune system. *J. Exp. Med.* *203*, 1435–1446.
- Walker, J.A., and McKenzie, A.N. (2013). Development and function of group 2 innate lymphoid cells. *Curr. Opin. Immunol.* *25*, 148–155.
- Wang, Y., Su, M.A., and Wan, Y.Y. (2011). An essential role of the transcription factor GATA-3 for the function of regulatory T cells. *Immunity* *35*, 337–348.
- Wansvee, F.M., Jelenčić, V., Valentić, S., Sestan, M., Wansvee, T.T., Theurich, S., Glasner, A., Mendrila, D., Štimac, D., Wunderlich, F.T., et al. (2015). NK cells link obesity-induced adipose stress to inflammation and insulin resistance. *Nat. Immunol.* *16*, 376–385.
- Winer, S., Chan, Y., Paltser, G., Truong, D., Tsui, H., Bahrami, J., Dorfman, R., Wang, Y., Zielinski, J., Mastroradi, F., et al. (2009). Normalization of obesity-associated insulin resistance through immunotherapy. *Nat. Med.* *15*, 921–929.
- Wiria, A.E., Sartono, E., Supali, T., and Yazdanbakhsh, M. (2014). Helminth infections, type-2 immune response, and metabolic syndrome. *PLoS Pathog.* *10*, e1004140.
- Wohlfert, E.A., Grainger, J.R., Bouladoux, N., Konkel, J.E., Oldenhove, G., Ribeiro, C.H., Hall, J.A., Yagi, R., Naik, S., Bhairavabhotla, R., et al. (2011). GATA3 controls Foxp3+ regulatory T cell fate during inflammation in mice. *J. Clin. Invest.* *121*, 4503–4515.
- Wood, P.M.D., Fieschi, C., Picard, C., Ottenhoff, T.H.M., Casanova, J.-L., and Kumararatne, D.S. (2005). Inherited defects in the interferon-gamma receptor or interleukin-12 signalling pathways are not sufficient to cause allergic disease in children. *Eur. J. Pediatr.* *164*, 741–747.
- Wood, I.S., Wang, B., and Trayhurn, P. (2009). IL-33, a recently identified interleukin-1 gene family member, is expressed in human adipocytes. *Biochem. Biophys. Res. Commun.* *384*, 105–109.
- Wu, D., Molofsky, A.B., Liang, H.-E., Ricardo-Gonzalez, R.R., Jouihan, H.A., Bando, J.K., Chawla, A., and Locksley, R.M. (2011). Eosinophils sustain adipose alternatively activated macrophages associated with glucose homeostasis. *Science* *332*, 243–247.
- Yang, Z., Grinchuk, V., Smith, A., Qin, B., Bohl, J.A., Sun, R., Notari, L., Zhang, Z., Sesaki, H., Urban, J.F., Jr., et al. (2013). Parasitic nematode-induced modulation of body weight and associated metabolic dysfunction in mouse models of obesity. *Infect. Immun.* *81*, 1905–1914.
- Yin, H., Li, X., Hu, S., Liu, T., Yuan, B., Gu, H., Ni, Q., Zhang, X., and Zheng, F. (2013). IL-33 accelerates cutaneous wound healing involved in upregulation of alternatively activated macrophages. *Mol. Immunol.* *56*, 347–353.
- Zeyda, M., Wernly, B., Demyanets, S., Kaun, C., Hämmerle, M., Hantusch, B., Schranz, M., Neuhofer, A., Itariu, B.K., Keck, M., et al. (2012). Severe obesity increases adipose tissue expression of interleukin-33 and its receptor ST2, both predominantly detectable in endothelial cells of human adipose tissue. *Int J Obes. (London)*.
- Zheng, Y., Chaudhry, A., Kas, A., deRoos, P., Kim, J.M., Chu, T.-T., Corcoran, L., Treuting, P., Klein, U., and Rudensky, A.Y. (2009). Regulatory T-cell suppressor program co-opts transcription factor IRF4 to control T(H)2 responses. *Nature* *458*, 351–356.

Regulatory T Cells in Tumor-Associated Tertiary Lymphoid Structures Suppress Anti-tumor T Cell Responses

Nikhil S. Joshi,¹ Elliot H. Akama-Garren,¹ Yisi Lu,¹ Da-Yae Lee,¹ Gregory P. Chang,¹ Amy Li,¹ Michel DuPage,¹ Tuomas Tammela,¹ Natanya R. Kerper,¹ Anna F. Farago,¹ Rebecca Robbins,¹ Denise M. Crowley,¹ Roderick T. Bronson,³ and Tyler Jacks^{1,2,*}

¹Koch Institute for Integrative Cancer Research and Department of Biology, Massachusetts Institute of Technology, Cambridge, MA 02142, USA

²Howard Hughes Medical Institute, Massachusetts Institute of Technology, Cambridge, MA 02142, USA

³Department of Pathology, Tufts University School of Medicine and Veterinary Medicine, North Grafton, MA 01536, USA

*Correspondence: tjacks@mit.edu

<http://dx.doi.org/10.1016/j.immuni.2015.08.006>

SUMMARY

Infiltration of regulatory T (Treg) cells into many tumor types correlates with poor patient prognoses. However, mechanisms of intratumoral Treg cell function remain to be elucidated. We investigated Treg cell function in a genetically engineered mouse model of lung adenocarcinoma and found that Treg cells suppressed anti-tumor responses in tumor-associated tertiary lymphoid structures (TA-TLSs). TA-TLSs have been described in human lung cancers, but their function remains to be determined. TLSs in this model were spatially associated with >90% of tumors and facilitated interactions between T cells and tumor-antigen-presenting dendritic cells (DCs). Costimulatory ligand expression by DCs and T cell proliferation rates increased in TA-TLSs upon Treg cell depletion, leading to tumor destruction. Thus, we propose that Treg cells in TA-TLSs can inhibit endogenous immune responses against tumors, and targeting these cells might provide therapeutic benefit for cancer patients.

INTRODUCTION

Non-small-cell lung cancer (NSCLC), including lung adenocarcinoma, accounts for ~25% of all cancer deaths (Jemal et al., 2010), and despite improvements in therapy, NSCLC mortality remains around 80% (<http://seer.cancer.gov/statfacts/html/lungb.html>). Immunotherapy uses the immune system to attack cancer and has demonstrated durable tumor regression in “immunogenic” tumor types such as melanoma (Pardoll, 2012). Yet, until recently, NSCLC was considered “non-immunogenic” because tumors responded poorly to immunotherapeutics (Raez et al., 2005). Furthermore, it was thought that compared to melanomas, lung tumors might not elicit strong endogenous T cell responses, even though these tumor types had similar numbers of mutations and predicted neoantigens

(Rajasagi et al., 2014; Vogelstein et al., 2013). The recent success of immune-checkpoint inhibitors in NSCLC patients demonstrates that anti-tumor T cell responses do exist in a significant fraction of lung cancer patients, but they are functionally inhibited by poorly understood immunosuppressive mechanisms (Pardoll, 2012). Overcoming these mechanisms will be essential for generating more-effective immunotherapies for this disease.

Regulatory T cell (Treg) deficiency, through mutation or deletion of X-linked forkhead box P3 (*Foxp3*), leads to a fatal lymphoproliferative disease (Josefowicz et al., 2012). However, Treg cells might also facilitate tumor progression by suppressing adaptive immunity against tumors. Treg cell depletion in transplantable, carcinogen-induced, and autochthonous tumor models demonstrates increased anti-tumor immune responses, even against previously established tumors, which results in reductions in tumor size (Sakaguchi, 2004; Bos et al., 2013; Teng et al., 2010). Yet, many questions remain about how and where Treg cells function in the context of developing tumors.

Treg cells suppress self-reactive T cells in secondary lymphoid organs (SLOs; e.g., lymph nodes [LNs] and spleen). Similarly, Treg cells can suppress anti-tumor responses in tumor-draining LNs (Boissonnas et al., 2010; Campbell and Koch, 2011). However, Treg cells inside tumor tissues might also be important in natural tumor progression. Treg cells are often enriched in tumor tissue, and a high ratio of intratumoral Treg cells to effector T cells generally predicts poor patient outcomes (Fridman et al., 2012). Furthermore, the ability of anti-CTLA-4 antibodies to deplete intratumoral, but not LN, Treg cells is critical for their efficacy in animal cancer models (Marabelle et al., 2013; Selby et al., 2013; Simpson et al., 2013). However, although previous data have suggested that intratumoral Treg cells promote tumor development, the mechanisms by which they do so remain to be fully determined.

In patients, across cancer types, lymphocytes can be found in LN-like, large, complex tumor-associated tertiary lymphoid structures (TA-TLSs; Fridman et al., 2012; Goc et al., 2013). Among patients with early-stage NSCLC, ~70% have TA-TLSs, which contain immune cells with an activated phenotype, as do TLSs observed after viral infection (Neyt et al., 2012; de

Chaisemartin et al., 2011; Dieu-Nosjean et al., 2008). TA-TLS presence also correlates with increased overall survival. Thus, it is thought that TA-TLSs promote anti-tumor responses. However, TA-TLSs have not been described in animal models, and their proposed functions have not been experimentally tested. It is also uncertain whether immunosuppressive pathways are active in TA-TLSs.

Genetically engineered mouse models (GEMMs) of cancer have greatly informed the understanding of tumor biology and therapy (Hayes et al., 2014; Kwon and Berns, 2013). Tumors in GEMMs develop from untransformed cells in their native microenvironment and, importantly, in the presence of a fully functional immune system. However, tumors in GEMMs are often poorly immunogenic, and consequentially, the use of GEMMs for tumor immunology studies has lagged (DuPage and Jacks, 2013). We previously programmed autochthonous sarcomas and lung adenocarcinomas in “KP” (*Kras*^{Lox-STOP-Lox(LSL)-G12D}*Trp53*^{flox/flox}) mice to express “LucOS,” firefly luciferase fused to a portion of ovalbumin (ova, encoding the potent T cell OT-I and OT-II antigens) and the antigenic 2C peptide (DuPage et al., 2011; DuPage et al., 2012). In both tumor types, tumor-specific T cells had a significant impact on tumor development, but disease outcomes differed. T cells prevented the development of LucOS-expressing sarcomas and, consequentially, only “edited” (LucOS-negative) sarcomas developed (DuPage et al., 2012). In contrast, although T cells restrained the growth of LucOS-expressing lung tumors early in the disease course, they could not prevent it (DuPage et al., 2011). Moreover, this initial impact on tumor growth was followed by immune suppression, despite the confirmed expression of LucOS by tumors. Therefore, whereas sarcomas escaped immune control via editing, lung tumors escaped because the anti-tumor response itself was suppressed. The mediators of immunosuppression in the lung adenocarcinoma model are unknown. Because Treg cells are prominent in early LucOS-expressing tumors (DuPage et al., 2011), we reasoned that they might be important in immune suppression in later-stage tumors. Here, we investigated the functions of intratumoral Treg cells in advanced lung adenocarcinomas.

RESULTS

Treg Cells Accumulate in Tumor-Bearing Lungs and Have an Activated Phenotype

To identify and deplete Treg cells in autochthonous lung tumors, we bred KP mice to *Foxp3*^{IRES-DTR-GFP} mice (Kim et al., 2007), in which all CD4⁺FoxP3⁺ Treg cells express diphtheria toxin receptor (DTR)-GFP fusion protein. Lung tumors in “KP-F” mice (F: *FoxP3*^{DTR-GFP/DTR-GFP} or *KP-FoxP3*^{DTR-GFP/y}) were initiated by intratracheal (i.t.) administration of non-replicating lentiviruses co-expressing LucOS and Cre-recombinase (LucOS/Cre LV; DuPage et al., 2011). In lung epithelial cells, Cre activates oncogenic *Kras*^{G12D} and deletes *Trp53*, resulting in the development of autochthonous lung adenocarcinomas over a period of months (Figure S1A; DuPage et al., 2011). After 20–24 weeks, KP-F mice had a mixture of low- and high-grade lung adenocarcinomas with few infiltrating lymphocytes (Figure S1B).

To identify circulating and lung-tissue Treg cells in flow cytometric analysis, we labeled the circulating cells with anti-CD45 (CD45^{PE-CF594}) antibodies injected prior to sacrifice (Figure S1C).

In control week-20 LucOS-infected P-F (*Kras*^{+/+}) mice, most “lung” CD4⁺ T cells or Treg cells were in the circulation (CD45^{PE-CF594+}), but in tumor-bearing animals, a large fraction of the CD4⁺ T cells and Treg cells were in the lung tissue (CD45^{PE-CF594+}; Figure 1A). This corresponded with a >20-fold increase in lung-tissue Treg cell numbers, whereas circulating Treg cell numbers remained unchanged (Figure 1B). Similar results were seen with excised tumors (data not shown).

Immunophenotyping demonstrated that ~60%–80% of the lung-tissue Treg cells in tumor-bearing mice expressed CD103 (integrin α E; Figure 1C), a Treg cell marker found in sites of inflammation (Feuerer et al., 2010; Sather et al., 2007; Suffia et al., 2005). Furthermore, ~50% of the CD103⁺ Treg cells also expressed killer cell lectin-like receptor G1 (KLRG1), which is typically associated with terminally differentiated immune cells (Beyersdorf et al., 2007; Cheng et al., 2012; Joshi et al., 2007; Robbins et al., 2005). In contrast, the presence of tumors did not affect CD103 and KLRG1 expression by Treg cells in the lung circulation, tumor-draining mediastinal LN (mLN), or control inguinal LNs (iLNs; Figure 1C). CD103⁺KLRG1⁺ double-positive (DP) Treg cells expressed high amounts of several additional molecules previously associated with activated Treg cells, including two markers of T cell activation, CD44 and CD69, and the ectonucleotidase CD39 (Figure 1D). DP Treg cells also expressed high amounts of the interleukin-2 (IL-2) high-affinity receptor IL-2R α (CD25), as well as the immunoinhibitory receptor PD-1 (Figure 1D). The expression of these markers by DP Treg cells was higher than that of CD103⁺KLRG1⁻ single-positive (SP) or CD103⁻KLRG1⁻ double-negative (DN) Treg cells in the lung tissue (Figure 1D). Treg cells in lung tissue also expressed higher amounts of CTLA-4 than did Treg cells in the mLN (Figure 1E). Together, these data suggest that similar to Treg cells found at sites of inflammation, tumor-infiltrating Treg cells exhibit an activated phenotype. Because few Treg cells with this phenotype were observed in the draining LN, it is likely that Treg cells acquired their activated phenotype within the tumor-bearing lung.

Treg Cells Actively Suppress Anti-tumor Responses Targeting Established Lung Adenocarcinomas

We next assessed the effect of Treg cell depletion on tumors in KP-F mice. Two intraperitoneal (i.p.) injections of diphtheria toxin (DT, 50 μ g/g) into tumor-bearing (~18–20 weeks after infection) or non-tumor-bearing KP-F mice efficiently eliminated Treg cells in the lungs and lymphoid tissues (Figures 2A, S2A, and S2B). However, *FoxP3*^{DTR} mice, but not *FoxP3*^{WT} mice, became moribund within ~2–3 weeks of depletion and required sacrifice (Figure S2C). Additionally, in tumor-bearing *KP-FoxP3*^{DTR-GFP/+} (KP-F/+) mice, in which only 50% of all Treg cells express DTR-GFP as a result of X inactivation (Figure S2D), DT treatment did not cause morbidity (data not shown). Therefore, the observed morbidity was caused by an autoimmune response triggered by transient Treg cell depletion and was not a side effect of DT treatment. Consistent with this, 12 days after depletion, in KP-F mice, but not in KP-F/+ mice, most T cells were activated (CD44^{hi}), there was dramatic lymphadenopathy and splenomegaly, and lymphocytes had infiltrated several tissues throughout the body (Figures S2E–S2H; Kim et al., 2007). Of note, regardless of tumor status, in Treg-cell-depleted mice we

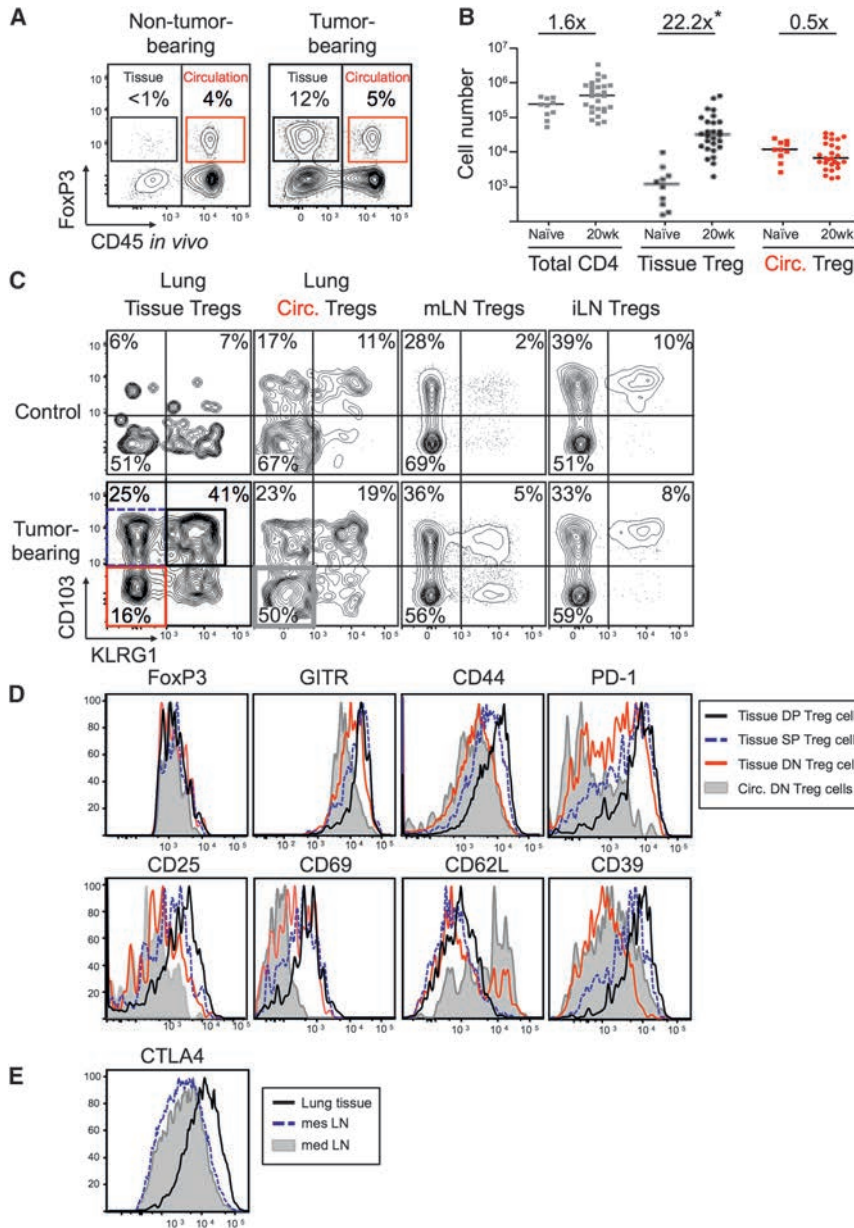


Figure 1. Treg Cells in Tumor-Bearing Lungs Have an Activated Phenotype

KP-F and P-F (control) mice were analyzed ~20 weeks (18–24 weeks) after LucOS/Cre LV infection by flow cytometry.

(A) FACS plots gated on lung CD4⁺ T cells. Tissue (black) and circulating (red) FoxP3⁺ Treg cell frequency is indicated. Note that control and uninfected (naive) lungs were indistinguishable. n > 30 mice.

(B) Graph of total CD4⁺ T cells and tissue and circulating Treg cell numbers in lungs from naive (n = 11) and tumor-bearing (week 20, n = 30) animals. Median and relative differences are indicated. *p = 0.03.

(C) CD103 and KLRG1 on the Treg cell populations in (A). n > 30 mice.

(D) Expression of indicated markers by circulating DN (filled gray line) and tissue DN, SP, and DP Treg cells (red, dashed blue, and black lines, respectively). Histograms are gated as shown in (C). n = 9–35 mice.

(E) CTLA-4 expression by mLN (gray filled line), mesenteric (mes) LN (dashed blue line), and lung-tissue Treg cells (black line). n = 7 mice.

observed lymphocytic infiltration near the major airways in the lungs and goblet cell metaplasia, similar to what is seen in FoxP3-deficient mice (Figures S2I and S2J; Lin et al., 2005). However, in non-tumor-bearing animals, the alveolar spaces in the lungs (where tumors normally develop) were free from infiltration.

To track tumor cell fate after Treg cell depletion, we bred KP-F mice to *Rosa26*^{LSL-tdTomato(tdT)} mice to generate “KPT-F” mice, in which Cre induces tdT expression in tumor cells (Figure S1A; Madisen et al., 2010). Immunofluorescence (IF) staining of tumors from untreated ~week-20 KPT-F mice demonstrated that they were composed of abundant, healthy-appearing tdT⁺ tumor cells that were arranged primarily in papillary structures with EpCAM staining junctions between adjacent tumor cells (Figure 2B). In contrast, day-12 Treg-cell-depleted tumors had a

range of cellular infiltration and disruption of regular tissue architecture (Figure 2B). Quantification of 85 control and 108 Treg-cell-depleted tumors showed that >80% of the Treg-cell-depleted tumors had moderate or severe disruption (Figure 2C). To visualize tumor destruction more comprehensively, we performed CLARITY (Chung et al., 2013) on lungs from control and Treg-cell-depleted KPT-F mice. This allowed whole-tumor 3D confocal imaging of 15 control and 10 Treg-cell-depleted tumors. Tumors from the Treg-cell-depleted mice showed extensive cellular infiltration (Figure 2D and Movie S1) and contained cavities filled with densely packed (non-tumor) cells. Furthermore, tumor cells in the Treg-cell-depleted mice were thin and elongated and no longer formed connections with adjacent tumor cells (Figures 2B and 2D). These data demonstrate that the cellular density and morphology of tumors were severely disrupted by Treg cell depletion.

Immunohistochemical (IHC) analysis showed that most of the infiltrating cells in Treg-cell-depleted tumors were CD45⁺ immune cells (Figure 2E). Infiltration was highly focused in the areas near tumors, given that distal areas were free of immune infiltrates (Figure S3A). Immune infiltration was not observed in tumors from Treg-cell-depleted KPT-F/+ mice, indicating that depletion of more than half of the Treg cell population was required for anti-tumor effects (Figure S3B). Fluorescence-activated cell sorting (FACS) analysis revealed that the number of CD4⁺ and CD8⁺ T cells in the lung increased after Treg cell depletion (Figure 2F). In contrast, the number of B cells did not

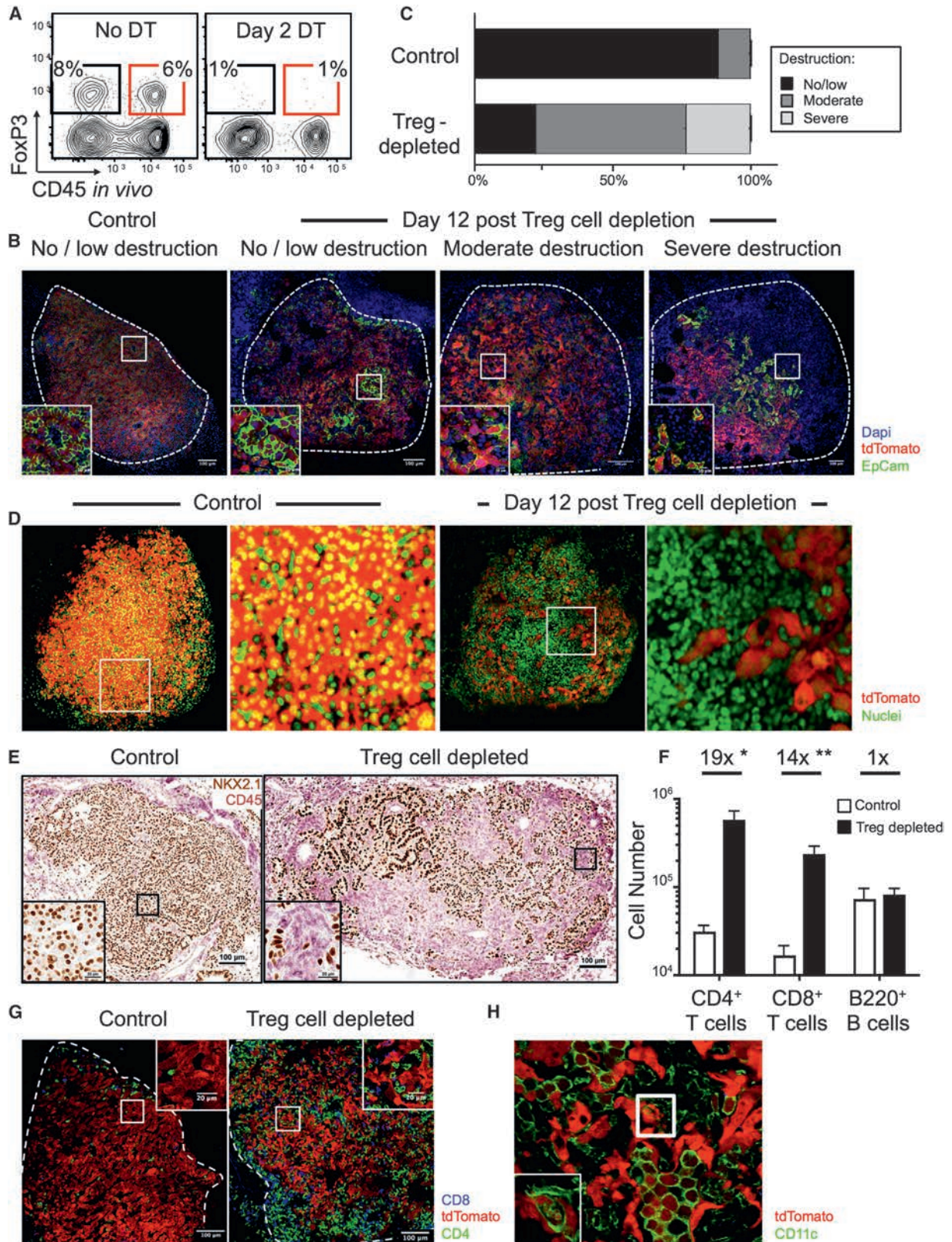


Figure 2. Treg Cells Maintain Immune Quiescence in Advanced Tumors

~Week-18 to week-20 LucOS/Cre-LV-infected KP-F (A) or KPT-F (B–H) mice were treated 1 × (A) or 2 × (B–H) with i.p. DT (50 ng/g) and analyzed 2 (A) or 12 (B–H) days later.

(legend continued on next page)

increase. IF analyses showed that in undepleted mice, CD3⁺ T cells in tumors were primarily located within or near blood vessels, and CD11c⁺ macrophages were located within airway-like pockets surrounded by tumor cells (Figures S4A and S4B). In contrast, in the absence of Treg cells, CD4⁺ and CD8⁺ T cells were located throughout the tumor parenchyma (Figure 2G), and tumors were heavily infiltrated by macrophages that were faintly positive for tdT (Figure 2H). Moreover, a small number of macrophages had tdT⁺ vesicles, suggesting phagocytosis of tumor cells. Together, these data demonstrate that Treg cells actively suppress immune destruction of established tumors.

Lung-Tissue Treg Cells Are Contained within TA-TLSs

We next investigated Treg cell localization in tumor-bearing lungs. Tumors in week-20 KP-F mice had few infiltrating Treg cells, and instead, most Treg cells (>80-fold increase) were located in perivascular immune cell patches resembling TLSs (Figures 3A and 3B). These structures also contained CD11c⁺ dendritic cells (DCs) and B220⁺ B cells, two cell types that have the potential to interact directly with Treg cells (Figure 3C). TA-TLSs have been observed in patients with lung adenocarcinoma (Fridman et al., 2012), but not in animal tumor models. Therefore, we quantified the extent to which TLSs were associated with tumors in this model and identified whether they displayed features of TA-TLSs in human cancers.

Because tumors span several hundred microns, we reasoned that analyses of thin (5- μ m) lung sections might underestimate the presence of TLSs in tumor-bearing lungs. Therefore, we quantified the presence of TLSs in 30- μ m-thick sections of tumor-bearing lungs from eight mice and counted the number of tumors that were associated with TLSs in three in-silico-reconstructed tumor-bearing lung lobes (Figure 3D). Analysis of the 30- μ m sections revealed that ~60% (18/31) of tumors were directly associated with at least one TLS (defined as B cell clusters of >10 cells directly associated with T cells), and analysis of the in-silico-reconstructed lungs showed at least one TLS associated with ~93% (70/75) of tumors analyzed (data not shown).

We next used IF to characterize the cellular and structural components of TLSs in thick sections of tumor-bearing lungs. TLSs varied greatly in size and complexity, although this might be due to the fact that individual sections only capture part of a given TLS. TA-TLSs in human cancers can have B and T cell zones organized by follicular dendritic cells (FDCs) and fibroblastic reticular cells (FRCs). Similarly, in this model, mature

TLSs had clearly defined B220⁺ B cell and CD3⁺ T cell areas, which were distinct from the NKX2.1⁺ tumor areas (Figures 3E–3I). Moreover, TLSs all contained Treg cells, which were primarily located in the T cell areas (Figure 3E-II). About 30% of the time, B cell areas in the TLSs contained detectable CR1⁺ cells with long processes that were morphologically similar to FDCs (Figure 3E-III). These cells also expressed the B cell chemoattractant CXCL13 and made direct contact with B cells (Figure 3E-III and Movie S2A). We also observed that many T cells in the T cell areas were in direct contact with ERTR-7⁺CCL21⁺ FRC-like cells (Figure 3E-IV and Movie S2B). The presence of FRC- and FDC-like cells in TA-TLSs suggests that they could help to organize and support infiltrating B and T cells.

Human TA-TLSs contain high endothelial venules (HEVs), which in LNs constitutively recruit B and T cells from the circulation (de Chaisemartin et al., 2011; Neyt et al., 2012). We noted prominent, large CD31⁺PNAd⁺ HEV-like structures, in many of which T cells in the lumen were associated with the vessel wall (Figures 3E–3V and Movie S2C). This indicates that HEV-like structures could be recruiting circulating T cells into TA-TLSs in this model, as has been hypothesized in humans. Together, these data demonstrate that TLSs associated with LucOS-expressing lung adenocarcinomas have hallmarks of LNs and phenotypically mirror TA-TLSs seen in cancer patients.

TLSs Facilitate T Cell Entry into and Activation in the Tumor Microenvironment

It has been speculated that TA-TLSs might be a site for local activation of tumor-specific T cells (Goc et al., 2013), but this possibility remains untested. Therefore, we focused on examining the function of TA-TLSs in vivo. Because LucOS/Cre LV encodes the antigenic portions of ova, we used ova-specific T cell receptor (TCR) transgenic (Tg) OT-I CD45.1⁺CD8⁺ T cells to analyze homing to and antigen presentation in TA-TLSs (outlined in Figure 4A). As a negative control, LCMV-specific P14 Tg CD45.1⁺CD8⁺ T cells were used because their TCR recognizes an antigen not present in LucOS. We activated the OT-I and P14 T cells in vitro to generate memory T cells, which are more sensitive for the presence of antigens (Kaech and Ahmed, 2001). Next, the OT-I and P14 T cells were labeled with the cell-proliferation dyes cell trace violet (CT-V) and eFluor670 (CT-670), respectively, mixed at a 1:1 ratio, and adoptively transferred into week-20 tumor-bearing CD45.2⁺ KP-F mice or control

(A) FACS plots show lung CD4⁺ T cells and are gated as in Figure 1A. n > 6 mice.

(B) Confocal IF images show the range (no or low, moderate, or severe) of tumor destruction in untreated (left panel) and Treg-cell-depleted (right three panels) mice. Red, tdTomato⁺; green, EpCAM; blue, DAPI; dashed line, tumor border.

(C) Quantitation of tumor destruction from images in (C). n = 85 and 13 control tumors and mice, respectively, and 108 and 17 Treg-cell-depleted tumors and mice, respectively.

(D) Control (left panels) and Treg-cell-depleted (right panels) lungs were optically cleared with CLARITY. Images show optical slices through tumors. Red, tdTomato⁺; green, YO-PRO-1. n = 15 and 7 control tumors and mice, respectively, and 10 and 3 Treg-cell-depleted tumors and mice, respectively. See also Movie S1.

(E) IHC images show control and Treg-cell-depleted tumors for lung (NKX2.1, brown) and immune (CD45, pink) cells. n = 71 and 11 control tumors and mice, respectively, and 55 and 9 Treg-cell-depleted tumors and mice, respectively.

(F) Graph of median lung-tissue CD4⁺ and CD8⁺ (Thy1.2⁺) T cell and (B220⁺ CD19⁺) B cell numbers in Treg-cell-depleted mice (black bars, n = 6) and control mice (white bars, n = 5) \pm SEM. *p = 0.0150, **p = 0.0175.

(G) Confocal IF images show control (n = 39) and Treg-cell-depleted (n = 15) tumors. Red, tdTomato⁺; green, CD4; blue, CD8⁺ T cells.

(H) Confocal IF image shows a Treg-cell-depleted tumor. Red, tdTomato⁺; green, CD11c⁺ macrophage (large round cells). The inset shows an optical slice of a macrophage with tdT⁺ vesicles (the z depth is different than in the larger image). n = 4 mice.

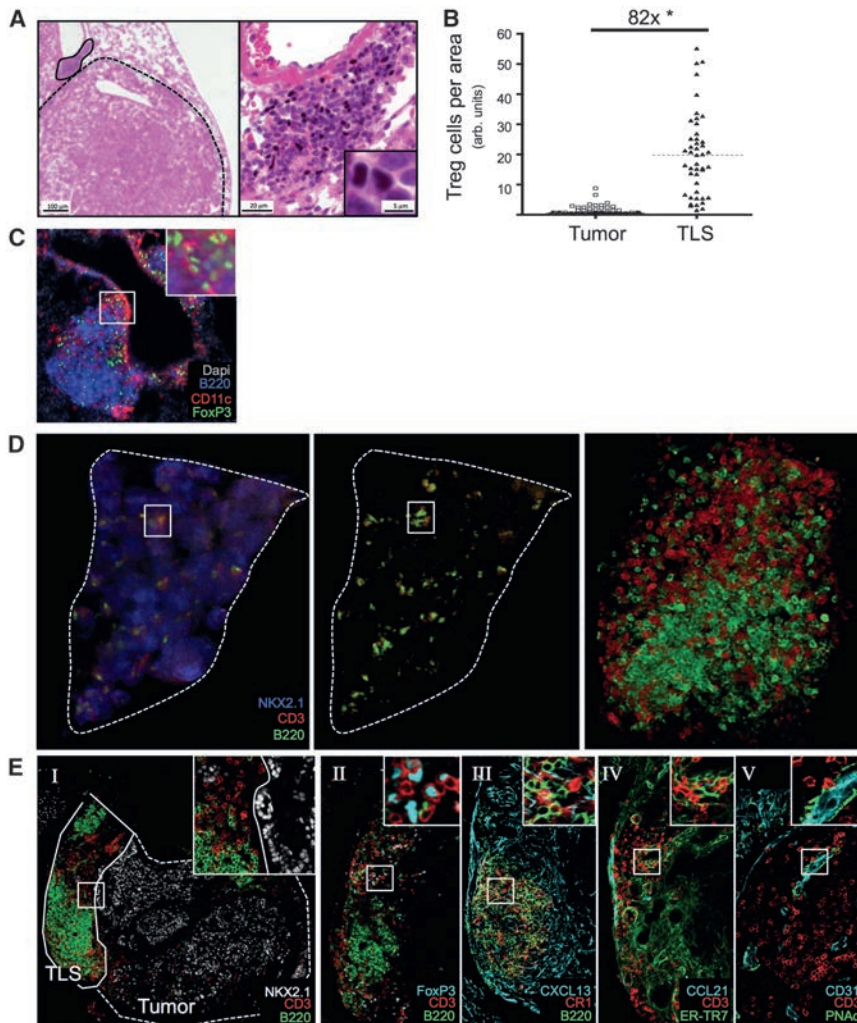


Figure 3. Treg Cells in Tumor-Bearing Lungs Are Located in TA-TLSs

KP-F or KPT-F mice were analyzed 18–20 weeks after LucOS/Cre LV infection.

(A) IHC images show FoxP3 (black), hematoxylin (blue), and eosin (pink). Tumor, dashed line; TLS, solid line; left panel, 4 \times ; right panel, 20 \times . $n = 10$ mice.

(B) Median Treg cell number in tumors ($n = 88$) and TLSs ($n = 45$) from 9 mice. Normalized by pixel area. * $p = 3.89 \times 10^{-25}$.

(C) IF image shows TLSs. Red, CD11c; green, FoxP3; blue, B220; white, DAPI. $n = 6$ mice.

(D) 3D rendering of an in-silico-reconstructed tumor-bearing lung lobe. ~ 20 IF sections (50 μM , ~ 1 -mm depth) were imaged by confocal microscopy. Blue, NKX2.1; red, CD3; green, B220. Center panel is the same as the left, except that NKX2.1 was removed. Right panel, TLS in box. $n = 3$ mice.

(E) Confocal IF images show a TLS in serial stained sections (30 μm) stained for indicated markers. The tumor border (dotted line) and TLS (solid line) are shown in (I). Images highlight (II) cyan FoxP3 $^+$ Treg cells, (III) red CR1 $^+$ FDCs, (IV) green ER-TR7 $^+$ FRCs, and (V) green PNAAd $^+$ CD31 $^+$ HEVs. $n = 16$ mice.

non-tumor-bearing CD45.2 $^+$ P-F mice. On days 2 and 3 after transfer, homing, proliferation, and activation status were assessed by FACS and IF. When OT-I and P14 T cells were transferred to control mice, neither cell type appreciably entered the lung tissue, consistent with a lack of TLSs in these mice (Figure 4B). In contrast, upon transfer into tumor-bearing hosts, both OT-I and P14 T cells entered the lung tissue. This suggests that like LNs, TLSs in this model have the capacity to recruit activated T cells from the circulation. Both P14 and OT-I T cells were found in the lung tissue, but by IF a greater fraction of the OT-I T cells were located in the TLS (Figure 4C and Figure S5A). Furthermore, OT-I T cells were observed to interact with DCs in the T cell areas of the TLSs (Figure 4D). To determine whether these contacts were functionally relevant, we assessed whether OT-I and P14 T cells form immunologic synapses *in vivo* with DCs. Sections were stained with γ -tubulin (a marker of the microtubule-organizing center [MTOC]) and CD11c, and immunologic synapses were quantified on the basis of MTOC position and interaction with a DC (Figure S5B). In cells forming synapses, the MTOC is repositioned to lie behind the synapse and, as such, can be used for determining the direction in which a T cell is oriented (Billadeau et al., 2007). According to this metric, along with

the accumulation of cell-proliferation dye (which non-specifically labels cellular protein) at the T-cell-DC interface, OT-I T cells formed 2.7-fold more synapses than did P14 T cells in TLSs (Figure 4E). A similar increase was seen among OT-I T cells transferred into LucOS/Cre-LV-infected versus Cre-LV-infected recipients, which have tumors that do not express LucOS (data not shown). Therefore, although OT-I and P14 T cells were both recruited into tumor-bearing lungs, OT-I T cells preferentially interacted with DCs in TLSs. This interaction had a meaningful effect on the OT-I T cells, such that they upregulated CD69, an early marker of T cell activation, and proliferated within lung tissue, whereas P14 T cells did not (Figure 4F). Similar activation and proliferation patterns were seen in the tumor-draining mLN, but not in the iLNs, spleen, or lung circulation (Figure 4F and data not shown). OT-I T cells did not upregulate CD69 or proliferate in the lung tissue or mLN when transferred into control P-F mice (data not shown). These data clearly demonstrate that infiltrating T cells can interact with tumor antigens in both the mLN and the TA-TLSs.

Because some DCs in the TLSs could have been directly infected by LucOS/Cre LV (20 weeks prior), and thus their presentation of antigens might not be tumor specific, we analyzed DCs in KPT-F mice for the presence of tdT by IF. Given that the highly active and ubiquitously expressed CAG promoter drives tdT expression after Cre-mediated recombination in KPT-F mice (Madisen et al., 2010), direct infection of any cell type results in strong tdT signal. 20 weeks after LucOS/Cre LV infection, directly infected round CD11c $^+$ macrophages were easily

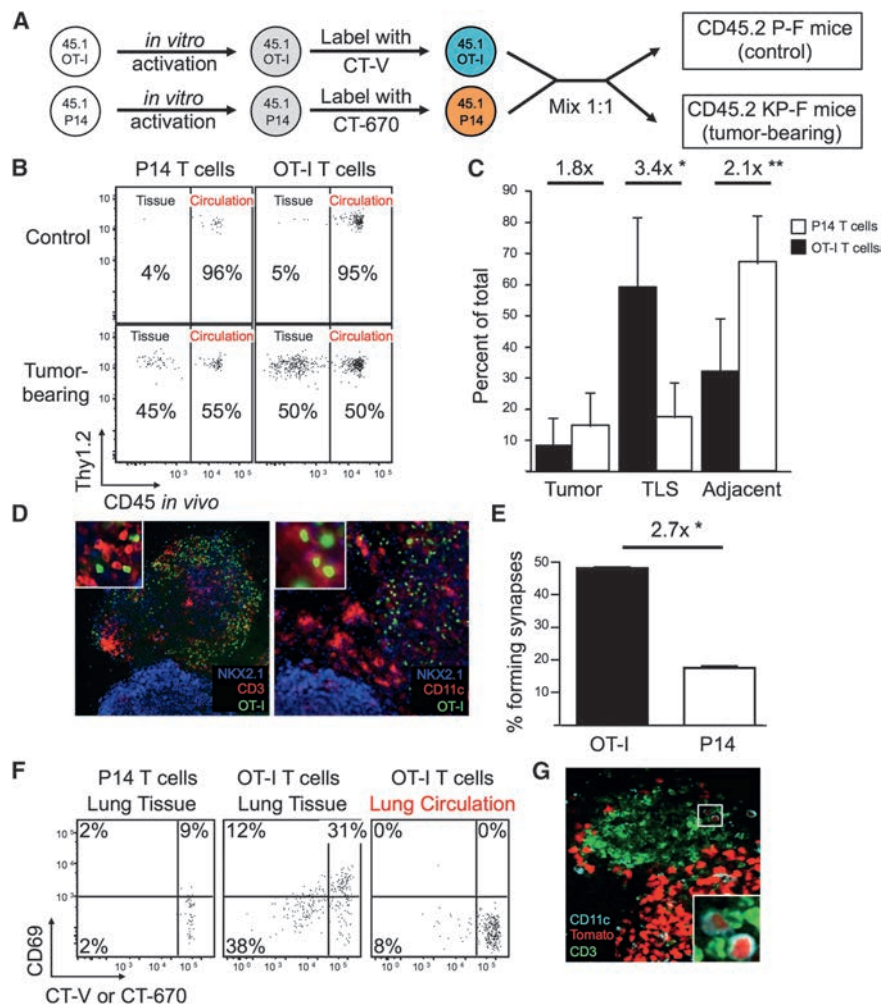


Figure 4. TLSs Serve as Local Sites of Tumor Antigen Presentation

(A) Schematic diagram for (B)–(F). In-vitro-activated CT-670⁺ P14 and CT-V⁺ OT-I Tg CD45.1⁺CD8⁺ T cells were transferred into ~week-20 LucOS/Cre-LV-infected CD45.2⁺ tumor-bearing KP-F and control P-F recipients.

(B) FACS plots show lung CD45.1⁺CD8⁺ P14 and OT-I T cells 2–3 days after transfer. n > 12 mice per group.

(C) Graph shows the median fraction (\pm SEM) of transferred OT-I (black bars, n = 620) or P14 (white bars, n = 238) CD8⁺ T cells in the indicated tissue (see also Figure S5A). *p = 1.89 \times 10⁻³, **p = 3.59 \times 10⁻³.

(D) Confocal IF images of a TLS. Green, CT-V (OT-I T cells); blue, NKX2.1; red, CD3 (left panel, n = 13) or CD11c (right panel, n > 20).

(E) Graph shows the mean fraction (\pm SEM) of OT-I (black bar, n = 231) or P14 (white bar, n = 122) T cells forming synapses (see also Figure S5B). *p = 5.62 \times 10⁻¹¹.

(F) FACS plots show transferred P14 or OT-I CD8⁺ T cells (gated as in Figure 5B). n > 12 recipients.

(G) Confocal IF image shows a tumor and TLS in ~week-20 LucOS/Cre-LV-infected KP-F mice. Green, CD3; cyan, CD11c (DCs are small cells); red, tdTomato. Note the signal-intensity difference between tumor cells and DCs. n = 5 mice.

identified on the basis of an abundant tdT signal, similar in intensity to that in tumor cells (data not shown). In contrast, some CD11c⁺ DCs (distinguished from macrophages on the basis of their smaller size and dendritic morphology; Thornton et al., 2012) had faint signal for tdT in TA-TLSs in KPT-F mice, implying that these cells had phagocytosed tumor-derived products (Figure 4G). Additionally, we sorted lung-tissue DCs from tumor-bearing lungs and confirmed that they could present tumor-derived antigens to naive OT-I CD8⁺ T cells in vitro (Figures S5C and S5D). Together, these data demonstrate that much like the tumor-draining LNs, TA-TLSs in this tumor model are functional structures capable of recruiting circulating CD8⁺ T cells and facilitating their interactions with antigen-presenting DCs.

Local Immune Responses in TA-TLSs after Treg Cell Depletion

We next assessed the impact of Treg cell depletion on tumor-associated TLSs. The area of the lung covered by TLSs from ~week-20 LucOS/Cre-LV-infected KP-F mice expanded ~7-fold in the 12 days after Treg cell depletion (Figure 5A). However, because it was unclear whether this increase was due to local lymphocyte expansion or recruitment, we analyzed TA-TLSs

for signs of immune activity at early time points after Treg cell depletion. Antigen-driven lymphocyte activation is strongly correlated with cell division; therefore, we treated mice with the nucleoside analog bromodeoxyuridine (BrdU) 4 hr before sacrifice to label proliferation of lymphocytes. IHC analysis

showed that the proportion of proliferating lymphocytes in TLSs was increased at days 4 and 6 after Treg cell depletion (Figures 5B and S6A). Moreover, analysis of BrdU incorporation by FACS and IF revealed that the increased rates of proliferation were largely among CD4⁺ and CD8⁺ T cells in TLSs, which increased ~5- and ~10-fold, respectively, after Treg cell depletion (Figures 5C and 5D). Collectively, these data suggest that TA-TLSs are local sites for T cell proliferation shortly after Treg cell depletion, although it is possible that some T cells proliferated elsewhere and migrated to TA-TLSs during the 4-hr window of our assay.

Treg cells directly regulate costimulatory molecules on DCs in SLOs (Kim et al., 2007), and we therefore reasoned that increased expression of costimulatory molecules on DCs immediately after Treg cell depletion could indicate sites of Treg cell function. Expression of CD80 (B7-1) and CD86 (B7-2) was examined on lung-tissue DCs 2 days after Treg cell depletion, when changes would most likely be due to direct effects in TLSs. FACS analysis of day-2 and day-6 Treg-cell-depleted mice revealed that lung-tissue DCs had higher expression of CD80 and CD86 at day 2 after depletion (Figure 5E). These data are consistent with the possibility that, as they do in other SLOs, Treg cells in TA-TLSs regulate DC

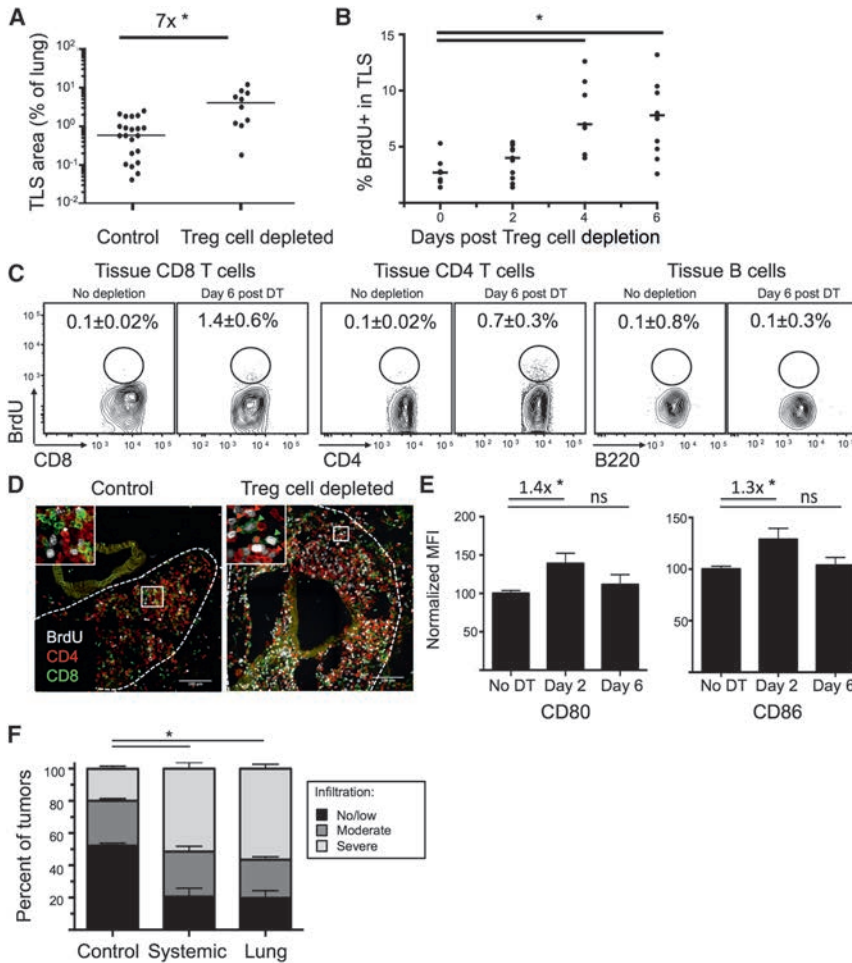


Figure 5. TLSs Are Sites of Immune Activation after Treg Cell Depletion

~week-20 LucOS/Cre-LV-infected KP-F mice received i.p. (A–F) or i.t. (F) DT injection. Mice were treated with BrdU for labeling proliferating cells (B–D).

(A) Graph quantifies TLS area (normalized to lung area) in 22 control and 10 day-12 Treg-cell-depleted mice. * $p = 1.8 \times 10^{-4}$.

(B) Graph shows the percent of BrdU⁺ lymphocytes in TLSs after Treg cell depletion. Day 0 indicates no DT. Points are the average of lymphocytes in all the TLSs in a section. Bars indicate the median. $n = 7$ (days 0 and 4) and 11 (days 2 and 6). * $p < 0.005$. See also Figure S6A.

(C) FACS plots show BrdU staining in lung-tissue CD8⁺ and CD4⁺ (FoxP3⁻) T cells and B220⁺CD19⁺ B cells. Data represent the average \pm SEM of three control and six Treg-cell-depleted mice.

(D) Confocal IF images show control ($n = 18$ TLSs and 9 mice) and day-6 Treg-cell-depleted ($n = 57$ TLSs and 12 mice) TLSs. Green, CD8; red, CD4; white, BrdU; arrowheads, BrdU⁺CD8⁺ (green) and CD4⁺ (red) T cells.

(E) Graphs show median (\pm SEM) CD80 and CD86 median fluorescence intensity on lung-tissue CD11b⁺CD11c⁺MHCII⁺ DCs. $n = 8$ (no DT), 12 (day 2), 13 (day 6). Relative change is indicated. ns, non-significant; * $p < 0.05$.

(F) Graph shows blind quantification of IHC on lung sections from control mice ($n = 630$ tumors and 23 mice), day-12 i.p.-DT-treated mice (systemic depletion, $n = 136$ tumors and 15 mice), and day-12 i.t.-DT-treated mice (lung-restricted depletion, $n = 266$ tumors and 11 mice) stained for CD45 and NKX2.1. No or low, <30% CD45⁺ cell infiltration; moderate, 30%–50%; severe, >50%. * $p < 0.005$.

function by reducing costimulatory levels. Furthermore, after Treg cell depletion, the overall microenvironment in the TA-TLSs might become more immunostimulatory to promote anti-tumor responses by T cells.

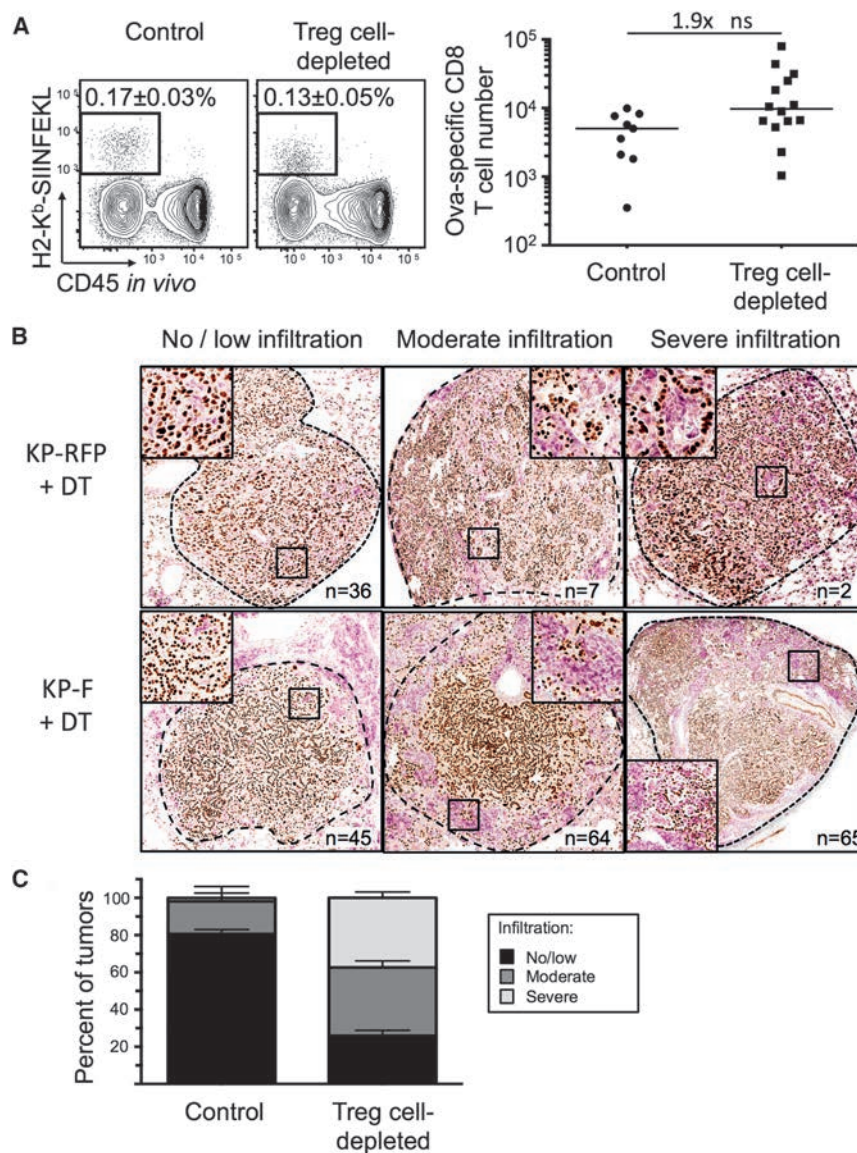
Local Treg Cell Depletion Triggers Anti-tumor Responses Targeting Established Lung Adenocarcinomas

Treating tumor-bearing KP-F mice with i.p. DT causes acute systemic Treg cell depletion throughout the mice. To verify that Treg cells in the local microenvironment of the lung suppress anti-tumor responses, we treated mice with repeated low doses of i.t. DT to deplete Treg cells locally within the lung. Week-20 LucOS/Cre-LV-infected KP-F mice were treated with six daily i.t. doses of 50 ng DT. Administering i.t. DT did not result in LN enlargement, with the exception of the lung-draining mLN, and no morbidity was observed (data not shown). Local Treg cell depletion triggered immune infiltration of ~80% of lung tumors (Figures 5F and S6B). Therefore, local Treg cell depletion was sufficient to trigger strong anti-tumor effects, consistent with the idea that Treg cells in the TLSs (and possibly in the mLNs) regulate local anti-tumor responses. Moreover, these data demonstrate that efficient, local Treg cell depletion could be an effective means of triggering endogenous anti-tumor immune re-

sponses without the systemic toxicity associated with whole-body Treg cell depletion.

Programmed Antigen Expression Is Not Required for Anti-tumor Responses after Treg Cell Depletion

We next examined whether Treg cell depletion enhanced responses by the CD8⁺ T cells targeting the potent T cell antigens in LucOS. Surprisingly, however, we found that the number of endogenous SIINFEKL-specific CD8⁺ T cells (identified with SIINFEKL-loaded H2-K^b MHC I tetramers) was not dramatically altered by Treg cell depletion (Figures 6A). Additionally, the responses of naive T cell OT-I CD8⁺ T cells transferred into tumor-bearing recipients were not enhanced by the absence of Treg cells (data not shown). These data suggest that programmed antigen expression by tumors is not required to elicit anti-tumor responses after Treg cell depletion. Thus, we infected KP-F and KP \times FoxP3^{IRES-RFP} (KP-RFP) mice with Cre LV (previously referred to as Lenti-X in DuPage et al., 2011), and ~18 weeks later, we treated them with DT. After 12 days, we analyzed lung tumors for infiltration by immune cells and evidence of tumor destruction. Treg cell depletion resulted in dramatic infiltration of lung tissues by CD45⁺ cells, particularly in the perivascular and peribronchiolar regions (data not shown). Moreover, ~75% of tumors in Treg-cell-depleted mice ($n = 174$



tumors from 10 mice) were moderately (immune infiltration in 30%–50% of the tumor area) or severely (greater than 50%) infiltrated, and most showed evidence of immune-mediated tumor disruption (Figures 6B and 6C). In contrast, ~20% of the tumors from DT-treated KP-RFP mice ($n = 45$ tumors from 6 mice) had moderate or severe immune infiltration (Figures 6B and 6C). Similarly, only 10% of non-DT-treated week-20 KP-F mice ($n = 58$ tumors from 5 mice) had severe or moderate infiltration. These data clearly demonstrate that the anti-tumor response seen after Treg cell depletion does not require the programmed expression of strong tumor antigens by tumors.

DISCUSSION

It is thought that the intratumoral Treg cells in cancer patients have important roles in immunosuppression, but it has not been possible to functionally explore these roles in humans. Here, we have demonstrated that Treg cells regulate anti-tumor immune

Figure 6. Overt Antigen Expression by Tumors Is Not Required for Anti-tumor Response after Treg Cell Depletion

(A) FACS plots and graph show endogenous ova-specific CD8⁺ T cells (identified with H2-K^b-SIINFEKL tetramer) in control ($n = 9$) and day-12 Treg-cell-depleted (i.p.; $n = 14$) ~week-20 LucOS/Cre-LV-infected KP-F mice. Plots are gated on CD8⁺ T cells. Median frequency of total \pm SEM is indicated on plots. Note that no tetramer staining was observed in Cre-LV-infected mice. ns, non-significant.

(B) IHC images show NKX2.1 (brown) and CD45 (pink) in ~week-18 Cre-LV-infected KP-F ($n = 15$) and KP-RFP (control, $n = 6$) mice 12 days after i.p. DT injection. No or low, <30% CD45⁺ cell infiltration; moderate, 30%–50%; severe, >50%. $n =$ tumor number.

(C) Graph quantifies IHC in (B). Control includes tumors from DT-treated KP-RFP mice ($n = 45$ tumors and 6 mice) and untreated KP-F mice ($n = 58$ tumors and 5 mice). $n = 174$ Treg-cell-depleted tumors from 10 mice.

responses in TA-TLSs in a mouse model of lung adenocarcinoma. We observed that TLSs recruit T cells from the circulation and facilitate their interaction with tumor-antigen-presenting DCs. Treg cells in TLSs actively suppress potent anti-tumor responses, and thus TLSs are a primary site for T cell expansion upon Treg cell depletion. Subsequently, T cells and macrophages infiltrate tumors, resulting in significant tumor destruction. Collectively, these data point to immunosuppressive Treg cell function within TLSs as one mechanism that prevents anti-tumor responses and allows continued tumor development.

TA-TLSs have been observed in several human cancer types (Fridman et al., 2012; Goc et al., 2013), but it is not known how they form or function. In this model, TA-TLSs formed during the course of tumor development and were closely associated with ~90% of the LucOS-expressing tumors. Interestingly, antigen expression by tumors might affect TLS formation given that TLSs in lungs from Cre-LV-infected mice appeared larger and were located centrally in the lungs, distal to tumors (N.S.J. and T.J., unpublished data).

In most studies, the presence of TA-TLSs correlates with better survival for cancer patients, suggesting that TA-TLSs have anti-tumor functions. However, one study found that high numbers of Treg cells in TA-TLSs, but not the tumor parenchyma, correlated with poor survival of breast cancer patients (Gobert et al., 2009). It has been difficult to study the function of TA-TLSs, including how immunosuppressive pathways, like Treg cells, influence anti-tumor responses from within these structures. In this model, we observed that Treg cells were prominent in TA-TLSs and that, upon Treg cell depletion, T cells within TA-TLSs proliferated, coincident with tumor infiltration. Thus, we

propose that TA-TLSs might serve both pro- and anti-tumor functions depending on the state of disease progression, as well as the presence of immunosuppressive cell types, including Treg cells. However, TA-TLSs also probably facilitate influx of new effector T cells into the tumor site after Treg cell depletion through HEVs and amplify the anti-tumor response. Therefore, TA-TLSs could be intimately involved in many aspects of the anti-tumor immune response, both at steady state and after therapeutic interventions.

The data presented here do not exclude the possibility that Treg cells in this model also suppress anti-tumor responses in the tumor-draining mLN. In contrast, because tumor antigens are presented in TA-TLSs and the mLN, regulation of anti-tumor immune responses most likely requires immunosuppression at both sites. Because Treg cells function through a variety of mechanisms (Josefowicz et al., 2012), Treg cells in TA-TLSs and LNs could rely on distinct effector pathways. Consistent with this idea, Treg cells in TA-TLSs were phenotypically more activated and expressed higher levels of multiple effector molecules. For example, Treg cells in our model (and others) expressed higher amounts of CTLA-4 in the tumor microenvironment than did tumor-draining LNs (Marabelle et al., 2013; McDermott et al., 2014; Selby et al., 2013; Simpson et al., 2013). In the steady state, Treg cells use CTLA-4 to reduce the amounts of costimulatory proteins on DCs, thus inhibiting T cell activation and preventing autoimmunity (Qureshi et al., 2011; Wing et al., 2008). Likewise, Treg cells in TLSs could use CTLA-4 to regulate anti-tumor responses through DCs. TA-TLS Treg cells also express high amounts of CD39, which, along with CD73, produces adenosine, a potent T cell inhibitor (Antonioli et al., 2013). Interestingly, chemical inhibition of CD39 has been shown to reduce early tumor growth in a Kras-driven *Atg5*-deficient mouse lung cancer model, possibly through Treg cell function (Rao et al., 2014). Further investigation will be required to more firmly establish the functional importance of these and other effector pathways active in Treg cells in TLSs and to determine whether these pathways can be therapeutically exploited for improving anti-tumor immune responses.

CD8⁺ T cell responses against the strong ova-antigen in LucOS were not dramatically enhanced by Treg cell depletion. This is perhaps because Treg cells preferentially suppress responses by T cells that have weak, lower-affinity interactions with their cognate antigen (Pace et al., 2012), more like those seen with self- or tumor-antigens (Aleksic et al., 2012). Therefore, in addition to responding to Cre-derived antigens, after Treg cell depletion, T cells could also have been responding to self-antigens expressed by tumors in this model. Overexpressed and abnormally expressed (non-mutated) antigens are frequent targets in human cancer (Finn, 2008), and advanced lung tumors in KP mice can express embryonic proteins and proteins normally found in other locations, such as the gut (Snyder et al., 2013). Responses against these antigens would be suppressed under steady-state conditions, but it is possible that Treg cell depletion permits responses by T cells with low affinity for these tumor-associated antigens. Identification of the types of tumor antigens recognized by T cells after Treg cell depletion will be helpful for guiding the development of future immune-based therapies.

Immune-checkpoint blockers have enormous potential for treating a variety of types of human cancers, but positive clinical responses correlate with immune-related adverse events (Pardoll, 2012). Because immune-checkpoint pathways are important for preventing naturally occurring autoimmune diseases, immunotherapies walk a fine line between promoting strong anti-cancer effects and minimizing autoimmune toxicity. Treg cells are prime immunotherapeutic targets. In our model, systemic Treg cell depletion unleashed a powerful anti-tumor response but also resulted in significant morbidity. Therefore, it seems possible that it could be difficult to control the autoimmune response triggered by systemic Treg cell depletion in patients once it is initiated. This concern underscores the need to identify mechanisms for localized therapeutic depletion or targeted blockade of Treg cells in the tumor microenvironment. For example, some CTLA-4 antibodies can deplete intratumoral Treg cells, and treatment of metastatic melanoma patients with a Treg-cell-depleting antibody, ipilimumab, provides an increase in overall survival, whereas treatment with a non-depleting antibody, tremelimumab, does not (Hodi et al., 2010; Ribas et al., 2013; Marabelle et al., 2013; McDermott et al., 2014; Selby et al., 2013; Simpson et al., 2013). From a therapeutic standpoint, specifically targeting immunosuppressive mediators in TA-TLSs (like Treg cells) could make it possible to promote local anti-tumor responses and maintain immune homeostasis outside of the tumor microenvironment. Our study supports the development of additional targets for local Treg cell inhibition within the tumor microenvironment as a strategy that could provide safer, more-effective therapy for patients with cancer.

EXPERIMENTAL PROCEDURES

Mice and Treatments

KP and *Foxp3*^{IRRES-DTR-GFP} mice have been previously described (DuPage et al., 2011; Kim et al., 2007). OT-I TCR Tg and *Rosa26*^{LSL-tDT} mice (B6.Cg-Gt(ROSA)26Sor^{tm14(CAG-tdTomato)Hze/J}) were purchased from the Jackson Laboratory, and P14 TCR Tg mice were purchased from Taconic. For systemic Treg cell depletion, mice received i.p. injection of 50 ng/g DT in PBS on days 0 and 1 (two doses). For lung-specific Treg cell depletion, mice received i.t. injection of 50 ng DT in 50–100 μ l PBS on days 0–5 (six doses). Mice tolerated i.t. DT well, and no morbidity or mortality was observed. Furthermore, i.t. DT did not trigger splenomegaly or lymphadenopathy, except in the lung-draining mediastinal LNs (data not shown). Details of BrdU labeling, in vivo labeling, and MRI are provided in the Supplemental Experimental Procedures. All studies were performed under an animal protocol approved by the Massachusetts Institute of Technology (MIT) Committee on Animal Care. Mice were assessed for morbidity according to guidelines set by the MIT Division of Comparative Medicine and were always humanely sacrificed prior to natural expiration.

Lentiviral Production

Mice received i.t. injection of 2.5×10^4 to 5×10^4 PFU of Cre or LucOS/Cre LV for tumor initiation. Details of the viruses and production are provided in the Supplemental Experimental Procedures.

Tissue Isolation, Immunohistochemistry, and Immunofluorescence

Lungs were isolated, flushed with bronchoalveolar lavage and/or lung circulatory perfusion, and then allocated for IHC, IF, FACS, and/or CLARITY. For IHC and IF, tissues were preserved overnight with paraformaldehyde-lysine-periodate fixative, embedded in paraffin (IHC) or cryoprotected with 30% sucrose in PBS (IF), and embedded in optimum cutting temperature compound (VWR). Details of isolation, fixation, and IF and IHC staining are provided in the Supplemental Experimental Procedures.

Confocal Imaging

Images were acquired on an Olympus FV1200 Laser Scanning Confocal Microscope or a Nikon A1R Ultra-Fast Spectral Scanning Confocal Microscope with 10 \times , 20 \times , and 30 \times objectives and analyzed with ImageJ (NIH) and Photoshop CS4 (Adobe Systems). For whole-lung reconstructions, individual sections were manually aligned with ImageJ and Photoshop as detailed in the Supplemental Experimental Procedures.

Flow Cytometry

Spleens and LNs were processed as described in Joshi et al. (2007). Lungs were prepared with a gentleMACS dissociator and C tubes (Miltenyi Biotec) as described in the Supplemental Experimental Procedures. Samples were analyzed with an LSR II (BD) and FlowJo software (Tree Star). Cell sorting was performed on a FACSAria III (BD).

Statistical Analyses and Quantifications

p values from unpaired two-tailed Student's t tests were used for all statistical comparisons. Tumor destruction based on the disruption of tumor morphology and infiltration by CD45⁺ immune cells was scored as described in the Supplemental Experimental Procedures.

In Vitro T Cell Activation and Adoptive Transfer

Splenocytes from OT-I or P14 TCR Tg mice were stimulated in vitro, stained with cell-proliferation dyes, and mixed at a 1:1 ratio as detailed in the Supplemental Experimental Procedures. 1×10^6 to 5×10^6 cells were then transferred intravenously into \sim week-20 LucOS/Cre-LV-infected recipient 45.2 KP-F mice.

Quantifying the Percentage of BrdU⁺ from IHC Sections

Sections of lungs were stained for BrdU by IHC, counterstained, and imaged with an Aperio slide scanner (Leica). TA-TLSs (distinct clusters of lymphocytes associated with blood vessels) were cropped with Adobe Photoshop. Cropped images were quantified by CellProfiler for nuclei and BrdU⁺ cells for determining the fraction of proliferating lymphocytes.

SUPPLEMENTAL INFORMATION

Supplemental Information includes six figures, Supplemental Experimental Procedures, and two movies and can be found with this article online at <http://dx.doi.org/10.1016/j.immuni.2015.08.006>.

AUTHOR CONTRIBUTIONS

N.S.J. and T.J. designed the study, and N.S.J. wrote the manuscript. N.S.J., E.H.A.-G., Y.L., D.-Y.L., G.P.C., A.L., R.R., D.M.C., and A.F.F. generated primary data. M.D. initiated the project. T.T. and N.R.K. established the CLARITY method in the laboratory. R.T.B. graded tumors. T.J. supervised data analysis and experiments.

ACKNOWLEDGMENTS

We thank Professor Alexander Rudensky (Memorial Sloan-Kettering Cancer Center) for the generous gift of *Foxp3*^{DTR-GFP} mice and T.J. lab members for reviewing the manuscript. We also thank the Swanson Biotechnology Center: Kathleen Cormier in the Hope Babette Tang (1983) Histology Facility, Eliza Vasile and Jeff Wyckoff in the Microscopy Facility, Scott Malmstrom in the Animal Imaging & Preclinical Testing Core Facility, Glenn Paradis in the Flow Cytometry Facility, and the KI Media Facility. This work was supported by NCI Cancer Center Support Grant P30-CA14051 and grants from the Howard Hughes Medical Institute (T.J.); NIH grants 1 U54 CA126515-01 (T.J.), R01-CA185020-01 (T.J.), and T32 GM007753 (A.L.); the Damon Runyon Cancer Foundation (N.S.J.); the Margaret A. Cunningham Immune Mechanisms in Cancer Research Fellowship Award (N.S.J.); and the Lung Cancer Research Foundation (N.S.J.). T.J. is a Howard Hughes Medical Institute Investigator and a Daniel K. Ludwig Scholar. This paper is dedicated to Professor Herman Eisen and to Officer Sean Collier for his caring service to the MIT community and for his sacrifice.

Received: June 2, 2015

Revised: June 2, 2015

Accepted: June 19, 2015

Published: September 1, 2015

REFERENCES

- Aleksic, M., Liddy, N., Molloy, P.E., Pumphrey, N., Vuidepot, A., Chang, K.M., and Jakobsen, B.K. (2012). Different affinity windows for virus and cancer-specific T-cell receptors: implications for therapeutic strategies. *Eur. J. Immunol.* **42**, 3174–3179.
- Antonoli, L., Pacher, P., Vizi, E.S., and Haskó, G. (2013). CD39 and CD73 in immunity and inflammation. *Trends Mol. Med.* **19**, 355–367.
- Beyersdorf, N., Ding, X., Tietze, J.K., and Hanke, T. (2007). Characterization of mouse CD4 T cell subsets defined by expression of KLRG1. *Eur. J. Immunol.* **37**, 3445–3454.
- Billadeau, D.D., Nolz, J.C., and Gomez, T.S. (2007). Regulation of T-cell activation by the cytoskeleton. *Nat. Rev. Immunol.* **7**, 131–143.
- Boissonnas, A., Scholer-Dahirel, A., Simon-Blancal, V., Pace, L., Valet, F., Kissenpfennig, A., Sparwasser, T., Malissen, B., Fétler, L., and Amigorena, S. (2010). Foxp3⁺ T cells induce perforin-dependent dendritic cell death in tumor-draining lymph nodes. *Immunity* **32**, 266–278.
- Bos, P.D., Plitas, G., Rudra, D., Lee, S.Y., and Rudensky, A.Y. (2013). Transient regulatory T cell ablation deters oncogene-driven breast cancer and enhances radiotherapy. *J. Exp. Med.* **210**, 2435–2466.
- Campbell, D.J., and Koch, M.A. (2011). Phenotypal and functional specialization of FOXP3⁺ regulatory T cells. *Nat. Rev. Immunol.* **11**, 119–130.
- Cheng, G., Yuan, X., Tsai, M.S., Podack, E.R., Yu, A., and Malek, T.R. (2012). IL-2 receptor signaling is essential for the development of KlrG1⁺ terminally differentiated T regulatory cells. *J. Immunol.* **189**, 1780–1791.
- Chung, K., Wallace, J., Kim, S.Y., Kalyanasundaram, S., Andalman, A.S., Davidson, T.J., Mirzabekov, J.J., Zalocusky, K.A., Mattis, J., Denisin, A.K., et al. (2013). Structural and molecular interrogation of intact biological systems. *Nature* **497**, 332–337.
- de Chaisemartin, L., Goc, J., Damotte, D., Validire, P., Magdeleinat, P., Alifano, M., Cremer, I., Fridman, W.H., Sautès-Fridman, C., and Dieu-Nosjean, M.C. (2011). Characterization of chemokines and adhesion molecules associated with T cell presence in tertiary lymphoid structures in human lung cancer. *Cancer Res.* **71**, 6391–6399.
- Dieu-Nosjean, M.C., Antoine, M., Danel, C., Heudes, D., Wislez, M., Poulot, V., Rabbe, N., Laurans, L., Tartour, E., de Chaisemartin, L., et al. (2008). Long-term survival for patients with non-small-cell lung cancer with intratumoral lymphoid structures. *J. Clin. Oncol.* **26**, 4410–4417.
- DuPage, M., and Jacks, T. (2013). Genetically engineered mouse models of cancer reveal new insights about the antitumor immune response. *Curr. Opin. Immunol.* **25**, 192–199.
- DuPage, M., Cheung, A.F., Mazumdar, C., Winslow, M.M., Bronson, R., Schmidt, L.M., Crowley, D., Chen, J., and Jacks, T. (2011). Endogenous T cell responses to antigens expressed in lung adenocarcinomas delay malignant tumor progression. *Cancer Cell* **19**, 72–85.
- DuPage, M., Mazumdar, C., Schmidt, L.M., Cheung, A.F., and Jacks, T. (2012). Expression of tumour-specific antigens underlies cancer immunoeediting. *Nature* **482**, 405–409.
- Feuerer, M., Hill, J.A., Kretschmer, K., von Boehmer, H., Mathis, D., and Benoist, C. (2010). Genomic definition of multiple ex vivo regulatory T cell subphenotypes. *Proc. Natl. Acad. Sci. USA* **107**, 5919–5924.
- Finn, O.J. (2008). Cancer immunology. *N. Engl. J. Med.* **358**, 2704–2715.
- Fridman, W.H., Pagès, F., Sautès-Fridman, C., and Galon, J. (2012). The immune contexture in human tumours: impact on clinical outcome. *Nat. Rev. Cancer* **12**, 298–306.
- Gobert, M., Treilleux, I., Bendriss-Vermare, N., Bachelot, T., Goddard-Leon, S., Arfi, V., Biota, C., Doffin, A.C., Durand, I., Olive, D., et al. (2009). Regulatory T cells recruited through CCL22/CCR4 are selectively activated

- in lymphoid infiltrates surrounding primary breast tumors and lead to an adverse clinical outcome. *Cancer Res.* 69, 2000–2009.
- Goc, J., Fridman, W.H., Sautès-Fridman, C., and Dieu-Nosjean, M.C. (2013). Characteristics of tertiary lymphoid structures in primary cancers. *Oncol Immunology* 2, e26836.
- Hayes, S.A., Hudson, A.L., Clarke, S.J., Molloy, M.P., and Howell, V.M. (2014). From mice to men: GEMMs as trial patients for new NSCLC therapies. *Semin. Cell Dev. Biol.* 27, 118–127.
- Hodi, F.S., O'Day, S.J., McDermott, D.F., Weber, R.W., Sosman, J.A., Haanen, J.B., Gonzalez, R., Robert, C., Schadendorf, D., Hassel, J.C., et al. (2010). Improved survival with ipilimumab in patients with metastatic melanoma. *N. Engl. J. Med.* 363, 711–723.
- Jemal, A., Siegel, R., Xu, J., and Ward, E. (2010). Cancer statistics, 2010. *CA Cancer J. Clin.* 60, 277–300.
- Josefowicz, S.Z., Lu, L.F., and Rudensky, A.Y. (2012). Regulatory T cells: mechanisms of differentiation and function. *Annu. Rev. Immunol.* 30, 531–564.
- Joshi, N.S., Cui, W., Chandele, A., Lee, H.K., Urso, D.R., Hagman, J., Gapin, L., and Kaech, S.M. (2007). Inflammation directs memory precursor and short-lived effector CD8(+) T cell fates via the graded expression of T-bet transcription factor. *Immunity* 27, 281–295.
- Kaech, S.M., and Ahmed, R. (2001). Memory CD8+ T cell differentiation: initial antigen encounter triggers a developmental program in naive cells. *Nat. Immunol.* 2, 415–422.
- Kim, J.M., Rasmussen, J.P., and Rudensky, A.Y. (2007). Regulatory T cells prevent catastrophic autoimmunity throughout the lifespan of mice. *Nat. Immunol.* 8, 191–197.
- Kwon, M.C., and Berns, A. (2013). Mouse models for lung cancer. *Mol. Oncol.* 7, 165–177.
- Lin, W., Truong, N., Grossman, W.J., Haribhai, D., Williams, C.B., Wang, J., Martín, M.G., and Chatila, T.A. (2005). Allergic dysregulation and hyperimmunoglobulinemia E in Foxp3 mutant mice. *J. Allergy Clin. Immunol.* 116, 1106–1115.
- Madisen, L., Zwingman, T.A., Sunkin, S.M., Oh, S.W., Zariwala, H.A., Gu, H., Ng, L.L., Palmiter, R.D., Hawrylycz, M.J., Jones, A.R., et al. (2010). A robust and high-throughput Cre reporting and characterization system for the whole mouse brain. *Nat. Neurosci.* 13, 133–140.
- Marabelle, A., Kohrt, H., Sagiv-Barfi, I., Ajami, B., Axtell, R.C., Zhou, G., Rajapaksa, R., Green, M.R., Torchia, J., Brody, J., et al. (2013). Depleting tumor-specific Tregs at a single site eradicates disseminated tumors. *J. Clin. Invest.* 123, 2447–2463.
- McDermott, D., Lebbé, C., Hodi, F.S., Maio, M., Weber, J.S., Wolchok, J.D., Thompson, J.A., and Balch, C.M. (2014). Durable benefit and the potential for long-term survival with immunotherapy in advanced melanoma. *Cancer Treat. Rev.* 40, 1056–1064.
- Neyt, K., Perros, F., GeurtsvanKessel, C.H., Hammad, H., and Lambrecht, B.N. (2012). Tertiary lymphoid organs in infection and autoimmunity. *Trends Immunol.* 33, 297–305.
- Pace, L., Tempez, A., Arnold-Schrauf, C., Lemaître, F., Bousso, P., Fétter, L., Sparwasser, T., and Amigorena, S. (2012). Regulatory T cells increase the avidity of primary CD8+ T cell responses and promote memory. *Science* 338, 532–536.
- Pardoll, D.M. (2012). The blockade of immune checkpoints in cancer immunotherapy. *Nat. Rev. Cancer* 12, 252–264.
- Qureshi, O.S., Zheng, Y., Nakamura, K., Attridge, K., Manzotti, C., Schmidt, E.M., Baker, J., Jeffery, L.E., Kaur, S., Briggs, Z., et al. (2011). Trans-endocytosis of CD80 and CD86: a molecular basis for the cell-extrinsic function of CTLA-4. *Science* 332, 600–603.
- Raez, L.E., Fein, S., and Podack, E.R. (2005). Lung cancer immunotherapy. *Clin. Med. Res.* 3, 221–228.
- Rajasagi, M., Shukla, S.A., Fritsch, E.F., Keskin, D.B., DeLuca, D., Carmona, E., Zhang, W., Sougnez, C., Cibulskis, K., Sidney, J., et al. (2014). Systematic identification of personal tumor-specific neoantigens in chronic lymphocytic leukemia. *Blood* 124, 453–462.
- Rao, S., Tortola, L., Perlot, T., Wirnsberger, G., Novatchkova, M., Nitsch, R., Sykacek, P., Frank, L., Schramek, D., Komnenovic, V., et al. (2014). A dual role for autophagy in a murine model of lung cancer. *Nat. Commun.* 5, 3056.
- Ribas, A., Kefford, R., Marshall, M.A., Punt, C.J., Haanen, J.B., Marmol, M., Garbe, C., Gogas, H., Schachter, J., Linette, G., et al. (2013). Phase III randomized clinical trial comparing tremelimumab with standard-of-care chemotherapy in patients with advanced melanoma. *J. Clin. Oncol.* 31, 616–622.
- Robbins, S.H., Tessmer, M.S., Van Kaer, L., and Brossay, L. (2005). Direct effects of T-bet and MHC class I expression, but not STAT1, on peripheral NK cell maturation. *Eur. J. Immunol.* 35, 757–765.
- Sakaguchi, S. (2004). Naturally arising CD4+ regulatory t cells for immunologic self-tolerance and negative control of immune responses. *Annu. Rev. Immunol.* 22, 531–562.
- Sather, B.D., Treuting, P., Perdue, N., Miazgowiec, M., Fontenot, J.D., Rudensky, A.Y., and Campbell, D.J. (2007). Altering the distribution of Foxp3(+) regulatory T cells results in tissue-specific inflammatory disease. *J. Exp. Med.* 204, 1335–1347.
- Selby, M.J., Engelhardt, J.J., Quigley, M., Henning, K.A., Chen, T., Srinivasan, M., and Korman, A.J. (2013). Anti-CTLA-4 antibodies of IgG2a isotype enhance antitumor activity through reduction of intratumoral regulatory T cells. *Cancer Immunol. Res.* 1, 32–42.
- Simpson, T.R., Li, F., Montalvo-Ortiz, W., Sepulveda, M.A., Bergerhoff, K., Arce, F., Roddie, C., Henry, J.Y., Yagita, H., Wolchok, J.D., et al. (2013). Fc-dependent depletion of tumor-infiltrating regulatory T cells co-defines the efficacy of anti-CTLA-4 therapy against melanoma. *J. Exp. Med.* 210, 1695–1710.
- Snyder, E.L., Watanabe, H., Magendanz, M., Hoersch, S., Chen, T.A., Wang, D.G., Crowley, D., Whittaker, C.A., Meyerson, M., Kimura, S., and Jacks, T. (2013). Nkx2-1 represses a latent gastric differentiation program in lung adenocarcinoma. *Mol. Cell* 50, 185–199.
- Suffia, I., Reckling, S.K., Salay, G., and Belkaid, Y. (2005). A role for CD103 in the retention of CD4+CD25+ Treg and control of Leishmania major infection. *J. Immunol.* 174, 5444–5455.
- Teng, M.W., Ngiow, S.F., von Scheidt, B., McLaughlin, N., Sparwasser, T., and Smyth, M.J. (2010). Conditional regulatory T-cell depletion releases adaptive immunity preventing carcinogenesis and suppressing established tumor growth. *Cancer Res.* 70, 7800–7809.
- Thornton, E.E., Looney, M.R., Bose, O., Sen, D., Sheppard, D., Locksley, R., Huang, X., and Krummel, M.F. (2012). Spatiotemporally separated antigen uptake by alveolar dendritic cells and airway presentation to T cells in the lung. *J. Exp. Med.* 209, 1183–1199.
- Vogelstein, B., Papadopoulos, N., Velculescu, V.E., Zhou, S., Diaz, L.A., Jr., and Kinzler, K.W. (2013). Cancer genome landscapes. *Science* 339, 1546–1558.
- Wing, K., Onishi, Y., Prieto-Martin, P., Yamaguchi, T., Miyara, M., Fehervari, Z., Nomura, T., and Sakaguchi, S. (2008). CTLA-4 control over Foxp3+ regulatory T cell function. *Science* 322, 271–275.

Introducing the China Gateway

The home for Chinese scientists



The new Cell Press China Gateway is the ultimate destination for Chinese scientists. Now highlights of the latest research, regional events, and featured content from Cell Press are accessible online, on a single webpage.

The Cell Press China Gateway was designed with you in mind. We hope you'll make yourself at home.

Visit us at www.cell.com/china

Distinct Commensals Induce Interleukin-1 β via NLRP3 Inflammasome in Inflammatory Monocytes to Promote Intestinal Inflammation in Response to Injury

Sang-Uk Seo,¹ Nobuhiko Kamada,² Raúl Muñoz-Planillo,¹ Yun-Gi Kim,¹ Donghyun Kim,¹ Yukiko Koizumi,¹ Mizuho Hasegawa,¹ Stephanie D. Himpfl,³ Hilary P. Browne,⁴ Trevor D. Lawley,⁴ Harry L.T. Mobley,³ Naohiro Inohara,¹ and Gabriel Núñez^{1,*}

¹Department of Pathology and Comprehensive Cancer Center

²Division of Gastroenterology, Department of Internal Medicine

³Department of Microbiology and Immunology

The University of Michigan Medical School, 1500 East Medical Center Drive, Ann Arbor, MI 48109, USA

⁴Bacterial Pathogenesis Laboratory, Wellcome Trust Sanger Institute, Wellcome Trust Genome Campus, Hinxton, Cambridgeshire CB10 1SA, UK

*Correspondence: gabriel.nunez@umich.edu

<http://dx.doi.org/10.1016/j.immuni.2015.03.004>

SUMMARY

The microbiota stimulates inflammation, but the signaling pathways and the members of the microbiota involved remain poorly understood. We found that the microbiota induces interleukin-1 β (IL-1 β) release upon intestinal injury and that this is mediated via the NLRP3 inflammasome. *Enterobacteriaceae* and in particular the pathobiont *Proteus mirabilis*, induced robust IL-1 β release that was comparable to that induced by the pathogen *Salmonella*. Upon epithelial injury, production of IL-1 β in the intestine was largely mediated by intestinal Ly6C^{high} monocytes, required chemokine receptor CCR2 and was abolished by deletion of IL-1 β in CCR2⁺ blood monocytes. Furthermore, colonization with *P. mirabilis* promoted intestinal inflammation upon intestinal injury via the production of hemolysin, which required NLRP3 and IL-1 receptor signaling in vivo. Thus, upon intestinal injury, selective members of the microbiota stimulate newly recruited monocytes to induce NLRP3-dependent IL-1 β release, which promotes inflammation in the intestine.

INTRODUCTION

The intestine is inhabited by trillions of resident bacteria that can provide beneficial effects to the host (Kamada et al., 2013). For example, bacterial metabolites including vitamins and short-chain fatty acids contribute to appropriate development of the host. Resident bacteria also confer resistance against pathogen infection and are critically involved in the development of lymphoid populations in the intestine (Kamada et al., 2013). Because commensal bacteria can stimulate the immune system, the host has evolved several mechanisms to prevent inappropriate activation of inflammatory responses in the intestine. For instance, the intestinal epithelium and resident macrophages

are hyporesponsive to bacterial Toll-like receptor ligands such as lipopolysaccharides (Lotz et al., 2006; Smythies et al., 2005). In addition, several barriers including the mucus layer and antimicrobial peptides limit the contact between microbes and the host immune system and contribute to gut homeostasis (Kamada and Núñez, 2014). A role for the microbiota in eliciting intestinal inflammation is supported by findings that chemically-induced and spontaneous colitis are reduced or abolished in antibiotic-treated mice and germ-free mice (Garrett et al., 2007; Hudcovic et al., 2001; Kirkland et al., 2012; Kitajima et al., 2001; Vijay-Kumar et al., 2007). In mouse models, certain members of the microbiota have been linked to inflammatory responses and intestinal pathology. For example, *Bacteroides* species and members of the *Enterobacteriaceae* family including *Klebsiella pneumoniae* and *Proteus mirabilis* can promote colitis (Bloom et al., 2011; Garrett et al., 2010). However, the signaling pathways by which resident bacteria stimulate the host immune system to induce inflammation in vivo remain poorly understood.

A critical step in the activation of inflammatory responses is the recognition of microbes or endogenous molecules produced in the setting of infection or cellular injury by host pattern-recognition receptors (Takeuchi and Akira, 2010). A major innate signaling pathway is the inflammasome, a multi-protein platform that activates caspase-1 leading to the proteolytic processing of pro-interleukin-1 β (IL-1 β) and pro-IL-18 into their mature active forms (Schroder and Tschopp, 2010). To date, four bona fide inflammasomes have been described, of which three, the NLRP1, NLRP3 and NLRC4 inflammasomes, contain a member of the intracellular Nod-like receptor (NLR) family (Franchi et al., 2012b). Among the NLR inflammasomes, NLRP3 is activated by multiple stimuli including bacterial pore-forming toxins, ATP, microbial RNA, and particulate matter (Hornung et al., 2008; Mariathasan et al., 2006). In contrast, NLRC4 activation is induced by several Gram-negative pathogens by the translocation of small amounts of flagellin or PrgJ-like rod proteins into the host cytosol (Franchi et al., 2006; Miao et al., 2010). In the intestine, NLRC4-dependent IL-1 β production is triggered by *Salmonella* in resident phagocytes, which contribute to host defense through the recruitment of neutrophils (Franchi et al., 2012a). The role of the NLRP3 inflammasome in intestinal

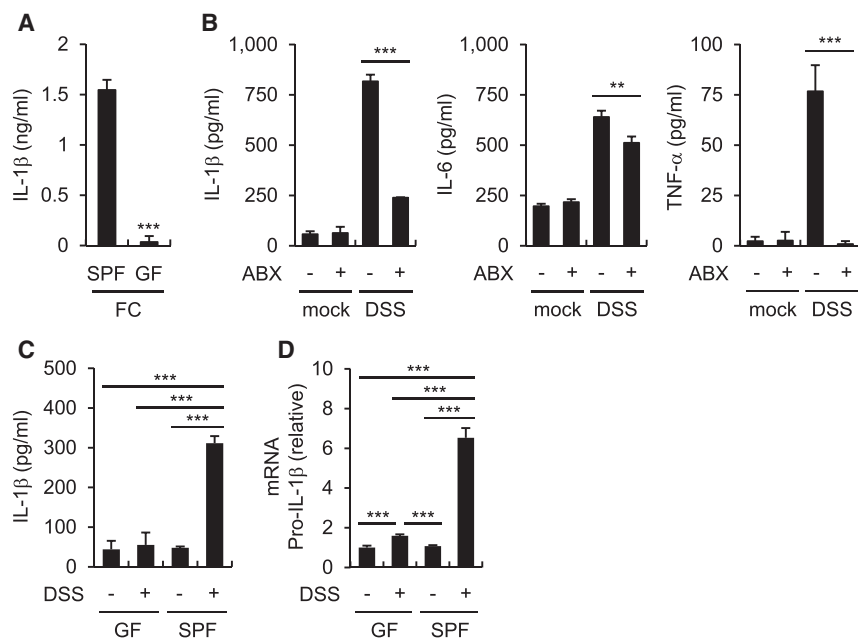


Figure 1. Commensal Bacteria Induce IL-1 β

(A) Fecal contents (FC) obtained from GF or SPF mice were used to stimulate BMDMs for 18 hr. IL-1 β was measured from culture supernatant by ELISA.

(B) Total LP cells were isolated from PBS or antibiotic cocktail (ABX)-treated mice on day 7 after mock or 2.5% DSS treatment and cultured for 3 hr. IL-1 β , IL-6, and TNF- α from culture supernatant were measured by ELISA.

(C and D) GF and SPF mice were treated with 2% DSS from day 0 to 6. Total LP cells were isolated on day 7. (C) Total LP cells were cultured for 3 hr and IL-1 β was measured by ELISA. (D) pro-IL-1 β mRNA expression was analyzed by qRT-PCR and normalized relative to GAPDH expression.

(A–D) Data are representative of at least two individual experiments and values represent mean of triplicate samples \pm SD. ** p < 0.01, *** p < 0.001.

Inflammation is controversial. For example, some studies showed that mice lacking NLRP3 or caspase-1 were less susceptible to chemically-induced colitis (Bauer et al., 2012; Bauer et al., 2010), whereas other authors reported increased susceptibility and worsened pathology (Allen et al., 2010; Zaki et al., 2010). The role of IL-1 β in colitis is also controversial. Some studies showed that blocking of IL-1 β signaling ameliorate intestinal inflammation in different animal colitis models (Coccia et al., 2012; Saitoh et al., 2008), but one study showed that IL-1 β -deficient mice are more susceptible to experimental colitis than wild-type (WT) mice (Bersudsky et al., 2014). The reasons for these contradictory results are unclear, but it might be caused, at least in part, by baseline differences in the gut microbiota (Bauer et al., 2012). While some intestinal commensals such as *Escherichia coli* can induce IL-1 β via the NLRP3 inflammasome in bone-marrow-derived macrophages (BMDMs), the ability of resident bacteria to induce IL-1 β in vivo and the innate immune cells involved in IL- β release in response to the intestinal microbiota remain unclear. In this study, we provide evidence that selective members of the microbiota and specifically *P. mirabilis* can induce robust IL-1 β production via the NLRP3 inflammasome and promote IL-1 β -dependent inflammation in the intestine. Production of IL-1 β by the microbiota is mediated by CCR2⁺ monocytes that are recruited to the intestine in response to epithelial injury.

RESULTS

Intestinal Resident Bacteria Induce IL-1 β Release and Promote Colitis via IL-1 β

To determine whether the fecal microbiota induce IL-1 β release, BMDMs were stimulated with fecal contents from conventionally reared mice and germ-free (GF) mice, and IL-1 β was assessed in the culture supernatants. The feces of conventionally raised specific pathogen-free (SPF) mice, but not GF mice, induced robust amounts of IL-1 β (Figure 1A). To determine whether the

microbiota induces IL-1 β in vivo, we treated mice with a cocktail of antibiotics or PBS and then orally with dextran sulfate sodium (DSS), a chemical that damages the epithelium resulting in exposure of lamina propria (LP) cells to luminal microbes. Treatment with antibiotics reduced the production of IL-1 β , IL-6, and tumor necrosis factor alpha (TNF- α) by LP cells when compared to PBS-treated mice (Figure 1B). Consistently, LP cells from SPF mice produced more IL-1 β and pro-IL-1 β mRNA than from GF mice after DSS administration (Figures 1C and 1D). To determine whether microbiota-induced IL-1 β is important for triggering intestinal inflammation in vivo, we assessed features associated with inflammation in WT and *Il1b*^{-/-} mice after DSS administration. IL-1 β deficiency was associated with reduced weight loss (Figure 2A) and lower disease activity index (DAI) (Figure 2A). In addition, WT mice had more colonic shortening, a marker of colitis (Figure 2B), and exhibited more inflammation in the colon upon DSS administration than *Il1b*^{-/-} mice (Figure 2C). Depletion of the microbiota by treatment with antibiotics abolished the phenotype associated with IL-1 β deficiency (Figures 2D–2F). These results indicate that the microbiota induces IL-1 β upon epithelial damage and IL-1 β promotes intestinal inflammation.

Commensal Bacteria Induce IL-1 β Release via the NLRP3 Inflammasome

To begin to understand how the intestinal microbiota induces the release of IL-1 β , we stimulated BMDMs from WT and mice deficient in caspase-1, the essential adaptor ASC and different sensors that activate the inflammasome with fecal contents. The production of IL-1 β , but not TNF- α , required caspase-1, NLRP3, or ASC (Figures 3A and 3B), but neither caspase-11 nor AIM2 or NLRC4 (Figures 3A and 3B). Consistently, caspase-1 activation as determined by the formation of the mature p20 subunit was induced by stimulation with fecal contents in WT, but not *Nlrp3*^{-/-} macrophages (Figure 3C). To determine whether the NLRP3 inflammasome is important for the induction of IL-1 β in vivo, we purified LP cells from DSS-treated WT mice

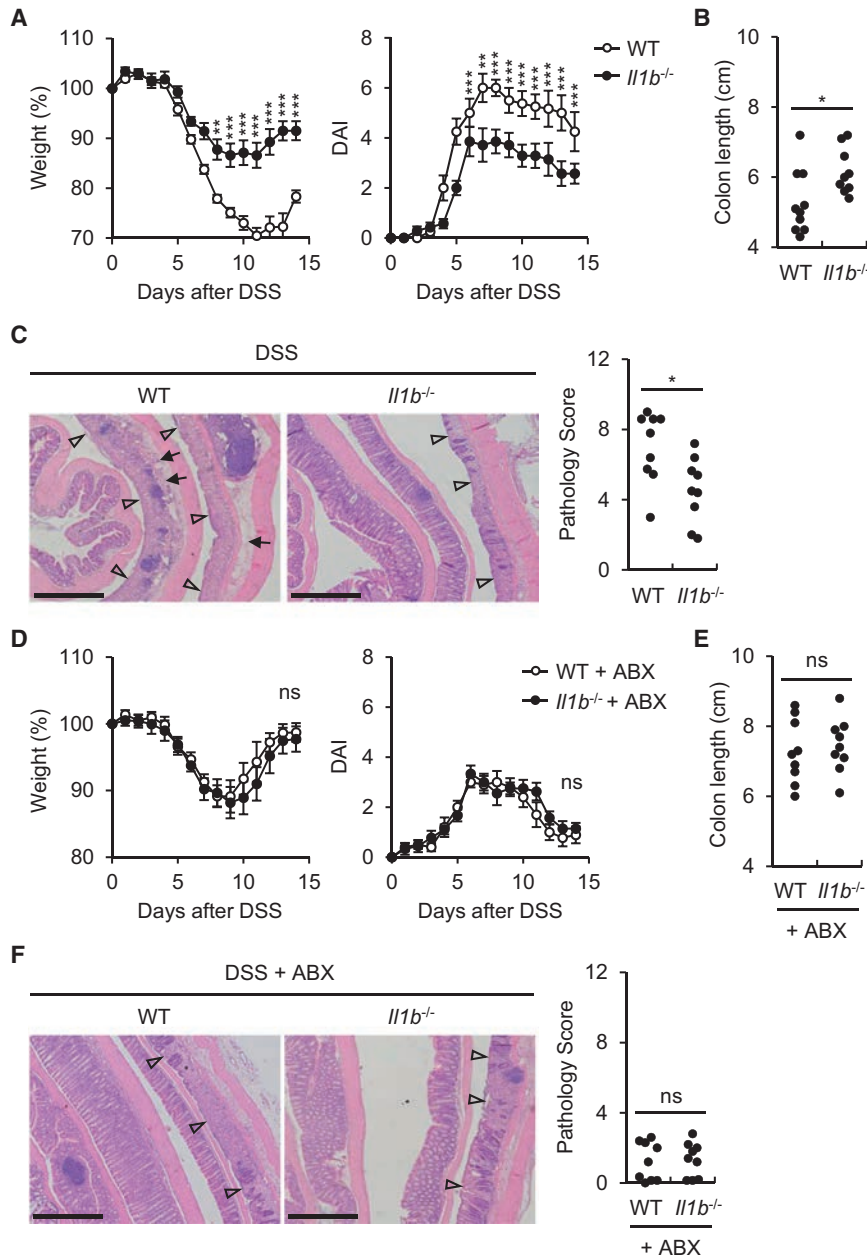


Figure 2. IL-1 β Induced by the Commensal Bacteria Promotes Colitis

(A) WT and *Il1b*^{-/-} mice were treated with 2% DSS from day 0 to day 6. Body weight and disease activity index (DAI) were measured daily for 2 weeks. Values represent means \pm SEM.

(B and C) WT and *Il1b*^{-/-} mice were treated with 2% DSS from day 0 to day 6 and euthanized at day 10. (B) Colon length was measured and (C) pathology score were assessed.

(D) WT and *Il1b*^{-/-} mice were treated with 2% DSS from day 0 to day 6 and received PBS or ABX daily by oral gavage from day -1 to 7. Body weight and disease activity index (DAI) were measured daily for 2 weeks. Values represent means \pm SEM.

(E and F) WT and *Il1b*^{-/-} mice were treated with 2% DSS from day 0 to day 6 and received PBS or ABX daily by oral gavage from day -1 to 7. Mice were euthanized at day 10. (E) Colon length was measured and (F) pathology score were assessed. (C and F) Representative images of the distal colon. Open arrowheads denote mucosal ulcer with total loss of epithelium. Solid arrows indicate presence of acute inflammatory cells and/or edema in the submucosa. Scale bar represents 500 μ m.

All data are pooled from two separate experiments ($n > 8$, each group). * $p < 0.05$, ** $p < 0.01$, *** $p < 0.001$.

Jung, 2013). We determined next which population of mononuclear phagocytic cells produces IL-1 β in response to the microbiota. We purified LP cells from naive mice and mice harboring CD11b⁺Ly6C^{high} inflammatory monocytes (IM) in response to DSS administration. In ex vivo experiments, intestinal phagocytic cells from DSS-treated mice, but not naive mice, spontaneously produced IL-1 β , which was further enhanced by the addition of ATP, a signal that activates the NLRP3 inflammasome (Figure 4A). In contrast, production of IL-6 was comparable in naive and DSS-treated mice and was not enhanced by ATP (Figure 4A). Notably, resident LP cells from naive

and mutant mice deficient in inflammasome components and assessed the release of IL-1 β by LP cells ex vivo. LP cells purified from the colonic LP of WT mice released spontaneously IL-1 β and this response was impaired in *Casp1*^{-/-}, *Nlrp3*^{-/-}, and *Pycard*^{-/-} mice (Figures 3D and 3E). These results indicate that the microbiota induces IL-1 β release via the NLRP3 inflammasome.

Recruited Monocytes Are the Major Source of IL-1 β Produced in Response to the Microbiota

The normal intestine contains large numbers of resident mononuclear phagocytes including macrophages and dendritic cells. In addition, blood monocytes are rapidly recruited to the intestinal tissue in response to inflammatory stimuli (Zigmond and

animals did not produce IL-1 β even after addition of exogenous ATP (Figure 4A). Production of IL-1 β by LP phagocytes was detected at day 3 and peaked around day 7 after DSS (Figure 4B). The kinetics of IL-1 β production by LP cells correlated with the number of IM (CD11b⁺Ly6C^{high}) recruited to the intestine (Figures 4B and 4C). To define the LP populations that produce IL-1 β in response to the microbiota, we sorted LP cells from DSS-treated mice into CD11b⁺Ly6C^{high} (IMs), CD11b⁺Ly6C^{low} (phagocytes), and CD11b⁻Ly6C⁻ (non-phagocytes). CD11b⁺Ly6C^{high} cells released more IL-1 β and expressed higher amounts of *Nlrp3* mRNA than phagocytes and non-phagocytic cells (Figure 4D). IMs isolated from the colon of DSS-treated *Nlrp3*^{-/-} and *Pycard*^{-/-} mice released less IL-1 β than WT, *Aim2*^{-/-}, and *Nlrp4*^{-/-} IMs (Figure 4E). The spontaneous release

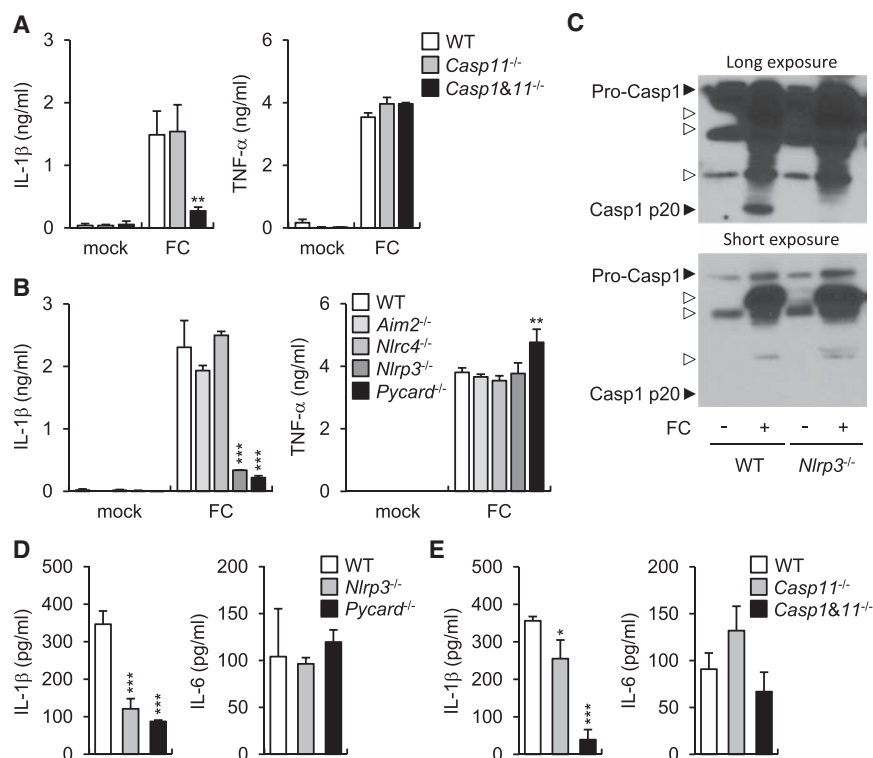


Figure 3. Commensal Bacteria Induce IL-1β through the NLRP3 Inflammasome

(A and B) Fecal contents (FC) obtained from SPF mice were used to stimulate WT, *Casp11^{-/-}*, *Casp1^{-/-}Casp11^{-/-}* BMDMs (A) and WT, *Aim2^{-/-}*, *Nlr3^{-/-}*, *Nlrp3^{-/-}*, *Pycard^{-/-}* BMDMs (B) for 18 hr. IL-1β and TNF-α were measured from culture supernatant.

(C) WT and *Nlrp3^{-/-}* BMDMs were stimulated with FC obtained from SPF mice and caspase-1 was detected by immunoblotting. Open arrow heads indicate non-specific bands.

(D and E) WT, *Casp11^{-/-}*, *Casp1^{-/-}Casp11^{-/-}*, *Nlrp3^{-/-}*, and *Pycard^{-/-}* mice were treated with 2.5% DSS from day 0 to 7. Total LP cells were cultured for 3 hr and IL-1β and IL-6 were measured in culture supernatant.

Values represent mean of triplicate samples ± SD. Data are representative for three experiments. *p < 0.05, **p < 0.01, ***p < 0.001.

analysis revealed comparable numbers of CD11b⁺Ly6C^{hi} IM in the LP of DT- and DSS-treated *Il1b^{+/+}Ccr2^{DTR/+}* and *Il1b^{-/-}Ccr2^{DTR/+}* mice (Figure S1D), ruling out that the impairment of IL-1β release was caused by defective intestinal recruitment of IM in *Il1b^{-/-}Ccr2^{DTR/+}*

of IL-1β by CD11b⁺Ly6C^{high} cells was largely triggered by the microbiota because it was greatly reduced in cells isolated from the intestine of DSS-treated GF mice (Figure 4F).

To further verify the role of recruited IM in microbiota-induced IL-1β release, we used mice deficient in CCR2, which is an essential chemokine receptor for emigration of Ly6C^{high} monocytes from the BM and recruitment to the intestine (Kim et al., 2011; Serbina and Pamer, 2006). *Ccr2^{-/-}* mice exhibited impaired recruitment of IM to the intestine in response to DSS administration (Figure S1A). CCR2 deficiency abolished the release of IL-1β by LP cells isolated from DSS-treated mice (Figure 4G). Given that IMs can produce various different inflammatory mediators capable of activating surrounding cells and contribute to develop DSS-induced colitis (Waddell et al., 2011) (Figure S1B), we used CCR2-diphtheria toxin receptor (*Ccr2^{DTR/+}*) deleter mice to determine the autonomous role of IMs in IL-1β production. We used *Ccr2^{DTR/+}* mice to generate mixed chimeras by transplanting mixtures of BM from WT or *Il1b^{-/-}* mice with BM from *Ccr2^{DTR/+}* mice at a 1:1 ratio into lethally-irradiated WT mice. Consistent with previous results (Hohl et al., 2009), we found efficient depletion (>90%) of CCR2⁺ monocytes after a single intraperitoneal (i.p.) administration of DT to *Ccr2^{DTR/+}* mice (Figure S1C). LP cells from recipient mice reconstituted with WT (*Il1b^{+/+}*) and *Ccr2^{DTR/+}* BM produced comparable amounts of IL-1β after DSS treatment regardless of DT treatment (Figure 4H). Consistent with mixed chimerism, LP cells from mice reconstituted with *Il1b^{-/-}* and *Ccr2^{DTR/+}* BM released less IL-1β than mice reconstituted with WT BM (Figure 4H). Notably, the release of IL-1β, but not TNF-α, by LP cells from mice reconstituted with *Il1b^{-/-}* and *Ccr2^{DTR/+}* bone marrow was abrogated after DT treatment (Figure 4H). Flow cytometric

chimeric mice. Collectively, these results indicate that IM recruited to the intestine are the major source of IL-1β produced in response to stimulation by the microbiota.

Selective Resident Bacteria Elicit Robust Release of IL-1β

To identify commensal bacteria that induce IL-1β release, we screened a panel of bacterial species isolated from the mouse intestine for their ability to trigger IL-1β production in macrophages at a low bacteria-macrophage ratio. Because fecal contents could induce IL-1β production under aerobic conditions, we first tested aerobic or facultative anaerobic commensal bacteria. All commensal bacteria tested could induce pro-IL-1β mRNA expression (Figure 5A, top panel). Notably, *P. mirabilis*, out of 13 tested, induced rapid and robust secretion of IL-1β (Figure 5A, middle panel). We also assessed the ability of *Bacteroides* and *Clostridium* species to induce IL-1β; however, these abundant anaerobic bacteria did not induce IL-1β release (data not shown). Remarkably, the kinetics and potency of *P. mirabilis* to induce IL-1β release was comparable to that of the pathogen *Salmonella enterica* Typhimurium (Figure 5A). After longer stimulation (18 hr), the commensal *E. coli* and the pathogen *Citrobacter rodentium* induced IL-1β secretion but in lower amounts than *P. mirabilis* (Figure S2). The link between *P. mirabilis* and IL-1β was highly specific in that most commensal bacteria triggered TNF-α (Figure 5A, lower panel, and Figure S2). To test specificity of *P. mirabilis* to induce IL-1β production in vivo, we mono-associated GF mice with *P. mirabilis*, *B. acidifaciens*, *C. sporogenes*, or *E. coli* and monitored their intestinal colonization in the feces before DSS treatment. Despite comparable bacterial colonization (Figure S3), LP cells

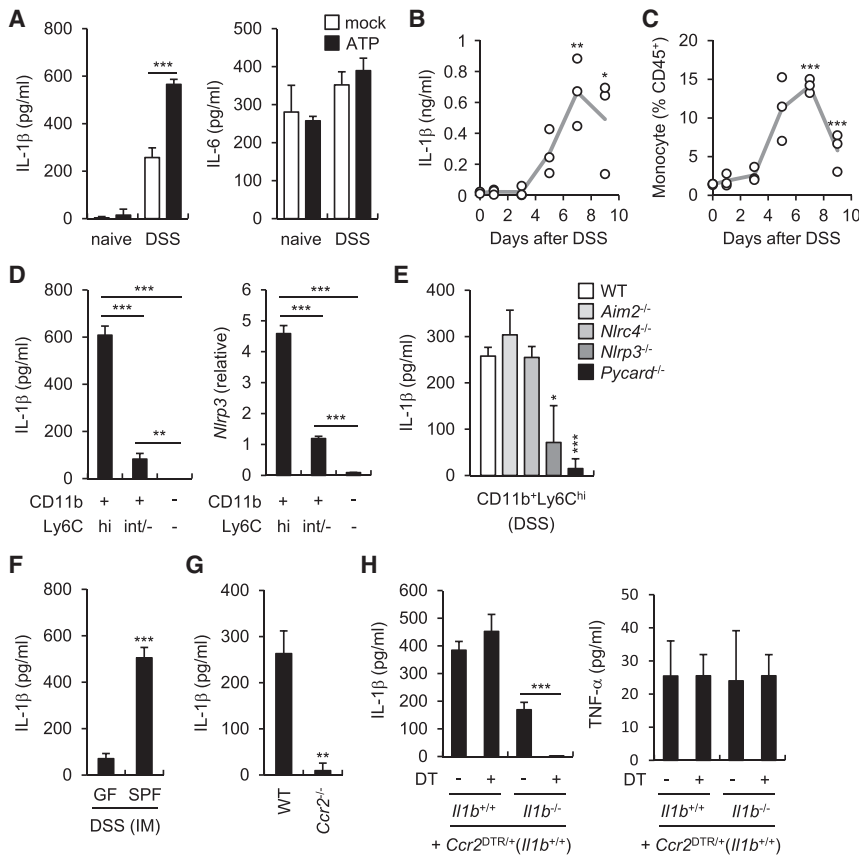


Figure 4. Recruited Inflammatory Monocytes Are the Main Source of IL-1β during DSS-Induced Colitis

(A) Total LP cells isolated on day 0 (naive) and on day 7 (DSS) after DSS treatment were cultured for 3 hr and left unstimulated or cultured in the presence of 5 mM ATP for the additional 30 min. IL-1β and IL-6 were measured from culture supernatant. (B and C) Total LP cells were isolated at indicated times from WT mice given 2.5% DSS from day 0 to day 7. (B) IL-1β was measured from culture supernatant after 3 hr of culture. (C) Percent of inflammatory monocytes (CD11b⁺Ly6C^{high}) in CD45⁺ LP cells was determined by flow cytometry. Open circles represents means of values from individual mice.

(D) Total LP cells were isolated from DSS-treated mice on day 7 after 2.5% DSS treatment and CD45⁺ cells were sorted according to CD11b and Ly6C expression. Sorted cells were cultured for 3 hr and IL-1β in culture supernatant and *Nlrp3* mRNA expression was analyzed by ELISA and qRT-PCR, respectively.

(E) WT, *Aim2*^{-/-}, *Nlr4*^{-/-}, *Nlrp3*^{-/-}, and *Pycard*^{-/-} mice were treated with 2.5% DSS for 7 days. Sorted inflammatory monocytes were cultured for 3 hr and IL-1β was measured in culture supernatant.

(F) GF and SPF mice were treated with 2% DSS for 6 days. Sorted inflammatory monocytes (IM) were cultured for 3 hr and IL-1β was measured in culture supernatant.

(G) WT and *Ccr2*^{-/-} mice were treated with 2.5% DSS for 7 days. Total LP cells were cultured for 3 hr and IL-1β was measured in culture supernatant.

(H) IL-1β release by total LP cells isolated from indicated chimera mice. Mice received PBS or DT

on day 0, 3, and 6. LP cells were isolated on day 7 and cultured for 3 hr to measure cytokine concentrations in culture supernatant. Data are representative of at least two experiments. Values are means of triplicate samples ± SD. *p < 0.05, **p < 0.01, ***p < 0.001. See also Figure S1.

isolated from mice mono-associated with *P. mirabilis* produced more IL-1β than LP cells from mice colonized with the other commensal bacteria (Figure 5B). Analyses of macrophages deficient in components of the inflammasome revealed that IL-1β release and caspase-1 activation, but not TNF-α, induced by *P. mirabilis* was abolished in *Nlrp3*^{-/-} and *Pycard*^{-/-} BMDMs (Figures 5C and 5D). Similarly, *P. mirabilis* induced IL-1β release in LP cells isolated from DSS-treated WT mice after 3 hr culture, and this response was largely dependent on caspase-1 and NLRP3, but much less on caspase-11 (Figures 5E and 5F). Consistent with previous results, *P. mirabilis* induced more IL-1β release than *E. coli* in LP cells (Figure 5F). LP cells isolated from *Ccr2*^{-/-} mice treated with DSS did not release IL-1β after *P. mirabilis* stimulation (Figure 5G). To determine whether *P. mirabilis* is sufficient to induce IL-1β production in vivo, we colonized GF mice with *P. mirabilis* and assessed the spontaneous production of IL-1β by LP cells purified from untreated and DSS-treated mice. Consistent with an important role for recruited monocytes, there was no or minimal IL-1β release by LP cells isolated from untreated mice colonized with *P. mirabilis* or GF mice treated with DSS (Figure 5H). In contrast, we found increased IL-1β production by LP cells from GF mice colonized with *P. mirabilis* and treated with DSS when compared to mice treated with the bacterium or DSS alone (Figure 5H).

***P. mirabilis* HpmA Hemolysin Is Required for the Activation of the NLRP3 Inflammasome**

We sequenced the genome of the mouse *P. mirabilis* referred here as strain UM001 to identify candidate genes that might be involved in triggering NLRP3 activation. We obtained a 3,950,860 base-pair (bp)-long genomic sequence of the *P. mirabilis* strain UM001 which revealed 3,579 putative protein-coding and 84 noncoding genes within 28 contigs (Figure S4A). Comprehensive comparison analysis of the genomic sequences by RAST showed that the mouse *P. mirabilis* genome contains several virulence genes that are also present in the reference human *P. mirabilis* strain H14320 (Aziz et al., 2008; Pearson et al., 2008). These genes included *cheW* (a regulator of chemotaxis), *fliF* (flagellin), *hpmA* (hemolysin), *mrpA* (fimbria), genes encoding essential proteins of a T3SS such as *spa47*, and *ureC* (urease) (Figure S4B). Notably, the human *P. mirabilis* strain H14320 also induced IL-1β release (Figure 6A). Analyses of several isogenic *P. mirabilis* mutants of H14320 revealed that *hpmA*, but not *cheW*, *cpsF*, *fliF*, *mrpA*, or *ureC*, was required for the induction of IL-1β release, but not of TNF-α (Figure 6A). Expression of the *hpmA* gene was detected in both the mouse and human *P. mirabilis* strains (Figure S4C). Comparison of the HpmA amino acid sequence from the mouse and human strains revealed that they were 99% identical (Figure S4D). Secretion of

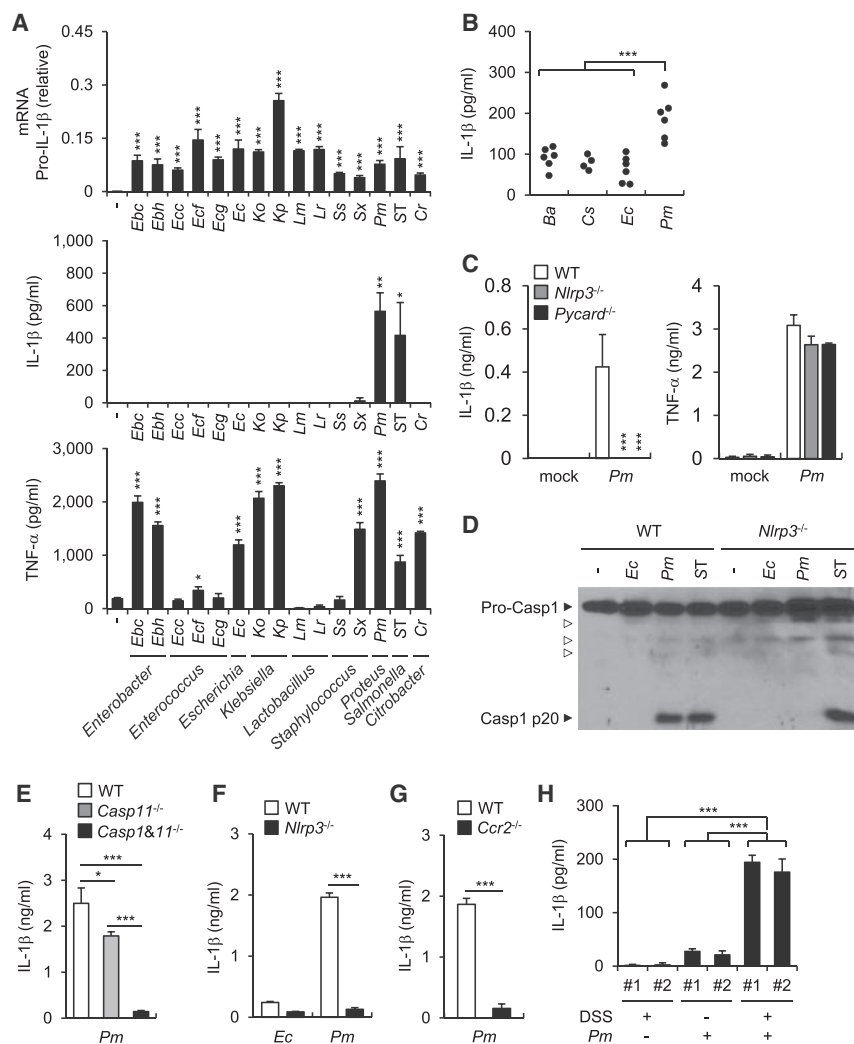


Figure 5. Selective Commensals Induce IL-1 β Release through the NLRP3 Inflammasome

(A) BMDMs were stimulated with indicated mouse commensal bacteria, *Citrobacter rodentium* (Cr), or *Salmonella enterica* serovar Typhimurium (ST) at a bacteria:macrophage ratio of 1. Abbreviations are as follows: *Ebc*, *Enterobacter cloacae*; *Ebh*, *E. hormaechei*; *Ecc*, *Enterococcus casseliflavus*; *Ecf*, *E. faecalis*; *Ecg*, *E. gallinarum*; *Ec*, *Escherichia coli*; *Ko*, *Klebsiella oxytoca*; *Kp*, *K. pneumoniae*; *Lm*, *Lactobacillus murinus*; *Lr*, *L. reuteri*; *Ss*, *Staphylococcus sciuri*; *Sx*, *S. xyloso*; *Pm*, *Proteus mirabilis*. Levels of cytokines in culture supernatant and pro-IL-1 β mRNA expression at 3 hr were determined by ELISA and qRT-PCR, respectively. Values represent means of triplicate samples \pm SD.

(B) GF mice were mono-associated with indicated mouse commensal bacteria. *Ba*, *Bacteroides acidifaciens*; *Cs*, *Clostridium sporogenes*; *Ec*, *E. coli*; *Pm*, *P. mirabilis*. Mice were treated with 1% DSS for 7 days and total LP cells were isolated and cultured for 3 hr to assess IL-1 β release in supernatant. Means of values from one or two mice are indicated. Results are pooled from three experiments with similar results.

(C) WT, *Nlrp3*^{-/-}, and *Pycard*^{-/-} BMDMs were stimulated with mouse *Pm* and cytokines were measured in culture supernatant after 3 hr. Values represent means of triplicate samples \pm SD.

(D) WT and *Nlrp3*^{-/-} BMDMs were stimulated with *Ec*, *Pm*, and ST for 3 hr and caspase-1 activation was detected by immunoblotting.

(E–G) WT or indicated mutant mice were treated with 2.5% DSS for 7 days and total LP cells were isolated and were stimulated with indicated bacteria at a bacteria:macrophage ratio of 1 for 3 hr. Values represent means of triplicate samples \pm SD.

(H) GF mice or gnotobiotic mice monocolonized with mouse *P. mirabilis* by oral gavage were treated with 2% DSS for 6 days. Total LP cells

were isolated on day 7 and IL-1 β was determined in culture supernatant after 3 hr. Values represent means of triplicate samples \pm SD.

Data are representative of at least two experiments. * $p < 0.05$, ** $p < 0.01$, *** $p < 0.001$. See also Figures S2 and S3.

IL-1 β via the NLRP3 inflammasome requires signal 1 that induces pro-IL-1 β and signal 2 that activates caspase-1 (Franchi et al., 2012b). To assess whether HpmA can provide signal 1 or signal 2, we stimulated BMDMs with Δ *hpmA* *P. mirabilis* or LPS as an inducer of signal 1 in absence or presence of ATP which provides signal 2 for inflammasome activation. Both Δ *hpmA* *P. mirabilis* and LPS induced the release of IL-1 β and caspase-1 activation, but only in the presence of ATP (Figures 6B and 6C). Together with results shown in Figure 6A, the data indicate that Δ *hpmA* *P. mirabilis* can only provide signal 1 and that HpmA is required for *P. mirabilis* to provide signal 2 for activation of the NLRP3 inflammasome. Complementation of the Δ *hpmA* mutant strain with a *hpmA* expression plasmid rescued the ability of the mutant strain to induce IL-1 β release, but it did not affect its ability to release TNF- α (Figure 6D). K⁺ efflux is a common event that is required for NLRP3 activation induced by multiple stimuli (Muñoz-Planillo et al., 2013). Consistently, WT *P. mirabilis*, but not the Δ *hpmA* mutant, induced K⁺ efflux which

was enhanced in the Δ *hpmA* mutant reconstituted with *hpmA* plasmid (Figure 6E). The enhanced induction of IL-1 β and K⁺ efflux by the complemented (Δ *hpmA*+*hpmA*) strain presumably results from the higher copy number of the plasmid-derived *hpmA* gene. Culture of macrophages in 45 mM K⁺ inhibited the ability of *P. mirabilis* to induce caspase-1 activation and the release of IL-1 β , but not that of TNF- α (Figures 6F and 6G). Collectively, these results indicate that activation of the NLRP3 inflammasome by *P. mirabilis* is mediated by the HpmA hemolysin.

***P. mirabilis* Colonization Enhances DSS-Induced Colitis via NLRP3-Mediated IL-1 Signaling**

To determine whether *P. mirabilis* can affect DSS-induced colitis, we generated a streptomycin-resistant *P. mirabilis* (Str^R *Pm*) strain by culturing the mouse *P. mirabilis* bacterium with streptomycin. Like the parental *P. mirabilis* strain, Str^R *Pm* induced IL-1 β release and exhibited swarming capacity

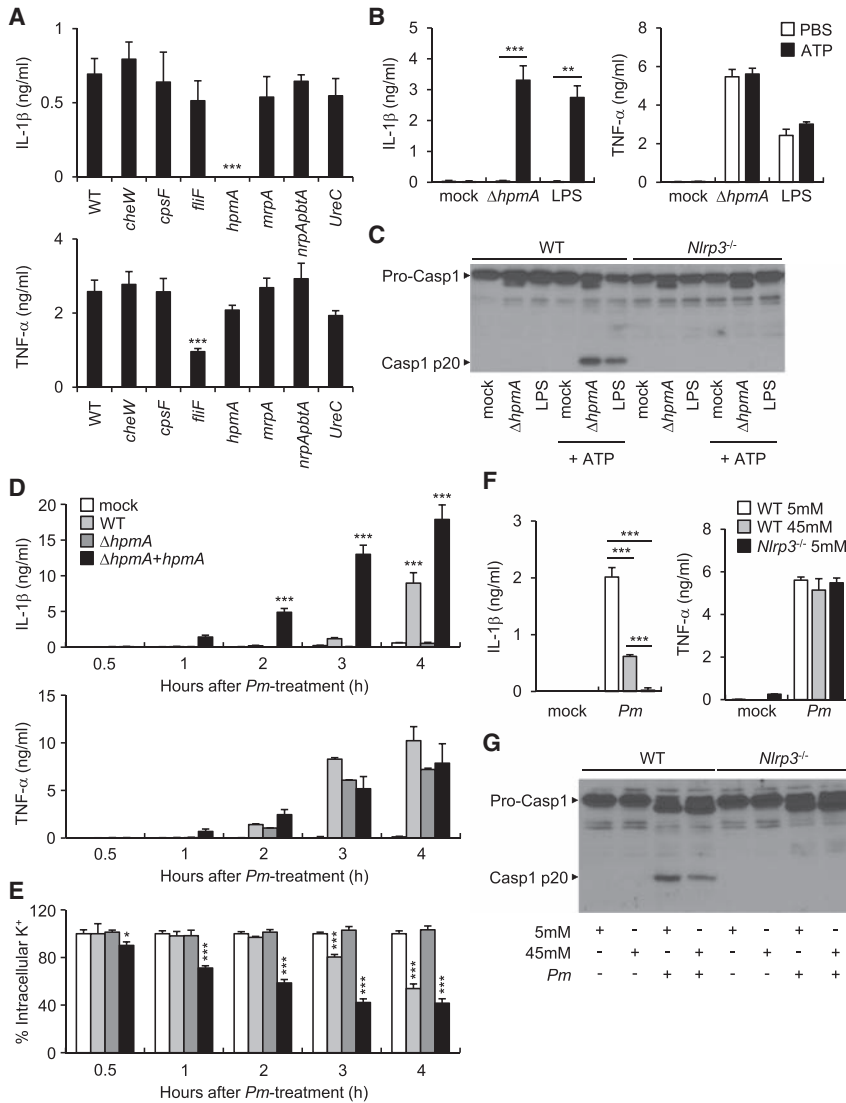


Figure 6. *P. mirabilis* HpmA Mediates NLRP3 Inflammasome Activation

(A) BMDMs were pre-incubated with LPS (100 ng/ml) for 3 hr and then stimulated with *P. mirabilis* HI4320 (WT) and indicated isogenic mutants for 3 hr at bacteria:macrophage ratio of 1. Cytokines were measured in culture supernatant after 3 hr culture. (B and C) WT or *Nlrp3*^{-/-} BMDMs were pre-incubated with *ΔhpmA Pm* or LPS (100 ng/ml) for 3 hr and left unstimulated or cultured in the presence of 5 mM ATP for additional 30 min. (B) IL-1β and TNF-α were measured from culture supernatant of WT BMDMs. (C) Caspase-1 activation was detected by immunoblotting.

(D and E) LPS-treated BMDMs were incubated with HpmA-deficient (*ΔhpmA Pm*) *P. mirabilis* mutant, and the same strain complemented with *hpmA* plasmid (*ΔhpmA+hpmA*). Cytokines in culture supernatant (D) and intracellular K⁺ concentrations (E) were measured at different time points.

(F and G) WT and *Nlrp3*^{-/-} BMDMs were stimulated with *P. mirabilis* (*Pm*) in culture medium containing the indicated concentration of extracellular K⁺. (F) Cytokine concentrations in culture supernatant were determined by ELISA. (G) Active caspase-1 in cell lysate and cell supernatant were detected by immunoblotting.

Values are means of triplicate samples ± SD. Data are representative of at least three experiments. *p < 0.05, **p < 0.01, ***p < 0.001. See also Figure S4.

observed in *Nlrp3*^{-/-} mice (Figures 7E–7G) and were reversed by treatment with Anakinra, an antagonist of IL-1 receptor signaling (Figures 7H–7J). In order to rule out the possibility that enhanced colitis merely reflect higher numbers of bacteria in *P. mirabilis* colonized mice, we inoculated mice with the same number of WT or *ΔhpmA P. mirabilis* by gavage. Analysis of fecal samples of WT and *ΔhpmA*

P. mirabilis showed comparable intestinal colonization (Figure S7). Importantly, colonization with *ΔhpmA P. mirabilis* resulted in less body weight loss and colonic shortening compared to colonization with WT *P. mirabilis* (Figure S7). Collectively, the results indicate *P. mirabilis* colonization enhances DSS-induced colitis via NLRP3-mediated IL-1 signaling in inflammatory monocytes.

DISCUSSION

Previous studies showed that the microbiota can promote intestinal inflammation and pathology in animal models (Hudcovic et al., 2001; Kirkland et al., 2012; Kitajima et al., 2001). A major inflammatory pathway induced in the intestine is that triggered by IL-1β. Clinical studies have suggested that IL-1β is important in disease because robust amounts of IL-1β are released by colonic LP cells from inflammatory bowel disease patients, which correlates with lesional disease activity (Ligumsky et al., 1990). However, the role of the microbiota and the mechanism

(Figure S5). When mice were treated with streptomycin and infected with Str^R *Pm*, colonization of the Str^R *Pm* strain was detected in the luminal contents of the ileum, cecum, and colon (Figure S6A) and the feces (Figure S6B). Notably, mice colonized with *P. mirabilis* did not display obvious signs of intestinal inflammation including loss of body weight, soft stools, or intestinal inflammation by histological examination (Figure S6C and S6D and data not shown). However, mice colonized with *P. mirabilis* exhibited more loss of body weight and colonic shortening than control mice after DSS administration (Figures 7A and 7B). The colitis induced by DSS is typically restricted to the distal colon in normal mice (Brown et al., 2007). Remarkably, mice colonized with *P. mirabilis* exhibited marked inflammation in the cecum upon DSS administration (Figures 7C and 7D). Consistent with the results in Figure 4, enhancement of DSS-colitis induced by *P. mirabilis* colonization was not detected in *Ccr2*^{-/-} mice (Figures S6E and S6F). Furthermore, the increase in body weight loss, colonic shortening, and enhanced tissue pathology associated with *P. mirabilis* colonization were not

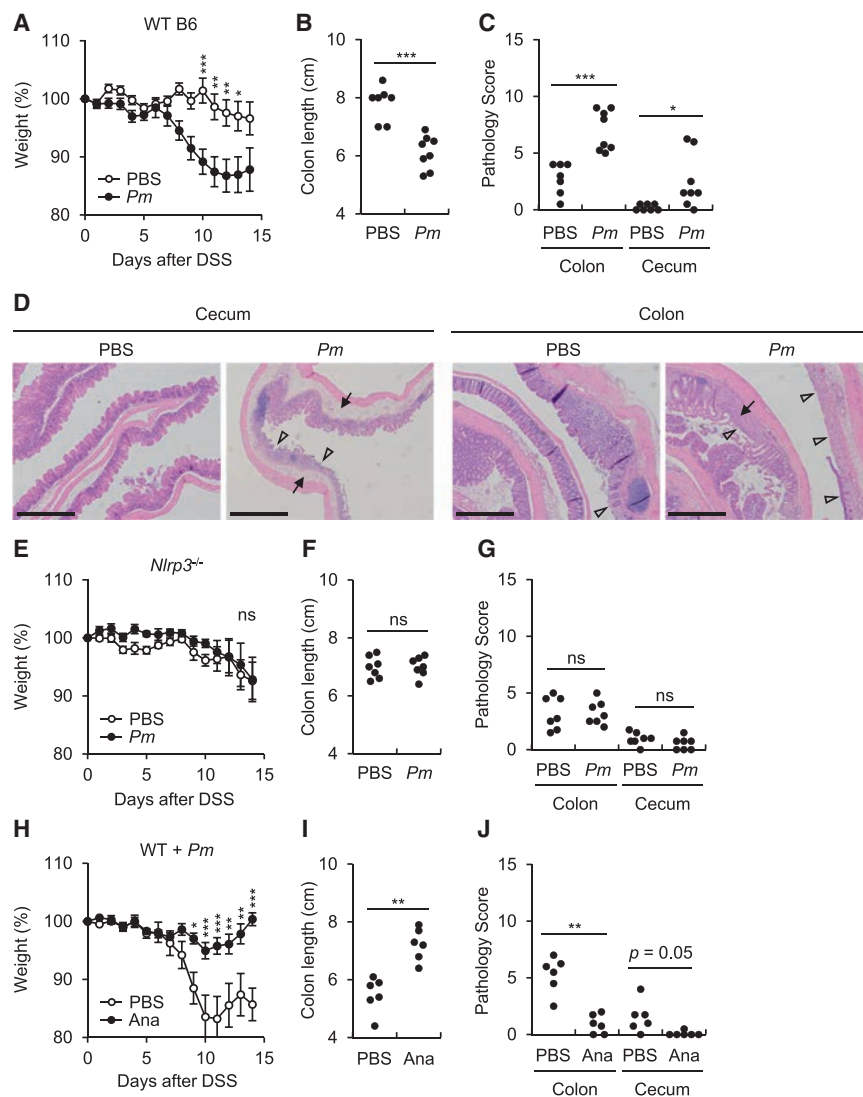


Figure 7. *P. mirabilis* Enhances DSS-Induced Inflammation via NLRP3 and IL-1R Signaling

Streptomycin-treated WT or *Nlrp3*^{-/-} mice were gavaged with 1×10^9 CFU of streptomycin-resistant *P. mirabilis* (*Pm*) on day 0, 4, and 8. Colitis was induced by administration of 1% DSS from day 0 to day 10. Mice were euthanized for analyses on day 15.

(A–C) WT mice injected with PBS ($n = 12$) or inoculated with *Pm* ($n = 15$).

(D) Representative histology of cecum and distal colon in WT mice in the absence and presence of *Pm* colonization after 1% DSS administration on day 15 after DSS administration. Open arrowheads denote damaged or ulcerated mucosa with total loss of epithelium, solid arrowheads indicate presence of inflammatory cells in the submucosa and edema. Scale bar represents 500 μm .

(E–G) *Nlrp3*^{-/-} mice injected with PBS ($n = 12$) or inoculated with *Pm* ($n = 11$).

(H–J) *Pm*-colonized WT mice were injected daily with PBS ($n = 9$) or Anakinra (Ana, 50 mg/kg, $n = 8$) from day 4.

Body weight data were pooled from three (A and E) or two (H) separate experiments. Values represent means \pm SEM. Colon length and pathology score were pooled from two experiments with similar results. * $p < 0.05$, ** $p < 0.01$, *** $p < 0.001$, ns; not significant. See also Figures S5–S7.

In the mouse model, *P. mirabilis* has been linked to the severity of colitis (Garrett et al., 2010). Thus, *P. mirabilis* acts as a pathobiont in mice and humans. Consistently, sequence analysis of the mouse *P. mirabilis* genome revealed that the commensal bacterium harbors multiple virulence genes shared with human uropathogenic *P. mirabilis* strains (Pearson et al., 2008).

One of the virulence genes, *hpmA*, was found to be critical for the activation of NLRP3 inflammasome. The *hpmA* gene encodes a secreted pore-forming cytolysin that is produced during bacterial growth and infection (Swihart and Welch, 1990). Although the function of HpmA in *P. mirabilis* is unknown, our study indicates that HpmA can induce K^+ efflux, and this activity is sensed by host macrophages to activate the NLRP3 inflammasome.

Several studies have assessed the role of the NLRP3 inflammasome in DSS-induced colitis with discordant results. For example, two studies reported increased susceptibility to DSS-induced colitis in *Nlrp3*^{-/-} mice, which was associated with decreased IL-1 β and IL-18 production, loss of epithelial integrity, and increased colonic inflammation (Allen et al., 2010; Zaki et al., 2010). In contrast, another group found lower concentrations of several cytokines including IL-1 β in colonic tissue and protection against colitis in *Nlrp3*^{-/-} mice (Bauer et al., 2010). These contradictory results are paralleled by observations in *Casp1*^{-/-} mice. For example, one study showed protection against DSS-induced colitis in *Casp1*^{-/-} mice, whereas another

involved in triggering IL-1 β production are unclear. On the basis of experiments in mice treated with antibiotics and GF mice, we show that the microbiota is critical for the induction of IL-1 β release and this response is mediated by the NLRP3 inflammasome in vitro and in vivo. Remarkably, the great majority of the resident bacteria isolated from the mouse intestine induce little or no release of IL-1 β , although they can elicit robust production of TNF- α . Although several intestinal bacteria including *P. mirabilis* and *E. coli* induce activation of the NLRP3 inflammasome in vitro, the ability of *P. mirabilis* to induce caspase-1 activation and IL-1 β release was striking in that it was comparable to that of pathogenic *Salmonella*. *P. mirabilis* was found to induce robust IL-1 β release; however, our results suggest that other bacteria including *E. coli* can induce IL-1 β in vitro and possibly in vivo. Furthermore, commensals other than *P. mirabilis*, some of which might be uncultivable, could be involved in regulating IL-1 β release in vivo. Although it is a member of the intestinal microbiota in humans and mice (Armbruster and Mobley, 2012; Garrett et al., 2010), *P. mirabilis* is a major cause of urinary tract infection in humans (Armbruster and Mobley, 2012).

groups showed the opposite (Allen et al., 2010; Siegmund et al., 2001; Zaki et al., 2010). Although it is difficult to ascertain the reason for these contradictory results, recent studies showed that protection of *Nlrp3*^{-/-} mice against colitis can be reversed by co-housing *Nlrp3*^{-/-} mice with WT mice (Bauer et al., 2012). The latter results suggest that the differences in results regarding the role of the NLRP3 inflammasome might be explained, at least in part, by baseline differences in the intestinal microbiota among mouse colonies. Given the marked variation in the ability of different intestinal bacteria to activate the NLRP3 inflammasome, it is likely that mice with different microbiota composition will differ in the intestinal activation of the inflammasome induced upon epithelial injury.

Intestinal bacteria belonging to the *Enterobacteriaceae* family have been linked to colitis in mice and humans. For example, *P. mirabilis* acts in concert with other intestinal bacteria to induce colitis in TRUC mice, a spontaneous model of ulcerative colitis (Garrett et al., 2010). Although the mechanism that is responsible for TRUC colitis is not fully understood, recent studies have revealed an important role for group 3 innate lymphoid cells (ILC3s) in the TRUC colitogenic phenotype (Powell et al., 2012). Because the activation of ILC3s is induced via IL-23 and IL-1 β (Coccia et al., 2012; Takatori et al., 2009), it is possible that *P. mirabilis* contributes to TRUC colitis through the activation of ILC3s and induction of colitogenic cytokines such as IL-17A. Although there is no evidence as yet that *P. mirabilis* contributes to colitis in humans, adherent and invasive *E. coli* (AIEC) strains that accumulate in the intestine of patients with inflammatory bowel disease induce robust IL-1 β release via the NLRP3 inflammasome (De la Fuente et al., 2014). Like *P. mirabilis*, AIEC is a pathobiont that expresses virulence factors and can enhance experimental colitis in mice (Drouet et al., 2012), although the host signaling pathways involved remain unclear. Because *P. mirabilis* colonization can promote colonic inflammation via NLRP3, we suggest that *Enterobacteriaceae* family members such as *P. mirabilis* and AIEC promote intestinal inflammation, at least in part, by inducing local IL-1 β release.

Colonization of conventionally reared mice or GF mice with *P. mirabilis* alone did not cause overt colitis. The latter can be explained by the requirement of intestinal injury and recruitment of inflammatory monocytes for the activation of the NLRP3 inflammasome and release of IL-1 β . It is possible that the HpmA is produced by *P. mirabilis* under steady-state conditions but its activity is antagonized by host factors such as intraluminal immunoglobulin A (IgA). Unlike resident mononuclear phagocytes that are hyporesponsive to commensal bacteria, inflammatory monocytes recruited to the intestine express NLRP3 and pro-IL-1 β in response to microbial stimulation and are responsive to NLRP3-activating signals such as ATP. Consistent with these studies, Ly6C^{high} inflammatory monocytes recruited to the intestine in response to DSS express pattern-recognition receptors such as TLR2 and NOD2 that sense bacteria and their deletion attenuates DSS-induced colitis (Zigmond et al., 2012). The lack of a functional NLRP3 inflammasome in resident phagocytes might ensure that inappropriate production of IL-1 β is not induced under steady-state conditions or when there is minimal epithelial injury. In contrast, resident intestinal macrophages constitutively express NLRC4 and pro-IL-1 β and release IL-1 β upon infection with enteric pathogens such

as *Salmonella* (Franchi et al., 2012a). These observations suggest that the NLRC4 inflammasome functions to detect pathogen invasion early, whereas the NLRP3 inflammasome is activated at later stages in inflammatory monocytes and might serve to boost immune responses against invasive pathogens and/or to enhance tissue repair in the intestine.

EXPERIMENTAL PROCEDURES

Mice

Six- to eight-week-old WT C57BL/6 (B6), *Aim2*^{-/-}, *Pycard*^{-/-}, *Casp1*^{-/-}, *Casp11*^{-/-}, *Casp11*^{-/-}, *Ccr2*^{-/-}, *Il1b*^{-/-}, *Nlr4*^{-/-}, and *Nlrp3*^{-/-} mice in B6 background were bred and kept under specific pathogen-free (SPF) conditions in University of Michigan Cancer Center. CCR2 deleter (*Ccr2*^{DTR/+}) mice were kindly provided by Dr. Eric Pamer, Memorial Sloan Kettering Cancer Center (Hohl et al., 2009). GF mice were bred and maintained at the GF Animal Core Facility of the University of Michigan. The animal studies were conducted under protocols approved by the University of Michigan Committee on Use and Care of Animals.

Bacteria

Commensal bacteria were isolated from the fecal content of B6 mice. For most commensals, the feces were suspended in PBS, plated on Brain Heart Infusion (BHI) plates at different dilutions under aerobic conditions, and individual colonies isolated and frozen in glycerol. *Lactobacillus* spp. were plated on de Man, Rogosa, and Sharpe (MRS) agar. For isolation of *Bacteroides* or *Clostridia* species, fecal samples were plated on Bacteroides Agar, and BHI agar plates containing 5% sheep blood, respectively, under anaerobic conditions. The bacterial species were verified by 16S rRNA sequencing. Most of bacteria were inoculated in Luria-Bertani (LB) broth (MP Biomedicals) and cultured overnight at 37°C with shaking. *Lactobacillus* spp. were inoculated in MRS broth (Difco) and cultured for 2 days under anaerobic conditions. *Bacteroides* and *Clostridium* were cultured in Chopped Meat Medium (Anaerobe Systems) for 2 days under anaerobic conditions. To generate streptomycin-resistant mouse-isolated *P. mirabilis*, we cultured multiple cycles of bacteria in broth containing increasing doses of streptomycin (Calbiochem). A single colony was picked from culture every two to three cycles using LB plates containing tetracycline (20 μ g/ml) and streptomycin (5 to 200 μ g/ml). *P. mirabilis* HI4320, a human urinary tract isolate has been described (Jones and Mobley, 1987). Isogenic *P. mirabilis* HI4320 mutants constructed using a TargeTron mutagenesis kit have been described (Alteri et al., 2013). To generate *hpmA*-complemented human *P. mirabilis* HI4320 strain (HI4320 Δ *hpmA*+pGEN*hpmA*), we transformed the mutant HI4320 Δ *hpmA* strain with pGEN plasmid expressing *hpmA* and the bacteria selected with ampicillin (20 μ g/ml).

Genomic Sequencing Analysis

Whole-genome sequencing of *P. mirabilis* UM001 was performed on the Illumina HiSeq 2000 platform using paired-end reads with 200–300 bp insert size and 100 bp read length. Assembly of the 5.25 million reads obtained was carried out using Velvet Optimizer (Zerbino and Birney, 2008) to produce a final genome assembly 3,950,860 bp in length composed of 28 contigs with a contig N50 of 377,567 bp. Annotation to identify coding sequences, assign predicted functions, and to predict RNA structures was generated using Prokka (Seemann, 2014).

DSS-Induced Colitis and *P. mirabilis* Colonization

Water containing 1%–2.5% DSS (molecular weight, 36,000–50,000; MP Biomedicals) was administered for 6–10 days and the mice were switched to regular water. Body weight and stool consistency were checked daily. In some experiments, mice were given an antibiotic cocktail (500 μ g of ampicillin, 250 μ g of vancomycin, 250 μ g of metronidazole, 250 μ g of gentamycin, and 500 μ g of neomycin) by gavage for 9 days starting 1 day prior to DSS treatment. For *P. mirabilis* colonization experiments, mice received 2 g/L streptomycin in the drinking water throughout the experiment starting 10 days before bacterial gavage. Mice were inoculated with 1 \times 10⁹ CFU of streptomycin-resistant *P. mirabilis* by gavage and all mouse groups received

water containing 1% DSS for 10 days to induce colitis. To antagonize IL-1 β , we intraperitoneally injected mice with Anakinra (50 mg/kg) daily from day 4 to day 14. Body weight measured every day and results are pool from 2 to 4 separate experiments, which used at least three mice per group. Disease activity index (DAI) was monitored every day in DSS-treated mice as described (Kamada et al., 2005). Briefly, loss of body weight (0, none; 1, 1%–5%; 2, 5%–10%; 3, 10%–20%; 4, >20%), stool consistency (0, normal stool; 2, loose stool; 4, diarrhea), hemocult (0, normal; 2, homocult positive; 4, gross blood). PBS-injected and *P. mirabilis*-infected mice were sacrificed on day 15 and histological score was evaluated blindly by one pathologist using a described scoring system (Chen et al., 2008). Briefly, severity of inflammation (0, none; 1, mild; 2, moderate; 3, severe), the level of involvement (0, none; 1, mucosa; 2, mucosa and submucosa; 3, transmural), and extent of epithelial/crypt damage (0, none; 1, basal 1/3; 2, basal 2/3; 3, crypt loss; 4, crypt and surface epithelial destruction). Each variable was then multiplied by a factor reflecting the percentage of the colon involved (0%–25%, 26%–50%, 51%–75%, 76%–100%), and then summed to obtain the overall score.

Preparation and Culture of Macrophage and Intestinal Phagocytes

BMDMs and LP cells were prepared as described (Franchi et al., 2012a). BMDMs (2×10^5 cells/well) were suspended in IMDM supplemented with 2% FBS and seeded in 48-multiwell plates. In some experiments, BMDMs were stimulated with Ultrapure *E. coli* LPS (100 ng/ml; Invivogen) for 3 hr. Feces from SPF or GF mice were suspended in sterile PBS (100 mg/ml), homogenized, and spun at 1,000 rpm for 5 s. Fecal contents were passed through 40 μ m cell strainer (BD Falcon) to remove aggregates and used to stimulate BMDMs at a 1:200 dilution. BMDMs were incubated with fecal contents for 3 hr, the medium was replaced with fresh medium containing gentamicin (100 μ g/ml) and the culture continued for an additional 15 hr. BMDMs were cultured with individual bacteria strains at a bacterial: macrophage ratio of 1 for 3 hr. For long-term stimulation, the medium was replaced with fresh medium containing gentamicin (100 μ g/ml) and the culture continued for an additional 15 hr. Isolated LP cells were resuspended in RPMI medium containing 10% heat-inactivated fetal bovine serum (FBS), 2- β -mercaptoethanol (50 μ M), L-glutamine (2 mM), sodium pyruvate (1 mM), MEM non-essential amino acids (GIBCO). LP cells were pooled from two or three mice per group, and total LP cells (2×10^5 cells/well) or sorted cells (1×10^5 cells/well) were seeded in 96-multiwell plates in triplicate. Cells were incubated for 3 hr in 5% CO₂ incubator and cell-free supernatant were subjected to further analysis. For *ex vivo* stimulation, cells were left unstimulated or incubated with 5 mM ATP for 30 min or with bacteria at bacteria:macrophage ratio of 1 for 3 hr.

Immunoblotting

Cells were lysed in buffer containing 1% NP-40 supplemented with complete protease inhibitor cocktail (Roche) and 2 mM dithiothreitol. Lysates were resolved by SDS-PAGE and transferred to PVDF membranes by electro-blotting. The rabbit anti mouse caspase-1 antibody has been described (Franchi et al., 2012a). Protein bands were revealed with goat anti-rabbit IgG antibody (Jackson ImmunoResearch Laboratories) and enhanced chemiluminescent substrate (Thermo Scientific).

Intracellular K⁺ Determination and Cytokine Detection

Intracellular K⁺ concentrations were measured as described previously (Muñoz-Planillo et al., 2013). Mouse cytokines were measured in culture supernatants by enzyme-linked immunosorbent assay (ELISA) kits (R&D Systems).

Flow Cytometry and Cell Sorting

LP cells were stained with the following antibodies: CD45 (30-F11), CD11b (M1/70), Ly6C (AL-21), Ly6G (1A8), all purchased from BD Pharmingen. Cells were stained and sorted using a FACSAria III instrument (BD Bioscience). Data were analyzed using FlowJo program (Tree Star).

Quantitative Real-Time PCR

RNA was extracted with E.Z.N.A. Total RNA Kit (Omega Biotek) according to the manufacturer's instructions. RNA was reverse transcribed using the High Capacity RNA-to-cDNA Kit (Applied Biosystems) and cDNA was then used

for quantitative PCR analysis using SYBR Green Gene-Expression Assay on an ABI 7900HT analyzer. The following primer sets were used for amplification: IL-1 β -F; 5'-GATCCACACTCTCCAGCTGCA, IL-1 β -R; 5'-CAACCAACAAGT GATATTCTCCATG, NLRP3-F; 5'-ATGGTATGCCAGGAGGACAG, NLRP3-R; 5'-ATGCTCCTTGACCAGTTGGA, GAPDH-F; 5'-TGCGACTTCAACAGCAAC TC, GAPDH-R; 5'-GCCTCTCTTGCTCAGTGTCC. Samples were run in triplicate for each experimental condition and mean values were used to calculate statistics.

Generation of Mixed Chimeric Mice

BM cells were obtained from *Ccr2*^{DTR/+} mice, mixed with equivalent number of WT or *Il1b*^{-/-} BM cells and 1×10^7 donor cells were injected into 8-week-old recipient WT mice that were lethally irradiated with 1,100 rads. Mice were used 8 weeks after reconstitution. To deplete CCR2⁺ cells, we intraperitoneally injected 10 μ g/kg diphtheria toxin (DT) on days 0, 3, 6.

Statistical Analysis

Statistical analysis was performed using GraphPad Prism program (GraphPad Software). Differences between two groups were evaluated using Student's t test. For multiple comparison, one-way ANOVA or Kruskal-Wallis test was used. For body weight and DAI comparisons, two-way ANOVA with Bonferroni posttest was used. $p < 0.05$ was considered significant.

ACCESSION NUMBERS

The ENA accession number for the genome sequence of mouse *Proteus mirabilis* strain UM001 reported in this paper is ERR832496.

SUPPLEMENTAL INFORMATION

Supplemental Information includes seven figures and can be found with this article online at <http://dx.doi.org/10.1016/j.immuni.2015.03.004>.

AUTHOR CONTRIBUTIONS

S.-U.S., N.K., and G.N. conceived the study. S.-U.S. performed most of the experiments. R.M.-P., Y.-G.K., D.K., Y.K., M.H., and S.D.H. provided critical reagents and helped with experiments. R.M.-P., H.L.T.M., H.P.B., T.D.L., and N.I. analyzed data. G.N. supervised all aspects of this study. S.-U.S. and G.N. wrote the manuscript with contributions from all authors.

ACKNOWLEDGMENTS

We thank Grace Chen for critical review of the manuscript and Eric Pamer for proving mutant mice. We thank the University of Michigan Host Microbiome Initiative for support. This work is supported by the Basic Science Research Program through the National Research Foundation of Korea funded by the Ministry of Education, Science and Technology 2013R1A6A3A03024348 (S.-U.S.), a Career Development award from the Crohn's and Colitis Foundation of America (N.K.), the Michigan Gastrointestinal Peptide Research Center NIDDK 5P30DK034933 (N.K.), grants 098051 and WT086418MA from the Wellcome Trust (T.D.L.) and DK091191 and DK095782 from the National Institutes of Health (G.N.).

Received: August 12, 2014

Revised: January 22, 2015

Accepted: February 20, 2015

Published: April 7, 2015

REFERENCES

- Allen, I.C., TeKippe, E.M., Woodford, R.M., Uronis, J.M., Holl, E.K., Rogers, A.B., Herfarth, H.H., Jobin, C., and Ting, J.P. (2010). The NLRP3 inflammasome functions as a negative regulator of tumorigenesis during colitis-associated cancer. *J. Exp. Med.* 207, 1045–1056.
- Alteri, C.J., Himpfl, S.D., Pickens, S.R., Lindner, J.R., Zora, J.S., Miller, J.E., Arno, P.D., Straight, S.W., and Mobley, H.L. (2013). Multicellular bacteria

- deploy the type VI secretion system to preemptively strike neighboring cells. *PLoS Pathog.* 9, e1003608.
- Armbruster, C.E., and Mobley, H.L. (2012). Merging mythology and morphology: the multifaceted lifestyle of *Proteus mirabilis*. *Nat. Rev. Microbiol.* 10, 743–754.
- Aziz, R.K., Bartels, D., Best, A.A., DeJongh, M., Disz, T., Edwards, R.A., Formsma, K., Gerdes, S., Glass, E.M., Kubal, M., et al. (2008). The RAST Server: rapid annotations using subsystems technology. *BMC Genomics* 9, 75.
- Bauer, C., Duewell, P., Mayer, C., Lehr, H.A., Fitzgerald, K.A., Dauer, M., Tschopp, J., Endres, S., Latz, E., and Schnurr, M. (2010). Colitis induced in mice with dextran sulfate sodium (DSS) is mediated by the NLRP3 inflammasome. *Gut* 59, 1192–1199.
- Bauer, C., Duewell, P., Lehr, H.A., Endres, S., and Schnurr, M. (2012). Protective and aggravating effects of Nlrp3 inflammasome activation in IBD models: influence of genetic and environmental factors. *Dig. Dis.* 30 (1), 82–90.
- Bersudsky, M., Luski, L., Fishman, D., White, R.M., Ziv-Sokolovskaya, N., Dotan, S., Rider, P., Kaplanov, I., Aychek, T., Dinarello, C.A., et al. (2014). Non-redundant properties of IL-1 α and IL-1 β during acute colon inflammation in mice. *Gut* 63, 598–609.
- Bloom, S.M., Bijanki, V.N., Nava, G.M., Sun, L., Malvin, N.P., Donermeyer, D.L., Dunne, W.M., Jr., Allen, P.M., and Stappenbeck, T.S. (2011). Commensal *Bacteroides* species induce colitis in host-genotype-specific fashion in a mouse model of inflammatory bowel disease. *Cell Host Microbe* 9, 390–403.
- Brown, S.L., Riehl, T.E., Walker, M.R., Geske, M.J., Doherty, J.M., Stenson, W.F., and Stappenbeck, T.S. (2007). Myd88-dependent positioning of Ptg2-expressing stromal cells maintains colonic epithelial proliferation during injury. *J. Clin. Invest.* 117, 258–269.
- Chen, G.Y., Shaw, M.H., Redondo, G., and Núñez, G. (2008). The innate immune receptor Nod1 protects the intestine from inflammation-induced tumorigenesis. *Cancer Res.* 68, 10060–10067.
- Coccia, M., Harrison, O.J., Schiering, C., Asquith, M.J., Becher, B., Powrie, F., and Maloy, K.J. (2012). IL-1 β mediates chronic intestinal inflammation by promoting the accumulation of IL-17A secreting innate lymphoid cells and CD4(+) Th17 cells. *J. Exp. Med.* 209, 1595–1609.
- De la Fuente, M., Franchi, L., Araya, D., Díaz-Jiménez, D., Olivares, M., Álvarez-Lobos, M., Golenbock, D., González, M.J., López-Kostner, F., Quera, R., et al. (2014). *Escherichia coli* isolates from inflammatory bowel diseases patients survive in macrophages and activate NLRP3 inflammasome. *Int. J. Med. Microbiol.* 304, 384–392.
- Drouet, M., Vignal, C., Singer, E., Djouina, M., Dubreuil, L., Cortot, A., Desreumaux, P., and Neut, C. (2012). AIEC colonization and pathogenicity: influence of previous antibiotic treatment and preexisting inflammation. *Inflamm. Bowel Dis.* 18, 1923–1931.
- Franchi, L., Amer, A., Body-Malapel, M., Kanneganti, T.D., Ozören, N., Jagirdar, R., Inohara, N., Vandenabeele, P., Bertin, J., Coyle, A., et al. (2006). Cytosolic flagellin requires Ipaf for activation of caspase-1 and interleukin 1 β in salmonella-infected macrophages. *Nat. Immunol.* 7, 576–582.
- Franchi, L., Kamada, N., Nakamura, Y., Burberry, A., Kuffa, P., Suzuki, S., Shaw, M.H., Kim, Y.G., and Núñez, G. (2012a). NLR4-driven production of IL-1 β discriminates between pathogenic and commensal bacteria and promotes host intestinal defense. *Nat. Immunol.* 13, 449–456.
- Franchi, L., Muñoz-Planillo, R., and Núñez, G. (2012b). Sensing and reacting to microbes through the inflammasomes. *Nat. Immunol.* 13, 325–332.
- Garrett, W.S., Lord, G.M., Punit, S., Lugo-Villarino, G., Mazmanian, S.K., Ito, S., Glickman, J.N., and Glimcher, L.H. (2007). Communicable ulcerative colitis induced by T-bet deficiency in the innate immune system. *Cell* 131, 33–45.
- Garrett, W.S., Gallini, C.A., Yatsunenkov, T., Michaud, M., DuBois, A., Delaney, M.L., Punit, S., Karlsson, M., Bry, L., Glickman, J.N., et al. (2010). Enterobacteriaceae act in concert with the gut microbiota to induce spontaneous and maternally transmitted colitis. *Cell Host Microbe* 8, 292–300.
- Hohl, T.M., Rivera, A., Lipuma, L., Gallegos, A., Shi, C., Mack, M., and Pamer, E.G. (2009). Inflammatory monocytes facilitate adaptive CD4 T cell responses during respiratory fungal infection. *Cell Host Microbe* 6, 470–481.
- Hornung, V., Bauernfeind, F., Halle, A., Samstad, E.O., Kono, H., Rock, K.L., Fitzgerald, K.A., and Latz, E. (2008). Silica crystals and aluminum salts activate the NALP3 inflammasome through phagosomal destabilization. *Nat. Immunol.* 9, 847–856.
- Hudcovic, T., Stěpánková, R., Cebra, J., and Tlaskalová-Hogenová, H. (2001). The role of microflora in the development of intestinal inflammation: acute and chronic colitis induced by dextran sulfate in germ-free and conventionally reared immunocompetent and immunodeficient mice. *Folia Microbiol. (Praha)* 46, 565–572.
- Jones, B.D., and Mobley, H.L. (1987). Genetic and biochemical diversity of ureases of *Proteus*, *Providencia*, and *Morganella* species isolated from urinary tract infection. *Infect. Immun.* 55, 2198–2203.
- Kamada, N., and Núñez, G. (2014). Regulation of the immune system by the resident intestinal bacteria. *Gastroenterology* 146, 1477–1488.
- Kamada, N., Inoue, N., Hisamatsu, T., Okamoto, S., Matsuoka, K., Sato, T., Chinen, H., Hong, K.S., Yamada, T., Suzuki, Y., et al. (2005). Nonpathogenic *Escherichia coli* strain Nissle1917 prevents murine acute and chronic colitis. *Inflamm. Bowel Dis.* 11, 455–463.
- Kamada, N., Seo, S.U., Chen, G.Y., and Núñez, G. (2013). Role of the gut microbiota in immunity and inflammatory disease. *Nat. Rev. Immunol.* 13, 321–335.
- Kim, Y.G., Kamada, N., Shaw, M.H., Warner, N., Chen, G.Y., Franchi, L., and Núñez, G. (2011). The Nod2 sensor promotes intestinal pathogen eradication via the chemokine CCL2-dependent recruitment of inflammatory monocytes. *Immunity* 34, 769–780.
- Kirkland, D., Benson, A., Mirpuri, J., Pifer, R., Hou, B., DeFranco, A.L., and Yarovsky, F. (2012). B cell-intrinsic MyD88 signaling prevents the lethal dissemination of commensal bacteria during colonic damage. *Immunity* 36, 228–238.
- Kitajima, S., Morimoto, M., Sagara, E., Shimizu, C., and Ikeda, Y. (2001). Dextran sodium sulfate-induced colitis in germ-free IqI/Jic mice. *Exp. Anim.* 50, 387–395.
- Ligumsky, M., Simon, P.L., Karmeli, F., and Rachmilewitz, D. (1990). Role of interleukin 1 in inflammatory bowel disease—enhanced production during active disease. *Gut* 31, 686–689.
- Lotz, M., Gütle, D., Walther, S., Ménard, S., Bogdan, C., and Hornef, M.W. (2006). Postnatal acquisition of endotoxin tolerance in intestinal epithelial cells. *J. Exp. Med.* 203, 973–984.
- Mariathasan, S., Weiss, D.S., Newton, K., McBride, J., O'Rourke, K., Roose-Girma, M., Lee, W.P., Weinrauch, Y., Monack, D.M., and Dixit, V.M. (2006). Cryopyrin activates the inflammasome in response to toxins and ATP. *Nature* 440, 228–232.
- Miao, E.A., Mao, D.P., Yudkovsky, N., Bonneau, R., Lorang, C.G., Warren, S.E., Leaf, I.A., and Aderem, A. (2010). Innate immune detection of the type III secretion apparatus through the NLR4 inflammasome. *Proc. Natl. Acad. Sci. USA* 107, 3076–3080.
- Muñoz-Planillo, R., Kuffa, P., Martínez-Colón, G., Smith, B.L., Rajendiran, T.M., and Núñez, G. (2013). K⁺ efflux is the common trigger of NLRP3 inflammasome activation by bacterial toxins and particulate matter. *Immunity* 38, 1142–1153.
- Pearson, M.M., Sebahia, M., Churcher, C., Quail, M.A., Seshasayee, A.S., Luscombe, N.M., Abdellah, Z., Arrosmith, C., Atkin, B., Chillingworth, T., et al. (2008). Complete genome sequence of uropathogenic *Proteus mirabilis*, a master of both adherence and motility. *J. Bacteriol.* 190, 4027–4037.
- Powell, N., Walker, A.W., Stolarczyk, E., Canavan, J.B., Gökmen, M.R., Marks, E., Jackson, I., Hashim, A., Curtis, M.A., Jenner, R.G., et al. (2012). The transcription factor T-bet regulates intestinal inflammation mediated by interleukin-7 receptor+ innate lymphoid cells. *Immunity* 37, 674–684.
- Saitoh, T., Fujita, N., Jang, M.H., Uematsu, S., Yang, B.G., Satoh, T., Omori, H., Noda, T., Yamamoto, N., Komatsu, M., et al. (2008). Loss of the autophagy

- protein Atg16L1 enhances endotoxin-induced IL-1 β production. *Nature* 456, 264–268.
- Schroder, K., and Tschopp, J. (2010). The inflammasomes. *Cell* 140, 821–832.
- Seemann, T. (2014). Prokka: rapid prokaryotic genome annotation. *Bioinformatics* 30, 2068–2069.
- Serbina, N.V., and Pamer, E.G. (2006). Monocyte emigration from bone marrow during bacterial infection requires signals mediated by chemokine receptor CCR2. *Nat. Immunol.* 7, 311–317.
- Siegmund, B., Lehr, H.A., Fantuzzi, G., and Dinarello, C.A. (2001). IL-1 β -converting enzyme (caspase-1) in intestinal inflammation. *Proc. Natl. Acad. Sci. USA* 98, 13249–13254.
- Smythies, L.E., Sellers, M., Clements, R.H., Mosteller-Barnum, M., Meng, G., Benjamin, W.H., Orenstein, J.M., and Smith, P.D. (2005). Human intestinal macrophages display profound inflammatory anergy despite avid phagocytic and bacteriocidal activity. *J. Clin. Invest.* 115, 66–75.
- Swihart, K.G., and Welch, R.A. (1990). Cytotoxic activity of the Proteus hemolysin HpmA. *Infect. Immun.* 58, 1861–1869.
- Takatori, H., Kanno, Y., Watford, W.T., Tato, C.M., Weiss, G., Ivanov, I.I., Littman, D.R., and O'Shea, J.J. (2009). Lymphoid tissue inducer-like cells are an innate source of IL-17 and IL-22. *J. Exp. Med.* 206, 35–41.
- Takeuchi, O., and Akira, S. (2010). Pattern recognition receptors and inflammation. *Cell* 140, 805–820.
- Vijay-Kumar, M., Sanders, C.J., Taylor, R.T., Kumar, A., Aitken, J.D., Sitaraman, S.V., Neish, A.S., Uematsu, S., Akira, S., Williams, I.R., and Gewirtz, A.T. (2007). Deletion of TLR5 results in spontaneous colitis in mice. *J. Clin. Invest.* 117, 3909–3921.
- Waddell, A., Ahrens, R., Steinbrecher, K., Donovan, B., Rothenberg, M.E., Munitz, A., and Hogan, S.P. (2011). Colonic eosinophilic inflammation in experimental colitis is mediated by Ly6C(high) CCR2(+) inflammatory monocyte/macrophage-derived CCL11. *J. Immunol.* 186, 5993–6003.
- Zaki, M.H., Boyd, K.L., Vogel, P., Kastan, M.B., Lamkanfi, M., and Kanneganti, T.D. (2010). The NLRP3 inflammasome protects against loss of epithelial integrity and mortality during experimental colitis. *Immunity* 32, 379–391.
- Zerbino, D.R., and Birney, E. (2008). Velvet: algorithms for de novo short read assembly using de Bruijn graphs. *Genome Res.* 18, 821–829.
- Zigmond, E., and Jung, S. (2013). Intestinal macrophages: well educated exceptions from the rule. *Trends Immunol.* 34, 162–168.
- Zigmond, E., Varol, C., Farache, J., Elmaliyah, E., Satpathy, A.T., Friedlander, G., Mack, M., Shpigel, N., Boneca, I.G., Murphy, K.M., et al. (2012). Ly6C hi monocytes in the inflamed colon give rise to proinflammatory effector cells and migratory antigen-presenting cells. *Immunity* 37, 1076–1090.

Spatiotemporally Distinct Interactions with Dendritic Cell Subsets Facilitates CD4⁺ and CD8⁺ T Cell Activation to Localized Viral Infection

Jyh Liang Hor,^{1,2,3} Paul G. Whitney,^{1,3} Ali Zaid,^{1,2} Andrew G. Brooks,^{1,4} William R. Heath,^{1,2,4} and Scott N. Mueller^{1,2,4,*}

¹Department of Microbiology and Immunology, The University of Melbourne, at the Peter Doherty Institute for Infection and Immunity, Parkville, VIC 3010, Australia

²The Australian Research Council Centre of Excellence in Advanced Molecular Imaging, The University of Melbourne, Parkville, VIC 3010, Australia

³Co-first author

⁴Co-senior author

*Correspondence: smue@unimelb.edu.au

<http://dx.doi.org/10.1016/j.immuni.2015.07.020>

SUMMARY

The dynamics of when and where CD4⁺ T cells provide help for CD8⁺ T cell priming and which dendritic cells (DCs) activate CD4⁺ T cells in vivo after localized infection are poorly understood. By using a cutaneous herpes simplex virus infection model combined with intravital 2-photon imaging of the draining lymph node (LN) to concurrently visualize pathogen-specific CD4⁺ and CD8⁺ T cells, we found that early priming of CD4⁺ T cells involved clustering with migratory skin DCs. CD8⁺ T cells did not interact with migratory DCs and their activation was delayed, requiring later clustering interactions with LN-resident XCR1⁺ DCs. CD4⁺ T cells interacted with these late CD8⁺ T cell clusters on resident XCR1⁺ DCs. Together, these data reveal asynchronous T cell activation by distinct DC subsets and highlight the key role of XCR1⁺ DCs as the central platform for cytotoxic T lymphocyte activation and the delivery of CD4⁺ T cell help.

INTRODUCTION

The priming of T cell responses to peripheral infections where the pathogen remains localized within the tissues requires the coordination of a variety of immune cells. Dendritic cells (DCs) are necessary to present antigens and provide appropriate costimulatory signals for the efficient activation of T cells. A number of phenotypically and functionally distinct subsets of DCs populate the lymphoid and non-lymphoid tissues and can play unique roles in T cell activation (Heath and Carbone, 2009; Merad et al., 2013). For example, the CD8 α ⁺ DCs, which reside in lymphoid organs, are specialized for the cross-presentation of antigens on major histocompatibility complex (MHC) class I for CD8⁺ T cell activation (Schnorrer et al., 2006), participate in viral immunity (Belz et al., 2004a, 2005), and belong to an XCR1⁺, Batf3-dependent lineage that is important for cytotoxic T

lymphocyte (CTL)- and T helper 1 (Th1) cell-mediated immunity (Edelson et al., 2010; Hildner et al., 2008). However, these lymph-node-resident DCs rarely act alone, especially during localized infections where they rely upon the activation and migration of tissue-associated DCs to deliver antigens to the lymph node (LN) (Allan et al., 2006; Belz et al., 2004b; Igyártó et al., 2011; Lee et al., 2009). Many vaccines and experimental infection models can, however, bypass a requirement for migratory DCs for T cell priming when injected antigens or pathogens drain directly to the LN via the lymphatic vessels (Gerner et al., 2015; Hickman et al., 2008; Itano et al., 2003; Kastenmüller et al., 2013).

The process of peripheral DC migration to LN can take multiple days, during which time different subsets of DCs emigrate from the tissues to the draining lymph node (dLN). In the skin after herpes simplex virus (HSV) infection, CD11b⁺ dermal DCs are the first to reach the dLN (Allan et al., 2006), followed by Langerhans cells, whereas CD103⁺ dermal DCs contribute appreciably to antigen presentation only after secondary spread of the virus across the skin (Bedoui et al., 2009). Some of these skin-migratory DCs are able to transfer antigens to LN-resident DCs, including CD8 α ⁺ DCs, facilitating CD8⁺ T cell activation (Allan et al., 2006). How this process of antigen handover occurs is not known, although the arrival of infected or antigen-carrying migratory DCs from the peripheral tissues might promote interactions with LN-resident DCs because recent migrants rapidly populate the LN paracortex after entering via the lymphatics (Braun et al., 2011; Kissenpfennig et al., 2005).

The current paradigm of T cell activation predicts that both CD8⁺ and CD4⁺ T cells will receive signals from DCs synchronously and become activated and divide with similar kinetics. Yet the involvement of different DC subsets in this process indicates that CD4⁺ and CD8⁺ T cells might not interact with DCs at the same time. Although such 3-cell interactions capably describe the existing model, temporally staggered interactions between CD4⁺ and CD8⁺ T cells and DCs have also been suggested (Ridge et al., 1998). Indeed, the discovery that multiple DC subsets can stimulate CD4⁺ T cells ex vivo after HSV infection, whereas CD8⁺ T cells can respond only to antigens presented by CD8 α ⁺ DCs in the early phase of the response (Allan et al., 2003; Bedoui et al., 2009), raises the possibility that

CD4⁺ T cells could be primed by a different subset of DCs and subsequently engage the DCs that prime CTLs. Furthermore, a number of infections require CD4⁺ T cell help via CD40L stimulation for maximal CD8⁺ T cell responses and memory (Wiesel and Oxenius, 2012), including HSV infection (Smith et al., 2004). Exactly how and when CD4⁺ T cells provide help to DCs remains poorly understood. CD4⁺ T cells might be required to provide help to DCs and then recruit naive CD8⁺ T cells to help DCs for more efficient priming (Castellino et al., 2006). One hypothesis arising from these observations is that CD4⁺ T cells that become activated early would be more capable of providing help to DCs and thus promoting CD8⁺ T cell responses.

A number of studies have focused on the initiation of immune responses subsequent to the drainage of lymph-borne antigens, particulates, or pathogens, revealing that subcapsular sinus-lining macrophages and DCs resident in this location can capture antigens (Carrasco and Batista, 2007; Gerner et al., 2015; Hickman et al., 2008; Junt et al., 2007; Phan et al., 2007). These antigen-presenting cells (APCs) can become infected by lymph-borne pathogens and present antigens directly to T cells. Assessment of the spatial and temporal aspects of T cell priming to such lymph-borne antigens have revealed that early CD8⁺ T cell interactions occur mainly in the peripheral paracortex and interfollicular regions (Gerner et al., 2015; Hickman et al., 2008; Kastenmüller et al., 2013). In contrast, the spatiotemporal dynamics of T cell priming after a localized infection where lymph-borne transport of pathogens is absent has not been examined. To determine the dynamics of CD4⁺ and CD8⁺ T cell priming after a localized peripheral virus infection and investigate interactions with DCs, here we have utilized cutaneous infection with HSV-1, a robust model of peripheral infection, combined with intravital 2-photon microscopy. We found that the activation of virus-specific CD4⁺ and CD8⁺ T cells, after localized infection, was temporally regulated by interactions with different subsets of DCs. CD4⁺ T cells interacted with migratory DCs arriving from the infected skin within 14 hr of infection and became activated. Conversely, CD8⁺ T cells were unable to see migratory APCs and were delayed in their interaction with LN-resident XCR1⁺ DCs. CD4⁺ T cells participated in dynamic clusters of CD8⁺ T cells on XCR1⁺ DCs that were the critical platform for CTL priming and the delivery of CD4⁺ T cell help. These findings reveal a previously unidentified level of control of T cell activation to peripheral infection.

RESULTS

Spatiotemporally Distinct Responses by Virus-Specific CD4⁺ and CD8⁺ T Cells after Localized Skin HSV Infection

To begin to explore the kinetics of both CD4⁺ and CD8⁺ T cell priming after localized infection, we utilized a well-characterized model of cutaneous HSV-1 infection of mice that induces robust CD4⁺ and CD8⁺ T cell responses and memory (Gebhardt et al., 2011; van Lint et al., 2004). Prior to infection, animals were adoptively transferred with CD4⁺ and CD8⁺ T cells from T cell receptor (TCR) transgenic mice. gDT-II CD4⁺ T cells specific for an HSV glycoprotein D epitope (Bedoui et al., 2009) and gBT-I CD8⁺ T cells specific for an HSV glycoprotein B epitope (Mueller et al., 2002a) were backcrossed onto mice ubiquitously express-

ing the fluorescent proteins GFP or DsRed to allow efficient tracking of small populations of cells by microscopy. Initial priming and expansion of T cells after flank HSV infection occurs in the draining brachial LN followed by emigration to the afferent axillary LN and release into the circulation (Eidsmo et al., 2012). When we examined gDT-II and gBT-I T cell numbers in the brachial LN 3 days after infection, we noted that CD4⁺ T cells began accumulating sooner than CD8⁺ T cells (Figure 1A). Both populations of virus-specific T cells peaked in number in the brachial LN 5–6 days after infection. CD4⁺ T cells then accumulated in the afferent axillary LN 3–4 days after infection, indicating egress from the brachial LN (Figure 1B). In contrast, gBT-I T cells entered the axillary LN only at day 5. In line with these observations, CD4⁺ T cells first appeared in the spleen at day 4, and CD8⁺ T cells 1 day later at day 5 (Figure 1C).

To ascertain whether these dissimilar CD4⁺ and CD8⁺ T cell response kinetics reflected differences in the location of the cells within the LN, we examined whole LN sections by microscopy. Tissues were co-stained with antibodies against LYVE-1 to detect lymphatics and B220 to visualize B cell follicles (Figure 1D). Both CD4⁺ and CD8⁺ T cells localized predominantly to the T cell zone 3 days after infection (Figures 1D and 1F). In contrast, 1 day later the virus-specific CD4⁺ T cells exhibited reduced accumulation in T cell zones and were observed in the medullary as well as at the subcapsular sinus (SCS) and within B cell follicles (Figures 1D, 1F, and S1). At this time point, the majority of the gBT-I CD8⁺ T cells remained in the deep T cell zone and interfollicular regions. Concomitant with this, CD4⁺ T cells were found concentrated in the medullary regions of the axillary LN, indicative of migration from the upstream brachial LN (Figure 1E). By day 5 of infection, CD8⁺ T cells displayed a similar pattern of intranodal migration, with many gBT-I T cells now observed in the medulla of the brachial LN and afferent axillary LN. This delayed pattern of CD8⁺ T cell migration was reflected in the systemic diaspora of the cells, whereby CD4⁺ T cells migrated to the spleen and the infected skin by day 4, yet CD8⁺ T cells were absent from these sites until day 5 of HSV infection (Figures 1G and 1H). These data indicate that CD4⁺ T cell responses in the draining LN and subsequent migration to infected peripheral tissues preceded that of the CD8⁺ T cells, potentially giving the helper T cells a temporal advantage.

Rapid CD4⁺ T Cell Priming in LN Follows Localized Virus Infection

The previous experiments suggested that CD4⁺ T cell responses developed more rapidly than CD8⁺ T cell responses after localized skin HSV infection. To examine whether this corresponded with initial activation and expansion of CD4⁺ T cells preceding CD8⁺ T cells, we labeled congenically marked gDT-II and gBT-I T cells with CellTrace Violet prior to adoptive transfer into mice. After skin HSV infection, virus-specific T cells were assessed for upregulation of the early activation marker CD69. Within 12 hr of infection, a proportion of gDT-II CD4⁺ T cells had upregulated CD69, whereas expression on the gBT-I CD8⁺ T cells remained undetectable until 24–48 hr after infection (Figures 2A and 2B). CD4⁺ T cells responding to the infection began dividing within 48 hr, demonstrated by CellTrace Violet dilution in a proportion of cells (Figures 2A and 2C). In contrast, CD8⁺ T cells showed delayed proliferation beginning 2–3 days after

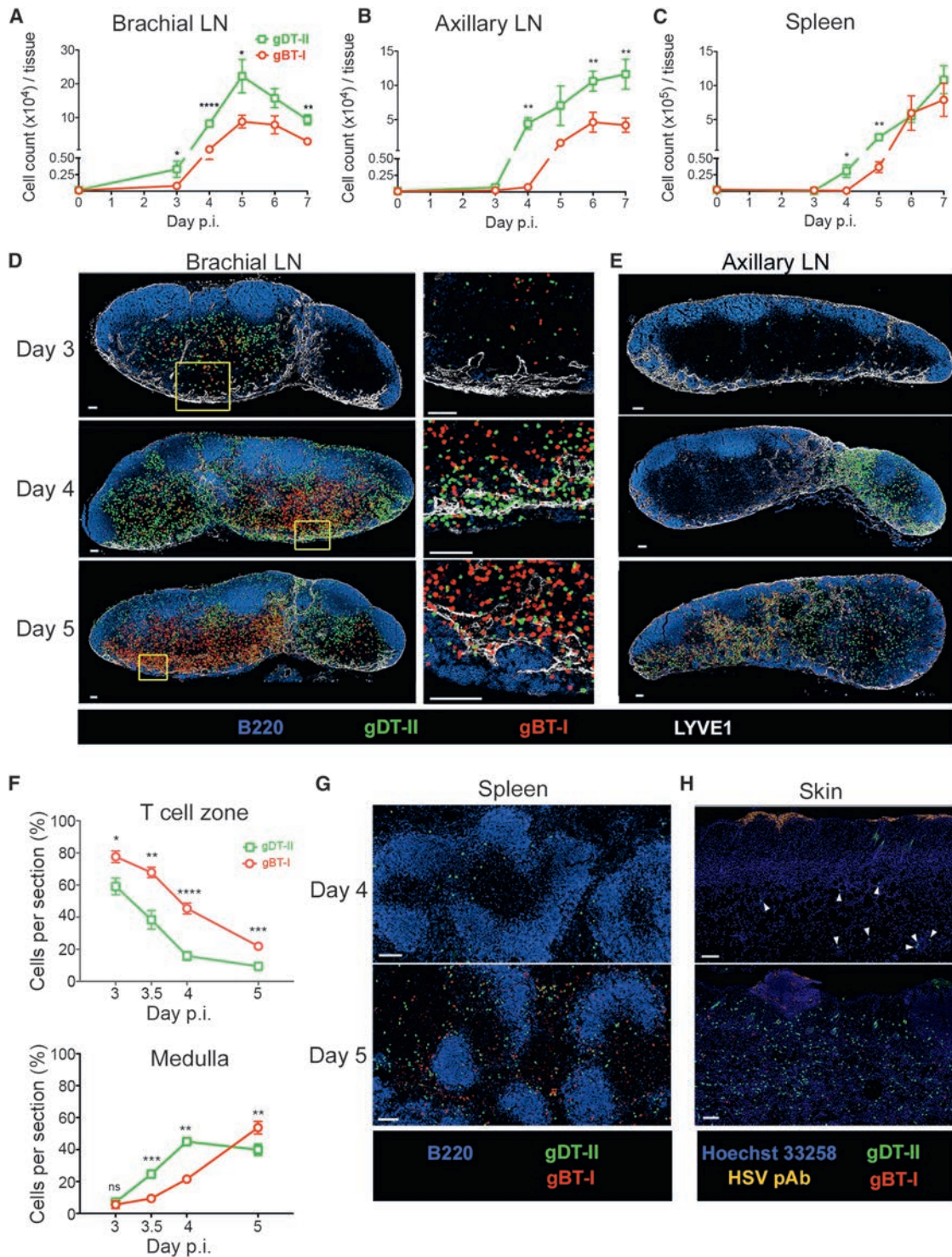


Figure 1. Distinct Kinetics and Spatiotemporal Distribution of CD4⁺ and CD8⁺ T Cells after Cutaneous HSV-1 Infection
 gDT-II CD4⁺ and gBT-I CD8⁺ T cells were cotransferred into recipient mice 1 day prior to epicutaneous HSV-1 infection. (A–C) Total number of gDT-II CD4⁺ (green) and gBT-I CD8⁺ (red) T cells recovered from draining brachial LN (A), downstream axillary LN (B), and the spleen (C) over the course of HSV-1 infection. Data pooled from 2 independent experiments; n = 5–7 mice for each time point. (D) Confocal images showing spatial distribution of gDT-II CD4⁺ (green) and gBT-I CD8⁺ (red) T cells in draining brachial LNs from days 3–5 p.i.; magnified regions of the medulla are shown in the panels on the right. LYVE-1⁺ lymphatic vessels are stained in white and B220⁺ B cells in blue. (E) Confocal images showing the infiltration of gDT-II CD4⁺ (green) and gBT-I CD8⁺ (red) T cells into the afferent axillary LNs from days 3–5 p.i.

(legend continued on next page)

infection. This could not be attributed to differential responsiveness of the two transgenic T cell subsets, because both responded after subcutaneous inoculation of titrated doses of peptide, with gBT-I cells displaying slightly greater sensitivity (Figure S2A). When we examined early CD8⁺ T cell activation in MHC-II-deficient mice where CD4⁺ T cell responses are absent, a further delay in CD69 upregulation by gBT-I CD8⁺ T cells was evident (Figure 2D). This showed that asynchronous activation of CD4⁺ and CD8⁺ T cells occurred after localized skin HSV infection. We have previously shown that CD4⁺ T cell help is required for optimal CD8⁺ T cell priming to HSV infection (Smith et al., 2004). These data further suggest that CD4⁺ T cell help is required to promote rapid CTL priming.

CD4⁺ T Cells Cluster in LN Early after Infection

We next sought to examine the dynamics of these early T cell priming events after HSV infection. To do this, we employed a modified flank HSV infection model that resulted in priming of the T cell responses in the draining inguinal LN. The kinetics of CD4⁺ and CD8⁺ T cell activation, proliferation, and migration was the same using this method compared to the standard site of flank infection (Figures S2B–S2D). We then utilized intravital 2-photon microscopy to visualize the behavior of responding gDT-II and gBT-I T cells in the draining LN early after infection. Within 12 hr of infection, we observed marked clustering of the gDT-II CD4⁺ T cells in the T cell zone that displayed a significantly reduced average velocity in comparison to T cells migrating in LN of naive uninfected mice (Figures 3A–3C, Movie S1). Most notably, gBT-I CD8⁺ T cells in the immediate vicinity of CD4⁺ T cell clusters showed no obvious change in motility or behavior. The CD8⁺ T cells did not cluster in the LN at this early time point, suggesting that they were ignorant of the APC driving CD4⁺ T cell activation. In accordance with the temporal proliferation data shown in Figure 2, these data indicated that DCs presenting antigen (Ag) on MHC-I were not yet present or accessible to the CD8⁺ T cells at this early stage.

When we examined CD4⁺ and CD8⁺ T cell behavior 40–48 hr after infection, we observed that both T cell subsets now formed dynamic clusters (Figures 3A and 3B, Movie S2). Both populations of cells displayed a reduced overall migrational velocity and greater mean confinement and a substantial proportion of each cell type participated in clusters within each imaging volume (Figures 3C–3E and S2E). We noted that many of the clusters contained mostly CD4⁺ or CD8⁺ T cells as opposed to relatively equal proportions of both cell types. Conspicuously, we also observed transient interactions between migrating CD4⁺ T cells that visited CD8⁺ T cells clusters. Clustering of the T cells was antigen specific—no clustering was observed among non-specific OT-II and OT-I T cells present in the LN at the same time (Figures 3F–3H and S2F, Movie S3). We did find that the OT-II CD4⁺ T cells showed a slightly reduced average velocity in the LN of HSV-infected mice. This indicated that the microenvironment of the inflamed LN also influenced T cell migration.

To enumerate T cell clustering in the LN, and because intravital 2-photon microscopy is restricted to the first few hundred microns of the tissue (preventing imaging of the deep paracortex), we imaged thick whole LN sections and quantitated CD4⁺ and CD8⁺ T cell clusters. As expected from our intravital movies, we observed extensive clustering of gDT-II T cells 18 hr after infection, with approximately 20% of the CD4⁺ T cells involved in clusters throughout the LN paracortex, whereas gBT-I T cells did not cluster (Figures 4A, 4B, and 4E). Similar numbers of gDT-II and gBT-I clusters were found 42 hr after infection (Figures 4C–4E). Given the dynamic nature of the clusters we observed by intravital 2-photon microscopy, whereby some cells were seen entering and exiting clusters, this static analysis of cluster frequency might reflect an underestimate of the true proportion of cells involved in clusters. When we assessed the composition of the clusters, we found that a substantial proportion was composed of only CD4⁺ or CD8⁺ T cells (Figure 4F). This supported our intravital imaging data, raising the possibility that the homogenous clusters of T cells were interacting with different DCs. Consistent with differential DC subset presentation, we also noted that CD8⁺ T cells formed clusters in more localized regions of the LN paracortex in all mice examined, as opposed to CD4⁺ T cells clusters that were distributed across one or both lobes of the draining LN (Figure 4D).

Migratory DCs Activate CD4⁺ T Cells Early after Infection

The above data suggested that the temporally and spatially segregated clusters of CD4⁺ and CD8⁺ T cells might be interacting with different APCs specializing in presentation of antigens on MHC class I or II. Although we observed predominantly CD4⁺ T cells clustering in the early phase of the response (12–24 hr), very rare CD8⁺ T cell clusters were observed in some of the mice (one to two clusters in two mice out of eight). Recent studies have shown that priming of CD8⁺ T cell responses to lymph-borne virus infection involves clustering of CD8⁺ T cells with infected cells (Hickman et al., 2011; Kastenmüller et al., 2013). We could not detect drainage of fluorescently labeled HSV from the site of infection on the flank to the draining LN after infection (Figures S3A and S3B). We were also unable to detect any virus in the LN within the first 3 days of HSV flank infection by microscopy or plaque assay. In contrast, after footpad inoculation, lymph-borne virus rapidly entered the draining LN and localized to the SCS where we could distinguish infected cells, including CD169⁺ SCS macrophages (Figure S3C). We observed CD8⁺ T cell clusters around virus-infected cells in the interfollicular regions and outer paracortex (cortical ridge) after lymph-borne infection (Figure S3D). Thus, CD8⁺ T cells clustered early with infected cells when virus drained to the LN. Moreover, proliferation of the CD4⁺ and CD8⁺ T cells proceeded synchronously after lymph-borne infection (Figures S3E and S3F). Taken together, this suggests that there was no significant contribution to T cell priming by directly infected cells in the LN after localized skin HSV infection, the focus of our studies.

(F) Proportion of gDT-II CD4⁺ (green) and gBT-I CD8⁺ (red) T cells occupying the T cell zone (top) and medulla (bottom) of the draining brachial LN from days 3–5 p.i., quantitated per LN section. Data pooled from 2 independent experiments; n = 5–6 mice per time point. See also Figure S1.

(G and H) Confocal images of the spleen (G) and infected skin (H) from days 4–5 p.i.

All scale bars denote 100 μm. Error bars represent mean ± SEM. *p < 0.05; **p < 0.01; ***p < 0.001; ****p < 0.0001; ns, not significant.

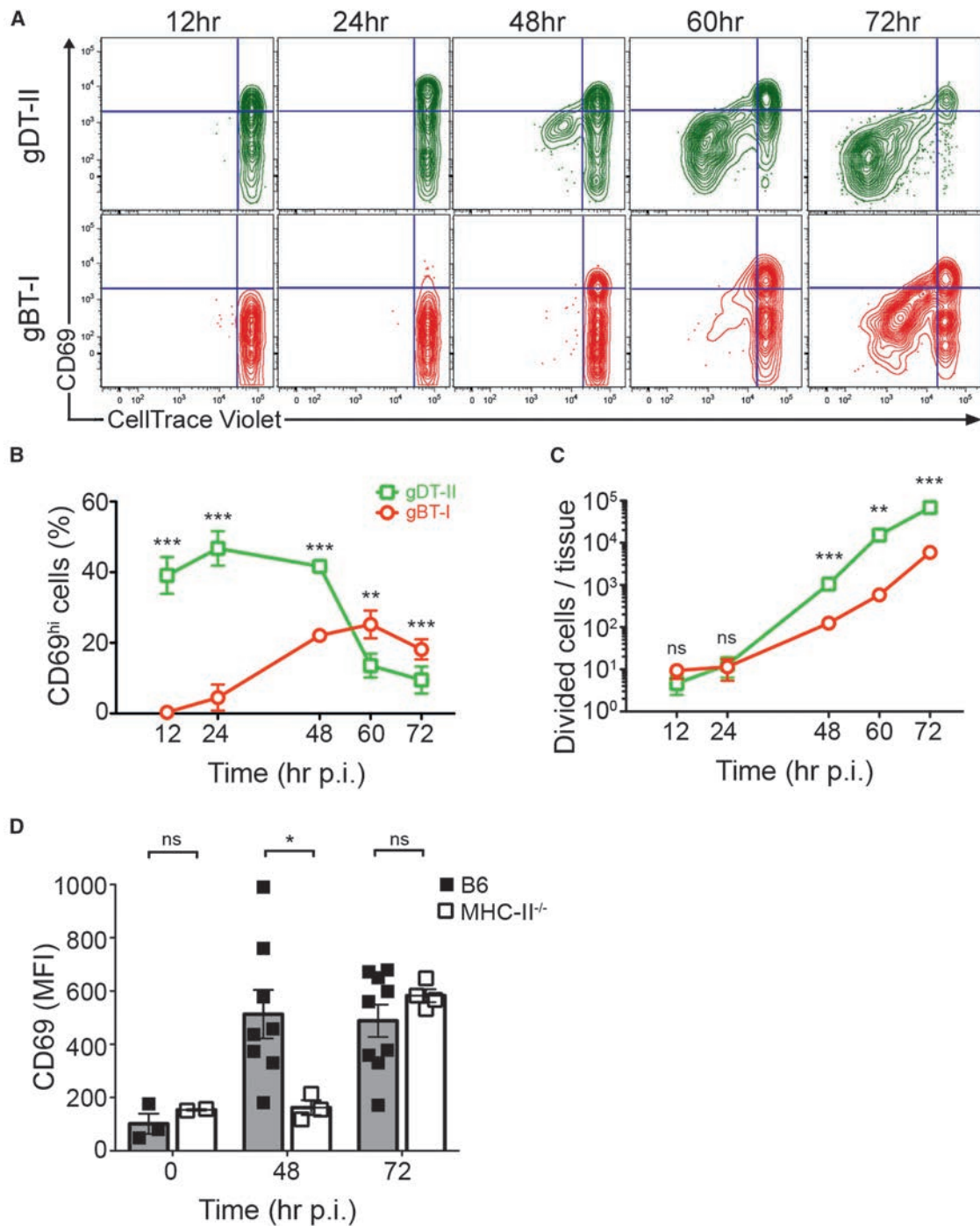


Figure 2. Differential Priming Kinetics of CD4⁺ and CD8⁺ T Cells after Cutaneous HSV-1 Infection

CellTrace Violet-labeled gDT-II CD4⁺ and gBT-I CD8⁺ T cells were adoptively transferred into recipient mice 1 day prior to epicutaneous HSV-1 infection.

(A) Upregulation of the early activation marker CD69 by gDT-II CD4⁺ (top, green) and gBT-I CD8⁺ (bottom, red) T cells in draining brachial LN from 12 to 72 hr p.i.

(B) Proportion of CD69^{hi} gDT-II CD4⁺ and gBT-I CD8⁺ T cells in draining brachial LN over 72 hr p.i.

(C) Number of divided cells (CellTrace Violet₀) recovered per draining brachial LN over 72 hr p.i.

(D) Mean fluorescence intensity of gBT-I CD8⁺ T cells in draining brachial LN of B6 and MHC-II^{-/-} mice at various time points after infection.

Data in (A)–(C) pooled from 2–3 independent experiments; n = 6–12 mice per time point. Error bars represent mean ± SEM. *p < 0.05; **p < 0.01; ***p < 0.001; ns, not significant. See also Figure S2.

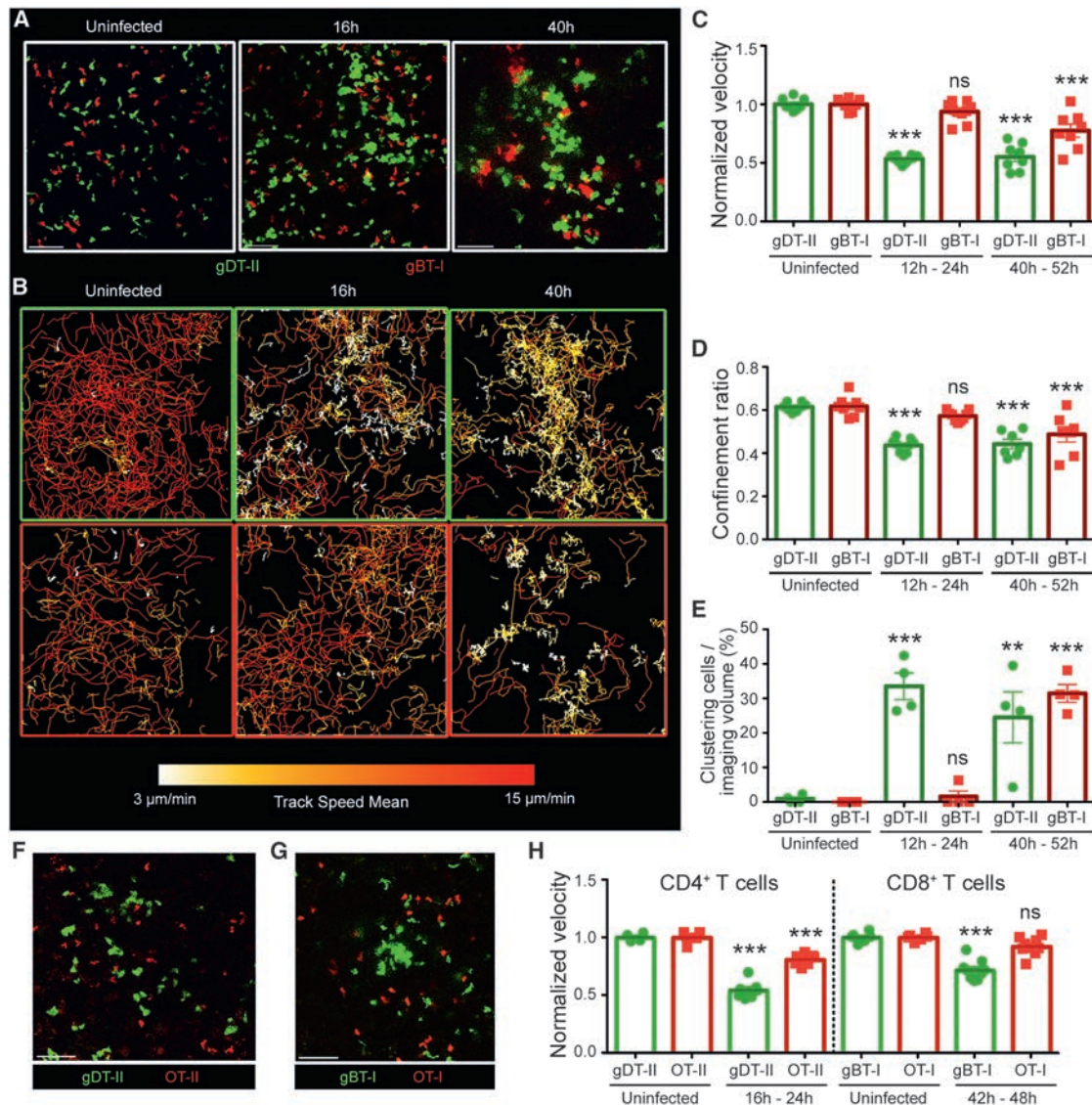
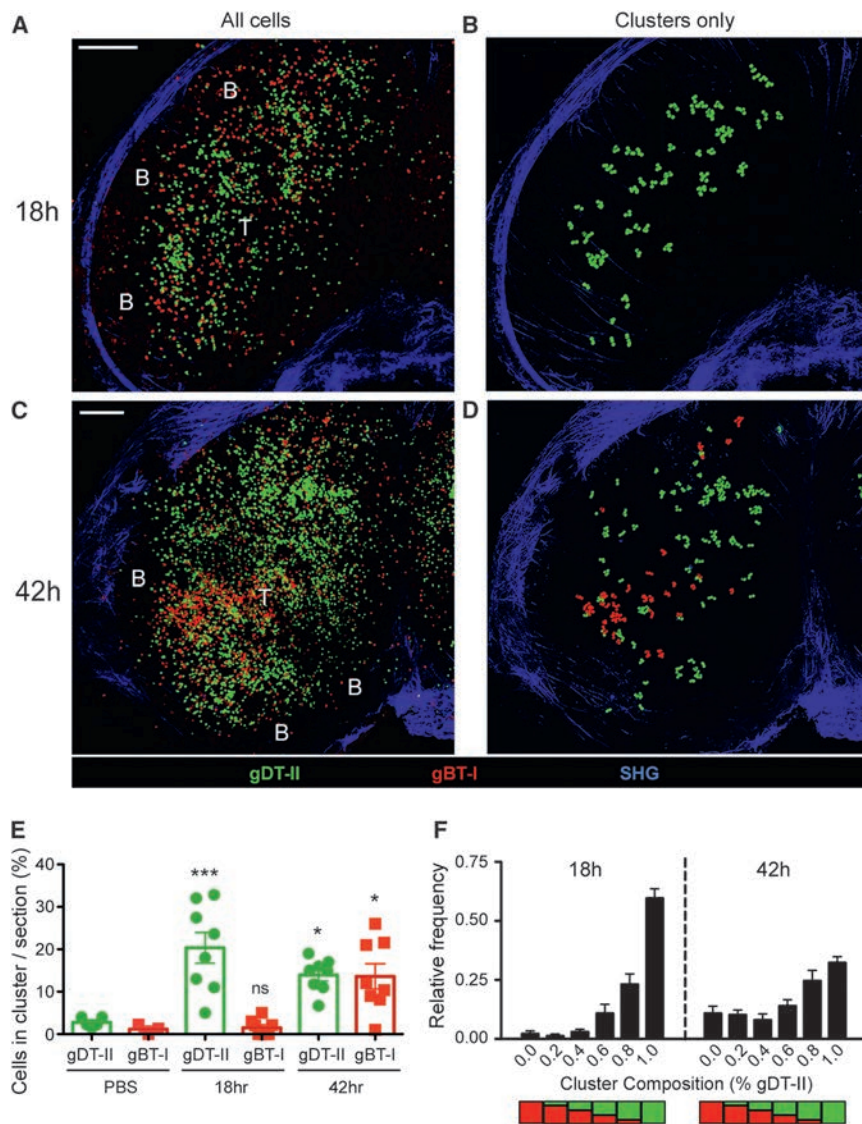


Figure 3. Early Clustering of HSV-Specific CD4⁺ T Cells in Draining LN

gDT-II.EGFP CD4⁺ and gBT-I.DsRed CD8⁺ T cells were adoptively transferred into recipient mice prior to epicutaneous HSV-1 infection. (A) Maximum intensity projection images showing clustering of gDT-II CD4⁺ (green) and gBT-I CD8⁺ (red) T cells in the T cell zone on the inguinal LN (imaging depth ~150–200 μm under LN capsule) at different phases of infection: uninfected (left), early (16 hr, middle), and late (40 hr, right). See also Movies S1 and S2. (B) Cell tracks of gDT-II CD4⁺ (top) and gBT-I CD8⁺ (bottom) color coded to display mean track velocity at the indicated time points. Red tracks correspond to higher track velocities and white tracks show slower cell tracks. Data from Movies S1 and S2. (C and D) Mean velocity (C) and mean confinement ratio (D) of cell tracks normalized to naive cells. Each data point represents the mean velocity (C) or confinement ratio (D) of all cell tracks per movie. Data pooled from at least two independent experiments; n = 2–4 movies each from 2–6 mice per time point. (E) Proportion of clustering cells in the LN after infection. Each data point represents the proportion of clustering gDT-II CD4⁺ and gBT-I CD8⁺ T cells in each imaging volume. Data pooled from 2 independent experiments; n = 4 mice per time point. (F and G) Maximum intensity projection images showing a snapshot of the behavior of (F) gDT-II and OT-II CD4⁺ T cells and (G) gBT-I and OT-I CD8⁺ T cells after infection. See also Movie S3. (H) Mean velocity of cell tracks normalized to migration in uninfected mice. Each data point represents the mean velocity of all cell tracks per movie. Data pooled from 2 independent experiments; n = 1–2 movies each from 4–7 mice. Error bars represent mean ± SEM. *p < 0.05; **p < 0.01; ***p < 0.001; ns, not significant. See also Figure S2.

The preceding experiments showed that temporally segregated antigen presentation occurred after flank HSV infection. Prior studies have shown that migratory subsets of DCs are essential for CD8⁺ T cell responses after skin HSV infection (Allan et al., 2006; Stock et al., 2004). To examine whether migratory

APCs were involved in the priming of the CD4⁺ T cell response *in vivo* after localized HSV infection, we painted the flank skin of mice with the fluorescent dye TRITC prior to virus inoculation. This enabled tracking and visualization of DCs migrating from the skin to the draining LN (Figure S4). Migratory TRITC⁺ APCs



entered the LN via the SCS and accumulated in the paracortex by 18 hr. By 40 hr after infection, the majority of the TRITC⁺ cells had migrated through the paracortex and were concentrated closer to medullary regions, similar to the path of intralymphatically injected DCs observed migrating through LN (Braun et al., 2011).

Clusters of gDT-II CD4⁺ T cells and TRITC⁺ cells formed early after infection (Figure 5A). Later in the response (40–48 hr), when both CD4⁺ and CD8⁺ T cell clusters were established, few clusters were directly associated with TRITC⁺ migratory APCs. These data indicated that early activation of CD4⁺ T cells, but not CD8⁺ T cells, probably involved interactions with migratory DCs. To test this hypothesis, we co-stained thick sections of LN tissue with antibodies against CD69 to visualize where the recently activated T cells localized. In the early phase of the response, CD69 was upregulated on gDT-II CD4⁺ T cells clustering around TRITC⁺ APCs (Figure 5B). At this time (20 hr), gBT-I CD8⁺ T cells remained CD69 negative. When we examined LNs a day later, CD69 was upregulated on CD8⁺ T cells, but these cells were not clustering with TRITC⁺ cells.

PBS (Figures 5C–5E, Movies S4 and S5). Together, these data reveal that CD4⁺ T cells were being activated by migratory APCs after localized skin HSV infection. In contrast, CD8⁺ T cells did not interact with migratory DCs and remained naive during the early phase of the response in the absence of direct virus drainage.

XCR1⁺ LN-Resident DCs Are Required for CD8⁺ T Cell Priming and CD4⁺ T Cell Help

Migratory APCs are necessary for CD8⁺ T cell priming after skin HSV infection (Allan et al., 2006; Stock et al., 2004). We hypothesized that migrants could present skin-acquired, virion-derived antigens on MHC-II, yet were unable to cross-present viral antigens to CD8⁺ T cells. In a prior study we found that antigen presentation for the immunodominant gBT-I epitope (gB₄₉₈₋₅₀₅) required de novo synthesis, yet expression was rapid and was detectable by CTL within 2 hr of infection (Mueller et al., 2003). When we infected mice on the skin with UV-inactivated HSV (UV-HSV), only gDT-II T cells were activated (Figure S5),

Figure 4. Spatial and Temporal Distribution of T Cell Clusters after Cutaneous HSV-1 Infection

gDT-II.EGFP CD4⁺ and gBT-I.DsRed CD8⁺ T cells were adoptively transferred into recipient mice 1 day prior to epicutaneous HSV-1 infection. (A and C) Maximum intensity projection images of thick inguinal LN sections (imaging volume 100–120 μ m thickness) showing the distribution of gDT-II CD4⁺ (green) and gBT-I CD8⁺ (red) cells during early (A) and late (C) phase of infection. (B and D) Location of clustering cells in ILN sections corresponding to (A) and (C), represented in green (gDT-II CD4⁺) or red (gBT-I CD8⁺) spots. (E) Percentage of clustering cells per LN section. (F) Composition of each cluster comprised of a minimum of four cells. A value of 1.0 represents homogenous (100%) gDT-II CD4⁺ T cell clusters and 0.0 represents 100% gBT-I CD8⁺ T cell clusters. Error bars represent mean \pm SEM. ***p* < 0.01; ****p* < 0.001; ns, not significant. Data pooled from 2 independent experiments; *n* = 4–8 mice per time point. See also Figure S3.

We next examined the dynamics of the virus-specific T cell interactions with the TRITC⁺ migratory APCs in the LN via intravital 2-photon microscopy. The gDT-II CD4⁺ T cells swarmed around a subset of TRITC⁺ migratory APCs (Figure 5C, Movies S4 and S5). CD4⁺ T cells participating in these dynamic clusters with TRITC⁺ APCs demonstrated both transient and stable interactions, with many cells remaining in contact with APC for >30 min (Figures 5D and 5E). As anticipated, CD8⁺ T cells engaged only transiently with the TRITC⁺ DCs and did not slow down, similar to that after mock infection with

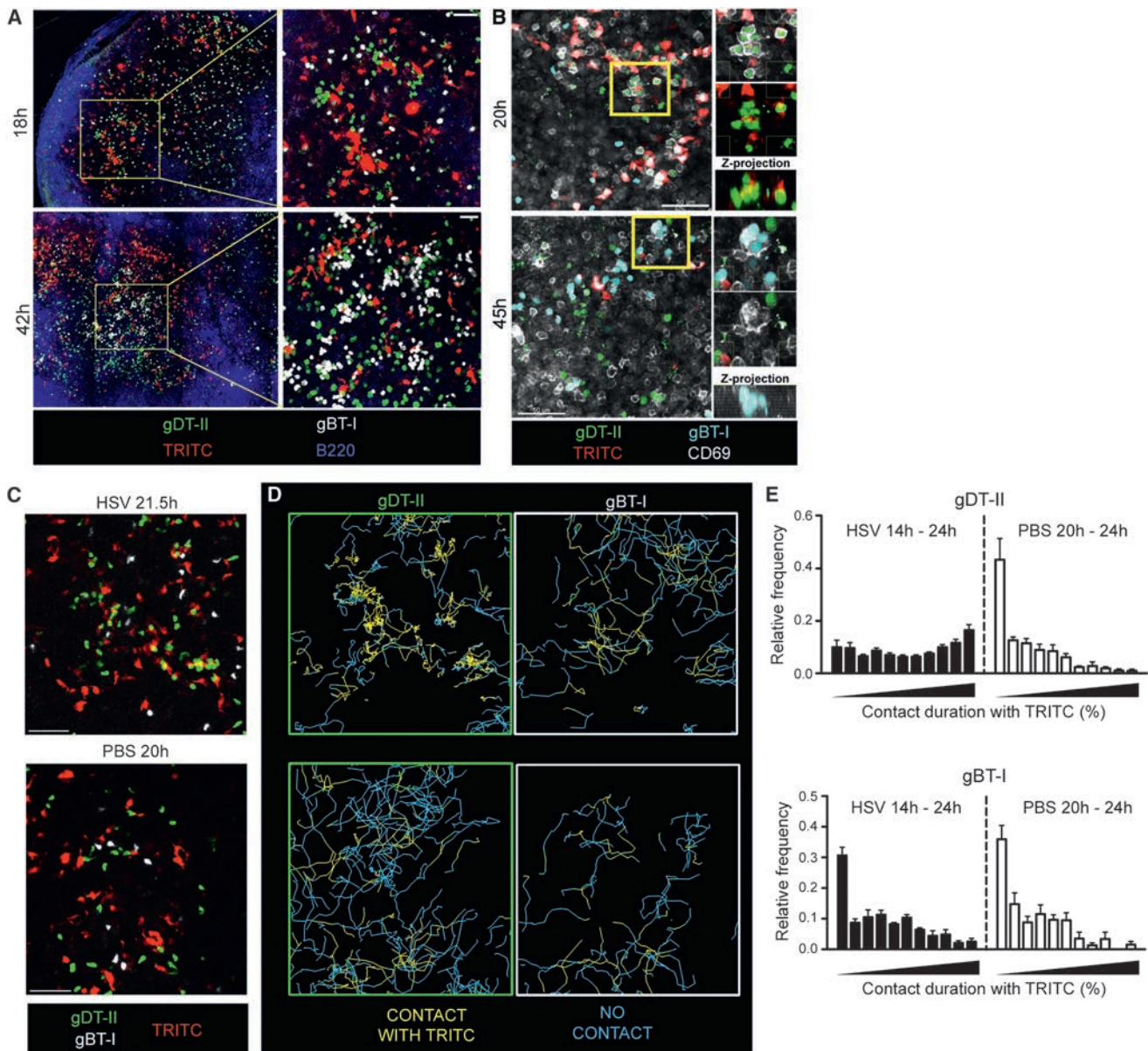


Figure 5. HSV-Specific CD4⁺ T Cells Preferentially Interact with Migratory APCs during Early HSV-1 Infection

(A) Maximum intensity projection images of thick inguinal LN sections showing the localization of TRITC⁺ cells (red), gDT-II CD4⁺ (green), and gBT-I CD8⁺ (white) T cells at early (top) and late (bottom) phases of infection. Scale bars represent 100 μ m.

(B) Maximum intensity projection images of thick inguinal LN sections showing anti-CD69 staining (white), gDT-II (green), gBT-I (cyan), and TRITC (red). Scale bars represent 50 μ m.

(C) Maximum intensity projection images from time-lapse movies showing interactions between gDT-II CD4⁺ (green) and gBT-I CD8⁺ (white) T cells with TRITC-painted cells (red) in early infected (top) or mock infected (bottom) mice. Scale bars represent 50 μ m. See also Movie S4.

(D) Cell tracks color-coded to show contact (yellow) or no contact (light blue) with TRITC⁺ DCs. gDT-II CD4⁺ (green box) and gBT-I CD8⁺ (white box) tracks correspond to Movie S4. See also Movie S5.

(E) Contact duration with TRITC⁺ cells by gDT-II CD4⁺ (left) and gBT-I CD8⁺ (right) T cells in early infected (black bars) and mock infected (white bars) mice. Data pooled from 1–2 independent experiments; n = 4–9 mice per time point. See also Figure S4. Error bars represent mean \pm SEM.

further supporting a requirement for de novo synthesis of gB for MHC-I presentation while demonstrating that virion-derived antigen could be presented on MHC-II. Thus, skin migratory CD11b⁺ DCs were unable to cross-present antigens on MHC-I and/or the availability of gB for cross-presentation was insufficient prior to viral protein synthesis.

The above data demonstrated that CD4⁺ T cells were activated by migratory DCs, yet we had previously shown that the LN-resident CD8 α ⁺ DCs are the only cells capable of stimulating CD8⁺ T cells ex vivo after HSV infection (Bedoui et al., 2009). We next examined the T cell-DC interactions driving CD8⁺ T cell clustering and activation by 2-photon microscopy in *Itgax*-EYFP mice

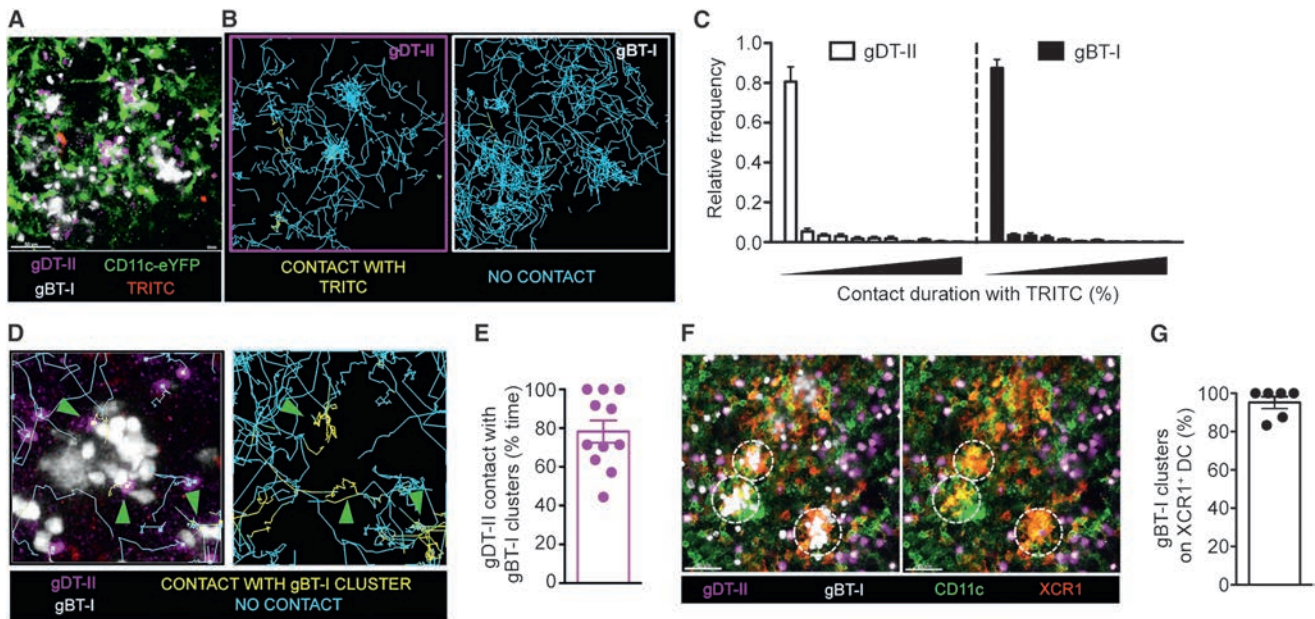


Figure 6. CD8⁺ T Cell Priming by XCR1⁺ LN-Resident DCs

(A) Maximum intensity projection images from time-lapse movies of ILN in HSV-infected *Itgax*-EYFP mice showing distinct clustering of gBT-I CD8⁺ T cells (white) with non-migratory DCs (green). Scale bars represent 50 μ m. See also Movie S6.

(B) Cell tracks color-coded to show contact (yellow) or no contact (light blue) with TRITC⁺ DCs. Tracks of gDT-II CD4⁺ (left) and gBT-I CD8⁺ (right) correspond to Movie S6.

(C) Duration of contact between gDT-II CD4⁺ and gBT-I CD8⁺ T cells with TRITC⁺ cells. Data pooled from 2 independent experiments, $n = 5$ –6 mice per group. Error bars represent mean \pm SEM.

(D) 2P image of inguinal LN showing gDT-II CD4⁺ T cells (purple) interacting with gBT-I CD8⁺ T cell clusters (white). Cell tracks color-coded to show contact with gBT-I clusters (yellow) and non-contact (blue) are depicted with a history of 20 frames. Full cell tracks are shown on the right panel. Green arrows denote CD4⁺ T cells in contact with gBT-I clusters. See also Movie S7.

(E) Proportion of time gDT-II CD4⁺ T cells were in contact with gBT-I CD8⁺ T cell clusters per movie. Only CD4⁺ T cells establishing contact for >5 min with gBT-I clusters were analyzed. Data from one representative experiment of two are shown.

(F) Maximum intensity projection images of thick inguinal LN sections showing localization of gBT-I CD8⁺ T cell clusters (white) relative to XCR1⁺ (red) CD11c⁺ (green) DCs. Dotted circles denote gBT-I clusters without gBT-I CD8⁺ T cells. Scale bars represent 40 μ m.

(G) Fraction of gBT-I CD8⁺ T cell clusters closely associated with XCR1⁺CD11c⁺ DCs per mouse. Data pooled from 2 independent experiments; $n = 6$ mice. See also Figure S5. Error bars represent mean \pm SEM.

(commonly known as CD11c-EYFP) to visualize both recent skin migrants (TRITC⁺CD11c⁺) and LN-resident DCs (TRITC⁻CD11c⁺). The gBT-I T cells clustered on TRITC⁻ cells in the draining LN 40–48 hr after HSV infection (Figure 6A and Movie S6). These DCs expressed less CD11c, indicative of mature DCs, which upregulate MHC-II and downregulate CD11c upon activation (Singh-Jasuja et al., 2013). Both gBT-I and gDT-II T cells interacted only minimally with TRITC⁺ migrants at this phase of the response (Figure 6C). Notably, the clusters of CD8⁺ T cells around CD11c⁺ DCs were frequently visited by CD4⁺ T cells that interacted with CD8⁺ T cells for substantial periods (Figures 6D and 6E and Movie S7). Thus, after activation by migratory DCs, CD4⁺ T cells access CD8⁺ T cell clusters on resident DCs, potentially to provide DC-licensing signals involved in CD8⁺ T cell priming.

We assessed the identity of the DCs involved in CD8⁺ T cell clustering. Because CD8 α ⁺ DCs are also defined by specific expression of the chemokine receptor XCR1 (Croizat et al., 2011; Dorner et al., 2009), we co-stained LN tissues with antibodies against XCR1 and CD11c. The clusters of CD8⁺ T cells in LN 42 hr after HSV infection occurred almost exclusively on XCR1⁺ DCs (Figures 6F and 6G). Thus, although migratory DCs

first prime CD4⁺ T cells after localized HSV infection, CD8⁺ T cell activation is delayed until resident CD8 α ⁺XCR1⁺ DCs acquire the capacity to stimulate CTLs. Such temporally separated priming of CD4⁺ T cells by DCs specialized in MHC-II presentation prior to providing help for CD8⁺ T cell responses highlights the key role played by XCR1⁺ DCs in CD8⁺ T cell activation and the provision of help.

DISCUSSION

The interactions between T cells and DCs and the requirements for T cell activation are increasingly being revealed through intravital imaging. Nevertheless, how both CD4⁺ and CD8⁺ T cell responses are initiated after infection and the involvement of different DC subsets in the coordination of T cell priming remains uncertain. To explore this, we utilized peripheral infection with HSV-1, a virus that remains localized within the tissues and requires antigen transport by migratory skin DCs to prime T cell responses in the LN. We found that activation of CD4⁺ and CD8⁺ T cells was temporally separated and involved antigen presentation by different subsets of DCs. CD4⁺ T cells clustered on

migratory DCs that arrived in the draining LN within 9 hr of infection, resulting in their activation. In contrast, CD8⁺ T cells needed to wait for XCR1⁺ LN-resident DCs to cross-present antigens and facilitate T cell clustering and activation. CD4⁺ T cells also interacted with late CD8⁺ T cell-XCR1⁺ DC clusters, defining these DCs as a critical platform for the delivery of CD4⁺ T cell help to CD8⁺ T cells.

These findings provide insight into the complex interactions involved in the priming of T cell responses to peripheral infection. Rapid activation of CD4⁺ T cells might enable these cells to provide help via the licensing of DCs. Although it is well established that CD4⁺ T cell help is required for maximal CD8⁺ T cell responses to infections including HSV, as well as for fully functional memory T cell populations, the mechanics of this process have not been determined. When and where this occurs, whether CD4⁺ T cells are activated by the same DCs through which they provide help, or through other DCs, are all questions that need answering. The provision of help requires that CD4⁺ T cells and CD8⁺ T cells interact with the same DCs, though whether this process involves simultaneous interactions by CD4⁺ and CD8⁺ T cells with DCs or sequential interactions is also not known. Moreover, in order to provide help, CD4⁺ T cells must first be activated and upregulate CD40L, implicating delayed kinetics of help for CTLs until the CD4⁺ T cells are activated and capable of licensing DCs.

Here we have provided substantial insight into these dynamic events and demonstrate that migratory DCs activated CD4⁺ T cells prior to the initiation of CD8⁺ T cell clustering on XCR1⁺ DCs. CD4⁺ T cells then interacted in a dynamic fashion with clusters of CD8⁺ T cells being stimulated by LN-resident DCs. These studies raise the possibility that pre-activated CD4⁺ T cells license CD8 α ⁺XCR1⁺ DCs during CD8⁺ T cell engagement, which differs for the model where CD4⁺ T cells attract naive CD8⁺ T cells to licensed DCs (Castellino et al., 2006). However, we also observed some clusters of CD4⁺ T cells on LN-resident DCs that did not involve CD8⁺ T cell clustering, suggesting that licensing of some DCs by CD4⁺ T cells could also occur prior to CD8⁺ T cell engagement. Importantly, our observations suggest that such CD4⁺-DC helper interactions are dynamic and short lived. Although we introduced a higher frequency of naive T cells to image these interactions, at lower precursor frequencies efficient licensing of multiple DCs by rare antigen-specific CD4⁺ T cells might necessitate that early-activated helper cells move rapidly between APCs for CTL priming.

The exact contribution of different DC subsets to CD4⁺ T cell priming is not known. Multiple migratory and lymphoid tissue-resident DC subsets have been shown to have the capacity to present antigen to CD4⁺ T cells *ex vivo* (Bedoui et al., 2009; Heath and Carbone, 2009; Kim and Braciale, 2009; Lee et al., 2009; Zhao et al., 2003). In our model, the migratory subset involved in antigen presentation early in the response is primarily the CD11b⁺ dermal DCs, whereas the skin CD103⁺ DC subset does not contribute until later in the response after secondary viral spread (Bedoui et al., 2009). Here we have shown that migratory DCs played a key role in activating CD4⁺ T cells, yet were unable to stimulate CD8⁺ T cell *in vivo*. Whether early CD4⁺ T cell activation by migratory DCs is sufficient for optimal effector cell generation or whether

signals from XCR1⁺ DCs are also required for complete maturation and the generation of a robust memory population will be important to determine.

The early activation of CD4⁺ T cells precipitated rapid intranodal reorganization to B cell follicles and medullary regions, egress to downstream lymph nodes, and more rapid accumulation at the site of infection. These data might help explain how CD4⁺ T cells facilitate recruitment of CD8⁺ T cells in the LN to the infected tissues early after infection (Kumamoto et al., 2011; Nakanishi et al., 2009). Though whether such a temporal difference occurs in other infections remains unclear given that we have shown here that lymph-borne infection after subcutaneous injection of virus resulted in synchronous kinetics of CD4⁺ and CD8⁺ T cell activation. The epicutaneous HSV-1 infection model used here represents a highly localized peripheral infection that primes robust T cell responses and memory formation. In contrast to beads applied to scarified skin (Gerner et al., 2015), we did not find detectable HSV infection in the LN after localized infection, only after subcutaneous inoculation. We found that the early events in T cell priming to localized infection differed slightly from that after lymph-borne spread of virus, the latter of which resulted in early activation of CD8⁺ T cells after clustering with infected cells. HSV binds efficiently to receptors in the skin and is restricted by the basement membrane and thus does not drain efficiently to LN (Mueller et al., 2002b; Weeks et al., 2000; Zhao et al., 2003). Infection of DCs in the LN has been shown to be negligible after skin HSV infection (Allan et al., 2006). Although we can't completely exclude that a small number of DCs in the LN are infected, our data suggest that cross presentation is the predominant pathway involved in priming the CD8⁺ T cell response via XCR1⁺ DCs.

Taken together, we have identified temporally staggered interactions with different DCs for the priming of CD4⁺ and CD8⁺ T cell responses to a localized virus infection. Our data suggest a model whereby migratory DCs transport antigens from the skin to the draining LN and activate CD4⁺ T cells. Yet, migratory skin DCs are unable to stimulate CD8⁺ T cells, which require antigen to be delivered to XCR1⁺ LN-resident DCs for cross-presentation. Crucially, CD8⁺ T cell clustering with LN-resident DCs involved concurrent interactions with CD4⁺ T cells, emphasizing the central role that XCR1⁺ DCs play in orchestrating both CTL priming and the delivery of help during localized infection.

EXPERIMENTAL PROCEDURES

Mice and Infections

C57BL/6, gBT-I (Mueller et al., 2002a), gBT-I.xB6.SJL-PtprcaPep3b/BoyJ (gBT-I.CD45.1), gBT-I.uGFP, gBT-I.dsRed, gDT-II (Bedoui et al., 2009), gDT-II.uGFP, gDT-II x B6.CD45.1, OT-I.uGFP, OT-II.dsRed, *Irgax*-EYFP, and MHC-II deficient (AB⁰) mice were bred in the Department of Microbiology and Immunology, The University of Melbourne. gBT-I and gDT-II encode transgenes expressing T cell receptor recognizing the HSV-1 glycoprotein B-derived epitope gB₄₉₈₋₅₀₅ and glycoprotein D-derived epitope gD₃₁₅₋₃₂₇, respectively. Animal experiments were approved by The University of Melbourne Animal Ethics Committee. Epicutaneous and subcutaneous infections with HSV-1 (KOS strain) were performed as described elsewhere (van Lint et al., 2004; Coles et al., 2002). For imaging experiments, scarification was performed at the hind flank, near the transition of torso-hind limb region to allow drainage to inguinal LN. See also Supplemental Experimental Procedures.

T Cell Enrichment, Labeling, and Adoptive Transfer

T cells were enriched from naive lymph nodes and/or spleens of female transgenic mice through negative enrichment of CD4⁺ or CD8⁺ T cells, for gDT-II and gBT-I, respectively. For gDT-II cells, further positive magnetic enrichment was performed as described elsewhere (Bedoui et al., 2009). See also Supplemental Experimental Procedures.

TRITC Painting

Tetramethylrhodamine-5-isothiocyanate (TRITC; Life Technologies) was dissolved in DMSO and diluted to 0.5% (v/v) in acetone. The TRITC solution was painted on a 1 cm² diameter region of skin in a 10 μ l volume on the depilated flank of anesthetized mice and allowed to dry. Mice were infected with HSV 4–6 hr after TRITC application.

Cell Isolation and Flow Cytometry

Single-cell suspensions were resuspended in PBS containing FCS (2%) and EDTA (5 mM) for antibody staining. For DC isolation, lymph nodes were disrupted with scalpel blade and incubated in 1 mg/ml collagenase type III (Worthington) and 20 μ g/ml DNase medium for 20 min before addition of 0.1 M EDTA. Cells were then filtered and resuspended as above for antibody staining. Propidium iodide was added to the samples prior to acquisition by flow cytometry (BD FACS Canto or BD Fortessa). Data were analyzed with FlowJo software (TreeStar). See also Supplemental Experimental Procedures.

Immunofluorescence and Confocal Microscopy

Lymph nodes and spleens were harvested and fixed in PLP fixative for 6–8 hr, washed in PBS twice for 10 min, and incubated in 20% sucrose overnight at 4°C. Tissue sections were cut at 12 μ m thickness with a cryostat (Leica CM3050S) and air-dried before being fixed in acetone for 5 min, dried, and then blocked for 20 min (Protein Block X0909, DAKO) at RT. Sections were then stained with primary antibodies for 1.5 hr, washed in PBS for 10 min, and stained with secondary antibodies for 30 min. Images were acquired with an LSM700 or LSM710 confocal microscope (Carl Zeiss) and processed with Imaris (Bitplane), ImageJ (NIH), and Photoshop (Adobe). Determination of the LN compartments was performed with masks for different regions that were generated semi-automatically with ImageJ (NIH) based on anti-B220 and anti-LYVE1 staining. See also Supplemental Experimental Procedures.

Intravital Two-Photon Microscopy

Surgically exposed left inguinal LNs were prepared for intravital imaging via a modified version of a published protocol (Miller et al., 2003; Qi et al., 2006), using an upright LSM710 NLO multiphoton microscope (Carl Zeiss) with a 20 \times /1.0 NA water immersion objective enclosed in an environmental chamber maintained at 35°C with heated air. Fluorescence excitation was provided by a Chameleon Vision II Ti:sapphire laser (Coherent) with dispersion correction and fluorescence emission detected using external non-descanned photomultiplier tubes. EGFP and DsRed were excited at 920 nm, EYFP and TRITC at 880 nm, and fluorescent probes at 800 nm. For four-dimensional datasets, three-dimensional stacks were captured every 30–45 s for 30–90 min. Raw imaging data were processed with Imaris 7 (Bitplane). Autofluorescence was removed via channel arithmetic function from Imaris XT (Bitplane). Cellular motion was tracked semi-automatically via built-in tracking functions aided by manual corrections. For tracking contact duration, spots and surfaces were generated for T cells and TRITC⁺ cells, respectively, and were tracked with custom MATLAB scripts interfaced with Imaris XT. Movies were generated in Imaris and composed in After Effects (Adobe). See also Supplemental Experimental Procedures.

Imaging Thick LN Sections

Harvested LNs were either fixed in PLP for 2–6 hr or left unfixed, prior to embedding in 2% agarose. Agarose blocks containing tissues were sliced using a VT1200 S vibratome (Leica Biosystems) into 200–250 μ m thick sections. For antibody staining, tissue sections were blocked for 1.5–2 hr before incubating with antibodies for 8–16 hr at 4°C. Sections were mounted on glass slides and images were acquired on a LSM710 NLO multiphoton microscope (Carl Zeiss). Post-acquisition processing was performed in Imaris (Bitplane). For cluster detection, spots were created with built-in spot detection function in Imaris and clusters detected with custom MATLAB scripts interfaced with Imaris XT. A cluster was defined as a minimum of 3 cells aggregating within

a distance of 15 μ m measured from the centroid of each cell. See also Supplemental Experimental Procedures.

Statistics

Comparison of data sets was performed using one-way analysis of variance with Tukey's post-test or two-tailed, paired t test where appropriate.

SUPPLEMENTAL INFORMATION

Supplemental Information includes five figures, seven movies, and Supplemental Experimental Procedures and can be found with this article online at <http://dx.doi.org/10.1016/j.immuni.2015.07.020>.

AUTHOR CONTRIBUTIONS

J.L.H. performed all imaging experiments; J.L.H., P.G.W., and A.Z. performed experiments and analyzed data; A.G.B., W.R.H., and S.N.M. designed the research and interpreted data; J.L.H. and S.N.M. prepared figures and movies; and S.N.M. wrote the manuscript.

ACKNOWLEDGMENTS

We thank S. Bedoui for discussions and C. Jones, G. Davey, and M. Damtsis for technical assistance. Supported by the National Health and Medical Research Council of Australia (P.G.W., A.G.B., W.R.H., and S.N.M.) and the Australian Research Council (W.R.H. and S.N.M.).

Received: May 9, 2015

Revised: June 16, 2015

Accepted: June 23, 2015

Published: August 18, 2015

REFERENCES

- Allan, R.S., Smith, C.M., Belz, G.T., van Lint, A.L., Wakim, L.M., Heath, W.R., and Carbone, F.R. (2003). Epidermal viral immunity induced by CD8 α ⁺ dendritic cells but not by Langerhans cells. *Science* 301, 1925–1928.
- Allan, R.S., Waithman, J., Bedoui, S., Jones, C.M., Villadangos, J.A., Zhan, Y., Lew, A.M., Shortman, K., Heath, W.R., and Carbone, F.R. (2006). Migratory dendritic cells transfer antigen to a lymph node-resident dendritic cell population for efficient CTL priming. *Immunity* 25, 153–162.
- Bedoui, S., Whitney, P.G., Waithman, J., Eidsmo, L., Wakim, L., Caminschi, I., Allan, R.S., Wojtasiak, M., Shortman, K., Carbone, F.R., et al. (2009). Cross-presentation of viral and self antigens by skin-derived CD103⁺ dendritic cells. *Nat. Immunol.* 10, 488–495.
- Belz, G.T., Smith, C.M., Eichner, D., Shortman, K., Karupiah, G., Carbone, F.R., and Heath, W.R. (2004a). Cutting edge: conventional CD8 α ⁺ dendritic cells are generally involved in priming CTL immunity to viruses. *J. Immunol.* 172, 1996–2000.
- Belz, G.T., Smith, C.M., Kleinert, L., Reading, P., Brooks, A., Shortman, K., Carbone, F.R., and Heath, W.R. (2004b). Distinct migrating and nonmigrating dendritic cell populations are involved in MHC class I-restricted antigen presentation after lung infection with virus. *Proc. Natl. Acad. Sci. USA* 101, 8670–8675.
- Belz, G.T., Shortman, K., Bevan, M.J., and Heath, W.R. (2005). CD8 α ⁺ dendritic cells selectively present MHC class I-restricted noncytolytic viral and intracellular bacterial antigens in vivo. *J. Immunol.* 175, 196–200.
- Braun, A., Worbs, T., Moschovakis, G.L., Halle, S., Hoffmann, K., Bölder, J., Münk, A., and Förster, R. (2011). Afferent lymph-derived T cells and DCs use different chemokine receptor CCR7-dependent routes for entry into the lymph node and intranodal migration. *Nat. Immunol.* 12, 879–887.
- Carrasco, Y.R., and Batista, F.D. (2007). B cells acquire particulate antigen in a macrophage-rich area at the boundary between the follicle and the subcapsular sinus of the lymph node. *Immunity* 27, 160–171.
- Castellino, F., Huang, A.Y., Altan-Bonnet, G., Stoll, S., Scheinecker, C., and Germain, R.N. (2006). Chemokines enhance immunity by guiding naive CD8⁺ T cells to sites of CD4⁺ T cell-dendritic cell interaction. *Nature* 440, 890–895.

- Coles, R.M., Mueller, S.N., Heath, W.R., Carbone, F.R., and Brooks, A.G. (2002). Progression of armed CTL from draining lymph node to spleen shortly after localized infection with herpes simplex virus 1. *J. Immunol.* *168*, 834–838.
- Crozat, K., Tamoutounour, S., Vu Manh, T.P., Fossum, E., Luche, H., Ardouin, L., Guillems, M., Azukizawa, H., Bogen, B., Malissen, B., et al. (2011). Cutting edge: expression of XCR1 defines mouse lymphoid-tissue resident and migratory dendritic cells of the CD8 α^+ type. *J. Immunol.* *187*, 4411–4415.
- Dorner, B.G., Dorner, M.B., Zhou, X., Opitz, C., Mora, A., Güttler, S., Hutloff, A., Mages, H.W., Ranke, K., Schaefer, M., et al. (2009). Selective expression of the chemokine receptor XCR1 on cross-presenting dendritic cells determines cooperation with CD8 $^+$ T cells. *Immunity* *31*, 823–833.
- Edelson, B.T., Kc, W., Juang, R., Kohyama, M., Benoit, L.A., Klekotka, P.A., Moon, C., Albring, J.C., Ise, W., Michael, D.G., et al. (2010). Peripheral CD103 $^+$ dendritic cells form a unified subset developmentally related to CD8 α^+ conventional dendritic cells. *J. Exp. Med.* *207*, 823–836.
- Eidsmo, L., Stock, A.T., Heath, W.R., Bedoui, S., and Carbone, F.R. (2012). Reactive murine lymph nodes uniquely permit parenchymal access for T cells that enter via the afferent lymphatics. *J. Pathol.* *226*, 806–813.
- Gebhardt, T., Whitney, P.G., Zaid, A., Mackay, L.K., Brooks, A.G., Heath, W.R., Carbone, F.R., and Mueller, S.N. (2011). Different patterns of peripheral migration by memory CD4 $^+$ and CD8 $^+$ T cells. *Nature* *477*, 216–219.
- Gener, M.Y., Torabi-Parizi, P., and Germain, R.N. (2015). Strategically localized dendritic cells promote rapid T cell responses to lymph-borne particulate antigens. *Immunity* *42*, 172–185.
- Heath, W.R., and Carbone, F.R. (2009). Dendritic cell subsets in primary and secondary T cell responses at body surfaces. *Nat. Immunol.* *10*, 1237–1244.
- Hickman, H.D., Takeda, K., Skon, C.N., Murray, F.R., Hensley, S.E., Loomis, J., Barber, G.N., Bennink, J.R., and Yewdell, J.W. (2008). Direct priming of antiviral CD8 $^+$ T cells in the peripheral interfollicular region of lymph nodes. *Nat. Immunol.* *9*, 155–165.
- Hickman, H.D., Li, L., Reynoso, G.V., Rubin, E.J., Skon, C.N., Mays, J.W., Gibbs, J., Schwartz, O., Bennink, J.R., and Yewdell, J.W. (2011). Chemokines control naive CD8 $^+$ T cell selection of optimal lymph node antigen presenting cells. *J. Exp. Med.* *208*, 2511–2524.
- Hildner, K., Edelson, B.T., Purtha, W.E., Diamond, M., Matsushita, H., Kohyama, M., Calderon, B., Schraml, B.U., Unanue, E.R., Diamond, M.S., et al. (2008). Batf3 deficiency reveals a critical role for CD8 α^+ dendritic cells in cytotoxic T cell immunity. *Science* *322*, 1097–1100.
- Igyártó, B.Z., Haley, K., Ortner, D., Bobr, A., Gerami-Nejad, M., Edelson, B.T., Zurawski, S.M., Malissen, B., Zurawski, G., Berman, J., and Kaplan, D.H. (2011). Skin-resident murine dendritic cell subsets promote distinct and opposing antigen-specific T helper cell responses. *Immunity* *35*, 260–272.
- Itano, A.A., McSorley, S.J., Reinhardt, R.L., Ehst, B.D., Ingulli, E., Rudensky, A.Y., and Jenkins, M.K. (2003). Distinct dendritic cell populations sequentially present antigen to CD4 T cells and stimulate different aspects of cell-mediated immunity. *Immunity* *19*, 47–57.
- Junt, T., Moseman, E.A., Iannaccone, M., Massberg, S., Lang, P.A., Boes, M., Fink, K., Henriksson, S.E., Shayakhmetov, D.M., Di Paolo, N.C., et al. (2007). Subcapsular sinus macrophages in lymph nodes clear lymph-borne viruses and present them to antiviral B cells. *Nature* *450*, 110–114.
- Kastenmüller, W., Brandes, M., Wang, Z., Herz, J., Egen, J.G., and Germain, R.N. (2013). Peripheral prepositioning and local CXCL9 chemokine-mediated guidance orchestrate rapid memory CD8 $^+$ T cell responses in the lymph node. *Immunity* *38*, 502–513.
- Kim, T.S., and Braciale, T.J. (2009). Respiratory dendritic cell subsets differ in their capacity to support the induction of virus-specific cytotoxic CD8 $^+$ T cell responses. *PLoS ONE* *4*, e4204.
- Kissenpfennig, A., Henri, S., Dubois, B., Laplace-Builhé, C., Perrin, P., Romani, N., Tripp, C.H., Douillard, P., Leserman, L., Kaiserlian, D., et al. (2005). Dynamics and function of Langerhans cells in vivo: dermal dendritic cells colonize lymph node areas distinct from slower migrating Langerhans cells. *Immunity* *22*, 643–654.
- Kumamoto, Y., Mattei, L.M., Sellers, S., Payne, G.W., and Iwasaki, A. (2011). CD4 $^+$ T cells support cytotoxic T lymphocyte priming by controlling lymph node input. *Proc. Natl. Acad. Sci. USA* *108*, 8749–8754.
- Lee, H.K., Zamora, M., Linehan, M.M., Iijima, N., Gonzalez, D., Haberman, A., and Iwasaki, A. (2009). Differential roles of migratory and resident DCs in T cell priming after mucosal or skin HSV-1 infection. *J. Exp. Med.* *206*, 359–370.
- Merad, M., Sathe, P., Helft, J., Miller, J., and Mortha, A. (2013). The dendritic cell lineage: ontogeny and function of dendritic cells and their subsets in the steady state and the inflamed setting. *Annu. Rev. Immunol.* *31*, 563–604.
- Miller, M.J., Wei, S.H., Cahalan, M.D., and Parker, I. (2003). Autonomous T cell trafficking examined in vivo with intravital two-photon microscopy. *Proc. Natl. Acad. Sci. USA* *100*, 2604–2609.
- Mueller, S.N., Heath, W., McLain, J.D., Carbone, F.R., and Jones, C.M. (2002a). Characterization of two TCR transgenic mouse lines specific for herpes simplex virus. *Immunol. Cell Biol.* *80*, 156–163.
- Mueller, S.N., Jones, C.M., Smith, C.M., Heath, W.R., and Carbone, F.R. (2002b). Rapid cytotoxic T lymphocyte activation occurs in the draining lymph nodes after cutaneous herpes simplex virus infection as a result of early antigen presentation and not the presence of virus. *J. Exp. Med.* *195*, 651–656.
- Mueller, S.N., Jones, C.M., Chen, W., Kawaoka, Y., Castrucci, M.R., Heath, W.R., and Carbone, F.R. (2003). The early expression of glycoprotein B from herpes simplex virus can be detected by antigen-specific CD8 $^+$ T cells. *J. Virol.* *77*, 2445–2451.
- Nakanishi, Y., Lu, B., Gerard, C., and Iwasaki, A. (2009). CD8 $^+$ T lymphocyte mobilization to virus-infected tissue requires CD4 $^+$ T-cell help. *Nature* *462*, 510–513.
- Phan, T.G., Grigorova, I., Okada, T., and Cyster, J.G. (2007). Subcapsular encounter and complement-dependent transport of immune complexes by lymph node B cells. *Nat. Immunol.* *8*, 992–1000.
- Qi, H., Egen, J.G., Huang, A.Y.C., and Germain, R.N. (2006). Extrafollicular activation of lymph node B cells by antigen-bearing dendritic cells. *Science* *312*, 1672–1676.
- Ridge, J.P., Di Rosa, F., and Matzinger, P. (1998). A conditioned dendritic cell can be a temporal bridge between a CD4 $^+$ T-helper and a T-killer cell. *Nature* *393*, 474–478.
- Schnorrer, P., Behrens, G.M., Wilson, N.S., Pooley, J.L., Smith, C.M., El-Sukkari, D., Davey, G., Kupresanin, F., Li, M., Maraskovsky, E., et al. (2006). The dominant role of CD8 $^+$ dendritic cells in cross-presentation is not dictated by antigen capture. *Proc. Natl. Acad. Sci. USA* *103*, 10729–10734.
- Singh-Jasuja, H., Thiolat, A., Ribon, M., Boissier, M.C., Bessis, N., Rammensee, H.G., and Decker, P. (2013). The mouse dendritic cell marker CD11c is down-regulated upon cell activation through Toll-like receptor triggering. *Immunobiology* *218*, 28–39.
- Smith, C.M., Wilson, N.S., Waithman, J., Villadangos, J.A., Carbone, F.R., Heath, W.R., and Belz, G.T. (2004). Cognate CD4 $^+$ T cell licensing of dendritic cells in CD8 $^+$ T cell immunity. *Nat. Immunol.* *5*, 1143–1148.
- Stock, A.T., Mueller, S.N., van Lint, A.L., Heath, W.R., and Carbone, F.R. (2004). Cutting edge: prolonged antigen presentation after herpes simplex virus-1 skin infection. *J. Immunol.* *173*, 2241–2244.
- van Lint, A., Ayers, M., Brooks, A.G., Coles, R.M., Heath, W.R., and Carbone, F.R. (2004). Herpes simplex virus-specific CD8 $^+$ T cells can clear established lytic infections from skin and nerves and can partially limit the early spread of virus after cutaneous inoculation. *J. Immunol.* *172*, 392–397.
- Weeks, B.S., Ramchandran, R.S., Hopkins, J.J., and Friedman, H.M. (2000). Herpes simplex virus type-1 and -2 pathogenesis is restricted by the epidermal basement membrane. *Arch. Virol.* *145*, 385–396.
- Wiesel, M., and Oxenius, A. (2012). From crucial to negligible: functional CD8 $^+$ T-cell responses and their dependence on CD4 $^+$ T-cell help. *Eur. J. Immunol.* *42*, 1080–1088.
- Zhao, X., Deak, E., Soderberg, K., Linehan, M., Spezzano, D., Zhu, J., Knipe, D.M., and Iwasaki, A. (2003). Vaginal submucosal dendritic cells, but not Langerhans cells, induce protective Th1 responses to herpes simplex virus-2. *J. Exp. Med.* *197*, 153–162.

The Cytokine GM-CSF Drives the Inflammatory Signature of CCR2⁺ Monocytes and Licenses Autoimmunity

Andrew L. Croxford,¹ Margit Lanzinger,¹ Felix J. Hartmann,¹ Bettina Schreiner,¹ Florian Mair,¹ Pawel Pelczar,¹ Björn E. Clausen,² Steffen Jung,³ Melanie Greter,¹ and Burkhard Becher^{1,*}

¹Institute of Experimental Immunology, University of Zürich, Zürich 8057, Switzerland

²Institute for Molecular Medicine, Johannes Gutenberg-University Mainz, 55131 Mainz, Germany

³Department of Immunology, Weizmann Institute of Science, 76100 Rehovot, Israel

*Correspondence: becher@immunology.uzh.ch

<http://dx.doi.org/10.1016/j.immuni.2015.08.010>

SUMMARY

Granulocyte-macrophage colony-stimulating factor (GM-CSF) has emerged as a crucial cytokine produced by auto-reactive T helper (Th) cells that initiate tissue inflammation. Multiple cell types can sense GM-CSF, but the identity of the pathogenic GM-CSF-responsive cells is unclear. By using conditional gene targeting, we systematically deleted the GM-CSF receptor (*Csf2rb*) in specific subpopulations throughout the myeloid lineages. Experimental autoimmune encephalomyelitis (EAE) progressed normally when either classical dendritic cells (cDCs) or neutrophils lacked GM-CSF responsiveness. The development of tissue-invading monocyte-derived dendritic cells (moDCs) was also unperturbed upon *Csf2rb* deletion. Instead, deletion of *Csf2rb* in CCR2⁺ Ly6C^{hi} monocytes phenocopied the EAE resistance seen in complete *Csf2rb*-deficient mice. High-dimensional analysis of tissue-infiltrating moDCs revealed that GM-CSF initiates a combination of inflammatory mechanisms. These results indicate that GM-CSF signaling controls a pathogenic expression signature in CCR2⁺ Ly6C^{hi} monocytes and their progeny, which was essential for tissue damage.

INTRODUCTION

Dysregulated cytokine activity is now recognized as a critical component of auto-inflammatory disorders and their respective preclinical models. This is highlighted by genome-wide association studies in which cytokines and their receptors represent important risk alleles shared among multiple autoimmune diseases (Cotsapas and Hafler, 2013). Among the tissue-directed autoimmune pathologies, multiple sclerosis (MS) affects the central nervous system (CNS) of young adults and represents the most common CNS inflammatory disorder. Experimental autoimmune encephalomyelitis (EAE) serves as the common animal model for MS and is among the most widely used T-cell-dependent models to study the roles of cytokines in chronic inflammatory disease. There is agreement that the cytokine interleukin-23 (IL-23) renders T helper (Th) cells pathogenic (Gyölvézi et al., 2009; McGeachy et al., 2009). The genes expressed after IL-23

receptor (IL-23R) engagement do not fall into a specific Th cell polarization pattern, but seem to represent a unique signature allowing for tissue entry and initiation of inflammation. The pro-inflammatory cytokine GM-CSF has non-redundant functions in several preclinical models of autoimmune disease including EAE (Codarri et al., 2011), and neutralization of GM-CSF is currently being tested in clinical trials for a number of diseases including MS (trial identifier NCT: NCT01517282) and rheumatoid arthritis (Burmester et al., 2011).

T cells do not respond to GM-CSF, and therefore activated Th cells must communicate with a GM-CSF-sensitive cell type to mediate pathology. Virtually all myeloid cells express the GM-CSF receptor (*Csf2ra* and *Csf2rb*) (Greter et al., 2012) and represent likely candidates for the critical GM-CSF-responsive entity. Microglia (Ponomarev et al., 2005, 2007), neutrophils (Kroenke et al., 2010), monocytes (Ko et al., 2014), dermal CD103⁺ dendritic cells (DCs) (King et al., 2010), and CNS-invading monocyte-derived DCs (moDCs) (King et al., 2009; Mildner et al., 2009) have been implicated in disease pathogenesis with an essential, GM-CSF-dependent role ascribed to them. When all reports are considered, exactly why GM-CSF is required for disease development is unknown. Questions also remain as to whether a single GM-CSF-responsive cell type is needed for EAE development, or whether multiple cell types act in concert.

In this report, we systematically addressed these questions via a conditional gene targeting approach. We exclude an obligatory GM-CSF-dependent function of microglia, conventional DCs (cDCs), and neutrophils. Instead, deletion of *Csf2rb* by specific and inducible delivery of Cre recombinase to CCR2⁺ myeloid cells fully phenocopied the resistance observed in *Csf2rb*-deficient mice. Lastly, we provide a high-dimensional GM-CSF-driven pathogenic expression signature in CNS-infiltrating moDCs, the progeny of Ly6C^{hi}CCR2⁺ monocytes, required for the initiation of tissue inflammation. Translating our findings to humans, we show that monocytes readily respond to GM-CSF by eliciting a pathogenic program characterized by IL-1 β expression. Therefore, the role of GM-CSF in autoimmune tissue damage can be traced to one specific myeloid cell population and the pathological mechanisms it controls.

RESULTS

Csf2rb^{LacZ/LacZ} and *Csf2rb*^{fl/fl} Mice Allow for Conditional and/or Inducible Targeting of *Csf2rb*

To unambiguously identify the GM-CSF-responsive cell type necessary for the induction of tissue inflammation, we generated

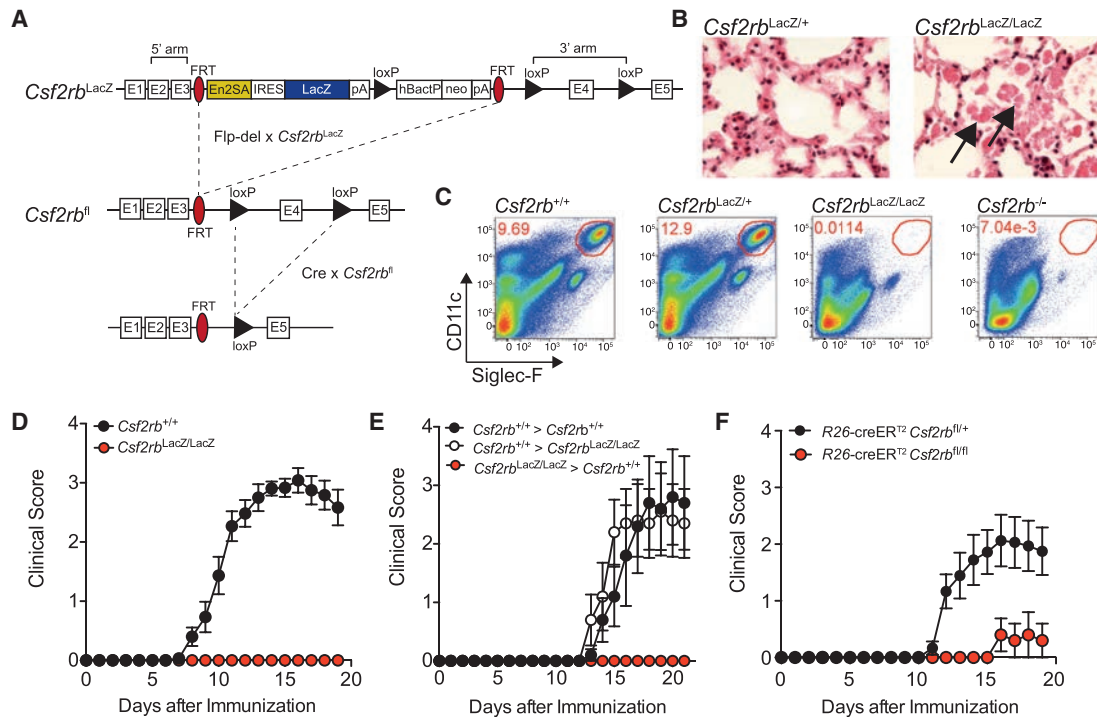


Figure 1. *Csf2rb*^{LacZ/LacZ} Mice Lack Functional *Csf2rb* Expression and GM-CSF Signaling Capability

(A) Schematic for the *Csf2rb*^{LacZ} knockout-first allele and its subsequent conversion to the conditional *Csf2rb*^{fl} using a flp-deleter strain. After Cre-mediated recombination, exon 4 of the *Csf2rb* gene is excised.

(B) Lung sections of *Csf2rb*^{LacZ/+} and *Csf2rb*^{LacZ/LacZ} mice were stained with hematoxylin and eosin. Arrows indicate surfactant aggregates in the alveoli of *Csf2rb*^{LacZ/LacZ} mice. Images represent three mice from each genotype and two experiments.

(C) Frequencies of CD11c^{hi}Siglec-F^{hi} alveolar macrophages (pre-gated on CD45⁺ cells) from lung tissue of indicated genotypes are shown in the dot plots. Data represent multiple experiments.

(D) *Csf2rb*^{+/+} (n = 15) and *Csf2rb*^{LacZ/LacZ} (n = 14) mice were actively immunized with MOG_{p35-55} emulsified in CFA (day 0, s.c.) and pertussis toxin (days 0 and 2) to induce EAE. The severity of clinical paralysis is plotted against time. Data shown are pooled from multiple experiments.

(E) Criss-cross BM chimeric mice were generated using the indicated host and donor genotypes. After 6 weeks, mice were actively immunized and scored for clinical EAE (n = 5 for all groups). Data represent two similar experiments.

(F) *Csf2rb*^{LacZ} mice were crossed to a flp-deleter strain to generate the *Csf2rb*^{fl} allele and subsequently crossed to the *R26-creER*^{T2}. *R26-creER*^{T2} *Csf2rb*^{fl/fl} (n = 7) and *R26-creER*^{T2} *Csf2rb*^{fl/+} control (n = 4) mice were placed on tamoxifen chow for 3 weeks, rested for a week, and then immunized to induce EAE. Clinical EAE scores represent two experiments with at least three mice per group. Error bars represent \pm SEM. See also Figure S1.

Csf2rb^{LacZ} transgenic mice to specifically manipulate GM-CSF responsiveness in vivo (Figure 1A). Bone marrow (BM) cells from *Csf2rb*^{LacZ/LacZ} mice lacked detectable expression of *Csf2rb* mRNA, whereas expression of *Csf2ra* remained unaltered (Figure S1A). *Csf2rb* is also required for IL-5 signaling and we observed a significant reduction of IL-5-dependent eosinophils in peripheral blood taken from *Csf2rb*^{LacZ/LacZ} mice (Figure S1B). Loss of GM-CSF or its receptor results in the absence of terminally differentiated alveolar macrophages (AMs) in the lungs of mutant mice (Guilliams et al., 2013; Shibata et al., 2001). Pulmonary alveolar proteinosis (PAP) was also clearly identifiable as surfactant aggregates in the alveoli of *Csf2rb*^{LacZ/LacZ} mice (Figure 1B). CD11c⁺Siglec-F⁺ AMs were absent in the lungs of both *Csf2rb*^{LacZ/LacZ} and *Csf2rb*^{-/-} mice (Figure 1C). Importantly, *Csf2rb*^{LacZ/LacZ} mice were also resistant to MOG-induced EAE (Figure 1D). *Csf2rb*^{+/+} host mice receiving *Csf2rb*^{LacZ/LacZ} bone marrow (BM) were also resistant, showing that a critical GM-CSF-responsive cell type is derived from the hematopoietic compartment (Figure 1E).

We performed allelic conversion (Figure 1A: Flp-mediated *Csf2rb*^{LacZ} \rightarrow *Csf2rb*^{fl}) and crossed the resulting conditional *Csf2rb*^{fl} allele with an inducible Cre-expressing strain targeting all cells and tissues (*R26-creER*^{T2}) (Ventura et al., 2007). After 3 weeks of tamoxifen feeding, mice were immunized to induce EAE. *R26-creER*^{T2}-*Csf2rb*^{fl/fl} mice were protected from EAE compared to control littermates (Figure 1F). Thus, allelic conversion from *Csf2rb*^{LacZ} \rightarrow *Csf2rb*^{fl} allows conditional and/or inducible targeting of *Csf2rb*.

GM-CSF Signaling in cDCs Is Dispensable for Autoimmunity

Numerous genes are regulated by GM-CSF signaling in cDCs (Kc et al., 2014). Indeed, both resident and migratory DCs derived from WT skin-draining lymph nodes (SLNs) were able to respond to exogenous GM-CSF by phosphorylating the transcription factor STAT5, in contrast to the same cells isolated from *Csf2rb*^{LacZ/LacZ} mice (Figures S1C and S1D). To analyze the requirement of GM-CSF signaling on cDCs during EAE, we

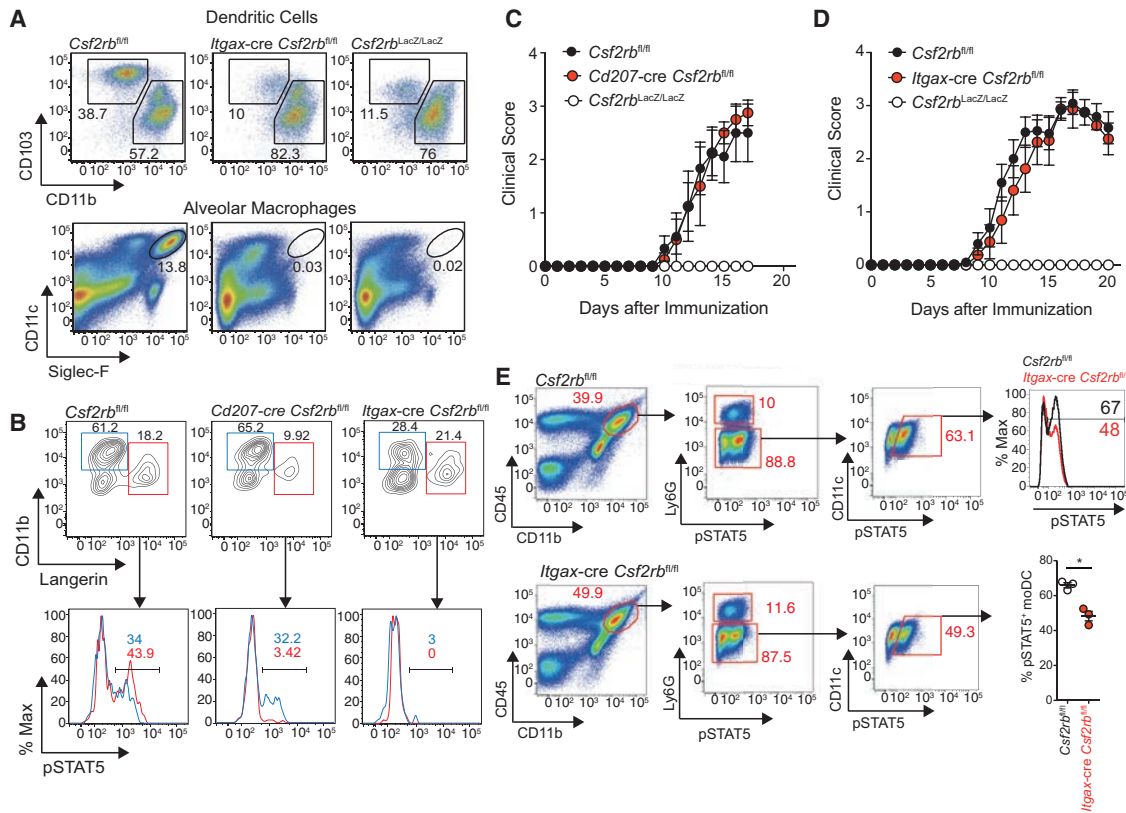


Figure 2. cDCs Do Not Require GM-CSF to Induce EAE

(A) Single-cell suspensions were prepared from lung tissue of *Csf2rb^{fl/fl}*, *Itgax-cre Csf2rb^{fl/fl}*, and *Csf2rb^{LacZ/LacZ}* mice. cDCs and AMs were identified by FACS staining for CD11c and Siglec-F (pre-gated on CD45), and DCs for CD11b and CD103 (pre-gated on CD45^{hi}MHC-II⁺CD11c⁺Siglec-F⁻). Data represent three experiments.

(B) SLNs from mice from the indicated genotypes were harvested, mechanically disrupted, and stained for the indicated markers (pre-gated on CD11c⁺MHC-II^{hi}) prior to a brief GM-CSF stimulation (20 ng/ml, 30 min) and intracellular staining (ICS) for pSTAT5. Frequencies of pSTAT5⁺ DCs are indicated in the gates and histograms. Data represent two experiments.

(C and D) Plots show the clinical scores of *Cd207-cre Csf2rb^{fl/fl}* and *Itgax-cre Csf2rb^{fl/fl}* mice s.c. immunized with MOG_{p35-55} emulsified in CFA, both representative of two experiments (C) or four experiments (D) with at least four mice per group.

(E) Inflamed CNS of indicated mice were harvested at peak disease and infiltrating cells were isolated and stimulated with GM-CSF before ICS for pSTAT5. Frequencies of pSTAT5⁺ inflammatory moDCs (CD45^{hi}CD11b⁺Ly6G⁻CD11c⁺pSTAT5⁺) are shown in the histogram and quantified in the graph. Statistical analysis was performed (*p < 0.05, **p < 0.01, ***p < 0.001, Student's t test, unpaired) and one of two independent experiments is shown. Error bars represent ± SEM. See also Figures S1 and S2.

crossed the *Csf2rb^{fl/fl}* with Cre-expressing strains targeting cDCs. The CD11c-Cre strain (*Itgax-cre*) shows a spectrum of activity across a variety of cell types, with deletion upward of 95% achievable in cDCs (Caton et al., 2007). Both *Itgax-cre Csf2rb^{fl/fl}* and *Csf2rb^{LacZ/LacZ}* mice presented with the anticipated decrease in lung-resident CD103⁺ DCs and CD11c⁺Siglec-F⁺ alveolar macrophages (Figure 2A), highlighting a successful targeting of CD11c-expressing myeloid cells in vivo.

Skin-resident CD103⁺ DCs are associated with the EAE resistance seen in GM-CSF-negative animals immunized in a subcutaneous (s.c.) manner (King et al., 2010). We therefore utilized both Langerin-Cre (*Cd207-cre*) and *Itgax-cre* mice crossed to the *Csf2rb^{fl/fl}* mice to determine whether GM-CSF signaling on Langerin⁺ DCs (CD103⁺ DCs and Langerhans cells [LCs]) or all cDCs, respectively, is required for EAE induction (Caton et al., 2007; Zahner et al., 2011). To determine the deletion efficiency of *Csf2rb* in cDCs, we analyzed GM-CSF-induced phosphoryla-

tion of STAT5. In *Cd207-cre Csf2rb^{fl/fl}* mice, STAT5 phosphorylation was selectively impaired in skin-derived Langerin⁺ DCs in response to GM-CSF (CD103⁺ DCs and LCs) (Figure 2B). In *Itgax-cre Csf2rb^{fl/fl}* mice, virtually all cDCs were rendered GM-CSF unresponsive and failed to phosphorylate STAT5 (Figure 2B). However, both *Cd207-cre Csf2rb^{fl/fl}* and *Itgax-cre Csf2rb^{fl/fl}* mice developed EAE, clearly demonstrating that GM-CSF signaling on cDCs is not required for tissue inflammation (Figures 2C and 2D).

Whereas cDCs populate tissues in the steady state, under inflammatory conditions, monocytes invade inflamed sites and differentiate into moDCs, characterized by upregulation of CD11c and MHC class II (MHC-II) (Serbina et al., 2003). Given the reported activity of *Itgax-cre* in subsets of myeloid cells other than cDCs (Caton et al., 2007), we isolated inflammatory infiltrates from *Itgax-cre Csf2rb^{fl/fl}* mice with EAE and assayed the infiltrating myeloid populations and their ability to respond to

GM-CSF. We observed a significant, though modest, reduction in the frequency of GM-CSF-responsive moDCs in *Itgax-cre Csf2rb^{fl/fl}* mice compared to controls (Figure 2E). This highlights that *Itgax-cre* effectively targets the *Csf2rb^{fl}* locus in cDCs, but conferred only a partial recombination in CNS-infiltrating inflammatory moDCs.

CNS-Invasive Neutrophils and Resident Microglia Do Not Require GM-CSF Signaling during EAE

Neutrophils and moDCs can respond to GM-CSF. During EAE, both cell types accumulate in the CNS, where they can rapidly phosphorylate STAT5 in response to GM-CSF (Figure S2A). The depletion of neutrophils was shown to abrogate clinical progression of EAE (Kroenke et al., 2010), but whether their essential effector function is controlled by GM-CSF has not been described. We crossed the *Csf2rb^{fl}* mice to the *LysM-Cre (Lyz2-cre)*, which shows high deletion in neutrophils and varying degrees of activity in Ly6C^{hi} monocytes and macrophages at different genomic loci (Clausen et al., 1999; Jakubzick et al., 2008; Schreiber et al., 2013). No apparent differences were observed in circulating neutrophils or Ly6C^{hi} monocytes in *Lyz2-cre Csf2rb^{fl/fl}* mice, although a reduction in CD131 staining intensity was observed on both neutrophils and total monocytes in peripheral blood (Figure 3A). Importantly, this translated into a marked reduction in GM-CSF sensitivity in circulating neutrophils (Figure 3B). However, 50% of monocytes in *Lyz2-cre Csf2rb^{fl/fl}* mice could still respond to GM-CSF in the steady state, indicative of incomplete deletion in this population.

CD115⁺ monocytes can be further characterized by their expression of Ly6C (either Ly6C^{hi} or Ly6C^{lo} monocytes) (Geissmann et al., 2010). We immunized *Lyz2-cre Csf2rb^{fl/fl}* mice and assayed blood neutrophils and Ly6C^{hi} and Ly6C^{lo} monocytes at day 7 after immunization. Despite an efficient targeting of neutrophils, Ly6C^{hi} monocytes largely retain their ability to respond to GM-CSF under inflammatory conditions, indicating poor deletion in this subset (Figure 3C). *Lyz2-cre Csf2rb^{fl/fl}* mice were susceptible to EAE and comparable myeloid infiltrates were consistently recovered from inflamed CNS tissue of both strains (Figure 3D). Of note, GM-CSF sensitivity of CNS-derived neutrophils was efficiently reduced in *Lyz2-cre Csf2rb^{fl/fl}* mice, where phosphorylation of STAT5 was reduced to background staining intensity (Figure 3E) and fully differentiated moDCs were also significantly targeted (Figure 3E). However, the robust GM-CSF responsiveness seen in blood Ly6C^{hi} monocytes of immunized *Lyz2-cre Csf2rb^{fl/fl}* mice still implicated these cells and their progeny as a potential target of GM-CSF during EAE.

Microglia are radiation resistant and are not replaced by BM-derived cells during disease progression (Greter et al., 2005). In addition to BM chimera experiments (Figure 1E), which excluded microglia as a critical GM-CSF responder cell, we formally discounted this cell type by using microglia-targeting *Cx3cr1-creER^{T2}* and *Cx3cr1-cre* strains crossed to the *Csf2rb^{fl}* strain (Yona et al., 2013). Both *Cx3cr1-cre Csf2rb^{fl/fl}* and tamoxifen-treated *Cx3cr1-creER^{T2} Csf2rb^{fl/fl}* mice were susceptible to EAE (Figures S2B and S2C). Interestingly, we again observed only a partial deletion of *Csf2rb* in Ly6C^{hi} monocytes, whereas Ly6C^{lo} monocytes of *Cx3cr1-cre Csf2rb^{fl/fl}* mice showed the expected loss of GM-CSF responsiveness (Figure S2D). Taken

together, GM-CSF signaling on cDCs, neutrophils, and microglia are not critical for the development of EAE. However, *Itgax-cre Csf2rb^{fl/fl}*, *Lyz2-cre Csf2rb^{fl/fl}*, and *Cx3cr1-cre Csf2rb^{fl/fl}* mice all failed to efficiently target *Csf2rb* in Ly6C^{hi} monocytes.

Csf2rb Expression in CCR2⁺Ly6C^{hi} Monocytes Is Critical for EAE Development

Numerous reports have described a crucial role for CCR2 and its ligand, CCL2/MCP-1, during EAE progression (Gaupp et al., 2003; Mahad and Ransohoff, 2003; Saederup et al., 2010). Given that Ly6C^{hi} monocytes strongly express CCR2, we generated the *Ccr2-creER^{T2}-mKate2* strain to specifically and inducibly target CCR2⁺ cell types. This mouse expresses CreER^{T2} and an mKate2 fluorescent reporter under the control of the *Ccr2* promoter, knocked into the 3' UTR of the murine gene *Ccr2* (Figure S3A). *Ccr2-creER^{T2} Csf2rb^{fl/fl}* mice were bred and immunized before administration of tamoxifen to induce *Csf2rb* deletion in CCR2-expressing cell types. Recombination efficiency was enhanced by homozygosity of the *Ccr2-creER^{T2}* allele, where tamoxifen administration targeted the *Csf2rb* locus in 90% of Ly6C^{hi} monocytes in *Ccr2-creER^{T2/+}-Csf2rb^{fl/fl}* mice (Figure S3B). Homozygous *Ccr2-creER^{T2/+}* mice show normal frequencies of CCR2⁺Ly6C^{hi} monocytes in peripheral blood and EAE susceptibility was maintained when immunized alongside *Ccr2^{-/-}* mice (Figures S3C and S3D).

The capacity of tissue-invading moDCs to mediate tissue damage has recently been demonstrated (Yamasaki et al., 2014), and we reasoned that GM-CSF licenses this pathogenic process. *Ccr2-creER^{T2/+} Csf2rb^{fl/fl}* and *Csf2rb^{fl/fl}* control mice were immunized and treated with tamoxifen to delete GM-CSF responsiveness in Ly6C^{hi} monocytes. *Ccr2-creER^{T2/+} Csf2rb^{fl/fl}* mice were fully resistant to EAE induction compared to control mice (Figure 4A). An extensive characterization of GM-CSF-responsive myeloid cell populations was performed on immunized *Ccr2-creER^{T2/+} Csf2rb^{fl/fl}* mice, ranging from BM precursors (macrophage and DC progenitors [MDPs] and common DC progenitors [CDPs]) to CNS-infiltrating moDCs. No significant reduction in STAT5 phosphorylation was observed in MDPs after tamoxifen treatment. However, recombination at the *Csf2rb* locus was apparent in CDPs from immunized *Ccr2-creER^{T2/+} Csf2rb^{fl/fl}* mice (Figure 4B). The targeting of CDPs led us to analyze the extent to which cDCs could potentially be targeted with the *Ccr2-creER^{T2}* strain. 48 hr after tamoxifen administration, migratory and resident DC populations in the SLN, cDCs in spleen, and blood-derived neutrophils all maintained the ability to respond to GM-CSF (Figures S4A–S4D). Using a fate mapping approach (*Ccr2-creER^{T2}-STOP-TdTomato*) (Madisen et al., 2010), we observed that 10 days after an initial tamoxifen administration, migratory and resident cDCs populations in the SLN were indeed partially targeted using the *Ccr2-creER^{T2}* strain (Figures S4E and S4F). Given the EAE susceptibility of *Itgax-cre Csf2rb^{fl/fl}* mice (Figure 2D) and the lack of requirement for CD103⁺ DCs in EAE (Edelson et al., 2011), we conclude that any potential long-term accumulation of targeted cDCs in *Ccr2-creER^{T2/+}-Csf2rb^{fl/fl}* mice did not contribute to resistance to EAE in this strain.

Blood-derived myeloid cells from immunized *Ccr2-creER^{T2/+} Csf2rb^{fl/fl}* mice were assayed for GM-CSF sensitivity. Although neutrophils maintained their ability to respond

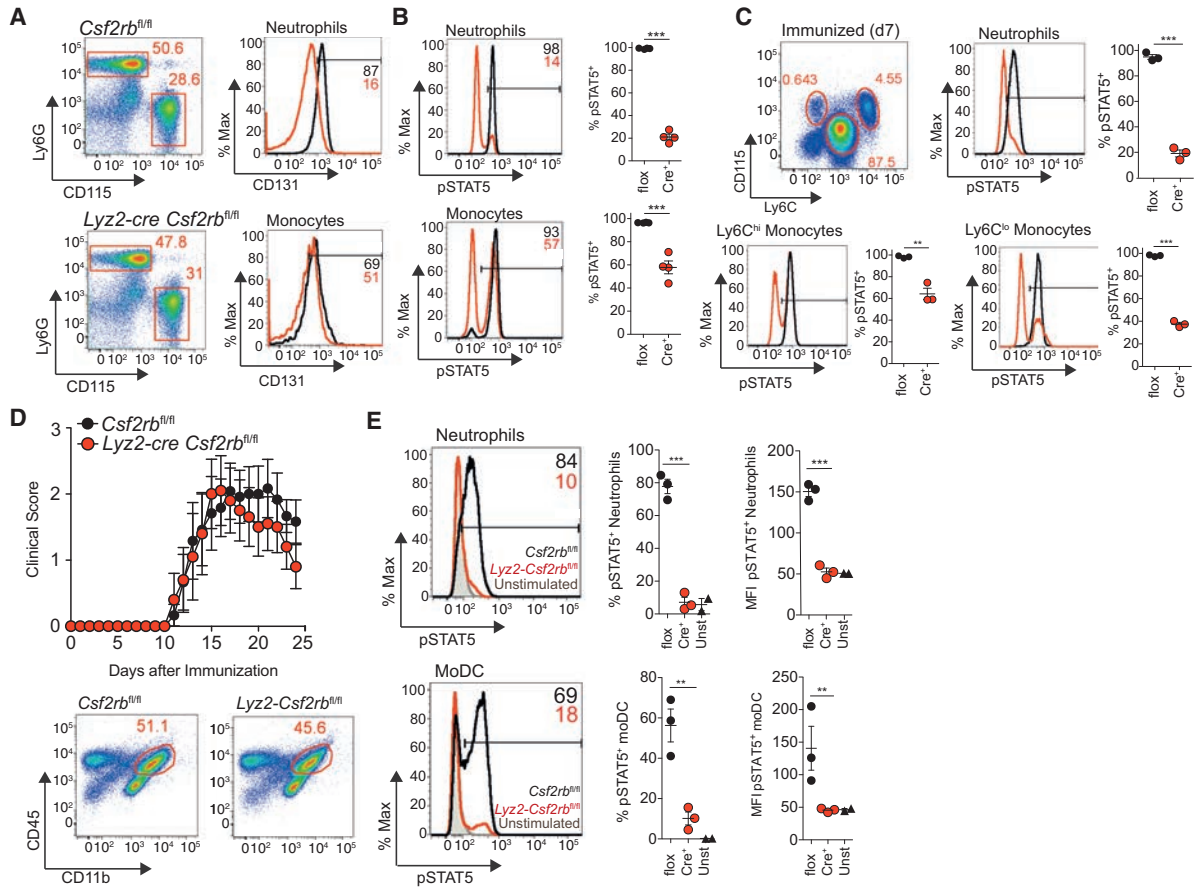


Figure 3. GM-CSF Signaling Is Not Required on moDCs and Neutrophils in the CNS to Mediate Paralysis

(A) Lysed whole blood from *Lyz2-cre Csf2rb^{fl/fl}* mice was stained for CD11b, Ly6G, Ly6C, and CD131 (GM-CSFR β). CD131 staining intensity for monocytes (CD11b⁺CD115⁺) and neutrophils (CD11b⁺Ly6G^{hi}) is shown for the indicated cell types and genotypes: *Csf2rb^{fl/fl}* (black) and *Lyz2-cre Csf2rb^{fl/fl}* (red). Data represent two experiments.

(B) Leukocytes from naive *Csf2rb^{fl/fl}* and *Lyz2-cre Csf2rb^{fl/fl}* blood were stimulated with GM-CSF in vitro (20 ng/ml, 30 min), surface stained as indicated followed by ICS for pSTAT5. Statistics for pSTAT5⁺ neutrophils (CD11b⁺Ly6G^{hi}) and monocytes (CD11b⁺CD115⁺) are shown and represent multiple experiments.

(C) *Lyz2-cre Csf2rb^{fl/fl}* and *Csf2rb^{fl/fl}* control mice were s.c. immunized with MOG_{p35-55} emulsified in CFA and Ptx on days 0 and 2. Mice were bled on day 7, stained for CD11b, Ly6G, Ly6C, and CD115, and stimulated with GM-CSF in vitro (20 ng/ml, 30 min) followed by ICS for pSTAT5. Data represent two experiments (n = 4 for both genotypes)

(D) *Csf2rb^{fl/fl}* (n = 6) and *Lyz2-cre Csf2rb^{fl/fl}* (n = 5) mice were s.c. immunized (as in C). Ascending clinical paralysis was then measured against time post-immunization. CNS of immunized mice was harvested (day 14) and infiltrating leukocytes isolated. Whole myeloid infiltrates (CD11b⁺CD45^{hi}) are shown. Clinical scores represent five independent experiments.

(E) Total inflammatory infiltrates (defined as either Ly6G^{hi} neutrophils or Ly6C^{hi}CD11c⁺MHC-II⁺ moDCs, pre-gated on CD11b⁺CD45^{hi}) were stimulated with GM-CSF (20 ng/ml, 30 min). Histograms show GM-CSF-induced phosphorylation of STAT5 in response to GM-CSF. Frequencies and MFI are shown in the histogram (black, *Csf2rb^{fl/fl}*; red, *Lyz2-cre Csf2rb^{fl/fl}*) for indicated populations and for the indicated genotypes shown in the accompanying bar charts. Closed triangles show unstimulated *Csf2rb^{fl/fl}* moDCs stained with anti-pSTAT5. *p < 0.05, **p < 0.01, ***p < 0.001 (Student's t test, unpaired). Two independent experiments with at least three mice per group were performed.

Error bars represent \pm SEM. See also Figures S2 and S7.

to GM-CSF, a 90% reduction of pSTAT5⁺Ly6C^{hi} monocytes present in peripheral blood was observed (Figure 4C). During EAE, active SLNs show accumulation of moDCs at the expense of migratory and resident cDCs, where they can respond to GM-CSF by secretion of proinflammatory factors such as IL-1 β (Figures S5A–S5C). In *Itgax-cre Csf2rb^{fl/fl}* and *Lyz2-cre Csf2rb^{fl/fl}* mice, no differences were noted in the generation of moDCs or cytokine-expressing T cells in the inflamed SLNs (Figures S5D–S5G). We assessed the ability of SLN moDCs from immunized *Ccr2-creER^{T2+/+} Csf2rb^{fl/fl}* mice

to respond to GM-CSF and observed a highly significant reduction of GM-CSF-responsive moDCs in the SLNs (Figure 4D). Functionally, moDCs isolated from immunized and tamoxifen-treated *Ccr2-creER^{T2+/+} Csf2rb^{fl/fl}* mice failed to up-regulate IL-1 β after exposure to GM-CSF (Figure 4E). Given that Ly6C^{hi}MHC-II^{hi} moDCs represent the most robust source of IL-1 β in the inflamed LN (Figure 4F), loss of GM-CSF signaling in moDCs therefore resulted in sub-optimal expression of IL-1 β at the site of T cell priming after subcutaneous immunization.

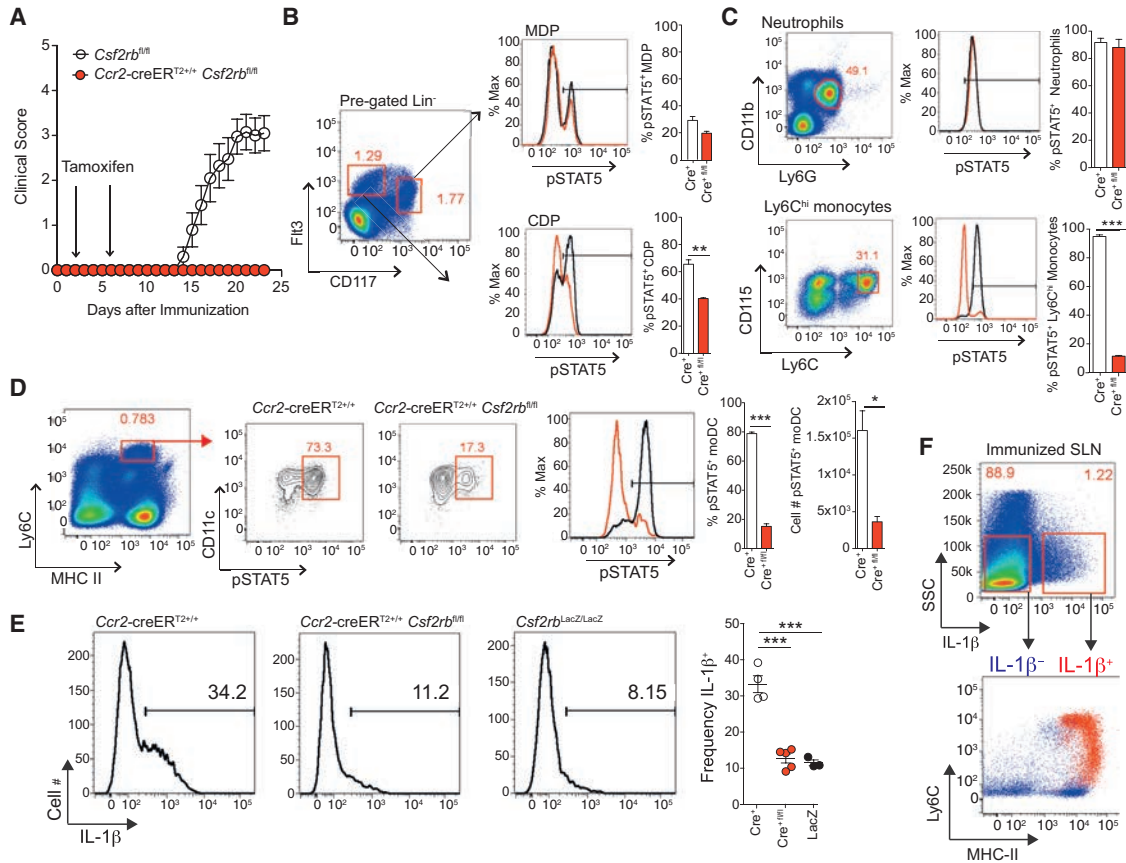


Figure 4. *Csf2rb* Expression in Ly6C^{hi}CCR2⁺ Monocytes Is Critical for EAE Induction

(A) *Ccr2-creER^{T2+/+} Csf2rb^{fl/fl}* mice were immunized to induce EAE and treated with tamoxifen (5 mg/dose) via oral gavage on days 2 and 6. Ascending clinical paralysis was then measured against identically treated control animals of indicated genotype. Data shown represents one of three independent experiments with similar EAE resistance observed.

(B) On day 7 after immunization and tamoxifen treatment (as in A), BM preparations from *Ccr2-creER^{T2+/+} Csf2rb^{fl/fl}* mice and controls were surface stained for lineage markers (B220, CD3, Ly6G, NK1.1, CD11c, MHC-II, Ly6C, CD11b) and GM-CSF-stimulated before ICS for pSTAT5. GM-CSF responsiveness of Lin⁻ (B220⁻Ly6G⁻Ly6C⁻CD11b⁻CD11c⁻MHC-II⁻CD3⁻) Fit3⁺CD117⁺ (MDPs) and Lin⁻Fit3⁺CD117⁻ (CDPs) was assayed and their frequencies shown in histograms and bar charts. Data represent two experiments.

(C) Blood (as in B) was analyzed on day 7, with the pSTAT5⁺ frequencies of Ly6C^{hi} monocytes (CD11b⁺Ly6G⁻CD115⁺Ly6C^{hi}) and Ly6G^{hi} neutrophils after GM-CSF stimulation shown in the histograms and bar charts. Data represent three similar experiments.

(D) Inflamed SLNs harvested on day 7 were analyzed for GM-CSF responsiveness. Frequencies and numbers of pSTAT5⁺ moDCs (Ly6C^{hi}MHC-II⁺CD11c⁺pSTAT5⁺) in the active SLNs are shown. Data represent two experiments.

(E) Ly6C^{hi}MHC-II⁺CD11c⁺ cells isolated from *Ccr2-creER^{T2+/+}* (open circles), *Ccr2-creER^{T2+/+} Csf2rb^{fl/fl}* (closed red circles), and *Csf2rb^{LacZ/LacZ}* (closed black circles) mice were stimulated with GM-CSF and monensin for 6 hr prior to ICS for IL-1β. Frequencies of Ly6C^{hi}MHC-II⁺IL-1β⁺ cells are shown in the histograms and bar charts. Data represent three experiments.

(F) SLNs of immunized WT mice excised at day 7 were cultured with GM-CSF and monensin for 6 hr prior to ICS. The distribution of IL-1β⁻ and IL-1β⁺ cells among Ly6C- and MHC-II-expressing cells are shown in the FACS plot (balanced numbers of each gate displayed). Data shown represent two experiments.

Significance between groups was calculated as *p < 0.05, **p < 0.01, ***p < 0.001 (Student's t test, unpaired for B–E). Open bars, *Ccr2-creER^{T2+/+}*; red bars, *Ccr2-creER^{T2+/+} Csf2rb^{fl/fl}*. Error bars represent ± SEM. See also Figures S3–S5 and S7.

Deletion of *Csf2rb* in CCR2⁺ Cells Reduces Established CNS Inflammation

Loss of *Csf2rb* on CCR2-expressing cells prior to disease onset results in abrogation of disease. We investigated whether this same deletion would provide a useful therapeutic intervention after the mice already had established clinical disease. *Ccr2-creER^{T2+/+} Csf2rb^{fl/fl}* mice and controls were immunized and at the first sign of clinical disease, tamoxifen was administered every 48 hr. Over a 2-week period, *Ccr2-creER^{T2+/+} Csf2rb^{fl/fl}* mice showed a reduced severity of EAE compared to controls

(Figure 5A). In the inflamed CNS, neutrophils maintained GM-CSF responsiveness, whereas Ly6C^{hi} infiltrates showed a highly significant reduction in GM-CSF sensitivity (Figures 5B and 5C). Lumbar spinal cords of EAE-affected, tamoxifen-treated *Ccr2-creER^{T2+/+} Csf2rb^{fl/fl}* mice showed significantly less demyelination compared to controls in a Luxol Fast Blue (LFB) histological analysis, both in terms of total area and percentage of white matter (Figure 5D). Therefore, maintained GM-CSF signaling on CCR2⁺ inflammatory infiltrates is required to maintain an inflammatory program that sustains the chronic phase of EAE.

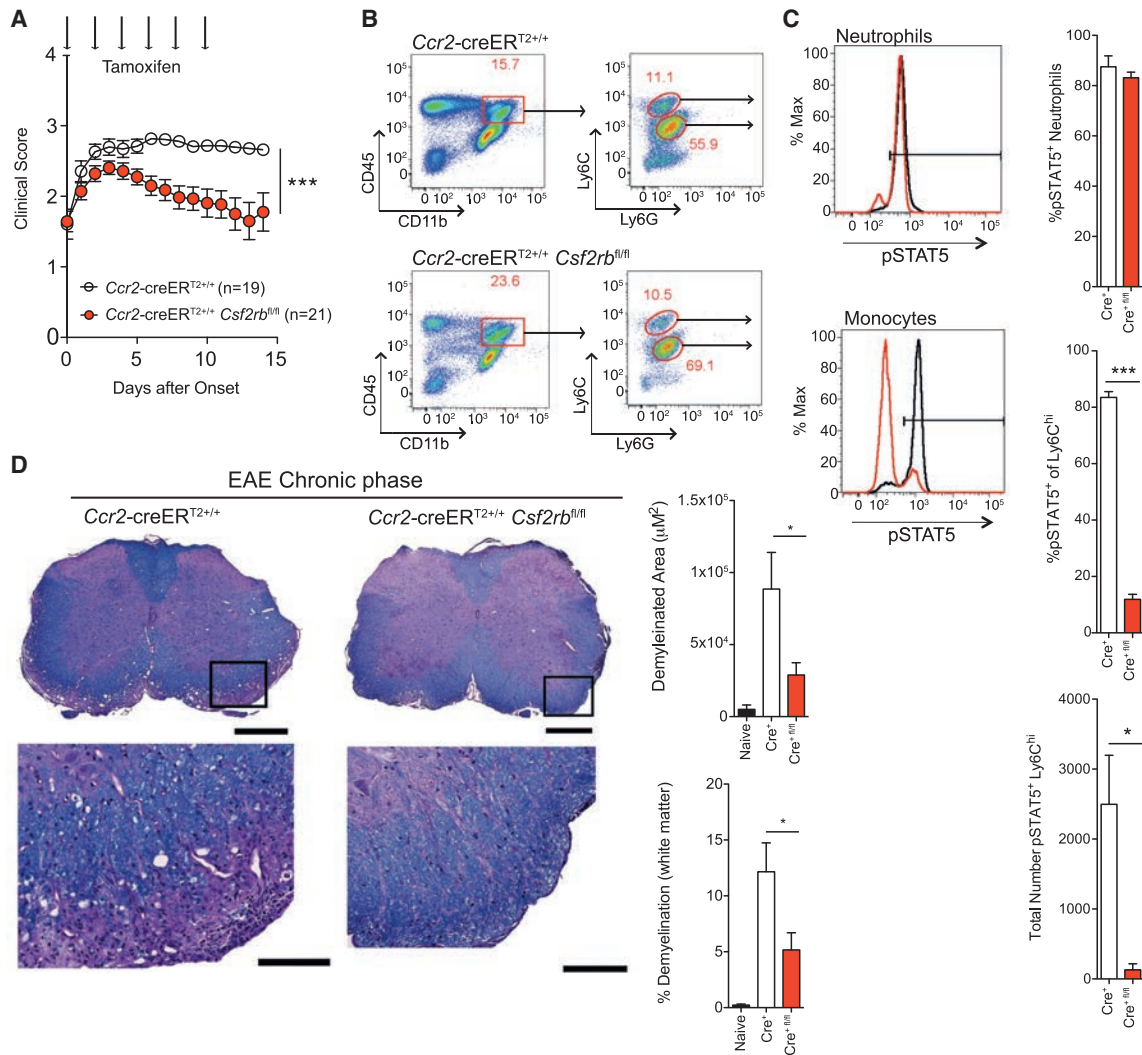


Figure 5. Deletion of *Csf2rb* in CCR2⁺ Cells Ameliorates Established Clinical EAE

(A) Multiple cohorts of *Ccr2-creER^{T2/+}* (pooled n = 19) and *Ccr2-creER^{T2/+} Csf2rb^{fl/fl}* (pooled n = 21) mice were immunized to induce EAE and monitored daily for onset of disease. Upon first sign of disease, mice received 5 mg tamoxifen via oral gavage and every 48 hr for the following 14 days (indicated as arrows). Disease for individual mice is normalized to the day of onset and statistical difference between curves calculated by two-way ANOVA. Data are pooled from three independent experiments.

(B) CNS infiltrates from sick, tamoxifen-treated mice (as in A) were isolated, stained for CD11b, CD45, Ly6C and Ly6G surface markers prior to GM-CSF stimulation (20 ng/ml GM-CSF, 30 min), and analyzed for GM-CSF responsiveness by pSTAT5 phosphorylation analysis.

(C) Frequencies of GM-CSF-responsive cells in the indicated gates are shown in the histograms and bar charts. Total numbers of Ly6C^{hi}pSTAT5⁺ cells isolated from CNS preparations of *Ccr2-creER^{T2/+}* (n = 3) and *Ccr2-creER^{T2/+} Csf2rb^{fl/fl}* (n = 3) are shown.

(D) Representative histopathological stainings and quantifications (pooled from two blinded analyses) of lumbar spinal cord sections from diseased, tamoxifen-treated mice (n = 7 for *Ccr2-creER^{T2/+}* [white bars], n = 9 for *Ccr2-creER^{T2/+} Csf2rb^{fl/fl}* [red bars], n = 3 for naive WT mice [black bars]) for myelin (LFB and PAS); scale bars represent 400 μm in the overview images and 100 μm in the insets.

*p < 0.05, **p < 0.01, ***p < 0.001 (Student's t test, unpaired, C and D). Error bars represent ± SEM. See also Figures S3, S4, S5, and S7.

GM-CSF and IL-1 Reciprocally Enhance Inflammation in the Inflamed CNS

The *Csf2rb*-mediated modulation of IL-1β expression in moDCs led us to characterize the interaction between GM-CSF and IL-1 during EAE pathogenesis. We immunized IL-1R-deficient mice and analyzed the quality of inflammation in the SLNs and CNS. As previously described (Lukens et al., 2012), *Il1r^{-/-}* mice were resistant to EAE (Figure S6A). Our data show that GM-CSF-expressing Th cell subsets are not generated in the SLN after im-

munization (Figure S6B). Given this profound defect, *Il1r^{-/-}* mice fail to develop CNS inflammation (Figure S6C). To study the interdependence of moDC-derived IL-1 and T-cell-derived GM-CSF within an inflamed CNS, we generated EAE-susceptible mixed BM chimeras. Chimeric mice bearing both *Csf2rb^{+/+}* (CD45.1) and *Csf2rb^{LacZ/LacZ}* (CD45.2) hematopoietic compartments were generated. At the peak of disease, CNS-infiltrating moDCs required a GM-CSF-mediated signal for optimal expression of IL-1α and IL-1β (Figures S6D and S6E). Chimeric mice

with mixed *Il1r^{+/+}* (CD45.1) and *Il1r^{-/-}* (CD45.2) BM were also immunized and T cells were isolated from the CNS at the peak of disease. We observed that GM-CSF-expressing pathogenic T cells require IL-1R (Figures S6F and S6G). Therefore, our data show that T-cell-derived GM-CSF acts on moDCs to enhance IL-1 expression, which in turn drives the expansion of GM-CSF-producing pathogenic T cells, leading to immune amplification and a continuation of inflammation in the CNS.

The GM-CSF-Dependent Expression Signature of CNS-Infiltrating moDCs

When all strains and myeloid cells analyzed in this report are considered, only *Ccr2-creER^{T2+/+} Csf2rb^{fl/fl}* mice provided a sufficient level of deletion in Ly6C^{hi} monocytes and, by virtue of the irreversibility of Cre-mediated recombination, in their progeny (Figure S7). We asked whether GM-CSF directly controls the wider inflammatory capacity of monocyte-derived inflammatory cells in vivo. *Csf2rb^{+/+}:Csf2rb^{LacZ/LacZ}* mixed chimeras were immunized and both *Csf2rb^{+/+}* and *Csf2rb^{LacZ/LacZ}* moDCs infiltrating the same inflamed CNS at the peak of disease were FACS sorted and mRNA was extracted. Next generation sequencing (NGS) was performed on these samples, and the genome-wide expression profiles were obtained and compared (Figures 6A and 6B). Of more than 22,000 genes expressed in these cells, we identified 1,490 significantly altered expression features between *Csf2rb^{+/+}* or *Csf2rb^{LacZ/LacZ}* cells conforming to a stringent significance threshold ($p < 0.001$). We confirmed the absence of *Csf2rb*, whereas the *Csf2ra* expression was not significantly altered. Furthermore, expression of GM-CSF-regulated PPAR γ (encoded by *Pparg*), a molecule required for the development and function of alveolar macrophages (Schneider et al., 2014), was highly upregulated by GM-CSF (Figure 6C).

Further in-depth analysis of the GM-CSF-induced transcriptome of tissue-infiltrating *Csf2rb^{LacZ/LacZ}* moDCs revealed a wide range of cellular mechanisms that were directly controlled by GM-CSF signaling. Expression of CCL6, CCL17, and CCL24 was strikingly reduced in moDCs lacking functional GM-CSF receptors (Figure 6D). The interactions of these chemokines with their receptors induce migration of phagocytic cells to inflammatory foci and have been shown to be critical for the development of EAE (Asensio et al., 1999; Forde et al., 2011; Rottman et al., 2000). These data show that GM-CSF directly modulates the expression of these chemoattractant proteins. The CD137L/CD137 interaction has been shown to be critically involved in development of EAE (Martínez Gómez et al., 2012). Although more classical costimulatory molecules including CD40, CD86, and CD80 were not induced by GM-CSF, CD137 (4-1BB, *Tnfrsf9*) was dramatically upregulated by GM-CSF in tissue-infiltrating moDCs.

Phagocytic moDCs in the CNS have been recently linked to EAE progression (Yamasaki et al., 2014). Genes including *Mfge8*, *Cd1d1*, *Pld1*, *Scarb1*, *Clec7a*, and *Anxa1* are involved in phagocytosis and require GM-CSF for optimal expression (Figure 6D). Manipulating inflammasome function has also been used successfully to dampen clinical EAE manifestations (Bordon, 2012). More specifically, key components of the NLRP3 inflammasome, namely ASC and NLRP3, play important roles in EAE pathogenesis (Inoue et al., 2012), and IL-1 expression has been linked to blood brain barrier integrity (Argaw

et al., 2006). We selected genes linked to inflammasome function and expression in tissue-infiltrating moDCs and assessed their dependence on GM-CSF. In addition to the NLRP3 inflammasome, we assessed the GM-CSF-mediated regulation of genes involved in NLRP1, IPAF, and AIM2 inflammasomes (Schroder and Tschopp, 2010). We observed that *Pycard*, encoding ASC, was significantly reduced in *Csf2rb^{LacZ/LacZ}* moDCs (Figure 6D). Thus, NLRP3 and AIM2 inflammasome function in moDCs is directly regulated by GM-CSF due to their requirement for ASC expression.

Collectively, GM-CSF is not required for the development of inflammatory monocyte-derived cells, but it has a fundamental impact on the capacity of these cells to coordinate tissue inflammation by inducing multiple, defined cellular pathways required for fulminant phagocytic function and proinflammatory responses. This dataset provides a full account of the transcriptome of GM-CSF-activated myeloid cells, which infiltrate the CNS and mediate tissue damage.

GM-CSF Regulates IL-1 Expression in Human Monocytes

The importance of GM-CSF in CNS inflammatory disease has recently also been translated to MS in humans (Hartmann et al., 2014; Noster et al., 2014; Rasouli et al., 2015). More specifically, it has been shown that MS patients have increased frequencies of GM-CSF-producing Th cells and this has been associated with increased disease activity and severity (Hartmann et al., 2014). To test whether our findings in EAE translate to the human system, we examined whether GM-CSF elicits similar pathogenic functions in human myeloid cells. For this purpose, we used mass cytometry, an emerging technology for the study of leukocyte subpopulations (Becher et al., 2014) and their cytokine responsiveness (Bendall et al., 2011). We analyzed the GM-CSF-induced response of whole human blood by examining the breadth of STAT5 phosphorylation after stimulation. Consistent with the respective populations in mice, we found that human monocytes, as well as granulocytes (basophils, neutrophils), strongly phosphorylated STAT5 in response to GM-CSF (Figures 7A and 7B). The obtained high-dimensional data were subjected to unsupervised dimensionality reduction (t-SNE) to identify and visualize the major leukocyte populations found in human peripheral blood (Figures 7C and 7D; Amir et al., 2013).

Next, we analyzed possible pathogenic mechanisms elicited by GM-CSF downstream of STAT5 phosphorylation. Human peripheral blood mononucleated cells (PBMCs) stimulated with GM-CSF showed a consistent upregulation of IL-1 β expression (Figure 7E). Taken together, our data indicate that also human monocytes readily respond to GM-CSF by STAT5 phosphorylation and elicit a pathogenic program, which is characterized by the expression of IL-1 β .

DISCUSSION

T-cell-mediated chronic inflammatory autoimmune disorders are initiated by dysregulated, autoantigen reactive Th cells. However, Th cells are not the major executors of tissue damage. Myeloid cells accumulate in abundance at inflammatory foci where they often represent the dominant cell type. We show that GM-CSF directly links the disease-initiating capacity of

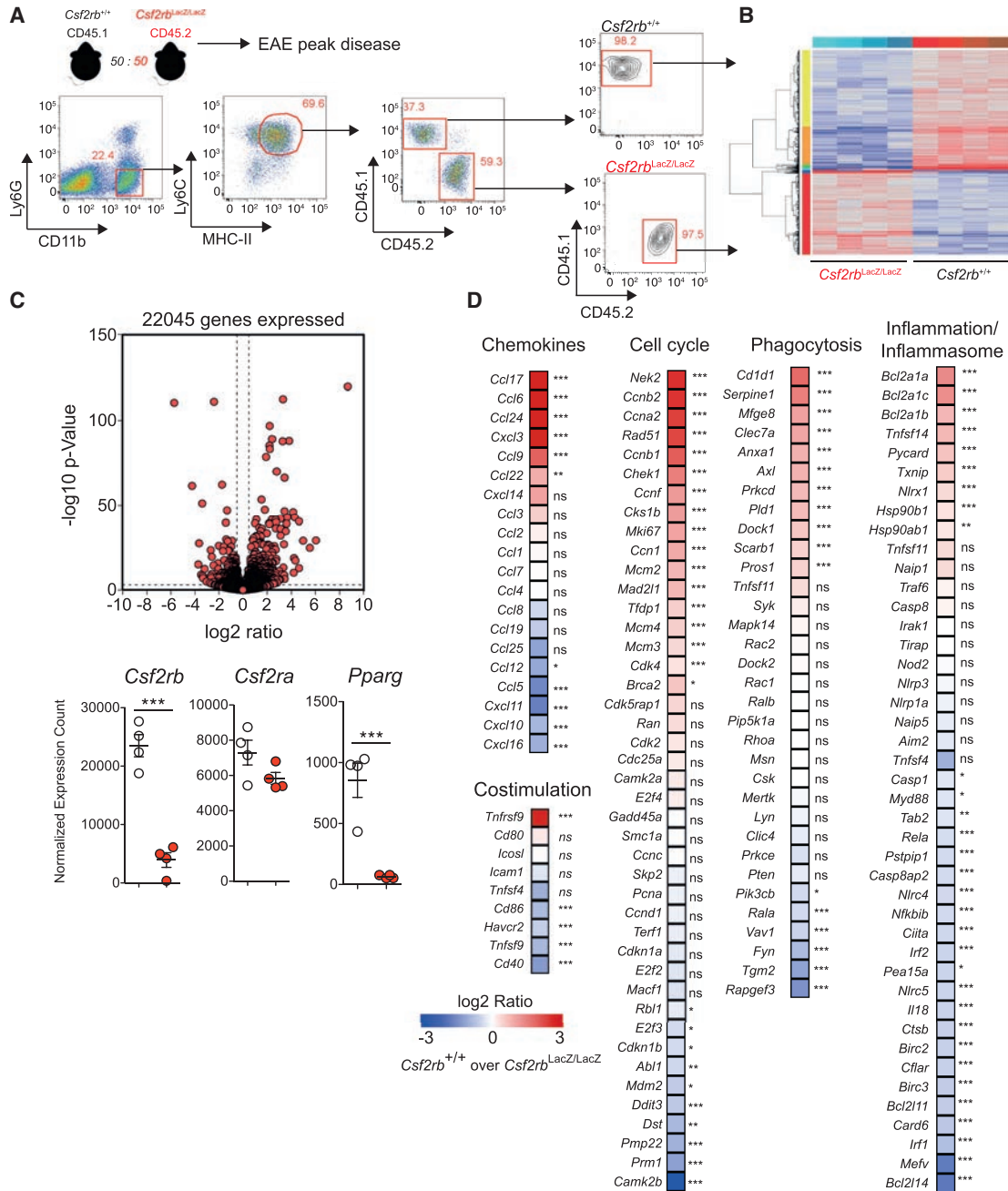


Figure 6. Identification of the GM-CSF-Dependent Expression Signature in CNS-Infiltrating moDCs

(A) Cohorts of 7–10 mixed BM chimeric mice (CD45.2 *Csf2rb*^{LacZ/LacZ}; CD45.1 *Csf2rb*^{+/+}) were immunized. At the peak of disease, mice were sacrificed and pooled and CNS-infiltrating moDCs were FACS sorted based on their expression of congenic CD45. One representative out of four independent FACS sorts is shown. (B) Next generation sequencing (NGS) was performed on RNA extracted from sorted cells of four independent EAE immunizations and CNS harvests. 1,490 genes are significantly altered to a minimum significance threshold of p < 0.001.

(C) Volcano plots showing the Log₂ ratio versus –log₁₀ p value (*Csf2rb*^{+/+}/*Csf2rb*^{LacZ/LacZ}). Normalized expression counts for the indicated genes (*Csf2rb*, *Csf2ra*, and *Pparg*) are shown. Each data point (open circles, *Csf2rb*^{+/+}; red circles, *Csf2rb*^{LacZ/LacZ}) represents a pooled value from 7–10 chimeric animals.

(D) Heat maps showing GM-CSF-regulated genes, clustered to their indicated pathways. Significance is shown alongside. *p < 0.05, **p < 0.01, ***p < 0.001 (Student's t test, unpaired).

Error bars represent ± SEM. See also Figure S6 and Accession Numbers.

pathogenic Th cells with the inflammatory signature of monocytes and their progeny. Since the initial observation that GM-CSF-deficient mice were resistant to EAE (McQualter et al.,

2001), numerous groups have investigated which responder cells mediate this phenotype. By systematic analysis, we could exclude a critical role for GM-CSF sensing in cDCs, neutrophils,

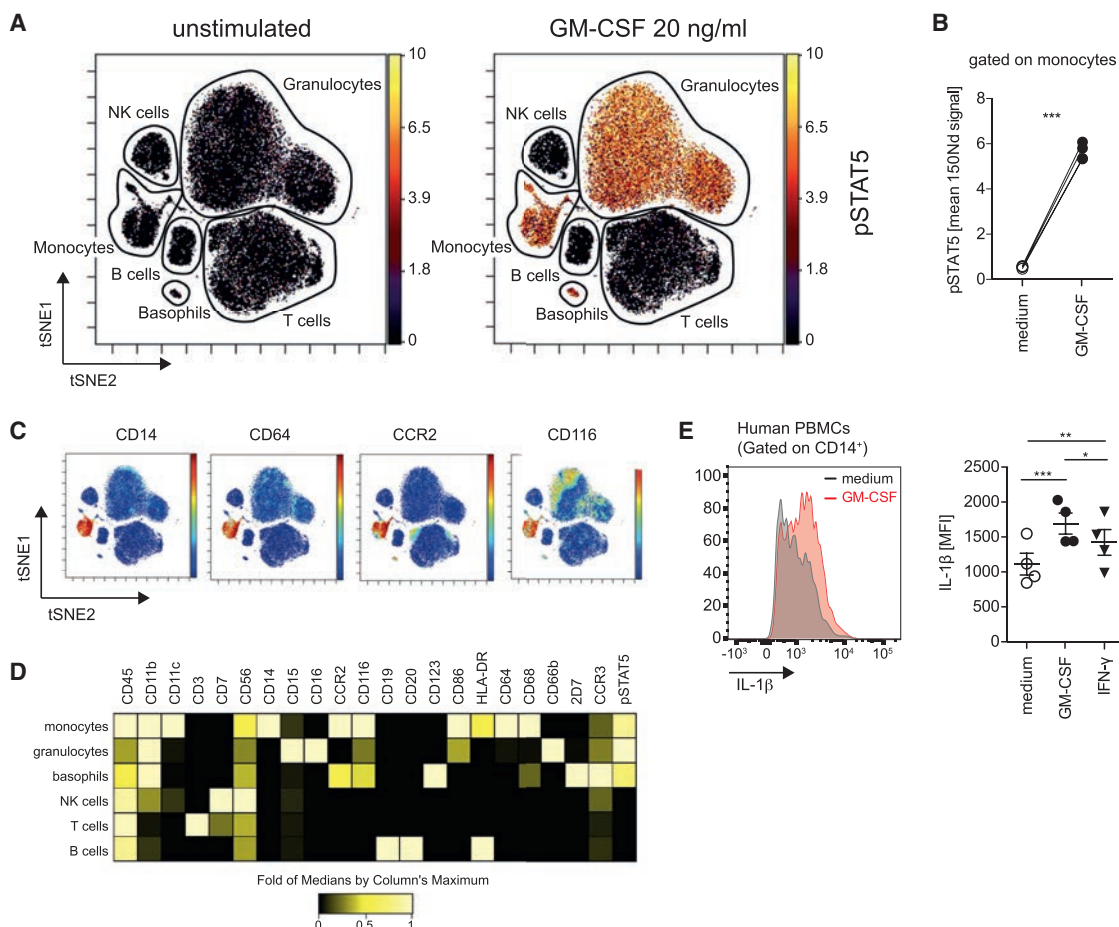


Figure 7. Human Monocytes Phosphorylate STAT5 and Produce IL-1 β in Response to GM-CSF Stimulation

(A) Annotated t-SNE map depicting the STAT5 phosphorylation (black to yellow gradient) upon GM-CSF stimulation in leukocyte populations from human whole blood. GM-CSF-stimulated whole blood was stained with heavy-metal labeled antibodies and acquired on a mass cytometer. Data represent two experiments. (B) Cumulative results of GM-CSF-induced pSTAT5 upregulation in human monocytes from four healthy individuals as shown overlaid in (A). (C) Selected channels used in the t-SNE analysis to identify monocytes are overlaid as a color-coded z-dimension. (D) Expression of all markers in the identified leukocyte populations (as seen in A) that were used for the t-SNE dimensionality reduction, plus the pSTAT5 staining intensity of GM-CSF-stimulated samples (not used for t-SNE). (E) Histogram and cumulative MFI of human PBMCs that were stimulated with or without 20 ng/ml GM-CSF or IFN- γ for 6 hr in the presence of monensin and analyzed for IL-1 β production. Data represent two experiments with similar GM-CSF-induced upregulation of IL-1 β observed. Error bars represent \pm SEM.

and microglia. Instead, we identified Ly6C^{hi}CCR2⁺ monocytes to be critically dependent on a specific signaling event that licenses a pathogenic gene expression signature, which in turn initiates a self-perpetuating inflammatory cascade within the tissue.

Our data confirm that cDCs respond readily to GM-CSF, which translates to the regulation of several hundred genes affecting survival and apoptosis (Kc et al., 2014). However, the role of cDCs in EAE has been challenged (Becher and Greter, 2012; Yogev et al., 2012). Moreover, *Batf3*^{-/-} mice, which lack CD8⁺ and CD103⁺ DCs, are not EAE resistant (Edelson et al., 2011). Thus, despite an active response to GM-CSF by cDCs, ablating GM-CSF responsiveness in these cells did not result in EAE resistance. We show that moDCs accumulate in the SLNs during early EAE. Our data suggest that GM-CSF-driven moDCs play a non-redundant role during the generation of pathogenic T cells through expression of polarizing cytokines

such as IL-1 β . A role for monocytes and monocyte-derived cells in antigen presentation is now also beginning to emerge (Jakubzick et al., 2013), suggesting that monocytes and their progeny (largely MHC-II⁺) can perform functions traditionally associated with cDCs. Their low expression of CD11c compared to cDCs might indeed allow a significant proportion of moDCs to escape traditional depletion systems using CD11c-linked diphtheria toxin receptor, particularly if CD11c-Cre is employed.

Neutrophils were also proposed to be essential in the pathogenesis of EAE (Kroenke et al., 2010). However, deletion of the GM-CSF signaling pathway in neutrophils (using the *Ly2z*-cre *Csf2rb*^{fl/fl} system) had no bearing on EAE progression. The data here do not challenge the relative importance of neutrophils per se, but exclude a critical role for GM-CSF for their pathogenicity. Neutrophils are also a major GM-CSF-responsive cell

type, with expression of genes involved in cell cycle, metabolism, host defense, and apoptosis activated after GM-CSF engagement (Kobayashi et al., 2005). Despite both cell types being present in the inflamed CNS, the inflammatory signature induced by GM-CSF in neutrophils is not essential for neuroinflammation.

CNS-invading moDCs were recently found to mediate demyelination during EAE (Yamasaki et al., 2014). Ly6C^{hi} monocytes and their progeny are critical for preclinical autoimmunity using *Ccr2*^{-/-} mice or diverse depletion systems (Ko et al., 2014; Mildner et al., 2009). We can conclude that GM-CSF plays no role in the phenotypic transition of monocyte to moDCs in terms of classical surface markers. During the course of the study, it proved essential to delete *Csf2rb* in CCR2⁺Ly6C^{hi} monocytes prior to their differentiation to moDCs using the *Ccr2-creER*^{T2+/+} *Csf2rb*^{fl/fl} mice. The susceptibility and progression of EAE in *Ly2z-cre Csf2rb*^{fl/fl} mice, despite largely efficient targeting of CNS-infiltrating moDCs, showed that the critical signal sent to monocytes by GM-CSF takes place prior to their terminal differentiation. More than half of Ly6C^{hi} monocytes in immunized *Ly2z-cre Csf2rb*^{fl/fl} mice retained their GM-CSF responsiveness, representing a significant window after migration into an inflamed site during which GM-CSF can initiate an inflammatory signature.

Among the GM-CSF-induced genes expressed by moDCs in the inflamed CNS, CCL6, CCL24, and CCL17 are also known to be critical for EAE development (Asensio et al., 1999; Forde et al., 2011; Rottman et al., 2000). Interestingly, their collective primary function is to recruit more myeloid cells into the inflammatory foci, highlighting a GM-CSF-driven immune amplification during neuroinflammation. Once arriving in the inflamed CNS, GM-CSF sustains the expression of the adaptor protein ASC in moDCs. Given that IL-1 expression is known to modulate blood brain barrier integrity (Argaw et al., 2006), a functional inflammatory response resulting in elevated, mature IL-1 within the CNS would contribute significantly to EAE progression. The role for IL-1 in the generation of Th17 cells during EAE has been proposed previously (Chung et al., 2009), and we add to this observation by highlighting the role of IL-1R for optimal GM-CSF expression by encephalitogenic Th cells in the inflamed brain. Therefore, therapeutic interventions aimed at targeting GM-CSF during inflammation will restrict not only the inflammatory myeloid responder cells but also the autoaggressive T cells providing GM-CSF.

The intention of this report is to bring consensus to the autoimmunity field and provide unambiguous evidence as to where and why GM-CSF has such an impact in tissue damage, and which cell types require a GM-CSF signaling event to mediate inflammation. Autoaggressive, pathogenic T cells license an inflammatory program in monocytes through GM-CSF, which become pathogenic moDCs. This cell population is in fact the most abundant cellular infiltrate in neuroinflammation and the best equipped to cause the tissue damage and demyelination observed in EAE. In addition to potential therapeutic benefits of targeting GM-CSF directly, a selection of GM-CSF-induced pathological mechanisms within tissue-destructive myeloid cells are outlined in this study. As such, not only GM-CSF itself, but also downstream effector proteins, are potentially open to inhibitory interventions.

EXPERIMENTAL PROCEDURES

Mice

To generate *Csf2rb*^{LacZ} mice, targeted JM8.A3 embryonic stem cells were obtained from EUCOMM (*Csf2rb*^{tm1a(EUCOMM)Hmg}; IKMC project: 80282). The L1L2_Bact_P cassette was placed upstream of exon 4. Usage of the EN2 (engrailed 2) splice acceptor results in a fusion message between the first three exons and the LacZ reporter sequence, resulting in a truncated *Csf2rb* message. Mice were further crossed to a flip-deleter strain, resulting in a LoxP-flanked exon 4 of *Csf2rb*, allowing for Cre-mediated conditional gene deletion. Primers for *Csf2rb*^{fl} PCR were as follows: forward, 5'-GAG AGA GGG TCC TTT TGG TC-3'; reverse, 5'-CCT CCC CTC TTC TGT ATC TTC-3'. Band size for WT was 297 bp; for *Csf2rb*^{fl}, 350 bp. Primers for *Csf2rb*^{LacZ} PCR (P1 and P2 = WT; P1 and P3 = LacZ) were as follows: P1, 5'-ACC ACC ACC AGC ATC CAA TC-3'; P2, 5'-CCC TCT TCT GTA TCT TCG CC-3'; P3, 5'-CAC TGA GTC TCT GGC ATC TC-3'.

The *Ccr2-creER*^{T2} mKate2 strain was generated upon request by Taconic-Artemis (PCR: forward, 5'-CTC TAC TTC ATC GCA TTC CTT GC-3'; reverse, 5'-GGT TGA TGA AGG TTT TGC TGC-3'; band size = 341 bp). *Ly2z-cre* and *Cd207-cre* mice were provided by Björn Clausen. *Itgax-cre* mice were provided by Boris Reizis. *Il1r*^{-/-} mice have been previously described (Glaccum et al., 1997), as have TdTomato reporter mice (Madisen et al., 2010) and *Csf2rb*^{-/-} mice (Robb et al., 1995). All cre strains were heterozygous unless otherwise indicated. All animal experiments performed in this study were approved by the Cantonal Veterinary Office Zurich.

EAE, Tamoxifen Treatment, and Bone Marrow Chimeras

EAE was induced and clinically scored as previously described (Codarri et al., 2011). Tamoxifen (Sigma) was dissolved in ethanol and corn oil to 25 mg/ml and administered in 200 μ l doses via oral gavage (5 mg/dose), or administered via tamoxifen-containing food (Harlan). For generation of BM chimeras, host animals received a split dose (2 \times 550 Rad with 24 hr interval) before receiving 5 \times 10⁶ donor BM cells i.v. injected. 50:50 mixed chimeras received 2.5 \times 10⁶ cells from BM donors of each genotype.

Flow Cytometry and Mass Cytometry

More detailed information on flow cytometry (including antibody clones), intracellular staining protocols, pSTAT phosphorylation/detection protocols, and CyTOF data handling can be found in the Supplemental Experimental Procedures.

Histopathological Analysis of EAE Tissue

LFB-PAS stainings were done according to standard protocols on 4% PFA-fixed, paraffin-embedded, and 2- μ m-thick tissue sections. We analyzed EAE histopathology on cross-sections (four to six per mouse) of lumbar spinal cords and recorded digital images of tissue sections with a Zeiss Axio Scan.Z1 Slide Scanner (Carl Zeiss, MicroImaging GmbH) with a 20 \times (air, NA 0.8) objective. Total demyelinated area of LFB- and PAS-stained sections was measured in μ m² by Fiji/ImageJ 1.46j software (NIH) and the area of demyelination calculated as percentage of the whole area of white matter within a given section.

Next Generation Sequencing

Chimeric mice were immunized and at peak diseases, moDCs were isolated from brain and spinal cord as described above and FACS sorted (BD FACSAria III). Total RNA from a minimum of 5 \times 10⁵ up to 1.2 \times 10⁶ cells was isolated with QIAGEN RNeasy Plus Micro Kit according to manufacturer's instructions resulting in RIN \geq 8. NGS was performed by the Functional Genomics Center Zurich (<http://www.fgc.zh.ch>).

Statistical Analysis

Mean values, SEM values, and Student's t test (unpaired) were calculated with Prism (GraphPad software). *p < 0.05, **p < 0.01, ***p < 0.001. Significance for pooled EAE experiments was performed by two-way ANOVA analysis.

ACCESSION NUMBERS

Sequencing information is available at the European Bioinformatics Institute (EBI) (ENA: PRJEB9884).

SUPPLEMENTAL INFORMATION

Supplemental Information includes seven figures and Supplemental Experimental Procedures and can be found with this article online at <http://dx.doi.org/10.1016/j.immuni.2015.08.010>.

AUTHOR CONTRIBUTIONS

A.L.C., M.G., M.L., F.J.H., and F.M. designed and performed the experiments, analyzed data, and prepared figure panels. P.P. coordinated the generation of the *Csf2rb*^{LacZ} mice. B.S. performed and analyzed histology. B.E.C. and S.J. provided mice used in the study and constructive criticism. A.L.C. and B.B. wrote the manuscript. B.B. directed and funded the study.

ACKNOWLEDGMENTS

This work was supported by grants from the Swiss national science foundation (PP00P3_144781 to M.G., 310030_146130 and 316030_150768 to B.B.), the European Union, FP7 ITN_NeuroKine and the European Union FP7 project TargetBrain (279017) (B.B.), the Swiss Multiple Sclerosis Society (B.B. and M.G.), and the University Priority Project Translational Cancer Research (B.B.). A.L.C. holds an EMBO Long term Fellowship (ALTF 508-2011) and was further supported by the Forschungskredit awarded by the University of Zürich. We thank Adriano Flora at TaconicArtemis for generating the *Ccr2-creER²* mKate2 strain, Lennart Opitz and Anna Bratus for performing the NGS analysis at the Functional Genomics Centre Zürich (FGCZ), Carsten Krieg for the labeling of antibodies used in CyTOF analyses, and Jennifer Jaberg, Jan Candreia, and Sabrina Nemetz for technical support.

Received: January 15, 2015

Revised: May 4, 2015

Accepted: June 1, 2015

Published: September 1, 2015

REFERENCES

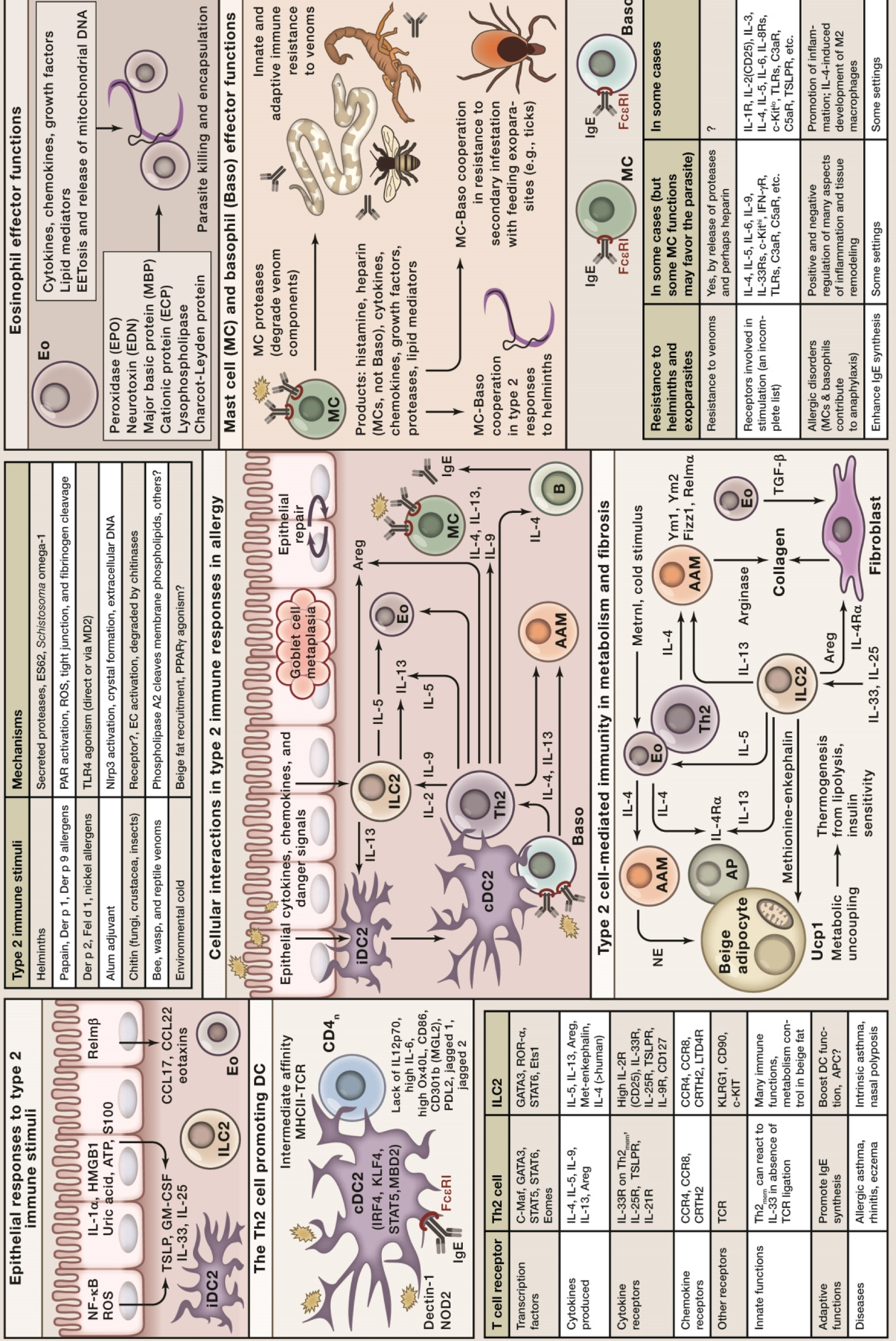
- Amir, A.D., Davis, K.L., Tadmor, M.D., Simonds, E.F., Levine, J.H., Bendall, S.C., Shenfeld, D.K., Krishnaswamy, S., Nolan, G.P., and Pe'er, D. (2013). viSNE enables visualization of high dimensional single-cell data and reveals phenotypic heterogeneity of leukemia. *Nat. Biotechnol.* **31**, 545–552.
- Argaw, A.T., Zhang, Y., Snyder, B.J., Zhao, M.L., Kopp, N., Lee, S.C., Raine, C.S., Brosnan, C.F., and John, G.R. (2006). IL-1beta regulates blood-brain barrier permeability via reactivation of the hypoxia-angiogenesis program. *J. Immunol.* **177**, 5574–5584.
- Asensio, V.C., Lassmann, S., Pagenstecher, A., Steffensen, S.C., Henriksen, S.J., and Campbell, I.L. (1999). C10 is a novel chemokine expressed in experimental inflammatory demyelinating disorders that promotes recruitment of macrophages to the central nervous system. *Am. J. Pathol.* **154**, 1181–1191.
- Becher, B., and Greter, M. (2012). Acquitting an APC: DCs found “not guilty” after trial by ablation. *Eur. J. Immunol.* **42**, 2551–2554.
- Becher, B., Schlitzer, A., Chen, J., Mair, F., Sumatoh, H.R., Teng, K.W., Low, D., Ruedl, C., Riccardi-Castagnoli, P., Poidinger, M., et al. (2014). High-dimensional analysis of the murine myeloid cell system. *Nat. Immunol.* **15**, 1181–1189.
- Bendall, S.C., Simonds, E.F., Qiu, P., Amir, A.D., Krutzik, P.O., Finck, R., Bruggner, R.V., Melamed, R., Trejo, A., Ornatsky, O.I., et al. (2011). Single-cell mass cytometry of differential immune and drug responses across a human hematopoietic continuum. *Science* **332**, 687–696.
- Bordon, Y. (2012). Autoimmunity: Inflammation dependency key for treating EAE. *Nat. Rev. Immunol.* **12**, 477.
- Burmester, G.R., Feist, E., Sleeman, M.A., Wang, B., White, B., and Magrini, F. (2011). Mavrilimumab, a human monoclonal antibody targeting GM-CSF receptor- α , in subjects with rheumatoid arthritis: a randomised, double-blind, placebo-controlled, phase I, first-in-human study. *Ann. Rheum. Dis.* **70**, 1542–1549.
- Caton, M.L., Smith-Raska, M.R., and Reizis, B. (2007). Notch-RBP-J signaling controls the homeostasis of CD8⁺ dendritic cells in the spleen. *J. Exp. Med.* **204**, 1653–1664.
- Chung, Y., Chang, S.H., Martinez, G.J., Yang, X.O., Nurieva, R., Kang, H.S., Ma, L., Watowich, S.S., Jetten, A.M., Tian, Q., and Dong, C. (2009). Critical regulation of early Th17 cell differentiation by interleukin-1 signaling. *Immunity* **30**, 576–587.
- Clausen, B.E., Burkhardt, C., Reith, W., Renkawitz, R., and Förster, I. (1999). Conditional gene targeting in macrophages and granulocytes using LysMcre mice. *Transgenic Res.* **8**, 265–277.
- Codarri, L., Gyölvésci, G., Tosevski, V., Hesse, L., Fontana, A., Magnenat, L., Suter, T., and Becher, B. (2011). ROR γ t drives production of the cytokine GM-CSF in helper T cells, which is essential for the effector phase of autoimmune neuroinflammation. *Nat. Immunol.* **12**, 560–567.
- Cotsapas, C., and Hafler, D.A. (2013). Immune-mediated disease genetics: the shared basis of pathogenesis. *Trends Immunol.* **34**, 22–26.
- Edelson, B.T., Bradstreet, T.R., Kc, W., Hildner, K., Herzog, J.W., Sim, J., Russell, J.H., Murphy, T.L., Unanue, E.R., and Murphy, K.M. (2011). Batf3-dependent CD11b(low/-) peripheral dendritic cells are GM-CSF-independent and are not required for Th cell priming after subcutaneous immunization. *PLoS ONE* **6**, e25660.
- Forde, E.A., Dogan, R.N., and Karpus, W.J. (2011). CCR4 contributes to the pathogenesis of experimental autoimmune encephalomyelitis by regulating inflammatory macrophage function. *J. Neuroimmunol.* **236**, 17–26.
- Gaupp, S., Pitt, D., Kuziel, W.A., Cannella, B., and Raine, C.S. (2003). Experimental autoimmune encephalomyelitis (EAE) in CCR2(-/-) mice: susceptibility in multiple strains. *Am. J. Pathol.* **162**, 139–150.
- Geissmann, F., Manz, M.G., Jung, S., Sieweke, M.H., Merad, M., and Ley, K. (2010). Development of monocytes, macrophages, and dendritic cells. *Science* **327**, 656–661.
- Glaccum, M.B., Stocking, K.L., Charrier, K., Smith, J.L., Willis, C.R., Maliszewski, C., Livingston, D.J., Peschon, J.J., and Morrissey, P.J. (1997). Phenotypic and functional characterization of mice that lack the type I receptor for IL-1. *J. Immunol.* **159**, 3364–3371.
- Greter, M., Heppner, F.L., Lemos, M.P., Odermatt, B.M., Goebels, N., Laufer, T., Noelle, R.J., and Becher, B. (2005). Dendritic cells permit immune invasion of the CNS in an animal model of multiple sclerosis. *Nat. Med.* **11**, 328–334.
- Greter, M., Helft, J., Chow, A., Hashimoto, D., Mortha, A., Agudo-Cantero, J., Bogunovic, M., Gautier, E.L., Miller, J., Leboeuf, M., et al. (2012). GM-CSF controls nonlymphoid tissue dendritic cell homeostasis but is dispensable for the differentiation of inflammatory dendritic cells. *Immunity* **36**, 1031–1046.
- Guilliams, M., De Kleer, I., Henri, S., Post, S., Vanhoutte, L., De Prijck, S., Deswarte, K., Malissen, B., Hammad, H., and Lambrecht, B.N. (2013). Alveolar macrophages develop from fetal monocytes that differentiate into long-lived cells in the first week of life via GM-CSF. *J. Exp. Med.* **210**, 1977–1992.
- Gyölvésci, G., Haak, S., and Becher, B. (2009). IL-23-driven encephalotropism and Th17 polarization during CNS-inflammation in vivo. *Eur. J. Immunol.* **39**, 1864–1869.
- Hartmann, F.J., Khademi, M., Aram, J., Ammann, S., Kockum, I., Constantinescu, C., Gran, B., Piehl, F., Olsson, T., Codarri, L., and Becher, B. (2014). Multiple sclerosis-associated IL2RA polymorphism controls GM-CSF production in human TH cells. *Nat. Commun.* **5**, 5056.
- Inoue, M., Williams, K.L., Gunn, M.D., and Shinohara, M.L. (2012). NLRP3 inflammasome induces chemotactic immune cell migration to the CNS in experimental autoimmune encephalomyelitis. *Proc. Natl. Acad. Sci. USA* **109**, 10480–10485.
- Jakubzick, C., Bogunovic, M., Bonito, A.J., Kuan, E.L., Merad, M., and Randolph, G.J. (2008). Lymph-migrating, tissue-derived dendritic cells are minor constituents within steady-state lymph nodes. *J. Exp. Med.* **205**, 2839–2850.
- Jakubzick, C., Gautier, E.L., Gibbings, S.L., Sojka, D.K., Schlitzer, A., Johnson, T.E., Ivanov, S., Duan, Q., Bala, S., Condon, T., et al. (2013). Minimal

- differentiation of classical monocytes as they survey steady-state tissues and transport antigen to lymph nodes. *Immunity* 39, 599–610.
- Kc, W., Satpathy, A.T., Rapaport, A.S., Briseño, C.G., Wu, X., Albring, J.C., Russler-Germain, E.V., Kretzer, N.M., Durai, V., Persaud, S.P., et al. (2014). L-Myc expression by dendritic cells is required for optimal T-cell priming. *Nature* 507, 243–247.
- King, I.L., Dickender, T.L., and Segal, B.M. (2009). Circulating Ly-6C+ myeloid precursors migrate to the CNS and play a pathogenic role during autoimmune demyelinating disease. *Blood* 113, 3190–3197.
- King, I.L., Kroenke, M.A., and Segal, B.M. (2010). GM-CSF-dependent, CD103+ dermal dendritic cells play a critical role in Th effector cell differentiation after subcutaneous immunization. *J. Exp. Med.* 207, 953–961.
- Ko, H.J., Brady, J.L., Ryg-Cornejo, V., Hansen, D.S., Vremec, D., Shortman, K., Zhan, Y., and Lew, A.M. (2014). GM-CSF-responsive monocyte-derived dendritic cells are pivotal in Th17 pathogenesis. *J. Immunol.* 192, 2202–2209.
- Kobayashi, S.D., Voyich, J.M., Whitney, A.R., and DeLeo, F.R. (2005). Spontaneous neutrophil apoptosis and regulation of cell survival by granulocyte macrophage-colony stimulating factor. *J. Leukoc. Biol.* 78, 1408–1418.
- Kroenke, M.A., Chensue, S.W., and Segal, B.M. (2010). EAE mediated by a non-IFN- γ /non-IL-17 pathway. *Eur. J. Immunol.* 40, 2340–2348.
- Lukens, J.R., Barr, M.J., Chaplin, D.D., Chi, H., and Kanneganti, T.D. (2012). Inflammasome-derived IL-1 β regulates the production of GM-CSF by CD4(+) T cells and $\gamma\delta$ T cells. *J. Immunol.* 188, 3107–3115.
- Madisen, L., Zwingman, T.A., Sunkin, S.M., Oh, S.W., Zariwala, H.A., Gu, H., Ng, L.L., Palmiter, R.D., Hawrylycz, M.J., Jones, A.R., et al. (2010). A robust and high-throughput Cre reporting and characterization system for the whole mouse brain. *Nat. Neurosci.* 13, 133–140.
- Mahad, D.J., and Ransohoff, R.M. (2003). The role of MCP-1 (CCL2) and CCR2 in multiple sclerosis and experimental autoimmune encephalomyelitis (EAE). *Semin. Immunol.* 15, 23–32.
- Martínez Gómez, J.M., Croxford, J.L., Yeo, K.P., Angeli, V., Schwarz, H., and Gasser, S. (2012). Development of experimental autoimmune encephalomyelitis critically depends on CD137 ligand signaling. *J. Neurosci.* 32, 18246–18252.
- McGeachy, M.J., Chen, Y., Tato, C.M., Laurence, A., Joyce-Shaikh, B., Blumenschein, W.M., McClanahan, T.K., O’Shea, J.J., and Cua, D.J. (2009). The interleukin 23 receptor is essential for the terminal differentiation of interleukin 17-producing effector T helper cells in vivo. *Nat. Immunol.* 10, 314–324.
- McQualter, J.L., Darwiche, R., Ewing, C., Onuki, M., Kay, T.W., Hamilton, J.A., Reid, H.H., and Bernard, C.C. (2001). Granulocyte macrophage colony-stimulating factor: a new putative therapeutic target in multiple sclerosis. *J. Exp. Med.* 194, 873–882.
- Mildner, A., Mack, M., Schmidt, H., Brück, W., Djukic, M., Zabel, M.D., Hille, A., Priller, J., and Prinz, M. (2009). CCR2+Ly-6Chi monocytes are crucial for the effector phase of autoimmunity in the central nervous system. *Brain* 132, 2487–2500.
- Noster, R., Riedel, R., Mashreghi, M.F., Radbruch, H., Harms, L., Haftmann, C., Chang, H.D., Radbruch, A., and Zielinski, C.E. (2014). IL-17 and GM-CSF expression are antagonistically regulated by human T helper cells. *Sci. Transl. Med.* 6, 241ra80.
- Ponomarev, E.D., Shriver, L.P., Maresz, K., and Dittel, B.N. (2005). Microglial cell activation and proliferation precedes the onset of CNS autoimmunity. *J. Neurosci. Res.* 81, 374–389.
- Ponomarev, E.D., Shriver, L.P., Maresz, K., Pedras-Vasconcelos, J., Verthelyi, D., and Dittel, B.N. (2007). GM-CSF production by autoreactive T cells is required for the activation of microglial cells and the onset of experimental autoimmune encephalomyelitis. *J. Immunol.* 178, 39–48.
- Rasouli, J., Ciric, B., Imitola, J., Gonnella, P., Hwang, D., Mahajan, K., Mari, E.R., Safavi, F., Leist, T.P., Zhang, G.X., and Rostami, A. (2015). Expression of GM-CSF in T cells is increased in multiple sclerosis and suppressed by IFN- β therapy. *J. Immunol.* 194, 5085–5093.
- Robb, L., Drinkwater, C.C., Metcalf, D., Li, R., Köntgen, F., Nicola, N.A., and Begley, C.G. (1995). Hematopoietic and lung abnormalities in mice with a null mutation of the common beta subunit of the receptors for granulocyte-macrophage colony-stimulating factor and interleukins 3 and 5. *Proc. Natl. Acad. Sci. USA* 92, 9565–9569.
- Rottman, J.B., Slavina, A.J., Silva, R., Weiner, H.L., Gerard, C.G., and Hancock, W.W. (2000). Leukocyte recruitment during onset of experimental allergic encephalomyelitis is CCR1 dependent. *Eur. J. Immunol.* 30, 2372–2377.
- Saederup, N., Cardona, A.E., Croft, K., Mizutani, M., Cotleur, A.C., Tsou, C.L., Ransohoff, R.M., and Charo, I.F. (2010). Selective chemokine receptor usage by central nervous system myeloid cells in CCR2-red fluorescent protein knock-in mice. *PLoS ONE* 5, e13693.
- Schneider, C., Nobs, S.P., Heer, A.K., Kurrer, M., Klinke, G., van Rooijen, N., Vogel, J., and Kopf, M. (2014). Alveolar macrophages are essential for protection from respiratory failure and associated morbidity following influenza virus infection. *PLoS Pathog.* 10, e1004053.
- Schreiber, H.A., Loschko, J., Karssemeijer, R.A., Escolano, A., Meredith, M.M., Mucida, D., Guernonprez, P., and Nussenzweig, M.C. (2013). Intestinal monocytes and macrophages are required for T cell polarization in response to *Citrobacter rodentium*. *J. Exp. Med.* 210, 2025–2039.
- Schroder, K., and Tschopp, J. (2010). The inflammasomes. *Cell* 140, 821–832.
- Serbina, N.V., Salazar-Mather, T.P., Biron, C.A., Kuziel, W.A., and Pamer, E.G. (2003). TNF/iNOS-producing dendritic cells mediate innate immune defense against bacterial infection. *Immunity* 19, 59–70.
- Shibata, Y., Berclaz, P.Y., Chronoes, Z.C., Yoshida, M., Whitsett, J.A., and Trapnell, B.C. (2001). GM-CSF regulates alveolar macrophage differentiation and innate immunity in the lung through PU.1. *Immunity* 15, 557–567.
- Ventura, A., Kirsch, D.G., McLaughlin, M.E., Tuveson, D.A., Grimm, J., Lintault, L., Newman, J., Reczek, E.E., Weissleder, R., and Jacks, T. (2007). Restoration of p53 function leads to tumour regression in vivo. *Nature* 445, 661–665.
- Yamasaki, R., Lu, H., Butovsky, O., Ohno, N., Rietsch, A.M., Cialic, R., Wu, P.M., Doykan, C.E., Lin, J., Cotleur, A.C., et al. (2014). Differential roles of microglia and monocytes in the inflamed central nervous system. *J. Exp. Med.* 211, 1533–1549.
- Yogev, N., Frommer, F., Lukas, D., Kautz-Neu, K., Karram, K., Ielo, D., von Stebut, E., Probst, H.C., van den Broek, M., Riethmacher, D., et al. (2012). Dendritic cells ameliorate autoimmunity in the CNS by controlling the homeostasis of PD-1 receptor(+) regulatory T cells. *Immunity* 37, 264–275.
- Yona, S., Kim, K.W., Wolf, Y., Mildner, A., Varol, D., Breker, M., Strauss-Ayali, D., Viukov, S., Guillems, M., Misharin, A., et al. (2013). Fate mapping reveals origins and dynamics of monocytes and tissue macrophages under homeostasis. *Immunity* 38, 79–91.
- Zahner, S.P., Kel, J.M., Martina, C.A., Brouwers-Haspels, I., van Roon, M.A., and Clausen, B.E. (2011). Conditional deletion of TGF- β 1 using Langerin-Cre mice results in Langerhans cell deficiency and reduced contact hypersensitivity. *J. Immunol.* 187, 5069–5076.

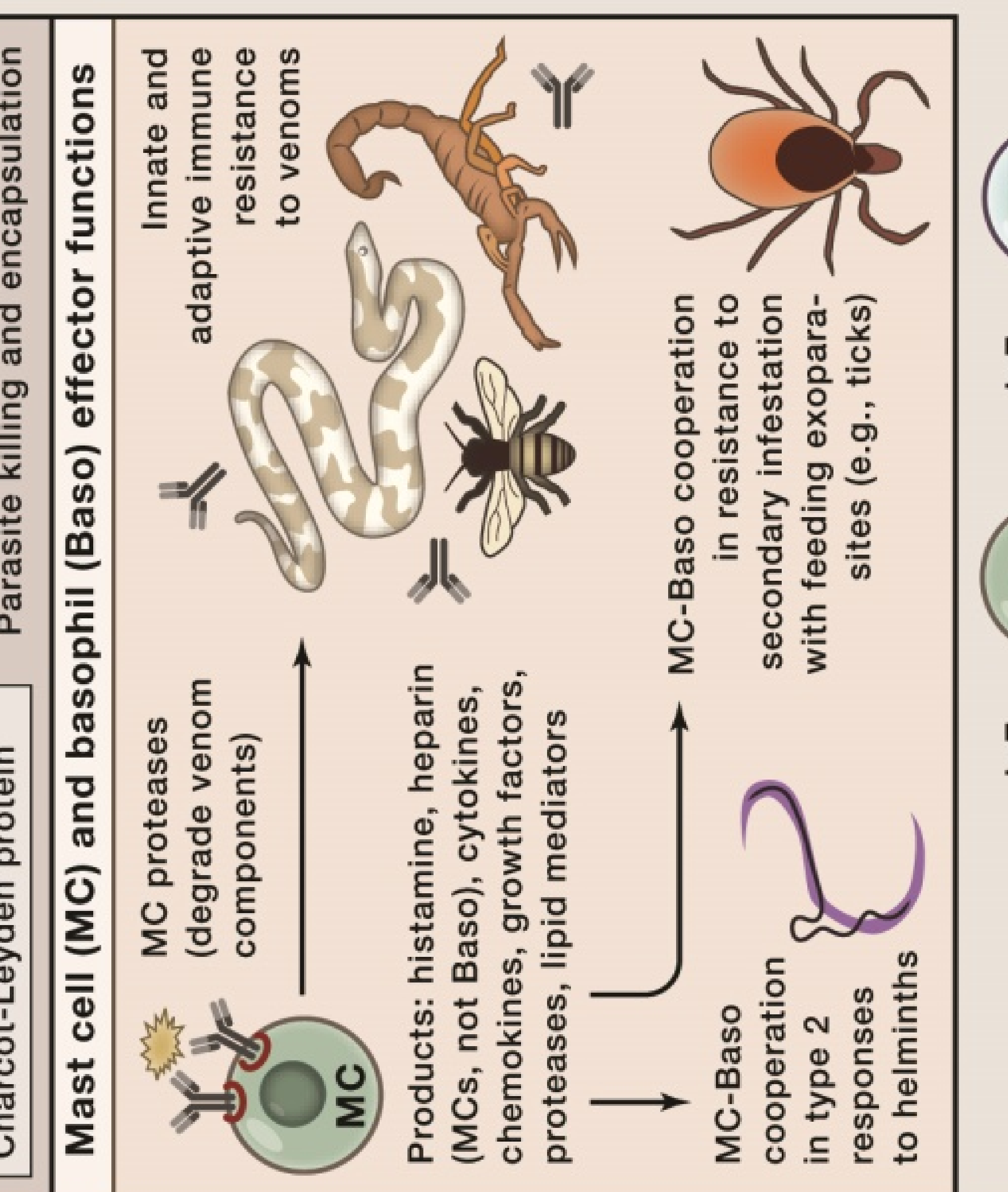
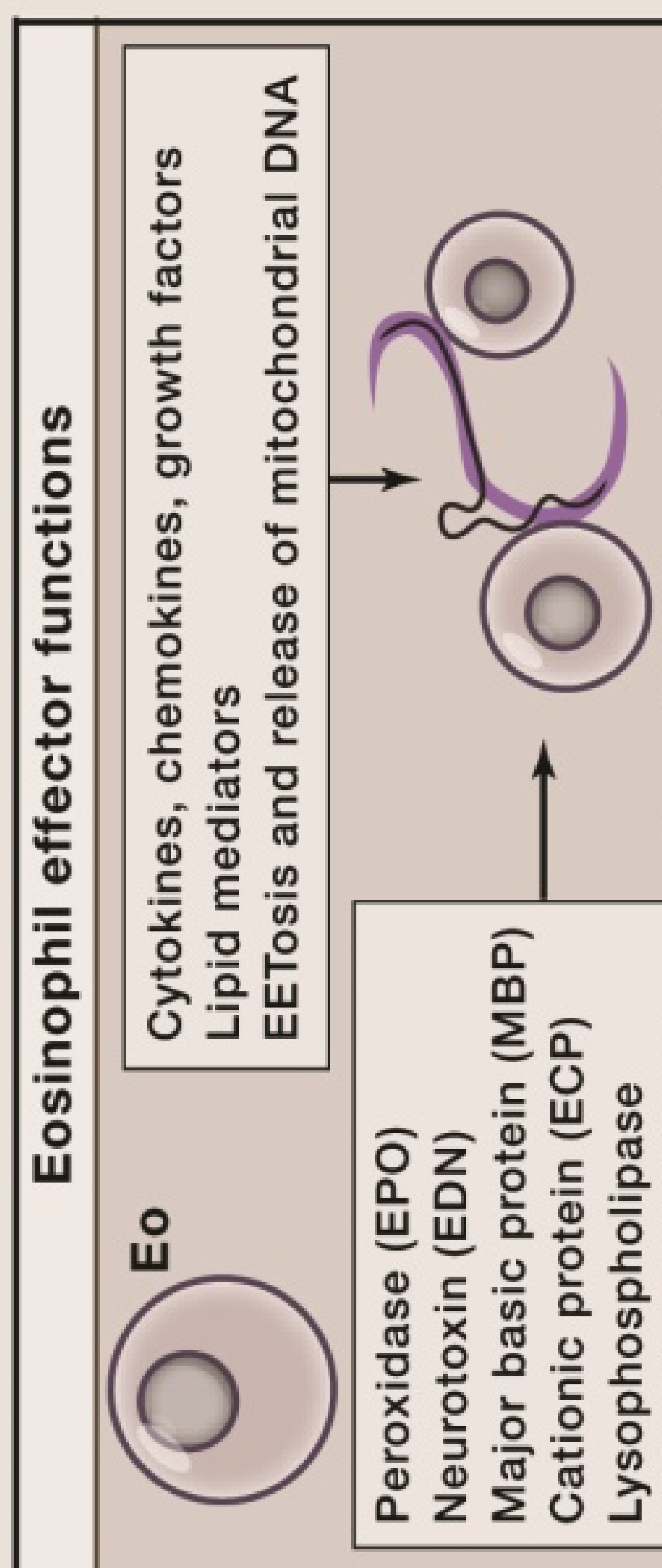
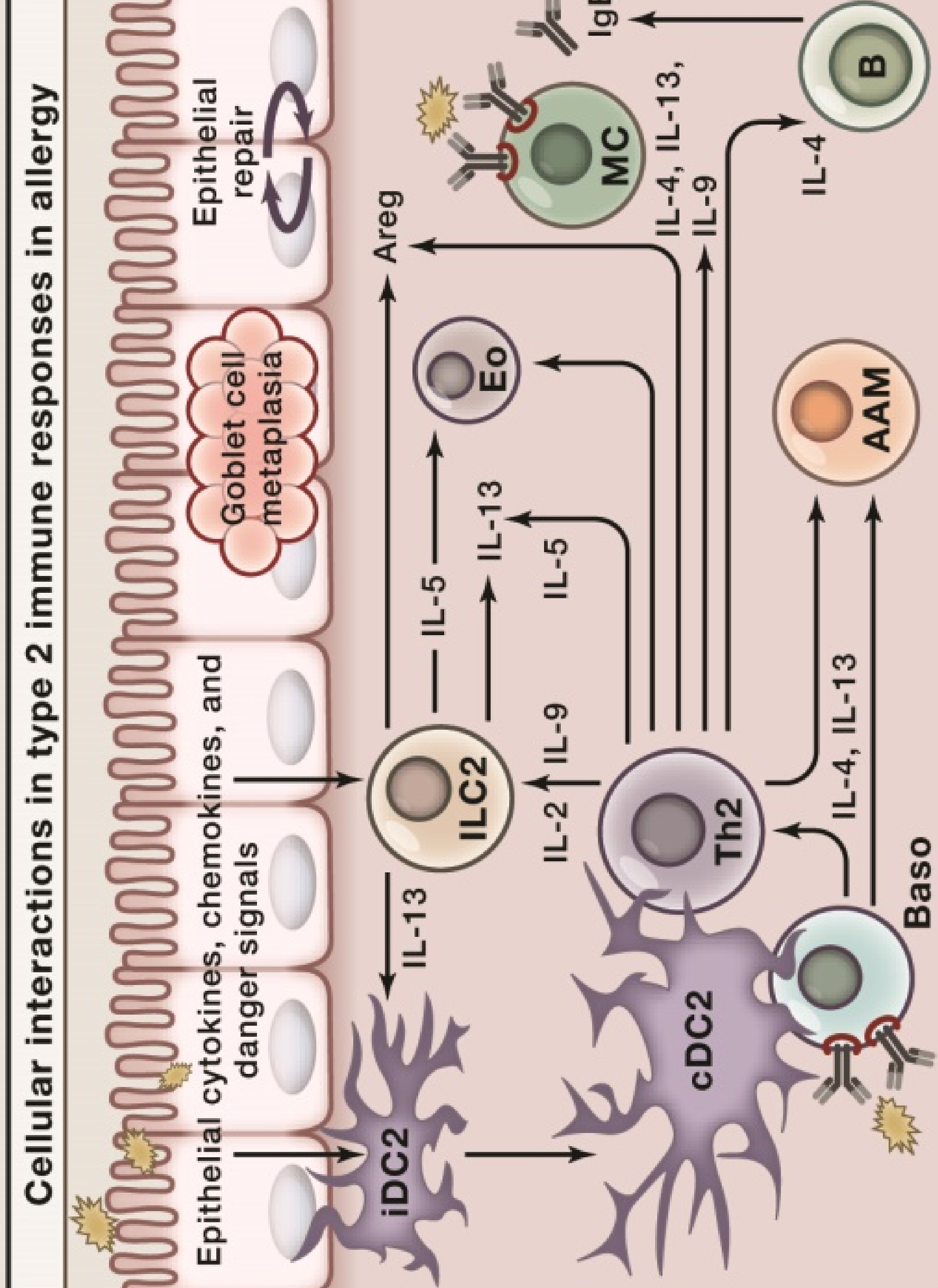
Snapshot: Integrated Type 2 Immune Responses Immunity

Bart N. Lambrecht^{1,2,3} and Stephen J. Galli⁴

¹VIB Inflammation Research Center, Ghent University, 9052 Belgium; ²Department of Respiratory Medicine, University Hospital Ghent, 9000 Belgium
³Department of Pulmonary Medicine, Erasmus MC, 3015 Rotterdam, the Netherlands; ⁴Departments of Pathology and of Microbiology and Immunology, and the Sean N. Parker Center for Allergy Research, Stanford University School of Medicine, Stanford, CA 94305, USA

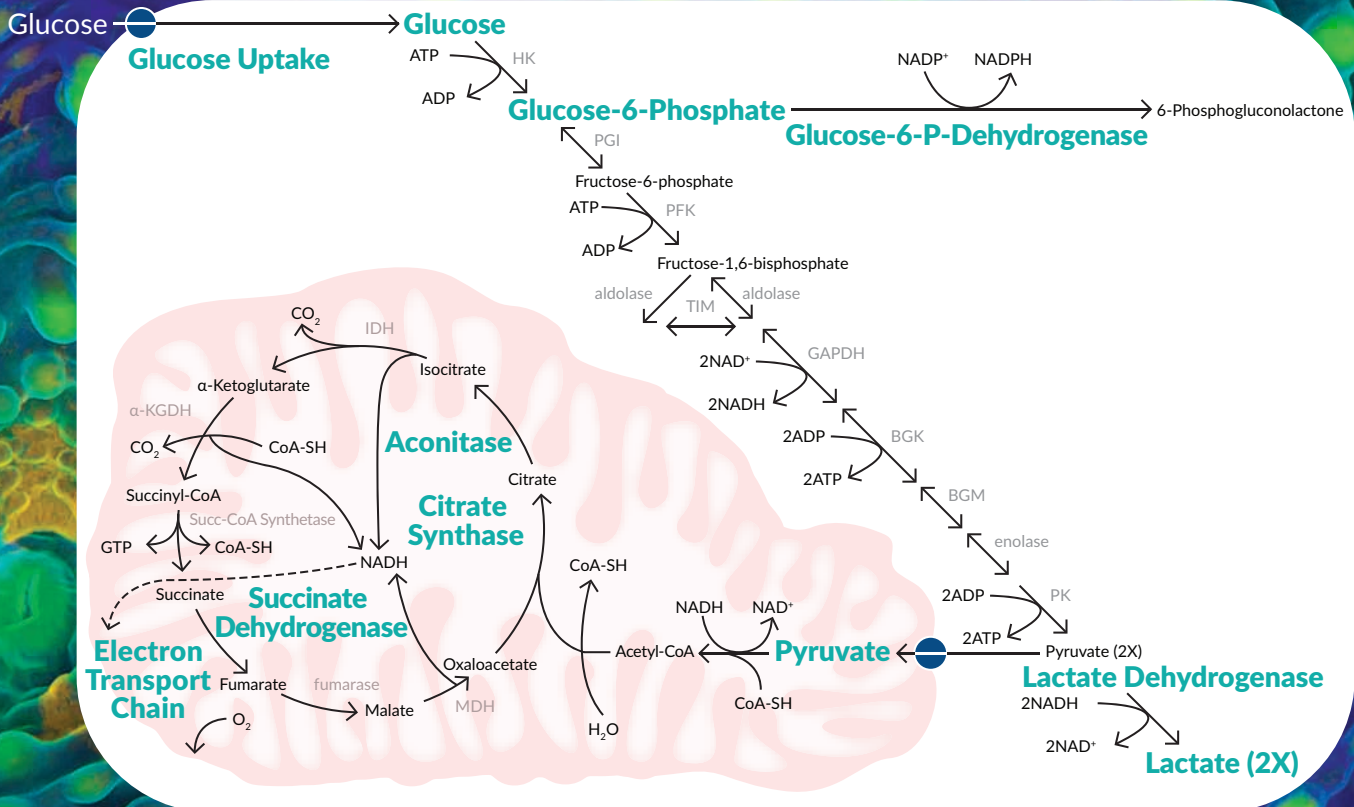


Type 2 immune stimuli	Mechanisms
Helminths	Secreted proteases, ES62, <i>Schistosoma</i> omega-1
Papain, Der p 1, Der p 9 allergens	PAR activation, ROS, tight junction, and fibrinogen cleavage
Der p 2, Fel d 1, nickel allergens	TLR4 agonism (direct or via MD2)
Alum adjuvant	Nlrp3 activation, crystal formation, extracellular DNA
Chitin (fungi, crustacea, insects)	Receptor?, EC activation, degraded by chitinases
Bee, wasp, and reptile venoms	Phospholipase A2 cleaves membrane phospholipids, others?
Environmental cold	Beige fat recruitment, PPARγ agonism?



Resistance to helminths and exoparasites	In some cases (but some MC functions may favor the parasite)	In some cases
Resistance to venoms	Yes, by release of proteases and perhaps heparin	?
Receptors involved in stimulation (an incomplete list)	IL-4, IL-5, IL-6, IL-9, IL-33Rs, c-Kit ^{hi} , IFN-γR, TLRs, C3aR, C5aR, etc.	IL-1R, IL-2(CD25), IL-3, IL-4, IL-5, IL-6, IL-8Rs, c-Kit ^{lo} , TLRs, C3aR, C5aR, TSLPR, etc.
Allergic disorders (MCs & basophils contribute to anaphylaxis)	Positive and negative regulation of many aspects of inflammation and tissue remodeling	Promotion of inflammation; IL-4-induced development of M2 macrophages
Enhance IgE synthesis	Some settings	Some settings

GLUCOSE METABOLISM

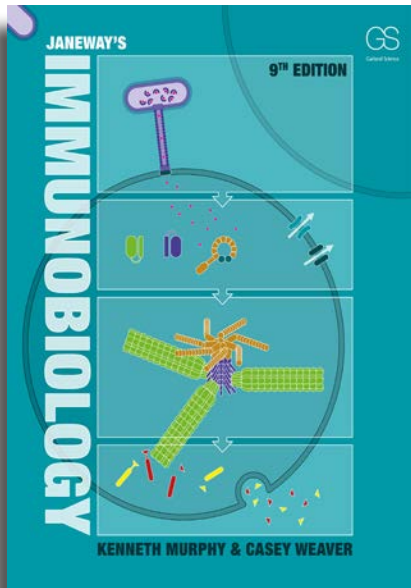


Assays available to measure:

- Glucose Uptake
- Glucose & Glucose-6-Phosphate
- Glucose-6-P-Dehydrogenase Activity
- Lactate Dehydrogenase Activity
- Lactate & Pyruvate
- Succinate Dehydrogenase Activity
- Citrate Synthase Activity
- Aconitase Activity
- Electron Transport Chain Activity
- Oxygen Consumption

New From Garland Science

JANEWAY'S IMMUNOBIOLOGY NINTH EDITION



Kenneth Murphy, Washington University School of Medicine
Casey Weaver, University of Alabama at Birmingham School of Medicine

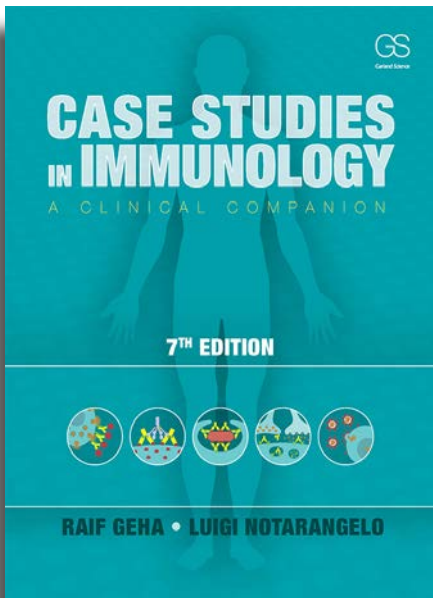
Janeway's Immunobiology is a textbook for students studying immunology at the undergraduate, graduate, and medical school levels. As an introductory text, students will appreciate the book's clear writing and informative illustrations, while advanced students and working immunologists will value its comprehensive scope and depth. **Janeway's Immunobiology** presents immunology from a consistent point of view throughout—that of the host's interaction with an environment full of microbes and pathogens. The Ninth Edition has been thoroughly revised bringing the content up-to-date with significant developments in the field, especially on the topic of innate immunity.

Also new to the Ninth Edition is a Question Bank available to adopting instructors, and the Garland Science Learning System which allows instructors to assign online tutorials with assessments on specific immunology topics and review the performance of the entire class, as well as individual students, via the instructor dashboard.

April 2016 • 928 pp • 621 illus
Loose-Leaf • 978-0-8153-4550-3 • \$95
Paperback • 978-0-8153-4505-3 • \$190
E-Books available for purchase and rental

To download a detailed table of contents and a chapter sample, please visit www.garlandscience.com/product/isbn/9780815345053

CASE STUDIES IN IMMUNOLOGY SEVENTH EDITION



Raif Geha, Harvard Medical School
Luigi Notarangelo, Harvard Medical School

Case Studies in Immunology, Seventh Edition is intended for medical students and undergraduate and graduate students in immunology. It presents major topics of immunology through a selection of clinical cases that reinforce and extend the basic science. Each case history is preceded by essential scientific facts about the immunological mechanisms of that specific disorder. The cases demonstrate how immunological problems are deconstructed in the clinic and each one is followed by a concise summary of the clinical finding and questions which can serve as discussion points.

The book includes a total of 55 cases and can be used as either a stand-alone text, review aid, or as a companion to **Janeway's Immunobiology, Ninth Edition** and **The Immune System, Fourth Edition**. Six new cases have been added to this edition: DOCK8 deficiency, activated PI3K delta syndrome, increased susceptibility to candida infections, LRBA deficiency, T cell signaling defects, and channelopathies.

February 2016 • 358 pp • 255 illus
Paperback • 978-0-8153-4512-1 • \$59
E-Books available for purchase and rental
Individual e-cases available for purchase

To view a list of all the cases and a sample case, please visit www.garlandscience.com/product/isbn/9780815345121

Visit us at the American Association of Immunologists Meeting in May

THE BENCHMARK IN ANTIBODIES

Since the day it was founded, Proteintech has been making all of its products to the highest standards possible while taking complete responsibility for the quality of each product.

- **Proteintech makes every single antibody in its 12,000-strong catalog.**
- **Each Proteintech product is unique and cannot be bought under a different label.**
- **Antibodies tested in siRNA knockdown experiment to demonstrate specificity.**
- **It works in any species and any application or get a full money-back refund.**